CALCIUM HOMEOSTASIS IN SKELETAL MUSCLE FUNCTION, PLASTICITY AND DISEASE

EDITED BY: Matias Mosqueira, Heinrich Brinkmeier and Enrique Jaimovich
PUBLISHED IN: Frontiers in Physiology

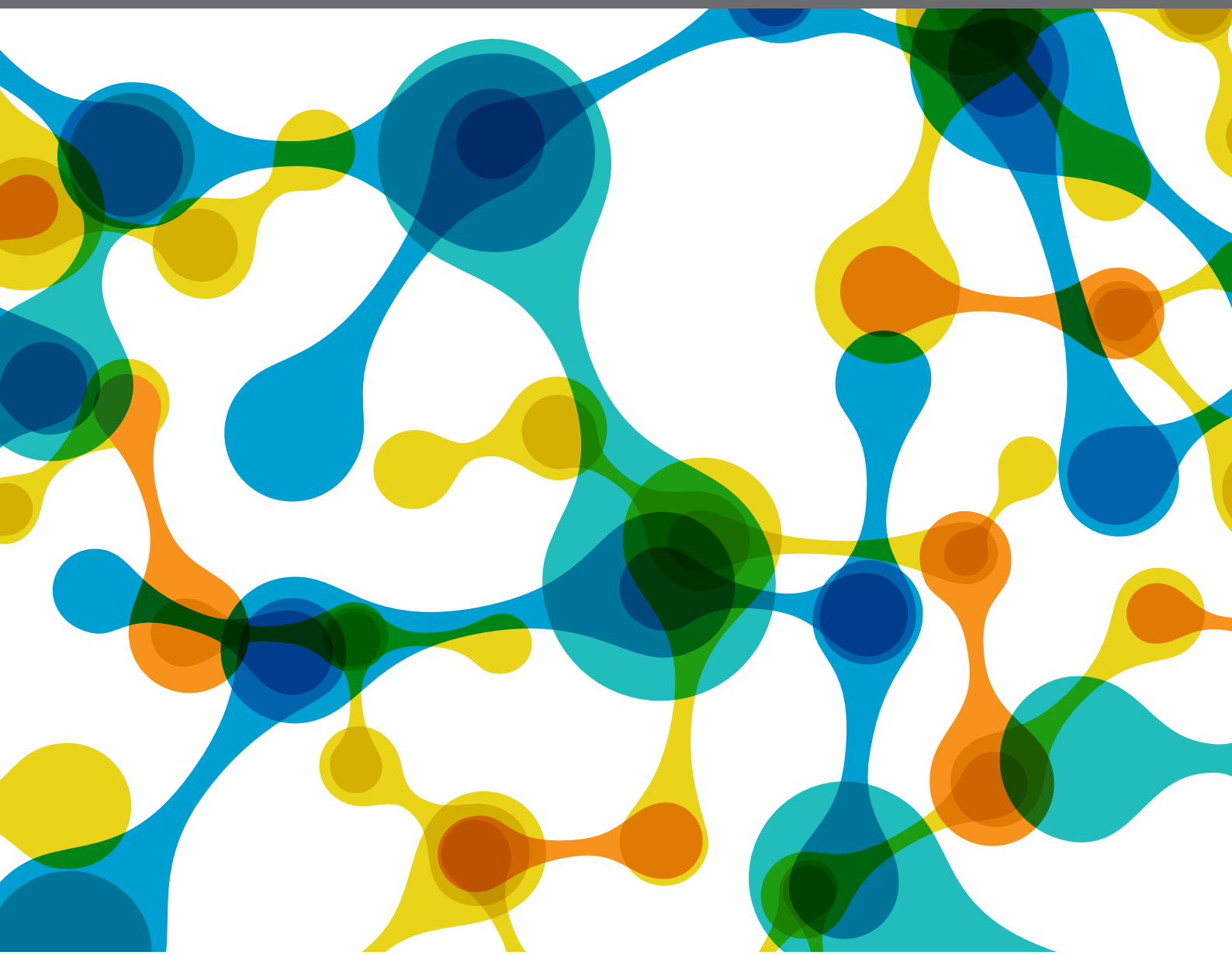

frontiers Research Topics

frontiers

ISSN 1664-8714
ISBN 978-2-88966-816-8
DOI 10.3389/978-2-88966-816-8

About Frontiers

Frontiers is more than just an open-access publisher of scholarly articles: it is a pioneering approach to the world of academia, radically improving the way scholarly research is managed. The grand vision of Frontiers is a world where all people have an equal opportunity to seek, share and generate knowledge. Frontiers provides immediate and permanent online open access to all its publications, but this alone is not enough to realize our grand goals.

Frontiers Journal Series

The Frontiers Journal Series is a multi-tier and interdisciplinary set of open-access, online journals, promising a paradigm shift from the current review, selection and dissemination processes in academic publishing. All Frontiers journals are driven by researchers for researchers; therefore, they constitute a service to the scholarly community. At the same time, the Frontiers Journal Series operates on a revolutionary invention, the tiered publishing system, initially addressing specific communities of scholars, and gradually climbing up to broader public understanding, thus serving the interests of the lay society, too.

Dedication to Quality

Each Frontiers article is a landmark of the highest quality, thanks to genuinely collaborative interactions between authors and review editors, who include some of the world's best academicians. Research must be certified by peers before entering a stream of knowledge that may eventually reach the public - and shape society; therefore, Frontiers only applies the most rigorous and unbiased reviews.
Frontiers revolutionizes research publishing by freely delivering the most outstanding research, evaluated with no bias from both the academic and social point of view. By applying the most advanced information technologies, Frontiers is catapulting scholarly publishing into a new generation.

What are Frontiers Research Topics?

Frontiers Research Topics are very popular trademarks of the Frontiers Journals Series: they are collections of at least ten articles, all centered on a particular subject. With their unique mix of varied contributions from Original Research to Review Articles, Frontiers Research Topics unify the most influential researchers, the latest key findings and historical advances in a hot research area! Find out more on how to host your own Frontiers Research Topic or contribute to one as an author by contacting the Frontiers Editorial Office: frontiersin.org/about/contact

CALCIUM HOMEOSTASIS IN SKELETAL MUSCLE FUNCTION, PLASTICITY AND DISEASE

Topic Editors:
Matias Mosqueira, Heidelberg University Hospital, Germany
Heinrich Brinkmeier, Universitätsmedizin Greifswald, Germany
Enrique Jaimovich, University of Chile, Chile

Citation: Mosqueira, M., Brinkmeier, H., Jaimovich, E., eds. (2021). Calcium Homeostasis in Skeletal Muscle Function, Plasticity and Disease. Lausanne: Frontiers Media SA. doi: 10.3389/978-2-88966-816-8

Table of Contents

05 ***Editorial: Calcium Homeostasis in Skeletal Muscle Function, Plasticity, and Disease***
Matias Mosqueira, Heinrich Brinkmeier and Enrique Jaimovich

08 ***Effects of Acute Exercise and Training on the Sarcoplasmic Reticulum Ca^{2+} Release and Uptake Rates in Highly Trained Endurance Athletes***
Kasper Degn Gejl, Erik P. Andersson, Joachim Nielsen, Hans-Christer Holmberg and Niels Ørtenbl

19 ***Dstac Regulates Excitation-Contraction Coupling in* Drosophila *Body Wall Muscles***
I-Uen Hsu, Jeremy W. Linsley, Lilly E. Reid, Richard I. Hume, Ari Leflein and John Y. Kuwada

30 ***Physiological Ca^{2+} Transients Versus Pathological Steady-State Ca^{2+} Elevation, Who Flips the ROS Coin in Skeletal Muscle Mitochondria***
Ang Li, Jianxun Yi, Xuejun Li and Jingsong Zhou

44 **STIM1/ORAI1** ***Loss-of-Function and Gain-of-Function Mutations Inversely Impact on SOCE and Calcium Homeostasis and Cause Multi-Systemic Mirror Diseases***
Roberto Silva-Rojas, Jocelyn Laporte and Johann Böhm

57 ***Multi-Cellular Functions of MG53 in Muscle Calcium Signaling and Regeneration***
Dathe Z. Benissan-Messan, Hua Zhu, Weina Zhong, Tao Tan, Jianjie Ma and Peter H. U. Lee

66 ***Phasic Store-Operated Ca^{2+} Entry During Excitation-Contraction Coupling in Skeletal Muscle Fibers From Exercised Mice***
Elena Lilliu, Karlheinz Hilber, Bradley S. Launikonis and Xaver Koenig

77 ***High Time Resolution Analysis of Voltage-Dependent and Voltage-Independent Calcium Sparks in Frog Skeletal Muscle Fibers***
Henrietta Cserne Szappanos, János Vincze, Dóra Bodnár, Beatrix Dienes, Martin F. Schneider, László Csernoch and Péter Szentesi

91 ***Disturbances in Calcium Homeostasis Promotes Skeletal Muscle Atrophy: Lessons From Ventilator-Induced Diaphragm Wasting***
Hayden W. Hyatt and Scott K. Powers

101 ***The Role of Orai1 in Regulating Sarcoplasmic Calcium Release, Mitochondrial Morphology and Function in Myostatin Deficient Skeletal Muscle***
Mónika Sztretye, Zoltán Singlár, Norbert Balogh, Gréta Kis, Péter Szentesi, Ágnes Angyal, Ildikó Balatoni, László Csernoch and Beatrix Dienes

116 ***Long-Term Exercise Reduces Formation of Tubular Aggregates and Promotes Maintenance of Ca^{2+} Entry Units in Aged Muscle***
Simona Boncompagni, Claudia Pecorai, Antonio Michelucci, Laura Pietrangelo and Feliciano Protasi

128 ***Senescence is Associated With Elevated Intracellular Resting [Ca^{2+}] in Mice Skeletal Muscle Fibers. An* in vivo *Study***
Alfredo Mijares, Paul D. Allen and Jose R. Lopez

138 ***Changes in Gene Expression of the MCU Complex Are Induced by Electrical Stimulation in Adult Skeletal Muscle***
Esteban R. Quezada, Alexis Díaz-Vegas, Enrique Jaimovich and Mariana Casas

148 ***Tissue-Engineered Skeletal Muscle Models to Study Muscle Function, Plasticity, and Disease***
Alastair Khodabukus

frontiers in Physiology

EDITORIAL
published: 26 March 2021
doi: 10.3389/fphys.2021.671292

Editorial: Calcium Homeostasis in Skeletal Muscle Function, Plasticity, and Disease

Matias Mosqueira[1]*, *Heinrich Brinkmeier*[2] *and Enrique Jaimovich*[3]

[1] *Institute of Physiology and Pathophysiology, Heidelberg University Hospital, Heidelberg, Germany,* [2] *Institute of Pathophysiology, University Medical Center Greifswald, Karlsburg, Germany,* [3] *Center for Exercise, Metabolism and Cancer Studies, Faculty of Medicine, University of Chile, Santiago, Chile*

Keywords: exercise, SOCE, ROS, MCU, Stac3 protein, MG53 (or TRIM72), mechanical ventilation, tissue engineering

Editorial on the Research Topic

Calcium Homeostasis in Skeletal Muscle Function, Plasticity, and Disease

The pivotal discovery of calcium as the only ion able to produce muscle contraction was made by Lewis Victor Heilbrunn in 1947. Since then, the role of calcium in the skeletal muscle has been expanded and clarified as the essential protagonist of intracellular signaling activity, metabolism, tissue formation, maturation, and regeneration. Physiological and biochemical effects of calcium are translated into cellular functions by the activity of calcium-binding proteins. Pathological conditions alter calcium's physiological role, making calcium a central target of therapeutic strategies. This Research Topic entitled "Calcium Homeostasis in Skeletal Muscle Function, Plasticity and Disease" collected new and relevant information on the role of calcium in skeletal muscle aiming to establish a new point of reference for future muscle research. For instance, Mijares et al. investigated the association of senescence with elevated intracellular resting [Ca^{2+}] in murine isolated single flexor digitorum brevis skeletal muscle fibers in parallel with an *in vivo* study. Using fluorescent ROS sensor CM-H2DCFDA in young (3 months-old), middle-aged (12 months-old), and aged (24 months-old) mice, they found an age-related increase in $[Ca^{2+}]_i$. When flufenamic acid, a non-steroidal anti-inflammatory was administered for several weeks the fluorescence levels were reduced in middle-aged and aged muscle fibers. This decrease was associated with a significant reduction of $[Ca^{2+}]_i$ as well as $[Na^{+}]_i$ and other pro-inflammatory markers.

It is known that Ca^{2+} plays a multifaceted role in mitochondrial function. During muscle contraction, Ca^{2+} influx into mitochondria activates multiple enzymes related to the tricarboxylic acid cycle and oxidative phosphorylation, resulting in increased ATP synthesis to meet the energy demand. Li et al. revised interesting mechanisms of how physiological Ca^{2+} transients vs. pathological steady-state Ca^{2+} elevation cause ROS increase in skeletal muscle mitochondria. Pathophysiological conditions such as skeletal muscle denervation or unloading also lead to elevated Ca^{2+} levels inside mitochondria. The outcomes of this steady-state elevation of mitochondrial Ca^{2+} level include exacerbated ROS generation, sensitized opening of mitochondrial permeability transition pore, induction of programmed cell death and ultimately muscle atrophy. However, both acute and long-term endurance exercise and electrical stimulation activate certain signaling pathways to counteract ROS production preventing apoptosis and alleviate muscle atrophy in denervated animal models and patients with motor impairment.

In this regard, Quezada et al. describe a new mechanism to explain the role of transient cytosolic Ca^{2+} signals and signaling pathways related to muscle plasticity by regulation of gene expression

OPEN ACCESS

Edited and reviewed by:
Paul M. L. Janssen,
The Ohio State University,
United States

***Correspondence:**
Matias Mosqueira
matias@physiologie.uni-heidelberg.de

Specialty section:
This article was submitted to Striated Muscle Physiology, a section of the journal Frontiers in Physiology

Received: *23 February 2021*
Accepted: *03 March 2021*
Published: *26 March 2021*

Citation:
Mosqueira M, Brinkmeier H and Jaimovich E (2021) Editorial: Calcium Homeostasis in Skeletal Muscle Function, Plasticity, and Disease. Front. Physiol. 12:671292. doi: 10.3389/fphys.2021.671292

of the MCU complex in adult skeletal muscle. The Authors report that the MCU complex can be regulated by electrical stimuli in a frequency-dependent manner. The changes observed in mRNA levels may be related to changes in the mitochondria, due to phenotypic transition from a fast to a slow muscle type. Exogenous ATP decreases the mRNA levels of the MCU complex while MCU levels increase when basal [ATP] is reduced, indicating that extracellular ATP may be a regulator of the MCU complex and part of the axes linking low-frequency stimulation with ATP/IP3/IP3R.

Store-operated calcium entry (SOCE) is a fast mechanism responsible for replenish SR with Ca^{2+} that is controlled by SR-located STIM1 and Orai1 present in the sarcolemma. In rat skeletal muscle, but not in mouse, a phasic SOCE can be activated upon single action potentials. Lilliu et al. demonstrating that pSOCE can be electrically triggered in EDL skinned murine muscle after 5–6 days of voluntary wheel-running successfully answered this issue. This simple strategy expands the use of genetically modified mouse models to further comprehending the physiology and pathophysiology of SOCE.

A second paper related to Orai1 has been published in this Research Topic, focusing on cell physiological consequences of reduced Orai1 gene expression. Sztretye et al. used two models, muscles from myostatin deficient mice and muscles from WT mice, gene silenced for Orai1. The authors present changes in mitochondrial function, altered ultrastructure of the neuromuscular junction and reduced postsynaptic Ca^{2+} transients. They suggest that reduced Orai1 gene expression may be related to certain types of muscle weakness and alleviated neuromuscular transmission.

Silva-Rojas et al. reviewed the remarkable diversity of phenotypes and disorders related to STIM/Orai proteins. STIM1 and Orai1 are required for the regulation and fine-tuning of the Ca^{2+} level in the sarco-/endoplasmic reticulum of many cell types. Both, loss of function and gain of function of either protein cause alterations of cellular functions leading to diseases. Early data on loss of function of Orai1 reported immune deficiency and muscle weakness in children. Recent findings revealed dysfunctions of eye movement, skin, bone and spleen abnormalities as well as blood coagulation defects due to mutations in the STIM1 and Orai1 genes.

Elementary calcium release events known as Ca^{2+}-sparks are observed in mammalian and non-mammalian skeletal muscle, characterizing the morphology and frequency of spontaneous Ca^{2+} release events. As in mammals, frogs also express two types of RyR. The α isoform is associated with DHPRs, while the β isoform is not connected with DHPR but sensitive to $[Ca^{2+}]_i$. Recording Ca^{2+}-sparks from isolated frog fibers at high-speed acquisition (15.4 μs/line), Szappanos et al. show that caffeine-dependent Ca^{2+}-spark are significantly larger and more frequently than the voltage-dependent. This result revealed the role of RyRβ in the generation of spontaneous Ca^{2+}-sparks and shedding light on the interaction of RyRα and RyRβ during Ca^{2+} release.

Tubular aggregates (TAs) are characterized by abnormal accumulation of packed SR tubes, a histopathological feature in TA myopathy (TAM). TAM is linked to gain-of-function mutations in both STIM1 and Orai1 and is commonly found in human muscle disorders, such as dyskalemia, periodic paralysis, or myotonic disorders. Boncompagni et al. evaluated the presence of TAs, STIM1-Orai1 localization and expression and fatigue resistance in intact wild-type murine EDL muscles at 4-month-old, aged (24-month-old) and in wheel-running trained for 15 months (starting from 9 months-old). Based on the evidence that long-term exercise significantly reduced aged-dependent TAs formation and accumulation of STIM1 and Orai1 in TAs and exercise restored the capability of aged EDL to use external Ca^{2+}, the Authors concluded that exercise maintains correct SOCE activity during aging.

New evidence of Ca^{2+} release's function during exercise is presented by Gejl et al. The Authors measured Ca^{2+} release from SR vesicles from muscles triceps brachii and vastus lateralis obtained from cross-country skiers and triathletes together with cyclists athletes 4-min single-bout of high-intensity exercise. The Authors showed reduced SR Ca^{2+} release after acute high-intensity training, which was further reduced when the athletes repeated the high-intensity exercise, without alteration on SERCA1 function. Together, this study demonstrated that short duration of high-intensity exercise adapts the EC-coupling reducing Ca^{2+} release without modifying Ca^{2+}-uptake.

In vertebrates, Stac3 protein is responsible for DHPR's function and localization. Mutants of Stac3 showed significant reduction in muscle function due to dysfunction and mis-localization of DHPR. Hsu et al. demonstrated in larvae of Drosophila that the Stac3 (Dstac) expression pattern correlated with the DHPR's pattern in the T-tubule and Stac3 knockout resulted in a significantly disarranged DHPR localization, but no alteration in the T-tubule disposition. Consequently, larval locomotion was significantly affected due to reduced Ca^{2+} transients. These results, as seen in vertebrates, suggest that Stac3 is relevant for the normal EC-coupling in skeletal muscles.

Benissan-Messan et al. revised the pivotal function of Mitsugumin-53 (MG53), a protein from tripartite motif (TRIM) family responsible for EC-coupling function such as enhancing Ca^{2+}-entry via SOCE and reducing RyR1 and SERCA activities as well at transcriptional level increasing TRPC3 and TRPC4 expressions and repair facilitating vesicle translocation to the plasma membrane after injury. MG53 also plays pivotal role on regeneration in different tissues besides skeletal muscle, resulting in an interesting key protein to be analyzed in several muscular dystrophies and aging.

Diaphragm' of patients under long-term mechanical ventilation (MV) reduce protein anabolism and increase protein catabolism, inducing diaphragmatic atrophy. This mechanism is known as ventilator-induced diaphragm dysfunction (VIDD). Hyatt and Powers reviewed new evidence of how mitochondrial ROS production during MV oxidates RyR1, leading to disassociation of calstabin1 from RyR1, resulting in Ca^{2+} leakage from the SR. Subsequently, high cytosolic Ca^{2+} triggers several proteolytic systems, which among them, calcium-activated protease calpain signaling pathway is the main responsible for VIDD. Therefore, it is relevant to control ROS production and re-establish Ca^{2+} homeostasis in the diaphragm during MV.

An interesting review by Khodabukus analyses the current evidence on tissue-engineered skeletal muscle models to study

muscle function, plasticity, and disease; although small animal models have been essential for elucidating the molecular mechanisms regulating skeletal muscle adaptation and plasticity, these models do not always accurately model human muscle disease. The potential of *in vitro* three-dimensional tissue-engineered skeletal muscle models is discussed, as well as the genetic, neural, and hormonal factors regulating skeletal muscle fiber-type *in vivo* and the ability of current *in vitro* models to study muscle fiber-type regulation.

In summary, this Research Topic highlighted the most recent function of Calcium in skeletal muscle, covering from the molecular level through signaling pathways up to the whole body with innovative models giving relevant information for physiological and pathophysiological conditions.

AUTHOR CONTRIBUTIONS

All authors listed have made a substantial, direct and intellectual contribution to the work, and approved it for publication.

Conflict of Interest: The authors declare that the research was conducted in the absence of any commercial or financial relationships that could be construed as a potential conflict of interest.

frontiers in Physiology

ORIGINAL RESEARCH
published: 07 July 2020
doi: 10.3389/fphys.2020.00810

Effects of Acute Exercise and Training on the Sarcoplasmic Reticulum Ca^{2+} Release and Uptake Rates in Highly Trained Endurance Athletes

Kasper Degn Gejl[1], Erik P. Andersson[2], Joachim Nielsen[1], Hans-Christer Holmberg[2,3] and Niels Ørtenblad[1]*

[1] Department of Sports Science and Clinical Biomechanics, University of Southern Denmark, Odense, Denmark, [2] Swedish Winter Sports Research Centre, Department of Health Sciences, Mid Sweden University, Östersund, Sweden, [3] Department of Physiology and Pharmacology, Biomedicum C5, Karolinska Institute, Stockholm, Sweden

OPEN ACCESS

Edited by:
Matias Mosqueira, Heidelberg University Hospital, Germany

Reviewed by:
Nicolas Place, University of Lausanne, Switzerland
Dae Yun Seo, Inje University College of Medicine, South Korea

***Correspondence:**
Kasper Degn Gejl
kgejl@health.sdu.dk

Specialty section:
This article was submitted to Striated Muscle Physiology, a section of the journal Frontiers in Physiology

Received: *29 April 2020*
Accepted: *18 June 2020*
Published: *07 July 2020*

Citation:
Gejl KD, Andersson EP, Nielsen J, Holmberg H-C and Ørtenblad N (2020) Effects of Acute Exercise and Training on the Sarcoplasmic Reticulum Ca^{2+} Release and Uptake Rates in Highly Trained Endurance Athletes. Front. Physiol. 11:810. doi: 10.3389/fphys.2020.00810

Little is presently known about the effects of acute high-intensity exercise or training on release and uptake of Ca^{2+} by the sarcoplasmic reticulum (SR). The aims here were to characterize this regulation in highly trained athletes following (1) repeated bouts of high-intensity exercise and (2) a period of endurance training including high-intensity sessions. Eleven cross-country skiers (25 ± 4 years, 65 ± 4 mL $O_2 \cdot kg^{-1} \cdot min^{-1}$) performed four self-paced sprint time-trials (STT 1-4) lasting ≈ 4 min each (STT 1–4) and separated by 45 min of recovery; while 19 triathletes and road cyclists (25 ± 4 years, 65 ± 5 mL $O_2 \cdot kg^{-1} \cdot min^{-1}$) completed 4 weeks of endurance training in combination with three sessions of high-intensity interval cycling per week. Release ($\mu mol \cdot g^{-1}$ prot$\cdot min^{-1}$) and uptake [tau (s)] of Ca^{2+} by SR vesicles isolated from m. *triceps brachii* and m. *vastus lateralis* were determined before and after STT 1 and 4 in the skiers and in m. *vastus lateralis* before and after the 4 weeks of training in the endurance athletes. The Ca^{2+} release rate was reduced by 17–18% in both limbs already after STT 1 (arms: 2.52 ± 0.74 to 2.08 ± 0.60; legs: 2.41 ± 0.45 to 1.98 ± 0.51, $P < 0.0001$) and attenuated further following STT 4 (arms: 2.24 ± 0.67 to 1.95 ± 0.45; legs: 2.13 ± 0.51 to 1.83 ± 0.36, $P < 0.0001$). Also, there was a tendency toward an impairment in the SR Ca^{2+} uptake from pre STT1 to post STT4 in both arms and legs (arms: from 22.0 ± 3.7 s to 25.3 ± 6.0 s; legs: from 22.5 ± 4.7 s to 25.5 ± 7.7 s, $P = 0.05$). Endurance training combined with high-intensity exercise increased the Ca^{2+} release rate by 9% (1.76 ± 0.38 to 1.91 ± 0.44, $P = 0.009$), without altering the Ca^{2+} uptake (29.6 ± 7.0 to 29.1 ± 8.7 s; $P = 0.98$). In conclusion, the Ca^{2+} release and uptake rates by SR in exercising limbs of highly trained athletes declines gradually by repetitive bouts of high-intensity exercise. We also demonstrate, for the first time, that the SR Ca^{2+} release rate can be enhanced by a specific program of training in highly trained athletes, which may have important implications for performance parameters.

Keywords: sarcoplasmic reticulum, fatigue, Ca^{2+} handling, athletes, exercise, training

INTRODUCTION

The functional capacity of skeletal muscles relies partly on intrinsic metabolic and mechanic properties and by repetitive contractions these may be disrupted leading to a reduction in skeletal muscle function and performance, i.e., fatigue (Allen et al., 2008). In most activation patterns and exercise tasks, a substantial part of the fatigue development is associated with impairments in the sequence of events at the muscle level leading to muscle activation and relaxation denoted the excitation-contraction (E-C) and relaxation coupling. The E-C and relaxation is a strictly coordinated regulation of the free cytosolic Ca^{2+} concentration in order to control the myofiber contraction and relaxation. This regulation is handled through an intracellular membrane-delimited organelle, the sarcoplasmic reticulum (SR). In response to muscle activation by action potential propagation throughout the t-tubules, the SR Ca^{2+} release channel [ryanodine receptor (RyR1)] opens, and Ca^{2+}-ions diffuse passively into the cytosol, elevating the cytosolic Ca^{2+} 10 to 20-fold (Ingalls et al., 1999; Bruton et al., 2003) activating the cross-bridge cycling. Concomitantly, Ca^{2+}-ions are re-sequestered back to the SR through another SR membrane protein [SR Ca^2 ATPase (SERCA)], leading to relaxation of the muscle fiber. Studies in intact single fibers of rodent and human skeletal muscle have repeatedly revealed that steps in the E-C coupling involving myofibrillar Ca^{2+} regulation are an important part of the decrease in force production following repeated contractions, with the underlying cellular mechanisms being, (i) an impaired SR Ca^{2+} release, (ii) a reduced myofibrillar Ca^{2+} sensitivity or (iii) a reduced maximal Ca^{2+} activated force production, with the importance of each depending on muscle activation pattern and duration (Allen et al., 2008). Further, these studies have revealed decreases in muscle fiber relaxation rate and rates of myofibrillar Ca^{2+} decline.

While myofibrillar Ca^{2+} levels have mainly been studied in rodent single fiber preparations, SR Ca^{2+} release and uptake rates can be measured directly in SR vesicles from human biopsies. In these studies, deteriorations in both SR vesicle Ca^{2+} release and uptake have repeatedly been reported in response to exercise. A decreased SR vesicle Ca^{2+} release and -uptake has been observed following short-term high-intensity exercise in untrained individuals (Hostrup et al., 2014) and following a single bout of short-term high-intensity knee-extension exercise or endurance exercise in both untrained (Booth et al., 1997; Tupling et al., 2000; Duhamel et al., 2006) and trained individuals (Li et al., 2002; Ørtenblad et al., 2011; Gejl et al., 2014). The few studies in highly trained individuals have shown consistent reductions in the SR vesicle Ca^{2+} release rate following exhaustive endurance exercise, whereas changes in SR Ca^{2+} uptake have been less consistent (Li et al., 2002; Ørtenblad et al., 2011; Gejl et al., 2014). In line with this, extensive fragmentation of the SR Ca^{2+} release channel was observed in recreationally active human subjects following repeated high-intensity exercise, while experiments on elite endurance athletes performing the same exercise showed no channel fragmentation (Place et al., 2015). However, the existing literature in trained humans has primarily focused on changes in SR function with acute endurance exercise, while little is known about changes during repeated high-intensity exercise and recovery.

A systematic change in function and demands posed on skeletal muscle will result in adaptations that increase performance toward the characteristics of the exercise stimulus (Bogdanis, 2012). Accordingly, adaptations that may reduce muscle fatigue during high-intensity exercise depend on the characteristics of the training program, i.e., type, intensity, frequency, and duration. While a salient response to training is increases in e.g., mitochondrial content and function (Granata et al., 2018) the antioxidant capacity (Hellsten et al., 1996; Ørtenblad et al., 1997) and muscle glycogen availability (Gejl et al., 2017a) little is known about effects of training on the SR Ca^{2+} handling properties *per se* in athletes. In untrained individuals, however, the SR Ca^{2+} ATPase activity has been shown to remain unaltered following sprint training (Ørtenblad et al., 2000) and resistance training (Green et al., 1998; Hunter et al., 1999) in some studies, while others have observed reductions following sprint training (Harmer et al., 2014) resistance training (Hunter et al., 1999) and aerobic training (Green et al., 2003). To the best of our knowledge, only one study has investigated the effects of exercise training on the SR Ca^{2+} release rate, and here a robust increase in SR vesicle Ca^{2+} release rate was observed following a 5-week period with sprint training (Ørtenblad et al., 2000). Based on these findings, high-intensity exercise seems necessary to improve the SR Ca^{2+} handling properties and it is highly relevant to investigate whether such adaptations in the SR Ca^{2+} handling are also present following exercise training involving high-intensity exercise in highly trained athletes. Accordingly, an optimization of the SR regulatory abilities may prevent myocellular disturbances in the Ca^{2+} homeostasis during exhaustive exercise.

Here, we examined changes in SR Ca^{2+} uptake and release in arm and leg muscles of highly trained athletes in response to acute exercise and training – i.e., cross-country skiers performing repeated high-intensity exercise and triathletes and road cyclists conducting 4 weeks of endurance training including high-intensity exercise, i.e., both interventions similar to their actual activities. We hypothesized that both acute and repeated high-intensity exercise impair SR Ca^{2+} handling, whereas a period of endurance training including high-intensity exercise improves SR function.

MATERIALS AND METHODS

Study Overview

The effects of both acute exercise and training on SR vesicle Ca^{2+} handling was determined in two groups of elite athletes performing exercise resembling "real-life" competition or training (**Figure 1** and **Table 1**). One group of highly trained cross-country skiers performed acute exercise consisting of four bouts of sprint time-trials (STTs) separated by 45 min. of recovery between bouts. The other group consisting of highly trained triathletes and road cyclists carried out both acute exercise and 4 weeks of endurance training including high-intensity exercise.

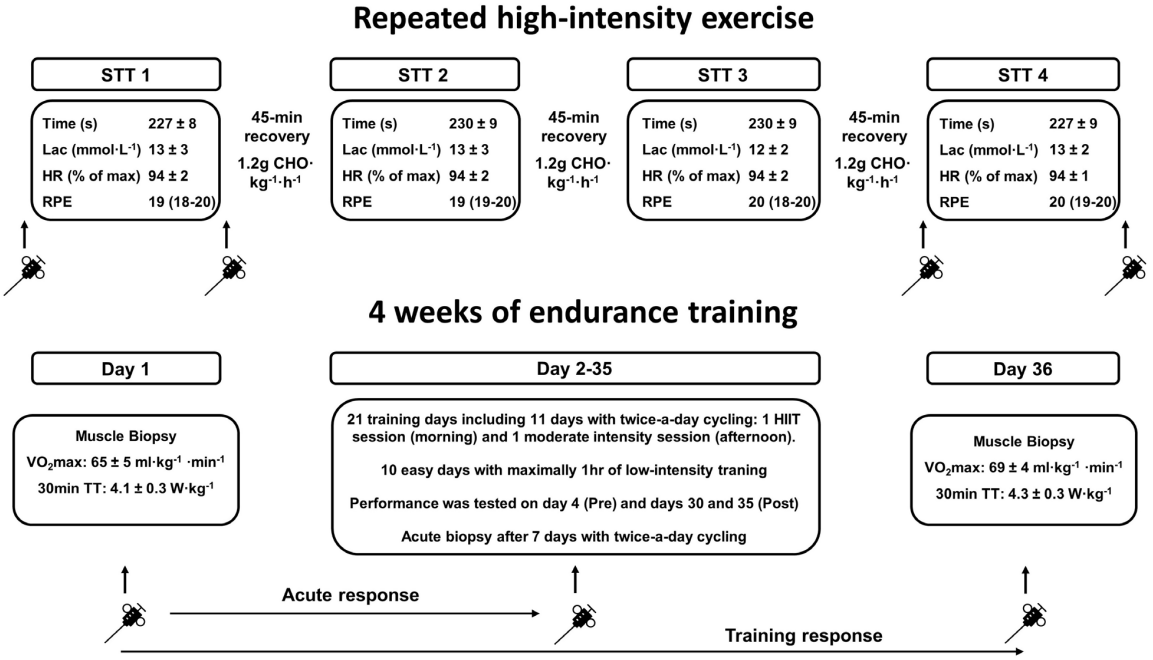

FIGURE 1 | Overview of the study protocol employed to examine the response of calcium handling by the sarcoplasmic reticulum in the muscles of the arms and legs to exercise. The **(upper)** section illustrates the four maximal 1300-m sprint time-trials (STT 1–4), separated by 45-min periods of recovery with intake of carbohydrate (CHO), performed by highly trained cross-country skiers, as well as associated analyzes. Muscle biopsies were obtained before and after the first (STT1) and fourth time-trials (STT4). Information about the time required to complete (time), blood lactate concentration (Lac) immediately after completion, average heart rate (HR) and RPE during each STT have been reported previously [values are mean ± SD, and for RPE as median (range)] (Andersson et al., 2016). The **(lower)** section illustrates the "real-life" training day and subsequent 34-day period of training by highly trained triathletes and road cyclists (described in detail in the section "Materials and Methods"). Information about changes in performance (i.e., VO2max and power output during the 30-min time-trial) following this training period have also been reported previously (Gejl et al., 2017b).

TABLE 1 | Subject characteristics.

	Repeated high- intensity exercise	Acute responses to endurance training	Long-term responses to endurance training
Group	Cross-country skiers	Triathletes and Cyclists	Triathletes and Cyclists
n	11	12	19
Age (years)	25 ± 4	24 ± 4	25 ± 5
Body mass (kg)	79 ± 6	76 ± 7	74 ± 7
Height (cm)	183 ± 9	184 ± 7	182 ± 6
VO_{2max} ($mL \cdot min^{-1}$)	5.1 ± 0.5	5.0 ± 0.6	4.8 ± 0.6
VO_{2max} ($mL \cdot kg^{-1} \cdot min^{-1}$)	65 ± 4	66 ± 6	65 ± 5
MHC Leg (% I; % IIa)	51 ± 8; 49 ± 8	53 ± 7; 47 ± 7	51 ± 8; 49 ± 8
MHC Arm (% I; % IIa)	39 ± 6; 61 ± 6		

Highly trained cross-country (CC) skiers underwent four bouts of high-intensity exercise with 45 min recovery, while highly trained triathletes and road cyclists performed exercise of moderate- to high intensity for 4 weeks. At different time-points during this period, SR Ca^{2+} handling of muscles in the arms and legs of the skiers and legs of the endurance athletes was examined. The values presented are means ± SD.

Subjects and Ethical Approval

The 11 cross-country skiers who performed STTs were highly trained male competitors in national and/or international sprint and distance races who trained 8–11 h each week during the period of the study (**Table 1**). The group performing endurance training was composed of 13 highly trained male triathletes and 6 elite male road cyclists. Among the triathletes, six were current members of the Danish National Team competing in international Olympic and sprint distances (the Olympic Games, World Triathlon Series, World Cup and Continental Cup), 7 participated in elite international and national competitions (at Olympic, 1/2 ironman and ironman distances), while the remaining two competed at a lower level (1/2 ironman and ironman distances). All 6 cyclists had A-licenses and competed at the elite national level (**Table 1**).

The participants were fully informed of potential risks associated with the experiments before verbal and written consents were obtained. The study was approved by the local Ethics Committee of Southern Denmark (Project-ID S-20150034) and Regional Ethics Review Board in Umeå, Sweden (#2013-59-31) and the experiments adhered to the standards of the *Declaration of Helsinki*. This study was part of a larger project described in part previously (Gejl et al., 2017b).

The STTs

The skiers were tested on a treadmill in the laboratory (Mid Sweden University, Östersund, Sweden) on separate days over 3 weeks, with at least 48 h between test days. These tests

are described in detail elsewhere (Andersson et al., 2016). Briefly, baseline height and body mass, as well as maximal oxygen uptake ($\dot{V}O_{2max}$) while performing both diagonal and double poling techniques were determined during the first visits, while the penultimate visit involved familiarization with the simulated competition protocol and on the final day the actual testing took place.

The protocol included four STTs, each 1300 m of supra-maximal roller-skiing (∼4 min. in duration), with 45 min. of recovery between successive STT's (**Figure 1**). Before undertaking STT 1, the skier warmed-up for 15-20 min., while STT 2-4 were preceded by a 5-min warm-up and STT 1–3 followed by a 5-min cool-down. Between cool-down and warm-up, the skiers rested passively for approximately 28 min.

Each 1300 m STT consisted of three flat sections (1° incline) to be skied employing the double poling technique (DP), with two intermediate uphill sections (7° incline) on which the diagonal stride sub-technique (DS) was utilized. The course was in total, 57% flat (1°), 23% uphill (7°), while the remaining 20% consisted of transitions from 1° to 7° or vice versa. This resulted in an average course incline of 2.8°. Skiers were encouraged to exert a maximal effort during each trial and were aided in doing so by continuous feedback concerning their speed and position on the course provided by a screen in front of the treadmill. The course was designed to simulate international cross-country sprint competitions (except downhill sections for safety reasons) and the total duration of the four STTs and recovery periods was 3 h, i.e., similar to the duration of actual sprint competitions.

Skiing speed, heart rate and $\dot{V}O_2$ were monitored continuously during the four STTs, and this data subsequently averaged (Andersson et al., 2016; Gejl et al., 2017a). Room temperature (∼22°C) and humidity (∼56%) were maintained throughout the experiment. The subjects were instructed to refrain from all physical activities of moderate to high intensity during the 48 h prior to testing.

During the 24 h prior to the first STT, each skier consumed three standardized CHO-enriched meals (on average, 18.000 kJ, 55% CHO, 30% fat, and 15% protein) and three snacks (8 g $CHO{\cdot}kg^{-1}$ $bw{\cdot}day^{-1}$), with the last meal being consumed in the laboratory 120 min. before the warm-up for STT1. During each of the 45-min. recovery periods the subjects consumed 1.2 g $CHO{\cdot}kg^{-1}$ $bw{\cdot}h^{-1}$, on average 40 g CHO in the form of a sport drink mixed with water and 30 g as an energy gel, with *ad libitum* intake of water. This CHO intake during the recovery periods was in accordance with the recommendations from the American College of Sports Medicine (Rodriguez et al., 2009).

Endurance Training

The triathletes and cyclists performed 4 weeks of routine training in combination with high-intensity interval cycling (HIIT). Skeletal muscle SR vesicle Ca^{2+} handling properties were examined at rest both before and after this 4-week intervention, as well as 1h following the moderate-intensity afternoon session on the seventh day of this intervention (**Figure 1**).

Originally, the study was designed to investigate the effects of periodized glycogen depletion on adaptations to training and for this purpose CHO intake during certain portions of the training period was manipulated. However, and as reported in companion papers, all acute responses (e.g., muscle glycogen, serum hormone levels, blood glucose) and training adaptations (e.g., performance, oxidative enzyme activity, VO_2max) were not different and similar between the intervention groups despite the CHO manipulation (Gejl et al., 2017b, 2018). This was also the case regarding SR Ca^{2+} handling, which allowed us to combine these two groups for the present analysis.

With the advice of exercise researchers and the Danish national triathlon coach, 4-week training plans were designed for the triathletes and cyclists, taking training history into account. On average, athletes trained 16 [12–20] hours per week and performed three HIIT sessions per week (11 times in total). The HIIT session was performed in the morning and consisted of eight 5-min cycling intervals separated by 2 min of active recovery, followed 7 h later by a moderate intensity cycling session. In connection with each session of HIIT, the first six 5-min intervals were conducted with a target intensity of 85% HR_{max}, while the final two consisted of five 15-s maximal sprints designed to recruit type II fibers, separated by 45-s of easy spinning. The afternoon session entailed 2 hrs of moderate cycling with a target intensity of 65% HR_{max}.

Both morning and afternoon sessions were carried out on personal bikes by use of turbo trainers (Tacx Bushido Smart T2780, Wassenaar, Netherlands). The three weekly double sessions comprised 30–50% of the total training volume. For the purposes of recovery, 1–2 weekly training days involved a maximum of 45 min of easy training. The remaining training days included two sessions of easy-to-moderate biking for the road cyclists (1.5–3.5 h at 65–75% of HR_{max}), or in the case of the triathletes, 2–4 sessions of easy-to-moderate swimming and 4–6 easy-to-moderate runs (65–85% of HR_{max}). Thus, in connection with this intervention, which was conducted during the pre-season, both the intensity of exercise during HIIT and the amount of high-intensity exercise were greater than normal for this period, whereas the total overall volume of training was maintained and similar to normal training during this period.

On the 11 days including two bikes sessions, all meals were provided to the subjects, while on the remaining days subjects were instructed to ingest CHO-enriched meals in the morning, for lunch and for dinner. To ensure dietary conformity, 3-day dietary recordings were collected both prior to and during the training period. A few athletes were asked to increase energy intake if their total intake of energy or CHO was less than recommended [1.8 PAL (0.0669bw + 2.28) $MJ{\cdot}day^{-1}$ or 5g CHO $kg^{-1}{\cdot}day^{-1}$]. Detailed information about training and dietary intake during the intervention has been described elsewhere (Gejl et al., 2017a).

Analytical Procedures

Muscle Biopsies

Using 5 mm Bergström needles, muscle biopsies of 100–150 mg were obtained from the *m. triceps brachii* and *m. vastus lateralis* in skiers and the *m. vastus lateralis* in the triathletes and cyclists. The procedure for the extraction of muscle tissue has been described in detail elsewhere (Gejl et al., 2017b). Muscle biopsies were obtained randomly from the right and left limb. In the skiers, biopsies were obtained before and after both STT 1 and

4. The first biopsy was extracted 35 min before STT 1 while the remaining biopsies were obtained 10–12 min after STT1 and 10–12 min before and after STT 4.

In the triathletes and cyclists, biopsies were obtained before (Pre) and after (Post) the 4 weeks of training as well as acutely (Acute) following the 7th day including both HIIT and moderate-intensity exercise. The pre- and post-biopsies were obtained in 19 subjects 1h after a standard meal and at identical time-points within each subject. The subjects received a standard diet for the last 24 h prior to the biopsy extraction (5 g CHO · kg bm^{-1}·d^{-1} with a total energy intake of 34.8 kcal · kg bm^{-1}). The final day with twice-a-day cycling was completed 36 h before extraction of the post-biopsy and athletes refrained from exercise during this recovery period. The acute biopsy was obtained in 12 subjects 1 h after completing the moderate-intensity afternoon session.

In both the skiers and the group of triathletes and cyclists, the muscle samples were placed on a filter paper on an ice-cooled ∼0°C petri dish and divided into several specimens. One part of the biopsy was immediately frozen in liquid nitrogen and stored at −80°C for subsequent analysis of glycogen content. Another part was manually homogenized with a potter-elvehjem glass-glass homogenizer (Kontes Glass Industry, Vineland, NJ, United States) for determination of SR vesicle Ca^{2+} release- and uptake and myosin heavy chain (MHC) distribution.

SR Vesicle Ca^{2+} Uptake and Release

The fluorescent dye technique was used to determine Ca^{2+} uptake and release rates in SR vesicles and it has been described in detail elsewhere (Ørtenblad et al., 2011; Gejl et al., 2014). Free [Ca^{2+}] was determined by the fluorescent Ca^{2+} indicator Indo-1 (1 μM) (20 Hz, Ratiomaster RCM; Photon Technology International, Brunswick, NJ, United States). SR vesicle Ca^{2+} uptake was initiated by adding 2 mM ATP to a final concentration of 5 mM and Ca^{2+} uptake was recorded for 3 min, before [Ca^{2+}] reached a plateau. The SR Ca^{2+} uptake rate was defined as the time for free [Ca^{2+}] to decrease by 63%. Upon measurements of Ca^{2+} uptake, the SR Ca^{2+} ATPase was blocked with cyclopiazonic acid before SR vesicle Ca^{2+} release was initiated by addition of 4-chloro-M-Cresol (4-CmC) (5 mM). Raw-data for [Ca^{2+}] were mathematically fitted using mono-exponential equations as previously described (Curve Fitting Toolbox version 1.1.1; The MathWorks, Natick, MA, United States) (Ørtenblad et al., 2011; Gejl et al., 2014). A representative example of measurements before and after STT 1 in the cross-country skiers is illustrated in **Figure 2**. Values obtained for SR Ca^{2+} release rates are relative and expressed as arbitrary units; Ca^{2+}·g $protein^{-1}$·min^{-1}. Assays of Ca^{2+} uptake and release were performed in triplicates (a few in duplicates due to limited tissue homogenate). Protein content in the muscle homogenate was measured in triplicates using a standard kit (Pierce BCA protein reagent no. 23225).

Muscle Glycogen and MHC Isoform

Muscle glycogen content was determined spectrophotometrically (Beckman DU 650) (Passonneau and Lowry, 1993; Gejl et al., 2014). Freeze-dried muscle tissue (1.5 mg) was boiled in 0.5 ml 1 M HCL for 150 min before it was quickly cooled, whirl-mixed and centrifuged at 3500 *g* for 10 min at 4°C. Forty μL of boiled muscle sample and 1 ml of reagent solution containing Tris-buffer (1M), distilled water, ATP (100 mM), $MgCl_2$ (1M), $NADP^+$ (100 mM) and G-6-PDH were mixed before the process was initiated by adding 10 μL of diluted hexokinase. Absorbance was recorded for 60 min before the glycogen content was calculated. Muscle glycogen was expressed as mmol·kg dw^{-1}.

Myosin heavy chain (MHC) composition was determined from homogenate using gel electrophoresis as previously described (Betto et al., 1986) and modified for humans (Ortenblad et al., 2000). Briefly, muscle homogenate (80 μL) was mixed with 200 μL of sample-buffer (10% glycerol, 5% 2-mercaptoethanol and 2.3% SDS, 62.5 mM Tris and 0.2% bromophenolblue at pH 6.8.), boiled in water at 100°C for 3 min and loaded (10–40 μL) on a SDS-PAGE gel [6% polyacrylmide (100:1 acrylmid : bis-acrylmid), 30% glycerol, 67.5 mM tris-base, 0.4% SDS, and 0.1 M glycine]. Gels were run at 80 V for at least 42 h at 4°C and MHC bands made visible by staining with Coomassie. The gels were scanned (Lino-scan 1400 scanner, Heidelberg, Germany) and MHC bands quantified densitometrically (Phoretix 1D, non-linear, Newcastle, United Kingdom) as an average of the three loaded protein amounts. MHC II was identified with Western blot using monoclonal antibody (Sigma M 4276) with the protocol Xcell IITM (Invitrogen, Carlsbad, CA, United States).

Statistical Analysis

All interactions or main effects were tested using a linear mixed-effects model, with time (and limb for the skiers) as fixed effects and individual subjects as random effect. Assumptions on heteroscedasticity and normal distribution were evaluated by inspecting the distribution of residuals and a standardized normal probability plot, respectively. Values are expressed as means ± SD and sample sizes are illustrated in the figure legends. Pearson's correlation analysis was used to analyze potential associations between variables. Analyzes demonstrating $P \leq 0.05$ were considered significant. All statistical analyzes were performed using Stata, version 16 (StataCorp LP, College Station, TX, United States). We have previously demonstrated a significant negative effect of exercise on the SR Ca^{2+} release rate (Gejl et al., 2014). Based on this data, with a mean reduction of −0.50 μmol · g $prot^{-1}$ · min^{-1} and a mean SD of 0.35, a minimum sample size of 5 subjects was calculated as needed to attain a power of 0.80.

RESULTS

SR Ca^{2+} Handling in Skiers Performing Repeated High-Intensity Exercise

The simulated sprint cross-country skiing competition, consisting of 4 × 4 min of high-intensity exercise interspersed with 45 min recovery periods, lead to significant fluctuations in the SR Ca^{2+} handling in both arms and legs (**Figures 3**, **4**).

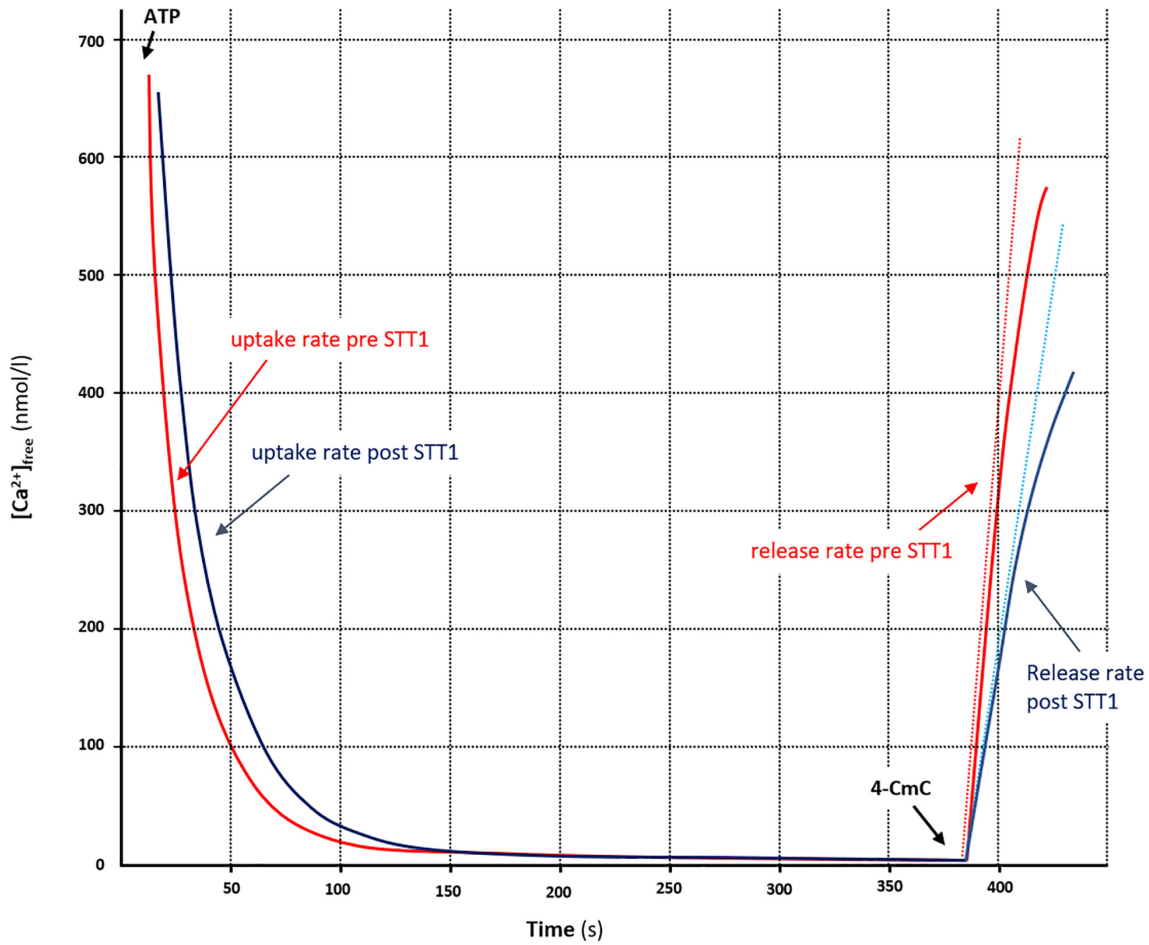

FIGURE 2 | Measurement of parameters associated with SR vesicle Ca^{2+} uptake and -release from representative examples of $[Ca^{2+}]$ traces in arm muscle, pre (STT1, red trace) and post (STT 2, blue trace) high-intensity exercise (~4 min. in duration). The free $[Ca^{2+}]$ was determined fluorometrically and the SR vesicle Ca^{2+} uptake was initiated by adding ATP (5 mM). When $[Ca^{2+}]$ reached a plateau, Ca^{2+} release was initiated by adding 4-CmC (5 mM). Curve fitting of Ca^{2+} uptake was performed with data points between a free $[Ca^{2+}]$ of 700 nM and the free $[Ca^{2+}]$ 20 s prior to initiating Ca^{2+} release. The time (τ) to reach 63% of the SR vesicle uptake (i.e., the initial free $[Ca^{2+}]$ minus nadir-Ca^{2+}) was calculated as 1/b from the equation; $[Ca^{2+}]_{free}$ = ae-bt +c (see section "Materials and Methods"). SR Ca^{2+} release rate was obtained by mathematically fitting the data points during the first 30 s of release to the equation: $y = x(1 - e\text{-}y(t\text{-}z)$, back-extrapolate to nadir-Ca^{2+} and then the rate of Ca^{2+} release was determined as the derivative of the initial release (dotted lines).

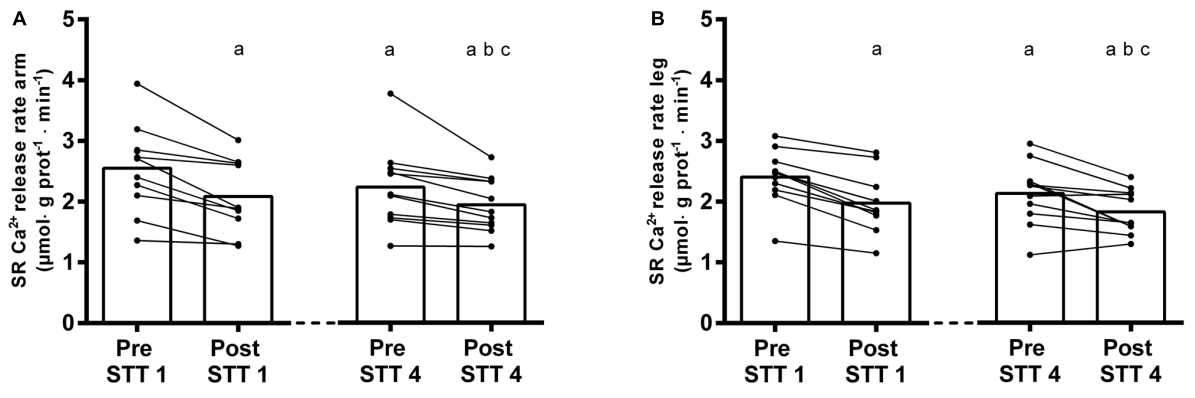

FIGURE 3 | SR Ca^{2+} release rates in arms **(A)** and legs **(B)** of elite cross-country skiers before (Pre) and after (Post) the first (STT 1, n = 10) and the fourth (STT 4, n = 11) bout of 1300-m high-intensity skiing. Each bout was interspersed with 45 min of recovery including carbohydrate intake. Both individual changes and mean values are shown; a different from Pre STT1, b different from Post STT1, c different from Pre STT4. See text for exact p-values.

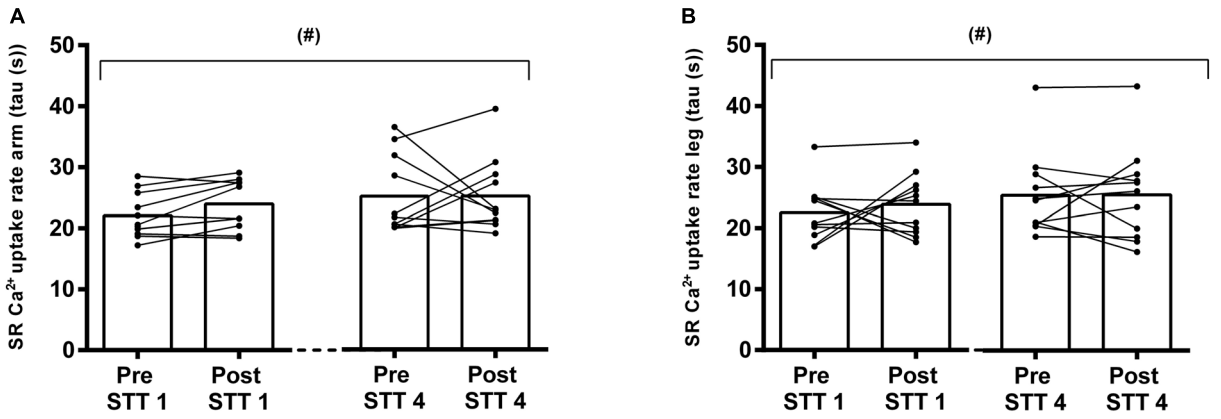

FIGURE 4 | SR Ca^{2+} uptake measured as the time for free [Ca^{2+}] to decrease by 63% in arms **(A)** and legs **(B)** of elite cross country skiers before (Pre) and after (Post) the first (STT 1, $n = 10$) and the fourth (STT 4, $n = 11$) bouts of 1300 m high-intensity skiing. Each bout was interspersed with 45 min of recovery including carbohydrate intake. Both individual changes and mean values are shown; (#) tendency to a main effect of time, $P = 0.053$.

SR Ca^{2+} Release Rate

The exposure to a single bout of 4 min high-intensity exercise (i.e., STT 1) induced a significant reduction in the SR Ca^{2+} release rate (arms: from 2.52 ± 0.74 to 2.08 ± 0.60 μmol · g $prot^{-1}$ · min^{-1}; legs: from 2.41 ± 0.45 to 1.98 ± 0.51 μmol · g $prot^{-1}$ · min^{-1}, Pre vs. Post: $P < 0.0001$ in both cases) (**Figures 3A,B**). After two additional bouts of high-intensity exercise (STT 2 and 3) and the intermediate 45 min periods of recovery, these rates were still depressed (arms: 2.24 ± 0.67 μmol · g $prot^{-1}$ · min^{-1}; legs: 2.13 ± 0.51 μmol · g $prot^{-1}$ · min^{-1}, $P < 0.0001$).

Moreover, during the fourth bout of high-intensity exercise (i.e., STT 4), the SR Ca^{2+} release rate were further reduced by 13–14% (arms: 1.95 ± 0.45 μmol · g $prot^{-1}$ · min^{-1}; legs: 1.83 ± 0.36 μmol · g $prot^{-1}$ · min^{-1}, $P < 0.0001$ in both cases) (**Figures 3A,B**). Although there was no limb × time interaction in this context ($P = 0.99$), the overall Ca^{2+} release rate was slightly higher in the arms than in the legs ($P = 0.04$).

SR Ca^{2+} Uptake

The Ca^{2+} uptake data from the skiers showed an unequal variance of the residuals across the time points. However, the tendency for a main time effect ($P = 0.053$) was confirmed after an inverse transformation of the data ($P = 0.098$), where equal variance was achieved (**Figures 4A,B**). In this context, there was no limb × time interaction ($P = 0.99$), and no differences between limbs ($P = 0.99$) (**Figures 4A,B**). Accordingly, there was a gradual numerical decline in the SR Ca^{2+} uptake from pre STT1 to post STT4 in both arms and legs (arms: from 22.0 ± 3.7 s to 25.3 ± 6.0 s; legs: from 22.5 ± 4.7 s to 25.5 ± 7.7 s).

"Real-Life" Endurance Exercise and SR Ca^{2+} Handling

Like the repeated high-intensity exercise, the conduction of a strenuous "real-life" training day in highly trained triathletes and cyclists lead to a significant depression of the SR Ca^{2+} release rate (from 1.82 ± 0.31 μmol · g $prot^{-1}$ · min^{-1} to 1.40 ± 0.23 μmol · g $prot^{-1}$ · min^{-1}, $P < 0.0001$), whereas the SR Ca^{2+} uptake was unaffected (26.6 ± 6.9 s to 31.6 ± 6.4 s, $P = 0.12$). Following the entire 4-week intervention, the SR Ca^{2+} release rate was elevated by 9% (from 1.76 ± 0.38 to 1.91 ± 0.44 μmol · g $prot^{-1}$ · min^{-1}, $P = 0.009$) (**Figure 5A**), still without any change in uptake (29.6 ± 7.0 versus 29.1 ± 8.7 s; $P = 0.98$) (**Figure 5B**).

Relationships Between SR Ca^{2+} Handling and Fiber Type Distribution and Endurance Performance

None of the groups demonstrated any association between the fiber type distribution (i.e., the relative MHC II content) and the SR Ca^{2+} release rate (cross-country skiers: $r^2 = 0.01$, $P = 0.80$; triathletes and cyclists: $r^2 = 0.01$, $P = 0.61$), or uptake rate (cross-country skiers: $r^2 = -0.16$, $P = 0.26$; triathletes and cyclists: $r^2 = 0.03$, $P = 0.21$). Nor was endurance performance (i.e., the time required by the skiers to complete STT1 or the power output by the endurance athletes during the 30-min time-trial, **Figure 1**) correlated to either Ca^{2+} release (cross-country skiers: $r^2 = 0.16$; triathletes and cyclists: $r^2 = 0.01$) or uptake (cross-country skiers: $r^2 = 0.25$; triathletes and cyclists: $r^2 = 0.16$) (Gejl et al., 2017b).

DISCUSSION

The present findings provide novel insights into the effects of acute and repeated high-intensity exercise, as well as a period of endurance training, on SR Ca^{2+} handling in the arm and leg muscles of highly trained athletes. While existing studies in endurance athletes have shown reduced SR Ca^{2+} release rates following single bouts of maximal leg-extension exercise (Li et al., 2002) and endurance exercise (Ørtenblad et al., 2011; Gejl et al., 2014) the present findings further extend this knowledge by demonstrating that as little as 4 min of whole-body high-intensity exercise attenuates the rate of SR Ca^{2+} release in both the arms and legs, with a further reduction when exercise is repeated. Moreover, short-term recovery (i.e., 45 min) appeared to partly

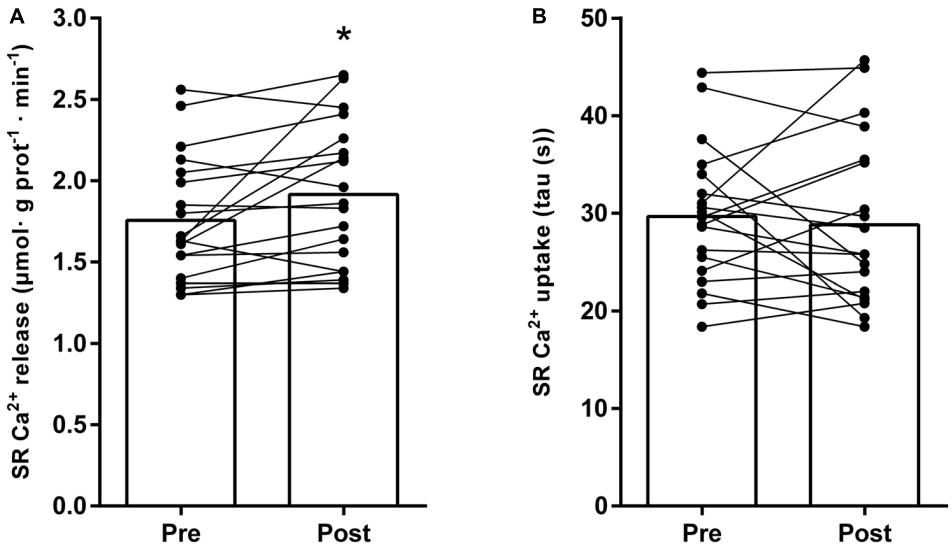

FIGURE 5 | Changes in SR vesicle Ca^{2+} release rate **(A)** and SR Ca^{2+} uptake **(B)**, measured as the time for free [Ca^{2+}] to decrease by 63%, during 4 weeks of endurance training in highly trained endurance athletes (n = 19). The training period included a mixture of low-, moderate-, and high-intensity exercise – *see* section "Materials and Methods" for details. Both individual and mean changes are shown. * different from pre, P = 0.009.

reverse this effect. In contrast, 4 weeks of endurance training including high-intensity exercise by highly trained endurance athletes increased the SR Ca^{2+} release rate.

SR Ca^{2+} uptake was less affected by acute high-intensity exercise, showing only a non-significant reduction in both arms and legs after one bout, but then a significant decline in both sets of limbs following 3 and 4 bouts. In the case of 4 weeks of endurance training including high-intensity exercise, the SR Ca^{2+} uptake rate was not changed either acutely after a single day of demanding training or at rest following the training period.

Effects of Acute Exercise on SR Ca^{2+} Handling

The maximal rate by which the SR releases Ca^{2+} can only be determined in SR vesicles and are carried out *in vitro* under apparently optimal conditions and demonstrate that once the SR is removed from the intracellular environment and not under normal voltage sensor control, changes in function persist. Thus, changes in the release rate can solely be explained by a modulation of the RyR1 opening probability and/or changes in the content of RyR1 in the muscle fibers. The underlying mechanism(s) explaining the present observations of a decreased SR vesicle Ca^{2+} release rate by acute exercise has been related to either oxidative modulations of the RYR1 and a fragmentation of the channel. Place and colleagues recently demonstrated that 6 × 30 s of "all-out" cycling exercise in untrained individuals led to a ROS-induced fragmentation of RyR1 and consequently an increased SR Ca^{2+} leak with reductions in SR Ca^{2+} release and power output (Place et al., 2015). Still, in elite endurance athletes the same exercise protocol was not associated with a RyR1 fragmentation, despite the power output being reduced (Place et al., 2015). Accordingly, the authors explained the structural maintenance of RyR1 in trained individuals by an increased ROS defense and a reduced ROS production during exercise (Place et al., 2015) and it was suggested that reductions in myofibrillar Ca^{2+} sensitivity could explain the reduction in performance (Westerblad and Allen, 2011). The present results support the absence of a RyR1 fragmentation by acute exposure to high-intensity exercise in trained individuals since the reduction in the SR Ca^{2+} release rate was partly reversed during recovery (**Figure 3**). However, as reported in a companion study (Gejl et al., 2016) the plasma redox status was disturbed during the repeated high-intensity exercise while the myofibrillar Ca^{2+} sensitivity was improved, possibly as a result of exercise-induced oxidation of the contractile apparatus. Since performance was maintained throughout the series of high-intensity exercise bouts, it is likely that the reductions in SR Ca^{2+} release were, at least partly, compensated for by increases in Ca^{2+} sensitivity (Andersson et al., 2016; Gejl et al., 2017a). Thus, it cannot be excluded that reductions in SR Ca^{2+} release rates were, at least partly, due to ROS-mediated RyR1 modifications. Previously, muscle glycogen depletion has been associated with impairments in SR Ca^{2+} handling (Gejl et al., 2017b) however, in the present studies muscle glycogen was not critically depleted during exercise, and no associations were observed between muscle glycogen availability and SR Ca^{2+} release rate acutely after exercise in any of the groups (r^2 = 0.00–0.29, P = 0.09–0.98). We have previously suggested that muscle glycogen depletion negatively affects the SR Ca^{2+} release when below 250–300 mmol · kg dw^{-1}, but in the present studies post-exercise glycogen levels were not significantly below this level (i.e., cross-country skiers: 290 mmol · kg dw^{-1}; endurance athletes:430 mmol · kg dw^{-1}) (Gejl et al., 2017a, 2018).

Concerning the acute effects of exhaustive exercise on SR Ca^{2+} uptake in highly trained athletes, the existing findings are inconsistent by showing impairments in the legs following

maximal leg extension exercise (Li et al., 2002) and 1 h of cross-country skiing (Ørtenblad et al., 2011) and maintenance of Ca^{2+} uptake in the legs following 4 h of cycling exercise (Gejl et al., 2014) and the arms following 1 h of cross-country skiing (Ørtenblad et al., 2011). The present findings extend this knowledge by showing that SR Ca^{2+} uptake is unaffected by 4 min of maximal whole-body exercise, whereas the four bouts of high-intensity exercise tended to exert a negative effect. Thus, the Ca^{2+} uptake seems relatively stable unless the muscle is exposed to a certain amount of high-intensity exercise. By investigating SR vesicles, the strong tendency to impairments observed with the repeated high-intensity exercise must be explained by modifications of the SR Ca^{2+}-ATPase itself or endogenous regulators of this enzyme. Apart from glycogen, which was not associated with SR Ca^{2+}-uptake following exercise in the present studies (r^2 = 0.00 – 0.15, P = 0.21–0.83), it is possible that the SR Ca^{2+}-ATPase activity was adversely affected by structural modifications of its nucleotide binding site (i.e., oxidation or nitrosylation) as a result of the ROS production during exercise (Klebl et al., 1998; Matsunaga et al., 2003; Tupling, 2004). In addition, high ADP concentrations or low local ATP concentrations in proximity to the SR Ca^{2+}-ATPase have been shown to adversely affect pump function *in vitro*, but the presence of such local changes *in vivo* is unknown (Tupling, 2004).

Effects of Exercise Training on SR Ca^{2+} Handling

Acute deteriorations in SR function, and particularly the SR Ca^{2+} release rate, has repeatedly been demonstrated as an important mechanism underlying the development of muscle fatigue (Li et al., 2002; Duhamel et al., 2006; Gejl et al., 2014; Place et al., 2015) and accordingly, improvements in the SR Ca^{2+} release rate with training could serve as a preventive mechanism, especially during high-intensity exercise. Interestingly, we here demonstrate that the exposure to routine endurance training, with superimposed high-intensity exercise, increased the SR Ca^{2+} release rate by 10% in already trained road cyclists and triathletes. To the best of our knowledge, only one study from our lab has elucidated the effect of high-intensity training on SR function in humans. In this study, a 9% increase in SR vesicle Ca^{2+} release rate was observed following 5 weeks of sprint training in untrained individuals (Ørtenblad et al., 2000). Furthermore, the data indicated that the 5-week sprint training induced an increase in the SR Ca^{2+} release rate, due to an enhanced SR content within the fiber. Altogether, these findings suggest that the muscle SR Ca^{2+} release rate increase in response to high-intensity exercise training, supporting the idea of an adaptation in SR function to counteract muscle fatigue and thereby improving athlete performance. We extracted the post-biopsy 36 h following the last training session, and since it has previously been shown that the RyR1 channel is not deteriorated 24 h following HIIT in endurance trained athletes, we assume that this training session did not affect our results (Place et al., 2015). However, if RyR1 was affected by the last training session, we may have slightly underestimated the positive effect of training.

Since MHC II fibers contain more SR and demonstrate higher SR Ca^{2+} release rates in comparison to MHC I fibers, a change in the fiber type composition could explain alterations in SR function (Rüegg, 1986). However, the fiber type distribution remained unchanged during the training period and, accordingly, this cannot explain the improved SR function in the present study (MHC I: 50 ± 9% to 51 ± 8%; MHC II: 50 ± 9% to 49 ± 8%). Based on previous findings from our lab, an enhanced Ca^{2+} release rate could instead be explained by an increase in the total number of RyR1 secondary to an increase in the total amount of SR per fiber (Ørtenblad et al., 2000). Interestingly, a pharmacologically induced increase in SR Ca^{2+} release rate, by β2-adrenergic stimulation, is associated with an increase in contractile force in non-fatigued muscle in trained men (Hostrup et al., 2014). Thus, increases in the SR Ca^{2+} release rate *per se* may improve muscle contractility as also demonstrated by the present and previous training effects.

Only a few previous studies have examined the SR Ca^{2+} uptake rate following a period of training and only resistance training in elderly women has previously been shown to increase rates of Ca^{2+} uptake, whereas resistance training (Hunter et al., 1999) as well as 5–7 weeks with sprint-training in young individuals (Ørtenblad et al., 2000; Harmer et al., 2014) does not seem induce changes in SR Ca^{2+} uptake. Since we did not observe any significant change following the 4 weeks of endurance training, the present findings are in agreement with previous findings in young untrained individuals. By contrast, 10 weeks of prolonged aerobic training has been shown to induce reductions in the SR Ca^{2+} uptake (Green et al., 2003). Although not measured in the present study, previous studies have reported that intensified training does not affect SR Ca^{2+}-ATPase content and -activity, and generally mechanisms related to the SR Ca^{2+} uptake seems less responsive to training in comparison to the SR Ca^{2+} release (Madsen et al., 1994; Green et al., 1998; Ørtenblad et al., 2000).

Implications of Changes in SR Function for Performance

As presented in a companion study, the repeated periods of high-intensity exercise were not associated with the development of fatigue since the time to complete the first and fourth bout of exercise was identical (STT1: 227 ± 8 s; STT4: 227 ± 9 s) (Gejl et al., 2017a). Interestingly, the performance was maintained despite the marked reductions in SR Ca^{2+} release and -uptake rates, which questions previous proposals of SR Ca^{2+} release rate as being an important mechanism underlying the development of muscle fatigue during exercise (Westerblad and Allen, 1991; Gejl et al., 2014; Place et al., 2015). As mentioned previously, reductions in SR Ca^{2+} release *per se* may compromise muscle function, but since other important steps in the E-C coupling may be improved (e.g., Ca^{2+} sensitivity) (Gejl et al., 2016; Lamboley et al., 2020) a net negative change in muscle function may not appear. Also, the exercise intensity during the repeated bouts of exercise as well as the endurance training day may have been too low to challenge the SR Ca^{2+} handling capacity and it cannot be excluded that the observed reductions in SR Ca^{2+} release

rate would compromise performance at even higher exercise intensities or longer durations.

According to the concept of symmorphosis, structures are developed to match the functional capacity of the system, and no single parameter has unnecessary excess capacity (Weibel et al., 1991). Here, we demonstrate a significant increase in the SR Ca^{2+} release rate by 4 weeks of endurance training including 11 high-intensity training sessions. An effect that, according to the concept of symmorphosis, is likely to enhance the maximal exercise capacity of the muscle. This may be particularly important in sports involving intermittent periods of high-intensity exercise and, accordingly, we have previously shown that the ability to perform maximal sprint exercise was reduced following 4 h of moderate intensity exercise concomitantly with a 15% reduction in SR Ca^{2+} release (Gejl et al., 2014).

Methodological Considerations

Importantly, SR function can only be analyzed *in vitro* and this reductionistic approach cannot account for interactions between different myocellular sites. Therefore, as changes in SR function with acute exercise and training were evident when it was removed from the *in vivo* conditions, it is important to consider the physiological relevance of these changes for whole muscle function. Using this method, it is herein an important assumption that the SR vesicle used for the *in vitro* measurements of SR function is functional apparent in *in vivo* muscles. First, the measures on SR vesicles represent functional measures of the Ca^{2+} uptake and release rates irrespective of possible changes present in the *in vivo* muscle, and changes in the SR function will reflect inherent changes in the SERCA pump and RyR channel, respectively (i.e., redox modifications or fragmentation of the RyR-channel). Second, these changes will be present in the athlete's muscle and conceivably affect muscle function, although it is not possible to estimate further modifications present in the *in vivo* milieu. Widening the present study to include an investigation of SR protein modifications could possibly have provided an explanation for the observed functional changes. However, the purpose of the present study was to investigate if exercise, that has previously been shown to induce mechanistic alterations in rodents and humans, ultimately affects SR on the functional level.

We have previously observed that SR function remained unchanged in the non-training control group of a 5-week training study (Ørtenblad et al., 2000). Thus, due to the difficulties associated with recruiting elite athletes to invasive studies involving muscle biopsies, and since the inclusion of a control group would comprise a 4-week period without training, which we assumed would not appeal to this specific group, we decided to conduct the project without a control group. Importantly, the included athletes had been training and competing on a high level for at least 2 years and since only the training approach was manipulated during the intervention period, we strongly believe that the observed changes were a result of this.

In conclusion, handling of Ca^{2+} by the SR in the arms and legs deteriorates following both a single bout and multiple bouts of high-intensity cross-country skiing by highly trained skiers. Moreover, we demonstrate that the rate of SR Ca^{2+} release in elite athletes can be enhanced by a specific program of training, which may have important implications for performance.

DATA AVAILABILITY STATEMENT

The data that support the findings of this study are available from the corresponding author upon reasonable request.

ETHICS STATEMENT

The studies involving human participants were reviewed and approved by the Ethics Committee of Southern Denmark (Project-ID S-20150034) Regional Ethics Review Board in Umeå, Sweden (#2013-59-31). The patients/participants provided their written informed consent to participate in this study.

AUTHOR CONTRIBUTIONS

KG, EA, NØ, and H-CH were responsible for the conception or design of the study. KG, NØ, and JN were responsible for acquisition, analysis, or interpretation of data. KG, EA, NØ, H-CH, and JN were responsible for drafting the manuscript or revising it critically for important intellectual content. All the authors have approved the final version of the manuscript. All persons designated as authors qualify for authorship.

FUNDING

The present study was supported financially by the Swedish National Centre for Research in Sports (CIF) (#FO2013-0033), The Danish Ministry of Culture (#TAKT2013-104), and Team Danmark.

REFERENCES

Allen, D. G., Lamb, G. D., and Westerblad, H. (2008). Skeletal muscle fatigue: cellular mechanisms. *Physiol. Rev.* 88, 287–332. doi: 10.1152/physrev.00015.2007

Andersson, E., Holmberg, H. C., Ortenblad, N., and Bjorklund, G. (2016). Metabolic responses and pacing strategies during successive sprint skiing time trials. *Med. Sci. Sports Exerc.* 48, 2544–2554. doi: 10.1249/mss.0000000000001037

Betto, D. D., Zerbato, E., and Betto, R. (1986). Type-1, type-2a and type-2b myosin heavy-chain electrophoretic analysis of rat muscle-fibers. *Biochem. Biophys. Res. Commun.* 138, 981–987. doi: 10.1016/s0006-291x(86)80592-7

Bogdanis, G. C. (2012). Effects of physical activity and inactivity on muscle fatigue. *Front. Physiol.* 3:142. doi: 10.3389/fphys.2012.00142

Booth, J., McKenna, M. J., Ruell, P. A., Gwinn, T. H., Davis, G. M., Thompson, M. W., et al. (1997). Impaired calcium pump function does not slow relaxation in human skeletal muscle after prolonged exercise. *J. Appl. Physiol.* 83, 511–521. doi: 10.1152/jappl.1997.83.2.511

Bruton, J., Tavi, P., Aydin, J., Westerblad, H., and Lannergren, J. (2003). Mitochondrial and myoplasmic [Ca2+] in single fibres from mouse limb muscles during repeated tetanic contractions. *J. Physiol.* 551, 179–190. doi: 10.1113/jphysiol.2003.043927

Duhamel, T. A., Perco, J. G., and Green, H. J. (2006). Manipulation of dietary carbohydrates after prolonged effort modifies muscle sarcoplasmic reticulum responses in exercising males. *Am. J. Physiol. Regul. Integr. Comp. Physiol.* 291, R1100–R1110. doi: 10.1152/ajpregu.00858.2005

Gejl, K. D., Hvid, L. G., Frandsen, U., Jensen, K., Sahlin, K., and Ortenblad, N. (2014). Muscle glycogen content modifies Sr Ca2+ release rate in elite endurance athletes. *Med. Sci. Sports Exerc.* 46, 496–505. doi: 10.1249/mss.0000000000000132

Gejl, K. D., Hvid, L. G., Willis, S. J., Andersson, E., Holmberg, H. C., Jensen, R., et al. (2016). Repeated high-intensity exercise modulates Ca(2+) sensitivity of human skeletal muscle fibers. *Scand. J. Med. Sci. Sports.* 26, 488–497. doi: 10.1111/sms.12483

Gejl, K. D., Ortenblad, N., Andersson, E., Plomgaard, P., Holmberg, H. C., and Nielsen, J. (2017a). Local depletion of glycogen with supramaximal exercise in human skeletal muscle fibres. *J. Physiol.* 595, 2809–2821. doi: 10.1113/jp273109

Gejl, K. D., Thams, L. B., Hansen, M., Rokkedal-Lausch, T., Plomgaard, P., Nybo, L., et al. (2017b). No superior adaptations to carbohydrate periodization in elite endurance athletes. *Med. Sci. Sports Exerc.* 49, 2486–2497. doi: 10.1249/MSS.0000000000001377

Gejl, K. D., Vissing, K., Hansen, M., Thams, L., Rokkedal-Lausch, T., Plomgaard, P., et al. (2018). Changes in metabolism but not myocellular signaling by training with cho-restriction in endurance athletes. *Physiol. Rep.* 6, e13847. doi: 10.14814/phy2.13847

Granata, C., Jamnick, N. A., and Bishop, D. J. (2018). Training-induced changes in mitochondrial content and respiratory function in human skeletal muscle. *Sports Med.* 48, 1809–1828. doi: 10.1007/s40279-018-0936-y

Green, H. J., Ballantyne, C. S., MacDougall, J. D., Tarnopolsky, M. A., and Schertzer, J. D. (2003). Adaptations in human muscle sarcoplasmic reticulum to prolonged submaximal training. *J. Appl. Physiol.* 94, 2034–2042. doi: 10.1152/japplphysiol.00244.2002

Green, H. J., Grange, F., Chin, C., Goreham, C., and Ranney, D. (1998). Exercise-induced decreases in sarcoplasmic reticulum Ca(2+)-atpase activity attenuated by high-resistance training. *Acta Physiol. Scand.* 164, 141–146. doi: 10.1046/j.1365-201X.1998.00425.x

Harmer, A. R., Ruell, P. A., Hunter, S. K., McKenna, M. J., Thom, J. M., Chisholm, D. J., et al. (2014). Effects of type 1 diabetes, sprint training and sex on skeletal muscle sarcoplasmic reticulum Ca2+ uptake and Ca2+-atpase activity. *J. Physiol.* 592, 523–535. doi: 10.1113/jphysiol.2013.261172

Hellsten, Y., Apple, F. S., and Sjodin, B. (1996). Effect of sprint cycle training on activities of antioxidant enzymes in human skeletal muscle. *J. Appl. Physiol.* 81, 1484–1487. doi: 10.1152/jappl.1996.81.4.1484

Hostrup, M., Kalsen, A., Ortenblad, N., Juel, C., Morch, K., Rzeppa, S., et al. (2014). Beta2-adrenergic stimulation enhances Ca2+ release and contractile properties of skeletal muscles, and counteracts exercise-induced reductions in Na+-K+-atpase vmax in trained men. *J. Physiol.* 592, 5445–5459. doi: 10.1113/jphysiol.2014.277095

Hunter, S. K., Thompson, M. W., Ruell, P. A., Harmer, A. R., Thom, J. M., Gwinn, T. H., et al. (1999). Human skeletal sarcoplasmic reticulum Ca2+ uptake and muscle function with aging and strength training. *J. Appl. Physiol.* 86, 1858–1865. doi: 10.1152/jappl.1999.86.6.1858

Ingalls, C. P., Warren, G. L., and Armstrong, R. B. (1999). Intracellular Ca2+ transients in mouse soleus muscle after hindlimb unloading and reloading. *J. Appl. Physiol.* 87, 386–390. doi: 10.1152/jappl.1999.87.1.386

Klebl, B. M., Ayoub, A. T., and Pette, D. (1998). Protein oxidation, tyrosine nitration, and inactivation of sarcoplasmic reticulum Ca2+-atpase in low-frequency stimulated rabbit muscle. *FEBS Lett.* 422, 381–384. doi: 10.1016/s0014-5793(98)00053-2

Lamboley, C. R., Rouffet, D. M., Dutka, T. L., McKenna, M. J., and Lamb, G. D. (2020). Effects of high-intensity intermittent exercise on the contractile properties of human type i and type ii skeletal muscle fibers *J. Appl. Physiol.* 128:1207–1216. doi: 10.1152/japplphysiol.00014.2020

Li, J. L., Wang, X. N., Fraser, S. F., Carey, M. F., Wrigley, T. V., and McKenna, M. J. (2002). Effects of fatigue and training on sarcoplasmic reticulum Ca(2+) regulation in human skeletal muscle. *J. Appl. Physiol.* 92, 912–922. doi: 10.1152/japplphysiol.00643.2000

Madsen, K., Franch, J., and Clausen, T. (1994). Effects of intensified endurance training on the concentration of Na,K-Atpase and Ca-atpase in human skeletal muscle. *Acta Physiol. Scand.* 150, 251–258. doi: 10.1111/j.1748-1716.1994.tb09684.x

Matsunaga, S., Inashima, S., Yamada, T., Watanabe, H., Hazama, T., and Wada, M. (2003). Oxidation of sarcoplasmic reticulum Ca(2+)-atpase induced by high-intensity exercise. *Pflugers. Arch.* 446, 394–399. doi: 10.1007/s00424-003-1040-0

Ortenblad, N., Lunde, P. K., Levin, K., Andersen, J. L., and Pedersen, P. K. (2000). Enhanced sarcoplasmic reticulum Ca2+ release following intermittent sprint training. *Am. J. Physiol. Regul. Integr. Comp. Physiol.* 279, R152–R160.

Ørtenblad, N., Lunde, P. K., Levin, K., Andersen, J. L., and Pedersen, P. K. (2000). Enhanced sarcoplasmic reticulum Ca(2+) release following intermittent sprint training. *Am. J. Physiol. Regul. Integr. Comp. Physiol.* 279, R152–R160. doi: 10.1152/ajpregu.2000.279.1.R152

Ørtenblad, N., Madsen, K., and Djurhuus, M. S. (1997). Antioxidant status and lipid peroxidation after short-term maximal exercise in trained and untrained humans. *Am. J. Physiol.* 272, R1258–R1263. doi: 10.1152/ajpregu.1997.272.4.R1258

Ørtenblad, N., Nielsen, J., Saltin, B., and Holmberg, H. C. (2011). Role of glycogen availability in sarcoplasmic reticulum Ca2+ kinetics in human skeletal muscle. *J. Physiol.* 589, 711–725. doi: 10.1113/jphysiol.2010.195982

Passonneau, J. V., and Lowry, O. H. (1993). *Enzymatic Analysis, A Practical Guide*. Totowa, NJ: Humana Press Inc.

Place, N., Ivarsson, N., Venckunas, T., Neyroud, D., Brazaitis, M., Cheng, A. J., et al. (2015). Ryanodine receptor fragmentation and sarcoplasmic reticulum Ca2+ leak after one session of high-intensity interval exercise. *Proc. Natl. Acad. Sci. U.S.A.* 112, 15492–15497. doi: 10.1073/pnas.1507176112

Rodriguez, N. R., Di Marco, N. M., and Langley, S. (2009). American college of sports medicine position stand. Nutrition and athletic performance. *Med. Sci. Sports Exerc.* 41, 709–731. doi: 10.1249/MSS.0b013e31890eb86

Rüegg, J. (1986). *Calcium in Muscle Activation. A Comparative Approach*. Berlin: Springer Verlag.

Tupling, A. R. (2004). The Sarcoplasmic reticulum in muscle fatigue and disease: role of the sarco(Endo)plasmic reticulum Ca2+-Atpase. *Can. J. Appl. Physiol.* 29, 308–329. doi: 10.1139/h04-021

Tupling, R., Green, H., Grant, S., Burnett, M., and Ranney, D. (2000). postcontractile force depression in humans is associated with an impairment in Sr Ca(2+) pump function. *Am. J. Physiol. Regul. Integr. Comp. Physiol.* 278, R87–R94. doi: 10.1152/ajpregu.2000.278.1.R87

Weibel, E. R., Taylor, C. R., and Hoppeler, H. (1991). The concept of symmorphosis: a testable hypothesis of structure-function relationship. *Proc. Natl. Acad. Sci. U.S.A.* 88, 10357–10361. doi: 10.1073/pnas.88.22.10357

Westerblad, H., and Allen, D. G. (1991). Changes of myoplasmic calcium concentration during fatigue in single mouse muscle fibers. *J. Gen. Physiol.* 98, 615–635. doi: 10.1085/jgp.98.3.615

Westerblad, H., and Allen, D. G. (2011). Emerging roles of Ros/Rns in muscle function and fatigue. *Antioxid. Redox. Signal.* 15, 2487–2499. doi: 10.1089/ars.2011.3909

Conflict of Interest: The authors declare that the research was conducted in the absence of any commercial or financial relationships that could be construed as a potential conflict of interest.

frontiers in Physiology

ORIGINAL RESEARCH
published: 06 October 2020
doi: 10.3389/fphys.2020.573723

Dstac Regulates Excitation-Contraction Coupling in *Drosophila* Body Wall Muscles

I-Uen Hsu[1†], Jeremy W. Linsley[1,2†], Lilly E. Reid[1], Richard I. Hume[1], Ari Leflein[1] and John Y. Kuwada[1,2]*

[1] Department of Molecular, Cellular, and Developmental Biology, University of Michigan, Ann Arbor, MI, United States,
[2] Cellular and Molecular Biology Program, University of Michigan, Ann Arbor, MI, United States

Stac3 regulates excitation-contraction coupling (EC coupling) in vertebrate skeletal muscles by regulating the L-type voltage-gated calcium channel (Ca_V channel). Recently a *stac*-like gene, *Dstac*, was identified in *Drosophila* and found to be expressed by both a subset of neurons and muscles. Here, we show that Dstac and Dmca1D, the *Drosophila* L-type Ca_V channel, are necessary for normal locomotion by larvae. Immunolabeling with specific antibodies against Dstac and Dmca1D found that Dstac and Dmca1D are expressed by larval body-wall muscles. Furthermore, Ca^{2+} imaging of muscles of Dstac and Dmca1D deficient larvae found that Dstac and Dmca1D are required for excitation-contraction coupling. Finally, Dstac appears to be required for normal expression levels of Dmca1D in body-wall muscles. These results suggest that Dstac regulates Dmca1D during EC coupling and thus muscle contraction.

Keywords: stac adaptor protein, *Drosophila*, muscle, L-type voltage-gated calcium channel, excitation-contraction coupling

OPEN ACCESS

Edited by:
Matias Mosqueira, Heidelberg University Hospital, Germany

Reviewed by:
Marta Campiglio, Innsbruck Medical University, Austria
Stefano Perni, University of Colorado Denver, United States

***Correspondence:**
John Y. Kuwada
kuwada@umich.edu

[†]These authors have contributed equally to this work

Specialty section:
This article was submitted to Striated Muscle Physiology, a section of the journal Frontiers in Physiology

Received: *17 June 2020*
Accepted: *15 September 2020*
Published: *06 October 2020*

Citation:
Hsu I-U, Linsley JW, Reid LE, Hume RI, Leflein A and Kuwada JY (2020) Dstac Regulates Excitation-Contraction Coupling in Drosophila Body Wall Muscles. Front. Physiol. 11:573723. doi: 10.3389/fphys.2020.573723

INTRODUCTION

Muscle contractions are initiated by depolarizations of muscle membrane potential due to the release of neurotransmitter at the neuromuscular junction. EC coupling is the process that transduces changes in membrane voltage to increases in cytosolic Ca^{2+} due to the release of Ca^{2+} from the sarcoplasmic reticulum (SR) and subsequently contraction. In vertebrate skeletal muscles EC coupling is thought to be mediated by a direct interaction between the L-type Ca_V channel, dihydropyridine receptor (DHPR), which is in the transverse tubule (T tubule) membrane and is the voltage sensor for EC coupling, and the ryanodine receptor (RyR), which is the Ca^{2+} release channel in the SR membrane (Schneider and Chandler, 1973; Rios and Brum, 1987; Tanabe et al., 1987; Block et al., 1988; Takeshima et al., 1989; Adams et al., 1990; Paolini et al., 2004).

Stac3 was identified as a novel adaptor protein that is required for EC coupling in zebrafish skeletal muscle and a missense mutation in *STAC3* is causal for the congenital Native American myopathy (Horstick et al., 2013). Stac3 also regulates EC coupling in murine skeletal muscles (Nelson et al., 2013) and murine muscle development (Ge et al., 2014; Cong et al., 2016). In zebrafish skeletal muscles Stac3 colocalizes with DHPR and RyR and regulates DHPR levels, stability and functionality, including the voltage response of DHPRs but not trafficking of DHPRs (Linsley et al., 2017a,b). Stac3 appears not to be required for normal levels or functionality of RyRs, however.

Recently, a *stac*-like gene, *Dstac*, was identified in *Drosophila* (Hsu et al., 2018). There is a single *stac* gene in *Drosophila* and it is expressed both by muscles and a subset of neurons including in the

lateral ventral neurons (LN_V) that express the neuropeptide, pigment dispersing factor (PDF), in the brain. Genetic manipulation of PDF demonstrated the necessity of PDF for circadian rhythm *in Drosophila* (Shafer and Taghert, 2009). Interestingly, knocking down *Dstac* specifically in PDF neurons disrupted circadian rhythm demonstrating the requirement of Dstac in PDF neurons for normal circadian rhythm (Hsu et al., 2018).

Dstac expression by muscles in *Drosophila* (Hsu et al., 2018) suggests that Dstac might regulate EC coupling in *Drosophila* muscles as does Stac3 in vertebrate skeletal muscles (Horstick et al., 2013; Nelson et al., 2013). As previously mentioned, EC coupling in vertebrate skeletal muscles involves the direct interaction of the L-type Ca_v channel, DHPR, in the T tubules with RyR in the SR. In mammalian skeletal muscles DHPR conducts Ca^{2+} from the external solution to the cytosol but this is not required for EC coupling (Dayal et al., 2017). Interestingly in teleost skeletal muscles EC coupling is similarly independent of Ca^{2+} influx from the exterior and DHPR appears to have evolved so that it no longer conducts Ca^{2+} (Schredelseker et al., 2010).

EC coupling in vertebrate cardiac and smooth muscles, however, does require an influx of Ca^{2+} through Ca_v channels which initiates Ca^{2+} induced Ca^{2+} release (CICR) from internal Ca^{2+} stores (Bolton et al., 1999). Similarly, EC coupling in invertebrate muscle appears to involve CICR (Györke and Palade, 1992; Maryon et al., 1998; Takekura and Franzini-Armstrong, 2002; Collet, 2009). CICR may also be necessary for EC coupling in *Drosophila* muscles. In *Drosophila* larvae RyR is expressed widely including the body wall muscles and systemic application of ryanodine and a partial loss-of-function *RyR* mutation both decreased locomotion by larvae (Sullivan et al., 2000), which is consistent with the involvement of CICR in body wall muscles for contractions. Furthermore, SERCA, the Ca^{2+}-ATPase in the ER/SR that pumps Ca^{2+} from the cytosol into the ER/SR, is expressed by muscles and a dominant heat inducible mutation of *SERCA* paralyzes larvae (Sanyal et al., 2005). Finally, *Dmca1D*, the *Drosophila* L-type Ca_v channel is widely expressed (Zheng et al., 1995). *Dmca1D* null embryos exhibit little movement and are larval lethal. Furthermore, pupae of *AR66* partial loss-of-function allele of *Dmca1D* do not eclose (Eberl et al., 1998). Dmca1D in larval muscle conduct voltage-dependent Ca^{2+} currents that are sensitive to dihydropyridines (Ren et al., 1998). These findings suggest that in *Drosophila* larval muscle Ca^{2+} influx via Dmca1D channels might initiate CICR. Here, locomotion analysis, *in vivo* Ca^{2+} imaging, and immunolabeling showed that Dstac and Dmca1D regulate Ca^{2+} transients in muscles and locomotion, and that Dstac is required for normal levels of Dmca1D in the muscles. Our finding suggests that Dstac regulates Dmca1D during the activation of *Drosophila* muscles.

MATERIALS AND METHODS

Drosophila melanogaster Strains

All crosses and larvae were kept at 25°C and supplied with food that uses molasses as sugar source (Food R purchased from LabExpress). The number of flies used in crosses was controlled so the vials were not overcrowded with larvae. All experiments used age and size matched larvae. *Dmca1D* knockdown experiments and *in vivo* Ca^{2+} imaging used 2nd instar larvae of both genders; all the other experiments used both female and male 3rd instar larvae. All experiments were conducted at room temperature (21–23.5°C). *UAS:Dcr-2* was present in all knockdown experiments using RNAi strains except for the TRiP RNAi lines that don't require Dcr-2. The fly stocks used in this study were: *Mef2:GAL4* (RRID:BDSC_27390), *UAS:Dcr-2* (RRID:BDSC_24651), *UAS:GCaMP6f* (RRID:BDSC_52869), *UAS:mCD4tdtomato* (From Bing Ye), *UAS:Dstac-RNAi* (VDRC 105848), *UAS:Dmca1D-RNAi* (RRID:BDSC_33413), *UAS:Luciferase-RNAi* (RRID:BDSC_31603), w^{1118} (RRID:BDSC_3605), $Dstac^{\Delta SH3}/CyO$ (Hsu, 2020).

Immunolabeling

3rd instar larvae were fileted in HL3 solution and fixed in 4% paraformaldehyde in PBS. Immunolabeling followed the procedure described previously (Hsu et al., 2018). The primary antibodies used were: chicken anti-Dmca1D (1:20 - 1:100) (Hsu, 2020), rabbit anti-Dstac (1:100 - 1:150) (Hsu et al., 2018), rabbit anti-DsRed (Millipore Sigma Cat # AB356483-25UG), mouse anti-discs large (anti-DLG) (DSHB Cat# 4F3, RRID:AB_528203). Secondary antibodies used were (1:1000): Donkey anti-chicken Alexa Fluor 488 (Jackson ImmunoResearch Labs Cat# 703-545-155, RRID:AB_2340375), Goat Anti-Chicken Alexa Fluor 647 (Abcam Cat # ab150175, RRID:AB_2732800), Donkey anti-chicken Alexa Fluor 633 (Sigma-Aldrich, SAB4600127), Goat anti-rabbit Alexa Fluor 647 (Thermo Fisher Scientific, Cat # A-21245, RRID:AB_2535813), Goat anti-rabbit Alexa Fluor 488 (Thermo Fisher Scientific, Cat # A-11034, RRID: AB_2576217), Goat anti-Mouse Alexa Fluor 568 (Thermo Fisher Scientific, Cat # A-11004, RRID:AB_2534072), Goat anti-Mouse Alexa Fluor Plus 647 (Thermo Fisher Scientific, Cat # A32728, RRID:AB_2633277), Goat anti-Mouse Alexa Fluor 488 (Thermo Fisher Scientific, Cat # A-11001, RRID:AB_2534069). Actin filaments were labeled with Alexa Fluor 647 Phalloidin (Thermo Fisher Scientific Cat # A12379) at 1:1000. Images were acquired with a Leica SP5 and SP8 confocal microscopes using a 100x or 63x oil objective. For comparisons of puncta labeled by anti-Dstac and anti-Dmca1D, images showing only the brightest 50% of the pixels were generated by adjusting the input levels in Photoshop.

Quantification of Dmca1D Immunostaining of Body-Wall Muscles

Images of muscle 4 from segments A3 to A5 were acquired at 1024 × 1024 pixels as z stacks (5 planes, 0.5 μm/focal plane) with a Leica SP8 confocal microscope with a 100× objective. Confocal settings were kept constant between controls and experimental groups. Images of Dmca1D immunolabeling was quantified in two ways. First, five focal plane images were stacked to a single image using imageJ. ROIs were drawn to encompass the striations labeled with anti-Dmca1D and the fluorescence intensities of the ROIs were measured using imageJ. Second, the anti-Dmca1D fluorescence of pixels in a line of pixels along the longitudinal

axis of each muscle that crossed multiple Dmca1D stripes was plotted. The intensities of the pixels along the line minus the background fluorescence of pixels between stripes were analyzed. This method has the advantage of avoiding the selection of ROIs.

Analysis of Eclosion

Third instar larvae were collected 5 days after the crosses were set. Between 7 and 10 days after the collection of larvae, the number of pupae and adult flies that enclosed were counted. All vials were kept at 25°C.

Motility Assay

Freely moving 3rd instar larvae were acclimated on a 10 cm 2% agar plate for 1 min and then recorded with a digital camera for 10 s at a frame rate of 7.5 Hz. Each larva was recorded 3 times which constituted a single trial. Larvae that hit the petri dish wall during the 10-s recording were excluded from the analysis. The assay was performed at 23.5°C. Larval movements were tracked by the "multitracker" plugin of imageJ that produced the (x,y) location of each larva in each frame. The distance between frames were calculated from the (x,y) locations and were summed to get the total distance traveled during the 10 s. The controls and experimental groups were coded to blind the genotypes. After completing the assay and analysis, the genotypes were unveiled.

In vivo Ca^{2+} Imaging

Live intact 2nd instar larvae of both genders selectively expressing GCaMP6f in body-wall muscles (*Mef2:GAL4 > UAS:GCaMP6f; UAS:mCD8tdTomato*) were placed into a microfluidics device (Ghannad-Rezaie et al., 2012) and GCaMP fluorescence was observed on a spinning disc confocal imaging system composed of an Olympus IX81 inverted microscope, a CSU-X1 scanner (Yokogawa), an iXon electron multiplying charge-coupled device camera (Andor), and MetaMorph Advanced Imaging acquisition software v.7.7.8.0 (Molecular Devices). Imaging was acquired with a 10X Olympus objective. The larvae were mounted on its side in the chamber in order to image muscle 4, 5, 8, 12, 21 that have some parts that don't overlap with other muscles. Images were captured every 0.5 sec for 5 min. The *mCD8tdTomato* expressed by *Mef2:GAL4* was used to locate the muscles. The larvae that moved a lot were not used. Region of interests (ROI) were drawn over parts of muscles that don't layer with other muscles and the position of the ROI was re-adjusted manually according to the movements of the samples. Time series analyzer v3 plugin of imageJ was used to measure fluorescence intensity of the ROI. Five frames of GCaMP6f fluorescence before and after the peaks were averaged and used as basal GCaMP6f level (F_{basal}) to calculate the fold change of GCaMP6f fluorescence intensity [$\Delta F/F = (F - F_{basal})/F_{basal}$]. Prism GraphPad was used to find the peak values. Basal GCaMP6f levels or Ca^{2+} peaks per muscles were averaged as one experiment sample. Both the experiments and analysis were done blind.

Statistical Analysis

Statistical analyses were performed using Prism GraphPad software. The normality of data distribution was tested by D'Agostino and Pearson test. If the data fit a normal distribution, unpaired *t* test was used. If the data were not normally distributed, the Mann-Whitney test was used. For experiments in which the change in results can be predicted by our hypothesis, one-tailed tests were performed; otherwise two-tailed tests were performed. In all figures, ns, *, **, ***, **** represent $P > 0.05$, $P < 0.05$, $P < 0.01$, $P < 0.001$, and $P < 0.0001$. Error bars are standard errors of the mean.

RESULTS

Dstac and Dmca1D Are Expressed by Larval Body Wall Muscles

In zebrafish skeletal muscles, the L-type calcium channel, DHPR, and cytosolic Stac3 colocalize at specialized junctions of the T tubules and SR (Horstick et al., 2013; Linsley et al., 2017a). To examine the expression pattern of Dstac and Dmca1D within larval body wall muscles, larvae were labeled with anti-Dstac (Hsu et al., 2018) and anti-Dmca1D (Hsu, 2020). The specificity of anti-Dstac was previously demonstrated by Western blot analysis (Hsu et al., 2018) and that of anti-Dmca1D by showing that anti-Dmca1D labeled the CNS in control embryos but no labeling of *Dmca1D* in null embryos (Hsu, 2020). Anti-Dstac and anti-Dmca1D labeled puncta organized as stripes orthogonal to the longitudinal axis of the muscles with the stripes centered on the muscle actin network and sarcomere Z-lines labeled by phalloidin (**Figures 1A,B**, **2A**). Furthermore, co-labeling with anti-Dstac and anti-Dmca1D found that Dstac and Dmca1D localized to the same stripes (**Figure 2B**) with some puncta co-labeled (arrowheads) for both Dstac and Dmca1D (**Figure 2C**). Previously, larvae expressing mCD8:GFP that labels the plasma membrane including the T tubules were found in similar stripes in larval muscles (Fujita et al., 2017). In fact, anti-Dmca1D labeled stripes were co-extensive with T tubules expressing mCD4-td-Tomato (**Figure 1C**), which is consistent with Dmca1D expression in the T tubules. Since anti-Dstac labels the same muscle stripes as anti-Dmca1D, these results are consistent with localization of both Dmca1D and Dstac within the T tubules.

Larvae With *Dstac* Knocked Down in Body Wall Muscles Exhibited Decreased Locomotion and Failed to Eclose

Previously we showed that *Dstac* mutant larvae showed decreased locomotion (Hsu, 2020). Since Dstac is expressed both by neurons and muscles (Hsu et al., 2018), the locomotion phenotype could be due to defects in neurons or muscles or both. To see if muscle Dstac is required for normal locomotion, we assayed larvae in which *Dstac* was selectively knocked down in body wall muscles using a muscle driver regulated RNAi line that was previously shown by Western analysis to knockdown *Dstac* selectively in body wall muscles (Hsu et al., 2018). These larvae exhibited decreased locomotion compared with control larvae (**Figure 3A**). To see if the locomotion defect could be due to defective morphology of muscles in $Dstac^{RNAi}$ larvae, we labeled

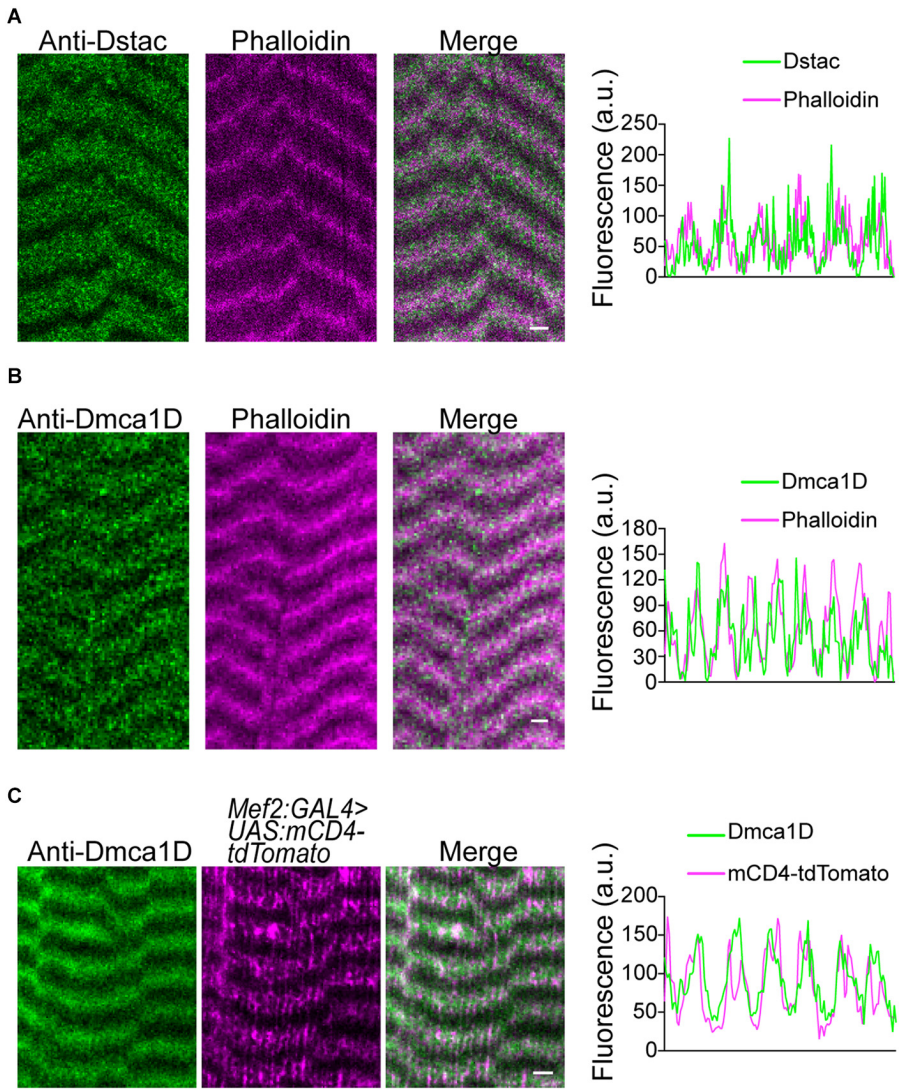

FIGURE 1 | Dstac and Dmca1D are expressed in stripes that are coextensive with T tubules in larval body wall muscles. **(A)** Anti-Dstac/phalloidin double labeling showed that Dstac is expressed in stripes centered on the actin network and Z line of larval muscles. The stripe pattern of the labeling along a muscle by anti-Dstac and phalloidin is quantified to show the extent of overlap of the labeling (right). **(B)** Anti-Dmca1D/phalloidin double labeling showed that Dmca1D is expressed in stripes centered on the actin network and Z line of larval muscles. The stripe pattern of the labeling along a muscle by anti-Dmca1D and phalloidin is quantified to show the overlap of the labeling (right). **(C)** Anti-Dmca1D labeling in *Mef2:GAL4 > UAS:mCD4-tdTomato* larvae showed that Dmca1D is found in the T tubules of larval muscles. The stripe pattern of Dmca1D and CD4-tdTomato along the muscle is quantified to show the overlap of the labeling with the T tubules (right). All images are a single plane. Scale bar, 3 μm.

muscles with anti-DLG, which recognizes the Disc-large protein, a membrane associated guanylate kinase that is localized to the postsynaptic membrane at the neuromuscular junctions (Lahey et al., 1994) and the longitudinal portions of the T tubules (Fujita et al., 2017). Anti-DLG labeling of the muscles of $Dstac^{RNAi}$ larvae were comparable with that in control larvae (**Figure 3B**). This result suggests that knockdown of Dstac in muscles does not lead to any obvious defects in body-wall muscles including the T tubules and thus the decreased locomotion may not be due to any morphological defect in the T tubules. $Dstac^{RNAi}$ larvae were able to develop to pupae that appeared similar to control pupae, but failed to eclose presumably due to decreased muscle function. The pharate adults released manually from the cocoon by dissection had apparent normal morphology (**Figure 3C**). Thus, Dstac in body wall muscles is required for normal locomotion.

Larvae With *Dmca1D* Knocked Down in Body Wall Muscles Exhibited Decreased Locomotion and Muscle Ca^{2+} Transients

Previously we showed that larvae that were homozygous for the ubiquitous *AR66* partial loss-of-function allele of *Dmca1D* exhibited decreased locomotion (Hsu, 2020). Dmca1D is expressed both by neurons including motor neurons (Hsu, 2020)

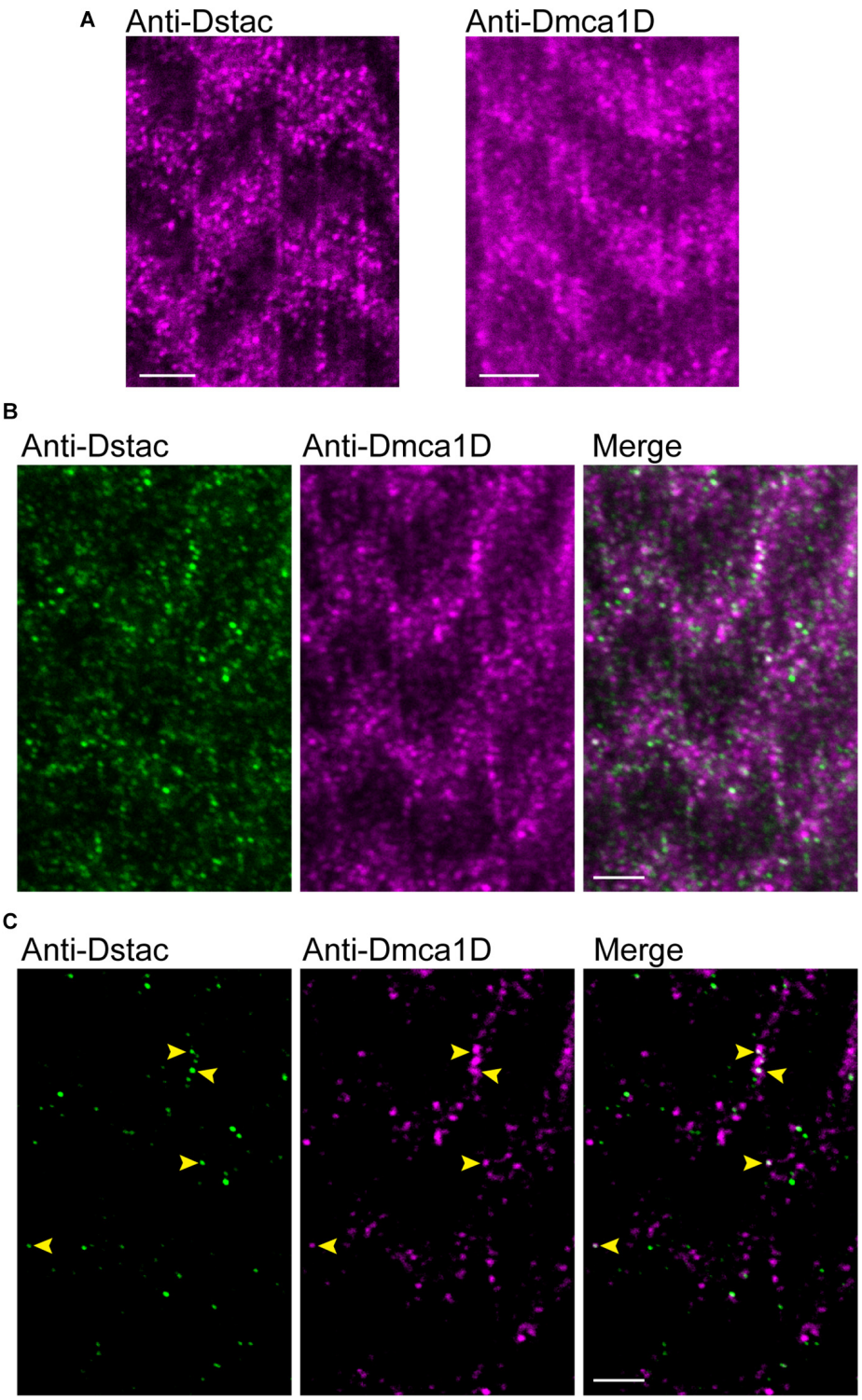

FIGURE 2 | Dstac and Dmca1D are co-expressed in larval muscle stripes. **(A)** Anti-Dstac (left) and anti-Dmca1D (right) labeling of 3rd instar body-wall muscles showed expression of Dstac and Dmca1D in stripes orthogonal to the longitudinal axis of the muscles. The images are a single focal plane. Scale bar, 3 μm. **(B)** Co-immunostaining of 3rd instar larval body wall muscles with anti-Dstac and anti-Dmca1D showed co-expression of Dstac and Dmca1D in the same stripes. The images are a single focal plane. Scale bar, 3 μm. **(C)** Same images as in **(B)** but showing only the puncta made up of the brightest 50% of pixels for easier comparison of the pattern of anti-Dstac and anti-Dmca1D labeling. Arrowheads indicate some puncta that co-labeled with anti-Dstac and anti-Dmca1D. The images are a single focal plane. Scale bar, 3 μm.

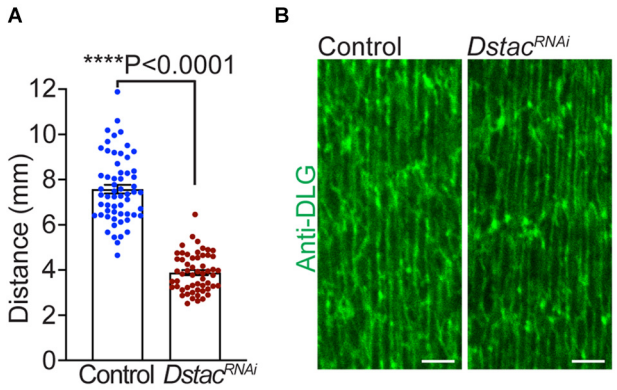

C

Genotype	Total # of Pupae	# of eclosion
Control	40	31
Dstac^{RNAi}	22	Zero

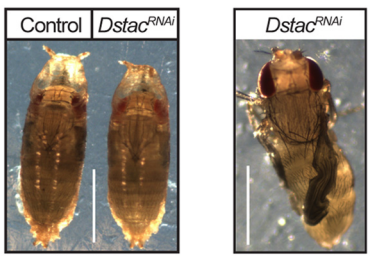

FIGURE 3 | Knockdown of *Dstac* in body wall muscles reduced larval locomotion. **(A)** *Dstac*^{RNAi} larvae in which *Dstac* was knocked down in body wall muscles (*Mef2:GAL4 > UAS:Dstac*^{RNAi}) showed decreased locomotion compared with control *Luciferase*^{RNAi} larvae (*Mef2:GAL4 > UAS:Luciferase*^{RNAi}). Control $n = 59$, *Dstac*^{RNAi} $n = 56$. One-tailed, unpaired *t* test. **(B)** Labeling T tubules of body-wall muscles with anti-DLG showed that T tubules of *Dstac*^{RNAi} larvae (*Mef2:GAL4 > UAS:Dstac*^{RNAi}) are similar in morphology and structure to control *Luciferase*^{RNAi} larvae (*Mef2:GAL4 > UAS:Luciferase*^{RNAi}). The images are a single focal plane. Scale bar, 3 μm. **(C)** *Dstac*^{RNAi} larvae in which *Dstac* was knocked down in body wall muscles (*Mef2:GAL4 > UAS:Dstac*^{RNAi}) could develop to mature pharate adults in the pupae but couldn't eclose. The left lower image shows a control *Luciferase*^{RNAi} pupa and a *Dstac*^{RNAi} pupa that are similar in morphology. The right lower image shows a pharate adult of *Dstac*^{RNAi} that was dissected out from its cocoon in which the wings are not inflated and did not survive. Scale bar, 1 mm. ****$P < 0.0001$.

and muscles and so the mutant phenotype could be due to a defect of *Dmca1D* in either neurons or muscles or both. To see if a muscle deficiency in Dmca1D could lead to decreased locomotion, we selectively knocked down *Dmca1D* in body wall muscles (*Mef2:GAL4 > UAS:Dmca1D*^{RNAi}). *Dmca1D*^{RNAi} larvae developed to the size of 2nd instar larvae and died approximately 10 days after hatching. Anti-Dmca1D labeling in body wall muscles was decreased in 2nd instar *Dmca1D*^{RNAi} larvae compared with size-matched control 2nd instar larvae (**Figure 4A**) suggesting that Dmca1D was indeed knocked down in muscles. We further analyzed the fluorescence levels of pixels along a longitudinal line of each muscle fiber in controls and *Dmca1D*^{RNAi} larvae and found that the difference in fluorescence of the peak pixels in the Dmca1D stripe and background fluorescence pixels in non-stripe regions was decreased in *Dmca1D*^{RNAi} larvae compared with controls (**Figure 4B**) confirming that Dmca1D was knocked down. Furthermore, *Dmca1D*^{RNAi} larvae showed reduced locomotion compared with size and age matched 2nd instar control larvae (**Figure 4C**). These results indicate that normal levels of Dmca1D in body-wall muscles are required for normal locomotion.

To see if the decreased locomotion of larvae with a muscle deficiency in Dmca1D was due to a defect in EC coupling, we examined transient increases in cytosolic Ca^{2+} in body wall muscles during locomotion in larvae selectively expressing GCaMP6f in muscles. Ca^{2+} imaging of body-wall muscles was performed in live, intact larvae placed in a microfluidics chamber designed to physically restrain larvae (Ghannad-Rezaie et al., 2012). Under these conditions, Ca^{2+} transient increases were observed within body-wall muscles of control (*Mef2:GAL4 > UAS:GCaMP6f; UAS:mCD8tdTomato; UAS-Luciferase*^{RNAi}) and *Dmca1D*^{RNAi} larvae (*Mef2:GAL4 > UAS:GCaMP6f; UAS:mCD8tdTomato; UAS-Dmca1D*^{RNAi}) (**Figure 4D**) that presumably were associated with muscle contractions. The basal GCaMP6f fluorescence levels when larvae were quiescent were similar in *Dmca1D*^{RNAi} larvae and control larvae (**Figure 4E**). Thus, expression of GCaMP6f was unaffected by the knockdown of Dmca1D in body wall muscles. However, the peak of the Ca^{2+} transients recorded from *Dmca1D*^{RNAi} larvae was decreased compared with controls (**Figure 4F**), but the frequency of transients was comparable (**Figure 4G**). These results showed that the output of the central pattern generator was not dependent on normal Dmca1D in muscles, but normal muscle Ca^{2+} transients during physiological activation of muscles were dependent on Dmca1D. Thus, it appears that EC coupling requires Dmca1D.

Muscle *Dstac* Deficiency Reduced *Dmca1D* Expression and Ca^{2+} Transients in Muscles During Locomotion

Since both Dmca1D and Dstac regulate larval locomotion and Dmca1D regulates Ca^{2+} transients during EC coupling, we asked if Dstac regulates Dmca1D. Immunolabeling the body wall muscles of wt and *Dstac*$^{\Delta SH3}$ mutant larvae (Hsu, 2020) with anti-Dmca1D showed that Dmca1D expression appeared to be reduced in *Dstac*$^{\Delta SH3}$ compared with wt larvae (**Figure 5A**). We further analyzed the fluorescence levels of pixels along a longitudinal line of anti-Dmca1D labeled muscle fibers in controls and *Dstac*$^{\Delta SH3}$ larvae and found that the difference in fluorescence of the peak pixels in the Dmca1D stripes and background fluorescence pixels in non-stripe regions was decreased in *Dstac*$^{\Delta SH3}$ larvae compared with controls (**Figure 5B**) confirming that Dmca1D was diminished in *Dstac*$^{\Delta SH3}$ larval muscles. The finding that there was no obvious defect in T tubules when Dstac is knocked down (**Figure 3B**) argues against the possibility that the decreased Dmca1D in *Dstac* mutants might be a by-product of a defect in the morphology/organization of the T tubules. Furthermore, although the intensity of anti-Dmca1D was reduced in *Dstac*$^{\Delta SH3}$

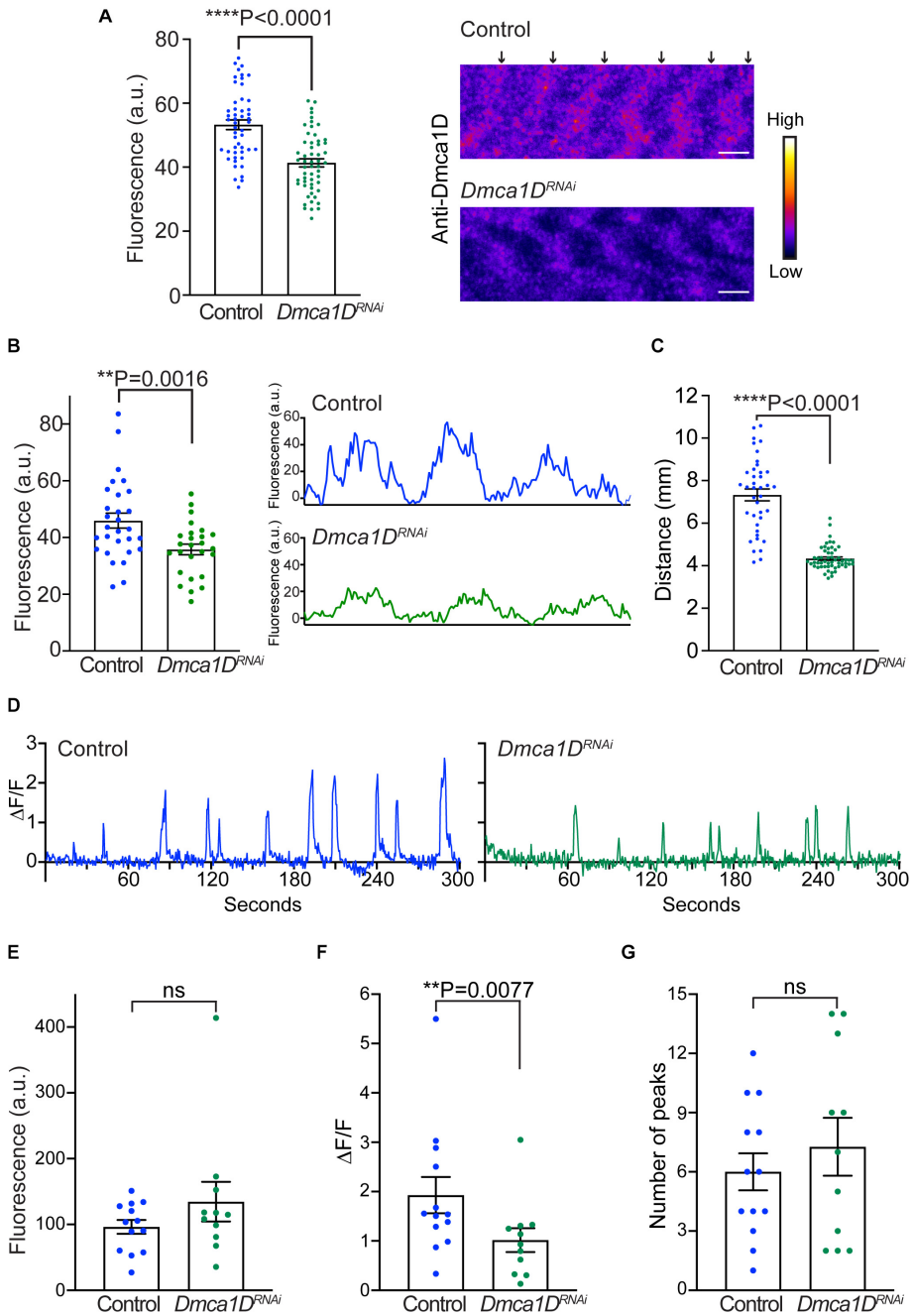

FIGURE 4 | Knockdown of *Dmca1D* selectively in muscles reduced larval locomotion and muscle Ca^{2+} transients. **(A)** Anti-Dmca1D labeling of muscles of larvae with Dmca1D knocked down selectively in body-wall muscles (*Mef2:GAL4 > UAS:Dmca1D*^{RNAi}) (n = 55 stripes from 11 muscles) confirmed that Dmca1D was knocked down compared with control muscles (*Mef2:GAL4 > UAS:Luciferase*^{RNAi}) (n = 50 stripes from 10 muscles). One-tailed, unpaired t test. Fluorescence was measured in ROIs that outlined each stripe. Right images are a single focal plane of muscle 4 of a control and a *Dmca1D*^{RNAi} larvae. Arrows denote the striations of Dmca1D clusters. Scale bar, 3 μm. **(B)** Same as in **(A)** except the peak fluorescence of stripes was measured. Fluorescence of individual pixels along a longitudinal line that crossed multiple stripes of muscle fibers was measured from *Mef2:GAL4 > UAS:Dmca1D*^{RNAi} (n = 26 stripes from 8 muscles) and control muscles (*Mef2:GAL4 > UAS:Luciferase*^{RNAi}) (n = 29 stripes from 9 muscles). One tailed, unpaired t test. Right images are examples of fluorescence measurements along the longitudinal line of wt and control muscles. **(C)** *Dmca1D*^{RNAi} larvae in which Dmca1D was knocked down in body-wall muscles (*Mef2:GAL4 > UAS:Dmca1D*^{RNAi}) showed decreased locomotion compared with control *Luciferase*^{RNAi} larvae (*Mef2:GAL4 > UAS:Luciferase*^{RNAi}). Control n = 39, Dmca1D^{RNAi} n = 54. One-tailed Mann-Whitney test. **(D)** Example of Ca^{2+} transients from a muscle in a control larva (*Mef2:GAL4 > UAS:GCaMP6f; UAS:mCD8tdTomato; UAS:Luciferase*^{RNAi}) and a *Dmca1D*^{RNAi} larva (*Mef2:GAL4 > UAS:GCaMP6f; UAS:mCD8tdTomato; UAS:Dmca1D*^{RNAi}). **(E)** Expression of GCaMP6f by muscles of *Dmca1D*^{RNAi} larvae was comparable to that of control. Mann-Whitney test. **(F)** The peaks of Ca^{2+} transients in the muscles of *Dmca1D*^{RNAi} larvae were smaller compared with controls. One-tailed, Mann-Whitney test. **(G)** The number of Ca^{2+} transients over 5 min in *Dmca1D*^{RNAi} and control muscles were comparable. Unpaired t test. Data in E-G were from 13 muscles of 7 control larvae and from 11 muscles of 6 *Dmca1D*^{RNAi} larvae. $^{**}P < 0.01$ and $^{****}P < 0.0001$.

mutants, the pattern of labeling was not, which is consistent with intact T tubules in mutants. This finding is consistent with the earlier finding that DHPR levels of skeletal muscles were reduced in mouse *stac3* knockout myotubes (Polster et al., 2016) and *stac3* null zebrafish (Linsley et al., 2017a). Thus, the Dmca1D immunolabeling of muscles in wt and $Dstac^{\Delta SH3}$ mutant larvae is consistent with the necessity of Dstac for normal expression of Dmca1D in muscles.

The decreased Dmca1D in body wall muscles predicts that Ca^{2+} transients should also be reduced when Dstac is knocked down in muscles (*Mef2:GAL4 > UAS:GCaMP6f; UAS:mCD8tdTomato; UAS-*$Dstac^{RNAi}$). As before Ca^{2+} transients were assayed in larvae selectively expressing GCaMP6f in body wall muscles (**Figure 5C**). The basal GCamP6f level when muscles were quiescent was higher in $Dstac^{RNAi}$ larvae compared with control larvae (**Figure 5D**), but peak Ca^{2+} transients were decreased (**Figure 5E**) but not their frequency (**Figure 5F**). Thus, Dstac appears to regulate Dmca1D to mediate normal Ca^{2+} transients during EC coupling.

DISCUSSION

In invertebrates, CICR appears to be important for muscle contraction (Györke and Palade, 1992; Collet, 2009). We found that *Drosophila* larvae in which *Dmca1D* was selectively knocked down in body wall muscles exhibited decreased muscle Ca^{2+} transients and locomotion. Thus, our results are consistent with the possibility that Ca^{2+} influx via Dmca1D might initiate CICR that leads to Ca^{2+} transients during EC coupling and thus muscle contraction.

In vertebrate skeletal muscles unlike in invertebrate muscles, EC coupling is independent of an influx of Ca^{2+} from calcium channels but rather involves direct interaction of DHPR, the voltage dependent L-type calcium channel in the T tubules, and the RyR Ca^{2+} release channel in the SR (Paolini et al., 2004; Dayal et al., 2017). Stac3 is a key regulator of EC coupling in vertebrate skeletal muscles that regulates the stability and voltage-response of DHPR in T tubules (Linsley et al., 2017a). Despite the differences in EC coupling of vertebrate and invertebrate muscles, the results in this study suggest that Dstac plays a conserved role as vertebrate Stac3 in regulating EC coupling. First, Dstac and Dmca1D are localized to the same stripes of the body wall muscles, which may also correspond with the T tubule network. Second, knockdown of Dstac in body-wall muscles reduced larval locomotion just as when Dmca1D is knocked down. Third, deficiency of Dstac in muscles decreased Ca^{2+} transients in body wall muscles during locomotion similar to that seen when Dmca1D is knocked down. Thus, Dstac is required for normal EC coupling. It appears that stac proteins regulate excitation-contraction coupling in both vertebrate skeletal muscles and invertebrate muscles due to their regulation of L-type calcium channels. In this regard, vertebrate cardiac myocytes that utilize CICR express low basal levels of Stac2, another stac protein (Niu et al., 2018) suggesting the possibility that stac proteins regulate excitation-contraction coupling in vertebrate cardiac muscles as well.

Our finding that the levels of Dmca1D in body wall muscles appeared to be decreased in *Dstac* mutants suggests that Dstac regulates Dmca1D. This finding corresponds with the regulation by Stac3 of the stability and thus the level of DHPRs in zebrafish skeletal muscles (Linsley et al., 2017a). Thus, it is possible that Dstac might regulate the stability of Dmca1D. Experiments such as live imaging of a fusion of Dmca1D with a photoconvertible protein will be needed to assay whether the stability of Dmca1D is regulated by Dstac. Stac3 also regulates the voltage response of DHPRs in zebrafish skeletal muscles (Linsley et al., 2017a). Whether Dstac also regulates the voltage response of Dmca1D await to be examined by voltage clamp experiments. In this regard, voltage-clamp analysis of L-type currents in motor neurons that also express Dstac and Dmca1D found that Dstac was required for normal voltage responses of Dmca1D channels (Hsu, 2020) suggesting that this might also be the case in body wall muscles.

Besides the Src Homology 3 (SH3) and cysteine-rich domain (CRD) that define the Stac proteins, Dstac has a putative BAR domain as do the other invertebrate Stac proteins but not the vertebrate Stac proteins (Hsu et al., 2018). The function of the putative BAR domain of Dstac is unknown. Amphiphysin, a protein containing a SH3 and a BAR domain but not a CRD domain, was found to regulate the development and organization of T tubules and thereby EC coupling (Razzaq et al., 2001). This result is consistent with a role for BAR domains for mediating membrane curvature (Salzer et al., 2017). However, what role the BAR domain of Dstac might play is unclear, but we did not detect any obvious defect in the T tubules of $Dstac^{RNAi}$ larvae. This finding appears to be consistent with no role of the Dstac BAR domain for the formation of T tubules. However, Dstac is alternatively spliced and $Dstac^{RNAi}$ targeted the linker sequence between the CRD and SH3 domains that is downstream of the BAR domain (Hsu et al., 2018). In fact, there are 13 transcripts containing a BAR domain and only 3 of these would have been targeted by the RNAi. Thus, any role of Dstac for the formation of T tubules will require further analysis.

Our results showed that $Dstac^{RNAi}$ larvae exhibited higher basal Ca^{2+} levels during the quiescent stage of locomotion. Control and $Dstac^{RNAi}$ larvae carried the same number of *GAL4* and *UAS* elements so this difference may not be due to differences in the expression level of GCaMP6f. The increased cytosolic Ca^{2+} levels in $Dstac^{RNAi}$ muscles could be explained by a decreased sequestration and/or storage of Ca^{2+} within the SR or through an increase in steady-state SR Ca^{2+} leak. However, in $Dmca1D^{RNAi}$ larvae, the elevated cytosolic Ca^{2+} when muscles were quiescent was not observed as it was in $Dstac^{RNAi}$ larvae. These results are consistent with the possibility that Dstac might regulate some Dmca1D-independent mechanisms to maintain cytosolic Ca^{2+} levels.

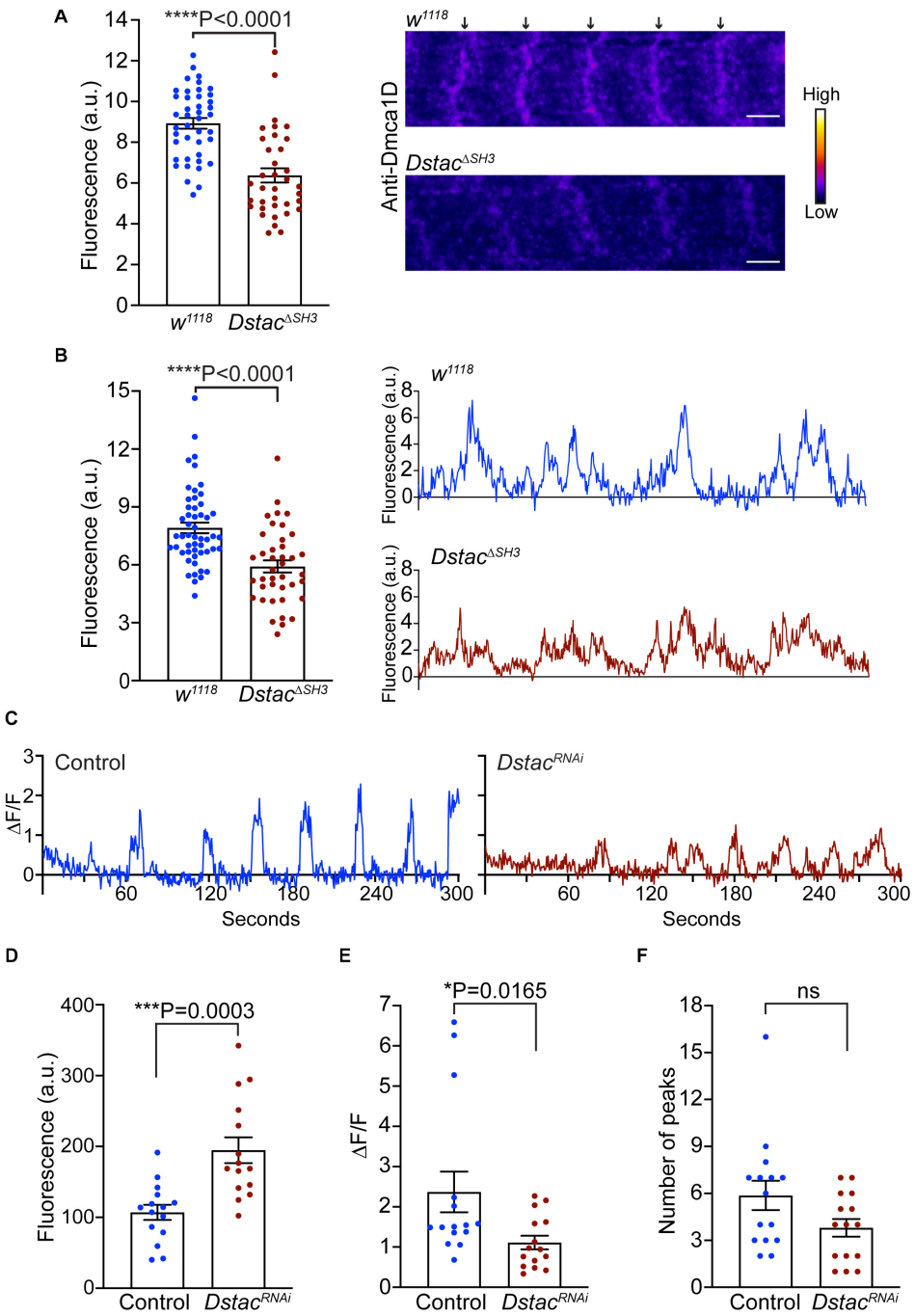

FIGURE 5 | Knockdown of *Dstac* in body-wall muscles reduced Dmca1D expression level and muscle Ca^{2+} transients. **(A)** Anti-Dmca1D labeling of $Dstac^{\Delta SH3}$ larval muscles (n = 36 stripes from 12 muscles) showed decreased level of Dmca1D at T tubules compared with wt (n = 42 stripes from 14 muscles). One-tailed Mann Whitney test. Right images are a single focal plane of muscle 4 of a wt and a $Dstac^{\Delta SH3}$ larvae. Arrows denote striations of Dmca1D clusters. Scale bar, 3 μm. **(B)** Same as in **(A)** except the peak fluorescence of stripes was measured. Fluorescence of individual pixels along a longitudinal line that crossed multiple stripes of muscle fibers was measured from $Dstac^{\Delta SH3}$ (n = 40 stripes from 13 muscles) and wt (n = 52 stripes from 14 muscles). One-tailed Mann Whitney test. Right images are examples of fluorescence measurements along the longitudinal line of wt and $Dstac^{\Delta SH3}$ muscles. **(C)** Example of Ca^{2+} transients from a muscle in a control larva (*Mef2:GAL4 > UAS:GCaMP6f; UAS:mCD8tdTomato; UAS:Luciferase*^{RNAi}) and a $Dstac^{RNAi}$ larva (*Mef2:GAL4 > UAS:GCaMP6f; UAS:mCD8tdTomato; UAS:Dstac*^{RNAi}). **(D)** The level of GCaMP6f fluorescence in muscles of $Dstac^{RNAi}$ larvae was higher than that of control. Unpaired t test. **(E)** The peaks of Ca^{2+} transients in the muscles of $Dstac^{RNAi}$ larvae were smaller compared with controls. One-tailed Mann-Whitney test. **(F)** The number of Ca^{2+} transients over 5 min in $Dstac^{RNAi}$ and control muscles were comparable. Mann-Whitney test. Data in D-F were from 15 muscles of 5 control larvae and from 15 muscles of 5 $Dstac^{RNAi}$ larvae. $^{*}P < 0.05$, $^{***}P < 0.001$, and $^{****}P < 0.0001$.

Electrophysiological analysis showed that *Drosophila* larval body-wall muscles express not only the L-type channel, *Dmca1D*, but also the T-type channel, *Dmca1G* (Gielow et al., 1995). Interestingly, vertebrate Stac1 was found to form a complex with a mammalian T-type Ca_V channel, $Ca_V3.2$, and is required for $Ca_V3.2$ expression at plasma membrane (Rzhepetskyy et al., 2016). It would be interesting to examine if Dstac also regulates Dmca1G as suggested by the Stac1/T-type Ca_V interactions.

DATA AVAILABILITY STATEMENT

The raw data supporting the conclusions of this article will be made available by the authors, without undue reservation.

AUTHOR CONTRIBUTIONS

I-UH, JL, and JK contributed to the conceptualization. I-UH and JK contributed to the methodology. I-UH contributed to the formal analysis. I-UH, JL, LR, AL, and JK contributed to the investigation. RH and JK contributed to the resources. I-UH and JK contributed to the writing of the original draft. JK contributed to the supervision. I-UH, JL, and JK contributed to the funding acquisition. All authors contributed to the article and approved the submitted version.

FUNDING

This project was funded by NIAMS (R01 AR063056) to JK and I-UH was supported by a Rackham International Student Fellowship, Rackham Barbour Scholarship, Rackham Predoctoral Fellowship, Rackham Research Grant and Rackham one-Term Fellowship from the University of Michigan. JL by a Rackham Merit Fellowship from the University of Michigan and NIGMS (T32 GM007315) and LR by Summer Research Fellowship from the University of Michigan.

ACKNOWLEDGMENTS

We thank Miranda Lum, Allison Orzel, Bethany Folk-Middlebrook for technical assistance, Catherine Collins and the Collins lab for advice and use of facilities for the genetics, Catherine Collins for comments on an earlier version of the manuscript and Gregg Sobocinski for expert assistance with confocal microscopy.

REFERENCES

Adams, B. A., Tanabe, T., Mikami, A., Numa, S., and Beam, K. G. (1990). Intramembrane charge movement restored in dysgenic skeletal muscle by injection of dihydropyridine receptor cDNAs. *Nature* 346, 569–572. doi: 10.1038/346569a0

Block, B. A., Imagawa, T., Campbell, K. P., and Franzini-Armstrong, C. (1988). Structural evidence for direct interaction between the molecular components of the transverse tubule/sarcoplasmic reticulum junction in skeletal muscle. *J. Cell Biol.* 107, 2587–2600. doi: 10.1083/jcb.107.6.2587

Bolton, T. B., Prestwich, S. A., Zholos, A. V., and Gordienko, D. V. (1999). Excitation-contraction coupling in gastrointestinal and other smooth muscles. *Annu. Rev. Physiol.* 61, 85–115. doi: 10.1146/annurev.physiol.61.1.85

Collet, C. (2009). Excitation-contraction coupling in skeletal muscle fibers from adult domestic honeybee. *Pflugers Arch.* 458, 601–612. doi: 10.1007/s00424-009-0642-6

Cong, X., Doering, J., Mazala, D. A. G., Chin, E. R., Grange, R. W., and Jiang, H. (2016). The SH3 and cysteine-rich domain 3 (Stac3) gene is important to growth, fiber composition, and calcium release from the sarcoplasmic reticulum in postnatal skeletal muscle. *Skelet. Muscle* 6:17.

Dayal, A., Schrötter, K., Pan, Y., Föhr, K., Melzer, W., and Grabner, M. (2017). The Ca2+ influx through the mammalian skeletal muscle dihydropyridine receptor is irrelevant for muscle performance. *Nat. Commun.* 8:475.

Eberl, D. F., Ren, D., Feng, G., Lorenz, L. J., Van Vactor, D., and Hall, L. M. (1998). Genetic and developmental characterization of Dmca1D, a calcium channel α1 subunit gene in *Drosophila melanogaster*. *Genetics* 148, 1159–1169.

Fujita, N., Huang, W., Lin, T.-H., Groulx, J.-F., Jean, S., Nguyen, J., et al. (2017). Genetic screen in Drosophila muscle identifies autophagy-mediated T-tubule remodeling and a Rab2 role in autophagy. *eLife* 6:e23367.

Ge, X., Zhang, Y., Park, S., Cong, X., Gerrard, D. E., and Jiang, H. (2014). Stac3 inhibits myoblast differentiation into myotubes. *PLoS One* 9:e95926. doi: 10.1371/journal.pone.0095926

Ghannad-Rezaie, M., Wang, X., Mishra, B., Collins, C., and Chronis, N. (2012). Microfluidic chips for *in vivo* imaging of cellular responses to neural injury in *Drosophila* larvae. *PLoS One* 7:e29869. doi: 10.1371/journal.pone.0029869

Gielow, M., Gu, G., and Singh, S. (1995). Resolution and pharmacological analysis of the voltage-dependent calcium channels of Drosophila larval muscles. *J. Neurosci.* 15, 6085–6093. doi: 10.1523/jneurosci.15-09-06085.1995

Györke, S., and Palade, P. (1992). Calcium-induced calcium release in crayfish skeletal muscle. *J. Physiol.* 457, 195–210. doi: 10.1113/jphysiol.1992.sp019373

Horstick, E. J., Linsley, J. W., Dowling, J. J., Hauser, M. A., Mcdonald, K. K., Ashley-Koch, A., et al. (2013). Stac3 is a component of the excitation-contraction coupling machinery and mutated in Native American myopathy. *Nat. Commun.* 4:1952.

Hsu, I. U. (2020). *Analysis of the Dstac Gene, a Novel Regulator of Neuronal Function and Behavior in Drosophila melanogaster*. Doctoral dissertation, University of Michigan, Ann Arbor, MI.

Hsu, I. U., Linsley, J. W., Varineau, J. E., Shafer, O. T., and Kuwada, J. Y. (2018). Dstac is required for normal circadian activity rhythms in *Drosophila*. *Chronobiol. Int.* 35, 1016–1026. doi: 10.1080/07420528.07422018.01454937

Lahey, T., Gorczyca, M., Jia, X.-X., and Budnik, V. (1994). The drosophila tumor suppressor gene dlg is required for normal synaptic bouton structure. *Neuron* 13, 823–835. doi: 10.1016/0896-6273(94)90249-6

Linsley, J. W., Hsu, I. U., Groom, L., Yarotskyy, V., Lavorato, M., Horstick, E. J., et al. (2017a). Congenital myopathy results from misregulation of a muscle Ca2+ channel by mutant Stac3. *Proc. Natl. Acad. Sci. U.S.A.* 114, E228–E236.

Linsley, J. W., Hsu, I. U., Wang, W., and Kuwada, J. Y. (2017b). Transport of the alpha subunit of the voltage gated L-type calcium channel through the sarcoplasmic reticulum occurs prior to localization to triads and requires the beta subunit but not Stac3 in skeletal muscles. *Traffic* 18, 622–632. doi: 10.1111/tra.12502

Maryon, E. B., Saari, B., and Anderson, P. (1998). Muscle-specific functions of ryanodine receptor channels in *Caenorhabditis elegans*. *J. Cell Sci.* 111(Pt 19), 2885–2895.

Nelson, B. R., Wu, F., Liu, Y., Anderson, D. M., Mcanally, J., Lin, W., et al. (2013). Skeletal muscle-specific T-tubule protein STAC3 mediates voltage-induced Ca2+ release and contractility. *Proc. Natl. Acad. Sci. U.S.A.* 110, 11881–11886. doi: 10.1073/pnas.1310571110

Niu, J., Dick, I. E., Yang, W., Bamgboye, M. A., Yue, D. T., Tomaselli, G., et al. (2018). Allosteric regulators selectively prevent Ca(2+)-feedback of CaV and NaV channels. *eLife* 7:e35222.

Paolini, C., Fessenden, J. D., Pessah, I. N., and Franzini-Armstrong, C. (2004). Evidence for conformational coupling between two calcium channels. *Proc. Natl. Acad. Sci. U.S.A.* 101, 12748–12752. doi: 10.1073/pnas.0404836101

Polster, A., Nelson, B. R., Olson, E. N., and Beam, K. G. (2016). Stac3 has a direct role in skeletal muscle-type excitation–contraction coupling that is disrupted by a myopathy-causing mutation. *Proc. Natl. Acad. Sci. U.S.A.* 113, 10986–10991. doi: 10.1073/pnas.1612441113

Razzaq, A., Robinson, I. M., Mcmahon, H. T., Skepper, J. N., Su, Y., Zelhof, A. C., et al. (2001). Amphiphysin is necessary for organization of the excitation-contraction coupling machinery of muscles, but not for synaptic vesicle endocytosis in *Drosophila*. *Genes Dev.* 15, 2967–2979. doi: 10.1101/gad.207801

Ren, D., Xu, H., Eberl, D. F., Chopra, M., and Hall, L. M. (1998). A mutation affecting dihydropyridine-sensitive current levels and activation kinetics in *Drosophila* muscle and mammalian heart calcium channels. *J. Neurosci.* 18, 2335–2341. doi: 10.1523/jneurosci.18-07-02335.1998

Rios, E., and Brum, G. (1987). Involvement of dihydropyridine receptors in excitation–contraction coupling in skeletal muscle. *Nature* 325, 717–720. doi: 10.1038/325717a0

Rzhepetskyy, Y., Lazniewska, J., Proft, J., Campiglio, M., Flucher, B. E., and Weiss, N. (2016). A $Ca_V3.2$/Stac1 molecular complex controls T-type channel expression at the plasma membrane. *Channels* 10, 346–354. doi: 10.1080/19336950.2016.1186318

Salzer, U., Kostan, J., and Djinović-Carugo, K. (2017). Deciphering the BAR code of membrane modulators. *Cell. Mol. Life Sci.* 74, 2413–2438. doi: 10.1007/s00018-017-2478-0

Sanyal, S., Consoulas, C., Kuromi, H., Basole, A., Mukai, L., Kidokoro, Y., et al. (2005). Analysis of conditional paralytic mutants in Drosophila sarco-endoplasmic reticulum calcium ATPase reveals novel mechanisms for regulating membrane excitability. *Genetics* 169, 737–750. doi: 10.1534/genetics.104.031930

Schneider, M. F., and Chandler, W. K. (1973). Voltage dependent charge movement in skeletal muscle: a possible step in excitation–contraction coupling. *Nature* 242, 244–246. doi: 10.1038/242244a0

Schredelseker, J., Shrivastav, M., Dayal, A., and Grabner, M. (2010). Non-Ca2+-conducting Ca2+ channels in fish skeletal muscle excitation-contraction coupling. *Proc. Natl. Acad. Sci. U.S.A.* 107, 5658–5663. doi: 10.1073/pnas.0912153107

Shafer, O. T., and Taghert, P. H. (2009). RNA-interference knockdown of *Drosophila* pigment dispersing factor in neuronal subsets: the anatomical basis of a neuropeptide's circadian functions. *PLoS One* 4:e8298. doi: 10.1371/journal.pone.0008298

Sullivan, K. M., Scott, K., Zuker, C. S., and Rubin, G. M. (2000). The ryanodine receptor is essential for larval development in *Drosophila melanogaster*. *Proc. Natl. Acad. Sci. U.S.A.* 97, 5942–5947. doi: 10.1073/pnas.110145997

Takekura, H., and Franzini-Armstrong, C. (2002). The structure of Ca(2+) release units in arthropod body muscle indicates an indirect mechanism for excitation-contraction coupling. *Biophys. J.* 83, 2742–2753. doi: 10.1016/s0006-3495(02)75284-3

Takeshima, H., Nishimura, S., Matsumoto, T., Ishida, H., Kangawa, K., Minamino, N., et al. (1989). Primary structure and expression from complementary DNA of skeletal muscle ryanodine receptor. *Nature* 339, 439–445. doi: 10.1038/339439a0

Tanabe, T., Takeshima, H., Mikami, A., Flockerzi, V., Takahashi, H., Kangawa, K., et al. (1987). Primary structure of the receptor for calcium channel blockers from skeletal muscle. *Nature* 328, 313–318. doi: 10.1038/328313a0

Zheng, W., Feng, G., Ren, D., Eberl, D. F., Hannan, F., Dubald, M., et al. (1995). Cloning and characterization of a calcium channel alpha 1 subunit from *Drosophila melanogaster* with similarity to the rat brain type D isoform. *J. Neurosci.* 15, 1132–1143. doi: 10.1523/jneurosci.15-02-01132.1995

Conflict of Interest: The authors declare that the research was conducted in the absence of any commercial or financial relationships that could be construed as a potential conflict of interest.

frontiers in Physiology

REVIEW
published: 22 October 2020
doi: 10.3389/fphys.2020.595800

Physiological Ca^{2+} Transients Versus Pathological Steady-State Ca^{2+} Elevation, Who Flips the ROS Coin in Skeletal Muscle Mitochondria

Ang Li, Jianxun Yi, Xuejun Li and Jingsong Zhou**

Department of Kinesiology, College of Nursing and Health Innovation, The University of Texas at Arlington, Arlington, TX, United States

OPEN ACCESS

Edited by:
Enrique Jaimovich, University of Chile, Chile

Reviewed by:
Takahiko Shimizu, National Center for Geriatrics and Gerontology (NCGG), Japan
Scott Powers, University of Florida, United States

***Correspondence:**
Ang Li
ang.li3@uta.edu
Jingsong Zhou
jingsong.zhou@uta.edu

Specialty section:
This article was submitted to Striated Muscle Physiology, a section of the journal Frontiers in Physiology

Received: *17 August 2020*
Accepted: *05 October 2020*
Published: *22 October 2020*

Citation:
Li A, Yi J, Li X and Zhou J (2020) Physiological Ca^{2+} Transients Versus Pathological Steady-State Ca^{2+} Elevation, Who Flips the ROS Coin in Skeletal Muscle Mitochondria. Front. Physiol. 11:595800. doi: 10.3389/fphys.2020.595800

Mitochondria are both the primary provider of ATP and the pivotal regulator of cell death, which are essential for physiological muscle activities. Ca^{2+} plays a multifaceted role in mitochondrial function. During muscle contraction, Ca^{2+} influx into mitochondria activates multiple enzymes related to tricarboxylic acid (TCA) cycle and oxidative phosphorylation, resulting in increased ATP synthesis to meet the energy demand. Pathophysiological conditions such as skeletal muscle denervation or unloading also lead to elevated Ca^{2+} levels inside mitochondria. However, the outcomes of this steady-state elevation of mitochondrial Ca^{2+} level include exacerbated reactive oxygen species (ROS) generation, sensitized opening of mitochondrial permeability transition pore (mPTP), induction of programmed cell death, and ultimately muscle atrophy. Previously, both acute and long-term endurance exercises have been reported to activate certain signaling pathways to counteract ROS production. Meanwhile, electrical stimulation is known to help prevent apoptosis and alleviate muscle atrophy in denervated animal models and patients with motor impairment. There are various mechanistic studies that focus on the excitation-transcription coupling framework to understand the beneficial role of exercise and electrical stimulation. Interestingly, a recent study has revealed an unexpected role of rapid mitochondrial Ca^{2+} transients in keeping mPTP at a closed state with reduced mitochondrial ROS production. This discovery motivated us to contribute this review article to inspire further discussion about the potential mechanisms underlying differential outcomes of physiological mitochondrial Ca^{2+} transients and pathological mitochondrial Ca^{2+} elevation in skeletal muscle ROS production.

Keywords: skeletal muscle, mitochondrial ROS, mitoflash, mitochondrial Ca^{2+} homeostasis, transitory mPTP opening, electric field stimulation

INTRODUCTION

Skeletal muscle carries out multiple critical functions of human body such as locomotion, metabolism, and thermogenesis (Block, 1994; Qiu et al., 2018). Thus, skeletal muscle atrophy, characterized by loss of muscle mass and strength, could have severe impact on daily living or even become life-threatening (Jackman and Kandarian, 2004). Human and animal studies revealed a variety of etiological factors for skeletal muscle atrophy, including disuse (limb immobilization, unloading) (Jackman and Kandarian, 2004), denervation (spinal motor neuron lesion in patients or surgical transection of motor nerves in animals) (Hoellwarth and Christian Hofer, 2005; Adhihetty et al., 2007), fasting (Qiu et al., 2018), lack of gravity (Fitts et al., 2001), aging (sarcopenia) (Dupont-Versteegden, 2005), cancer (cachexia) (Tisdale, 2010), neuromuscular diseases such as amyotrophic lateral sclerosis (ALS), and spinal muscular atrophy (Fischer et al., 2004; Monani, 2005). Accumulating evidence highlights programmed cell death (apoptosis) as a major cause of muscle fiber loss in skeletal muscle atrophy (Borisov and Carlson, 2000; Tews, 2002; Siu and Alway, 2005; Adhihetty et al., 2007), potentially implicating mitochondrial abnormality as a shared pathological feature underlying muscle atrophy induced by different etiological factors.

Mitochondria take up around 10–15% volume of mammalian skeletal muscle fibers (Eisenberg, 2010), with a certain degree of compositional and function differences observed between the subsarcolemmal, interfibrillar and peri-nuclear subpopulations (Cogswell et al., 1993; Díaz-Vegas et al., 2019). Mitochondria, especially the interfibrillar subpopulation, not only serve as the primary energy provider but also are intimately involved in apoptosis (Adhihetty et al., 2005; Siu and Alway, 2005; Chabi et al., 2008; Wang and Youle, 2009). The connections between mitochondria and apoptosis include:

1. Multiple proapoptotic proteins are located within mitochondria, such as cytochrome c (Cyto c) (Liu et al., 1996), apoptosis-inducing factor (AIF) (Susin et al., 1999), second mitochondria-derived activator of caspase/direct IAP (inhibitor-of apoptosis) binding protein (Smac/Diablo) (Du et al., 2000), Endonuclease G (EndoG) (Li et al., 2001), and high temperature requirement protein A2 (HtraA2) (Hegde et al., 2002).

2. Although healthy mitochondria are not the major contributor to cytosolic ROS in skeletal muscle during contractile activities (Sakellariou et al., 2013; Powers et al., 2016; Henríquez-Olguin et al., 2019), they can significantly contribute to ROS production under pathological conditions (Pottecher et al., 2013; Lejay et al., 2014). Upon overwhelming the cellular antioxidants' neutralizing capacity, ROS causes oxidative damages to lipids, proteins, and DNA (Bandyopadhyay et al., 1999). Elevated ROS production is frequently observed as an early event of the apoptotic process (Fernandez et al., 2002).

3. Long-term elevation of mitochondrial matrix Ca^{2+} ($[Ca^{2+}]_{mito}$) can induce cell apoptosis through increasing the release of proapoptotic proteins and mitochondrial permeability transition pore (mPTP) opening (Haworth and Hunter, 1979; Hirsch et al., 1997; De Giorgi et al., 2002; Borutaite et al., 2003). It is worth noticing that interfibrillar mitochondria are more prone to release proapoptotic factors upon ROS stimulation, potentially due to higher probability of mPTP opening than subsarcolemmal mitochondria (Adhihetty et al., 2005). The detailed mechanisms will be discussed later in this review.

Although long-term $[Ca^{2+}]_{mito}$ elevation is closely associated with excessive ROS production (Adam-Vizi and Starkov, 2010; Peng and Jou, 2010), we observed an interesting phenomenon that mitochondrial Ca^{2+} transients induced by the electrical stimulation can decrease ROS production in denervated skeletal muscle fibers within a minute (Karam et al., 2017). This phenomenon is different from the excitation–transcription coupling events that help skeletal muscle cope with ROS during exercise or electrical stimulation, which usually occur in the time frame of hours or longer (Tsuboyama-Kasaoka et al., 1998; Cortright et al., 1999; Pilegaard et al., 2003; Egan et al., 2010). Although the underlying molecular mechanism of the instant ROS suppression by the rapid mitochondrial Ca^{2+} influx remains elusive, through this review we hope to inspire more thoughts and discussion about how Ca^{2+} temporal profile differentially influences mitochondrial ROS production and cell death.

Abbreviations: AAV, adeno-associated virus; AIF, apoptosis-inducing factor; ALS, amyotrophic lateral sclerosis; AMPK, AMP-activated protein kinase; ANT, adenine nucleotide translocator; CaMK, Ca^{2+}/calmodulin-dependent protein kinase; CDK, cyclin-dependent kinase; CsA, Cyclosporin A; CypD, cyclophilin D; Diablo, direct IAP (inhibitor-of apoptosis) binding protein with low pI; EC-coupling, excitation contraction-coupling; EDL, extensor digitorum longus; EMRE, essential MCU regulator; EndoG, endonuclease G; ERK, extracellular signal-regulated kinase; FAK, focal adhesion kinase; FDB, flexor digitorum brevis; GPDH, glycerol phosphate dehydrogenase; HtraA2, high temperature requirement protein A2; ICDH, isocitrate dehydrogenase; ILK, integrin-linked kinase; IMM, inner mitochondrial membrane; JNK, c-Jun N-terminal kinase; MAPK, mitogen-activated protein kinase; mCa2, mitochondrial calcium channel type 2; MCU, mitochondrial Ca^{2+} uniporter; MICU, mitochondrial Ca^{2+} uptake; mPTP, mitochondrial permeability transition pore; mTOR, mammalian target of rapamycin; NCLX, $Na^{+}/Ca^{2+}/Li^{+}$ exchanger; OMM, outer mitochondrial membrane; OSCP, oligomycin sensitivity-conferring protein; OXPHOS, oxidative phosphorylation; PKA, protein kinase A; PKC, protein kinase C; PDH, pyruvate dehydrogenase; RaM, rapid mode of mitochondrial Ca^{2+} uptake; PiC, phosphate carrier; RaM, rapid mode of mitochondrial Ca^{2+} uptake; ROS, reactive oxygen species; RYR, ryanodine receptor; SIRT, sirtuin; Smac, second mitochondria-derived activator of caspase; SR, sarcoplasmic reticulum.

Crucial Regulators of Ca^{2+} Homeostasis in Mitochondria

This review does not intend to comprehensively cover all players involved in mitochondrial Ca^{2+} handling. However, a brief introduction is needed for meaningful discussions about the connections between $[Ca^{2+}]_{mito}$, ROS, apoptosis, and muscle atrophy (**Figure 1**).

Mitochondria are constantly involved in modulating spatiotemporal profiles of cytosolic Ca^{2+} ($[Ca^{2+}]_{cyto}$) in different types of cells under physiological and pathological conditions (Gunter et al., 2004; Szabadkai and Duchen, 2008; Demaurex and Guido, 2017), including cardiac and skeletal muscle (Zhou et al., 1998;Maack et al., 2006; Rizzuto and Pozzan, 2006; Sedova et al., 2006; Csordás and Hajnóczky, 2009; Yi et al., 2011). This is due to their abilities to uptake and extrude Ca^{2+}, as well as retain Ca^{2+} in their matrix

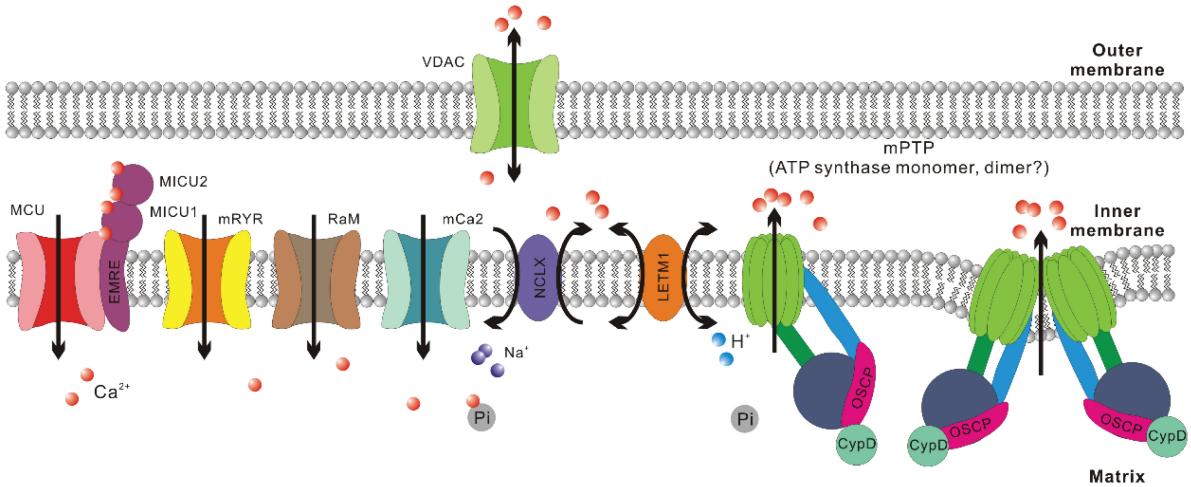

FIGURE 1 | Crucial regulators of Ca^{2+} homeostasis in mitochondria. For mitochondrial Ca^{2+} uptake, the major routes include mitochondrial Ca^{2+} uniporter (MCU), mitochondrial ryanodine receptor (mRYR), rapid mode of mitochondrial Ca^{2+} uptake (RaM), and mitochondrial calcium channel type 2 (mCa2). The most crucial regulatory subunits of MCU include mitochondrial calcium uptake 1, 2 (MICU1, MICU2) and essential MCU regulator (EMRE). For mitochondrial Ca^{2+} extrusion, the major routes include $Na^+/Ca^{2+}/Li^+$ exchanger (NCLX), mitochondrial H^+/Ca^{2+} exchanger (LETM1), and mitochondrial permeability transition pore (mPTP). Voltage-dependent anion channel (VDAC) is suggested to be the outer mitochondrial membrane (OMM) component of mPTP. Recently, ATP synthase has been confirmed to be the inner mitochondrial membrane (IMM) component of mPTP. There are still debates about whether mPTP is formed by ATP synthase dimer or monomer. Cyclophilin (Cyp) D is a crucial regulator of mPTP opening and interacts with ATP synthase through the oligomycin sensitivity-conferring protein (OSCP) subunit. As to Ca^{2+} retention in mitochondrial matrix, inorganic phosphate (Pi) helps sequester free Ca^{2+} in solid precipitates, which could serve as an MCU independent source of mitochondrial Ca^{2+} upon matrix acidification.

(Szabadkai and Duchen, 2008). Indeed, mitochondrial Ca^{2+} uptake has been first observed *in vivo* during skeletal muscle contraction induced by motor nerve stimulation (Rudolf et al., 2004) and later quantified in isolated individual muscle fibers during E-C coupling (Yi et al., 2011; Karam et al., 2017). The Ca^{2+} uptake routes in mitochondria include mitochondrial Ca^{2+} uniporter (MCU), mitochondrial ryanodine receptor (mRYR), as well as two other channels with unknown molecular nature: rapid mode of mitochondrial Ca^{2+} uptake (RaM) and mitochondrial calcium channel type 2 (mCa2) (Buntinas et al., 2001; Kirichok et al., 2004; Altschafl et al., 2007; Michels et al., 2009; Hoppe, 2010). In skeletal muscle, the presence of uptake routes other than MCU still waits to be confirmed. Overexpression of MCU in adult mouse flexor digitorum brevis (FDB) muscle led to notable enhancement in caffeine-induced mitochondrial Ca^{2+} influx as well as a moderate elevation of the resting $[Ca^{2+}]_{mito}$ level (Mammucari et al., 2015). In contrast, transfection of FDB muscle with short hairpin (sh) RNA against MCU resulted in marked reduction of both resting $[Ca^{2+}]_{mito}$ level and caffeine-induced mitochondrial Ca^{2+} influx (Mammucari et al., 2015). Furthermore, extensor digitorum longus (EDL) muscle infected by adeno-associated virus (AAV) carrying shRNA against MCU exhibited decreased pyruvate dehydrogenase (PDH) activity (Mammucari et al., 2015), which is known to be dependent on $[Ca^{2+}]_{mito}$ level (Wan et al., 1989; Denton, 2009). Consistently, in skeletal muscles from $MCU^{-/-}$ mice, resting $[Ca^{2+}]_{mito}$ level seems reduced when compared to wild-type controls, while the phosphorylation of PDH, which is negatively correlated with the activity of Ca^{2+} sensitive phosphatase PDP1, significantly increased (Pan et al., 2013).

The activity of MCU is regulated by MICU1-MICU2 heterodimer, which senses $[Ca^{2+}]_{cyto}$ level (Mallilankaraman et al., 2012; Csordás et al., 2013; Kamer and Mootha, 2014; Patron et al., 2014; Wang et al., 2014). MICU1 is suggested to function as the cooperative activator of MCU, while MICU2 is believed to keep MCU closed at low $[Ca^{2+}]_{cyto}$ level (Patron et al., 2014). Skeletal muscle expresses a unique alternative splice isoform of MICU1, which is more sensitive to Ca^{2+} than the isoform expressed in other tissues and hence allows activation of MCU at a lower $[Ca^{2+}]_{cyto}$ level (Reane et al., 2016). This is likely an evolutionary adaption to the astounding amount of ATP consumed during muscle contraction since the activities of multiple enzymes involved in ATP synthesis are stimulated by Ca^{2+} (Wan et al., 1989; Das and Harris, 1990; Murphy et al., 1990; Denton, 2009; Glancy et al., 2013). Indeed, $[Ca^{2+}]_{mito}$ transients in skeletal muscle are larger than those measured in other tissues based on mitoplast patch clamp results (Fieni et al., 2012). Other MCU regulatory subunits include EMRE and MCUb. EMRE helps tether MICU1 and MICU2 to the transmembrane region of MCU, while MCUb is a paralog of MCU that is suggested to negatively regulate MCU complex in a direct manner (Raffaello et al., 2013; Tsai et al., 2016).

The Ca^{2+} extrusion routes include $Na^+/Ca^{2+}/Li^+$ exchanger (NCLX), mPTP and arguably mitochondrial H^+/Ca^{2+} exchanger (LETM1) (Jiang et al., 2009; Hoppe, 2010; Palty et al., 2010; Nowikovsky et al., 2012). NCLX is more intensively expressed in skeletal muscle compared to many other tissues such as cardiac muscle (Palty et al., 2004, 2010). This is accompanied by an ultrafast Ca^{2+} efflux rate of skeletal muscle mitochondria, which is 2-3 orders faster than cardiac muscle (Rudolf et al., 2004;

Palty et al., 2010). mPTP is a nonselective, large conductance megachannel mediating solute (<1.5 kDa) exchange between mitochondrial matrix and the outside milieu (Haworth and Hunter, 1979; Hunter and Haworth, 1979a,b; Kinnally et al., 1992; Szabó and Zoratti, 1992). The opening of mPTP is sensitive to Ca^{2+}, cyclophilin (Cyp) D, oxidizing agents, thiol reagents, depletion of ADP, while its inhibitors include Mg^{2+}, ADP, NADH, antioxidants, and cyclosporin (Cs) A (through interacting with CypD) (Haworth and Hunter, 1979; Hunter and Haworth, 1979a,b; Kinnally et al., 1992; Szabó and Zoratti, 1992). mPTP opening is widely known for its central role in cell death induction under multiple pathological conditions (Bonora et al., 2020). Osmotic influx of water into mitochondrial matrix through these pores results in swollen matrix, dissipated IMM potential and ceased ATP production. ATP dependent ion exchangers/pumps fail to maintain cellular ion homeostasis and finally lead to necrosis (Bonora et al., 2015). Additionally, mPTP opening has also been implied to facilitate the release of intermembrane space factors activating apoptotic pathway (Hirsch et al., 1997; De Giorgi et al., 2002; Borutaite et al., 2003). While the irreversible, high conductance mPTP opening upon $[Ca^{2+}]_{mito}$ overload is detrimental (Ichas et al., 1997; Hoppe, 2010; Karch and Molkentin, 2018), the transient and low conductance mPTP opening is considered a Ca^{2+} extrusion route that may carry out physiological functions (Ichas and Mazat, 1998; Elrod et al., 2010; Elrod and Molkentin, 2013).

The molecular composition of mPTP has remained elusive for over 60 years (Urbani et al., 2019). Previously mPTP was suggested to form from adenine nucleotide translocator (ANT) or phosphate carrier (PiC) on IMM, as well as voltage-dependent anion channel (VDAC) on OMM (Halestrap and Davidson, 1990; Szabó et al., 1993; Baines, 2009; Halestrap, 2009). However, further researches indicate that they are not the pore forming unit of mPTP, but could be regulatory components (Kokoszka et al., 2004; Krauskopf et al., 2006; Baines et al., 2007). In recent decades, CypD was reported to physically interact with oligomycin sensitivity-conferring protein (OSCP) within ATP synthase (complex V of OXPHOS) (Giorgio et al., 2009) and ATP synthase increases the permeability of IMM to different solutes upon $[Ca^{2+}]_{mito}$ overload (Giorgio et al., 2013, 2017; Alavian et al., 2014). However, the argument about whether it is the monomer or dimer of ATP synthase that carries out the megachannel function has not been settled yet (Mnatsakanyan et al., 2019).

The Ca^{2+} retention capacity of mitochondrial matrix is believed to heavily rely on the inorganic phosphate (Pi) entered mainly through mitochondrial phosphate carrier (PiC) (Szabadkai and Duchen, 2008; Seifert et al., 2015). Pi can buffer Ca^{2+} through the formation of osmotically neutral precipitates such as hydroxyapatite and whitlockite (Carafoli, 2010; Chinopoulos and Adam-Vizi, 2010), which theoretically should enable additional Ca^{2+} uptake through MCU, suppress Ca^{2+} efflux through NCLX and desensitize mPTP (Zoccarato and Nicholls, 1982; Szabadkai and Duchen, 2008; Seifert et al., 2015). However, these assumptions were challenged as opposite results were observed in PiC knockdown cells and PiC knockout mice (Varanyuwatana and Halestrap, 2012; Kwong et al., 2014). Meanwhile Pi is a long known sensitizer of mPTP (Zoratti and Szabò, 1995). Thus the precise role of the PiC in $[Ca^{2+}]_{mito}$ regulation still waits to be addressed. In addition, Ca–Pi precipitates can dissolve upon acidification and IMM potential disruption, enabling MCU-independent elevation of $[Ca^{2+}]_{mito}$ (Greenawalt et al., 1964; Wolf et al., 2017; Hernansanz-Agustín et al., 2020). For example, in cells experiencing acute hypoxia, complex I of OXPHOS in mitochondria undergoes conformational changes that lead to proton accumulation inside the matrix, dissolution of Ca–Pi precipitates, elevation of $[Ca^{2+}]_{mito}$ and activation of NCLX (Hernansanz-Agustín et al., 2020).

Associations Between Steady-State Elevation of Mitochondrial Ca^{2+} Level and ROS Production

Elevation of $[Ca^{2+}]_{mito}$ level could result in enhanced ROS production through multiple mechanisms (**Figure 2**):

1. Elevation of $[Ca^{2+}]_{mito}$ stimulates Ca^{2+} sensitive dehydrogenases, including glycerol phosphate dehydrogenase (GPDH), PDH, isocitrate dehydrogenase (ICDH), and α-ketoglutarate dehydrogenase (α-KGDH) (Wan et al., 1989; Denton, 2009). There is also evidence that Ca^{2+} increases activities of complexes I, III, IV, and V of OXPHOS (Das and Harris, 1990; Glancy et al., 2013). The faster O_2 consumption rate results in increased ROS production under certain circumstances, although the opposite situation also exists (Barja, 2007; Neretti et al., 2009; Silva et al., 2009).

2. Elevation of $[Ca^{2+}]_{mito}$ stimulates mitochondrial nitric oxide synthase (NOS) to produce more nitric oxide (NO). NO can compete with O_2 for binding sites on cytochrome c oxidase (complex IV of OXPHOS), which hinders the electron flow and decreases mitochondrial O_2 consumption (Giulivi, 2003; Ghafourifar and Cadenas, 2005). The hindrance of the electron flow and the increase of local O_2 may boost ROS production (Brookes et al., 2004). On the other hand, NO reacts readily with superoxide and generates peroxynitrite ($ONOO^-$), which is a more potent ROS that causes Cyto c release, lipid peroxidation and oxidative damage to other vulnerable targets (Ghafourifar and Cadenas, 2005).

3. Elevated $[Ca^{2+}]_{mito}$ promotes the opening of mPTP. mPTP opening can lead to changes of ionic strength and hence disrupt the electrostatic interaction between Cyto c and cardiolipin in mitochondrial intermembrane space. Cyto c is required for the activity of ubiquinol-cytochrome c oxidoreductase (complex III of OXPHOS) (Ott et al., 2002). The blockage of complex III activity enhances ROS production by increasing the accumulation of the one-electron donor ubisemiquinone (Turrens et al., 1985; Muller et al., 2002, 2003). mPTP opening also seems to induce conformation changes in NADH-ubiquinone oxidoreductase (complex I of OXPHOS), resulting in increased ROS production (Batandier et al., 2004).

4. $[Ca^{2+}]_{mito}$ overload may stimulate Cyto c release from cardiolipin through competing for cardiolipin binding sites (Grijalba et al., 1999), which affects complex III activity and hence promotes ROS generation.

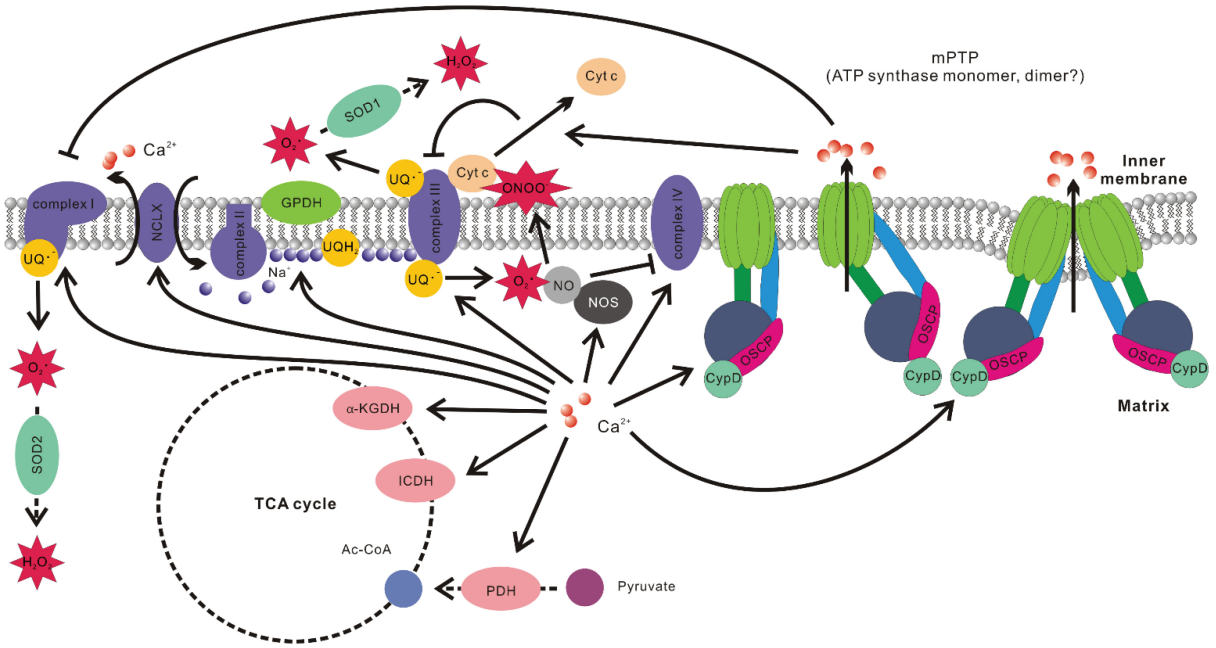

FIGURE 2 | Associations between mitochondrial Ca^{2+} level and ROS production. Ca^{2+} promotes the activities of multiple Ca^{2+} sensitive dehydrogenase such as glycerol phosphate dehydrogenase (GPDH), pyruvate dehydrogenase (PDH), isocitrate dehydrogenase (ICDH), and α-ketoglutarate dehydrogenase (α-KGDH). It also elevates the efficiency of complexes I, III, IV, and V of OXPHOS. Ca^{2+}-induced activation of NCLX results in Na^+ influx into the matrix and Na^+ interacts with phospholipid in the inner leaflet of IMM, decreases its fluidity, and slows down ubiquinol (UQH_2) diffusion. This results in uncoupling of Q cycle and increased ROS production at Q_o site in complex III. Ca^{2+} stimulation of nitric oxide synthase (NOS) increases nitric oxide (NO) production, which inhibits complex IV by competing with O_2. NO also readily react with superoxide to form peroxynitrite ($ONOO^-$), which promotes cytochrome c (Cyt c) release. Cyt c release would disrupt the activity of complex III, increase the level of ubisemiquinone (UQ^-), which provide one electron to O_2 to form superoxide. Ca^{2+} is also the major stimulant of mPTP opening. The subsequent change of ion strength in mitochondrial intermembrane space disrupts electrostatic interactions between Cyt c and membrane lipid cardiolipin, leading to Cyt c release and hindrance of complex III activity. mPTP opening has also been implicated in inducing conformation changes of complex I, resulting in elevated ROS production.

5. During acute hypoxia, elevation of $[Ca^{2+}]_{mito}$ due to matrix acidification activates NCLX, promoting the import of Na^+. Matrix Na^+ interacts with phospholipids in the IMM (such as phosphatidylcholine), reducing membrane fluidity, slowing down the diffusion of ubiquinol from glyceraldehyde 3-phosphate dehydrogenase (GAPDH) or complex II to complex III of OXPHOS, resulting in elevated ROS production of complex III at Q_o site (Hernansanz-Agustín et al., 2020).

Transient Mitochondrial Ca^{2+} Influx Diminishes Denervation-Induced ROS Production and mPTP Opening in Skeletal Muscle

The cytosolic Ca^{2+} transients are spatiotemporally well-controlled Ca^{2+} release events from the sarcoplasmic reticulum (SR) responding to the motor nerve activation in a skeletal muscle fiber during excitation contraction (EC)-coupling. Skeletal muscle inactivity including neuromuscular diseases, spinal cord injury, and muscle unloading, etc., could partially or completely disrupt EC-coupling and eliminate cytosolic Ca^{2+} transients. A pathological hallmark of prolonged muscle inactivity is the enhanced ROS production in muscle fibers (Muller et al., 2007; Powers et al., 2012; Xiao et al., 2018). It is very well established that mitochondria are a major source of ROS production in prolonged muscle inactivity (Powers et al., 2012). Prolonged muscle unloading leads to an elevated resting $[Ca^{2+}]_{cyto}$ (Tischler et al., 1990; Ingalls et al., 1999), which in turn could overload mitochondria, increase the propensity of mPTP opening and stimulate ROS production (Csukly et al., 2006). However, the initial cause of mitochondrial ROS production in inactivated skeletal muscle remains elusive (Hyatt et al., 2019). One question is whether the cessation of physiological Ca^{2+} transients is an initiating factor for promoting mitochondria ROS production.

Transgenic mouse model expressing a mitochondria-targeted biosensor (mt-cpYFP) allowed a real-time measurement of a ROS-related mitochondrial signal, termed "mitoflash" (Wang et al., 2008; Ding et al., 2015). Although mitoflash activities could be composed of multifaceted signals including matrix alkalization, superoxide, and arguably some other oxidants (Wang et al., 2008, 2016; Schwarzländer et al., 2012; Wei-LaPierre et al., 2013), the mechanism underlying mitoflash events is believed to be linked to transitory opening of mPTP due to the high spatiotemporal correlations between mitoflash events and IMM depolarization (Wang et al., 2008, 2016). Besides transitory opening of mPTP, there are also other potential causes of IMM depolarization during mitoflash events, such as the activation of uncoupling proteins UCP2 and UCP3. However, inhibition

of UCP2 by chemical blocker or RNA interference slightly increased, rather than decreased the mitoflash incidence (Wang et al., 2017). Skeletal muscle fibers derived from UCP3 knockout mice exhibited no changes in mitoflash frequency, amplitude or duration compared to wild type controls, while the average area of mitoflash events mildly reduced (McBride et al., 2019). Thus, these functional perturbation experiments do not support the hypothesis of UCP2/3 mediated uncoupling activities as the major contributor of mitoflash signals.

Using this transgenic mouse model, Karam et al detected a fourfold increase of mitoflash activity in skeletal muscle following a short period (24 h) of sciatic nerve transection (Karam et al., 2017). This denervation-induced mitoflash activity could be attenuated by the application of CsA, an established inhibitor of mPTP opening (Giorgio et al., 2018), further suggesting that mitoflash events reflect real-time opening of mPTP in denervated muscle fibers. Consistently, the increased mitoflash activity is associated with an elevated mitochondrial superoxide level reported with MitoSOX Red (Mukhopadhyay et al., 2007) in muscle fibers 24 h after the denervation. Similar results were also reported for muscle fibers derived from the ALS mouse model ($SOD1^{G93A}$) at a stage before disease symptom onset (Xiao et al., 2018), when motor neuron axon terminal withdrawal (denervation) start to occur in individual muscle fibers (Frey et al., 2000; Fischer et al., 2004).

Due to lack of neuronal impulses, the action potential and physiological $[Ca^{2+}]_{cyto}$ transients are abolished in denervated skeletal muscle. Thus, a hypothesis was proposed that dynamic Ca^{2+} transients were required to keep mPTP at its closed state and maintain mitochondrial ROS production at the physiological level in skeletal muscle (Karam et al., 2017). Remarkably, when muscle fibers from denervated (24 h) mouse model were exposed to a brief electrical stimulation (40 Hz, 0.5 ms pulses at 8–12 V for a total duration of 350 ms) to restore physiological cytosolic and mitochondrial Ca^{2+} transients, the area and amplitude of mitoflash events dramatically reduced within a minute to a level comparable to the unstimulated sham muscle fibers (Karam et al., 2017). Importantly, after treating the denervated muscle fibers with Ru360 to block MCU for mitochondrial Ca^{2+} uptake, electrical stimulation no longer had significant impact on mitoflash activities. Additionally, the levels of mitochondrial superoxide (indicated by MitoSOX Red) also exhibited the same trend of changes under these conditions (Karam et al., 2017). Thus, mitochondrial Ca^{2+} influxes triggered by physiological cytosolic Ca^{2+} transients, even brief ones, seems to be capable of inhibiting transitory mPTP opening and ROS generation in mitochondria.

The above results are in line with previous discoveries that electrical stimulations help prevent apoptosis, retard muscle atrophy and improve muscle strength in denervated animal models (Mokrusch et al., 1990; Arakawa et al., 2010; Nakagawa et al., 2017) and patients with motor impairment caused by spinal cord injury or stroke (Dudley et al., 1999; Crameri et al., 2000, 2002; Doucet et al., 2012; Nascimento et al., 2014). However, the studies of the mechanisms underlying these phenomena usually focus on relatively long-term molecular changes, such as gene expression regulation, which usually takes tens of minutes to hours to occur (Voytik et al., 1993; Kostrominova et al., 2005; Arakawa et al., 2010; Peviani et al., 2010; Russo et al., 2010). The events occurred within a minute after electrical stimulation were rarely investigated.

One potential mechanism underlying the role of physiological Ca^{2+} transients in inhibition of mitochondrial ROS production could be that mitochondrial Ca^{2+} influxes induced by cytosolic Ca^{2+} transients suddenly boost the electron flow rate along the respiratory chain, decreasing the reduced state of ROS generators, such as ubisemiquinone generated by complex III of OXPHOS. Meanwhile, the sudden boost of respiratory chain activity also increases O_2 consumption rate, decreasing the amount of local O_2 available for forming superoxide. These two factors may both contribute to a quick attenuation of superoxide formation. Similar situation also occurs during sudden transition of state 4 respiration to state 3 respiration in isolated mitochondria (Barja, 2007).

Additionally, as illustrated in **Figure 3**, we propose a second hypothetical mechanism that key mPTP components have two sets of Ca^{2+} responding structures with different affinities that trigger opposite changes in the propensity of mPTP opening based on the temporal profile of mitochondrial Ca^{2+} influxes in skeletal muscle fibers. Under this scenario, a steady-state increase of $[Ca^{2+}]_{mito}$ (a likely outcome of steady-state $[Ca^{2+}]_{cyto}$ elevation after denervation or neuronal degenerative disease) promotes mPTP opening through a relatively higher affinity Ca^{2+} responding structure. The second Ca^{2+} responding structure with relatively lower Ca^{2+} binding affinity may respond to the spike of mitochondrial Ca^{2+} influx following the cytosolic Ca^{2+} transient during EC-coupling activated by neuronal input or electrical field stimulation and quickly shut down the opening of mPTP in skeletal muscle. More than a coincidence, previous studies identified two binding sites for divalent cations (including Ca^{2+}) on the F1 catalytic domain of ATP synthase. One located in the nucleotide binding pocket within the αβ cleft, the other located in the superficial loop of the β subunit and contains the acidic sequence DELSEED (Hubbard and McHugh, 1996; Giorgio et al., 2017, 2018). The first one is implicated as the "trigger site" of mPTP opening. More specifically, the occupancy of this site by Ca^{2+} (instead of Mg^{2+}) is proposed to elevate the rigidity of F1 domain and transmit mechanical energy to OSCP, the peripheral stalk and finally to the IMM, leading to the formation of mPTP by ATP synthase dimers (Giorgio et al., 2017, 2018). Interestingly, the physiological role of the other Ca^{2+} binding site remains unknown. Due to the low affinity nature of this Ca^{2+} binding site, it may serve as the potential link between mitochondrial Ca^{2+} transients and quick mPTP shut down. It is also possible that the second Ca^{2+} responding structure locates on molecules other than ATP synthase, which acts as an accessory safe guard against mPTP opening upon Ca^{2+} binding during rapid mitochondrial Ca^{2+} influx. Further structural and functional studies are needed to validate those hypotheses. Nevertheless, the results reported in Karam et al. suggest that the physiological

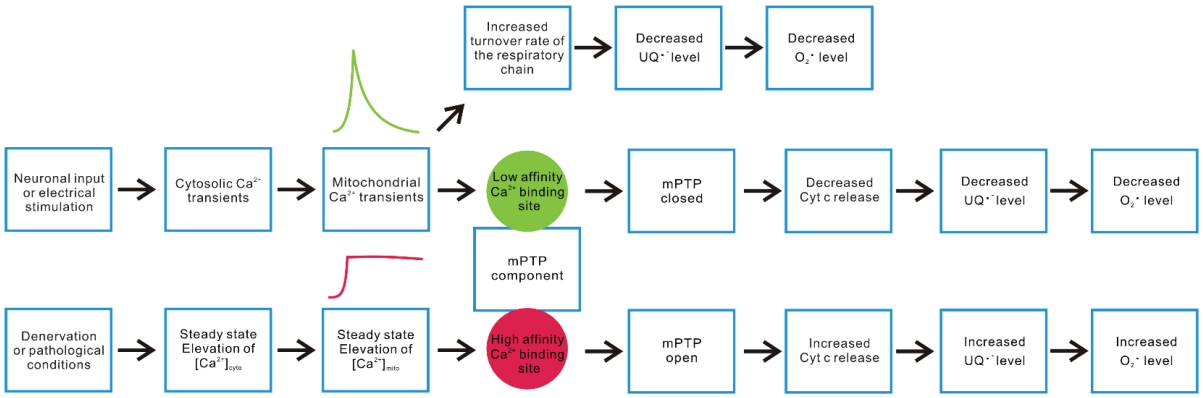

FIGURE 3 | Hypothetical mechanisms underlying differential mitochondrial Ca^{2+} dynamics and ROS production. Neuronal or electrical stimulation-induced cytosolic Ca^{2+} transient can result in rapid Ca^{2+} influx into mitochondria, serving as a stimulant of multiple enzyme complex in OXPHOS that accelerate electron flux along the respiratory chain, leading to decreased accumulation of ubisemiquinone (UQ) and lower O_2 partial pressure. Both factors contribute to alleviated superoxide production. On the other hand, we hypothesize that a key mPTP component may have two sets of Ca^{2+} sensory structures with different Ca^{2+} affinities, resulting in distinct responses to rapid versus steady-state elevation of $[Ca^{2+}]_{mito}$. Steady-state elevation of $[Ca^{2+}]_{mito}$ resulting from denervation or other pathological conditions may predominantly trigger the response mediated by a relatively higher affinity structure (such as the Ca^{2+} binding site within the F1 domain nucleotide binding pockets of ATP synthase), which promotes mPTP opening, enhances Cyt c release, disrupts complex III activity, and increases superoxide production. The rapid mitochondrial Ca^{2+} transients induced by motor neuron input or electrical stimulation may predominantly activate the response mediated by a relatively lower affinity Ca^{2+} responding structure, shutting down mPTP and decrease ROS production.

cytosolic and mitochondrial Ca^{2+} transients induced during EC-coupling are vital to keep mPTP in a closed status in skeletal muscle fibers.

Exercise-Induced Signaling Involved in Mitochondrial ROS Regulation

During exercise, muscle contraction dramatically increases ATP turnover rate, which could be more than 100-fold that of the basal rate (Hochachka and McClelland, 1997). To cope with such large demand of ATP, Ca^{2+} influx into mitochondrial matrix activates multiple enzymes related to TCA cycle and oxidative phosphorylation, elevating the synthesis of ATP in skeletal muscle (Wan et al., 1989; Das and Harris, 1990; Denton, 2009). The high O_2 consumption rate and elevated $[Ca^{2+}]_{mito}$ level do not necessarily increase ROS production (Barja, 2007; Silva et al., 2009), which could be at least partially attributable to the exercise-induced signaling pathways, such as AMP-activated protein kinase (AMPK), protein kinase A (PKA), Ca^{2+}/calmodulin-dependent protein kinase (CaMK), mitogen-activated protein kinase (MAPK), protein kinase C (PKC), focal adhesion kinase (FAK), and mammalian target of rapamycin (mTOR), cyclin-dependent kinase (CDK), integrin-linked kinase (ILK), and sirtuin (SIRT) family of protein deacetylases (Sakamoto and Goodyear, 2002; Egan and Zierath, 2013; Hoffman et al., 2015). Although some of these pathways are preferentially induced by acute exercise while the others mediate physiological adaptation to long-term endurance exercise, both of them involve transcriptional regulation and hence belong to excitation-transcription coupling framework (Egan and Zierath, 2013). It is beyond the scope of this review to systematically go through these pathways. But we would like to highlight some of them directly or indirectly involved in ROS regulation (**Figure 4A**).

The three best-characterized MAPK subfamilies are c-Jun N-terminal kinase (JNK), extracellular signal-regulated kinase (ERK), and p38 MAPK (Chen et al., 2001). All three subfamilies have been shown to be activated by oxidative stress (Torres and Forman, 2003; Li et al., 2005). Among them, p38 MAPK signaling has been reported to participate in contraction-induced PGC-1α gene expression in skeletal muscle (Akimoto et al., 2004). PGC-1α is a "master regulator" of mitochondrial biogenesis and promotes the expression of OXPHOS enzymes and uncoupling proteins (UCP2 and UCP3) (Wu et al., 1999; Zhou et al., 2000). Uncoupling proteins function to mildly depolarize IMM by increasing proton backflow into the matrix in a fatty acid (FA)-dependent manner (Brand and Esteves, 2005). This process could be described by an FA futile cycling model, in which UCP exports FA^- anions into intermembrane space. The anion diffuses away and gets protonated. Then, the protonated FA flip-flops across the membrane to deliver protons electro-neutrally back to the matrix (Jabůrek et al., 1999). UCP2 and UCP3 are not involved in thermogenesis adapting to cold temperature as UCP1 (Brand and Esteves, 2005). Instead, they are believed to serve as a cellular defense mechanism against superoxide formation, which works through accelerating the rates of proton pumping and electron flux along the respiratory chain, decreasing the level of one-electron donors (to O_2) generated by complex I and III of OXPHOS (Brand, 2000; Zhou et al., 2000; Echtay et al., 2002; Brand and Esteves, 2005; Ježek et al., 2018). The expression of UCP3 is particularly high in skeletal muscle (Boss et al., 1997; Matsuda et al., 1997; Vidal-Puig et al., 1997; Liu et al., 1998) and is further induced by exercise or fasting (Gong et al., 1997; Tsuboyama-Kasaoka et al., 1998; Cortright et al., 1999). In contrast, denervation of skeletal muscle decreases the expression of UCP3 (Tsuboyama-Kasaoka et al., 1998).

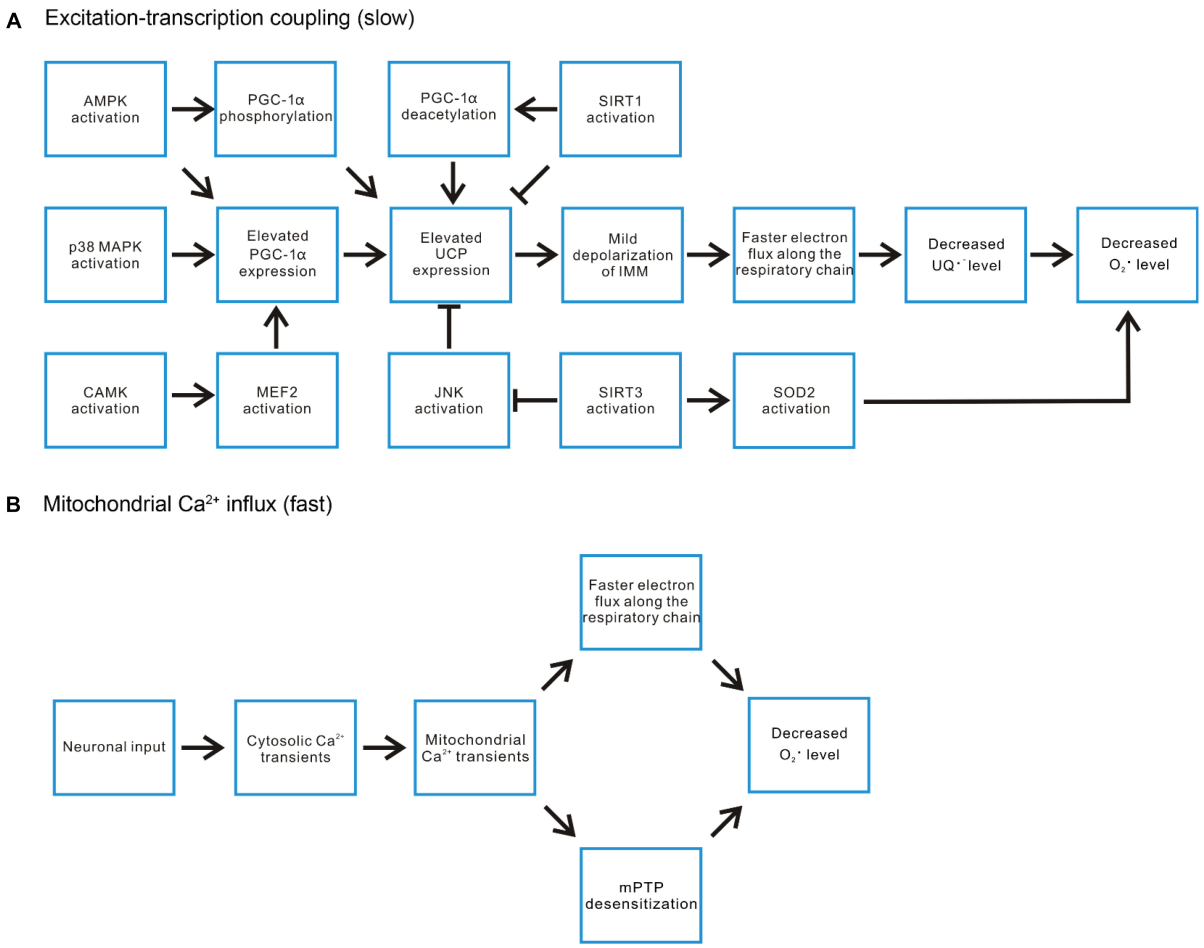

FIGURE 4 | Exercise-induced signaling pathways regulate mitochondrial ROS level. **(A)** In the aspect of the excitation-transcription events, the ATP deficit during exercise induces AMPK activation, which can both directly phosphorylate and increase the expression of PGC-1α, the pivotal player in countering ROS-related damages. P38 MAPK and certain CAMKs have also been demonstrated to be activated by exercise and induce PGC-1α expression. SIRT1 activation promotes deacetylation of PGC-1α, enhancing its transcriptional activities. On the other hand, SIRT1 represses the expression of uncoupling protein (UCP2, UCP3). UCP induced mild depolarization of IMM accelerates electron flux along the respiratory chain, decreases the level of ubisemiquinone (UQ) and hence reduces superoxide production. Thus, the impact of SIRT1 activation on ROS level is mixed. In contrast, another SIRT family member SIRT3 promotes UCP expression by inhibiting JNK activation. It also promotes superoxide removal through deacetylating SOD2. **(B)** The rapid mitochondrial Ca^{2+} flux induced by motor neuron input may decrease ROS production through increasing the turnover rate of the respiratory chain or suppressing mPTP opening.

AMPK can also be activated by ROS indirectly through ATP deficit, more specifically the increase of AMP/ATP and creatine/phosphocreatine ratios (Kahn et al., 2005; Irrcher et al., 2009). Acute exercise, due to the increased turnover of ATP, promotes AMPK activation in an intensity dependent manner (Wojtaszewski et al., 2000; Egan et al., 2010). AMPK activation has been report to mediate direct phosphorylation of PGC-1α and transcriptional upregulation of PGC-1α expression (Jäger et al., 2007; Irrcher et al., 2008). Meanwhile acute exercise induced UCP3 expression has also been demonstrated to involve AMPK (Zhou et al., 2000).

CaMKs are implicated in muscle fiber type switch adapting to long-term endurance exercise (Wu et al., 2000). Additionally, they have also been suggested to regulate mitochondrial biogenesis independent of fiber type transformation (Wu et al., 2002). Transgenic mice expressing constitutively active CaMKIV in skeletal muscle exhibited improved resistance to fatigue during repetitive contraction, augmented mitochondrial biogenesis, increased expression of OXPHOS genes (such as subunits of complex I) and PGC-1α (Wu et al., 2002). PGC-1α is a target gene of myocyte-specific enhancer factor 2 (MEF2), one of the transcription factors activated by CaMKIV (Passier et al., 2000). Furthermore, CaMKII has also been suggested to induce PGC-1α expression due to the activation of MEF2 (Liu et al., 2005; Egan and Zierath, 2013).

SIRTs are a family of protein deacetylases sensitive to elevated $[NAD^+]$ or NAD^+/NADH ratio (Egan and Zierath, 2013). Their activities are closely linked with cellular metabolic status (Schwer and Verdin, 2008). SIRT1 mediated deacetylation is suggested to activate PGC-1α transcriptional activity on other genes (Gerhart-Hines et al., 2007; Gurd, 2011). However, SIRT1 also serves a potent repressor of UCP2 and UCP3 gene

expression (Amat et al., 2007, 2009; Schwer and Verdin, 2008). Thus, SIRT1 exerts both positive and negative impact on ROS production. SIRT3 is a major deacetylase for mitochondrial proteins (Jing et al., 2011). In SIRT3 knockout mice, O_2 consumption rate decreases while oxidative stress increases, accompanied by enhanced activation of JNK pathway (Jing et al., 2011). Consistently, knocking down SIRT3 in cultured myoblast also led to defective mitochondrial respiration capacity, increased ROS production and JNK pathway activation (Jing et al., 2011). Furthermore, SIRT3 has been shown to deacetylate SOD2, leading to increase in the SOD2 enzymatic activity to convert superoxide into hydrogen peroxide (Tao et al., 2014). Thus, the SIRT3 activity overall helps mitigate ROS accumulation (Tao et al., 2010, 2014).

It is also worth noticing that PGC-1α has an isoform termed PGC-1α4 resulted from alternative promoter usage and splicing (Ruas et al., 2012). This isoform is preferentially induced in mouse and human muscle during resistance exercise training (Ruas et al., 2012). Different from PGC-1α, it does not regulate OXPHOS genes but specifically induces IGF1 and represses myostatin, resulting in muscle hypertrophy (Ruas et al., 2012). Studies have indicated that the induction of PGC-1α4 requires MCU mediated Ca^{2+} uptake (Mammucari et al., 2015).

Although most studies concerning the beneficiary effect of exercise on ROS control focus on the excitation-transcription coupling framework, there is evidence directly linking acute exercise with improved mitochondrial functions such as decreased susceptibility to mPTP opening and increased O_2 respiration rate in cardiac and skeletal muscle (Ascensão et al., 2011; Yoo et al., 2019a,b). These reports are consistent with the mechanisms we proposed underlying the instant decrease of mitochondrial ROS production in denervated skeletal muscle upon electrical stimulation. These two mechanisms may also explain why mitochondria were not the major contributor of ROS during electrical stimulation induced muscle contractions (Sakellariou et al., 2013). Thus, we propose that beside the excitation-transcription coupling framework, the rapid mitochondrial Ca^{2+} transients generated during exercise serve as a parallel mechanism contributing to prevent excessive ROS production, either through accelerating the turnover rate of the respiratory chain or suppressing mPTP opening (**Figure 4B**). The rapid mitochondrial Ca^{2+} influxes could also be one reason why there is no significant mitochondrial contribution to cytosolic ROS level in contractile skeletal muscle fibers.

SUMMARY AND FUTURE PERSPECTIVES

The elevations of $[Ca^{2+}]_{mito}$ induced by muscle contraction or muscle inactivity share many Ca^{2+} regulators in common, yet the outcomes are dramatically different in skeletal muscle ROS production. Additionally, electrical stimulation not only rapidly inhibits ROS production in an MCU dependent manner in skeletal muscle, but also prevents apoptosis, retards muscle atrophy in a longer term. These phenomena imply that $[Ca^{2+}]_{mito}$ temporal profile, likely in combination with steady-state $[Ca^{2+}]_{mito}$ level, serves as a toggle switch flipping between the beneficiary versus destructive outcomes. The players downstream of this toggle switch, aside from those relatively slower excitation-transcription coupling events, also include processes that modulate ROS production within the time frame of seconds to minutes. In this review, we proposed two potential mechanisms underlying this rapid process, such as direct regulation of the turnover rate of the respiratory chain and mPTP desensitization. Further experiments are needed to evaluate the validity of these hypotheses.

AUTHOR CONTRIBUTIONS

AL and JZ designed the scheme of this review. All authors contributed to editing the article and approved the submitted version.

FUNDING

Research in our laboratory has been supported by the Muscular Dystrophy Association Grant MDA-4351, NIH AR057404, NIH R01HL138570, NIH R01NS105621, DOD AL170061, the ALS Association (16-IIP-288), Victor E. Speas Foundation, a startup fund from Kansas City University of Medicine and Bioscience, and startup funds from the University of Texas at Arlington to JZ.

REFERENCES

Adam-Vizi, V., and Starkov, A. A. (2010). Calcium and mitochondrial reactive oxygen species generation: how to read the facts. *J. Alzheimers Dis.* 20, S413–S426. doi: 10.3233/JAD-2010-100465

Adhihetty, P. J., Ljubicic, V., Menzies, K. J., and Hood, D. A. (2005). Differential susceptibility of subsarcolemmal and intermyofibrillar mitochondria to apoptotic stimuli. *Am. J. Physiol. Cell Physiol.* 289, C994–C1001. doi: 10.1152/ajpcell.00031.2005

Adhihetty, P. J., O'leary, M. F., Chabi, B., Wicks, K. L., and Hood, D. A. (2007). Effect of denervation on mitochondrially mediated apoptosis in skeletal muscle. *J. Appl. Physiol.* 102, 1143–1151. doi: 10.1152/japplphysiol.00768.2006

Akimoto, T., Sorg, B. S., and Yan, Z. (2004). Real-time imaging of peroxisome proliferator-activated receptor-γ coactivator-1α promoter activity in skeletal muscles of living mice. *Am. J. Physiol. Cell Physiol.* 287, C790–C796. doi: 10.1152/ajpcell.00425.2003

Alavian, K. N., Beutner, G., Lazrove, E., Sacchetti, S., Park, H.-A., Licznerski, P., et al. (2014). An uncoupling channel within the c-subunit ring of the F1FO ATP synthase is the mitochondrial permeability transition pore. *Proc. Natl. Acad. Sci. U.S.A.* 111, 10580–10585. doi: 10.1073/pnas.1401591111

Altschafl, B. A., Beutner, G., Sharma, V. K., Sheu, S.-S., and Valdivia, H. H. (2007). The mitochondrial ryanodine receptor in rat heart: a pharmaco-kinetic profile. *Biochim. Biophys. Acta Biomembr.* 1768, 1784–1795. doi: 10.1016/j.bbamem.2007.04.011

Amat, R., Planavila, A., Chen, S. L., Iglesias, R., Giralt, M., and Villarroya, F. (2009). SIRT1 controls the transcription of the peroxisome proliferator-activated receptor-γ co-activator-1α (PGC-1α) gene in skeletal muscle through

the PGC-1α autoregulatory loop and interaction with MyoD. *J. Biol. Chem.* 284, 21872–21880. doi: 10.1074/jbc.M109.022749

Amat, R., Solanes, G., Giralt, M., and Villarroya, F. (2007). SIRT1 is involved in glucocorticoid-mediated control of uncoupling protein-3 gene transcription. *J. Biol. Chem.* 282, 34066–34076. doi: 10.1074/jbc.M707114200

Arakawa, T., Katada, A., Shigyo, H., Kishibe, K., Adachi, M., Nonaka, S., et al. (2010). Electrical stimulation prevents apoptosis in denervated skeletal muscle. *NeuroRehabilitation* 27, 147–154. doi: 10.3233/NRE-2010-0591

Ascensão, A., Lumini-Oliveira, J., Machado, N. G., Ferreira, R. M., Gonçalves, I. O., Moreira, A. C., et al. (2011). Acute exercise protects against calcium-induced cardiac mitochondrial permeability transition pore opening in doxorubicin-treated rats. *Clin. Sci.* 120, 37–49. doi: 10.1042/CS20100254

Baines, C. P. (2009). The molecular composition of the mitochondrial permeability transition pore. *J. Mol. Cell. Cardiol.* 46, 850–857. doi: 10.1016/j.yjmcc.2009.02.007

Baines, C. P., Kaiser, R. A., Sheiko, T., Craigen, W. J., and Molkentin, J. D. (2007). Voltage-dependent anion channels are dispensable for mitochondrial-dependent cell death. *Nat. Cell Biol.* 9, 550–555. doi: 10.1038/ncb1575

Bandyopadhyay, U., Das, D., and Banerjee, R. K. (1999). Reactive oxygen species: oxidative damage and pathogenesis. *Curr. Sci.* 77, 658–666.

Barja, G. (2007). Mitochondrial oxygen consumption and reactive oxygen species production are independently modulated: implications for aging studies. *Rejuvenat. Res.* 10, 215–224. doi: 10.1089/rej.2006.0516

Batandier, C., Leverve, X., and Fontaine, E. (2004). Opening of the mitochondrial permeability transition pore induces reactive oxygen species production at the level of the respiratory chain complex I. *J. Biol. Chem.* 279, 17197–17204. doi: 10.1074/jbc.M310329200

Block, B. A. (1994). Thermogenesis in muscle. *Annu. Rev. Physiol.* 56, 535–577. doi: 10.1146/annurev.ph.56.030194.002535

Bonora, M., Patergnani, S., Ramaccini, D., Morciano, G., Pedriali, G., Kahsay, A. E., et al. (2020). Physiopathology of the permeability transition pore: molecular mechanisms in human pathology. *Biomolecules* 10:998. doi: 10.3390/biom10070998

Bonora, M., Wieckowski, M. R., Chinopoulos, C., Kepp, O., Kroemer, G., Galluzzi, L., et al. (2015). Molecular mechanisms of cell death: central implication of ATP synthase in mitochondrial permeability transition. *Oncogene* 34, 1475–1486. doi: 10.1038/onc.2014.96

Borisov, A. B., and Carlson, B. M. (2000). Cell death in denervated skeletal muscle is distinct from classical apoptosis. *Anat. Rec.* 258, 305–318. doi: 10.1002/(SICI)1097-0185(20000301)258:3<305::AID-AR10>3.0.CO;2-A

Borutaite, V., Jekabsone, A., Morkuniene, R., and Brown, G. C. (2003). Inhibition of mitochondrial permeability transition prevents mitochondrial dysfunction, cytochrome c release and apoptosis induced by heart ischemia. *J. Mol. Cell. Cardiol.* 35, 357–366. doi: 10.1016/S0022-2828(03)00005-1

Boss, O., Samec, S., Paoloni-Giacobino, A., Rossier, C., Dulloo, A., Seydoux, J., et al. (1997). Uncoupling protein-3: a new member of the mitochondrial carrier family with tissue-specific expression. *FEBS Lett.* 408, 39–42. doi: 10.1016/S0014-5793(97)00384-0

Brand, M. (2000). Uncoupling to survive? The role of mitochondrial inefficiency in ageing. *Exp. Gerontol.* 35, 811–820. doi: 10.1016/S0531-5565(00)00135-2

Brand, M. D., and Esteves, T. C. (2005). Physiological functions of the mitochondrial uncoupling proteins UCP2 and UCP3. *Cell Metab.* 2, 85–93. doi: 10.1016/j.cmet.2005.06.002

Brookes, P. S., Yoon, Y., Robotham, J. L., Anders, M., and Sheu, S.-S. (2004). Calcium, ATP, and ROS: a mitochondrial love-hate triangle. *Am. J. Physiol. Cell Physiol.* 287, C817–C833. doi: 10.1152/ajpcell.00139.2004

Buntinas, L., Gunter, K. K., Sparagna, G. C., and Gunter, T. E. (2001). The rapid mode of calcium uptake into heart mitochondria (RaM): comparison to RaM in liver mitochondria. *Biochim. Biophys. Acta Bioenerg.* 1504, 248–261. doi: 10.1016/S0005-2728(00)00254-1

Carafoli, E. (2010). The fateful encounter of mitochondria with calcium: how did it happen? *Biochim. Biophys. Acta Bioenerg.* 1797, 595–606. doi: 10.1016/j.bbabio.2010.03.024

Chabi, B., Ljubicic, V., Menzies, K. J., Huang, J. H., Saleem, A., and Hood, D. A. (2008). Mitochondrial function and apoptotic susceptibility in aging skeletal muscle. *Aging cell* 7, 2–12. doi: 10.1111/j.1474-9726.2007.00347.x

Chen, Z., Gibson, T. B., Robinson, F., Silvestro, L., Pearson, G., Xu, B.-E., et al. (2001). MAP kinases. *Chem. Rev.* 101, 2449–2476. doi: 10.1021/cr000241p

Chinopoulos, C., and Adam-Vizi, V. (2010). Mitochondrial Ca2+ sequestration and precipitation revisited. *FEBS J.* 277, 3637–3651. doi: 10.1111/j.1742-4658.2010.07755.x

Cogswell, A. M., Stevens, R. J., and Hood, D. A. (1993). Properties of skeletal muscle mitochondria isolated from subsarcolemmal and intermyofibrillar regions. *Am. J. Physiol. Cell Physiol.* 264, C383–C389. doi: 10.1152/ajpcell.1993.264.2.C383

Cortright, R. N., Zheng, D., Jones, J. P., Fluckey, J. D., Dicarlo, S. E., Grujic, D., et al. (1999). Regulation of skeletal muscle UCP-2 and UCP-3 gene expression by exercise and denervation. *Am. J. Physiol. Endocrinol. Metab.* 276, E217–E221. doi: 10.1152/ajpendo.1999.276.1.E217

Crameri, R., Weston, A., Climstein, M., Davis, G., and Sutton, J. (2002). Effects of electrical stimulation-induced leg training on skeletal muscle adaptability in spinal cord injury. *Scand. J. Med. Sci. Sports* 12, 316–322. doi: 10.1034/j.1600-0838.2002.20106.x

Crameri, R. M., Weston, A. R., Rutkowski, S., Middleton, J. W., Davis, G. M., and Sutton, J. R. (2000). Effects of electrical stimulation leg training during the acute phase of spinal cord injury: a pilot study. *Eur. J. Appl. Physiol.* 83, 409–415. doi: 10.1007/s004210000263

Csordás, G., Golenár, T., Seifert, E. L., Kamer, K. J., Sancak, Y., Perocchi, F., et al. (2013). MICU1 controls both the threshold and cooperative activation of the mitochondrial Ca2+ uniporter. *Cell Metab.* 17, 976–987. doi: 10.1016/j.cmet.2013.04.020

Csordás, G., and Hajnóczky, G. (2009). SR/ER–mitochondrial local communication: calcium and ROS. *Biochim. Biophys. Acta Bioenerg.* 1787, 1352–1362. doi: 10.1016/j.bbabio.2009.06.004

Csukly, K., Ascah, A., Matas, J., Gardiner, P. F., Fontaine, E., and Burelle, Y. (2006). Muscle denervation promotes opening of the permeability transition pore and increases the expression of cyclophilin D. *J. Physiol.* 574, 319–327. doi: 10.1113/jphysiol.2006.109702

Das, A. M., and Harris, D. A. (1990). Control of mitochondrial ATP synthase in heart cells: inactive to active transitions caused by beating or positive inotropic agents. *Cardiovasc. Res.* 24, 411–417. doi: 10.1093/cvr/24.5.411

De Giorgi, F., Lartigue, L., Bauer, M. K., Schubert, A., Grimm, S., Hanson, G. T., et al. (2002). The permeability transition pore signals apoptosis by directing Bax translocation and multimerization. *FASEB J.* 16, 607–609. doi: 10.1096/fj.01-0269fje

Demaurex, N., and Guido, D. (2017). "The role of mitochondria in the activation/maintenance of SOCE: membrane contact sites as signaling hubs sustaining store-operated Ca 2+ entry," in *Store-Operated Ca2+ Entry (SOCE) Pathways*, eds K. Groschner, W. Graier, and C. Romanin (Cham: Springer), 277–296. doi: 10.1007/978-3-319-57732-6_15

Denton, R. M. (2009). Regulation of mitochondrial dehydrogenases by calcium ions. *Biochim. Biophys. Acta Bioenerg.* 1787, 1309–1316. doi: 10.1016/j.bbabio.2009.01.005

Díaz-Vegas, A., Eisner, V., and Jaimovich, E. (2019). Skeletal muscle excitation-metabolism coupling. *Arch. Biochem. Biophys.* 664, 89–94. doi: 10.1016/j.abb.2019.01.037

Ding, Y., Fang, H., Shang, W., Xiao, Y., Sun, T., Hou, N., et al. (2015). Mitoflash altered by metabolic stress in insulin-resistant skeletal muscle. *J. Mol. Med.* 93, 1119–1130. doi: 10.1007/s00109-015-1278-y

Doucet, B. M., Lam, A., and Griffin, L. (2012). Neuromuscular electrical stimulation for skeletal muscle function. *Yale J. Biol. Med.* 85:201.

Du, C., Fang, M., Li, Y., Li, L., and Wang, X. (2000). Smac, a mitochondrial protein that promotes cytochrome c–dependent caspase activation by eliminating IAP inhibition. *Cell* 102, 33–42. doi: 10.1016/S0092-8674(00)00008-8

Dudley, G., Castro, M., Rogers, S., and Apple, D. Jr. (1999). A simple means of increasing muscle size after spinal cord injury: a pilot study. *Eur. J. Appl. Physiol. Occup. Physiol.* 80, 394–396. doi: 10.1007/s004210050609

Dupont-Versteegden, E. E. (2005). Apoptosis in muscle atrophy: relevance to sarcopenia. *Exp. Gerontol.* 40, 473–481. doi: 10.1016/j.exger.2005.04.003

Echtay, K. S., Roussel, D., St-Pierre, J., Jekabsons, M. B., Cadenas, S., Stuart, J. A., et al. (2002). Superoxide activates mitochondrial uncoupling proteins. *Nature* 415, 96–99. doi: 10.1038/415096a

Egan, B., Carson, B. P., Garcia-Roves, P. M., Chibalin, A. V., Sarsfield, F. M., Barron, N., et al. (2010). Exercise intensity-dependent regulation of peroxisome proliferator-activated receptor γ coactivator-1α mRNA abundance is associated with differential activation of upstream signalling kinases in human skeletal muscle. *J. Physiol.* 588, 1779–1790. doi: 10.1113/jphysiol.2010.188011

Egan, B., and Zierath, J. R. (2013). Exercise metabolism and the molecular regulation of skeletal muscle adaptation. *Cell Metab.* 17, 162–184. doi: 10.1016/j.cmet.2012.12.012

Eisenberg, B. R. (2010). Quantitative ultrastructure of mammalian skeletal muscle. *Comp. Physiol.* 73–112. doi: 10.1002/cphy.cp100103

Elrod, J. W., and Molkentin, J. D. (2013). Physiologic functions of cyclophilin D and the mitochondrial permeability transition pore. *Circ. J.* 77, 1111–1122. doi: 10.1253/circj.CJ-13-0321

Elrod, J. W., Wong, R., Mishra, S., Vagnozzi, R. J., Sakthievel, B., Goonasekera, S. A., et al. (2010). Cyclophilin D controls mitochondrial pore–dependent Ca 2+ exchange, metabolic flexibility, and propensity for heart failure in mice. *J. Clin. Invest.* 120, 3680–3687. doi: 10.1172/JCI43171

Fernandez, M. G., Troiano, L., Moretti, L., Nasi, M., Pinti, M., Salvioli, S., et al. (2002). Early changes in intramitochondrial cardiolipin distribution during apoptosis. *Cell Growth Differ.* 13, 449–455.

Fieni, F., Lee, S. B., Jan, Y. N., and Kirichok, Y. (2012). Activity of the mitochondrial calcium uniporter varies greatly between tissues. *Nat. Commun.* 3, 1–12. doi: 10.1038/ncomms2325

Fischer, L. R., Culver, D. G., Tennant, P., Davis, A. A., Wang, M., Castellano-Sanchez, A., et al. (2004). Amyotrophic lateral sclerosis is a distal axonopathy: evidence in mice and man. *Exp. Neurol.* 185, 232–240. doi: 10.1016/j.expneurol.2003.10.004

Fitts, R. H., Riley, D. R., and Widrick, J. J. (2001). Functional and structural adaptations of skeletal muscle to microgravity. *J. Exp. Biol.* 204, 3201–3208.

Frey, D., Schneider, C., Xu, L., Borg, J., Spooren, W., and Caroni, P. (2000). Early and selective loss of neuromuscular synapse subtypes with low sprouting competence in motoneuron diseases. *J. Neurosci.* 20, 2534–2542. doi: 10.1523/JNEUROSCI.20-07-02534.2000

Gerhart-Hines, Z., Rodgers, J. T., Bare, O., Lerin, C., Kim, S. H., Mostoslavsky, R., et al. (2007). Metabolic control of muscle mitochondrial function and fatty acid oxidation through SIRT1/PGC-1α. *EMBO J.* 26, 1913–1923. doi: 10.1038/sj.emboj.7601633

Ghafourifar, P., and Cadenas, E. (2005). Mitochondrial nitric oxide synthase. *Trends Pharmacol. Sci.* 26, 190–195. doi: 10.1016/j.tips.2005.02.005

Giorgio, V., Bisetto, E., Soriano, M. E., Dabbeni-Sala, F., Basso, E., Petronilli, V., et al. (2009). Cyclophilin D modulates mitochondrial F0F1-ATP synthase by interacting with the lateral stalk of the complex. *J. Biol. Chem.* 284, 33982–33988. doi: 10.1074/jbc.M109.020115

Giorgio, V., Burchell, V., Schiavone, M., Bassot, C., Minervini, G., Petronilli, V., et al. (2017). Ca2+ binding to F-ATP synthase β subunit triggers the mitochondrial permeability transition. *EMBO Rep.* 18, 1065–1076. doi: 10.15252/embr.201643354

Giorgio, V., Guo, L., Bassot, C., Petronilli, V., and Bernardi, P. (2018). Calcium and regulation of the mitochondrial permeability transition. *Cell Calcium* 70, 56–63. doi: 10.1016/j.ceca.2017.05.004

Giorgio, V., Von Stockum, S., Antoniel, M., Fabbro, A., Fogolari, F., Forte, M., et al. (2013). Dimers of mitochondrial ATP synthase form the permeability transition pore. *Proc. Natl. Acad. Sci. U.S.A.* 110, 5887–5892. doi: 10.1073/pnas.1217823110

Giulivi, C. (2003). Characterization and function of mitochondrial nitric-oxide synthase. *Free Radic. Biol. Med.* 34, 397–408. doi: 10.1016/S0891-5849(02)01298-4

Glancy, B., Willis, W. T., Chess, D. J., and Balaban, R. S. (2013). Effect of calcium on the oxidative phosphorylation cascade in skeletal muscle mitochondria. *Biochemistry* 52, 2793–2809. doi: 10.1021/bi3015983

Gong, D.-W., He, Y., Karas, M., and Reitman, M. (1997). Uncoupling protein-3 is a mediator of thermogenesis regulated by thyroid hormone, β3-adrenergic agonists, and leptin. *J. Biol. Chem.* 272, 24129–24132. doi: 10.1074/jbc.272.39.24129

Greenawalt, J. W., Rossi, C. S., and Lehninger, A. L. (1964). Effect of active accumulation of calcium and phosphate ions on the structure of rat liver mitochondria. *J. Cell Biol.* 23, 21–38. doi: 10.1083/jcb.23.1.21

Grijalba, M. T., Vercesi, A. E., and Schreier, S. (1999). Ca2+-induced increased lipid packing and domain formation in submitochondrial particles. A possible early step in the mechanism of Ca2+-stimulated generation of reactive oxygen species by the respiratory chain. *Biochemistry* 38, 13279–13287. doi: 10.1021/bi9828674

Gunter, T. E., Yule, D. I., Gunter, K. K., Eliseev, R. A., and Salter, J. D. (2004). Calcium and mitochondria. *FEBS Lett.* 567, 96–102. doi: 10.1016/j.febslet.2004.03.071

Gurd, B. J. (2011). Deacetylation of PGC-1α by SIRT1: importance for skeletal muscle function and exercise-induced mitochondrial biogenesis. *Appl. Physiol. Nutr. Metab.* 36, 589–597. doi: 10.1139/h11-070

Halestrap, A. P. (2009). What is the mitochondrial permeability transition pore? *J. Mol. Cell. Cardiol.* 46, 821–831. doi: 10.1016/j.yjmcc.2009.02.021

Halestrap, A. P., and Davidson, A. M. (1990). Inhibition of Ca2+-induced large-amplitude swelling of liver and heart mitochondria by cyclosporin is probably caused by the inhibitor binding to mitochondrial-matrix peptidyl-prolyl cis-trans isomerase and preventing it interacting with the adenine nucleotide translocase. *Biochem. J.* 268, 153–160. doi: 10.1042/bj2680153

Haworth, R. A., and Hunter, D. R. (1979). The Ca2+-induced membrane transition in mitochondria: II. Nature of the Ca2+ trigger site. *Arch. Biochem. Biophys.* 195, 460–467. doi: 10.1016/0003-9861(79)90372-2

Hegde, R., Srinivasula, S. M., Zhang, Z., Wassell, R., Mukattash, R., Cilenti, L., et al. (2002). Identification of Omi/HtrA2 as a mitochondrial apoptotic serine protease that disrupts inhibitor of apoptosis protein-caspase interaction. *J. Biol. Chem.* 277, 432–438. doi: 10.1074/jbc.M109721200

Henríquez-Olguin, C., Knudsen, J. R., Raun, S. H., Li, Z., Dalbram, E., Treebak, J. T., et al. (2019). Cytosolic ROS production by NADPH oxidase 2 regulates muscle glucose uptake during exercise. *Nat. Commun.* 10, 1–11. doi: 10.1038/s41467-019-12523-9

Hernansanz-Agustín, P., Choya-Foces, C., Carregal-Romero, S., Ramos, E., Oliva, T., Villa-Piña, T., et al. (2020). Na+ controls hypoxic signalling by the mitochondrial respiratory chain. *Nature* 586, 287–291. doi: 10.1038/s41586-020-2551-y

Hirsch, T., Marzo, I., and Kroemer, G. (1997). Role of the mitochondrial permeability transition pore in apoptosis. *Biosci. Rep.* 17, 67–76. doi: 10.1023/A:1027339418683

Hochachka, P., and McClelland, G. (1997). Cellular metabolic homeostasis during large-scale change in ATP turnover rates in muscles. *J. Exp. Biol.* 200, 381–386.

Hoellwarth, U., and Christian Hofer, D. (2005). Muscle biopsies show that FES of denervated muscles reverses human muscle degeneration from permanent spinal motoneuron lesion. *J. Rehabil. Res. Dev.* 42(Suppl. 1), 43–53. doi: 10.1682/JRRD.2004.05.0061

Hoffman, N. J., Parker, B. L., Chaudhuri, R., Fisher-Wellman, K. H., Kleinert, M., Humphrey, S. J., et al. (2015). Global phosphoproteomic analysis of human skeletal muscle reveals a network of exercise-regulated kinases and AMPK substrates. *Cell Metab.* 22, 922–935. doi: 10.1016/j.cmet.2015.09.001

Hoppe, U. C. (2010). Mitochondrial calcium channels. *FEBS Lett.* 584, 1975–1981. doi: 10.1016/j.febslet.2010.04.017

Hubbard, M. J., and McHugh, N. J. (1996). Mitochondrial ATP synthase F1-β-subunit is a calcium-binding protein. *FEBS Lett.* 391, 323–329. doi: 10.1016/0014-5793(96)00767-3

Hunter, D. R., and Haworth, R. A. (1979a). The Ca2+-induced membrane transition in mitochondria: I. The protective mechanisms. *Arch. Biochem. Biophys.* 195, 453–459. doi: 10.1016/0003-9861(79)90371-0

Hunter, D. R., and Haworth, R. A. (1979b). The Ca2+-induced membrane transition in mitochondria: III. Transitional Ca2+ release. *Arch. Biochem. Biophys.* 195, 468–477. doi: 10.1016/0003-9861(79)90373-4

Hyatt, H., Deminice, R., Yoshihara, T., and Powers, S. K. (2019). Mitochondrial dysfunction induces muscle atrophy during prolonged inactivity: a review of the causes and effects. *Arch. Biochem. Biophys.* 662, 49–60. doi: 10.1016/j.abb.2018.11.005

Ichas, F., Jouaville, L. S., and Mazat, J.-P. (1997). Mitochondria are excitable organelles capable of generating and conveying electrical and calcium signals. *Cell* 89, 1145–1153. doi: 10.1016/S0092-8674(00)80301-3

Ichas, F., and Mazat, J.-P. (1998). From calcium signaling to cell death: two conformations for the mitochondrial permeability transition pore. Switching from low-to high-conductance state. *Biochim. Biophys. Acta Bioenerg.* 1366, 33–50. doi: 10.1016/S0005-2728(98)00119-4

Ingalls, C. P., Warren, G. L., and Armstrong, R. (1999). Intracellular Ca2+ transients in mouse soleus muscle after hindlimb unloading and reloading. *J. Appl. Physiol.* 87, 386–390. doi: 10.1152/jappl.1999.87.1.386

Irrcher, I., Ljubicic, V., and Hood, D. A. (2009). Interactions between ROS and AMP kinase activity in the regulation of PGC-1α transcription in skeletal muscle cells. *Am. J. Physiol. Cell Physiol.* 296, C116–C123. doi: 10.1152/ajpcell.00267.2007

Irrcher, I., Ljubicic, V., Kirwan, A. F., and Hood, D. A. (2008). AMP-activated protein kinase-regulated activation of the PGC-1α promoter in skeletal muscle cells. *PLoS One* 3:e3614. doi: 10.1371/journal.pone.0003614

Jabůrek, M., VařEcha, M., Gimeno, R. E., Dembski, M., JežEk, P., Zhang, M., et al. (1999). Transport function and regulation of mitochondrial uncoupling proteins 2 and 3. *J. Biol. Chem.* 274, 26003–26007. doi: 10.1074/jbc.274.37.26003

Jackman, R. W., and Kandarian, S. C. (2004). The molecular basis of skeletal muscle atrophy. *Am. J. Physiol. Cell Physiol.* 287, C834–C843. doi: 10.1152/ajpcell.00579.2003

Jäger, S., Handschin, C., Pierre, J. S., and Spiegelman, B. M. (2007). AMP-activated protein kinase (AMPK) action in skeletal muscle via direct phosphorylation of PGC-1α. *Proc. Natl. Acad. Sci. U.S.A.* 104, 12017–12022. doi: 10.1073/pnas.0705070104

Ježek, P., Holendová, B., Garlid, K. D., and Jabůrek, M. (2018). Mitochondrial uncoupling proteins: subtle regulators of cellular redox signaling. *Antioxid. Redox Signal.* 29, 667–714. doi: 10.1089/ars.2017.7225

Jiang, D., Zhao, L., and Clapham, D. E. (2009). Genome-wide RNAi screen identifies Letm1 as a mitochondrial Ca2+/H+ antiporter. *Science* 326, 144–147. doi: 10.1126/science.1175145

Jing, E., Emanuelli, B., Hirschey, M. D., Boucher, J., Lee, K. Y., Lombard, D., et al. (2011). Sirtuin-3 (Sirt3) regulates skeletal muscle metabolism and insulin signaling via altered mitochondrial oxidation and reactive oxygen species production. *Proc. Natl. Acad. Sci. U.S.A.* 108, 14608–14613. doi: 10.1073/pnas.1111308108

Kahn, B. B., Alquier, T., Carling, D., and Hardie, D. G. (2005). AMP-activated protein kinase: ancient energy gauge provides clues to modern understanding of metabolism. *Cell Metab.* 1, 15–25. doi: 10.1016/j.cmet.2004.12.003

Kamer, K. J., and Mootha, V. K. (2014). MICU1 and MICU2 play nonredundant roles in the regulation of the mitochondrial calcium uniporter. *EMBO Rep.* 15, 299–307. doi: 10.1002/embr.201337946

Karam, C., Yi, J., Xiao, Y., Dhakal, K., Zhang, L., Li, X., et al. (2017). Absence of physiological Ca 2+ transients is an initial trigger for mitochondrial dysfunction in skeletal muscle following denervation. *Skeletal Muscle* 7:6. doi: 10.1186/s13395-017-0123-0

Karch, J., and Molkentin, J. D. (2018). Identity of the elusive mitochondrial permeability transition pore: what it might be, what it was, and what it still could be. *Curr. Opin. Physiol.* 3, 57–62. doi: 10.1016/j.cophys.2018.03.001

Kinnally, K. W., Antonenko, Y. N., and Zorov, D. B. (1992). Modulation of inner mitochondrial membrane channel activity. *J. Bioenerg. Biomembr.* 24, 99–110. doi: 10.1007/BF00769536

Kirichok, Y., Krapivinsky, G., and Clapham, D. E. (2004). The mitochondrial calcium uniporter is a highly selective ion channel. *Nature* 427:360. doi: 10.1038/nature02246

Kokoszka, J. E., Waymire, K. G., Levy, S. E., Sligh, J. E., Cai, J., Jones, D. P., et al. (2004). The ADP/ATP translocator is not essential for the mitochondrial permeability transition pore. *Nature* 427, 461–465. doi: 10.1038/nature02229

Kostrominova, T. Y., Dow, D. E., Dennis, R. G., Miller, R. A., and Faulkner, J. A. (2005). Comparison of gene expression of 2-mo denervated, 2-mo stimulated-denervated, and control rat skeletal muscles. *Physiol. Genomics* 22, 227–243. doi: 10.1152/physiolgenomics.00210.2004

Krauskopf, A., Eriksson, O., Craigen, W. J., Forte, M. A., and Bernardi, P. (2006). Properties of the permeability transition in VDAC1−/− mitochondria. *Biochim. Biophys. Acta Bioenerg.* 1757, 590–595. doi: 10.1016/j.bbabio.2006.02.007

Kwong, J., Davis, J., Baines, C., Sargent, M., Karch, J., Wang, X., et al. (2014). Genetic deletion of the mitochondrial phosphate carrier desensitizes the mitochondrial permeability transition pore and causes cardiomyopathy. *Cell Death Differ.* 21, 1209–1217. doi: 10.1038/cdd.2014.36

Lejay, A., Meyer, A., Schlagowski, A.-I., Charles, A.-L., Singh, F., Bouitbir, J., et al. (2014). Mitochondria: mitochondrial participation in ischemia–reperfusion injury in skeletal muscle. *Int. J. Biochem. Cell Biol.* 50, 101–105. doi: 10.1016/j.biocel.2014.02.013

Li, L. Y., Luo, X., and Wang, X. (2001). Endonuclease G is an apoptotic DNase when released from mitochondria. *Nature* 412, 95–99. doi: 10.1038/35083620

Li, Y.-P., Chen, Y., John, J., Moylan, J., Jin, B., Mann, D. L., et al. (2005). TNF-α acts via p38 MAPK to stimulate expression of the ubiquitin ligase atrogin1/MAFbx in skeletal muscle. *FASEB J.* 19, 362–370. doi: 10.1096/fj.04-2364com

Liu, Q., Bai, C., Chen, F., Wang, R., Macdonald, T., Gu, M., et al. (1998). Uncoupling protein-3: a muscle-specific gene upregulated by leptin in ob/ob mice. *Gene* 207, 1–7. doi: 10.1016/S0378-1119(97)00596-9

Liu, X., Kim, C. N., Yang, J., Jemmerson, R., and Wang, X. (1996). Induction of apoptotic program in cell-free extracts: requirement for dATP and cytochrome c. *Cell* 86, 147–157. doi: 10.1016/S0092-8674(00)80085-9

Liu, Y., Randall, W. R., and Schneider, M. F. (2005). Activity-dependent and-independent nuclear fluxes of HDAC4 mediated by different kinases in adult skeletal muscle. *J. Cell Biol.* 168, 887–897. doi: 10.1083/jcb.200408128

Maack, C., Cortassa, S., Aon, M. A., Ganesan, A. N., Liu, T., and O'rourke, B. (2006). Elevated cytosolic Na+ decreases mitochondrial Ca2+ uptake during excitation-contraction coupling and impairs energetic adaptation in cardiac myocytes. *Circ. Res.* 99, 172–182. doi: 10.1161/01.RES.0000232546.92777.05

Mallilankaraman, K., Doonan, P., Cárdenas, C., Chandramoorthy, H. C., Müller, M., Miller, R., et al. (2012). MICU1 is an essential gatekeeper for MCU-mediated mitochondrial Ca2+ uptake that regulates cell survival. *Cell* 151, 630–644. doi: 10.1016/j.cell.2012.10.011

Mammucari, C., Gherardi, G., Zamparo, I., Raffaello, A., Boncompagni, S., Chemello, F., et al. (2015). The mitochondrial calcium uniporter controls skeletal muscle trophism in vivo. *Cell Rep.* 10, 1269–1279. doi: 10.1016/j.celrep.2015.01.056

Matsuda, J., Hosoda, K., Itoh, H., Son, C., Doi, K., Tanaka, T., et al. (1997). Cloning of rat uncoupling protein-3 and uncoupling protein-2 cDNAs: their gene expression in rats fed high-fat diet. *FEBS Lett.* 418, 200–204. doi: 10.1016/S0014-5793(97)01381-1

McBride, S., Wei-Lapierre, L., Mcmurray, F., Macfarlane, M., Qiu, X., Patten, D., et al. (2019). Skeletal muscle mitoflashes, pH, and the role of uncoupling protein-3. *Arch. Biochem. Biophys.* 663, 239–248. doi: 10.1016/j.abb.2019.01.018

Michels, G., Khan, I. F., Endres-Becker, J., Rottlaender, D., Herzig, S., Ruhparwar, A., et al. (2009). Regulation of the human cardiac mitochondrial Ca2+ uptake by 2 different voltage-gated Ca2+ channels. *Circulation* 119:2435. doi: 10.1161/CIRCULATIONAHA.108.835389

Mnatsakanyan, N., Llaguno, M. C., Yang, Y., Yan, Y., Weber, J., Sigworth, F. J., et al. (2019). A mitochondrial megachannel resides in monomeric F 1 FO ATP synthase. *Nat. Commun.* 10, 1–11. doi: 10.1038/s41467-019-13766-2

Mokrusch, T., Engelhardt, A., Eichhorn, K.-F., Prischenk, G., Prischenk, H., Sack, G., et al. (1990). Effects of long-impulse electrical stimulation on atrophy and fibre type composition of chronically denervated fast rabbit muscle. *J. Neurol.* 237, 29–34. doi: 10.1007/BF00319664

Monani, U. R. (2005). Spinal muscular atrophy: a deficiency in a ubiquitous protein; a motor neuron-specific disease. *Neuron* 48, 885–895. doi: 10.1016/j.neuron.2005.12.001

Mukhopadhyay, P., Rajesh, M., Yoshihiro, K., Haskó, G., and Pacher, P. (2007). Simple quantitative detection of mitochondrial superoxide production in live cells. *Biochem. Biophys. Res. Commun.* 358, 203–208. doi: 10.1016/j.bbrc.2007.04.106

Muller, F., Crofts, A. R., and Kramer, D. M. (2002). Multiple Q-cycle bypass reactions at the Qo site of the cytochrome bc 1 complex. *Biochemistry* 41, 7866–7874. doi: 10.1021/bi025581e

Muller, F. L., Roberts, A. G., Bowman, M. K., and Kramer, D. M. (2003). Architecture of the Qo site of the cytochrome bc 1 complex probed by superoxide production. *Biochemistry* 42, 6493–6499. doi: 10.1021/bi0342160

Muller, F. L., Song, W., Jang, Y. C., Liu, Y., Sabia, M., Richardson, A., et al. (2007). Denervation-induced skeletal muscle atrophy is associated with increased mitochondrial ROS production. *Am. J. Physiol. Regul. Integr. Comp. Physiol.* 293, R1159–R1168. doi: 10.1152/ajpregu.00767.2006

Murphy, A. N., Kelleher, J., and Fiskum, G. (1990). Submicromolar Ca2+ regulates phosphorylating respiration by normal rat liver and AS-30D hepatoma mitochondria by different mechanisms. *J. Biol. Chem.* 265, 10527–10534.

Nakagawa, K., Tamaki, H., Hayao, K., Yotani, K., Ogita, F., Yamamoto, N., et al. (2017). Electrical stimulation of denervated rat skeletal muscle retards capillary and muscle loss in early stages of disuse atrophy. *Biomed Res. Int.* 2017:5695217. doi: 10.1155/2017/5695217

Nascimento, L. R., Michaelsen, S. M., Ada, L., Polese, J. C., and Teixeira-Salmela, L. F. (2014). Cyclical electrical stimulation increases strength and improves activity after stroke: a systematic review. *J. Physiother.* 60, 22–30. doi: 10.1016/j.jphys.2013.12.002

Neretti, N., Wang, P.-Y., Brodsky, A. S., Nyguyen, H. H., White, K. P., Rogina, B., et al. (2009). Long-lived Indy induces reduced mitochondrial reactive oxygen species production and oxidative damage. *Proc. Natl. Acad. Sci. U.S.A.* 106, 2277–2282. doi: 10.1073/pnas.0812484106

Nowikovsky, K., Pozzan, T., Rizzuto, R., Scorrano, L., and Bernardi, P. (2012). The pathophysiology of LETM1. *J. Gen. Physiol.* 139, 445–454. doi: 10.1085/jgp.201110757

Ott, M., Robertson, J. D., Gogvadze, V., Zhivotovsky, B., and Orrenius, S. (2002). Cytochrome c release from mitochondria proceeds by a two-step process. *Proc. Natl. Acad. Sci. U.S.A.* 99, 1259–1263. doi: 10.1073/pnas.241655498

Palty, R., Ohana, E., Hershfinkel, M., Volokita, M., Elgazar, V., Beharier, O., et al. (2004). Lithium-calcium exchange is mediated by a distinct potassium-independent sodium-calcium exchanger. *J. Biol. Chem.* 279, 25234–25240. doi: 10.1074/jbc.M401229200

Palty, R., Silverman, W. F., Hershfinkel, M., Caporale, T., Sensi, S. L., Parnis, J., et al. (2010). NCLX is an essential component of mitochondrial Na+/Ca2+ exchange. *Proc. Natl. Acad. Sci. U.S.A.* 107, 436–441. doi: 10.1073/pnas.0908099107

Pan, X., Liu, J., Nguyen, T., Liu, C., Sun, J., Teng, Y., et al. (2013). The physiological role of mitochondrial calcium revealed by mice lacking the mitochondrial calcium uniporter. *Nat. Cell Biol.* 15, 1464–1472. doi: 10.1038/ncb2868

Passier, R., Zeng, H., Frey, N., Naya, F. J., Nicol, R. L., Mckinsey, T. A., et al. (2000). CaM kinase signaling induces cardiac hypertrophy and activates the MEF2 transcription factor in vivo. *J. Clin. Invest.* 105, 1395–1406. doi: 10.1172/JCI8551

Patron, M., Checchetto, V., Raffaello, A., Teardo, E., Reane, D. V., Mantoan, M., et al. (2014). MICU1 and MICU2 finely tune the mitochondrial Ca2+ uniporter by exerting opposite effects on MCU activity. *Mol. Cell* 53, 726–737. doi: 10.1016/j.molcel.2014.01.013

Peng, T. I., and Jou, M. J. (2010). Oxidative stress caused by mitochondrial calcium overload. *Ann. N. Y. Acad. Sci.* 1201, 183–188. doi: 10.1111/j.1749-6632.2010.05634.x

Peviani, S. M., Russo, T. L., Durigan, J. L., Vieira, B. S., Pinheiro, C. M., Galassi, M. S., et al. (2010). Stretching and electrical stimulation regulate the metalloproteinase-2 in rat denervated skeletal muscle. *Neurol. Res.* 32, 891–896. doi: 10.1179/174313209X459093

Pilegaard, H., Saltin, B., and Neufer, P. D. (2003). Exercise induces transient transcriptional activation of the PGC-1α gene in human skeletal muscle. *J. Physiol.* 546, 851–858. doi: 10.1113/jphysiol.2002.034850

Pottecher, J., Guillot, M., Belaidi, E., Charles, A.-L., Lejay, A., Gharib, A., et al. (2013). Cyclosporine A normalizes mitochondrial coupling, reactive oxygen species production, and inflammation and partially restores skeletal muscle maximal oxidative capacity in experimental aortic cross-clamping. *J. Vasc. Surg.* 57, 1100–1108.e2. doi: 10.1016/j.jvs.2012.09.020

Powers, S. K., Radak, Z., and Ji, L. L. (2016). Exercise-induced oxidative stress: past, present and future. *J. Physiol.* 594, 5081–5092. doi: 10.1113/JP270646

Powers, S. K., Wiggs, M. P., Duarte, J. A., Zergeroglu, A. M., and Demirel, H. A. (2012). Mitochondrial signaling contributes to disuse muscle atrophy. *Am. J. Physiol. Endocrinol. Metab.* 303, E31–E39. doi: 10.1152/ajpendo.00609.2011

Qiu, J., Fang, Q., Xu, T., Wu, C., Xu, L., Wang, L., et al. (2018). Mechanistic role of reactive oxygen species and therapeutic potential of antioxidants in denervation-or fasting-induced skeletal muscle atrophy. *Front. Physiol.* 9:215. doi: 10.3389/fphys.2018.00215

Raffaello, A., De Stefani, D., Sabbadin, D., Teardo, E., Merli, G., Picard, A., et al. (2013). The mitochondrial calcium uniporter is a multimer that can include a dominant-negative pore-forming subunit. *EMBO J.* 32, 2362–2376. doi: 10.1038/emboj.2013.157

Reane, D. V., Vallese, F., Checchetto, V., Acquasaliente, L., Butera, G., De Filippis, V., et al. (2016). A MICU1 splice variant confers high sensitivity to the mitochondrial Ca2+ uptake machinery of skeletal muscle. *Mol. Cell* 64, 760–773. doi: 10.1016/j.molcel.2016.10.001

Rizzuto, R., and Pozzan, T. (2006). Microdomains of intracellular Ca2+: molecular determinants and functional consequences. *Physiol. Rev.* 86, 369–408. doi: 10.1152/physrev.00004.2005

Ruas, J. L., White, J. P., Rao, R. R., Kleiner, S., Brannan, K. T., Harrison, B. C., et al. (2012). A PGC-1α isoform induced by resistance training regulates skeletal muscle hypertrophy. *Cell* 151, 1319–1331. doi: 10.1016/j.cell.2012.10.050

Rudolf, R. D., Mongillo, M., Magalhães, P. J., and Pozzan, T. (2004). In vivo monitoring of Ca2+ uptake into mitochondria of mouse skeletal muscle during contraction. *J. Cell Biol.* 166, 527–536. doi: 10.1083/jcb.200403102

Russo, T. L., Peviani, S. M., Durigan, J. L., Gigo-Benato, D., Delfino, G. B., and Salvini, T. F. (2010). Stretching and electrical stimulation reduce the accumulation of MyoD, myostatin and atrogin-1 in denervated rat skeletal muscle. *J. Muscle Res. Cell Motil.* 31, 45–57. doi: 10.1007/s10974-010-9203-z

Sakamoto, K., and Goodyear, L. J. (2002). Invited review: intracellular signaling in contracting skeletal muscle. *J. Appl. Physiol.* 93, 369–383. doi: 10.1152/japplphysiol.00167.2002

Sakellariou, G. K., Vasilaki, A., Palomero, J., Kayani, A., Zibrik, L., Mcardle, A., et al. (2013). Studies of mitochondrial and nonmitochondrial sources implicate nicotinamide adenine dinucleotide phosphate oxidase (s) in the increased skeletal muscle superoxide generation that occurs during contractile activity. *Antioxid. Redox Signal.* 18, 603–621. doi: 10.1089/ars.2012.4623

Schwarzländer, M., Murphy, M. P., Duchen, M. R., Logan, D. C., Fricker, M. D., Halestrap, A. P., et al. (2012). Mitochondrial 'flashes': a radical concept repHined. *Trends Cell Biol.* 22, 503–508. doi: 10.1016/j.tcb.2012.07.007

Schwer, B., and Verdin, E. (2008). Conserved metabolic regulatory functions of sirtuins. *Cell Metab.* 7, 104–112. doi: 10.1016/j.cmet.2007.11.006

Sedova, M., Dedkova, E. N., and Blatter, L. A. (2006). Integration of rapid cytosolic Ca2+ signals by mitochondria in cat ventricular myocytes. *Am. J. Physiol. Cell Physiol.* 291, C840–C850. doi: 10.1152/ajpcell.00619.2005

Seifert, E. L., Ligeti, E., Mayr, J. A., Sondheimer, N., and Hajnóczky, G. (2015). The mitochondrial phosphate carrier: role in oxidative metabolism, calcium handling and mitochondrial disease. *Biochem. Biophys. Res. Commun.* 464, 369–375. doi: 10.1016/j.bbrc.2015.06.031

Silva, L. A., Pinho, C. A., Scarabelot, K. S., Fraga, D. B., Volpato, A. M., Boeck, C. R., et al. (2009). Physical exercise increases mitochondrial function and reduces oxidative damage in skeletal muscle. *Eur. J. Appl. Physiol.* 105, 861–867. doi: 10.1007/s00421-008-0971-8

Siu, P. M., and Alway, S. E. (2005). Mitochondria-associated apoptotic signalling in denervated rat skeletal muscle. *J. Physiol.* 565, 309–323. doi: 10.1113/jphysiol.2004.081083

Susin, S. A., Lorenzo, H. K., Zamzami, N., Marzo, I., Snow, B. E., Brothers, G. M., et al. (1999). Molecular characterization of mitochondrial apoptosis-inducing factor. *Nature* 397, 441–446. doi: 10.1038/17135

Szabadkai, G., and Duchen, M. R. (2008). Mitochondria: the hub of cellular Ca2+ signaling. *Physiology* 23, 84–94. doi: 10.1152/physiol.00046.2007

Szabó, I., Pinto, V. D., and Zoratti, M. (1993). The mitochondrial permeability transition pore may comprise VDAC molecules: II. The electrophysiological properties of VDAC are compatible with those of the mitochondrial megachannel. *FEBS Lett.* 330, 206–210. doi: 10.1016/0014-5793(93)80274-X

Szabó, I., and Zoratti, M. (1992). The mitochondrial megachannel is the permeability transition pore. *J. Bioenerg. Biomembr.* 24, 111–117. doi: 10.1007/BF00769537

Tao, R., Coleman, M. C., Pennington, J. D., Ozden, O., Park, S.-H., Jiang, H., et al. (2010). Sirt3-mediated deacetylation of evolutionarily conserved lysine 122 regulates MnSOD activity in response to stress. *Mol. Cell* 40, 893–904. doi: 10.1016/j.molcel.2010.12.013

Tao, R., Vassilopoulos, A., Parisiadou, L., Yan, Y., and Gius, D. (2014). Regulation of MnSOD enzymatic activity by Sirt3 connects the mitochondrial acetylome signaling networks to aging and carcinogenesis. *Antioxid. Redox Signal.* 20, 1646–1654. doi: 10.1089/ars.2013.5482

Tews, D. (2002). Apoptosis and muscle fibre loss in neuromuscular disorders. *Neuromuscul. Disord.* 12, 613–622. doi: 10.1016/S0960-8966(02)00030-5

Tischler, M. E., Rosenberg, S., Satarug, S., Henriksen, E. J., Kirby, C. R., Tome, M., et al. (1990). Different mechanisms of increased proteolysis in atrophy induced by denervation or unweighting of rat soleus muscle. *Metabolism* 39, 756–763. doi: 10.1016/0026-0495(90)90113-Q

Tisdale, M. J. (2010). Cancer cachexia. *Curr. Opin. Gastroenterol.* 26, 146–151. doi: 10.1097/MOG.0b013e3283347e77

Torres, M., and Forman, H. J. (2003). Redox signaling and the MAP kinase pathways. *Biofactors* 17, 287–296. doi: 10.1002/biof.5520170128

Tsai, M.-F., Phillips, C. B., Ranaghan, M., Tsai, C.-W., Wu, Y., Williams, C., et al. (2016). Dual functions of a small regulatory subunit in the mitochondrial calcium uniporter complex. *eLife* 5:e15545. doi: 10.7554/eLife.15545.019

Tsuboyama-Kasaoka, N., Tsunoda, N., Maruyama, K., Takahashi, M., Kim, H., Ikemoto, S., et al. (1998). Up-regulation of uncoupling protein 3 (UCP3) mRNA by exercise training and down-regulation of UCP3 by denervation in skeletal muscles. *Biochem. Biophys. Res. Commun.* 247, 498–503. doi: 10.1006/bbrc.1998.8818

Turrens, J. F., Alexandre, A., and Lehninger, A. L. (1985). Ubisemiquinone is the electron donor for superoxide formation by complex III of heart mitochondria. *Arch. Biochem. Biophys.* 237, 408–414. doi: 10.1016/0003-9861(85)90293-0

Urbani, A., Giorgio, V., Carrer, A., Franchin, C., Arrigoni, G., Jiko, C., et al. (2019). Purified F-ATP synthase forms a Ca 2+-dependent high-conductance channel matching the mitochondrial permeability transition pore. *Nat. Commun.* 10, 1–11. doi: 10.1038/s41467-019-12331-1

Varanyuwatana, P., and Halestrap, A. P. (2012). The roles of phosphate and the phosphate carrier in the mitochondrial permeability transition pore. *Mitochondrion* 12, 120–125. doi: 10.1016/j.mito.2011.04.006

Vidal-Puig, A., Solanes, G., Grujic, D., Flier, J. S., and Lowell, B. B. (1997). UCP3: an uncoupling protein homologue expressed preferentially and abundantly in skeletal muscle and brown adipose tissue. *Biochem. Biophys. Res. Commun.* 235, 79–82. doi: 10.1006/bbrc.1997.6740

Voytik, S. L., Przyborski, M., Badylak, S. F., and Konieczny, S. F. (1993). Differential expression of muscle regulatory factor genes in normal and denervated adult rat hindlimb muscles. *Dev. Dyn.* 198, 214–224. doi: 10.1002/aja.1001980307

Wan, B., Lanoue, K., Cheung, J., and Scaduto, R. (1989). Regulation of citric acid cycle by calcium. *J. Biol. Chem.* 264, 13430–13439.

Wang, C., and Youle, R. J. (2009). The role of mitochondria in apoptosis. *Annu. Rev. Genet.* 43, 95–118. doi: 10.1146/annurev-genet-102108-134850

Wang, L., Yang, X., Li, S., Wang, Z., Liu, Y., Feng, J., et al. (2014). Structural and mechanistic insights into MICU1 regulation of mitochondrial calcium uptake. *EMBO J.* 33, 594–604. doi: 10.1002/embj.201386523

Wang, W., Fang, H., Groom, L., Cheng, A., Zhang, W., Liu, J., et al. (2008). Superoxide flashes in single mitochondria. *Cell* 134, 279–290. doi: 10.1016/j.cell.2008.06.017

Wang, W., Zhang, H., and Cheng, H. (2016). Mitochondrial flashes: from indicator characterization to in vivo imaging. *Methods* 109, 12–20. doi: 10.1016/j.ymeth.2016.06.004

Wang, X., Zhang, X., Wu, D., Huang, Z., Hou, T., Jian, C., et al. (2017). Mitochondrial flashes regulate ATP homeostasis in the heart. *eLife* 6:e23908. doi: 10.7554/eLife.23908

Wei-LaPierre, L., Gong, G., Gerstner, B. J., Ducreux, S., Yule, D. I., Pouvreau, S., et al. (2013). Respective contribution of mitochondrial superoxide and pH to mitochondria-targeted circularly permuted yellow fluorescent protein (mt-cpYFP) flash activity. *J. Biol. Chem.* 288, 10567–10577. doi: 10.1074/jbc.M113.455709

Wojtaszewski, J. F., Nielsen, P., Hansen, B. F., Richter, E. A., and Kiens, B. (2000). Isoform-specific and exercise intensity-dependent activation of 5′-AMP-activated protein kinase in human skeletal muscle. *J. Physiol.* 528, 221–226. doi: 10.1111/j.1469-7793.2000.t01-1-00221.x

Wolf, S. G., Mutsafi, Y., Dadosh, T., Ilani, T., Lansky, Z., Horowitz, B., et al. (2017). 3D visualization of mitochondrial solid-phase calcium stores in whole cells. *eLife* 6:e29929. doi: 10.7554/eLife.29929.029

Wu, H., Kanatous, S. B., Thurmond, F. A., Gallardo, T., Isotani, E., Bassel-Duby, R., et al. (2002). Regulation of mitochondrial biogenesis in skeletal muscle by CaMK. *Science* 296, 349–352. doi: 10.1093/emboj/19.9.1963

Wu, H., Naya, F. J., Mckinsey, T. A., Mercer, B., Shelton, J. M., Chin, E. R., et al. (2000). MEF2 responds to multiple calcium-regulated signals in the control of skeletal muscle fiber type. *EMBO J.* 19, 1963–1973. doi: 10.1016/S0092-8674(00)80611-X

Wu, Z., Puigserver, P., Andersson, U., Zhang, C., Adelmant, G., Mootha, V., et al. (1999). Mechanisms controlling mitochondrial biogenesis and respiration through the thermogenic coactivator PGC-1. *Cell* 98, 115–124.

Xiao, Y., Karam, C., Yi, J., Zhang, L., Li, X., Yoon, D., et al. (2018). ROS-related mitochondrial dysfunction in skeletal muscle of an ALS mouse model during the disease progression. *Pharmacol. Res.* 138, 25–36.

Yi, J., Ma, C., Li, Y., Weisleder, N., Ríos, E., Ma, J., et al. (2011). Mitochondrial calcium uptake regulates rapid calcium transients in skeletal muscle during excitation-contraction (EC) coupling. *J. Biol. Chem.* 286, 32436–32443.

Yoo, S.-Z., No, M.-H., Heo, J.-W., Chang, E., Park, D.-H., Kang, J.-H., et al. (2019a). Effects of a single bout of exercise on mitochondria-mediated apoptotic signaling in rat cardiac and skeletal muscles. *J. Exer. Rehabil.* 15:512.

Yoo, S.-Z., No, M.-H., Heo, J.-W., Park, D.-H., Kang, J.-H., Kim, J.-H., et al. (2019b). Effects of acute exercise on mitochondrial function, dynamics, and mitophagy in rat cardiac and skeletal muscles. *Int. Neurourol. J.* 23:S22.

Zhou, M., Lin, B.-Z., Coughlin, S., Vallega, G., and Pilch, P. F. (2000). UCP-3 expression in skeletal muscle: effects of exercise, hypoxia, and AMP-activated protein kinase. *Am. J. Physiol. Endocrinol. Metab.* 279, E622–E629.

Zhou, Z., Matlib, M. A., and Bers, D. M. (1998). Cytosolic and mitochondrial Ca2+ signals in patch clamped mammalian ventricular myocytes. *J. Physiol.* 507, 379–403.

Zoccarato, F., and Nicholls, D. (1982). The role of phosphate in the regulation of the independent calcium-efflux pathway of liver mitochondria. *Eur. J. Biochem.* 127, 333–338.

Zoratti, M., and Szabò, I. (1995). The mitochondrial permeability transition. *Biochim. Biophys. Acta Rev. Biomembr.* 1241, 139–176.

Conflict of Interest: The authors declare that the research was conducted in the absence of any commercial or financial relationships that could be construed as a potential conflict of interest.

frontiers in Physiology

REVIEW
published: 04 November 2020
doi: 10.3389/fphys.2020.604941

STIM1/ORAI1 Loss-of-Function and Gain-of-Function Mutations Inversely Impact on SOCE and Calcium Homeostasis and Cause Multi-Systemic Mirror Diseases

Roberto Silva-Rojas†, Jocelyn Laporte† and Johann Böhm*†*

Institut de Génétique et de Biologie Moléculaire et Cellulaire (IGBMC), Inserm U1258, CNRS UMR 7104, Université de Strasbourg, Illkirch, France

OPEN ACCESS

Edited by:
Enrique Jaimovich, University of Chile, Chile

Reviewed by:
Vincenzo Sorrentino, University of Siena, Italy
D. George Stephenson, La Trobe University, Australia

***Correspondence:**
Jocelyn Laporte
jocelyn@igbmc.fr
Johann Böhm
johann@igbmc.fr

†ORCID:
Roberto Silva-Rojas
orcid.org/0000-0002-0349-4283
Jocelyn Laporte
orcid.org/0000-0001-8256-5862
Johann Böhm
orcid.org/0000-0001-8019-9504

Specialty section:
This article was submitted to Striated Muscle Physiology, a section of the journal Frontiers in Physiology

Received: *10 September 2020*
Accepted: *15 October 2020*
Published: *04 November 2020*

Citation:
Silva-Rojas R, Laporte J and Böhm J (2020) STIM1/ORAI1 Loss-of-Function and Gain-of-Function Mutations Inversely Impact on SOCE and Calcium Homeostasis and Cause Multi-Systemic Mirror Diseases. Front. Physiol. 11:604941. doi: 10.3389/fphys.2020.604941

Store-operated Ca^{2+} entry (SOCE) is a ubiquitous and essential mechanism regulating Ca^{2+} homeostasis in all tissues, and controls a wide range of cellular functions including keratinocyte differentiation, osteoblastogenesis and osteoclastogenesis, T cell proliferation, platelet activation, and muscle contraction. The main SOCE actors are STIM1 and ORAI1. Depletion of the reticular Ca^{2+} stores induces oligomerization of the luminal Ca^{2+} sensor STIM1, and the oligomers activate the plasma membrane Ca^{2+} channel ORAI1 to trigger extracellular Ca^{2+} entry. Mutations in *STIM1* and *ORAI1* result in abnormal SOCE and lead to multi-systemic disorders. Recessive loss-of-function mutations are associated with CRAC (Ca^{2+} release-activated Ca^{2+}) channelopathy, involving immunodeficiency and autoimmunity, muscular hypotonia, ectodermal dysplasia, and mydriasis. In contrast, dominant *STIM1* and *ORAI1* gain-of-function mutations give rise to tubular aggregate myopathy and Stormorken syndrome (TAM/STRMK), forming a clinical spectrum encompassing muscle weakness, thrombocytopenia, ichthyosis, hyposplenism, short stature, and miosis. Functional studies on patient-derived cells revealed that CRAC channelopathy mutations impair SOCE and extracellular Ca^{2+} influx, while TAM/STRMK mutations induce excessive Ca^{2+} entry through SOCE over-activation. In accordance with the opposite pathomechanisms underlying both disorders, CRAC channelopathy and TAM/STRMK patients show mirror phenotypes at the clinical and molecular levels, and the respective animal models recapitulate the skin, bones, immune system, platelet, and muscle anomalies. Here we review and compare the clinical presentations of CRAC channelopathy and TAM/STRMK patients and the histological and molecular findings obtained on human samples and murine models to highlight the mirror phenotypes in different tissues, and to point out potentially undiagnosed anomalies in patients, which may be relevant for disease management and prospective therapeutic approaches.

Keywords: SOCE, calcium, STIM1, ORAI1, CRAC channelopathy, tubular aggregate myopathy, Stormorken syndrome

INTRODUCTION

Calcium (Ca^{2+}) is an elemental factor regulating a multitude of metabolic processes, signaling pathways, and cellular functions in all tissues, and mediates muscle contraction, nerve conduction, hormone release, and blood coagulation. Consistently, normal tissue and organ physiology strictly depends on the precise control of Ca^{2+} entry, storage, and release, while abnormal Ca^{2+} homeostasis induces various rare and common disorders affecting skeletal muscle, heart, bones, brain, skin, or the immune and hormonal systems (Peacock, 2010; Gattineni, 2014).

Ca^{2+} is mainly stored in the endoplasmic/sarcoplasmic reticulum (ER/SR), and refilling of the stocks is initiated by store-operated Ca^{2+} entry (SOCE), a ubiquitous mechanism driven by the concerted action of STIM1 and ORAI1 (Zhang et al., 2005; Feske et al., 2006). STIM1 contains an intraluminal region with EF hands sensing the reticular Ca^{2+} concentration, and a cytosolic part interacting with the plasma membrane CRAC (Ca^{2+} release-activated Ca^{2+}) channel ORAI1 (Stathopulos et al., 2006, 2008). Ca^{2+} store depletion induces STIM1 unfolding and oligomerization, and the STIM1 oligomers hence activate ORAI1 to trigger extracellular Ca^{2+} entry (Stathopulos et al., 2008; Prakriya and Lewis, 2015; Stathopulos and Ikura, 2017).

Abnormal SOCE has been associated with different human disorders. Recessive *STIM1* and *ORAI1* loss-of-function (LoF) mutations resulting in insufficient SOCE cause CRAC channelopathies characterized by severe combined immunodeficiency (SCID) involving recurrent and chronic infections, autoimmunity, muscular hypotonia, ectodermal dysplasia, anhidrosis, and mydriasis (Feske et al., 2006; Picard et al., 2009; Lacruz and Feske, 2015). The majority of the LoF mutations involve a total loss of STIM1 or ORAI1 (Lacruz and Feske, 2015), but single point mutations disrupting the STIM1 function and interfering with the STIM1-ORAI1 interaction (R426C, R429C) (Fuchs et al., 2012; Wang et al., 2014) or generating an obstructed ORAI1 channel (R91W) (Feske et al., 2006) have also been described (**Figure 1**). In contrast, dominant *STIM1* and *ORAI1* gain-of-function (GoF) mutations inducing excessive Ca^{2+} entry through SOCE over-activation were found in patients with tubular aggregate myopathy (TAM) and Stormorken syndrome (STRMK) (Bohm et al., 2013; Misceo et al., 2014; Morin et al., 2014; Nesin et al., 2014). TAM and STRMK form a clinical continuum characterized by progressive muscle weakness and myalgia predominantly affecting the lower limbs (Chevessier et al., 2005), and most patients manifest a varying degree of additional multi-systemic signs as miosis, ichthyosis, short stature, hyposplenism, thrombocytopenia, and dyslexia (Endo et al., 2015; Markello et al., 2015; Walter et al., 2015; Bohm et al., 2017; Garibaldi et al., 2017; Noury et al., 2017; Bohm and Laporte, 2018; Morin et al., 2020). All GoF mutations are missense mutations affecting highly conserved amino acids in the Ca^{2+}-binding EF hands (H72Q, N80T, G81D, D84G, D84E, S88G, L92V, L96V, Y98C, F108I, F108L; H109N, H109R, H109Y, I115F) (Bohm et al., 2013, 2014; Hedberg et al., 2014; Markello et al., 2015; Walter et al., 2015; Harris et al., 2017; Noury et al., 2017; Li et al., 2019; Claeys et al., 2020; Morin et al., 2020) or in the luminal coiled-coil domains of STIM1 (R304W, R304Q) (Misceo et al., 2014; Morin et al., 2014; Nesin et al., 2014; Markello et al., 2015; Harris et al., 2017; Alonso-Jimenez et al., 2018; Borsani et al., 2018; Sura et al., 2020), or in the ORAI1 transmembrane domains forming the channel pore or concentric rings surrounding the pore (G97C, G98S, V107M, L138F, T184M, P245L) (Nesin et al., 2014; Endo et al., 2015; Bohm et al., 2017; Garibaldi et al., 2017; **Figure 1**). Missense mutations in the muscle-specific SR Ca^{2+} buffer calsequestrin (*CASQ1*) have moreover been reported in patients with late-onset muscle weakness and myalgia, forming the mild end of the TAM/STRMK spectrum (Barone et al., 2017; Bohm et al., 2018; **Figure 1**).

Animal models for CRAC channelopathy and TAM/STRMK exist and widely recapitulate the clinical signs of the human disorders. Mice lacking STIM1 or ORAI1 die perinatally (Baba et al., 2008; Oh-Hora et al., 2008), and the tissue-specific deletion of *Stim1* or *Orai1* or the generation of chimeras through transplantation of hematopoietic $Stim1^{-/-}$ or $Orai1^{-/-}$ stem cells results in defective T cell activation and Treg suppression (Gwack et al., 2008; Oh-Hora et al., 2008, 2013; McCarl et al., 2010), splenomegaly (Oh-Hora et al., 2008, 2013), autoimmunity (Oh-Hora et al., 2008, 2013), reduced platelet activation and thrombus formation (Varga-Szabo et al., 2008; Bergmeier et al., 2009; Braun et al., 2009; Ahmad et al., 2011), anhidrosis (Concepcion et al., 2016), amelogenesis imperfecta (Gwack et al., 2008), and muscle weakness with reduced resistance to fatigue (Stiber et al., 2008; Srikanth et al., 2010; Li et al., 2012; Wei-Lapierre et al., 2013; Carrell et al., 2016; Sampieri et al., 2018). Mice harboring the *Stim1* GoF mutations D84G, I115F, or R304W show a varying degree of multi-systemic disease signs including small size (Cordero-Sanchez et al., 2019; Silva-Rojas et al., 2019), eye movement defects (Silva-Rojas et al., 2019), skin and spleen anomalies (Grosse et al., 2007; Cordero-Sanchez et al., 2019; Silva-Rojas et al., 2019), bleeding diathesis with thrombocytopenia (Grosse et al., 2007; Cordero-Sanchez et al., 2019; Silva-Rojas et al., 2019), and muscle weakness (Cordero-Sanchez et al., 2019; Silva-Rojas et al., 2019). SOCE deficiency in drosophila resulting from *Stim* or *Orai* downregulation impairs the flight capacities (Venkiteswaran and Hasan, 2009; Agrawal et al., 2010), and zebrafish embryos injected with mRNA containing *STIM1* or *ORAI1* GoF mutations display thrombocytopenia (Nesin et al., 2014), highlighting the conservation of SOCE in specific tissues.

The present review aims to provide an update on the current knowledge of CRAC channelopathy and TAM/STRMK, to highlight the molecular and/or clinical mirror phenotypes caused by either LoF or GoF mutations in the SOCE key players, and to provide an overview of the available animal models recapitulating the human disorders. We thoroughly and stepwise compare the eye, skin, bone, enamel, spleen, immune, platelet, and muscle phenotypes in human and mouse, and we detail the inverse mutational effects and pathomechanisms underlying CRAC channelopathy and TAM/STRMK, and their impact on the sequence of events leading to the diverging clinical manifestations and mirror-image anomalies in most affected tissues. We also point to clinical signs that are potentially underdiagnosed in patients, and may be relevant

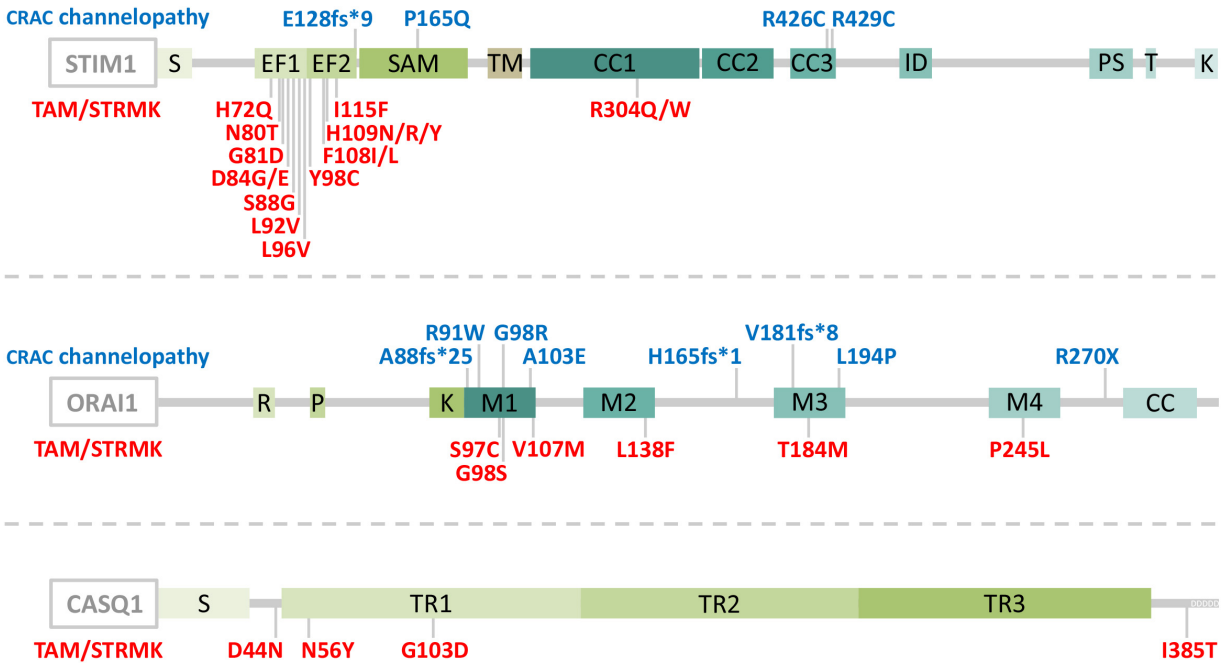

FIGURE 1 | Schematic representation of STIM1, ORAI1, and CASQ1 with position of the CRAC channelopathy and TAM/STRMK mutations. STIM1 is composed of a luminal part with a reticular signal sequence (S), Ca^{2+}-binding EF-hands and a SAM domain, a transmembrane domain (TM), and a cytosolic part with coiled-coil (CC) domains 1–3, an inhibitory domain (ID), a proline/serine-rich region (PS), a TRIP domain (T), and a lysine-rich region (K). ORAI1 contains arginine (R), proline (P), and lysine (K)-rich regions, four transmembrane domains (M1-M4), and a coiled-coil domain (CC), and calsequestrin (CASQ1) contains a reticular signal sequence (S), three thioredoxin domains (TR1-3), and an N-terminal stretch of Ca^{2+}-binding aspartic acid residues (DDDDD). CRAC channelopathy mutations are depicted in blue and TAM/STRMK mutations in red. Note that an additional *STIM1* splice site mutation (c.970-1G>A) generates unstable transcripts and causes CRAC channelopathy.

for diagnosis and disease management, and disclose treatment options. A schematic illustration opposing the clinical pictures of CRAC channelopathy versus TAM/STRMK is shown in **Figure 2**, and is supported by a detailed description in **Table 1**.

PHENOTYPIC TRAITS IN CRAC CHANNELOPATHY AND TAM/STRMK PATIENTS AND MICE

CRAC channelopathy and TAM/STRMK are multi-systemic disorders, and patients with either disease can manifest impairments of pupillary function, eye movement, skin, enamel, bones, immune system, spleen, coagulation, and skeletal muscle. The following chapter provides a comparative overview of the clinical anomalies and the molecular and mechanistic causes, and also refers to the phenotypic traits of diverse CRAC channelopathy and TAM/STRMK mouse models.

Pupillary Dysfunction and Eye Movement Limitations

Vision is primarily a photochemical process, and can be adapted to the lighting conditions through iris constriction/dilatation and eye movement, both governed by Ca^{2+}-dependent muscle contraction. Ca^{2+} release from the reticulum activates the contractile apparatus, which generates force, causing the shortening of the muscle cells (Ebashi, 1974). The iris acts as a diaphragm controlling the amount of light entering the eye through the pupil, and SOCE substantially sustains the muscle tonus for the steady contraction of the smooth sphincter and dilator muscles for an appropriate view in brightness and obscurity (Eckstein et al., 2017; Feldman et al., 2017).

Pupillary dysfunction is a main clinical sign of CRAC channelopathy and TAM/STRMK. While CRAC channelopathy patients typically show iris dilatation (mydriasis) (Feske et al., 2006; Picard et al., 2009; Fuchs et al., 2012; Lian et al., 2018), the inverse phenotype of light-insensitive iris hypercontraction (miosis) is a hallmark of TAM/STRMK, and results in migraine and reduced night vision (Misceo et al., 2014; Morin et al., 2014, 2020; Nesin et al., 2014; Markello et al., 2015; Bohm et al., 2017; Garibaldi et al., 2017; Harris et al., 2017; Alonso-Jimenez et al., 2018; Borsani et al., 2018; Claeys et al., 2020; Sura et al., 2020). Mydriasis and miosis have, however, not been described in murine models for CRAC channelopathy or TAM/STRMK. They may have been missed, or may reflect physiological differences between the species. Indeed, mice are nocturnal animals, and murine pupil constriction is essentially triggered by a light-dependent mechanism known as local pupillary reflex that is absent in humans (Xue et al., 2011).

Eye movement relies on the rapid and concerted contraction of six striated extraocular muscles, and ophthalmoplegia

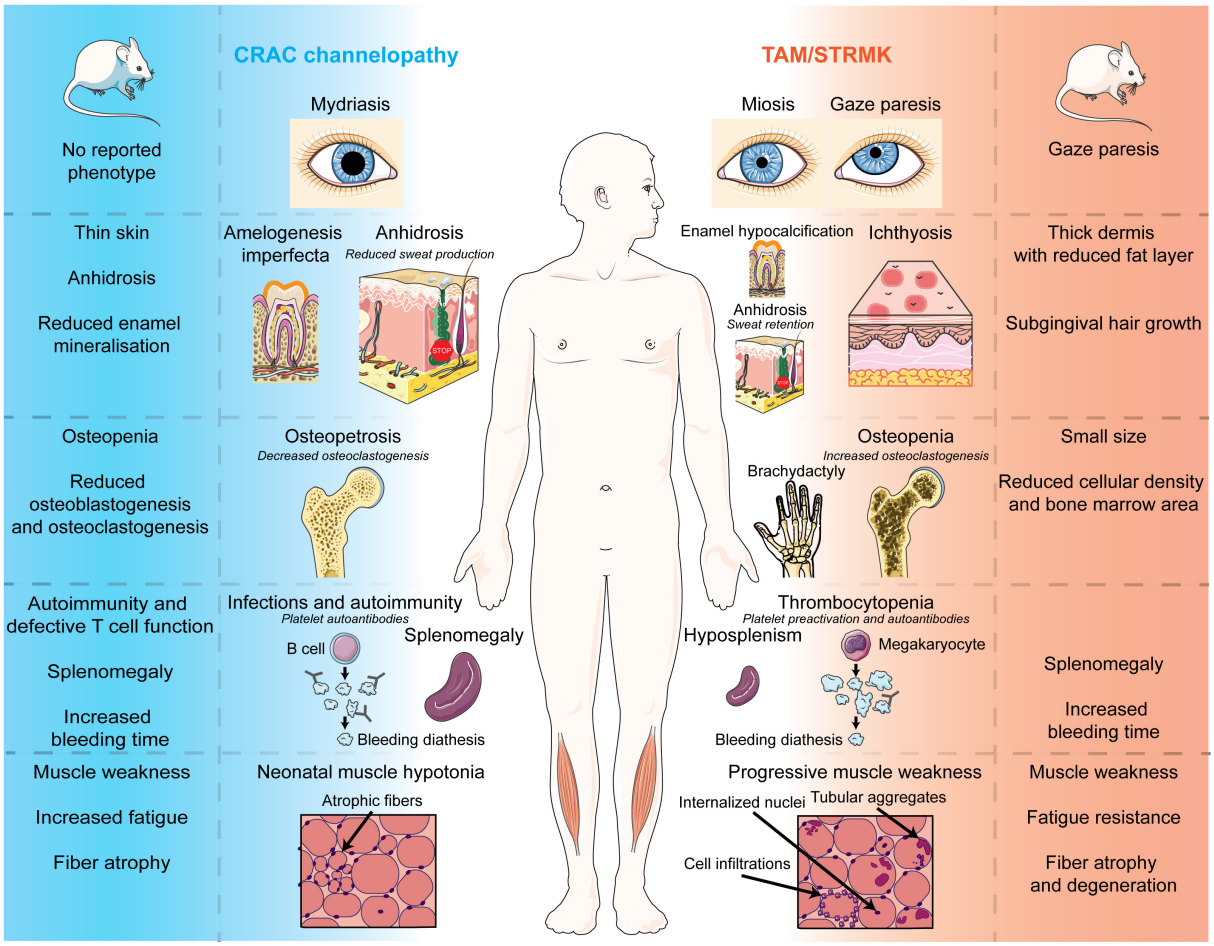

FIGURE 2 | Phenotypes of CRAC channelopathy and TAM/STRMK in patients and mouse models. Schematic overview of the clinical and molecular phenotypes of eyes, skin, teeth, spleen, immune system, and skeletal muscle in CRAC channelopathy and TAM/STRMK. The figure uses modified images from Servier Medical Art Commons Attribution 3.0 Unported License (http://smart.servier.com).

including upward gaze paresis (Bohm et al., 2013; Noury et al., 2017), lateral gaze paresis (Morin et al., 2020), or reduced lateral and/or upward gaze (Bohm et al., 2014; Hedberg et al., 2014; Markello et al., 2015; Walter et al., 2015; Harris et al., 2017; Noury et al., 2017) is commonly seen in TAM/STRMK patients. In accordance, the TAM/STRMK mouse model harboring the most common STIM1 GoF mutation R304W also features an upward gaze paresis (Silva-Rojas et al., 2019).

Skin Anomalies and Enamel Defects

Skin forms the first defense barrier to protect from external agents, and also plays a pivotal role in thermoregulation by sweat production. Keratinocytes are the principal components of the outermost skin layer, the epidermis, and their growth, differentiation, and migration is driven by SOCE in both humans and mice (Numaga-Tomita and Putney, 2013; Vandenberghe et al., 2013). SOCE also triggers the opening of the Ca^{2+}-activated chloride channel TMEM16A in the sweat glands, and thereby enables chloride secretion and sweat production (Concepcion et al., 2016). In the absence of SOCE, CRAC channelopathy patients present with thermoregulatory instability and anhidrosis accompanied by heat intolerance, dry skin, and eczema (Feske et al., 2006; Fuchs et al., 2012; Schaballie et al., 2015; Lian et al., 2018). Skin anomalies including eczema and ichthyosis are also commonly seen in TAM/STRMK patients (Misceo et al., 2014; Morin et al., 2014, 2020; Bohm et al., 2017; Harris et al., 2017; Claeys et al., 2020), and one patient additionally manifested anhidrosis (Ishitsuka et al., 2019). Histological examinations of the skin biopsy revealed an obstruction of the spiral duct in the eccrine gland, the acrosyringia, resulting in sweat retention. This is different from CRAC channelopathy patients, where the sweat glands display a reduced lumen due the lack of sweat production (Lian et al., 2018). Noteworthy, the ectodermal barrier protein proflaggrin was found to be aggregated in the acrosyringia of the TAM/STRMK patient. Loss of proflaggrin is a major predisposing factor of idiopathic ichthyosis (Palmer et al., 2006), indicating that the skin phenotype in TAM/STRMK patients may be a direct consequence of the abnormal proflaggrin accumulation in the sweat glands.

TABLE 1 | Descriptive comparison of the clinical signs and physiological defects in CRAC channelopathy and TAM/STRMK patients and mouse models.

		CRAC channelopathy Reduced SOCE		TAM/STRMK Increased SOCE	
		Mouse models	**Patients**	**Patients**	**Mouse models**
Eye	Pupils	Not reported	Mydriasis	Miosis	Not reported
	Eye movement	Not reported	Not reported	Upward/lateral gaze paresis	Upward gaze paresis (*Stim1*$^{R304W/+}$)
Ectodermal tissues	Skin	Thin skin (*Orai1*$^{-/-}$), anhidrosis (*Orai1*$^{-/-}$, *Stim1*$^{-/-}$*Stim2*$^{-/-}$)	Anhidrosis	Anhidrosis, ichthyosis	Thick dermis, reduced subcutaneous fat layer (*Stim1*$^{R304W/+}$)
	Teeth	Reduced enamel mineralization (*Orai1*$^{-/-}$)	Amelogenesis imperfecta	Enamel hypocalcification	Subgingival hair growth (*Stim1*$^{R304W/+}$)
Bones	Clinical signs	Not reported	Facial dysmorphism	Short stature brachydactyly, syndactyly, Klippel-Feil anomaly	Small size (*Stim1*$^{R304W/+}$), reduced number of ribs (*Stim1*$^{R304W/R304W}$), thin and compact bones (*Stim1*$^{R304W/R304W}$)
	Molecular findings	Reduced osteoblastogenesis and osteoclastogenesis, osteopenia (*Orai1*$^{-/-}$)	Osteopetrosis, reduced osteoclasteogenesis	Osteopenia, increased osteoclasteogenesis	Reduced cellular density, reduced bone marrow area (*Stim1*$^{R304W/+}$)
Immune system	Clinical signs	Autoimmunity, splenomegaly (*Stim1*$^{-/-}$*Stim2*$^{-/-}$, *Orai1*$^{R93W/R93W}$)	Recurrent and chronic infections, autoimmunity, splenomegaly	Hyposplenism	Splenomegaly (*Stim1*$^{D84G/+}$, *Stim1*$^{I115F/+}$ and *Stim1*$^{R304W/+}$)
	Molecular findings	Reduced cytokine expression (*Stim1*$^{-/-}$, *Orai1i*$^{-/-}$, *Stim1*$^{-/-}$*Stim2*$^{-/-}$, *Orai1*$^{R93W/R93W}$), reduced suppressive function of NKT and Treg cells (*Stim1*$^{-/-}$*Stim2*$^{-/-}$, *Orai1*$^{R93W/R93W}$)	Reduced T cell proliferation, cytokine expression, immunoglobulin production, iNKT and Treg cells, presence of anti-platelet autoantibodies	Lymphoproliferation, presence of anti-platelet autoantibodies	Reduced Treg and NK cells, increased neutrophils and monocytes (*Stim1*$^{R304W/+}$)
Coagulation	Clinical signs	Slightly increased bleeding time (*Stim1*$^{-/-}$, *Orai1*$^{-/-}$)	Mild bleeding diathesis	Bleeding diathesis	Increased bleeding time (*Stim1*$^{D84G/+}$)
	Molecular findings	Reduced platelet activation (*Stim1*$^{-/-}$, *Orai1*$^{-/-}$, *Stim1*$^{-/-}$*Orai1*$^{-/-}$, *Orai1*$^{R93W/R93W}$), reduced thrombus formation (*Stim1*$^{-/--}$, *Orai1*$^{-/-}$, *Stim1*$^{-/-}$*Orai1*$^{-/-}$)	Reduced platelet activation, reduced thrombus formation	Thrombocytopenia, Platelet pre-activation, aberrant size and morphology, reduced platelet-platelet adhesion	Thrombocytopenia (*Stim1*$^{D84G/+}$, *Stim1*$^{I115F/+}$, *Stim1*$^{R304W/+}$), platelet pre-activation, increased platelet clearance (*Stim1*$^{D84G/+}$)
Skeletal muscle	Clinical signs	Muscle weakness (*Stim1*$^{-/-}$, *Orai1*$^{-/-}$), increased fatigue (*Stim1*$^{-/-}$, *Orai1*$^{-/-}$)	Neonatal hypotonia, muscle weakness	Muscle weakness, cramps, myalgia	Muscle weakness, increased resistance to fatigue (*Stim1*$^{I115F/+}$, *Stim1*$^{R304W/+}$)
	Molecular findings	Fiber atrophy, swollen mitochondria (*Stim1*$^{-/-}$, *Orai1*$^{-/-}$)	Type I predominance, type II fiber atrophy	Tubular aggregates, type I fiber predominance, type II fiber atrophy, internalized nuclei, vacuoles, fibrosis, elevated serum CK	Fiber atrophy and degeneration, type I fiber predominance, swollen mitochondria, elevated serum CK (*Stim1*$^{I115F/+}$, *Stim1*$^{R304W/+}$)

Alike skin and sweat glands, teeth derive from the ectoderm, and CRAC channelopathy patients also manifest dental maturation defects including major enamel loss, discoloration and poor mineralization of both deciduous and permanent teeth (Feske et al., 2006; McCarl et al., 2009; Picard et al., 2009; Fuchs et al., 2012; Wang et al., 2014; Schaballie et al., 2015; Lian et al., 2018), highlighting the importance of SOCE in ameloblast formation and mineralization (Wang et al., 2014). In contrast, amelogenesis imperfecta is not a typical feature of TAM/STRMK, and enamel hypocalcification was only noted in a single patient (Noury et al., 2017).

CRAC channelopathy and TAM/STRMK animal models partially recapitulate the human enamel and skin phenotypes. Mice lacking ORAI1 manifest reduced enamel mineralization (Robinson et al., 2012) and thinner skin with elongated keratinocytes and smaller vibrissae follicles (Gwack et al., 2008), and the ectodermal-specific knockout of *Orai1* or *Stim1*/*Stim2* impairs SOCE and results in anhidrosis and a reduced sweat gland lumen (Concepcion et al., 2016). The TAM/STRMK mouse harboring the STIM1 R304W mutation shows a thickened dermis and a reduction of the subcutaneous fat layer (Silva-Rojas et al., 2019), and a subset of the animals additionally exhibit subgingival hair growth on the lower incisors (Gamage et al., 2020).

Bone Anomalies

Bones represent 15% of the total body weight and are essential for motion, mineral storage, and hematopoiesis. Bone deposition and resorption are dynamic and balanced processes driven by bone-forming osteoblasts and bone-resorbing osteoclasts (Florencio-Silva et al., 2015), and their growth and differentiation is regulated by SOCE-dependent Ca^{2+} homeostasis (Eapen et al., 2010; Blair et al., 2011; Chen et al., 2018). Bone resorption by osteoclasts generates a local increment of extracellular Ca^{2+}, inducing the activation of the calcineurin/NFAT signaling pathway, and resulting in osteoblastogenesis (Zayzafoon, 2006). Calcineurin/NFAT signaling is also essential for osteoclastogenesis and T cell activation, and the inhibition of this pathway with cyclosporine A to prevent transplant rejection is associated with an increased incidence of bone fractures (Zayzafoon, 2006).

Overt bone anomalies are largely absent in CRAC channelopathy and TAM/STRMK patients with exception of individual cases with facial dysmorphism (McCarl et al., 2009), fusion of the cervical vertebrae (Klippel-Feil anomaly) (Morin et al., 2020), brachydactyly (Morin et al., 2020), or syndactyly of the second and third toes (Borsani et al., 2018). Bone mineralization was found to be increased in two CRAC channelopathy patients (osteopetrosis) and decreased in a single TAM/STRMK patient (osteopenia), and accordingly, functional studies demonstrated a decreased osteoclastogenesis in bone marrow mononuclear macrophages from the CRAC channelopathy patients, and an increased osteoclastogenesis in cells derived from the TAM/STRMK patient (Huang et al., 2020). Of note, a number of TAM/STRMK patients exhibit a short stature (Misceo et al., 2014; Morin et al., 2014, 2020; Noury et al., 2017; Borsani et al., 2018), and other more subtle or late-onset bone disorders might have been overlooked in CRAC channelopathy and TAM/STRMK patients. This is supported by the impaired differentiation and function of osteoblasts and osteoclasts leading to osteopenia with decreased bone density and trabecular bone volume in ORAI1-deficient mice (Hwang et al., 2012; Robinson et al., 2012). Alike patients, TAM/STRMK mice are smaller than their littermates, and micro-CT analyses revealed a decreased cellular density and a reduced bone marrow area in femur and tibia, potentially affecting bone strength and stiffness (Silva-Rojas et al., 2019). Surviving mice carrying the STIM1 R304W mutation at the homozygous state show a more severe skeletal phenotype with thinner and more compact bones, and also feature a reduced number of ribs (Gamage et al., 2020).

Immune System and Spleen Anomalies

The immune system is an essential and complex defense network, and SOCE directs the fate and function of diverse cells of the innate and adaptive immune system, including dendritic cell maturation (Felix et al., 2013), neutrophil activation (Zhang et al., 2014), lymphocyte cytotoxicity and cytokine production (Maul-Pavicic et al., 2011), as well as T cell proliferation, differentiation, and metabolism (Vaeth et al., 2017; Vaeth and Feske, 2018). T cells play a pivotal role in the adaptive immune system and act as effector, memory, suppressor, or helper cells in response to external agents. The antigen recognition by the T cell receptors activates a signaling cascade resulting in the continuous depletion of the reticular Ca^{2+} stores and a durable extracellular Ca^{2+} entry via SOCE to initiate the Ca^{2+}-dependent transcriptional program necessary for T cell function (Feske, 2007).

Recurrent infections and autoimmunity are the predominant clinical traits of CRAC channelopathy (Feske et al., 2006; McCarl et al., 2009; Picard et al., 2009; Byun et al., 2010; Fuchs et al., 2012; Wang et al., 2014; Chou et al., 2015; Lacruz and Feske, 2015; Schaballie et al., 2015; Badran et al., 2016; Lian et al., 2018), and hematological examinations of affected individuals revealed normal levels of T cells, while functional investigations detected a reduced T cell proliferation and cytokine expression, and an impaired production of immunoglobulins in response to antigens (Feske et al., 1996, 2006; Fuchs et al., 2012; Lian et al., 2018). Invariant natural killer T cells (iNKT) and/or regulatory T cells (Treg) were reduced (Schaballie et al., 2015; Badran et al., 2016; Lian et al., 2018), suggesting a defect in self-tolerance as in autoimmune disorders (Dejaco et al., 2006; Novak and Lehuen, 2011; Josefowicz et al., 2012). In accordance with the immune cell dysregulation in patients, cytokine expression is impaired in mice with T CD4+ cell-specific deletion of *Stim1* or *Orai1*, and chimeric $Orai1^{R93W/R93W}$ animals (corresponding to R91W in humans) and *Stim1* and *Stim2* double knockout mice additionally show a reduced suppressive function of Treg and NKT cells and an associated autoimmunity and splenomegaly (Gwack et al., 2008; Oh-Hora et al., 2008, 2013; McCarl et al., 2010).

The spleen is the largest lymphoid organ and functions as a blood filter, and ensures the biogenesis and storage of white and red blood cells, as well as the phagocytosis of circulating microorganisms (de Porto et al., 2010). CRAC channelopathy patients develop hepatosplenomegaly (Picard et al., 2009; Byun et al., 2010; Schaballie et al., 2015; Lian et al., 2018), while asplenia or hyposplenia is a clinical hallmark of TAM/STRMK (Morin

et al., 2020). As an indication of abnormal spleen function, Howell-Jolly bodies have moreover been found on peripheral blood film in several affected individuals (Misceo et al., 2014; Morin et al., 2014; Markello et al., 2015; Harris et al., 2017; Noury et al., 2017), but an increased rate of infections has nevertheless not been reported. Contrasting the patients, the TAM/STRMK mouse models present with splenomegaly, and histological investigations of the spleen revealed megakaryocyte hypoplasia (Grosse et al., 2007; Silva-Rojas et al., 2019). This is possibly related to a physiological difference between both species, as hematopoiesis lowers with age in humans, while it is maintained throughout life in mice (Bronte and Pittet, 2013). Of note, hematological analyses disclosed abnormal B, NK, and Treg counts in the STIM1 R304W mouse (Silva-Rojas et al., 2019), indicating that disturbances of the immune system may also occur in TAM/STRMK patients and potentially contribute to the spleen, platelet, and skin anomalies. This is sustained by the detection of lymphoproliferation and circulating antibodies against platelets in a single patient with STIM1 R304W mutation (Sura et al., 2020).

Coagulation Defects

Hemostasis prevents and stops bleeding through the formation of a thrombus, which is ultimately resolved in the process of wound healing. Platelets play an essential role in thrombus formation, and the activation of platelets is induced by the presence of the subcortical component collagen in the blood flow following vessel wall damage (Bye et al., 2016). The collagen fragments bind to glycoprotein VI (GPVI) at the surface of the platelets and trigger a signaling cascade involving SOCE and leading to the Ca^{2+}-dependent exposure of phosphatidylserine (PS) and the secretion of alpha granules containing thrombotic factors (Berna-Erro et al., 2016; van der Meijden and Heemskerk, 2019), which will then prompt the coagulation process and modulate inflammation and angiogenesis in the injured area (Blair and Flaumenhaft, 2009).

As a result of SOCE deficiency, PS exposure and alpha granule secretion is reduced in platelets from CRAC channelopathy patients, impeding platelet aggregation and thrombus formation (Nakamura et al., 2013). In consequence of the overall reduction of Treg cells, high titers of anti-platelet autoantibodies are detectable in the serum of the patients, lead to hemolytic anemia, and contribute to mild or intermittent susceptibility to bleed in several affected individuals (Picard et al., 2009; Byun et al., 2010; Fuchs et al., 2012; Lian et al., 2018). Bleeding diathesis associated with thrombocytopenia is a major clinical feature of TAM/STRMK (Misceo et al., 2014; Morin et al., 2014, 2020; Nesin et al., 2014; Markello et al., 2015; Bohm et al., 2017; Harris et al., 2017; Noury et al., 2017; Alonso-Jimenez et al., 2018; Borsani et al., 2018; Li et al., 2019; Claeys et al., 2020; Sura et al., 2020), and the analysis of blood samples from patients revealed increased platelet activation markers and enhanced secretion of alpha granules in unstimulated platelets (Misceo et al., 2014). Despite this pre-activation state caused by elevated resting Ca^{2+}, the platelet-platelet adhesion is impaired, and platelets often appeared with aberrant size and morphology (Markello et al., 2015), suggesting that the coagulation defect in TAM/STRMK patients results from a combination of platelet loss and platelet dysfunction.

In analogy to CRAC channelopathy patients, PS exposure and secretion of alpha granules is diminished in mice with platelet-specific deletion of *Stim1* and in chimeric $Orai1^{R93W/R93W}$ animals (Bergmeier et al., 2009; Ahmad et al., 2011). Chimeric $Stim1^{-/-}$ and $Orai1^{-/-}$ mice additionally show impaired platelet aggregation and thrombus formation, leading to a slight increase in bleeding time (Varga-Szabo et al., 2008; Braun et al., 2009; Gilio et al., 2010). The murine TAM/STRMK models similarly recapitulate the coagulation defects seen in the patients, as thrombocytopenia is evident in all three STIM1 D84G, I115F, and R304W models (Grosse et al., 2007; Cordero-Sanchez et al., 2019; Silva-Rojas et al., 2019). Further analyses on the STIM1 D84G mice uncovered that the pre-activation state of the platelets increases platelet clearance, and thereby prevents efficient platelet aggregation (Grosse et al., 2007). If and to what extent the bleeding diathesis is exacerbated by the immune system defects in TAM/STRMK mice and potentially in patients remains to be determined.

Muscle Weakness

Skeletal muscles maintain posture and allow movements under the voluntary control of the somatic nervous system, and also regulate body temperature and nutrition storage. SOCE activation and extracellular Ca^{2+} entry is significantly faster in myofibers compared with other cell types, occurring within milliseconds after each action potential (Launikonis et al., 2009; Edwards et al., 2010). This is believed to be related to the presence of the muscle-specific STIM1L isoform forming pre-activated Ca^{2+} entry units with ORAI1 at the SR/plasma membrane junction (Darbellay et al., 2011). Refilling of the Ca^{2+} stores is mediated by the ATP-dependent SERCA pumps to maintain high Ca^{2+} gradients across the SR membrane, thus limiting the SR depletion of Ca^{2+} during repetitive tetanic stimulations (Pan et al., 2002; Zhao et al., 2005).

CRAC channelopathy patients manifest neonatal hypotonia and generalized muscle weakness, and show delayed motor milestones and reduced walking distance in infancy, with additional respiratory insufficiency in individual cases (Feske et al., 2006; McCarl et al., 2009; Picard et al., 2009; Fuchs et al., 2012; Chou et al., 2015; Schaballie et al., 2015; Badran et al., 2016; Lian et al., 2018). Histological investigations were performed on muscle biopsies from two patients, and revealed fiber type I fiber predominance and type II atrophy (McCarl et al., 2009; Lian et al., 2018). Muscle weakness and exercise intolerance are primary clinical features of TAM/STRMK, and the onset and severity depend on the causative gene and correlate with the position of the mutation (Morin et al., 2020). In most cases, disease onset is during infancy or childhood, and first and foremost affects the proximal muscles of the lower limbs. Muscle weakness is generally accompanied by elevated serum creatine kinase (CK) levels, indicating moderate fiber degeneration, and myalgia and cramps are often observed as secondary features, but can also occur as isolated signs (Bohm et al., 2013; Bohm et al., 2014, 2017, 2018; Hedberg et al., 2014; Misceo et al., 2014; Morin et al., 2014, 2020; Nesin et al., 2014;

Endo et al., 2015; Markello et al., 2015; Walter et al., 2015; Barone et al., 2017; Garibaldi et al., 2017; Harris et al., 2017; Noury et al., 2017; Alonso-Jimenez et al., 2018; Borsani et al., 2018; Li et al., 2019; Claeys et al., 2020). Noteworthy, Ca^{2+} overload in skeletal muscle fibers has been shown to disrupt excitation-contraction coupling (ECC) (Lamb et al., 1995), which possibly contributes to the reduced muscle force in TAM/STRMK patients. Muscle sections from affected individuals typically show tubular aggregates appearing in red on Gomori trichrome staining, and adopting a honeycomb structure of densely packed tubules on electron microscopy (Chevessier et al., 2004, 2005; Bohm and Laporte, 2018). The tubular aggregates are highly Ca^{2+}-rich, and immunofluorescence studies have shown that they essentially contain SR proteins such as STIM1, calsequestrin, triadin, or RyR1, indicating that they are of reticular origin (Chevessier et al., 2004, 2005; Bohm et al., 2013, 2017; Endo et al., 2015). It has been suggested that the abundance of Ca^{2+} in muscle fibers may cause SR protein misfolding and aggregation, leading to the formation of membrane stacks as precursors of tubular aggregates (Morin et al., 2020). Alternatively, the occurrence of tubular aggregates may reflect the attempt to regenerate a functional triad, a specialized membrane complex in skeletal muscle hosting the ECC machinery. This is supported by the observation that Ca^{2+} excess induces the proteolysis of junctophilins, which tether the SR membrane to deep plasma membrane invaginations known as T-tubules to form the triad (Murphy et al., 2013). Further histopathological signs on TAM/STRMK biopsies encompass fiber size variability, type I fiber predominance, type II fiber atrophy, internalized nuclei, vacuoles, and fibrosis (Bohm et al., 2013, 2014, 2017, 2018; Hedberg et al., 2014; Morin et al., 2014, 2020; Nesin et al., 2014; Endo et al., 2015; Markello et al., 2015; Walter et al., 2015; Harris et al., 2017; Noury et al., 2017; Borsani et al., 2018; Li et al., 2019; Claeys et al., 2020).

Stim1 KO and *Orai1* KO Mice die perinatally (Baba et al., 2008; Gwack et al., 2008; Oh-Hora et al., 2008), and the muscle-specific invalidation of either gene results in diminished cellular Ca^{2+} transients following stimulation, and interferes with muscle contractility and the production of force (Stiber et al., 2008; Li et al., 2012; Wei-Lapierre et al., 2013; Carrell et al., 2016). The mice also show an increased susceptibility to fatigue (Stiber et al., 2008; Wei-Lapierre et al., 2013; Carrell et al., 2016), and histological and ultrastructural investigations of muscle samples uncovered a reduction in fiber size and overall muscle mass, and swollen mitochondria (Stiber et al., 2008; Li et al., 2012; Wei-Lapierre et al., 2013; Carrell et al., 2016). The STIM1 I115F and R304W TAM/STRMK mouse models exhibit reduced muscle force (Cordero-Sanchez et al., 2019; Silva-Rojas et al., 2019), and continuous muscle stimulation evidenced a slower force decay compared with WT littermates, presumably reflecting an increased resistance to fatigue (Silva-Rojas et al., 2019). The animals exhibit elevated serum CK levels, and histological examinations of muscle samples revealed an increased proportion of type I fibers, an overall reduction of fiber diameter with signs of muscle fiber degeneration and regeneration, and electron microscopy uncovered swollen mitochondria (Cordero-Sanchez et al., 2019; Silva-Rojas et al., 2019). Most strikingly, tubular aggregates are absent from muscles in both murine TAM/STRMK models, highlighting a major structural difference between human and mouse muscle pathologies despite the concordance of the overall clinical picture. Considering the observation that dystrophic signs are more prominent in TAM/STRMK mice than in patients, the tubular aggregates may protect the human muscle fibers from degeneration by bundling excessive free Ca^{2+}. Another STIM1 R304W mouse model does not show functional or structural skeletal muscle aberrations (Gamage et al., 2018), and a potential muscle phenotype of the STIM1 D84G mouse was not assessed (Grosse et al., 2007).

SOCE REGULATORS, ASSOCIATED DISEASES AND ANIMAL MODELS

Ca^{2+} controls a multitude of metabolic processes, signaling pathways, and cellular functions including transcription, proliferation, differentiation, and exocytosis. As a major regulator of Ca^{2+} homeostasis, SOCE takes a central role in the physiology of all tissues and organs, and needs to be adaptable to the Ca^{2+} sensitivity and Ca^{2+} balance of the individual cell types forming an organism.

The STIM1 homologue STIM2 has been shown to modulate SOCE activity (Darbellay et al., 2011; Miederer et al., 2015), and several additional regulators either promoting or restricting extracellular Ca^{2+} entry are known. Positive effectors encompass CRACR2A and septins, facilitating STIM1-ORAI1 coupling (Srikanth et al., 2010; Sharma et al., 2013), STIMATE, favoring STIM1 clustering (Jing et al., 2015), and the inositol triphosphate receptor (IP_3R), lowering the local Ca^{2+} levels in proximity to the STIM1 EF hands (Sampieri et al., 2018). Negative regulators include SARAF and calsequestrin, both hampering STIM1 oligomerization (Palty et al., 2012; Jha et al., 2013; Wang et al., 2015), Golli-MBP, binding and dispersing the STIM1-ORAI1 complex (Feng et al., 2006; Walsh et al., 2010), ORMLD3, fostering STIM1-ORAI1 uncoupling following Ca^{2+} influx (Carreras-Sureda et al., 2013), and ALG2, ALG14, DPAGT1, GFPT1, and GMPPB, all mediating post-translational modifications repressing the activity of STIM1 and ORAI1 (Belaya et al., 2012, 2015; Guergueltcheva et al., 2012; Cossins et al., 2013). To date, IP_3R, calsequestrin, ALG2, ALG14, DPAGT1, GFPT1, and GMPPB have been associated with human pathologies, suggesting that mutations in the other SOCE regulators may similarly impact on Ca^{2+} homeostasis and cause CRAC channelopathy, TAM/STRMK, or related disorders. It is, however, possible that potential physiological anomalies remain within the normal range of tissue and organ functionality due to a marginal effect on the intracellular Ca^{2+} balance, and are therefore hardly detectable.

LoF mutations in *ITPR1*, encoding IP_3R type 1, cause Gillepsie syndrome (GLSP), characterized by muscular hypotonia, mydriasis, ataxia, and intellectual disability (Gerber et al., 2016), and *Itpr1*-null mice manifest severe ataxia and epileptic seizures (Matsumoto et al., 1996). Mutations in *ITPR2* and *ITRP3*, respectively, encoding IP_3R types 2 and 3, are associated with

anhidrosis in patients (Klar et al., 2014; Kerkhofs et al., 2018), and the same phenotype is also observed in *Itpr2* and *Itpr3* double knockout mice (Futatsugi et al., 2005). This is in accordance with the idea that the reduction of SOCE through the loss of the positive effector IP_3R results in a clinical phenotype resembling CRAC channelopathy. In the same line, *STING* GoF mutations are found in patients with systemic inflammatory syndrome and autoimmunity (Jeremiah et al., 2014), and a mouse model carrying a patient mutation recapitulates the clinical signs (Bouis et al., 2019). STING is a signaling adaptor residing in the ER, and is retained in an inactive state through direct interaction with STIM1. In response to DNA pathogens, STING translocates to the ER-Golgi intermediate compartment to trigger an interferon response through the STING-TBK1-IRF3 pathway (Ishikawa and Barber, 2008, 2011). Loss of STIM1 in mouse and human CRAC channelopathy cell lines induces a spontaneous activation of STING and an enhanced expression of type 1 interferons under sterile conditions, thereby stimulating the immune system even in the absence of pathogens (Srikanth et al., 2019).

Calsequestrin (CASQ1) is the major Ca^{2+} buffering protein in the sarcoplasmic reticulum in skeletal muscle, and polymerizes with increasing luminal Ca^{2+} concentrations (Manno et al., 2017). In turn, Ca^{2+} store depletion promotes depolymerization, and the calsequestrin monomers sequester STIM1 and hence negatively regulate SOCE (Wang et al., 2015). Specific missense mutations in *CASQ1* interfere with the polymerization and depolymerization dynamics of calsequestrin, lower the Ca^{2+} buffer capacities of the reticulum and impair calsequestrin monomerization, leading to an increase in SOCE activity (Barone et al., 2017; Bohm et al., 2018). As calsequestrin expression is restricted to skeletal muscle, patients with *CASQ1* mutations show a mild form of TAM/STRMK with late-onset muscle weakness, myalgia, and abundant tubular aggregates, but without additional multi-systemic signs (Bohm and Laporte, 2018; Bohm et al., 2018). A murine model harboring a *CASQ1* mutation found in patients does not exist, and the total loss of calsequestrin generates a malignant hyperthermia phenotype with an increased risk of sudden death in mice (Protasi et al., 2009). Noteworthy, CASQ1 null mice show an increased expression of STIM1 and ORAI1 associated with enhanced SOCE activity, possibly reflecting a compensatory mechanism to ensure the maintenance of contractile force despite the reduction of bound and releasable Ca^{2+} in the SR (Michelucci et al., 2020). Tubular aggregates containing STIM1 and calsequestrin are also seen on muscle biopsies from patients with limb-girdle congenital myasthenic syndrome (LG-CMS), marked by fluctuating muscle weakness and fatigability (Evangelista et al., 2015). LG-CMS is caused by the impaired transmission at the neuromuscular junction, the relay between motor neuron and muscle fiber, and results from LoF mutations in *ALG2*, *ALG14*, *DPAGT1*, *GFPT1*, or *GMPP8* (Belaya et al., 2012, 2015; Guergueltcheva et al., 2012; Cossins et al., 2013). All five genes code for proteins of the glycosylation pathway and procure posttranslational modifications to a wide variety of proteins including STIM1 and ORAI1. Hypoglycosylation of STIM1 and ORAI1 stimulates SOCE and extracellular Ca^{2+} influx (Selcen et al., 2014), and the muscle-specific deletion of *Gfpt1* in mice causes myasthenia and the occurrence of tubular aggregates in muscle fibers (Issop et al., 2018). These examples show that the dysfunction of proteins directly or indirectly associated with STIM1 and ORAI1 can cause human pathologies overlapping with TAM/STRMK at the clinical and histological level.

CONCLUSION AND PERSPECTIVES

LoF mutations in *STIM1* and *ORAI1* impair SOCE and cause CRAC channelopathy, while GoF mutations in both genes involve SOCE over-activation and result in TAM/STRMK (Lacruz and Feske, 2015; Bohm and Laporte, 2018). In agreement with the opposite mutational effects and pathomechanisms leading to either CRAC channelopathy or TAM/STRMK, both disorders by and large show clinical mirror phenotypes affecting the eyes, bones, immune system, platelets, and skeletal muscle. While CRAC channelopathy is characterized by mydriasis, increased bone mineralization, immunodeficiency, splenomegaly, impaired platelet activation, and muscle hypotonia, TAM/STRMK patients typically present with miosis, decreased bone mineralization, hyposplenism, platelet pre-activation, and muscle cramping. A single TAM/STRMK patient was additionally diagnosed with lymphoproliferation (Sura et al., 2020), indicating an over-active immune system. Investigations on TAM/STRMK mouse models confirmed a dysregulation of various immune system cells, which may account for the skin phenotype in humans and mice (Silva-Rojas et al., 2019). It is interesting to note that the clinical anomalies of platelets and skeletal muscle are similar in CRAC channelopathy and TAM/STRMK patients despite the inverse pathogenic effect of *STIM1* and *ORAI1* LoF and GoF mutations at the molecular level, highlighting the importance of strict SOCE regulation for normal tissue physiology. Thrombus formation is impaired in both disorders and enhances the tendency to bleed following injury. This is due to the reduced activation of platelets in CRAC channelopathy (Nakamura et al., 2013), and results from the impaired adhesion between platelets in TAM/STRMK (Markello et al., 2015). Similarly, muscle weakness either arises from the incapacity to sustain a sufficient muscle tonus in the absence of Ca^{2+} store refill in CRAC channelopathy, or from cytosolic Ca^{2+} excess disrupting excitation-contraction coupling and/or restraining proper muscle relaxation in TAM/STRMK.

CRAC channelopathy and TAM/STRMK mouse models recapitulate the main clinical signs of the human disorders, and are valuable and powerful tools to understand the importance of Ca^{2+} balance and the impact of Ca^{2+} imbalance on eye, bones, enamel, skin, platelets, spleen, immune system, and skeletal muscle physiology. Patients are usually examined by specialized physicians with a major focus on the principal handicap, and additional phenotypic anomalies might be overlooked, especially in the context of multi-systemic disorders with mild to moderate involvement of specific tissues. In contrast, murine models generally undergo unbiased phenotyping and offer the possibility for a detailed analysis of all organs to provide an overview of the disease. As an example, the complete characterization

of the STIM1 R304W TAM/STRMK mouse model unveiled anomalies of the glucose metabolism, hepatic function, and the immune system (Silva-Rojas et al., 2019), which have not been described in patients yet, but might be of medical importance. Conversely, psychiatric diseases including confusion (Misceo et al., 2014; Harris et al., 2017), Capgras syndrome (Harris et al., 2017), and manic psychosis (Harris et al., 2017) have only been reported in individual TAM/STRMK cases, and thorough investigations on the mouse model might help to determine if these anomalies are disease-related or unrelated. Lastly, the mouse models faithfully recapitulating CRAC channelopathy and TAM/STRMK can serve for the assessment of therapeutic approaches, which may also be relevant for other Ca^{2+}-related disorders affecting the bones, platelets, spleen, immune system, or skeletal muscle.

AUTHOR CONTRIBUTIONS

RS-R and JB wrote the manuscript. All authors contributed to the article and approved the submitted version.

FUNDING

This work was supported by INSERM, CNRS, University of Strasbourg, Agence Nationale de la Recherche (ANR-10-LABX-0030-INRT) within the Investissements d'Avenir program (10-IDEX-0002), and Association Française contre les Myopathies (AFM 17088, 20323). RS-R was funded by a Fondation pour la Recherche Médicale doctoral fellowship (FRM, PLP20170939073).

REFERENCES

Agrawal, N., Venkiteswaran, G., Sadaf, S., Padmanabhan, N., Banerjee, S., and Hasan, G. (2010). Inositol 1,4,5-trisphosphate receptor and dSTIM function in *Drosophila* insulin-producing neurons regulates systemic intracellular calcium homeostasis and flight. *J. Neurosci.* 30, 1301–1313. doi: 10.1523/JNEUROSCI.3668-09.2010

Ahmad, F., Boulaftali, Y., Greene, T. K., Ouellette, T. D., Poncz, M., Feske, S., et al. (2011). Relative contributions of stromal interaction molecule 1 and CalDAG-GEFI to calcium-dependent platelet activation and thrombosis. *J. Thromb. Haemost.* 9, 2077–2086. doi: 10.1111/j.1538-7836.2011.04474.x

Alonso-Jimenez, A., Ramon, C., Dols-Icardo, O., Roig, C., Gallardo, E., Clarimon, J., et al. (2018). Corpus callosum agenesis, myopathy and pinpoint pupils: consider Stormorken syndrome. *Eur. J. Neurol.* 25, e25–e26. doi: 10.1111/ene.13545

Baba, Y., Nishida, K., Fujii, Y., Hirano, T., Hikida, M., and Kurosaki, T. (2008). Essential function for the calcium sensor STIM1 in mast cell activation and anaphylactic responses. *Nat. Immunol.* 9, 81–88. doi: 10.1038/ni1546

Badran, Y. R., Massaad, M. J., Bainter, W., Cangemi, B., Naseem, S. U., Javad, H., et al. (2016). Combined immunodeficiency due to a homozygous mutation in ORAI1 that deletes the C-terminus that interacts with STIM 1. *Clin. Immunol.* 166-167, 100–102. doi: 10.1016/j.clim.2016.03.012

Barone, V., Del, Re, V., Gamberucci, A., Polverino, V., Galli, L., et al. (2017). Identification and characterization of three novel mutations in the CASQ1 gene in four patients with tubular aggregate myopathy. *Hum. Mutat.* 38, 1761–1773. doi: 10.1002/humu.23338

Belaya, K., Finlayson, S., Slater, C. R., Cossins, J., Liu, W. W., Maxwell, S., et al. (2012). Mutations in DPAGT1 cause a limb-girdle congenital myasthenic syndrome with tubular aggregates. *Am. J. Hum. Genet.* 91, 193–201. doi: 10.1016/j.ajhg.2012.05.022

Belaya, K., Rodriguez Cruz, P. M., Liu, W. W., Maxwell, S., McGowan, S., Farrugia, M. E., et al. (2015). Mutations in GMPPB cause congenital myasthenic syndrome and bridge myasthenic disorders with dystroglycanopathies. *Brain* 138(Pt 9), 2493–2504. doi: 10.1093/brain/awv185

Bergmeier, W., Oh-Hora, M., McCarl, C. A., Roden, R. C., Bray, P. F., and Feske, S. (2009). R93W mutation in Orai1 causes impaired calcium influx in platelets. *Blood* 113, 675–678. doi: 10.1182/blood-2008-08-174516

Berna-Erro, A., Jardin, I., Smani, T., and Rosado, J. A. (2016). Regulation of platelet function by Orai, STIM and TRP. *Adv. Exp. Med. Biol.* 898, 157–181. doi: 10.1007/978-3-319-26974-0_8

Blair, H. C., Robinson, L. J., Huang, C. L., Sun, L., Friedman, P. A., Schlesinger, P. H., et al. (2011). Calcium and bone disease. *Biofactors* 37, 159–167. doi: 10.1002/biof.143

Blair, P., and Flaumenhaft, R. (2009). Platelet alpha-granules: basic biology and clinical correlates. *Blood Rev.* 23, 177–189. doi: 10.1016/j.blre.2009.04.001

Bohm, J., Bulla, M., Urquhart, J. E., Malfatti, E., Williams, S. G., O'Sullivan, J., et al. (2017). ORAI1 mutations with distinct channel gating defects in tubular aggregate myopathy. *Hum. Mutat.* 38, 426–438. doi: 10.1002/humu.23172

Bohm, J., Chevessier, F., Koch, C., Peche, G. A., Mora, M., Morandi, L., et al. (2014). Clinical, histological and genetic characterisation of patients with tubular aggregate myopathy caused by mutations in STIM1. *J. Med. Genet.* 51, 824–833. doi: 10.1136/jmedgenet-2014-102623

Bohm, J., Chevessier, F., Maues, De Paula, A., Koch, C., Attarian, S., et al. (2013). Constitutive activation of the calcium sensor STIM1 causes tubular-aggregate myopathy. *Am. J. Hum. Genet.* 92, 271–278. doi: 10.1016/j.ajhg.2012.12.007

Bohm, J., and Laporte, J. (2018). Gain-of-function mutations in STIM1 and ORAI1 causing tubular aggregate myopathy and Stormorken syndrome. *Cell Calc.* 76, 1–9. doi: 10.1016/j.ceca.2018.07.008

Bohm, J., Lornage, X., Chevessier, F., Birck, C., Zanotti, S., Cudia, P., et al. (2018). CASQ1 mutations impair calsequestrin polymerization and cause tubular aggregate myopathy. *Acta Neuropathol.* 135, 149–151. doi: 10.1007/s00401-017-1775-x

Borsani, O., Piga, D., Costa, S., Govoni, A., Magri, F., Artoni, A., et al. (2018). Stormorken syndrome caused by a p.*R304W* STIM1 mutation: the first italian patient and a review of the literature. *Front. Neurol.* 9:859. doi: 10.3389/fneur.2018.00859

Bouis, D., Kirstetter, P., Arbogast, F., Lamon, D., Delgado, V., Jung, S., et al. (2019). Severe combined immunodeficiency in stimulator of interferon genes (STING) V154M/wild-type mice. *J. Allergy Clin. Immunol.* 143, 712.e5–725.e5. doi: 10.1016/j.jaci.2018.04.034

Braun, A., Varga-Szabo, D., Kleinschnitz, C., Pleines, I., Bender, M., Austinat, M., et al. (2009). Orai1 (CRACM1) is the platelet SOC channel and essential for pathological thrombus formation. *Blood* 113, 2056–2063. doi: 10.1182/blood-2008-07-171611

Bronte, V., and Pittet, M. J. (2013). The spleen in local and systemic regulation of immunity. *Immunity* 39, 806–818. doi: 10.1016/j.immuni.2013.10.010

Bye, A. P., Unsworth, A. J., and Gibbins, J. M. (2016). Platelet signaling: a complex interplay between inhibitory and activatory networks. *J. Thromb. Haemost.* 14, 918–930. doi: 10.1111/jth.13302

Byun, M., Abhyankar, A., Lelarge, V., Plancoulaine, S., Palanduz, A., Telhan, L., et al. (2010). Whole-exome sequencing-based discovery of STIM1 deficiency in a child with fatal classic Kaposi sarcoma. *J. Exp. Med.* 207, 2307–2312. doi: 10.1084/jem.20101597

Carrell, E. M., Coppola, A. R., McBride, H. J., and Dirksen, R. T. (2016). Orai1 enhances muscle endurance by promoting fatigue-resistant type I fiber content but not through acute store-operated Ca2+ entry. *FASEB J.* 30, 4109–4119. doi: 10.1096/fj.201600621R

Carreras-Sureda, A., Cantero-Recasens, G., Rubio-Moscardo, F., Kiefer, K., Peinelt, C., Niemeyer, B. A., et al. (2013). ORMDL3 modulates store-operated calcium entry and lymphocyte activation. *Hum. Mol. Genet.* 22, 519–530. doi: 10.1093/hmg/dds450

Chen, Y., Ramachandran, A., Zhang, Y., Koshy, R., and George, A. (2018). The ER Ca(2+) sensor STIM1 can activate osteoblast and odontoblast differentiation in mineralized tissues. *Connect Tissue Res.* 59(Suppl. 1), 6–12. doi: 10.1080/03008207.2017.1408601

Chevessier, F., Bauche-Godard, S., Leroy, J. P., Koenig, J., Paturneau-Jouas, M., Eymard, B., et al. (2005). The origin of tubular aggregates in human myopathies. *J. Pathol.* 207, 313–323. doi: 10.1002/path.1832

Chevessier, F., Marty, I., Paturneau-Jouas, M., Hantai, D., and Verdiere-Sahuque, M. (2004). Tubular aggregates are from whole sarcoplasmic reticulum origin: alterations in calcium binding protein expression in mouse skeletal muscle during aging. *Neuromuscul. Disord.* 14, 208–216. doi: 10.1016/j.nmd.2003.11.007

Chou, J., Badran, Y. R., Yee, C. S., Bainter, W., Ohsumi, T. K., Al-Hammadi, S., et al. (2015). A novel mutation in ORAI1 presenting with combined immunodeficiency and residual T-cell function. *J. Allergy Clin. Immunol.* 136, 479.e1–482.e1. doi: 10.1016/j.jaci.2015.03.050

Claeys, T., Goosens, V., Race, V., Theys, T., Thal, D. R., Depuydt, C. E., et al. (2020). Clinical and muscle MRI features in a family with tubular aggregate myopathy and novel STIM1 mutation. *Neuromuscul. Disord.* 30, 709–718. doi: 10.1016/j.nmd.2020.07.010

Concepcion, A. R., Vaeth, M., Wagner, L. E. II, Eckstein, M., Hecht, L., Yang, J., et al. (2016). Store-operated Ca2+ entry regulates Ca2+-activated chloride channels and eccrine sweat gland function. *J. Clin. Invest.* 126, 4303–4318. doi: 10.1172/JCI89056

Cordero-Sanchez, C., Riva, B., Reano, S., Clemente, N., Zaggia, I., Ruffinatti, F. A., et al. (2019). A luminal EF-hand mutation in STIM1 in mice causes the clinical hallmarks of tubular aggregate myopathy. *Dis. Model Mech.* 13:dmm041111. doi: 10.1242/dmm.041111

Cossins, J., Belaya, K., Hicks, D., Salih, M. A., Finlayson, S., Carboni, N., et al. (2013). Congenital myasthenic syndromes due to mutations in ALG2 and ALG14. *Brain* 136(Pt 3), 944–956. doi: 10.1093/brain/awt010

Darbellay, B., Arnaudeau, S., Bader, C. R., Konig, S., and Bernheim, L. (2011). STIM1L is a new actin-binding splice variant involved in fast repetitive Ca2+ release. *J. Cell Biol.* 194, 335–346. doi: 10.1083/jcb.201012157

de Porto, A. P., Lammers, A. J., Bennink, R. J., ten Berge, I. J., Speelman, P., and Hoekstra, J. B. (2010). Assessment of splenic function. *Eur. J. Clin. Microbiol. Infect. Dis.* 29, 1465–1473. doi: 10.1007/s10096-010-1049-1

Dejaco, C., Duftner, C., Grubeck-Loebenstein, B., and Schirmer, M. (2006). Imbalance of regulatory T cells in human autoimmune diseases. *Immunology* 117, 289–300. doi: 10.1111/j.1365-2567.2005.02317.x

Eapen, A., Sundivakkam, P., Song, Y., Ravindran, S., Ramachandran, A., Tiruppathi, C., et al. (2010). Calcium-mediated stress kinase activation by DMP1 promotes osteoblast differentiation. *J. Biol. Chem.* 285, 36339–36351. doi: 10.1074/jbc.M110.145607

Ebashi, S. (1974). Regulatory mechanism of muscle contraction with special reference to the Ca-troponin-tropomyosin system. *Essays Biochem.* 10, 1–36.

Eckstein, M. K., Guerra-Carrillo, B., Miller Singley, A. T., and Bunge, S. A. (2017). Beyond eye gaze: what else can eyetracking reveal about cognition and cognitive development? *Dev. Cogn. Neurosci.* 25, 69–91. doi: 10.1016/j.dcn.2016.11.001

Edwards, J. N., Murphy, R. M., Cully, T. R., von Wegner, F., Friedrich, O., and Launikonis, B. S. (2010). Ultra-rapid activation and deactivation of store-operated Ca(2+) entry in skeletal muscle. *Cell Calc.* 47, 458–467. doi: 10.1016/j.ceca.2010.04.001

Endo, Y., Noguchi, S., Hara, Y., Hayashi, Y. K., Motomura, K., Miyatake, S., et al. (2015). Dominant mutations in ORAI1 cause tubular aggregate myopathy with hypocalcemia via constitutive activation of store-operated Ca(2)(+) channels. *Hum. Mol. Genet.* 24, 637–648. doi: 10.1093/hmg/ddu477

Evangelista, T., Hanna, M., and Lochmuller, H. (2015). Congenital myasthenic syndromes with predominant limb girdle weakness. *J. Neuromuscul. Dis.* 2(Suppl. 2), S21–S29. doi: 10.3233/JND-150098

Feldman, C. H., Grotegut, C. A., and Rosenberg, P. B. (2017). The role of STIM1 and SOCE in smooth muscle contractility. *Cell Calc.* 63, 60–65. doi: 10.1016/j.ceca.2017.02.007

Felix, R., Crottes, D., Delalande, A., Fauconnier, J., Lebranchu, Y., Le Guennec, J. Y., et al. (2013). The Orai-1 and STIM-1 complex controls human dendritic cell maturation. *PLoS One* 8:e61595. doi: 10.1371/journal.pone.0061595

Feng, J. M., Hu, Y. K., Xie, L. H., Colwell, C. S., Shao, X. M., Sun, X. P., et al. (2006). Golli protein negatively regulates store depletion-induced calcium influx in T cells. *Immunity* 24, 717–727. doi: 10.1016/j.immuni.2006.04.007

Feske, S. (2007). Calcium signalling in lymphocyte activation and disease. *Nat. Rev. Immunol.* 7, 690–702. doi: 10.1038/nri2152

Feske, S., Gwack, Y., Prakriya, M., Srikanth, S., Puppel, S. H., Tanasa, B., et al. (2006). A mutation in Orai1 causes immune deficiency by abrogating CRAC channel function. *Nature* 441, 179–185. doi: 10.1038/nature04702

Feske, S., Muller, J. M., Graf, D., Kroczek, R. A., Drager, R., Niemeyer, C., et al. (1996). Severe combined immunodeficiency due to defective binding of the nuclear factor of activated T cells in T lymphocytes of two male siblings. *Eur. J. Immunol.* 26, 2119–2126. doi: 10.1002/eji.1830260924

Florencio-Silva, R., Sasso, G. R., Sasso-Cerri, E., Simoes, M. J., and Cerri, P. S. (2015). Biology of bone tissue: structure, function, and factors that influence bone cells. *Biomed. Res. Int.* 2015:421746. doi: 10.1155/2015/421746

Fuchs, S., Rensing-Ehl, A., Speckmann, C., Bengsch, B., Schmitt-Graeff, A., Bondzio, I., et al. (2012). Antiviral and regulatory T cell immunity in a patient with stromal interaction molecule 1 deficiency. *J. Immunol.* 188, 1523–1533. doi: 10.4049/jimmunol.1102507

Futatsugi, A., Nakamura, T., Yamada, M. K., Ebisui, E., Nakamura, K., Uchida, K., et al. (2005). IP3 receptor types 2 and 3 mediate exocrine secretion underlying energy metabolism. *Science* 309, 2232–2234. doi: 10.1126/science.1114110

Gamage, T. H., Gunnes, G., Lee, R. H., Louch, W. E., Holmgren, A., Bruton, J. D., et al. (2018). STIM1 R304W causes muscle degeneration and impaired platelet activation in mice. *Cell Calc.* 76, 87–100. doi: 10.1016/j.ceca.2018.10.001

Gamage, T. H., Lengle, E., Gunnes, G., Pullisaar, H., Holmgren, A., Reseland, J. E., et al. (2020). STIM1 R304W in mice causes subgingival hair growth and an increased fraction of trabecular bone. *Cell Calc.* 85:102110. doi: 10.1016/j.ceca.2019.102110

Garibaldi, M., Fattori, F., Riva, B., Labasse, C., Brochier, G., Ottaviani, P., et al. (2017). A novel gain-of-function mutation in ORAI1 causes late-onset tubular aggregate myopathy and congenital miosis. *Clin. Genet.* 91, 780–786. doi: 10.1111/cge.12888

Gattineni, J. (2014). Inherited disorders of calcium and phosphate metabolism. *Curr. Opin. Pediatr.* 26, 215–222. doi: 10.1097/MOP.0000000000000064

Gerber, S., Alzayady, K. J., Burglen, L., Bremond-Gignac, D., Marchesin, V., Roche, O., et al. (2016). Recessive and dominant De Novo ITPR1 mutations cause gillespie syndrome. *Am. J. Hum. Genet.* 98, 971–980. doi: 10.1016/j.ajhg.2016.03.004

Gilio, K., van Kruchten, R., Braun, A., Berna-Erro, A., Feijge, M. A., Stegner, D., et al. (2010). Roles of platelet STIM1 and Orai1 in glycoprotein VI- and thrombin-dependent procoagulant activity and thrombus formation. *J. Biol. Chem.* 285, 23629–23638. doi: 10.1074/jbc.M110.108696

Grosse, J., Braun, A., Varga-Szabo, D., Beyersdorf, N., Schneider, B., Zeitlmann, L., et al. (2007). An EF hand mutation in Stim1 causes premature platelet activation and bleeding in mice. *J. Clin. Invest.* 117, 3540–3550. doi: 10.1172/JCI32312

Guergueltcheva, V., Muller, J. S., Dusl, M., Senderek, J., Oldfors, A., Lindbergh, C., et al. (2012). Congenital myasthenic syndrome with tubular aggregates caused by GFPT1 mutations. *J. Neurol.* 259, 838–850. doi: 10.1007/s00415-011-6262-z

Gwack, Y., Srikanth, S., Oh-Hora, M., Hogan, P. G., Lamperti, E. D., Yamashita, M., et al. (2008). Hair loss and defective T- and B-cell function in mice lacking ORAI1. *Mol. Cell Biol.* 28, 5209–5222. doi: 10.1128/MCB.00360-08

Harris, E., Burki, U., Marini-Bettolo, C., Neri, M., Scotton, C., Hudson, J., et al. (2017). Complex phenotypes associated with STIM1 mutations in both coiled coil and EF-hand domains. *Neuromuscul. Disord.* 27, 861–872. doi: 10.1016/j.nmd.2017.05.002

Hedberg, C., Niceta, M., Fattori, F., Lindvall, B., Ciolfi, A., D'Amico, A., et al. (2014). Childhood onset tubular aggregate myopathy associated with de novo STIM1 mutations. *J. Neurol.* 261, 870–876. doi: 10.1007/s00415-014-7287-x

Huang, Y., Li, Q., Feng, Z., and Zheng, L. (2020). STIM1 controls calcineurin/Akt/mTOR/NFATC2-mediated osteoclastogenesis induced by RANKL/M-CSF. *Exp. Therap. Med.* 20, 736–747. doi: 10.3892/etm.2020.8774

Hwang, S. Y., Foley, J., Numaga-Tomita, T., Petranka, J. G., Bird, G. S., and Putney, J. W. Jr. (2012). Deletion of Orai1 alters expression of multiple genes during osteoclast and osteoblast maturation. *Cell Calc.* 52, 488–500. doi: 10.1016/j.ceca.2012.10.001

Ishikawa, H., and Barber, G. N. (2008). STING is an endoplasmic reticulum adaptor that facilitates innate immune signalling. *Nature* 455, 674–678. doi: 10.1038/nature07317

Ishikawa, H., and Barber, G. N. (2011). The STING pathway and regulation of innate immune signaling in response to DNA pathogens. *Cell. Mol. Life Sci.* 68, 1157–1165. doi: 10.1007/s00018-010-0605-2

Ishitsuka, Y., Inoue, S., Furuta, J., Koguchi-Yoshioka, H., Nakamura, Y., Watanabe, R., et al. (2019). Sweat retention anhidrosis associated with tubular aggregate myopathy. *Br. J. Dermatol.* 181, 1104–1106. doi: 10.1111/bjd.18175

Issop, Y., Hathazi, D., Khan, M. M., Rudolf, R., Weis, J., Spendiff, S., et al. (2018). GFPT1 deficiency in muscle leads to myasthenia and myopathy in mice. *Hum. Mol. Genet.* 27, 3218–3232. doi: 10.1093/hmg/ddy225

Jeremiah, N., Neven, B., Gentili, M., Callebaut, I., Maschalidi, S., Stolzenberg, M. C., et al. (2014). Inherited STING-activating mutation underlies a familial inflammatory syndrome with lupus-like manifestations. *J. Clin. Invest.* 124, 5516–5520. doi: 10.1172/JCI79100

Jha, A., Ahuja, M., Maleth, J., Moreno, C. M., Yuan, J. P., Kim, M. S., et al. (2013). The STIM1 CTID domain determines access of SARAF to SOAR to regulate Orai1 channel function. *J. Cell Biol.* 202, 71–79. doi: 10.1083/jcb.201301148

Jing, J., He, L., Sun, A., Quintana, A., Ding, Y., Ma, G., et al. (2015). Proteomic mapping of ER-PM junctions identifies STIMATE as a regulator of Ca(2)(+) influx. *Nat. Cell Biol.* 17, 1339–1347. doi: 10.1038/ncb3234

Josefowicz, S. Z., Lu, L. F., and Rudensky, A. Y. (2012). Regulatory T cells: mechanisms of differentiation and function. *Annu. Rev. Immunol.* 30, 531–564. doi: 10.1146/annurev.immunol.25.022106.141623

Kerkhofs, M., Seitaj, B., Ivanova, H., Monaco, G., Bultynck, G., and Parys, J. B. (2018). Pathophysiological consequences of isoform-specific IP3 receptor mutations. *Biochim. Biophys. Acta Mol. Cell Res.* 1865(11 Pt B), 1707–1717. doi: 10.1016/j.bbamcr.2018.06.004

Klar, J., Hisatsune, C., Baig, S. M., Tariq, M., Johansson, A. C., Rasool, M., et al. (2014). Abolished InsP3R2 function inhibits sweat secretion in both humans and mice. *J. Clin. Invest.* 124, 4773–4780. doi: 10.1172/JCI70720

Lacruz, R. S., and Feske, S. (2015). Diseases caused by mutations in ORAI1 and STIM1. *Ann. N. Y. Acad. Sci.* 1356, 45–79. doi: 10.1111/nyas.12938

Lamb, G. D., Junankar, P. R., and Stephenson, D. G. (1995). Raised intracellular [Ca2+] abolishes excitation-contraction coupling in skeletal muscle fibres of rat and toad. *J. Physiol.* 489(Pt 2), 349–362. doi: 10.1113/jphysiol.1995.sp021056

Launikonis, B. S., Stephenson, D. G., and Friedrich, O. (2009). Rapid Ca2+ flux through the transverse tubular membrane, activated by individual action potentials in mammalian skeletal muscle. *J. Physiol.* 587(Pt 10), 2299–2312. doi: 10.1113/jphysiol.2009.168682

Li, A., Kang, X., Edelman, F., and Waclawik, A. J. (2019). Stormorken syndrome: a rare cause of myopathy with tubular aggregates and dystrophic features. *J. Child Neurol.* 34, 321–324. doi: 10.1177/0883073819829389

Li, T., Finch, E. A., Graham, V., Zhang, Z. S., Ding, J. D., Burch, J., et al. (2012). STIM1-Ca(2+) signaling is required for the hypertrophic growth of skeletal muscle in mice. *Mol. Cell Biol.* 32, 3009–3017. doi: 10.1128/MCB.06599-11

Lian, J., Cuk, M., Kahlfuss, S., Kozhaya, L., Vaeth, M., Rieux-Laucat, F., et al. (2018). ORAI1 mutations abolishing store-operated Ca(2+) entry cause anhidrotic ectodermal dysplasia with immunodeficiency. *J. Allergy Clin. Immunol.* 142, 1297.e11–1310.e11. doi: 10.1016/j.jaci.2017.10.031

Manno, C., Figueroa, L. C., Gillespie, D., Fitts, R., Kang, C., Franzini-Armstrong, C., et al. (2017). Calsequestrin depolymerizes when calcium is depleted in the sarcoplasmic reticulum of working muscle. *Proc. Natl. Acad. Sci. U.S.A.* 114, E638–E647. doi: 10.1073/pnas.1620265114

Markello, T., Chen, D., Kwan, J. Y., Horkayne-Szakaly, I., Morrison, A., Simakova, O., et al. (2015). York platelet syndrome is a CRAC channelopathy due to gain-of-function mutations in STIM1. *Mol. Genet. Metab.* 114, 474–482. doi: 10.1016/j.ymgme.2014.12.307

Matsumoto, M., Nakagawa, T., Inoue, T., Nagata, E., Tanaka, K., Takano, H., et al. (1996). Ataxia and epileptic seizures in mice lacking type 1 inositol 1,4,5-trisphosphate receptor. *Nature* 379, 168–171. doi: 10.1038/379168a0

Maul-Pavicic, A., Chiang, S. C., Rensing-Ehl, A., Jessen, B., Fauriat, C., Wood, S. M., et al. (2011). ORAI1-mediated calcium influx is required for human cytotoxic lymphocyte degranulation and target cell lysis. *Proc. Natl. Acad. Sci. U.S.A.* 108, 3324–3329. doi: 10.1073/pnas.1013285108

McCarl, C. A., Khalil, S., Ma, J., Oh-hora, M., Yamashita, M., Roether, J., et al. (2010). Store-operated Ca2+ entry through ORAI1 is critical for T cell-mediated autoimmunity and allograft rejection. *J. Immunol.* 185, 5845–5858. doi: 10.4049/jimmunol.1001796

McCarl, C. A., Picard, C., Khalil, S., Kawasaki, T., Rother, J., Papolos, A., et al. (2009). ORAI1 deficiency and lack of store-operated Ca2+ entry cause immunodeficiency, myopathy, and ectodermal dysplasia. *J. Allergy Clin. Immunol.* 124, 1311.e7–1318.e7. doi: 10.1016/j.jaci.2009.10.007

Michelucci, A., Boncompagni, S., Pietrangelo, L., Takano, T., Protasi, F., and Dirksen, R. T. (2020). Pre-assembled Ca2+ entry units and constitutively active Ca2+ entry in skeletal muscle of calsequestrin-1 knockout mice. *J. Gen. Physiol.* 152:e202012617. doi: 10.1085/jgp.202012617

Miederer, A. M., Alansary, D., Schwar, G., Lee, P. H., Jung, M., Helms, V., et al. (2015). A STIM2 splice variant negatively regulates store-operated calcium entry. *Nat. Commun.* 6:6899. doi: 10.1038/ncomms7899

Misceo, D., Holmgren, A., Louch, W. E., Holme, P. A., Mizobuchi, M., Morales, R. J., et al. (2014). A dominant STIM1 mutation causes Stormorken syndrome. *Hum. Mutat.* 35, 556–564. doi: 10.1002/humu.22544

Morin, G., Biancalana, V., Echaniz-Laguna, A., Noury, J. B., Lornage, X., Moggio, M., et al. (2020). Tubular aggregate myopathy and Stormorken syndrome: mutation spectrum and genotype/phenotype correlation. *Hum. Mutat.* 41, 17–37. doi: 10.1002/humu.23899

Morin, G., Bruechle, N. O., Singh, A. R., Knopp, C., Jedraszak, G., Elbracht, M., et al. (2014). Gain-of-function mutation in STIM1 (P.*R304W*) is associated with Stormorken Syndrome. *Hum. Mutat.* 35, 1221–1232. doi: 10.1002/humu.22621

Murphy, R. M., Dutka, T. L., Horvath, D., Bell, J. R., Delbridge, L. M., and Lamb, G. D. (2013). Ca2+-dependent proteolysis of junctophilin-1 and junctophilin-2 in skeletal and cardiac muscle. *J. Physiol.* 591, 719–729. doi: 10.1113/jphysiol.2012.243279

Nakamura, L., Sandrock-Lang, K., Speckmann, C., Vraetz, T., Buhrlen, M., Ehl, S., et al. (2013). Platelet secretion defect in a patient with stromal interaction molecule 1 deficiency. *Blood* 122, 3696–3698. doi: 10.1182/blood-2013-08-522037

Nesin, V., Wiley, G., Kousi, M., Ong, E. C., Lehmann, T., Nicholl, D. J., et al. (2014). Activating mutations in STIM1 and ORAI1 cause overlapping syndromes of tubular myopathy and congenital miosis. *Proc. Natl. Acad. Sci. U.S.A.* 111, 4197–4202. doi: 10.1073/pnas.1312520111

Noury, J. B., Bohm, J., Peche, G. A., Guyant-Marechal, L., Bedat-Millet, A. L., Chiche, L., et al. (2017). Tubular aggregate myopathy with features of Stormorken disease due to a new STIM1 mutation. *Neuromuscul. Disord.* 27, 78–82. doi: 10.1016/j.nmd.2016.10.006

Novak, J., and Lehuen, A. (2011). Mechanism of regulation of autoimmunity by iNKT cells. *Cytokine* 53, 263–270. doi: 10.1016/j.cyto.2010.11.001

Numaga-Tomita, T., and Putney, J. W. (2013). Role of STIM1- and Orai1-mediated Ca2+ entry in Ca2+-induced epidermal keratinocyte differentiation. *J. Cell Sci.* 126(Pt 2), 605–612. doi: 10.1242/jcs.115980

Oh-Hora, M., Komatsu, N., Pishyareh, M., Feske, S., Hori, S., Taniguchi, M., et al. (2013). Agonist-selected T cell development requires strong T cell receptor signaling and store-operated calcium entry. *Immunity* 38, 881–895. doi: 10.1016/j.immuni.2013.02.008

Oh-Hora, M., Yamashita, M., Hogan, P. G., Sharma, S., Lamperti, E., Chung, W., et al. (2008). Dual functions for the endoplasmic reticulum calcium sensors STIM1 and STIM2 in T cell activation and tolerance. *Nat. Immunol.* 9, 432–443. doi: 10.1038/ni1574

Palmer, C. N., Irvine, A. D., Terron-Kwiatkowski, A., Zhao, Y., Liao, H., Lee, S. P., et al. (2006). Common loss-of-function variants of the epidermal barrier protein filaggrin are a major predisposing factor for atopic dermatitis. *Nat. Genet.* 38, 441–446. doi: 10.1038/ng1767

Palty, R., Raveh, A., Kaminsky, I., Meller, R., and Reuveny, E. (2012). SARAF inactivates the store operated calcium entry machinery to prevent excess calcium refilling. *Cell* 149, 425–438. doi: 10.1016/j.cell.2012.01.055

Pan, Z., Yang, D., Nagaraj, R. Y., Nosek, T. A., Nishi, M., Takeshima, H., et al. (2002). Dysfunction of store-operated calcium channel in muscle cells lacking mg29. *Nat. Cell Biol.* 4, 379–383. doi: 10.1038/ncb788

Peacock, M. (2010). Calcium metabolism in health and disease. *Clin. J. Am. Soc. Nephrol.* 5(Suppl. 1), S23–S30. doi: 10.2215/CJN.05910809

Picard, C., McCarl, C. A., Papolos, A., Khalil, S., Luthy, K., Hivroz, C., et al. (2009). STIM1 mutation associated with a syndrome of immunodeficiency and autoimmunity. *N. Engl. J. Med.* 360, 1971–1980. doi: 10.1056/NEJMoa0900082

Prakriya, M., and Lewis, R. S. (2015). Store-operated calcium channels. *Physiol. Rev.* 95, 1383–1436. doi: 10.1152/physrev.00020.2014

Protasi, F., Paolini, C., and Dainese, M. (2009). Calsequestrin-1: a new candidate gene for malignant hyperthermia and exertional/environmental heat stroke. *J. Physiol.* 587(Pt 13), 3095–3100. doi: 10.1113/jphysiol.2009.171967

Robinson, L. J., Mancarella, S., Songsawad, D., Tourkova, I. L., Barnett, J. B., Gill, D. L., et al. (2012). Gene disruption of the calcium channel Orai1 results

in inhibition of osteoclast and osteoblast differentiation and impairs skeletal development. *Lab. Invest.* 92, 1071–1083. doi: 10.1038/labinvest.2012.72

Sampieri, A., Santoyo, K., Asanov, A., and Vaca, L. (2018). Association of the IP3R to STIM1 provides a reduced intraluminal calcium microenvironment, resulting in enhanced store-operated calcium entry. *Sci. Rep.* 8:13252. doi: 10.1038/s41598-018-31621-0

Schaballie, H., Rodriguez, R., Martin, E., Moens, L., Frans, G., Lenoir, C., et al. (2015). A novel hypomorphic mutation in STIM1 results in a late-onset immunodeficiency. *J. Allergy Clin. Immunol.* 136, 816.e4–819.e4. doi: 10.1016/j.jaci.2015.03.009

Selcen, D., Shen, X. M., Brengman, J., Li, Y., Stans, A. A., Wieben, E., et al. (2014). DPAGT1 myasthenia and myopathy: genetic, phenotypic, and expression studies. *Neurology* 82, 1822–1830. doi: 10.1212/WNL.0000000000000435

Sharma, S., Quintana, A., Findlay, G. M., Mettlen, M., Baust, B., Jain, M., et al. (2013). An siRNA screen for NFAT activation identifies septins as coordinators of store-operated Ca2+ entry. *Nature* 499, 238–242. doi: 10.1038/nature12229

Silva-Rojas, R., Treves, S., Jacobs, H., Kessler, P., Messaddeq, N., Laporte, J., et al. (2019). STIM1 over-activation generates a multi-systemic phenotype affecting the skeletal muscle, spleen, eye, skin, bones and immune system in mice. *Hum. Mol. Genet.* 28, 1579–1593. doi: 10.1093/hmg/ddy446

Srikanth, S., Jung, H. J., Kim, K. D., Souda, P., Whitelegge, J., and Gwack, Y. (2010). A novel EF-hand protein, CRACR2A, is a cytosolic Ca2+ sensor that stabilizes CRAC channels in T cells. *Nat. Cell Biol.* 12, 436–446. doi: 10.1038/ncb2045

Srikanth, S., Woo, J. S., Wu, B., El-Sherbiny, Y. M., Leung, J., Chupradit, K., et al. (2019). The Ca(2+) sensor STIM1 regulates the type I interferon response by retaining the signaling adaptor STING at the endoplasmic reticulum. *Nat. Immunol.* 20, 152–162. doi: 10.1038/s41590-018-0287-8

Stathopulos, P. B., and Ikura, M. (2017). Store operated calcium entry: from concept to structural mechanisms. *Cell Calc.* 63, 3–7. doi: 10.1016/j.ceca.2016.11.005

Stathopulos, P. B., Li, G. Y., Plevin, M. J., Ames, J. B., and Ikura, M. (2006). Stored Ca2+ depletion-induced oligomerization of stromal interaction molecule 1 (STIM1) via the EF-SAM region: an initiation mechanism for capacitive Ca2+ entry. *J. Biol. Chem.* 281, 35855–35862. doi: 10.1074/jbc.M608247200

Stathopulos, P. B., Zheng, L., Li, G. Y., Plevin, M. J., and Ikura, M. (2008). Structural and mechanistic insights into STIM1-mediated initiation of store-operated calcium entry. *Cell* 135, 110–122. doi: 10.1016/j.cell.2008.08.006

Stiber, J., Hawkins, A., Zhang, Z. S., Wang, S., Burch, J., Graham, V., et al. (2008). STIM1 signalling controls store-operated calcium entry required for development and contractile function in skeletal muscle. *Nat. Cell Biol.* 10, 688–697. doi: 10.1038/ncb1731

Sura, A., Jacher, J., Neil, E., McFadden, K., Walkovich, K., and Hannibal, M. (2020). Chronic thrombocytopenia as the initial manifestation of STIM1-related disorders. *Pediatrics* 145:e20192081. doi: 10.1542/peds.2019-2081

Vaeth, M., and Feske, S. (2018). NFAT control of immune function: new frontiers for an abiding trooper. *F1000Res* 7:260. doi: 10.12688/f1000research.13426.1

Vaeth, M., Maus, M., Klein-Hessling, S., Freinkman, E., Yang, J., Eckstein, M., et al. (2017). Store-Operated Ca(2+) entry controls clonal expansion of t cells through metabolic reprogramming. *Immunity* 47, 664.e6–679.e6. doi: 10.1016/j.immuni.2017.09.003

van der Meijden, P. E. J., and Heemskerk, J. W. M. (2019). Platelet biology and functions: new concepts and clinical perspectives. *Nat. Rev. Cardiol.* 16, 166–179. doi: 10.1038/s41569-018-0110-0

Vandenberghe, M., Raphael, M., Lehen'kyi, V., Gordienko, D., Hastie, R., Oddos, T., et al. (2013). ORAI1 calcium channel orchestrates skin homeostasis. *Proc. Natl. Acad. Sci. U.S.A.* 110, E4839–E4848. doi: 10.1073/pnas.1310394110

Varga-Szabo, D., Braun, A., Kleinschnitz, C., Bender, M., Pleines, I., Pham, M., et al. (2008). The calcium sensor STIM1 is an essential mediator of arterial thrombosis and ischemic brain infarction. *J. Exp. Med.* 205, 1583–1591. doi: 10.1084/jem.20080302

Venkiteswaran, G., and Hasan, G. (2009). Intracellular Ca2+ signaling and store-operated Ca2+ entry are required in Drosophila neurons for flight. *Proc. Natl. Acad. Sci. U.S.A.* 106, 10326–10331. doi: 10.1073/pnas.0902982106

Walsh, C. M., Doherty, M. K., Tepikin, A. V., and Burgoyne, R. D. (2010). Evidence for an interaction between Golli and STIM1 in store-operated calcium entry. *Biochem. J.* 430, 453–460. doi: 10.1042/BJ20100650

Walter, M. C., Rossius, M., Zitzelsberger, M., Vorgerd, M., Muller-Felber, W., Ertl-Wagner, B., et al. (2015). 50 years to diagnosis: autosomal dominant tubular aggregate myopathy caused by a novel STIM1 mutation. *Neuromuscul. Disord.* 25, 577–584. doi: 10.1016/j.nmd.2015.04.005

Wang, L., Zhang, L., Li, S., Zheng, Y., Yan, X., Chen, M., et al. (2015). Retrograde regulation of STIM1-Orai1 interaction and store-operated Ca2+ entry by calsequestrin. *Sci. Rep.* 5:11349. doi: 10.1038/srep11349

Wang, S., Choi, M., Richardson, A. S., Reid, B. M., Seymen, F., Yildirim, M., et al. (2014). STIM1 and SLC24A4 are critical for enamel maturation. *J. Dent. Res.* 93(7 Suppl), 94S–100S. doi: 10.1177/0022034514527971

Wei-Lapierre, L., Carrell, E. M., Boncompagni, S., Protasi, F., and Dirksen, R. T. (2013). Orai1-dependent calcium entry promotes skeletal muscle growth and limits fatigue. *Nat. Commun.* 4:2805. doi: 10.1038/ncomms3805

Xue, T., Do, M. T., Riccio, A., Jiang, Z., Hsieh, J., Wang, H. C., et al. (2011). Melanopsin signalling in mammalian iris and retina. *Nature* 479, 67–73. doi: 10.1038/nature10567

Zayzafoon, M. (2006). Calcium/calmodulin signaling controls osteoblast growth and differentiation. *J. Cell Biochem.* 97, 56–70. doi: 10.1002/jcb.20675

Zhang, H., Clemens, R. A., Liu, F., Hu, Y., Baba, Y., Theodore, P., et al. (2014). STIM1 calcium sensor is required for activation of the phagocyte oxidase during inflammation and host defense. *Blood* 123, 2238–2249. doi: 10.1182/blood-2012-08-450403

Zhang, S. L., Yu, Y., Roos, J., Kozak, J. A., Deerinck, T. J., Ellisman, M. H., et al. (2005). STIM1 is a Ca2+ sensor that activates CRAC channels and migrates from the Ca2+ store to the plasma membrane. *Nature* 437, 902–905. doi: 10.1038/nature04147

Zhao, X., Yoshida, M., Brotto, L., Takeshima, H., Weisleder, N., Hirata, Y., et al. (2005). Enhanced resistance to fatigue and altered calcium handling properties of sarcalumenin knockout mice. *Physiol. Genomics* 23, 72–78. doi: 10.1152/physiolgenomics.00020.2005

Conflict of Interest: The authors declare that the research was conducted in the absence of any commercial or financial relationships that could be construed as a potential conflict of interest.

frontiers in Physiology

REVIEW
published: 06 November 2020
doi: 10.3389/fphys.2020.583393

Multi-Cellular Functions of MG53 in Muscle Calcium Signaling and Regeneration

Dathe Z. Benissan-Messan[1], Hua Zhu[1], Weina Zhong[1], Tao Tan[1], Jianjie Ma[1] and Peter H. U. Lee[1,2,3]**

[1] Department of Surgery, The Ohio State University, Columbus, OH, United States, [2] Department of Pathology and Laboratory Medicine, Brown University, Providence, RI, United States, [3] Department of Cardiothoracic Surgery, Southcoast Health, Fall River, MA, United States

Since its identification in 2009, multiple studies have indicated the importance of MG53 in muscle physiology. The protein is produced in striated muscles but has physiologic implications reaching beyond the confines of striated muscles. Roles in muscle regeneration, calcium homeostasis, excitation-contraction coupling, myogenesis, and the mitochondria highlight the protein's wide-reaching impact. Numerous therapeutic applications could potentially emerge from these physiologic roles. This review summarizes the current literature regarding the role of MG53 in the skeletal muscle. Therapeutic applications are discussed.

Keywords: metabolic syndrome, skeletal muscle regeneration, myogenesis, insulin resistance, mitochondria, calcium homeostasis, plasma membrane repair, TRIM72

OPEN ACCESS

Edited by:
Matias Mosqueira, Heidelberg University Hospital, Germany

Reviewed by:
Margaret Westfall, University of Michigan, United States
Marco P. Brotto, University of Texas at Arlington, United States

****Correspondence:***
Jianjie Ma
Jianjie.Ma@osumc.edu
Peter H. U. Lee
Peter_Lee@brown.edu

Specialty section:
This article was submitted to Striated Muscle Physiology, a section of the journal Frontiers in Physiology

Received: *14 July 2020*
Accepted: *09 October 2020*
Published: *06 November 2020*

Citation:
Benissan-Messan DZ, Zhu H, Zhong W, Tan T, Ma J and Lee PHU (2020) Multi-Cellular Functions of MG53 in Muscle Calcium Signaling and Regeneration. Front. Physiol. 11:583393. doi: 10.3389/fphys.2020.583393

INTRODUCTION

More than 70 TRIM family proteins exist. They are characterized by the presence of a tripartite motif composed of a RING finger, B-box motifs, and a coiled coil region at their N-terminus. Among them is a 53 kD protein named Mitsugumin 53 (MG53) (Cai et al., 2009a; McNeil, 2009). MG53, also known as TRIM72, was cloned in 2009 using an immunoproteomic library in an attempt to identify proteins involved in myogenesis, calcium signaling, and striated muscle integrity (Weisleder et al., 2008; Tan et al., 2016). Since its identification, multiple physiologic functions have been attributed to this protein, which have made it an attractive candidate in translational medicine as a potential therapeutic agent. The protein is primarily expressed in striated muscles. This review of literature details the current understanding of the role of MG53 in skeletal muscle. Therapeutic applications of the protein relative to skeletal muscle diseases are discussed.

THE SKELETAL MUSCLE

Skeletal muscles are made of bundles of contractile units called myofibers. Myofibers are made of myofibrils which are in turn composed of longitudinal thick and thin filaments (Ciciliot and Schiaffino, 2010). Myofibers form fascicles and bundles of fascicles form muscle tissue (Mukund and Subramaniam, 2020). Myofibers arise during development from the fusion of mononucleate precursor cells known as myoblasts and satellites cells which are stem cells that

are activated during regeneration following muscle injury to proliferate and differentiate into myofibers (Blanco-Bose et al., 2001). Skeletal muscles are highly vascularized and innervated (Mukund and Subramaniam, 2020).

Contraction of muscle fibers occur following conduction of impulses through motor neurons via neuromuscular junctions through excitation-contraction (EC) coupling (Takeshima et al., 1994; Mukund and Subramaniam, 2020). Acetylcholine receptors in the plasma membrane of skeletal muscle cells are activated by the release of acetylcholine from motor neurons and leads to membrane depolarization (Lee, 2010; Ahn et al., 2016). The membrane potential induced through depolarization is propagated to the interior of muscle cells via transverse tubules (T-tubules) and leads to the activation of dihydropyridine receptors (DHPR), which in turn activate ryanodine receptor 1 (RyR1), a calcium channel on the sarcoplasmic reticulum membrane (Ahn et al., 2016). RyR1 is responsible for the release of calcium ions into the cytosol (Takeshima et al., 1994). Calcium ions in the cytosol further activate more RyR1 to release more calcium into the cytosol, a phenomenon referred to as calcium-ion induced calcium release (Takeshima et al., 1994). Entry of extracellular calcium into the cell through store-operated calcium entry (SOCE) via Orai1 or through the transient receptor potential canonical (TRPC) channels also contribute to the calcium supply during skeletal muscle contraction (Ahn et al., 2016). Following contraction, the sarcoplasmic endoplasmic reticulum calcium ion ATPase 1a (SERCA1a) uptakes cytosolic calcium and leads to a return to a resting level and a replenishment of the calcium content of the sarcoplasmic reticulum (Ahn et al., 2016).

In addition to being a contractile machine, the skeletal muscle is considered an endocrine organ and secretes several myokines that modulate tissue function (Iizuka et al., 2014; Karstoft and Pedersen, 2016; Giudice and Taylor, 2017; Hoffmann and Weigert, 2017; Bian et al., 2019). Striated muscles are constantly subjected to stress and an active injury-repair mechanism is necessary for their optimum function. Repeated use, stress, diseases, and other injuries would otherwise impair muscle function and movement. The repair of the plasma membrane following injury requires the translocation of intracellular vesicles to the site of injury (Cai et al., 2009a,b). These vesicles fuse with the plasma membrane in a calcium dependent manner (Cai et al., 2009a). Dysferlin and caveolae are essential components of the membrane repair machinery and participate in vesicle fusion to the plasma membrane (Bansal et al., 2003; Glover and Brown, 2007).

MG53 IN THE SKELETAL MUSCLE

MG53 is composed of a TRIM domain at the N-terminus, a PRY domain (associated with SPRY), and a SPRY domain (sequence repeat in the dual-specificity kinase sp1A and ryanodine receptor) at the C-terminus (Cai et al., 2009a; Ahn et al., 2016). Generally, TRIM containing proteins control important cellular processes in intracellular signaling, innate immunity, transcription, autophagy, and carcinogenesis (Hatakeyama, 2017). Genetic analysis of the TRIM domain reveals that it is made up of a Really Interesting New Gene (RING) domain with ubiquitin E3 ligase activity, a B-box with a zinc-binding domain, and coiled-coil moieties (Ozato et al., 2008; Cai et al., 2009a; Tan et al., 2016). The RING finger domain is a zinc finger motif containing a $Cys_3HisCys_4$ amino acid motif which binds two zinc cations (Zhang et al., 2017). The E3 ubiquitin ligase activity of the RING domain catalyzes ubiquitin conjugation which targets proteins for degradation (Hatakeyama, 2017). The B-box domains are zinc binding as well and have been shown to play roles in the innate immune system defense (Ozato et al., 2008). The coiled-coil domain mediates interactions among TRIM proteins which leads to protein assembly into high molecular mass complexes (Ozato et al., 2008; Zhang et al., 2017). The PRY domain is involved in protein binding and has been suggested to be an interface for the protein-protein interaction of MG53 with other proteins (Ahn et al., 2016). At the C-terminus, MG53 has a SPRY domain, which is responsible for the binding of target proteins (Zhang et al., 2017). MG53 is primarily produced in cardiac and skeletal muscles (Cai et al., 2009a; Hu and Xiao, 2018). RNA analysis has revealed expression in the lung and kidney (Cai et al., 2009a; Jia et al., 2014; Duann et al., 2015). The protein was also noted to be expressed by macrophages (Sermersheim et al., 2020). Recombinant human MG53 (rhMG53) has been purified and is available for therapeutic applications (Weisleder et al., 2012; Jia et al., 2014; Duann et al., 2015; Li et al., 2015; Liu J.et al., 2015; Zhu et al., 2015; Yao et al., 2016; Adesanya et al., 2019; Bian et al., 2019; Chandler et al., 2019; Guan et al., 2019a,b; Liu et al., 2020; Sermersheim et al., 2020).

The Role of MG53 in Skeletal Muscle Calcium Homeostasis and EC Coupling

MG53 binds to Orai1 via its PRY-SPRY region and co-localizes with Orai1 to the plasma membranes of skeletal muscles to enhance extracellular calcium entry via by SOCE, while reducing intracellular calcium release through RyR1, and increasing the expression of TRPC3, TRPC4, and calmodulin 1(CaM1) (**Figure 1A**; Ahn et al., 2016). MG53 also attenuates SERCA1a activity, leading to a rise in cytosolic calcium (Lee et al., 2012). The TRIM and PRY domains of MG53 constitute the binding region to SERCA1a and the interaction of MG53 and SERCA1a reduces the activity of SERCA1a, which takes up calcium from the cytosol to the sarcoplasmic reticulum (Lee et al., 2012; Ahn et al., 2016). Together, this leads to a transient increase in cytosolic calcium, which results in efficient skeletal muscle contractions (Ahn et al., 2016).

The Role of MG53 in the Mitochondria

Studies in high fat diet (HFD)-induced metabolic syndrome mouse models have demonstrated an aggregation of MG53 around the mitochondria of skeletal muscle in the presence of reactive oxygen species (ROS) which suggests a role for the protein as a mitochondrial guardian (**Figure 1B**; Ma et al., 2015). Since HFD feeding induces an elevation in mitochondrial activity as a result of increased production of ROS, MG53

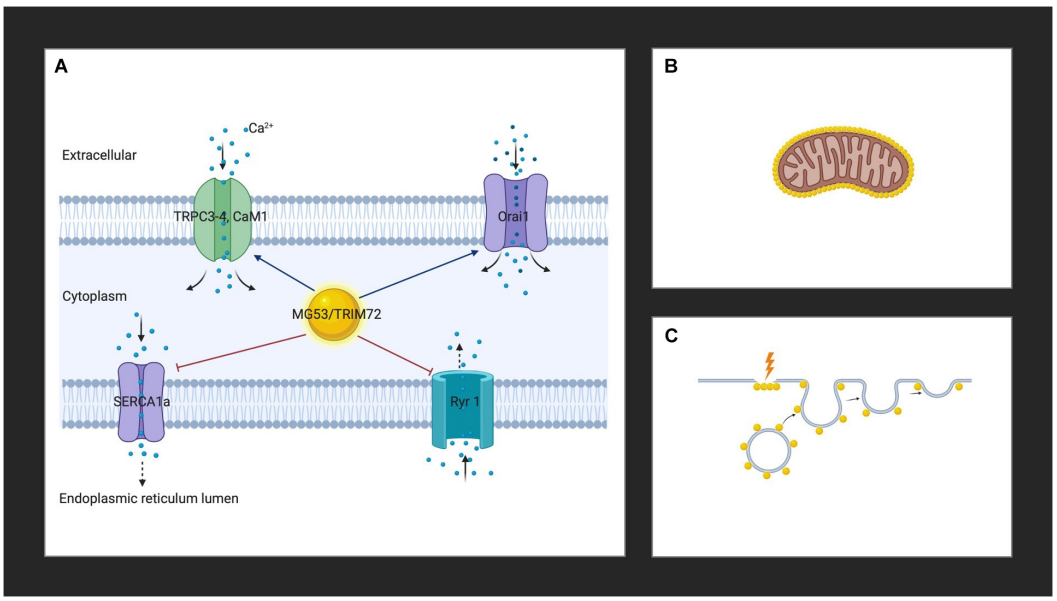

FIGURE 1 | (A) MG53 controls cytosolic calcium through interactions with Orai1, RyR1, TRPC3, TRPC4, CaM1, and SERCA. **(B)** MG53 aggregates around the mitochondria of skeletal muscle in the presence of reactive oxygen species. **(C)** MG53 promotes plasma membrane repair by facilitating vesicle translocation following injury. Golden spheres represent MG53. Created with BioRender.com.

is thought to play a protective role (Ma et al., 2015). More recently, MG53 overexpression was also suggested to promote mitochondrial autophagy to help remove damaged mitochondria to relieve CKD-induced muscle atrophy in skeletal muscle cells by upregulating autophagy and beclin 1 regulator 1 (Ambra1), a key regulator involved in autophagosome formation (Lijie et al., 2019). These studies herald the opening of new avenues regarding the widening reach of the activity of MG53. Further studies will undoubtedly elucidate the role of the protein in the mitochondria.

The Role of MG53 in Plasma Membrane Repair

The role of MG53 in the plasma membrane was one of the first discovered physiological functions of the protein. It is now well established that MG53 facilitates vesicle translocation to the plasma membrane where it leads to repair following injury (**Figure 1C**; Cai et al., 2009a). Cholesterol exposure in the plasma membrane following skeletal muscle injury is thought to mediate the translocation of MG53 upon membrane damage (Han, 2011; Zhu et al., 2011). The protein appears as a monomer in the reduced environment of the cytoplasm of an intact cell, and acute muscle plasma membrane disruption leads to exposure of the cell interior to the external oxidized environment (Cai et al., 2009a). A change in the oxidation state of MG53 ensues, which initiates oligomerization (Cai et al., 2009a; McNeil, 2009). Targeted mutagenesis revealed that MG53 oligomer formation requires a conserved cystidine residue (C242) and mutations in C242 do not result in the formation of oligomers (Matsuda et al., 2012). Oligomerization of MG53 through oxidation of the thiol group of cysteine at 242 and a leucine zipper motif between the two coiled-coil domains induces the nucleation of intracellular vesicles coated with MG53, the trafficking of vesicles to the injury sites, and the resealing of the injured membranes (Hwang et al., 2011; Ahn et al., 2016). At the membrane, MG53 concentrates at the site of injury in damaged adult muscle fibers (Cai et al., 2009a; Weisleder et al., 2012; Lek et al., 2013). The protein binds to phosphatidylserine in the plasma membrane to mediate vesicle accumulation at the site of injury (Cai et al., 2009a; Tan et al., 2016). Polymerase I and transcript release factor (PTRF; also known as cavin-1) recognize cholesterol at the injury site and act as a docking protein to tether MG53 together with its associated vesicles to the damage site (Zhu et al., 2011). Once associated with intracellular vesicles and the inner leaflet of the sarcolemma of striated muscle, fusion is mediated through membrane proteins such as caveolin-3 (Cav-3) (Weisleder et al., 2009). While the exact interaction of MG53 with Cav-3 to control intracellular vesicle trafficking and membrane remodeling in muscle is unknown, the binding of Cav-3 to MG53 is known to be essential for vesicle fusion (Cai et al., 2009b). Together with dysferlin, PTRF, and non-muscle myosin type IIA, MG53 constitute the membrane repair system (Cai et al., 2009c; Zhu et al., 2011; Lin et al., 2012). The ensuing vesicle fusion to the plasma membrane requires the presence of calcium and results in the formation of a membrane patch which seals the site of injury (Cai et al., 2009b; Weisleder et al., 2009; Lek et al., 2013). A recently proposed novel model of membrane repair including MG53 involves the formation of cap and shoulder proteins (Demonbreun and McNally, 2016; Demonbreun et al., 2016). Following membrane disruption, annexins proteins (A1, A2, A5, and A6) bind phospholipids in the presence of calcium ions to form a "cap" at the site of damage (Demonbreun et al., 2016). Repair "shoulder" proteins, such as dysferlin, Epsin 15

homology domain-containing proteins (EHD1, EHD2), MG53, and BIN1 then localizes adjacent to the repair cap to form a membrane repair complex system and seals the injured site (Demonbreun et al., 2016).

The Role of MG53 in Myogenesis

Mammalian skeletal muscles are made of multinucleated myofibers formed during development by fusion of mononucleated muscle progenitors (Ciciliot and Schiaffino, 2010). Myogenic differentiation is a tightly regulated process in which mononucleated myoblasts expressing myogenic marker proteins [MyoD, Myogenin, Myosin Heavy Chain (MyHC), and others] proliferate and fuse to form multinucleated myotubes. Matured myotubes convert into contractile myofibers (Okino et al., 2020). The formation of new myofibers or myofiber segments following necrosis is called muscle regeneration (Ciciliot and Schiaffino, 2010). Mature skeletal muscle tissues possess the ability to regenerate from the interaction of satellite cells and their surrounding microenvironment (Mukund and Subramaniam, 2020). Satellite cells are characterized by the expression of transcription factors PAX3 and PAX7 and are located between the basal lamina and the sarcolemma (Relaix et al., 2006; Buckingham, 2007; von Maltzahn et al., 2013). Muscle regeneration following injury is characterized by an inflammatory reaction dominated by the invasion of macrophages, followed by the activation, migration, and proliferation of satellite cells, and their differentiation and fusion into muscle fibers (Ciciliot and Schiaffino, 2010). The maturation of these newly formed myofibers and the remodeling of the regenerated muscle follows (Ciciliot and Schiaffino, 2010). Local apoptosis seen in atrophic muscle can also lead to an increase in the number of satellite cells (Ciciliot and Schiaffino, 2010).

Quiescent satellite cells are marked by the expression of PAX7 as well as several other molecular markers, and is notable for the absence of Myogenic Regulatory Factor (MRF), Myogenic Differentiation1 (MYOD1) and Myogenin (MYOG) (Rocheteau et al., 2015; Mukund and Subramaniam, 2020). Skeletal muscle-specific TGFb family member, myostatin, suppresses satellite cell activation (McCroskery et al., 2003). Sprouty1 (SPRY1), a tyrosine inhibitor kinase, is necessary for maintenance and re-entry of PAX7 satellite cells into quiescence (Shea et al., 2010). Satellite cells are activated in response to injury. Activated satellite cells are characterized by PAX7 and the expression of MRFs [MYOD1, MYOG, and Myogenic Factor (MYF)5] (Mukund and Subramaniam, 2020). PAX7 is absolutely required for normal function of satellite cells in regenerative myogenesis in both neonatal and adult skeletal cells (von Maltzahn et al., 2013). Deficiency in PAX7 results in cell-cycle arrest and precocious differentiation (von Maltzahn et al., 2013). The migration to an injury site and proliferation of satellite cells is governed by chemo-attractants released from the extracellular matrix or inflammatory cells (Mukund and Subramaniam, 2020).

Insulin-like growth factors, IGF-I and IGF-II, are essential for skeletal muscle development, hypertrophy, and regeneration. IGF-I plays a key role in the differentiation of satellite cells and the development, hypertrophy, and regeneration of skeletal muscles (Zhang et al., 2017). Likewise, satellite cells lose their muscle differentiation activity when treated with anti-IGF-II antibody or antisense IGF-II, whereas IGF-I overexpression in mice leads to hypertrophy and hyperplasia, leading to increased muscle mass and force generation (Jung and Ko, 2010). IGF-I and IGF-II transduce cellular signaling through the IGF-I receptor (IGFR) that subsequently recruits insulin receptor substrate-1 (IRS-1) (Yi et al., 2013). The recruited IRS-1 can activate the phosphoinositide 3 kinase (PI(3)K)/Akt and Ras/Raf/MEK/ERK pathways. The Ras/Raf/MEK/ERK pathway controls muscle fiber type whereas the PI(3)K/Akt pathway induces muscle differentiation and hypertrophy (Jung and Ko, 2010). The activated Akt targets a mammalian target of rapamycin (mTOR), glycogen synthase kinase 3β (GSK3β), and Forkhead box O (FOXO) (Jung and Ko, 2010). mTOR activity is not involved in muscle differentiation (Jung and Ko, 2010). Phosphorylated GSK3β and FOXO stimulate muscle hypertrophy and suppress muscle atrophy. IRS-1 overexpression inhibits myogenic differentiation through continuous FOXO inhibition and causes repression of MyHC during differentiation (Okino et al., 2020). Additionally, IRS-1 and insulin signaling is reduced during myogenesis, and myoblasts with higher IRS-1 levels are eliminated during differentiation (Bian et al., 2019; Okino et al., 2020).

Intracellularly, evidence suggests that MG53 is a negative regulator of IGF-induced myogenesis (Jung and Ko, 2010; Lee et al., 2010). The MG53 promoter contains E-boxes [which are short DNA motifs within myogenic *cis*-regulatory element (CREs)] and a Myocyte Enhancer Factor (MEF)-binding site for the myogenic transcription factors MyoD and MEF (Jung and Ko, 2010; Soleimani et al., 2018). MG53 is gradually expressed during myogenesis because the transcription of MG53 requires MyoD and Akt (Jung and Ko, 2010; Hong et al., 2016). MG53 then acts as an E3 ligase, targeting the insulin receptor and IRS-1 for ubiquitin-dependent degradation (Song et al., 2013; Yi et al., 2013). This negatively regulates skeletal myogenesis by reducing IGF-I-initiated IRS-1 tyrosine phosphorylation and Akt phosphorylation without affecting IGF-I-elicited IGFR tyrosine phosphorylation and ERK1/2 phosphorylation (Yi et al., 2013). Myogenesis and IGF-I-induced IRS-1 tyrosine phosphorylation were prevented in C2C12 myoblasts by MG53 overexpression but enhanced by MG53 knockdown (Jung and Ko, 2010). The RING domain of MG53 with E3 ligase activity is necessary for the inhibition of IGF-I-elictied IRS-1 phosphorylation (Yi et al., 2013). MG53-induced ubiquitination and degradation of another kinase, focal adhesion kinase (FAK), is also thought to inhibit myogenesis (Nguyen et al., 2014). FAK regulates heterochromatin remodeling to modulate myogenin expression during skeletal myogenesis and regulate the expression of genes involved in membrane fusion, including caveolae (Nguyen et al., 2014). Its inhibition by MG53 is also thought to reduce myogenesis (Nguyen et al., 2014).

Meanwhile, exogenous MG53 has been noted to facilitate the differentiation of C2C12 skeletal myoblasts to myotubes by enhancing vesicle trafficking and membrane fusion (Cai et al., 2009a; Bian et al., 2019). A recent study published by Bian et al. provided evidence that increased levels of MG53 in circulation do not negatively impact myogenesis (Bian et al., 2019). Transgenic mice with sustained elevation of MG53 in circulation (tPA-MG53) have a longer lifespan

compared to their wild type counterparts due to enhanced repair capacity after injury and enhanced muscle regeneration (Bian et al., 2019). The authors also did not observe any changes in IRS-1 activity in the skeletal muscles as a result of MG53 overexpression. MG53 was noted to restore satellite cell proliferation in MG53 knockout ($mg53^{-/-}$) mice (Bian et al., 2019). This evidence led to the hypothesis that MG53 may improve muscle regeneration by modulating the activity of satellite cells (Bian et al., 2019). This resulting dichotomous functions between the intracellular mechanism of MG53 and the effect of extracellular MG53 application remains to be elucidated.

MG53 in Skeletal Muscle Disease Related Therapies

MG53 is an endogenous protein and therefore therapies based on its use are less likely to elicit an immune system reaction. The recombinant human form of the protein (rhMG53) is readily available for therapeutic application and studies have shown limited toxicity (Weisleder et al., 2012; Alloush and Weisleder, 2013; Jia et al., 2014; Duann et al., 2015; Liu J.et al., 2015; Tan et al., 2016). Here, we present a few studies highlighting the potential therapeutic applications for MG53.

When applied intravenously, rhMG53 can potentially treat multiple pathologies in rodent and large animal disease models (Weisleder et al., 2012; Jia et al., 2014; Duann et al., 2015; Liu J.et al., 2015; Zhu et al., 2015). The myokine has been shown to play a protective role in skeletal muscles, kidneys, lungs, brains, skin, hearts, and corneas (He et al., 2012; Weisleder et al., 2012; Jia et al., 2014; Duann et al., 2015; Li et al., 2015; Yao et al., 2016; Adesanya et al., 2019; Chandler et al., 2019). Exogenously administered rhMG53 travels in the circulation and concentrates at the healing edge of injury sites and contributes to regeneration following injury (Weisleder et al., 2012; Bian et al., 2019). Muscle cells and tissues treated with rhMG53 show resistance to mechanical, chemical, and ultraviolet damage (Weisleder et al., 2012). Intravenous injection of the protein protects skeletal muscles against acute and chronic insults (Weisleder et al., 2012; Zhu et al., 2015; Bian et al., 2019). Weisleder et al. (2012) noted in mouse models that 300 nM rhMG53 was sufficient to protect muscle cells against mechanical damage and prevent muscle injury.

The importance of the protein in membrane repair has been highlighted by multiple studies. MG53-/- mice with targeted protein deletion develop progressive muscle pathology with age characterized by defects in skeletal muscle contractility after injury and defective membrane repair (Cai et al., 2009a). Morphologically, a pathologic increase in the number of central nuclei, a measure of defective muscle repair, and decreased diameter of muscle fibers, were observed in isolated skeletal muscles of older mg53-/- mice when compared to younger counterparts and wild type littermates (Cai et al., 2009a). Following cardiotoxin-induced muscle injury, genetically enhanced tPA-MG53 mice overexpressing MG53 displayed enhanced regeneration when compared to wild type and mg53-/- mice (Bian et al., 2019). The regenerative ability of MG53 is thought to be mediated via satellite cell proliferation (Bian et al., 2019).

Muscular dystrophies are an inherited group of disorders characterized by progressive muscle weakness and atrophy and linked to a loss of function of dystrophin and its associated proteins (Glover and Brown, 2007). Muscular dystrophies can be caused by genetic mutations in over thirty different genes, many of which encode for proteins essential for the integrity of muscle cell structure and membranes (He et al., 2012). Mutations in the dystrophin gene in Duchenne muscular dystrophy (DMD) and Becker muscular dystrophy (BMD), or sarcoglycan genes in limb-girdle muscular dystrophies (LGMDs) lead to muscle sarcolemma destabilization and fragility (He et al., 2012). DMD is an X-linked inherited muscle wasting disorder with limited treatment options characterized by compromised muscle structure and decreased muscle function (Burkin and Wuebbles, 2012; Weisleder et al., 2012). Dysferlinopathies are a heterogenous group of progressive muscular dystrophies characterized by mutations in the DYSF gene, leading to reduced or null expression of the dysferlin protein and resulting in varied phenotypes (Flix et al., 2013). Dysferlin is a type II muscle surface membrane, expressed in the sarcolemma, in intracellular vesicles, and in T-tubules (Glover and Brown, 2007; Han, 2011; Flix et al., 2013). Although dysferlin is important in membrane repair, dysferlin itself does not participate in the recruitment of intracellular vesicles for membrane repair and dysferlin -/- muscle retains accumulation of vesicles near membrane damage sites. Dysferlin is known to interact with several proteins including AHNAK, MG53, and Cav3 (Flix et al., 2013). MG53 and AHNAK interact directly with dysferlin (Flix et al., 2013). Like dysferlin, many mutations of Cav3 have been linked to muscular dystrophy (Cai et al., 2009c). Additionally, Cav3 has also been shown to be essential for MG53-mediated vesicle translocation (Cai et al., 2009c).

Cav3 binds to MG53, which in turn interacts with dysferlin (Flix et al., 2013). In the absence of dystrophin, there is weakening of the attachment of the muscle cells to the surrounding basal lamina, which results in reduced force transmission, loss of muscle integrity, altered cell signaling, and weakened sarcolemma that is easily damaged during muscle contraction (Burkin and Wuebbles, 2012). MG53 interacts with dysferlin to facilitate vesicle trafficking to sites of membrane damage (Cai et al., 2009c). Systemic delivery and muscle specific overexpression of the human MG53 gene by recombinant adeno-associated virus (AAV) vectors enhanced membrane repair, ameliorated pathology, and improved muscle and heart functions in δ-sarcoglycan (δ-sarcoglycan) deficient TO-s hamsters (He et al., 2012). Overexpression of MG53 increased dysferlin levels and facilitated its trafficking to the muscle membrane through the participation of Cav3 (He et al., 2012). In addition, MG53 protected muscle cells by activating cell survival kinases, such as Akt, extracellular signal-regulated kinases (ERK1/2), and glycogen synthase kinase-3β (GSK-3β), and inhibiting proapoptotic protein like Bax (He et al., 2012). Even though MG53 delivery would not constitute a cure for dysferlonopathies, a palliation of pathology could be obtained through its delivery in some sarcoglyconopathies.

Maintenance of plasma membrane integrity is vital for cell survival. The constant stress imposed on the skeletal muscle system over time requires a regular system of maintenance to

ensure that it continuously fulfills its mechanical and endocrine functions. Aging, cachexia, sarcopenia and disease states such as cancers are conditions associated with compromised muscle integrity and muscle atrophy where MG53 could play a therapeutic role. An increase in MG53 expression level and other plasma membrane repair proteins has already been observed in sedentary *ad libitum* aging in animal studies by Hord et al. (2016). The authors postulated that the increased requirement for phospholipid membrane repair in the aging skeletal muscle necessitated the increased presence of these proteins. The study of the function of MG53 in these diseases states and conditions could further shed light on the restoration of muscle integrity and function. Given its protective roles, MG53 is an ideal candidate therapeutic agent for maintaining skeletal muscle health.

Controversial Role of MG53 in Diabetes

Skeletal muscles play an important role in glucose control. They are responsible for 70–90% of insulin-stimulated glucose metabolism (Song et al., 2013; Tan et al., 2016). Song et al. reported increased MG53 expression in animal models and human patients with diabetes (Song et al., 2013). They also showed that an upregulation of MG53 occurred before the onset of diabetes (Song et al., 2013). They proposed that an upregulation of MG53 causes insulin insensitivity through the degradation of IRS-1. These observations have not been substantiated by other investigators, and many others failed to observe an upregulation of MG53 in diabetic animals and humans (Ma et al., 2013, 2015, 2017; Xu et al., 2013; Yi et al., 2013; Yuan et al., 2013; Zabielski et al., 2016). Rather, serum samples from high fat diet induced diabetic mice (Ma et al., 2015) and db/db mice (Wang et al., 2020) showed reduced levels of MG53. It is also well-known that a loss of IRS-1 does not directly result in diabetes, owing to a robust compensatory mechanism among the different IRS subtypes (Tamemoto et al., 1994; Terauchi et al., 1997; Laustsen et al., 2002). A recent proteomic study specifically examined the interactions of IRS-1 in skeletal muscle from normal individuals, obese insulin-resistant non-diabetic control subjects, and patients with type 2 diabetes before and after insulin infusion, and failed to identify an enhancement of MG53 (Caruso et al., 2014). Thus, the mounting evidence do not support the proposed role of MG53 in the regulation of IRS-1 in diabetes.

Liu F.et al. (2015) proposed a different mechanism of MG53 mediated diabetes in 2015. The researchers generated transgenic mice by using the alpha myosin heavy chain (α-MHC) promoter to drive expression of MG53 and found that overexpression of MG53 was powerful enough to induce whole body insulin resistance and compromised glucose uptake (Liu F.et al., 2015). MG53 was posited to enter the nucleus and serve as a transcription factor to activate the peroxisome proliferation-activated receptor alpha (PPAR-α) which in turn mediated excessive lipid uptake induced cytotoxicity. Our group successfully generated a MG53 transgenic mouse line to achieve sustained elevation of circulating MG53 by fusing a tPA secretory peptide at the N-terminus of the MG53 protein (tPA-MG53) (Yao et al., 2016; Bian et al., 2019). tPA-MG53 mice live a healthy lifespan with enhanced tissue repair and regeneration capacity (Yao et al., 2016; Bian et al., 2019). To test the role of elevated circulating MG53 in the development of diabetes, we crossed tPA-MG53 mice with db/db mice and found that tPA-MG53/db/db mice develop diabetes at a rate similar to its db/db littermates, suggesting overexpression of MG53 has negligible effects on the development of diabetes (Wang et al., 2020). A separate transgenic mouse model with overexpression of MG53 was generated by Ham and Mahoney (2013). While they used the same α-MHC promoter to drive overexpression of MG53 as Liu F.et al. (2015), they observed that IRS-1 protein levels were higher in transgenic animals when compared to that of their wild type littermates (Ham and Mahoney, 2013). This observation suggests that a feedback mechanism compensates for the downregulation of IRS-1 by MG53. Other studies with mg*53-/-*, tPA-MG53, and their wild type littermates also failed to show alteration of PPAR-α (Bian et al., 2019).

Wu et al. (2019) recently implicated MG53 in the development of diabetes. They showed that the binding affinity between MG53 and insulin receptor (IR) is over threefold higher than that of insulin and insulin receptor (Kd: MG53 and IR is 8 nM vs. insulin and IR is 28 nM) (Wu et al., 2019). Thus, MG53 serves as a novel agonist of IR and a competitive antagonist of insulin. If this hypothesis holds true, not only would the authors have successfully identified the receptor for MG53 but they would also have shown that targeting endogenous MG53 could treat diabetes. This would also imply that the high levels of circulating MG53 present in tPA-MG53 mice could block the insulin pathway and greatly facilitate the development of diabetes. However, as mentioned above, tPA-MG53 mice live a healthy lifespan and when crossed with db/db mice, tPA-MG53/db/db mice are indistinguishable from db/db littermates in terms of growth rate, glucose tolerance test, and insulin tolerance test (Bian et al., 2019; Wang et al., 2020). These studies highlight the deep controversies surrounding the protein that will need to be resolved by future studies.

CONCLUSION

Much is still unknown regarding the physiologic impact of MG53 in skeletal muscle despite the presence of numerous studies involving the protein. MG53 undoubtedly plays an important role in several arenas of physiology. It is involved in calcium homeostasis, muscle contraction, and regeneration. Its role as an agent in plasma membrane repair is uncontested. Emerging roles in mitochondrial protection further highlight the fact that not all is known about the protein. The therapeutic applications of the protein in treating skeletal muscle pathologies are numerous and include the use of the protein as an agent of repair, in providing a treatment for certain types of dystrophies, and in modulating muscle regeneration.

AUTHOR CONTRIBUTIONS

DB-M, JM, and PL designed the manuscript. DB, HZ, WZ, TT, JM, and PL wrote, read, edited, and approved the final version of manuscript. All authors contributed to the article and approved the submitted version.

FUNDING

This work was partially supported by a postdoctoral Ruth L. Kirschstein National Research Service Award to DB-M (2T32AI106704-06) from ARTIST, a K08-GM126315 grant to PL, and R01-AG056919, R01-AR061385, R01-AR070752, R01-DK106394, and R01-HL138570, as well as by DOD grant W81XWH-18-1-0787 to JM.

REFERENCES

Adesanya, T. M. A., Russell, M., Park, K. H., Zhou, X., Sermersheim, M. A., Gumpper, K., et al. (2019). MG 53 protein protects aortic valve interstitial cells from membrane injury and fibrocalcific remodeling. *J. Am. Heart Assoc.* 8:e009960. doi: 10.1161/jaha.118.009960

Ahn, M. K., Lee, K. J., Cai, C., Huang, M., Cho, C. H., Ma, J., et al. (2016). Mitsugumin 53 regulates extracellular Ca(2+) entry and intracellular Ca(2+) release via Orai1 and RyR1 in skeletal muscle. *Sci. Rep.* 6:36909. doi: 10.1038/srep36909

Alloush, J., and Weisleder, N. (2013). TRIM proteins in therapeutic membrane repair of muscular dystrophy. *JAMA Neurol.* 70, 928–931. doi: 10.1001/jamaneurol.2013.469

Bansal, D., Miyake, K., Vogel, S. S., Groh, S., Chen, C. C., Williamson, R., et al. (2003). Defective membrane repair in dysferlin-deficient muscular dystrophy. *Nature* 423, 168–172. doi: 10.1038/nature01573

Bian, Z., Wang, Q., Zhou, X., Tan, T., Park, K. H., Kramer, H. F., et al. (2019). Sustained elevation of MG53 in the bloodstream increases tissue regenerative capacity without compromising metabolic function. *Nat. Commun.* 10:4659. doi: 10.1038/s41467-019-12483-0

Blanco-Bose, W. E., Yao, C. C., Kramer, R. H., and Blau, H. M. (2001). Purification of mouse primary myoblasts based on alpha 7 integrin expression. *Exp. Cell Res.* 265, 212–220. doi: 10.1006/excr.2001.5191

Buckingham, M. (2007). Skeletal muscle progenitor cells and the role of Pax genes. *C. R. Biol.* 330, 530–533. doi: 10.1016/j.crvi.2007.03.015

Burkin, D. J., and Wuebbles, R. D. (2012). A molecular bandage for diseased muscle. *Sci. Transl. Med.* 4:139fs119. doi: 10.1126/scitranslmed.3004082

Cai, C., Masumiya, H., Weisleder, N., Matsuda, N., Nishi, M., Hwang, M., et al. (2009a). MG53 nucleates assembly of cell membrane repair machinery. *Nat. Cell Biol.* 11, 56–64. doi: 10.1038/ncb1812

Cai, C., Masumiya, H., Weisleder, N., Pan, Z., Nishi, M., Komazaki, S., et al. (2009b). MG53 regulates membrane budding and exocytosis in muscle cells. *J. Biol. Chem.* 284, 3314–3322. doi: 10.1074/jbc.M808866200

Cai, C., Weisleder, N., Ko, J. K., Komazaki, S., Sunada, Y., Nishi, M., et al. (2009c). Membrane repair defects in muscular dystrophy are linked to altered interaction between MG53, caveolin-3, and dysferlin. *J. Biol. Chem.* 284, 15894–15902. doi: 10.1074/jbc.M109.009589

Caruso, M., Ma, D., Msallaty, Z., Lewis, M., Seyoum, B., Al-janabi, W., et al. (2014). Increased interaction with insulin receptor substrate 1, a novel abnormality in insulin resistance and type 2 diabetes. *Diabetes* 63, 1933–1947. doi: 10.2337/db13-1872

Chandler, H. L., Tan, T., Yang, C., Gemensky-Metzler, A. J., Wehrman, R. F., Jiang, Q., et al. (2019). MG53 promotes corneal wound healing and mitigates fibrotic remodeling in rodents. *Commun. Biol.* 2:71. doi: 10.1038/s42003-019-0316-7

Ciciliot, S., and Schiaffino, S. (2010). Regeneration of mammalian skeletal muscle: basic mechanisms and clinical implications. *Curr. Pharmaceutical Design* 16, 906–914. doi: 10.2174/138161210790883453

Demonbreun, A. R., and McNally, E. M. (2016). Plasma membrane repair in health and disease. *Curr. Top. Membr.* 77, 67–96. doi: 10.1016/bs.ctm.2015.10.006

Demonbreun, A. R., Quattrocelli, M., Barefield, D. Y., Allen, M. V., Swanson, K. E., and McNally, E. M. (2016). An actin-dependent annexin complex mediates plasma membrane repair in muscle. *J. Cell Biol.* 213, 705–718. doi: 10.1083/jcb.201512022

Duann, P., Li, H., Lin, P., Tan, T., Wang, Z., Chen, K., et al. (2015). MG53-mediated cell membrane repair protects against acute kidney injury. *Sci. Transl. Med.* 7:279ra236. doi: 10.1126/scitranslmed.3010755

Flix, B., De La Torre, C., Castillo, J., Casal, C., Illa, I., and Gallardo, E. (2013). Dysferlin interacts with calsequestrin-1, myomesin-2 and dynein in human skeletal muscle. *Int. J. Biochem. Cell Biol.* 45, 1927–1938. doi: 10.1016/j.biocel.2013.06.007

Giudice, J., and Taylor, J. M. (2017). Muscle as a paracrine and endocrine organ. *Curr. Opin. Pharmacol.* 34, 49–55. doi: 10.1016/j.coph.2017.05.005

Glover, L., and Brown, R. H. Jr. (2007). Dysferlin in membrane trafficking and patch repair. *Traffic* 8, 785–794. doi: 10.1111/j.1600-0854.2007.00573.x

Guan, F., Huang, T., Wang, X., Xing, Q., Gumpper, K., Li, P., et al. (2019a). The TRIM protein Mitsugumin 53 enhances survival and therapeutic efficacy of stem cells in murine traumatic brain injury. *Stem Cell Res. Ther.* 10:352. doi: 10.1186/s13287-019-1433-4

Guan, F., Zhou, X., Li, P., Wang, Y., Liu, M., Li, F., et al. (2019b). MG53 attenuates lipopolysaccharide-induced neurotoxicity and neuroinflammation via inhibiting TLR4/NF-kappaB pathway in vitro and in vivo. *Prog. Neuropsychopharmacol. Biol. Psychiatry* 95:109684. doi: 10.1016/j.pnpbp.2019.109684

Ham, Y. M., and Mahoney, S. J. (2013). Compensation of the AKT signaling by ERK signaling in transgenic mice hearts overexpressing TRIM72. *Exp. Cell Res.* 319, 1451–1462. doi: 10.1016/j.yexcr.2013.02.016

Han, R. (2011). Muscle membrane repair and inflammatory attack in dysferlinopathy. *Skelet Muscle* 1:10. doi: 10.1186/2044-5040-1-10

Hatakeyama, S. (2017). TRIM family proteins: roles in autophagy, immunity, and carcinogenesis. *Trends Biochem. Sci.* 42, 297–311. doi: 10.1016/j.tibs.2017.01.002

He, B., Tang, R. H., Weisleder, N., Xiao, B., Yuan, Z., Cai, C., et al. (2012). Enhancing muscle membrane repair by gene delivery of MG53 ameliorates muscular dystrophy and heart failure in delta-Sarcoglycan-deficient hamsters. *Mol. Ther.* 20, 727–735. doi: 10.1038/mt.2012.5

Hoffmann, C., and Weigert, C. (2017). Skeletal muscle as an endocrine organ: the role of myokines in exercise adaptations. *Cold Spring Harb. Perspect. Med.* 7:a029793. doi: 10.1101/cshperspect.a029793

Hong, J., Park, J. S., Lee, H., Jeong, J., Hyeon Yun, H., Yun Kim, H., et al. (2016). Myosin heavy chain is stabilized by BCL-2 interacting cell death suppressor (BIS) in skeletal muscle. *Exp. Mol. Med.* 48:e225. doi: 10.1038/emm.2016.2

Hord, J. M., Botchlett, R., and Lawler, J. M. (2016). Age-related alterations in the sarcolemmal environment are attenuated by lifelong caloric restriction and voluntary exercise. *Exp. Gerontol.* 83, 148–157. doi: 10.1016/j.exger.2016.08.006

Hu, X., and Xiao, R. P. (2018). MG53 and disordered metabolism in striated muscle. *Biochim. Biophys. Acta Mol. Basis Dis.* 1864(5 Pt B), 1984–1990. doi: 10.1016/j.bbadis.2017.10.013

Hwang, M., Ko, J. K., Weisleder, N., Takeshima, H., and Ma, J. (2011). Redox-dependent oligomerization through a leucine zipper motif is essential for MG53-mediated cell membrane repair. *Am. J. Physiol. Cell Physiol.* 301, C106–C114. doi: 10.1152/ajpcell.00382.2010

Iizuka, K., Machida, T., and Hirafuji, M. (2014). Skeletal muscle is an endocrine organ. *J. Pharmacol. Sci.* 125, 125–131. doi: 10.1254/jphs.14r02cp

Jia, Y., Chen, K., Lin, P., Lieber, G., Nishi, M., Yan, R., et al. (2014). Treatment of acute lung injury by targeting MG53-mediated cell membrane repair. *Nat. Commun.* 5:4387. doi: 10.1038/ncomms5387

Jung, S. Y., and Ko, Y. G. (2010). TRIM72, a novel negative feedback regulator of myogenesis, is transcriptionally activated by the synergism of MyoD (or myogenin) and MEF2. *Biochem. Biophys. Res. Commun.* 396, 238–245. doi: 10.1016/j.bbrc.2010.04.072

Karstoft, K., and Pedersen, B. K. (2016). Skeletal muscle as a gene regulatory endocrine organ. *Curr. Opin. Clin. Nutr. Metab. Care* 19, 270–275. doi: 10.1097/mco.0000000000000283

Laustsen, P. G., Michael, M. D., Crute, B. E., Cohen, S. E., Ueki, K., Kulkarni, R. N., et al. (2002). Lipoatrophic diabetes in Irs1(-/-)/Irs3(-/-) double knockout mice. *Genes Dev.* 16, 3213–3222. doi: 10.1101/gad.1034802

Lee, C. S., Yi, J. S., Jung, S. Y., Kim, B. W., Lee, N. R., Choo, H. J., et al. (2010). TRIM72 negatively regulates myogenesis via targeting insulin receptor substrate-1. *Cell Death Differ* 17, 1254–1265. doi: 10.1038/cdd.2010.1

Lee, E. H. (2010). Ca2+ channels and skeletal muscle diseases. *Prog. Biophys. Mol. Biol.* 103, 35–43. doi: 10.1016/j.pbiomolbio.2010.05.003

Lee, K. J., Park, C. S., Woo, J. S., Kim, D. H., Ma, J., and Lee, E. H. (2012). Mitsugumin 53 attenuates the activity of sarcoplasmic reticulum Ca(2+)-ATPase 1a (SERCA1a) in skeletal muscle. *Biochem. Biophys. Res. Commun.* 428, 383–388. doi: 10.1016/j.bbrc.2012.10.063

Lek, A., Evesson, F. J., Lemckert, F. A., Redpath, G. M., Lueders, A. K., Turnbull, L., et al. (2013). Calpains, cleaved mini-dysferlinC72, and L-type channels underpin calcium-dependent muscle membrane repair. *J. Neurosci.* 33, 5085–5094. doi: 10.1523/jneurosci.3560-12.2013

Li, H., Duann, P., Lin, P. H., Zhao, L., Fan, Z., Tan, T., et al. (2015). Modulation of wound healing and scar formation by MG53 protein-mediated cell membrane repair. *J. Biol. Chem.* 290, 24592–24603. doi: 10.1074/jbc.M115.680074

Lijie, G., Yueyue, Z., Nan, Z., Ling, W., Xuan, W., and Weijie, Y. (2019). Mitsugumin 53 promotes mitochondrial autophagy through regulating Ambra1 expression in C2C12 myoblast cells. *Cell Biol. Int.* 43, 290–298. doi: 10.1002/cbin.11097

Lin, P., Zhu, H., Cai, C., Wang, X., Cao, C., Xiao, R., et al. (2012). Nonmuscle myosin IIA facilitates vesicle trafficking for MG53-mediated cell membrane repair. *Faseb J.* 26, 1875–1883. doi: 10.1096/fj.11-188599

Liu, C., Hu, Y. H., Han, Y., Wang, Y. B., Zhang, Y., Zhang, X. Q., et al. (2020). MG53 protects against contrast-induced acute kidney injury by reducing cell membrane damage and apoptosis. *Acta Pharmacol. Sin.* doi: 10.1038/s41401-020-0420-8 [Epub ahead of print].

Liu, F., Song, R., Feng, Y., Guo, J., Chen, Y., Zhang, Y., et al. (2015). Upregulation of MG53 induces diabetic cardiomyopathy through transcriptional activation of peroxisome proliferation-activated receptor alpha. *Circulation* 131, 795–804. doi: 10.1161/circulationaha.114.012285

Liu, J., Zhu, H., Zheng, Y., Xu, Z., Li, L., Tan, T., et al. (2015). Cardioprotection of recombinant human MG53 protein in a porcine model of ischemia and reperfusion injury. *J. Mol. Cell Cardiol.* 80, 10–19. doi: 10.1016/j.yjmcc.2014.12.010

Ma, H., Liu, J., Bian, Z., Cui, Y., Zhou, X., Zhang, B., et al. (2015). Effect of metabolic syndrome on mitsugumin 53 expression and function. *PLoS One* 10:e0124128. doi: 10.1371/journal.pone.0124128

Ma, L. L., Kong, F. J., Guo, J. J., Zhu, J. B., Shi, H. T., Li, Y., et al. (2017). Hypercholesterolemia abrogates remote ischemic preconditioning-induced cardioprotection: role of reperfusion injury salvage kinase signals. *Shock* 47, 363–369. doi: 10.1097/shk.0000000000000737

Ma, L. L., Zhang, F. J., Qian, L. B., Kong, F. J., Sun, J. F., Zhou, C., et al. (2013). Hypercholesterolemia blocked sevoflurane-induced cardioprotection against ischemia-reperfusion injury by alteration of the MG53/RISK/GSK3beta signaling. *Int. J. Cardiol.* 168, 3671–3678. doi: 10.1016/j.ijcard.2013.06.037

Matsuda, C., Miyake, K., Kameyama, K., Keduka, E., Takeshima, H., Imamura, T., et al. (2012). The C2A domain in dysferlin is important for association with MG53 (TRIM72). *PLoS Curr.* 4:e5035add8caff4. doi: 10.1371/5035add8caff4

McCroskery, S., Thomas, M., Maxwell, L., Sharma, M., and Kambadur, R. (2003). Myostatin negatively regulates satellite cell activation and self-renewal. *J. Cell Biol.* 162, 1135–1147. doi: 10.1083/jcb.200207056

McNeil, P. (2009). Membrane repair redux: redox of MG53. *Nat. Cell Biol.* 11, 7–9. doi: 10.1038/ncb0109-7

Mukund, K., and Subramaniam, S. (2020). Skeletal muscle: a review of molecular structure and function, in health and disease. *Wiley Interdiscip Rev. Syst. Biol. Med.* 12:e1462. doi: 10.1002/wsbm.1462

Nguyen, N., Yi, J. S., Park, H., Lee, J. S., and Ko, Y. G. (2014). Mitsugumin 53 (MG53) ligase ubiquitinates focal adhesion kinase during skeletal myogenesis. *J. Biol. Chem.* 289, 3209–3216. doi: 10.1074/jbc.M113.525154

Okino, R., Usui, A., Yoneyama, Y., Takahashi, S. I., and Hakuno, F. (2020). Myoblasts with higher IRS-1 levels are eliminated from the normal cell layer during differentiation. *Front. Endocrinol. (Lausanne)* 11:96. doi: 10.3389/fendo.2020.00096

Ozato, K., Shin, D. M., Chang, T. H., and Morse, H. C. III (2008). TRIM family proteins and their emerging roles in innate immunity. *Nat. Rev. Immunol.* 8, 849–860. doi: 10.1038/nri2413

Relaix, F., Montarras, D., Zaffran, S., Gayraud-Morel, B., Rocancourt, D., Tajbakhsh, S., et al. (2006). Pax3 and Pax7 have distinct and overlapping functions in adult muscle progenitor cells. *J. Cell Biol.* 172, 91–102. doi: 10.1083/jcb.200508044

Rocheteau, P., Vinet, M., and Chretien, F. (2015). Dormancy and quiescence of skeletal muscle stem cells. *Results Probl. Cell Differ.* 56, 215–235. doi: 10.1007/978-3-662-44608-9_10

Sermersheim, M., Lin, P., Kenney, A., McMichael, T., Cai, C., Gumpper, K., et al. (2020). MG53 suppresses interferon-β and inflammation via regulation of ryanodine receptor-mediated intracellular calcium signaling. *Nat. Commun.* 11:3624.

Shea, K. L., Xiang, W., LaPorta, V. S., Licht, J. D., Keller, C., Basson, M. A., et al. (2010). Sprouty1 regulates reversible quiescence of a self-renewing adult muscle stem cell pool during regeneration. *Cell Stem Cell* 6, 117–129. doi: 10.1016/j.stem.2009.12.015

Soleimani, V. D., Nguyen, D., Ramachandran, P., Palidwor, G. A., Porter, C. J., Yin, H., et al. (2018). Cis-regulatory determinants of MyoD function. *Nucleic Acids Res.* 46, 7221–7235. doi: 10.1093/nar/gky388

Song, R., Peng, W., Zhang, Y., Lv, F., Wu, H. K., Guo, J., et al. (2013). Central role of E3 ubiquitin ligase MG53 in insulin resistance and metabolic disorders. *Nature* 494, 375–379. doi: 10.1038/nature11834

Takeshima, H., Iino, M., Takekura, H., Nishi, M., Kuno, J., Minowa, O., et al. (1994). Excitation-contraction uncoupling and muscular degeneration in mice lacking functional skeletal muscle ryanodine-receptor gene. *Nature* 369, 556–559. doi: 10.1038/369556a0

Tamemoto, H., Kadowaki, T., Tobe, K., Yagi, T., Sakura, H., Hayakawa, T., et al. (1994). Insulin resistance and growth retardation in mice lacking insulin receptor substrate-1. *Nature* 372, 182–186. doi: 10.1038/372182a0

Tan, T., Ko, Y. G., and Ma, J. (2016). Dual function of MG53 in membrane repair and insulin signaling. *BMB Rep.* 49, 414–423. doi: 10.5483/bmbrep.2016.49.8.079

Terauchi, Y., Iwamoto, K., Tamemoto, H., Komeda, K., Ishii, C., Kanazawa, Y., et al. (1997). Development of non-insulin-dependent diabetes mellitus in the double knockout mice with disruption of insulin receptor substrate-1 and beta cell glucokinase genes. Genetic reconstitution of diabetes as a polygenic disease. *J. Clin. Invest.* 99, 861–866. doi: 10.1172/JCI119250

von Maltzahn, J., Jones, A. E., Parks, R. J., and Rudnicki, M. A. (2013). Pax7 is critical for the normal function of satellite cells in adult skeletal muscle. *Proc. Natl. Acad. Sci. U.S.A.* 110, 16474–16479. doi: 10.1073/pnas.1307680110

Wang, Q., Bian, Z., Jiang, Q., Wang, X., Zhou, X., Park, K. H., et al. (2020). MG53 does not manifest the development of diabetes in db/db mice. *Diabetes* 69, 1052–1064. doi: 10.2337/db19-0807

Weisleder, N., Takeshima, H., and Ma, J. (2008). Immuno-proteomic approach to excitation–contraction coupling in skeletal and cardiac muscle: molecular insights revealed by the mitsugumins. *Cell Calcium* 43, 1–8. doi: 10.1016/j.ceca.2007.10.006

Weisleder, N., Takeshima, H., and Ma, J. (2009). Mitsugumin 53 (MG53) facilitates vesicle trafficking in striated muscle to contribute to cell membrane repair. *Commun. Integr. Biol.* 2, 225–226. doi: 10.4161/cib.2.3.8077

Weisleder, N., Takizawa, N., Lin, P., Wang, X., Cao, C., Zhang, Y., et al. (2012). Recombinant MG53 protein modulates therapeutic cell membrane repair in treatment of muscular dystrophy. *Sci. Transl. Med.* 4:139ra185. doi: 10.1126/scitranslmed.3003921

Wu, H. K., Zhang, Y., Cao, C. M., Hu, X., Fang, M., Yao, Y., et al. (2019). Glucose-sensitive myokine/cardiokine MG53 regulates systemic insulin response and metabolic homeostasis. *Circulation* 139, 901–914. doi: 10.1161/circulationaha.118.037216

Xu, Y., Ma, L. L., Zhou, C., Zhang, F. J., Kong, F. J., Wang, W. N., et al. (2013). Hypercholesterolemic myocardium is vulnerable to ischemia-reperfusion injury and refractory to sevoflurane-induced protection. *PLoS One* 8:e76652. doi: 10.1371/journal.pone.0076652

Yao, Y., Zhang, B., Zhu, H., Li, H., Han, Y., Chen, K., et al. (2016). MG53 permeates through blood-brain barrier to protect ischemic brain injury. *Oncotarget* 7, 22474–22485. doi: 10.18632/oncotarget.7965

Yi, J. S., Park, J. S., Ham, Y. M., Nguyen, N., Lee, N. R., Hong, J., et al. (2013). MG53-induced IRS-1 ubiquitination negatively regulates skeletal myogenesis and insulin signalling. *Nat. Commun.* 4:2354. doi: 10.1038/ncomms3354

Yuan, H., Niu, Y., Liu, X., Yang, F., Niu, W., and Fu, L. (2013). Proteomic analysis of skeletal muscle in insulin-resistant mice: response to 6-week aerobic exercise. *PLoS One* 8:e53887. doi: 10.1371/journal.pone.0053887

Zabielski, P., Lanza, I. R., Gopala, S., Heppelmann, C. J., Bergen, H. R. III, Dasari, S., et al. (2016). Altered skeletal muscle mitochondrial proteome as the basis of disruption of mitochondrial function in diabetic mice. *Diabetes* 65, 561–573. doi: 10.2337/db15-0823

Zhang, Y., Wu, H. K., Lv, F., and Xiao, R. P. (2017). MG53: biological function and potential as a therapeutic target. *Mol. Pharmacol.* 92, 211–218. doi: 10.1124/mol.117.108241

Zhu, H., Hou, J., Roe, J. L., Park, K. H., Tan, T., Zheng, Y., et al. (2015). Amelioration of ischemia-reperfusion-induced muscle injury by the recombinant human MG53 protein. *Muscle Nerve* 52, 852–858. doi: 10.1002/mus.24619

Zhu, H., Lin, P., De, G., Choi, K. H., Takeshima, H., Weisleder, N., et al. (2011). Polymerase transcriptase release factor (PTRF) anchors MG53 protein to cell injury site for initiation of membrane repair. *J. Biol. Chem.* 286, 12820–12824. doi: 10.1074/jbc.C111.221440

Conflict of Interest: JM was the founder of TRIM-edicine, Inc., a university spin-off biotechnology company that is developing recombinant MG53 protein as a therapeutic reagent for regenerative medicine. Patents on the use of MG53 are held by Rutgers University and The Ohio State University.

The remaining authors declare that the research was conducted in the absence of any commercial or financial relationships that could be construed as a potential conflict of interest.

frontiers in Physiology

ORIGINAL RESEARCH
published: 12 November 2020
doi: 10.3389/fphys.2020.597647

Phasic Store-Operated Ca^{2+} Entry During Excitation-Contraction Coupling in Skeletal Muscle Fibers From Exercised Mice

*Elena Lilliu[1], Karlheinz Hilber[1], Bradley S. Launikonis[2] and Xaver Koenig[1]**

[1] Department of Neurophysiology and Pharmacology, Center for Physiology and Pharmacology, Medical University of Vienna, Vienna, Austria, [2] School of Biomedical Sciences, The University of Queensland, Brisbane, QLD, Australia

Store-operated calcium entry (SOCE) plays a pivotal role in skeletal muscle physiology as, when impaired, the muscle is prone to early fatigue and the development of different myopathies. A chronic mode of slow SOCE activation is carried by stromal interaction molecule 1 (STIM1) and calcium-release activated channel 1 (ORAI1) proteins. A phasic mode of fast SOCE (pSOCE) occurs upon single muscle twitches in synchrony with excitation-contraction coupling, presumably activated by a local and transient depletion at the terminal cisternae of the sarcoplasmic reticulum Ca^{2+}-stores. Both SOCE mechanisms are poorly understood. In particular, pSOCE has not been described in detail because the conditions required for its detection in mouse skeletal muscle have not been established to date. Here we report the first measurements of pSOCE in mouse extensor digitorum longus muscle fibers using electrical field stimulation (EFS) in a skinned fiber preparation. We show moderate voluntary wheel running to be a prerequisite to render muscle fibers reasonably susceptible for EFS, and thereby define an experimental paradigm to measure pSOCE in mouse muscle. Continuous monitoring of the physical activity of mice housed in cages equipped with running wheels revealed an optimal training period of 5–6 days, whereby best responsiveness to EFS negatively correlated with running distance and speed. A comparison of pSOCE kinetic data in mouse with those previously derived from rat muscle demonstrated very similar properties and suggests the existence and similar function of pSOCE across mammalian species. The new technique presented herein enables future experiments with genetically modified mouse models to define the molecular entities, presumably STIM1 and ORAI1, and the physiological role of pSOCE in health and under conditions of disease.

Keywords: store-operated Ca^{2+}-entry, skeletal muscle, mouse, exercise, electrical field stimulation

OPEN ACCESS

Edited by:
Matias Mosqueira, Heidelberg University Hospital, Germany

Reviewed by:
Antonio Michelucci, University of Studies G. d'Annunzio Chieti – Pescara, Italy
Vincent Jacquemond, Centre National de la Recherche Scientifique (CNRS), France

****Correspondence:***
Xaver Koenig
xaver.koenig@meduniwien.ac.at

Specialty section:
This article was submitted to Striated Muscle Physiology, a section of the journal Frontiers in Physiology

Received: *21 August 2020*
Accepted: *20 October 2020*
Published: *12 November 2020*

Citation:
Lilliu E, Hilber K, Launikonis BS and Koenig X (2020) Phasic Store-Operated Ca^{2+} Entry During Excitation-Contraction Coupling in Skeletal Muscle Fibers From Exercised Mice. Front. Physiol. 11:597647. doi: 10.3389/fphys.2020.597647

INTRODUCTION

Store-operated calcium entry (SOCE) is a widespread cellular mechanism, by which calcium (Ca^{2+}) influx across the plasma membrane is triggered by a depletion of the Endo/Sarcoplasmic reticulum (ER/SR) Ca^{2+} stores (Prakriya and Lewis, 2015). Stromal interaction molecule (STIM) acts as the SR Ca^{2+} sensor (Roos et al., 2005; Dirksen, 2009; Prakriya and Lewis, 2015) to orchestrate the

activation of Ca^{2+}-release activated Ca^{2+} channel (ORAI) in the plasma membrane (Feske et al., 2006; Vig et al., 2006; Dirksen, 2009). STIM1 and ORAI1 are highly expressed in skeletal muscle (Stiber et al., 2008; Vig et al., 2008), and deficiency of either protein abolished SOCE (Lyfenko and Dirksen, 2008). Loss as well as gain of function mutations within STIM1 and ORAI1 affect SOCE and result in the development of skeletal myopathy (Feske et al., 2006; Stiber et al., 2008; McCarl et al., 2009; Böhm et al., 2013, 2014, 2017; Endo et al., 2015).

Store-operated calcium entry is well understood, e.g., in the course of immune cell activation (Prakriya and Lewis, 2015), but its role in skeletal muscle remains elusive. While SOCE is a relatively slow process in non-excitable cells (Launikonis et al., 2010; Trebak et al., 2013) it presents with extraordinary fast kinetics in skeletal muscle (Launikonis and Ríos, 2007; Edwards et al., 2010; Launikonis et al., 2010; Koenig et al., 2018, 2019) suggesting a close juxtaposition or even physical association of STIM1 and ORAI1 within the triads (Dirksen, 2009; Launikonis et al., 2010; Wei-Lapierre et al., 2013; Koenig et al., 2018). Recently, we demonstrated that SOCE is activated upon individual action potentials (APs) in rat skeletal muscle cells (Koenig et al., 2018, 2019), a mode of SOCE that we named phasic SOCE (pSOCE), because it showed comparable kinetics to excitation-contraction coupling.

Action potentials in the transverse tubular system (t-system) of skinned skeletal muscle fibers can be triggered by electrical field stimulation (EFS), and respective muscle twitches are indistinguishable from twitches in intact fibers (Posterino et al., 2000; Posterino and Lamb, 2003). While EFS works well in rat extensor digitorum longus (EDL) muscle fibers, respective experiments presented challenging in mice. The reason for that is unknown, but might relate to the fact that only fibers derived from rats express high enough numbers of voltage-gated sodium channels (VGSCs) within the t-tubular system to enable sufficient membrane depolarization and subsequent activation of the voltage-sensor to trigger Ca^{2+}-release from the SR via the ryanodine receptor. Importantly, until now, this has precluded the assessment of pSOCE in mice, and thereby the study of its functional and pathophysiological relevance in skeletal muscle by genetically modified mouse models.

Here we report that moderate physical training of mice by voluntary wheel running for several days enabled successful EFS of skinned mouse EDL fibers in a manner fully comparable to EFS of skinned rat EDL fibers. The EFS- triggered release of SR Ca^{2+} induced an activation of pSOCE, which was indistinguishable from that observed in rat EDL fibers. Our results demonstrate the existence of pSOCE in skeletal muscle fibers across animal species and open the door for future experiments on genetically modified mice to study the role of pSOCE in health and disease.

MATERIALS AND METHODS

Ethics Statement

The current study conforms to the guiding principles of the Declaration of Helsinki and coincides with the rules of the Animal Welfare Committee at the Medical University of Vienna. The current study is covered by the animal ethics vote BMBWF 2020-0.499.046 granted by the Federal Ministry of the Republic of Austria.

Animal Model and Skinned Fiber Preparation

Male C57BL/6 mice at an age of 10–15 weeks were used throughout this study. Data derived from rat, as presented in **Figure 5**, are taken from previous work (Koenig et al., 2018), with permission. On the day of experiment animals were killed by cervical dislocation and the EDL muscle was rapidly excised. Isolation of single fibers and mechanical "skinning" of the fibers was performed as previously described (Cully et al., 2016; Koenig et al., 2018, 2019). Briefly, EDL muscle was transferred to a glass petri dish filled with paraffin oil and with the bottom covered by a layer of Sylgard. Immersed in paraffin oil, muscle was manually dissected into small bundles of fibers. Single fibers were isolated from the small bundles and the sarcolemma was mechanically removed with forceps. Fibers were cut at up to 1 cm in length and knots were tied on both ends of the skinned fiber using 10-0 nylon or silk suture, which enabled proper handling of the single fiber with forceps (Fine science tools, Dumont #5) and also served to mount the skinned fiber in a custom built experimental chamber. After skinning, fibers isolated in the paraffin oil filled petri dish were plotted dry on Whatman filter paper and transferred to the experimental chamber filled with internal solution (see below). The chamber had a diameter of about 1.5 cm and was based on top of a 1.5 coverslip. Two parallel Minutien Pins (Fine science tools) glued down onto the coverslip served to hold the fiber by clamping down the suture knot tied at the fiber ends. Once the fiber was fixed in the chamber the preparation was immediately mounted onto the stage of an inverted microscope (Nikon Eclipse Ti-E). The whole procedure, from sacrificing the animal ($t = 0$ min), to the excision of the EDL muscle ($t = 15$ min), the isolation and skinning of single fibers ($t = 35$ min), a possible incubation with Rhod-5N ($t = 50$ min), and the mounting of the fiber within the experimental chamber ($t = 60$ min), allocates a total time of about 1 h, with approximated time points given in brackets. Due to experiments were performed in a sequential manner, subsequent fibers were isolated only after confocal imaging on the preceding fiber was finished, with respective additive temporal delays. To improve preparation quality, room temperature was constantly maintained at 22 degrees and muscle, which was not used immediately, was remained immersed in paraffin oil and kept on ice. Under these conditions successful EFS can be obtained several hours after excision of the muscle. Once mounted into the recording chamber, individual skinned fibers loaded with rhod-5N and fluo-4 that respond to EFS were typically recorded over a time span of several minutes, but we haven't investigated how stable the preparation is over longer time periods.

To load the t-system with rhod-5N, small bundles of fibers were dissected with fine forceps under paraffin oil from the EDL muscle. Before skinning, a small bundle was exposed to a single drop of Ringer solution containing 2.5 mM of the Ca^{2+}-sensitive dye rhod-5N applied by a micro capillary. The drop was left on

the fiber bundle for at least 10 min before single fibers were mechanically isolated and skinned. By skinning the fiber the t-system re-seals and traps rhod-5N within its lumen (Lamb et al., 1995; Cully et al., 2016).

Voluntary Running Wheel Training

Mice were kept in cages equipped with running wheels (ACT-551-MS-SS, Coulbourn Instruments). Mouse running activity was monitored by counting wheel rotations by using a magnetic switch, which was connected to a breakout box (ACT-553, Coulbourn Instruments) through a pair of banana jacks. The breakout box was further connected to an interface (ACT-556a, Coulbourn), which communicated via USB with the recording software (Clocklab; ACT-500, Coulbourn). Recorded data were read and analyzed using the ClockLab analysis toolbox in MATLAB R2015a and Microsoft Excel.

EFS-Score

We defined the EFS-score as an overall measure of how well fibers isolated from one animal preparation could be electrically stimulated. The EFS-score takes integer values ranging from 0 to 4 based on the following criteria: 0, defines fibers that could not be stimulated at all; 1, only very small fiber segments responded, or small segments with weak Ca^{2+}-release; 2, half or less of the fiber responding to EFS with weak Ca^{2+} release; 3, almost complete excitation along the whole fiber length with strong Ca^{2+} release, or excitation along the entire fiber but with weaker release of Ca^{2+}; 4, a strong release of Ca^{2+} along the whole fiber. Respective EFS-score levels were assigned if at least one fiber from one animal preparation met the required criterion. The intensity of Ca^{2+} release was determined from the fluo-4 peak amplitude upon stimulation with a cut off at $F/F_0 = 1.5$; weak Ca^{2+} release defined being lower and strong Ca^{2+} release defined being larger, respectively.

Experimental Solutions

Skinned fibers were bathed in an internal salt solution detailed in previous work (Cully et al., 2016; Koenig et al., 2018). It consisted of (in mM): 90 HEPES, 10 EGTA, 40 HDTA (1,6-diaminohexane-N,N,N′,N′-tetraacetic acid), 8.77 MgO, 1.94 CaCO3, 8 Na2ATP, 10 Na2CP (creatine phosphate). pH was adjusted to 7.1 ± 0.1 with KOH. Free cytosolic Ca^{2+} concentration was calculated to 67 nM assuming a pre-determined K_d of EGTA for Ca^{2+} of 200 nM (Cully et al., 2016). Free cytosolic Mg^{2+} concentration was 1 mM. BTS (4-methyl-*N*-(phenylmethyl)benzenesulfonamide; #1870, Tocris Bio-Techne) was dissolved in dimethyl sulfoxide (DMSO) and added at a final concentration of 50 μM to inhibit fiber contraction during EFS. Fluo-4 (F14200, ThermoFisher) was dissolved in DMSO at a stock concentration of 5 mM, stored in aliquots, and was added at a final concentration of 10 μM. All solutions were made up freshly on the day of experiment.

Calibration of fluo-4 and rhod-5N Fluorescence

K_{d_Ca} values for fluo-4 and rhod-5N, 1 μM and 0.872 mM, respectively, were taken from previously published work on rat EDL skinned fibers (Koenig et al., 2018). Fluorescence values of fluo-4 and rhod-5N were converted to $[Ca^{2+}]_{cyto}$ and $[Ca^{2+}]_{t\text{-}sys}$ using the following formula for single wavelength dyes assuming quasi steady-state conditions of Ca^{2+}-binding to the fluorophore for every acquired image within the obtained image series (Grynkiewicz et al., 1985; Royer et al., 2008; Cully et al., 2016),

$$\left[Ca^{2+}\right] = K_d * (F - F_{min}) \,/\, (F_{max} - F), \quad (1)$$

with $[Ca^{2+}]$ is free Ca^{2+} concentration, K_d is fluorophore dissociation constant for Ca^{2+}, F is fluorophore fluorescence, F_{min} and F_{max} is fluorophore fluorescence under Ca^{2+} free or high Ca^{2+} conditions in the presence of the ionophores ionomycin (25 μM) and calcimycin (A23187, 25 μM) (Cully et al., 2016). Calibration solution for F_{max} contained (in mM): 5 $CaCl_2$, 140 NaCl, 1 $MgCl_2$, 10 HEPES, 4 KCl, 5 glucose, pH 7.4 with NaOH/HCl, with added ionophores and 100 μM BTS. F_{min} was Ca^{2+} free and contained: 90 HEPES, 10 EGTA, 40 HDTA, 10.3 MgO, 1.94 $CaCO_3$, 8 Na_2ATP, 10 Na_2CP. pH was adjusted to 7.1 ± 0.1 with KOH; with added ionophores and 50 μM BTS.

To determine $[Ca^{2+}]_{t\text{-}sys}$ (t), Eq. (1) was used, which required determining F_{min} and F_{max} for each fiber. F_{min} was determined at the end of each experiment. F_{max} was determined by rearranging Eq. (1):

$$F_{max} = F + (F - F_{min}) * K_d \,/\, \left[Ca^{2+}\right],$$

with F, the fluorescence before EFS, and $[Ca^{2+}]$, the respective free Ca^{2+} concentration in the cytoplasm (67 nM) and the t-system (calibrated in an independent set of experiments), respectively. Independent calibration of the t-system was necessary because exposure of the skinned fibers to the F_{max} solutions frequently induced the formation of vacuoles, mostly in the longitudinal t-system, which could not be identified on the recordings from the resonant scanner due to its poor spatial resolution. Moreover, due to the high frequency sampling, rhod-5N fluorescence bleaches over time, roughly by about 20% during 2 min of recording, which would induce a large calibration error. Therefore, we performed $n = 5$ experiment using low speed recordings with high spatial resolution that allowed us to identify vacuoles and to exclude these regions from the calibration process. In this way we calibrated $[Ca^{2+}]_{t\text{-}sys}$ before EFS in the presence of 67 nM $[Ca^{2+}]_{cyto}$ and confirmed it to be 1.4 mM in mouse; as determined previously in rat EDL muscle fibers (Cully et al., 2016).

Electrical Field Stimulation

Electrical field stimulation was applied via a pair of platinum electrodes placed in parallel to the long axis and on opposing sides of a skinned fiber set about 1 cm apart. Monophasic square voltage pulses with amplitudes of 60 V and durations of 2–4 ms were generated by a GRASS S48 square pulse stimulator box and delivered at a frequency of 1, 2, 5, or 10 Hz.

Confocal Imaging

The fibers were imaged as previously described (Koenig et al., 2019), using a 20× water (Nikon, CFI APO 20× WI λS, long working distance, NA 0.95, or Plan Apo λ 20× NA

0.75) immersion objective on a Nikon laser scanning confocal microscope system (Nikon A1R+ system on an inverted Nikon Ti-E microscope) equipped with a 12 kHz resonant scanner and high-sensitivity GaAsP detectors. Rhod-5N and fluo-4 were excited at 488 and 561 nm at a laser power of 0.4–1% and 0.4–0.8%, and emitted light was collected at 525/50 nm and 595/50 nm, respectively. The pinhole was set to 4–7 Airy units. Acquired image series (xyt) had a physical dimension of $x = 512$ pixel and $y = 32$–128 pixel, resulting in a temporal resolution of $\Delta t = 4$–16 ms, or 250–62 frames s^{-1}. Fluorescence was averaged across a region of interest to improve the signal to noise ratio, in particular necessary to monitor rhod-5N fluorescence in the t-system.

Statistical Analysis and Data Fitting

Throughout the manuscript data are presented as means ± SEM. The number of mice used in this study is indicated by *N*, while the number of fibers is denoted by n.

Mean data of the rate constants and $[Ca^{2+}]_{t\text{-}sys}$ in **Figure 5** were fit with single exponential functions of the form, $y = y0 + \left(Plateau - y0\right) * \left(1 - \exp\left(-k * x\right)\right)$, were y represents the ordinate values, rate and $[Ca^{2+}]_{t\text{-}sys}$, respectively, and x the abscissa value frequency. $y0$ denotes the initial value at zero frequency, which were constrained to 0 and 1.4 for rate and $[Ca^{2+}]_{t\text{-}sys}$, respectively, reflecting no depletion and a constant level of $[Ca^{2+}]_{t\text{-}sys}$ if no EFS was applied. Plateau reflects the y value in the limit of infinite frequency, and k the exponential rate constant. To compare data from mouse with those derived from rat, respective fits were compared with an Extra sum-of-square F-test. A p value <0.05 was considered significant.

Rights and Permissions

Data from rat EDL muscle fibers were taken from Koenig et al. (2018) published under CreativeCommons BY 4.0 license.

RESULTS

In rat, EFS can trigger APs in the sealed t-system and subsequent Ca^{2+} release from the SR in skinned, fast-twitch EDL muscle fibers (Posterino et al., 2000; Posterino and Lamb, 2003; Goodman et al., 2008; Launikonis et al., 2009; Koenig et al., 2018, 2019). In contrast, EFS works much inferior in skinned fibers from rat and mouse slow-twitch soleus muscle and, importantly, in skinned fibers from mouse EDL muscle. The reason for that is unknown. The inability to use mouse mechanically skinned muscle fibers for EFS represents an impediment to research efforts. We suspected that the inability of mouse skinned skeletal muscle fibers to respond to EFS arose from a significant physical inactivity of experimental mice housed in standard cages, which substantially restrains their natural running behavior. To overcome this, we provided the mice with voluntary running wheels for 1 to 14 days and tested the excitability in mechanically skinned fibers prepared from the EDL muscles thereafter. Continuous monitoring of the physical activity revealed a status of significant de-training in conventionally housed mice (**Figure 1A–C**). Thus, at the beginning of training, mice ran a distance of about ∼2 km/day (**Figure 1A**) at an average speed of ∼0.5 km/h (**Figure 1B**). These values are considerably lower than commonly published values, where mice typically travel distances of 4 km/day at an average speed of about 1 km/h (Coleman et al., 1998; Manzanares et al., 2019). Respective activity values increased considerably with continuous training times (**Figures 1A,B**) confirming our hypothesis that mice housed in standard cages show signs of substantial de-training. Running times on the other hand did not change during the whole training period (**Figure 1C**), and recorded values matched previously published ones (Coleman et al., 1998; Manzanares et al., 2019).

Electrical Field Stimulation Induces SR Ca^{2+} Release in Skeletal Muscle Fibers of Trained Mice

To test if the physical training of mice would result in skinned muscle fibers that respond to EFS we isolated single fibers of EDL muscle derived from animals that had used a voluntary running wheel (**Figure 1**). These fibers were mechanically skinned by removing the sarcolemma with forceps, which causes the t-system to seal and leaves the fiber's cytoplasm accessible to the surrounding bath solution but preserves the fiber structure and function otherwise (Lamb and Stephenson, 1994; Dutka et al., 2008; Cully et al., 2017). Subsequently, these skinned fibers were immersed in a physiological salt solution mimicking the cytoplasmic environment of the cell, with free Ca^{2+} strongly buffered by 10 mM EGTA. The added Ca^{2+}-sensitive dye fluo-4 allowed for real-time imaging of changes in the cytosolic free calcium concentration with confocal microscopy, while EFS was applied by a pair of platinum electrodes placed in parallel to the longitudinal axis of the fiber (Posterino et al., 2000; Koenig et al., 2018, 2019). **Figure 2**, shows one of the first successful EFS in a skinned EDL fiber from a trained mouse. Individual electrical field pulses elicited clearly discernible transient rises in fluo-4 fluorescence indicating a respective increase in free cytosolic Ca^{2+} ($[Ca^{2+}]_{cyto}$) due to SR Ca^{2+} release. The placing of the stimulating electrodes in parallel to the fiber's long axis led to an induction of APs in the sealed t-system (Posterino et al., 2000) simultaneously across sarcomeres, as evidenced by a uniform excitation pattern across the whole fiber length (**Figure 2A**). The high EGTA buffering in the cytosol led to Ca^{2+}-transients of brief duration and with only a small increase in baseline fluorescence after release (**Figure 2B**). The fiber could successfully be stimulated at frequencies of 1, 2, 5, and 10 Hz with the higher frequencies leading to an increase of baseline Ca^{2+} levels during trains of stimulation (**Figure 2C**).

Moderate but Not Excessive Exercise Enables Successful Electrical Field Stimulation of Mouse Skinned Skeletal Muscle Fibers

Without training we were consistently struggling to obtain robust responses to EFS in mouse EDL muscle fibers. However, already a few days of voluntary wheel running led to a convincing

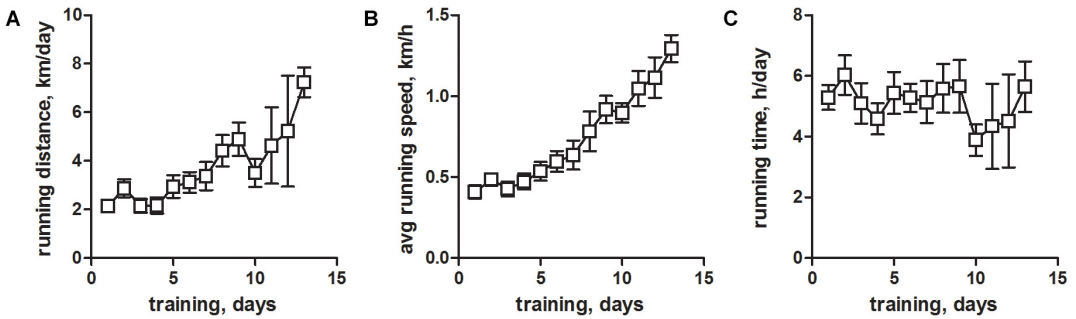

FIGURE 1 | Voluntary running wheel parameters of housed mice. Male C57BL/6 mice at an age of 10–15 weeks were trained between 1 and 14 days by providing a running wheel in their cages. Training parameters of voluntary wheel running were monitored continuously for individual animals. **(A)** Total daily running distance (kilometers per day), **(B)** average daily running speed (kilometers per hour), and **(C)** total daily running time (hours per day). All values are given as means ± SEM and are derived from $N = 29$ mice.

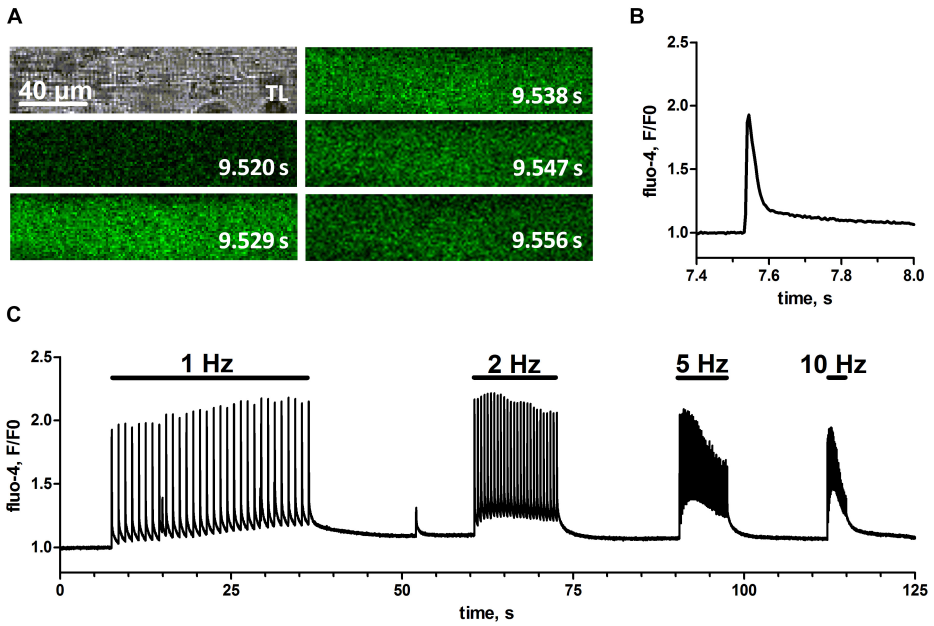

FIGURE 2 | Cytosolic Ca^{2+}-transients upon electrical field stimulation in skinned mouse skeletal muscle fibers. EFS was applied via two platinum electrodes in parallel to the fiber's long-axis by rectangular monophasic voltage steps of 60 V with 4 ms duration. A skinned mouse EDL muscle fiber was bathed in a solution containing endogenous free Ca^{2+}, Mg^{2+}, and ATP concentrations. **(A)** Original transmitted light image of the skinned fiber (top left) and respective image series of fluo-4 fluorescence with indicated time stamps referring to the time course of single EFS pulse induced Ca^{2+}-transient (left to right, top to bottom). Scale bar refers to *x*- and *y*-dimension. Note that, in order to obtain a maximal imaging speed, recorded image series were restricted to a narrow rectangular region of interest within the fiber; therefore no area surrounding the fiber can be seen. **(B)** Profile of the fluo-4 fluorescence plotted as fluorescence over baseline fluorescence (F/F_0) during the first delivered EFS pulse. **(C)** Profile of fluo-4 fluorescence (F/F_0) during trains of EFS delivered at different frequencies of 1, 2, 5, and 10 Hz. Original image series and respective fluo-4 profile were obtained from one representative fiber.

stimulation of mouse EDL skinned fibers (**Figure 2**). In order to systematically derive optimal training conditions, we sacrificed animals that had been trained for between 1 and 14 days. We assessed the benefit of training by counting the number of fibers within one preparation (one animal per experiment day) that responded positively to EFS (**Figure 3A**). As a second readout, we defined a specific score (EFS-score; see section "Materials and Methods" for definition details), that provided a measure to estimate the overall EFS quality of individual preparations (**Figure 3B**). Both parameters indicated similar training times for an optimal response to EFS, peaking between 5 to 6 days of training (**Figures 3A,B**). Surprisingly, longer training periods did not further improve the response to EFS, but led to a reduction in fiber excitability. Taken together, voluntary running on a wheel for 5 to 6 days not only led to an approximately two-fold improvement of the number of EFS positive fibers (**Figure 3A**) but also increased the quality of respective EFS responses by almost three-fold (**Figure 3B**).

We next analyzed which of the training parameters (see **Figure 1**) would have the strongest impact on the obtained

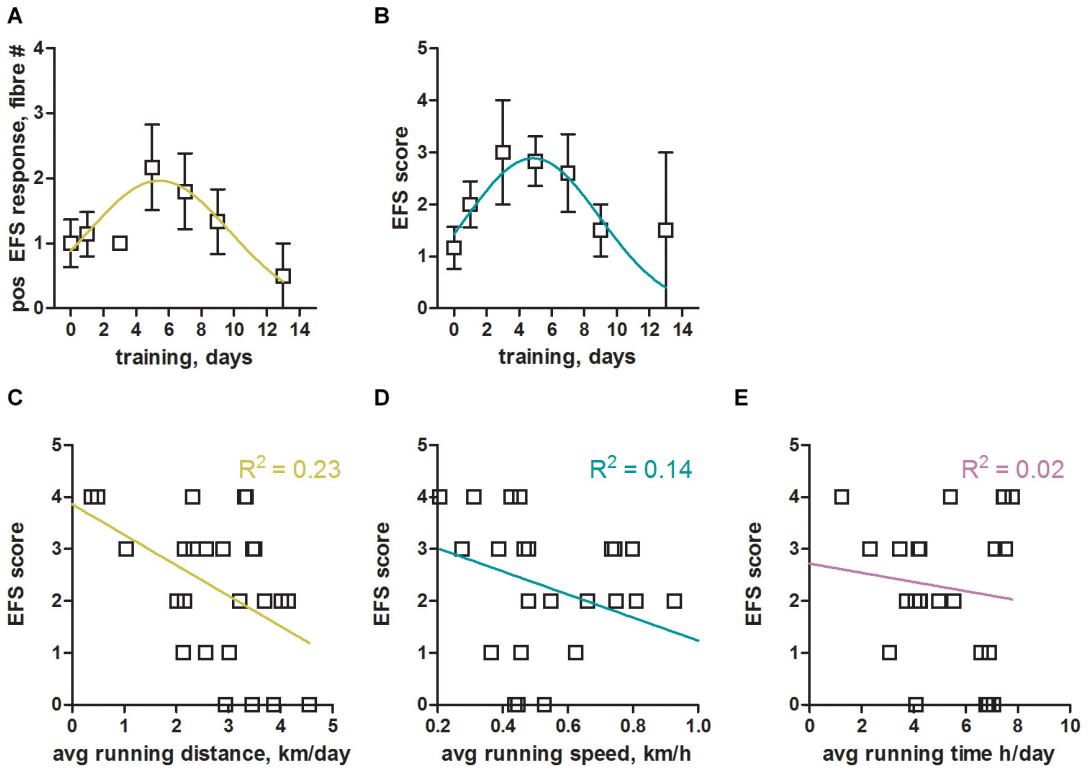

FIGURE 3 | Optimal training parameters for successful electrical field stimulation of mouse skeletal muscle fibers. **(A)** Total number of mouse EDL fibers from one experiment day (one animal) with positive response to EFS plotted over the number of training days (voluntary wheel running). Data were binned into two day intervals, [1–2], [3–4], [5–6], [7–8], [9–10], [11–12], and [13–14], with the number of mice in these intervals being 7, 3, 6, 5, 6, 0, 2, respectively. Data from $N = 6$ non-trained mice (no running wheel) were included as control at 0 training days. A Gaussian fit to the binned data revealed a maximum (mean ± SEM) at 5.4 ± 0.9 days of training; The Gaussian fit was the preferred model when compared to a straight line ($p < 0.05$, Extra sum-of-squares F-test). On average we tested 5 fibers per animal, so that a value of 2 would indicate that 40% of fibers showed a positive response to EFS. **(B)** EFS-score, a measure of the quality of EFS induced SR Ca^{2+} release (see section "Materials and Methods" for details) estimated from all fibers derived from one animal, plotted over the number of training days. Data were binned into two day intervals as in **(A)**. A Gaussian fit to the binned data revealed a maximum (mean ± SEM) at 4.9 ± 0.6 days of training. The Gaussian fit was the preferred model when compared to a straight line ($p < 0.05$, Extra sum-of-squares F-test). **(C–E)** EFS-score plotted over the average running distance, speed, and time of respective mice. Linear regression lines with respective R^2 values are shown in color. Data were derived from $N = 29$ trained and $N = 6$ non-trained mice.

results. To this end we plotted the EFS-score over the running distance, running speed, and running time (**Figures 3C–E**) to derive potential correlations. The EFS-score correlated weakly in a negative fashion with the average running distance (**Figure 3C**) and running speed (**Figure 3D**) of mice, indicating that fibers from mice that exercised more intensely were less likely to respond to EFS. No correlation was observed for the EFS-score with the average running time of the mice (**Figure 3E**).

Skeletal Muscle Fibers From Trained Mice Show Phasic SOCE

Next, we were interested if the EFS triggered SR Ca^{2+} release was associated with activation of pSOCE, as we previously observed in rat EDL skinned fibers (Koenig et al., 2018, 2019). To this end we loaded the t-system and the cytoplasm of EDL muscle fibers derived from trained mice with the Ca^{2+}-sensitive dyes, rhod-5N and fluo-4, respectively (Cully et al., 2016; Koenig et al., 2018, 2019). The dual loading allowed us to track the Ca^{2+} movements in both of these compartments simultaneously, while triggering Ca^{2+} release from the SR. Thus, EFS triggered SR Ca^{2+}-release with each stimulation pulse applied (**Figure 4**, gray traces), as observed originally in fibers loaded with fluo-4 only (**Figure 2**). In addition, each stimulation pulse resulted in an abrupt depletion of free Ca^{2+} in the t-system ($[Ca^{2+}]_{t\text{-}sys}$; **Figure 4** black traces). Repeated stimulation at a frequency of 1 Hz (**Figure 4A**, black bar) led to a step-wise depletion of steady-state $[Ca^{2+}]_{t\text{-}sys}$ with respect to the level before the start of EFS. The loss of $[Ca^{2+}]_{t\text{-}sys}$ upon individual EFS pulses was partially recovered by a re-uptake of Ca^{2+} into the t-system in between stimulation pulses, which is most likely carried by the sodium-calcium exchanger (Cully et al., 2018). The single depletion and re-uptake steps generated a case like depletion pattern in $[Ca^{2+}]_{t\text{-}sys}$, which, dependent on pulse frequency, converged toward a new steady-state level with prolonged stimulation. The dynamic equilibrium was reached faster at higher stimulation frequencies of 2, 5 and 10 Hz compared to 1 Hz, and led to a deeper overall depletion of the $[Ca^{2+}]_{t\text{-}sys}$ during continuous EFS (**Figures 4B–D**). Overall, the EFS-induced staircase like depletion pattern appeared very

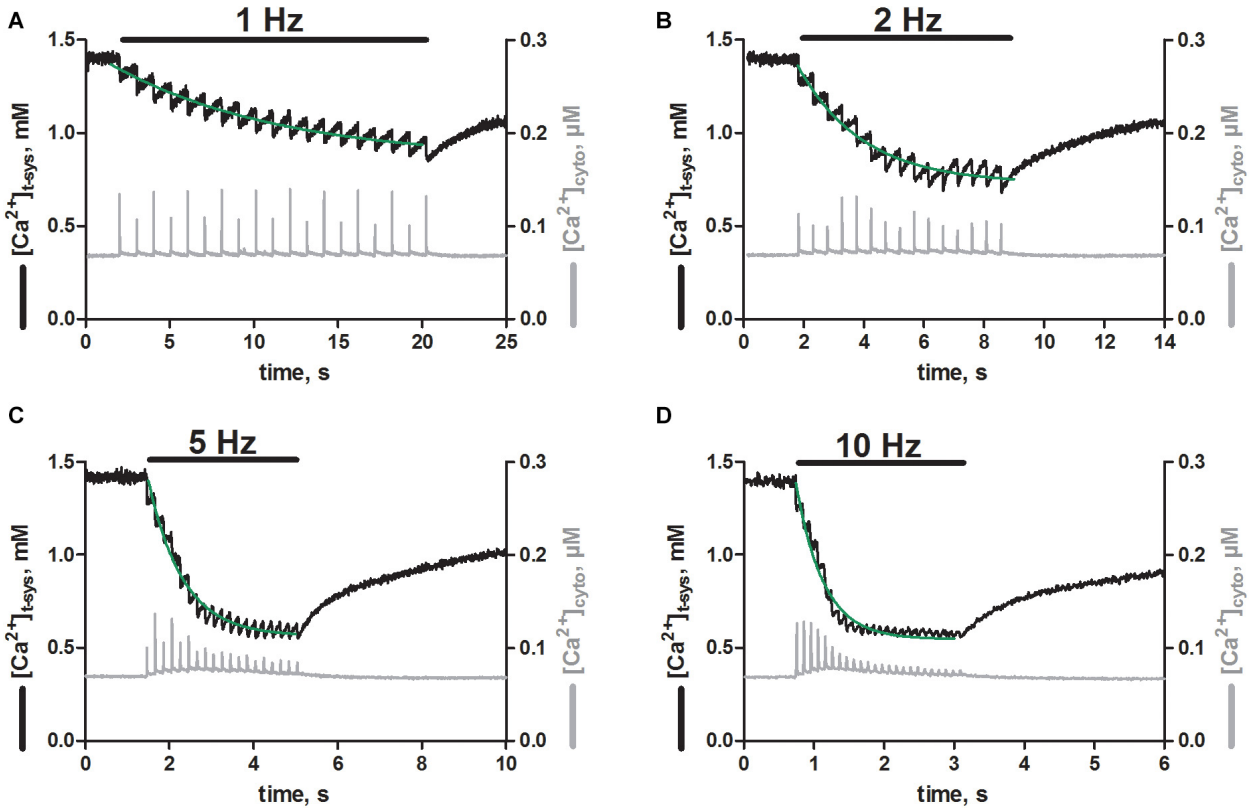

FIGURE 4 | Skeletal muscle fibers from trained mice show phasic SOCE upon electrical field stimulation. Typical recordings of $[Ca^{2+}]_{t\text{-}sys}$ (black traces, left axes) and $[Ca^{2+}]_{cyto}$ (gray traces, right axes) over time as derived from skinned mouse EDL fibers during EFS. xyt image series were acquired simultaneously for the fluorescent signals of rhod-5N and fluo-4 trapped in the t-system and loaded into the cytosol, respectively. Both signals were spatially averaged over a region of interest, in which the fiber was responding optimal to EFS. Signals were further calibrated by determining the fluorescent values under conditions of minimal and maximal Ca^{2+} concentrations in the presence of ionophores (see section "Materials and Methods"). Electrical stimulation at 1 **(A)**, 2 **(B)**, 5 **(C)**, and 10 Hz **(D)** as indicated by the black bars was started shortly after beginning of the recording and was continued until a new steady state in the t-system was reached. Of note, sampling below the Nyquist criterion resulted in an apparent modulation of cytosolic Ca^{2+} transient amplitudes, best seen in A. Green lines represent mono-exponential fits to the decaying phase of $[Ca^{2+}]_{t\text{-}sys}$ upon stimulation. Original profiles of $[Ca^{2+}]_{t\text{-}system}$ and$[Ca^{2+}]_{cyto}$ were obtained from one representative fiber.

similar to what we had previously described in rat EDL skinned muscle fibers (Koenig et al., 2018, 2019).

Phasic SOCE Is Similar in Rat and Mouse EDL Fibers

Next, we compared the characteristics of pSOCE in mouse EDL skinned fibres (the present study) to those previously established in rat EDL skinned fibres (Koenig et al., 2018). **Figure 5** shows a comparison of the rate of depletion and the new steady-state levels of $[Ca^{2+}]_{t\text{-}sys}$ induced by pSOCE during trains of EFS in mouse and rat fibers. Respective values were derived by fitting the staircase-like depletion pattern with a single exponential function to obtain the rate and steady-state values for different stimulation frequencies (1, 2, 5, and 10 Hz). Mean ± SEM values from a total of $n = 3$ mouse EDL fibers (**Figures 5A,B**, in olive green), together with the respective data from $n = 10$ rat EDL fibers (in black; taken from Koenig et al., 2018 with permission), were displayed on top of each other for comparison. Overall it can be observed that rat and mouse show very similar characteristics. These results suggest that phasic SOCE is a common mechanism in mammalian skeletal muscle, occurring with similar kinetics.

DISCUSSION

Within this work we have relied on the assumption that mouse limb muscle is de-trained when animals are housed in cages not supporting their natural running behavior and that this can be overcome by providing running wheels. While this approach clearly led to efficient EFS of mouse EDL skinned fibers, in a manner comparable to previous experiments in rat EDL skinned fibers, our study cannot provide a respective rational explanation. Thus, we can only speculate about possible underlying reasons.

Voluntary wheel running affects fiber type composition (Wernig et al., 1990; Allen et al., 2001), whereby a typical effect of endurance training in fast-twitch muscle is a relative switch to more oxidative fiber types. This conversion could render the fibers more susceptible to EFS. This, however, seems unlikely because of two points. First, we have consistently failed to obtain

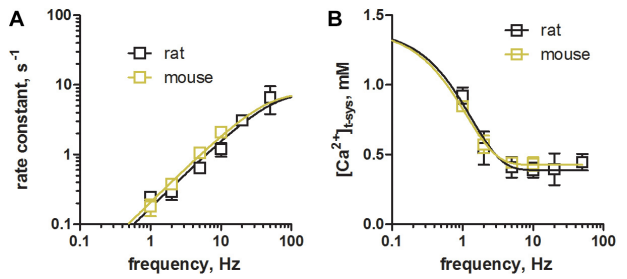

FIGURE 5 | Comparison of phasic SOCE between mouse and rat skeletal muscle fibers. Skinned EDL muscle fibers were derived from rats and trained mice using identical experimental protocols. **(A)** Comparison of the rate constants during a train of EFS at different frequencies as shown in **Figure 4**. Rate constants were derived from mono-exponential fits to the overall staircase like depletion pattern of $[Ca^{2+}]_{t\text{-}sys}$ (green fits, **Figure 4**). Mean ± SEM data derived from mouse fibers ($N = 3$ animals) as obtained within this study are shown in olive green, while data derived from rat fibers ($N = 5$ animals, in black), were taken from our previous work (Koenig et al., 2018, CC BY 4.0 license). **(B)** Comparison of the new steady-state $[Ca^{2+}]_{t\text{-}sys}$ levels during repeated stimulation as determined by the dynamic equilibrium between depletion and reuptake fluxes. Data from mouse (olive green) and rat (black) EDL muscle fibers are derived from the same sources as in **(A)**. Exponential fits to the data derived in mice and rats were compared using an Extra sum-of-square *F*-test. Calculated p values of 0.26 and 0.89 for the rate constant and for $[Ca^{2+}]_{t\text{-}sys}$, respectively, suggested the preferred model to have the same fit parameters for the two data sets.

successful EFS in skinned fibres from mouse and rat soleus muscles, which express almost exclusively slow-twitch fibers. Second, training of 5 to 6 days only, the optimal training period determined in **Figure 3**, is likely insufficient to allow for a considerable fiber type switch, given that respective adaptations take several weeks to occur (Wernig et al., 1990; Allen et al., 2001).

An alternative explanation why EFS improves in moderately exercised mouse muscle might be associated with molecular changes underlying the excitability of the fiber. (i) EFS works equally well in intact (e.g., Fryer and Neering, 1989) and skinned rat EDL fibers (Posterino et al., 2000; Koenig et al., 2018, 2019). Accordingly, VGSCs within the t-system and not the sarcolemma have been identified as respective EFS response elements (Posterino et al., 2000). VGSCs cluster at the entry points of the t-system (Murphy et al., 2009) and protrude into the sub-sarcolemma region (Clausen, 2003). It is thus conceivable that, while some of these channels are removed during the skinning procedure, a significant fraction of channels remains functional in sub-sarcolemma regions of the fiber. Upon exercise, an increased AP upstroke was observed in rat soleus fibers, suggesting a larger density of VGSCs or an increased fraction of non-refractory channels (Broch-Lips et al., 2011). If this holds true for fast twitch muscle and for shorter training periods then it might serve as an explanation for why EDL muscle fibers of trained mice do successfully respond to EFS. (ii) Fibers from trained animals were more resistant to depolarizations by high K^+ indicating a more robust t-system membrane potential as caused, e.g., by an increase in Na^+/K^+ pump activity (Clausen, 2003; Broch-Lips et al., 2011). Indeed, an increased Na^+/K^+-ATPase content was detected in muscle fibers derived from trained compared to sedentary rats (Xu et al., 2018). (iii) Training induced a lower resting conductance, possibly carried by Cl^- (Broch-Lips et al., 2011), which is in line with an observed increased Cl^- conductance in sedentary muscle (Pierno et al., 2007). Importantly, a reduction in resting Cl^- currents was shown to improve fiber excitability (Coonan and Lamb, 1998; Pedersen et al., 2005). While it is unclear if these adaptions occur already after a few days of voluntary wheel running, it is conceivable that the aforementioned and possibly additional unknown factors might contribute to the observed increase in excitability of mouse EDL skinned fibers upon moderate training.

Moderate exercise on a running wheel for 5–6 days led to a significant improvement of the number of EFS positive fibers (**Figure 3A**) as well as the quality of respective EFS responses (**Figure 3B**). Thus, 5–6 days of moderate excise in mice offers an about six-fold improvement in EFS, making EC coupling and dual EC coupling - pSOCE experiments feasible in mouse skinned fibres. A somewhat paradoxical finding was that training times longer than 5–6 days led to an apparent decline in fiber excitability (**Figures 3A,B**). The reasons for that are unknown. Training times, frequency and performance differ substantially among individual mice on voluntary running wheels. A more standardized approach, e.g. using a treadmill, may help define such parameters in EFS success.

Physiological Relevance

Chronic SOCE (cSOCE), as induced by thorough depletion of the SR Ca^{2+}-stores, has been observed in skeletal muscle across mammalian species (Kurebayashi and Ogawa, 2001; Stiber et al., 2008; Cully et al., 2016), including human (Cully et al., 2018), and there is little doubt that cSOCE is carried by STIM1 and Orai1 proteins (Lyfenko and Dirksen, 2008; Stiber et al., 2008; Dirksen, 2009). Phasic SOCE (pSOCE), on the other hand, as activated by individual APs during EC-coupling (Koenig et al., 2018, 2019), was only observed in rat EDL muscle fibers to date, and its molecular nature is still unresolved. Although it seems reasonable to assume that pSOCE is mediated by the same protein machinery (Koenig et al., 2018), a direct proof of this hypothesis remains outstanding.

To provide an explanation for the extraordinary fast activation of pSOCE (Launikonis and Ríos, 2007; Edwards et al., 2010; Koenig et al., 2018, 2019) a direct and permanent physical coupling of STIM1 and ORAI1 has been proposed (Edwards et al., 2010; Launikonis et al., 2010) in combination with a nanodomain Ca^{2+} depletion within the terminal cisternae of the SR (Koenig et al., 2019) upon opening of the ryanodine receptor during EC-coupling. This notion was supported by respective co-localization of STIM1 and ORAI1 at the triad membranes (Darbellay et al., 2011; Wei-Lapierre et al., 2013; Tammineni et al., 2020), and encouraged by the discovery of a long STIM1 isoform (STIM1L) with supplemental actin binding properties and the ability to form permanent STIM1L/ORAI1-clusters (Darbellay et al., 2011; Saüc et al., 2015). However, others have questioned that idea based on results derived from an (uncalibrated) STIM1/ORAI1 complementation assay (Wei-Lapierre et al., 2013).

Store-operated calcium entry plays an important role in muscle growth and development, is involved in fatigue resistance, and causes different forms of myopathy when impaired (Feske, 2009). The underlying mechanisms are poorly understood. Partly, this might be caused by the fact that chronic, long-lasting activation of SOCE does not reflect the natural activation patterns of skeletal muscle, which occur as brief twitches induced by very transient releases of SR Ca^{2+}. The temporal presentation of SOCE in working, intact skeletal muscle should not be assumed from experimental conditions where SOCE and SR Ca^{2+} release are not simultaneous measured or there is SR Ca^{2+} depletion due to inhibition of the SR Ca^{2+} pump or removal of extracellular Ca^{2+}. Also, an increase in persistent Ca^{2+} leak through the ryanodine receptor is required to activate cSOCE (Cully et al., 2018), which is more likely to be associated with disease conditions (Cully et al., 2018; Rebbeck et al., 2020) or the post-exercise period (Place et al., 2015; Ivarsson et al., 2019). In this light it seems reasonable to assume that pSOCE rather than cSOCE actually represents the more relevant physiological manifestation of this important Ca^{2+} flux in prevailing skeletal muscle function.

Mouse models, genetically engineered to target the proposed key proteins of SOCE, have already been generated, but the inability to efficiently use mechanically skinned muscle fibers from mouse for EFS has presented significant impediment to research efforts. With the here presented protocol of moderate exercise, providing a running wheel to otherwise physically restrained mice, we have provided a tool to measure pSOCE in mouse muscle during single muscle twitches. Genetically modified mouse models can now be put forward to test the molecular nature and physiological role of pSOCE. Furthermore, a new platform is provided to study this sophisticated type of Ca^{2+}-influx in skeletal myopathies, in which pSOCE presumable plays a prominent role.

pSOCE in Intact and Skinned Fibers

Phasic SOCE has been demonstrated directly in skinned fibers (Koenig et al., 2018). The skinned fiber preparation provides means to simultaneously measure t-system Ca^{2+} influx and SR Ca^{2+} release during EC coupling with a high signal: noise ratio and temporal resolution for detecting Ca^{2+} entry (Launikonis and Ríos, 2007; Koenig et al., 2018, 2019). In intact fiber preparations, resolving brief Ca^{2+} entry is difficult (Launikonis et al., 2009). However, there is evidence from indirect measurements in intact fiber preparations of a "pSOCE" (Bianchi and Shanes, 1959; Curtis, 1966; Gissel and Clausen, 1999). For example, Gissel and Clausen (1999) showed that a continuous, low-frequency EFS of intact muscle for several hours led to a significant influx and accumulation of radioactive Ca^{2+} consistent with stimulation frequency that was resistant to nifedipine. Studies of SOCE in intact fibers with high frequency EFS have suggested SOCE is involved in the continuing Ca^{2+} release response. The indirect nature of the measure of SOCE in these studies (no measure of Ca^{2+} entry during EC coupling) means we need to apply what we have measured in skinned fibers to help determine what is happening in the intact system. The use of genetically manipulated mice in skinned fiber EFS experiments, using the protocols developed here, will provide a more solid platform to tie results from intact and skinned fibers together, and advance the field.

DATA AVAILABILITY STATEMENT

The raw data supporting the conclusions of this article will be made available by the authors, without undue reservation.

ETHICS STATEMENT

The animal study was reviewed and approved by the Animal Welfare Committee at the Medical University of Vienna and is covered by licence BMBWF 2020-0.499.046 granted by the Federal Ministry of the Republic of Austria.

AUTHOR CONTRIBUTIONS

XK and BL contributed to the conception and design. EL and XK performed the experiments and analyzed the data. EL and BL contributed reagents, materials, and analysis tools. XK, KH, and BL wrote the manuscript and contributed to the data interpretation and manuscript revision. All authors contributed to the article and approved the submitted version.

FUNDING

This work was supported by the Austrian Science Fund (FWF) P31563FW to XK, the "Österreichische Muskelforschung" (ÖMF) supported by the "Harley Davidson Charity Fonds" AP00845OFF/KP00845OFF to XK, and an Australian Research Council (ARC) Discovery Project Grant DP200100435 to BL.

REFERENCES

Allen, D. L., Harrison, B. C., Maass, A., Bell, M. L., Byrnes, W. C., and Leinwand, L. A. (2001). Cardiac and skeletal muscle adaptations to voluntary wheel running in the mouse. *J. Appl. Physiol.* 90, 1900–1908. doi: 10.1152/jappl.2001.90.5.1900

Bianchi, C. P., and Shanes, A. M. (1959). Calcium influx in skeletal muscle at rest, during activity, and during potassium contracture. *J. Gen. Physiol.* 42, 803–815. doi: 10.1085/jgp.42.4.803

Böhm, J., Bulla, M., Urquhart, J. E., Malfatti, E., Williams, S. G., O'Sullivan, J., et al. (2017). ORAI1 mutations with distinct channel gating defects in tubular aggregate myopathy. *Hum. Mut.* 38, 426–438. doi: 10.1002/humu.23172

Böhm, J., Chevessier, F., Koch, C., Peche, G. A., Mora, M., Morandi, L., et al. (2014). Clinical, histological and genetic characterisation of patients with tubular aggregate myopathy caused by mutations in STIM1. *J. Med. Genet.* 51, 824–833. doi: 10.1136/jmedgenet-2014-102623

Böhm, J., Chevessier, F., Maues De Paula, A., Koch, C., Attarian, S., Feger, C., et al. (2013). Constitutive activation of the calcium sensor STIM1 causes tubular-aggregate myopathy. *Am. J. Hum. Genet.* 92, 271–278. doi: 10.1016/j.ajhg.2012.12.007

Broch-Lips, M., de Paoli, F., Pedersen, T. H., Overgaard, K., and Nielsen, O. B. (2011). Effects of 8 Wk of voluntary unloaded wheel running on K+ tolerance and excitability of soleus muscles in rat. *J. Appl. Physiol.* 111, 212–220. doi: 10.1152/japplphysiol.00687.2010

Clausen, T. (2003). Na+-K+ pump regulation and skeletal muscle contractility. *Physiol. Rev.* 83, 1269–1324. doi: 10.1152/physrev.00011.2003

Coleman, M. A., Garland, T. Jr., Marler, C. A., Newton, S. S., Swallow, J. G., and Carter, P. A. (1998). Glucocorticoid response to forced exercise in laboratory house mice (*Mus domesticus*). *Physiol. Behav.* 63, 279–285. doi: 10.1016/S0031-9384(97)00441-441

Coonan, J. R., and Lamb, G. D. (1998). Effect of transverse-tubular chloride conductance on excitability in skinned skeletal muscle fibres of rat and toad. *J. Physiol.* 509, 551–564. doi: 10.1111/j.1469-7793.1998.551bn.x

Cully, T. R., Choi, R. H., Bjorksten, A. R., George Stephenson, D., Murphy, R. M., and Launikonis, B. S. (2018). Junctional membrane Ca2+ dynamics in human muscle fibers are altered by malignant hyperthermia causative RyR mutation. *Proc. Natl. Acad. Sci. U.S.A.* 115, 8215–8220. doi: 10.1073/pnas.1800490115

Cully, T. R., Edwards, J. N., Murphy, R. M., and Launikonis, B. S. (2016). A quantitative description of tubular system Ca2+handling in fast- and slow-twitch muscle fibres. *J. Physiol.* 594, 2795–2810. doi: 10.1113/JP271658

Cully, T. R., Murphy, R. M., Roberts, L., Raastad, T., Fassett, R. G., Coombes, J. S., et al. (2017). Human skeletal muscle plasmalemma alters its structure to change its Ca2+ handling following heavy-load resistance exercise. *Nat. Commun.* 8, 1–10. doi: 10.1038/ncomms14266

Curtis, B. A. (1966). Ca fluxes in single twitch muscle fibers. *J. Gen. Physiol.* 50, 255–267. doi: 10.1085/jgp.50.2.255

Darbellay, B., Arnaudeau, S., Bader, C. R., Konig, S., and Bernheim, L. (2011). STIM1L is a new actin-binding splice variant involved in fast repetitive Ca 2+ release. *J. Cell Biol.* 194, 335–346. doi: 10.1083/jcb.201012157

Dirksen, R. T. (2009). Checking your SOCCs and feet: the molecular mechanisms of Ca2+ entry in skeletal muscle. *J. Physiol.* 587, 3139–3147. doi: 10.1113/jphysiol.2009.172148

Dutka, T. L., Murphy, R. M., Stephenson, D. G., and Lamb, G. D. (2008). Chloride conductance in the transverse tubular system of rat skeletal muscle fibres: importance in excitation-contraction coupling and fatigue. *J. Physiol.* 586, 875–887. doi: 10.1113/jphysiol.2007.144667

Edwards, J. N., Murphy, R. M., Cully, T. R., von Wegner, F., Friedrich, O., and Launikonis, B. S. (2010). Ultra-rapid activation and deactivation of store-operated Ca2+entry in skeletal muscle. *Cell Calc.* 47, 458–467. doi: 10.1016/j.ceca.2010.04.001

Endo, Y., Noguchi, S., Hara, Y., Hayashi, Y. K., Motomura, K., Miyatake, S., et al. (2015). Dominant mutations in ORAI1 cause tubular aggregate myopathy with Hypocalcemia via constitutive activation of store-operated Ca2+ channels. *Hum. Mol. Genet.* 24, 637–648. doi: 10.1093/hmg/ddu477

Feske, S. (2009). ORAI1 and STIM1 deficiency in human and mice: roles of store-operated Ca2+ entry in the immune system and beyond. *Immunol. Rev.* 231, 189–209. doi: 10.1111/j.1600-065X.2009.00818.x

Feske, S., Gwack, Y., Prakriya, M., Srikanth, S., Puppel, S. H., Tanasa, B., et al. (2006). A mutation in Orai1 causes immune deficiency by abrogating CRAC channel function. *Nature* 441, 179–185. doi: 10.1038/nature04702

Fryer, M. W., and Neering, I. R. (1989). Actions of caffeine on fast- and slow-twitch muscles of the rat. *J. Physiol.* 416, 435–454. doi: 10.1113/jphysiol.1989.sp017770

Gissel, H., and Clausen, T. (1999). Excitation-induced Ca2+ uptake in rat skeletal muscle. *Am. J. Physiol. Regul. Integr. Compar. Physiol.* 276, 24–52.

Goodman, C. A., Blazev, R., Kemp, J., and Stephenson, G. M. M. (2008). E-C coupling and contractile characteristics of mechanically skinned single fibres from young rats during rapid growth and maturation. *Pflug. Arch. Eur. J. Physiol.* 456, 1217–1228. doi: 10.1007/s00424-008-0474-479

Grynkiewicz, G., Poenie, M., and Tsien, R. Y. (1985). A new generation of Ca2+ indicators with greatly improved fluorescence properties. *J. Biol. Chem.* 260, 3440–3450.

Ivarsson, N., Mattsson, C. M., Cheng, A. J., Bruton, J. D., Ekblom, B., Lanner, J. T., et al. (2019). SR Ca2+ leak in skeletal muscle fibers acts as an intracellular signal to increase fatigue resistance. *J. Gen. Physiol.* 151, 567–577. doi: 10.1085/jgp.201812152

Koenig, X., Choi, R. H., and Launikonis, B. S. (2018). Store-operated Ca2+ entry is activated by every action potential in skeletal muscle. *Commun. Biol.* 1:31. doi: 10.1038/s42003-018-0033-37

Koenig, X., Choi, R. H., Schicker, J., Singh, D. P., Hilber, K., and Launikonis, B. S. (2019). Mechanistic insights into store-operated Ca2+ entry during excitation-contraction coupling in skeletal muscle. *Biochim. Biophys. Acta Mol. Cell Res.* 1866, 1239–1248. doi: 10.1016/j.bbamcr.2019.02.014

Kurebayashi, N., and Ogawa, Y. (2001). Depletion of Ca2 + in the sarcoplasmic reticulum stimulates Ca2 + entry into mouse skeletal muscle fibres. *J. Physiol.* 533, 185–199. doi: 10.1111/j.1469-7793.2001.0185b.x

Lamb, G. D., Junankar, P. R., and Stephenson, D. G. (1995). Raised Intracellular [Ca2+] abolishes excitation-contraction coupling in skeletal muscle Fibres of rat and toad. *J. Physiol.* 489, 349–362. doi: 10.1113/jphysiol.1995.sp021056

Lamb, G. D., and Stephenson, D. G. (1994). Effects of intracellular pH and [Mg^{2+}] on excitation-contraction coupling in skeletal muscle fibres of the rat. *J. Physiol.* 478, 331–339. doi: 10.1113/jphysiol.1994.sp020253

Launikonis, B. S., George Stephenson, D., and Friedrich, O. (2009). Rapid Ca2+ Flux through the transverse tubular membrane, activated by individual action potentials in mammalian skeletal muscle. *J. Physiol.* 587(Pt 10), 2299–2312. doi: 10.1113/jphysiol.2009.168682

Launikonis, B. S., Murphy, R. M., and Edwards, J. N. (2010). Toward the roles of store-operated Ca2+ entry in skeletal muscle. *Pflug. Arch. Eur. J. Physiol.* 460, 813–823. doi: 10.1007/s00424-010-0856-857

Launikonis, B. S., and Ríos, E. (2007). Store-operated Ca2+ entry during intracellular Ca2+ release in mammalian skeletal muscle. *J. Physiol.* 583(Pt 1), 81–97. doi: 10.1113/jphysiol.2007.135046

Lyfenko, A. D., and Dirksen, R. T. (2008). Differential dependence of store-operated and excitation-coupled Ca2+ entry in skeletal muscle on STIM1 and Orai1. *J. Physiol.* 586(Pt 20), 4815–4824. doi: 10.1113/jphysiol.2008.160481

Manzanares, G., Brito-Da-Silva, G., and Gandra, P. G. (2019). Voluntary wheel running: patterns and physiological effects in mice. *Braz. J. Med. Biol. Res.* 52, 1–9. doi: 10.1590/1414-431X20187830

McCarl, C. A., Picard, C., Khalil, S., Kawasaki, T., Röther, J., Papolos, A., et al. (2009). ORAI1 deficiency and lack of store-operated Ca2+ entry cause immunodeficiency, myopathy, and ectodermal dysplasia. *J. Allerg. Clin. Immunol.* 124:7. doi: 10.1016/j.jaci.2009.10.007

Murphy, R. M., Larkins, N. T., Mollica, J. P., Beard, N. A., and Lamb, G. D. (2009). Calsequestrin content and SERCA determine normal and maximal Ca2+ storage levels in sarcoplasmic reticulum of fast- and slow-twitch fibres of rat. *J. Physiol.* 587, 443–460. doi: 10.1113/jphysiol.2008.163162

Pedersen, T. H., De Paoli, F., and Nielsen, O. B. (2005). Increased excitability of acidified skeletal muscle: role of chloride conductance. *J. Gen. Physiol.* 125, 237–246. doi: 10.1085/jgp.200409173

Pierno, S., Desaphy, J. F., Liantonio, A., De Luca, A., Zarrilli, A., Mastrofrancesco, L., et al. (2007). Disuse of rat muscle in vivo reduces protein kinase C activity controlling the sarcolemma chloride conductance. *J. Physiol.* 584, 983–995. doi: 10.1113/jphysiol.2007.141358

Place, N., Ivarsson, N., Venckunas, T., Neyroud, D., Brazaitis, M., Cheng, A. J., et al. (2015). Ryanodine receptor fragmentation and sarcoplasmic reticulum Ca2+ leak after one session of high-intensity interval exercise. *Proc. Natl. Acad. Sci. U.S.A.* 112, 15492–15497. doi: 10.1073/pnas.1507176112

Posterino, G. S., and Lamb, G. D. (2003). Effect of sarcoplasmic reticulum Ca2+ content on action potential-induced Ca2+ Release in rat skeletal muscle fibres. *J. Physiol.* 551, 219–237. doi: 10.1113/jphysiol.2003.040022

Posterino, G. S., Lamb, G. D., and Stephenson, D. G. (2000). Twitch and tetanic force responses and longitudinal propagation of action potentials in skinned skeletal muscle fibres of the rat. *J. Physiol.* 527(Pt 1), 131–137. doi: 10.1111/j.1469-7793.2000.t01-2-00131.x

Prakriya, M., and Lewis, R. S. (2015). Store-operated calcium channels. *Physiol. Rev.* 4, 1383–1436. doi: 10.1016/B978-0-12-378630-2.00301-7

Rebbeck, R. T., Singh, D. P., Janicek, K. A., Bers, D. M., Thomas, D. D., Launikonis, B. S., et al. (2020). RyR1-targeted drug discovery pipeline integrating FRET-based high-throughput screening and human myofiber dynamic Ca2+ assays. *Sci. Rep.* 10, 1–13. doi: 10.1038/s41598-020-58461-58461

Roos, J., DiGregorio, P. J., Yeromin, S. V., Ohlsen, K., Lioudyno, M., Zhang, S., et al. (2005). STIM1, an essential and conserved component of store-operated Ca 2+ channel function. *J. Cell Biol.* 169, 435–445. doi: 10.1083/jcb.200502019

Royer, L., Pouvreau, S., and Ríos, E. (2008). Evolution and modulation of intracellular calcium release during long-lasting, depleting depolarization in mouse muscle. *J. Physiol.* 586, 4609–4629. doi: 10.1113/jphysiol.2008.157990

Saüc, S., Bulla, M., Nunes, P., Orci, L., Marchetti, A., Antigny, F., et al. (2015). STIM1L traps and gates orai1 channels without remodeling the cortical ER. *J. Cell Sci.* 128, 1568–1579. doi: 10.1242/jcs.164228

Stiber, J., Hawkins, A., Zhang, Z. S., Wang, S., Burch, J., Graham, V., et al. (2008). STIM1 signalling controls store-operated calcium entry required for development and contractile function in skeletal muscle. *Nat. Cell Biol.* 10, 688–697. doi: 10.1038/ncb1731

Tammineni, E. R., Kraeva, N., Figueroa, L., Manno, C., Ibarra, C., Klip, A., et al. (2020). Intracellular calcium leak lowers glucose storage in human muscle, promoting hyperglycemia and diabetes. *eLife* 9:e053999. doi: 10.7554/eLife.53999

Trebak, M., Zhang, W., Ruhle, B., Henkel, M. M., González-Cobos, J. C., Motiani, R. K., et al. (2013). What role for store-operated Ca2+ entry in muscle? *Microcirculation* 20, 330–336. doi: 10.1111/micc.12042

Vig, M., DeHaven, W. I., Bird, G. S., Billingsley, J. M., Wang, H., Rao, P. E., et al. (2008). Defective mast cell effector functions in mice lacking the CRACM1 pore subunit of store-operated calcium release-activated calcium channels. *Nat. Immunol.* 9, 89–96. doi: 10.1038/ni1550

Vig, M., Peinelt, C., Beck, A., Koomoa, D. L., Rabah, D., Koblan-Huberson, M., et al. (2006). CRACM1 is a plasma membrane protein essential for store-operated Ca2+ entry. *Science* 312, 1220–1223. doi: 10.1017/CBO9781107415324.004

Wei-Lapierre, L., Carrell, E. M., Boncompagni, S., Protasi, F., and Dirksen, R. T. (2013). Orai1-dependent calcium entry promotes skeletal muscle growth and limits fatigue. *Na. Commun.* 4:2805. doi: 10.1038/ncomms3805

Wernig, A., Irintchev, A., and Weisshaupt, P. (1990). Muscle injury, cross-sectional area and fibre type distribution in mouse soleus after intermittent wheel-running. *J. Physiol.* 428, 639–652. doi: 10.1113/jphysiol.1990.sp018232

Xu, H., Ren, X., Lamb, G. D., and Murphy, R. M. (2018). Physiological and biochemical characteristics of skeletal muscles in sedentary and active rats. *J. Mus. Res. Cell Motil.* 39, 1–16. doi: 10.1007/s10974-018-9493-9490

Conflict of Interest: The authors declare that the research was conducted in the absence of any commercial or financial relationships that could be construed as a potential conflict of interest.

frontiers in Physiology

ORIGINAL RESEARCH
published: 15 December 2020
doi: 10.3389/fphys.2020.599822

High Time Resolution Analysis of Voltage-Dependent and Voltage-Independent Calcium Sparks in Frog Skeletal Muscle Fibers

*Henrietta Cserne Szappanos[1,2], János Vincze[2], Dóra Bodnár[2], Beatrix Dienes[2], Martin F. Schneider[1], László Csernoch[2] and Péter Szentesi[2]**

[1] Department of Biochemistry and Molecular Biology, School of Medicine, University of Maryland, Baltimore, Baltimore, MD, United States, [2] Department of Physiology, Faculty of Medicine, University of Debrecen, Debrecen, Hungary

OPEN ACCESS

Edited by:
Heinrich Brinkmeier, Universitätsmedizin Greifswald, Germany

Reviewed by:
Isabelle Marty, Institut National de la Santé et de la Recherche Médicale (INSERM), France
Gustavo Brum, Universidad de la República, Uruguay

***Correspondence:**
Péter Szentesi
szentesi.peter@med.unideb.hu

Specialty section:
This article was submitted to Striated Muscle Physiology, a section of the journal Frontiers in Physiology

Received: 28 August 2020
Accepted: 25 November 2020
Published: 15 December 2020

Citation:
Cserne Szappanos H, Vincze J, Bodnár D, Dienes B, Schneider MF, Csernoch L and Szentesi P (2020) High Time Resolution Analysis of Voltage-Dependent and Voltage-Independent Calcium Sparks in Frog Skeletal Muscle Fibers. Front. Physiol. 11:599822. doi: 10.3389/fphys.2020.599822

In amphibian skeletal muscle calcium (Ca^{2+}) sparks occur both as voltage-dependent and voltage-independent ligand-activated release events. However, whether their properties and their origin show similarities are still in debate. Elevated K^+, constant Cl^- content solutions were used to initiate small depolarizations of the resting membrane potential to activate dihydropyridine receptors (DHPR) and caffeine to open ryanodine receptors (RyR) on intact fibers. The properties of Ca^{2+} sparks observed under control conditions were compared to those measured on depolarized cells and those after caffeine treatment. Calcium sparks were recorded on intact frog skeletal muscle fibers using high time resolution confocal microscopy (x-y scan: 30 Hz). Sparks were elicited by 1 mmol/l caffeine or subthreshold depolarization to different membrane potentials. Both treatments increased the frequency of sparks and altered their morphology. Images were analyzed by custom-made computer programs. Both the amplitude (in $\Delta F/F_0$; 0.259 ± 0.001 vs. 0.164 ± 0.001; n = 24942 and 43326, respectively; mean ± SE, $p < 0.001$) and the full width at half maximum (FWHM, in μm; parallel with fiber axis: 2.34 ± 0.01 vs. 1.92 ± 0.01, $p < 0.001$; perpendicular to fiber axis: 2.08 ± 0.01 vs. 1.68 ± 0.01, $p < 0.001$) of sparks was significantly greater after caffeine treatment than on depolarized cells. 9.8% of the sparks detected on depolarized fibers and about one third of the caffeine activated sparks (29.7%) overlapped with another one on the previous frame on x-y scans. Centre of overlapping sparks travelled significantly longer distances between consecutive frames after caffeine treatment then after depolarization (in μm; 1.66 ± 0.01 vs. 0.95 ± 0.01, $p < 0.001$). Our results suggest that the two types of ryanodine receptors, the junctional RyRs controlled by DHPRs and the parajunctional RyRs are activated independently, using alternate ways, with the possibility of cooperation between neighboring release channels.

Keywords: skeletal muscle, frog, excitation-contraction coupling, ryanodine receptor, calcium-induced calcium release, membrane depolarization, calcium spark, caffeine

INTRODUCTION

Calcium ion is a ubiquitous second messenger in many intracellular signaling pathways, but it also regulates highly specialized cellular processes such as contraction in muscle cells. Ca^{2+} sparks are the openings of a local cluster of ryanodine receptors (RyR) which are the Ca^{2+}-release channels of the sarcoplasmic reticulum (SR; Wang et al., 2004). Sparks in amphibians are elementary events igniting global Ca^{2+} release during depolarization (Klein et al., 1997). Thus, the study of Ca^{2+} sparks provides useful information about the Ca^{2+} release process itself and the gating kinetics of RyR Ca^{2+} release channels.

Elementary calcium release events were first found in cardiac myocytes (Cheng et al., 1993), then in many other cell types as smooth (Nelson et al., 1995) and skeletal muscle (Tsugorka et al., 1995; Klein and Schneider, 2006). Morphology and frequency of calcium release events in various cell types, or from different species show marked alterations. One of the possible explanations could be the difference in the expression pattern of calcium release channels. In non-mammalian and embryonic mammalian skeletal muscle fibers two RyR isoforms coexist in almost equal amounts in contrast to fibers from adult mammals where the RyR1 isoform predominates (Sutko and Airey, 1996; Ogawa et al., 1999; Felder and Franzini-Armstrong, 2002). Interestingly mammalian skeletal muscle express the RyR3 isoform embryonically and certain muscles in adult, like diaphragm and soleus, and lower levels in abdominal muscles and tibialis anterior (Ogawa et al., 1999). The frog RyR isoforms (RyRα and RyRβ) are similar to mammalian RyR1 and RyR3, both in terms of their amino acid sequence and functional properties (Franzini-Armstrong and Protasi, 1997).

The α isoform is closely associated with the voltage sensor dihydropyridine receptors (DHPRs) located in the transverse (T-) tubule, and is voltage controlled. The β isoform is not connected with DHPRs, but even a small increase in intracellular calcium concentration can open it (Rodney and Schneider, 2003; Zhou et al., 2004; Pouvreau et al., 2007). The response to caffeine reportedly varies depending on animal species, muscle type, and age, with characteristically higher sensitivity and responsiveness reported on frog muscles than mammalian muscles which do not express RyR3 or just very low level (Ogawa et al., 1999; Rossi et al., 2001, Kashiyama et al., 2010).

Electron microscopic studies showed highly organized pattern of RYR receptors, called 'feet' on the SR membrane oriented toward the DHPR receptors in the T-tubule. Muscles expressing RyRβ/3 have additional clusters in the SR membrane. These are segregated from junctional RyRα/1s and are located in a parajunctional position (Felder and Franzini-Armstrong, 2002). This observation led to the hypothesis of two different mechanisms of RyR activation: a voltage-controlled intracellular calcium release through the RYRα/1s and the voltage-independent or calcium induced calcium release (CICR) pathway via the opening of RyRβ/3s (Rios and Pizarro, 1988; Franzini-Armstrong, 2004).

Previously, frog skeletal muscle Ca^{2+} sparks were shown to occur both in a voltage-dependent and voltage-independent, ligand-activated manner. Voltage-dependent sparks can be evoked experimentally by a subthreshold depolarization of a skeletal muscle fiber, and the frequency of Ca^{2+} sparks increases steeply with increasing depolarization (Klein et al., 1996). Voltage dependent activation of SR Ca^{2+} release in skeletal muscle is regulated by intramembrane voltage sensors, the dihydropyridine receptors (Franzini-Armstrong, 2004) in the transverse tubule membrane. The voltage dependence of intramembrane charge movement indicates that changes in membrane potential lead to the redistribution of these voltage sensors between intramembrane locations according to the Boltzmann relationship (Schneider and Ward, 2002). Voltage-independent sparks were ignited by endogenous ligands of RyRs via Ca^{2+}-induced Ca^{2+} release mechanisms (Klein et al., 1996). Caffeine was used to activate RyRs and increase the frequency of the calcium release events on skeletal muscle fibers (Brum et al., 2000; Gonzalez et al., 2000a,b). In these studies increased frequency, higher amplitude and eccentricity was distinctive to the caffeine induced events.

Skeletal muscle fibers expressing both RyR isotype show a higher incidence of spontaneous calcium release events, than fibers missing the RyRβ/3 isotype. It was also found that spontaneous sparks remain visible in fully depolarized (voltage clamped to 0 mV) frog fiber, or blocking DHPRs (nifedipine, Klein et al., 1996, Cd^{2+}/La^{3+} Perez et al., 2003). Although these applications could abolish the calcium movement through the voltage sensor DHPR, it was also demonstrated, that non-conducting DHPRs remain functional as voltage sensor for conformational EC coupling (Dayal et al., 2017).

Previous studies have also demonstrated that a chemical or mechanical skinning procedure results in a partial destabilization of the coupling between the DHPR–RyR that leads to the appearance of calcium release events (Kirsch et al., 2001; Zhou et al., 2003; Szappanos et al., 2005). Isaeva et al. (2005) found that the contents of the cytosol of skinned fibers were washed out and the number of the calcium release events changed consequently. Hollingworth et al. (2001) concluded in their studies that properties of spontaneous and voltage-activated sparks were similar in intact muscle fibers. They controlled membrane potential by using extracellular Ringer's solutions with different potassium ion concentrations like as used in this study with some modification (see in "Materials and Methods").

In our previous experiments using voltage clamped cut frog skeletal muscle fibers (Klein et al., 1996) we concluded that the amplitude of spontaneous sparks measured at the holding potential (–90 mV) was much smaller than that of voltage-dependent sparks during small depolarizations. Distribution of the amplitude of voltage-dependent sparks could be fitted by the sum of Gaussian functions with means being multiples of the unitary amplitude of the spontaneous sparks.

To re-examine the difference between voltage-dependent and independent sparks, as well as to characterize the voltage dependence of spark frequency, we have reinvestigated the properties of Ca^{2+} sparks performing a high time resolution analysis. To this end a Zeiss LSM 5 Live laser scanning confocal microscope system was used, with a maximum data acquisition

speed up to 15.4 μs/line to record sparks in intact fibers isolated from frog toe muscle.

We found significant differences in the amplitude of the voltage-dependent and -independent sparks. Their spatial and temporal properties were different, similarly to the results of our previous experiments performed on cut fibers.

The novelty in our experiments are the high resolution data acquisition and the analysis. Using the high speed confocal microscopic technique with about 50 times faster acquisition rates at high resolution allowed us to study the spatial and temporal characteristics of sparks with minimal photo-toxicity. Part of this work was presented to the Biophysical Society (Vincze et al., 2013, 2014).

MATERIALS AND METHODS

Fiber Preparation and Solutions

Frogs (*Rana pipiens*) were placed into crushed ice-water slurry for 30 min then killed by decapitation followed by spinal cord destruction according to protocols approved by the University of Maryland Institutional Animal Care and Use Committee. Toe muscles (*flexor digitorum brevis*) were removed, and individual muscle fibers were enzymatically isolated (8 mg/ml neutral dispase II, 1.3 mg/ml collagenase A, at 37°C, 1 h), in nominally calcium-free Ringer solution (in mM: 115 NaCl, 2.5 KCl, 1 $MgCl_2$, 10 HEPES, pH 7.0). The separated, intact fibers were plated on extracellular matrix covered, glass bottom dishes, in Ringer solution containing 1.8 mM $CaCl_2$. Before each experiments the cells were incubated with 20 μM Fluo-4 AM at room temperature for 30 min, followed by 20 min de-esterification.

To initiate voltage activated sparks in intact fibers we used high concentration potassium ion (K^+) containing extracellular solutions (**Table 1**). Stepwise solution change with increased K^+ content allowed us to reach small depolarizations between -70 and -60 mV while avoiding transient intracellular calcium level increase and subsequent contractions. The Goldman-Hodgkin-Katz equation was used to estimate the actual membrane potential in each K^+ containing solutions. Methane sulfonic acid was used to keep the concentration of Cl^- constant in all solutions and so the ionic strength and the osmolality of the depolarization solutions.

Caffeine in 1 mM concentration was used to increase the appearance of sparks.

Individual fibers were monitored and fibers with increased overall fluorescence or physical deformities following laser exposure or solution change were not used for spark recording. The basic spontaneous activity was also recorded for 10 and 5 fibers before introducing small depolarizations, or 1 mM caffeine, respectively. All measures were taken to avoid photo damage or photo bleaching therefore subsequent images were taken on the same fiber after repositioning. To avoid movement artifacts no local perfusion was used during recordings. This is demonstrated by combining all images in a time-series to show that structural elements did not move (**Supplementary Figures 1C,D** and **Supplementary Video 1**).

TABLE 1 | Composition of the external solution to induce different depolarizations.

In mM	Ringer (−90 mV)	−70 mV	−65 mV	−60 mV
NaCl	115	115	115	115
KCl	2.5	0	0	0
$CaCl_2$	1.8	1.8	1.8	1.8
$MgCl_2$	1	1	1	1
Hepes	10	10	10	10
K methane sulfonate	–	10.2	13.8	18.1

High Speed Recording and Analysis of Ca^{2+} Sparks in Intact Fiber

The fibers were imaged using a Zeiss LSM 5 LIVE laser scanning confocal microscope (Zeiss, Oberkochen, Germany). Instead of imaging the specimen pixel by pixel, it scans along a whole line at the same time, obtaining high temporal resolution image at high acquisition speed. Two dimensional (x-y) image series were taken with speed of 30 or 60 frame per second (FPS), the pixel (line) acquisition time was 47.4 and 15.4 μs. The 512 × 512 pixel image corresponds to 106 μm × 106 μm image size in our experimental setting (pinhole 17 μm, objective: 63X water, NA: 1.2). Fluo-4 was excited with an Argon ion laser (at 488 nm), emitted light was collected through a beam-path filter and digitized at 12 bit. The images were normalized to events excluded baseline fluorescence (F_0).

Identification of Cell Structure and Calcium Sparks on x-y Images

The x-y image sequences containing spontaneous elementary calcium release events (**Figure 1A**) were evaluated using a homemade computer program developed in Borland Delphi (Borland Software Co., Austin, TX, United States). The program allows full automatic analysis of the sequence of images without human intervention.

As the first step in image analysis, the baseline fluorescence value for each pixel of the image was determined. To obtain this value, the average fluorescence value of the points in the time domain for a given pixel that are below $Mean + NormCri \cdot \sigma$ values for all pixel was calculated, where Mean and σ correspond to the average and standard deviation of the fluorescence values of a given pixel in the time domain, respectively. The optimal value of *NormCri* was 1.1. As a next step, the components of the time series belonging to each pixel was determined by the single-dimensional stationary wavelet transformation (Szabo et al., 2010) and then a high pass filtering was applied. Finally, the changes in calcium levels with very slow kinetics not caused by spark formation was removed by dividing all the data of the time-series with the value of the 4th wavelet level (see Szabo et al., 2010, **Figure 1**).

The area belonging to the cell was determined from an image with good signal-to-noise ratio created from the baseline fluorescence values for each pixel (**Figure 1B**). The fluorescence of the cell-associated pixels was much higher than the fluorescence of the extracellular image points; the distribution of intensity was distinctly bimodal. The optimal cut between the

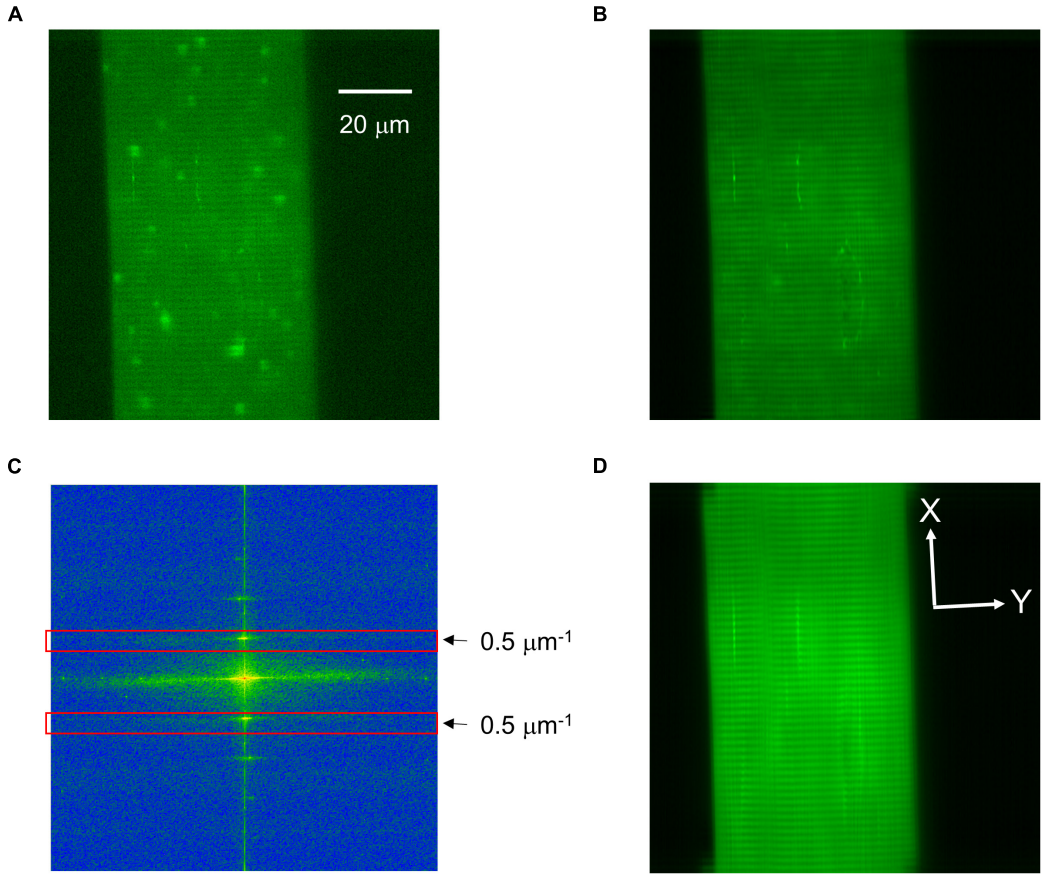

FIGURE 1 | Identification of the cell structure in a representative x-y image. **(A)** An original x-y image of an intact frog skeletal muscle fiber loaded with Fluo-4 displaying calcium release events. **(B)** The picture of the basic fluorescence values of each pixel showing good signal-to-noise ratio for static image elements, such as Z-lines. **(C)** Fast Fourier transform showing the frequency spectrum of the image in panel **(B)**. At 0.5 μm^{-1} (and at its inverse, red rectangles) the sharp band corresponding to one sarcomere is clearly visible. **(D)** The result of the inverse Fourier transformation, where the Z-lines are excellently traceable. White lines perpendicular (X) and parallel (Y) to the Z-lines determine the directions of FWHMs. Scale of panels **(B,D)** is identical to that in panel **(A)**.

two sets of pixels was determined with iterative method, then the area above the threshold was defined as the cell.

After the removal of all variable elements (i.e., calcium sparks) from the image series Z-lines became even more pronounced with some other constant features being present. The structural elements of the cell were determined by the Fourier transform of longitudinally oriented cell areas (**Figure 1C**). The values observed at 0.5 μm^{-1} corresponded to the expected (approximately 2 μm) sarcomere length. Except this peak and the center area of the frequency components all other coefficients were set to zero and an inverse Fourier transformation was performed. In the resulting picture only the components corresponding to the structural elements remained (**Figure 1D**). The Z-lines were determined by searching for the local maximum at columns. With this method the incidentally breaking Z-lines could have also been followed and the parameters of the events could be determined in directions perpendicular (X) and parallel (Y) to the Z-lines (**Figure 1D**).

The efficiency of Z-line identification was tested with images containing artificially created fiber structures. The inclination angle of fibers was determined from the orientation of Z-lines and was compared to the pre-defined creation angle. The developed method gave back almost identical inclination angles (**Supplementary Figure 2**).

Before identifying the ROIs and defining their parameters, high-efficiency Wavelet noise filtering (δ = 3; Szabo et al., 2010) was performed on each normalized image. To identify ROIs corresponding to elemental calcium release events a modified double-threshold method (Cheng et al., 1999) was used in the analysis (**Figure 2**). Contiguous areas with values over *Mean* + *LoCri*·σ that contained at least one pixel with a value greater than *Mean* + *HiCri*·σ were identified as events. The optimal value of *LoCri* and *HiCri* in our case was 1.7 and 2.8, respectively.

To test the method a spark free x-y image with sarcomeric structure and some higher intensity areas throughout the experiment, was merged with artificial Gaussian sparks with different amplitudes (**Supplementary Figure 3A**). Sparks were added to the image by convolving the function producing two-dimensional Gaussian curves with the image containing

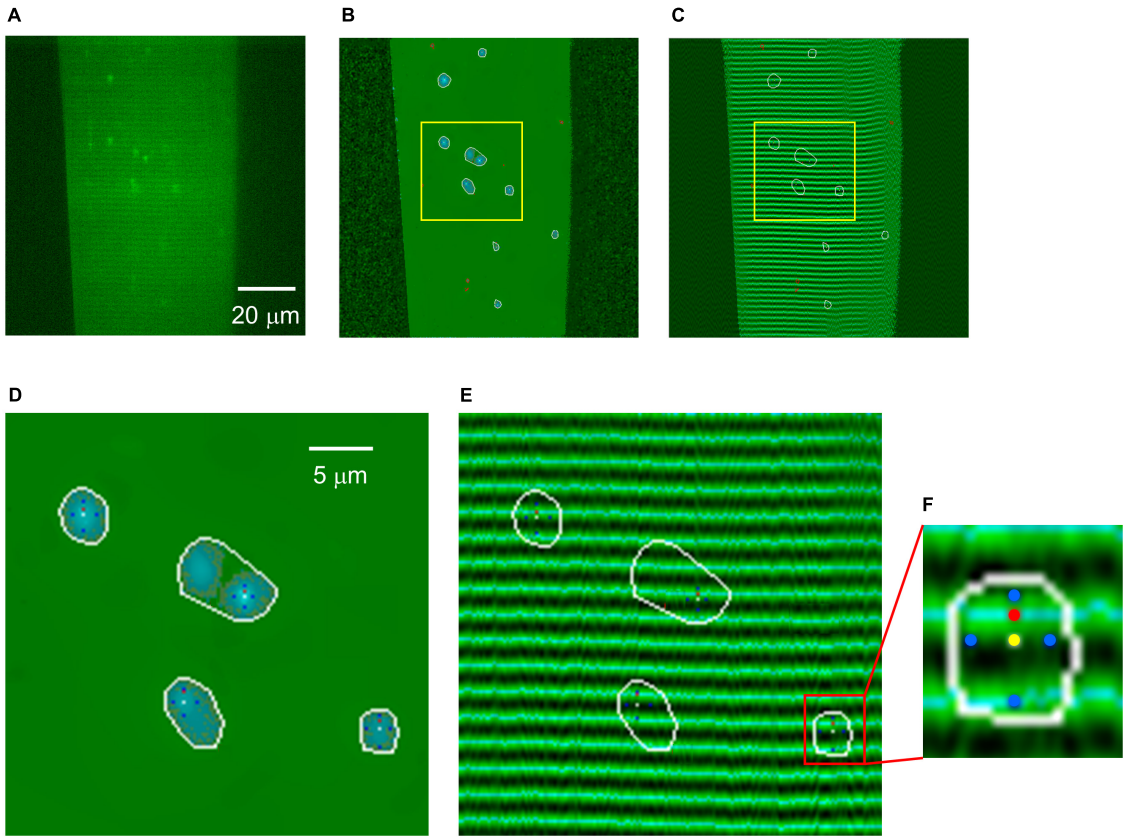

FIGURE 2 | Generation of structure-free normalized image for spark identification and localization. **(A)** Original x-y image. **(B)** F/F_0 image to show that the structure was removed and only the sparks are visible. **(C)** Fiber structure superimposed with areas of sparks. **(D)** Part of the image in **(B)** showing four events at high magnification. White curves encircle the areas corresponding to the identified events. Yellow dots present the position of the maxima, while the four blue dots in each event show the orientation of the two axis (perpendicular and parallel to the Z-lines) within the spark. Red pixels represent the position of the fluorescence maximum of Fluo-4, and thus the distance between yellow and red pixels was used to calculate the distance of the center of the spark from the nearest Z-line. **(E)** Same area as in panel **(B)** enlarged from panel **(C)** showing the superimposed Z-lines. The dark bands mark the triads at the Z-lines. **(F)** A spark enlarged from panel **(E)** showing the location of color dots described above. Light blue lines show the fluorescence maximum (i.e., the middle of a sarcomere).

no sparks at random locations (minimal distance of sparks was 4 μm). Number of sparks per frame (30) and spatial parameters corresponded to the averages found under control conditions (Full-width at half maximum in the X direction, FWHM-X = 1.74 μm; Full-width at half maximum in the Y direction, FWHM-Y = 1.52 μm). The amplitude ranged between 0.15 and 0.6. The sensitivity of the wavelet based detection method was proven, all events with amplitude higher than 0.2 were identified (**Supplementary Figure 3B**). Events with amplitude of 0.2 were captured with around 0.6 sensitivity while events with smaller amplitude were lost. The positive predicted curve (**Supplementary Figure 3C**) was, however, very sharp, all events with amplitude higher than 0.15 were identified correctly. According to these findings events with amplitude less than 0.15 were excluded from all further evaluation. Due to the large number of sparks in x-y images analyzed, small sparks not found due to the chosen thresholds did not cause any significant drop in the analysis and considered as out of focus events.

Within all identified ROI a 3 × 3 area with the highest average amplitude was determined and the center was defined as the center of the event (**Figure 2D**). The difference between the fluorescence intensity of this point and the baseline was used to calculate the amplitude of the spark. The program also considered this point as focal point in the direction parallel and perpendicular to the Z-lines. Where the average intensity of three points reached half of the amplitude value of the spark, the program identified these points as the boundaries of FWHM-X and FWHM-Y. The distance for each event from the nearest Z-line was assessed by calculating the difference of the estimated half sarcomere length and the distance from the nearest fluorescence maximum (**Figure 2E**). The position of the center of the spark was identified on each consecutive image and was used to calculate the movement of the spark, if present, in the X and Y directions.

The effects of the amplitude on the other parameters of the spark were also tested. Images (n = 40) containing artificial sparks with different amplitudes (n = 30) were evaluated and the amplitude and FWHM in both directions were calculated. The program slightly under estimated the original amplitudes (**Supplementary Figure 4A**). Calculated FWHMs at

both directions were the most accurate at 0.25 amplitude. At smaller amplitudes both FWHMs were under estimated, while at higher amplitudes they were overestimated (**Supplementary Figures 4B,C**). We also tested the effects of the orientation of fiber in the image on FWHMs. By limiting the ROI to the central part of the events, the FWHM values (**Supplementary Figure 5**) and eccentricity of sparks (**Supplementary Figure 6B**; see below) were not affected by fiber orientation.

Ca^{2+} spark frequency was calculated from the number of sparks during the recording period divided by the area of the fiber and the duration of the acquisition (number of sparks per area per time) at each conditions.

Signal mass (SM) was calculated as follows:

$$SM = 1.206 \times (FWHM - X) \times (FWHM - Y) \times \left(\frac{(FWHM - X)}{2} + \frac{(FWHM - Y)}{2}\right), \quad (1)$$

where Amp is the amplitude, while FWHM-X and FWHM-Y have their usual meaning (Hollingworth et al., 2001). The spark was assumed to be a spherical 3D object with different X, Y and Z diameters. The diameter in the Z direction was estimated as the average of the X and Y diameter.

To assess the shape of the recorded spark a modified eccentricity value was calculated defined as:

$$E = 1 - \left(\frac{FWHM - Y}{FWHM - X}\right)^2, \quad (2)$$

Note that this is different from the classical definition of eccentricity for an ellipsis (see **Supplementary Figure 6**) to account for the case when FWHM-Y is greater than FWHM-X.

Chemicals and Statistical Analysis

Chemicals, unless otherwise stated, were purchased from Sigma (St. Louis, CA, United States) and were of analytical grade.

Pooled data were expressed as mean ± standard error (SE) of the mean. The differences between control and treatments was assessed using one-way analysis of variance (ANOVA) and all pair wise multiple comparison procedures (Student-Newman-Keuls Method). F test was used to test the significance and a p value of less than 0.05 was considered statistically significant.

RESULTS

Event Frequency and Parameters of Sparks in Different Conditions

Both caffeine treatment and depolarization increased the frequency, the amplitude, the spatial dimensions, and the signal mass of sparks in frog skeletal muscle fibers (**Table 2** and **Figures 3**, **4**). Using incremental depolarization steps, the highest frequency was found at -60 mV (**Table 2**). In the presence of 1 mM caffeine sparks occurred at higher frequency. Depolarization and caffeine treatment together led to even more sparks (**Table 2**). Simultaneously applied depolarization and caffeine gave the highest frequency at -65 mV. However, at this voltage both the amplitude, the spatial spread, and the signal mass were significantly reduced. This was likely due to the fact that the depolarization induced a partial inactivation of the voltage sensors (e.g., Huang, 1996) and the large frequency of sparks induced a partial depletion of calcium in the SR thus 1./greater depolarizations in the presence of caffeine were not explored in detail and 2./except for **Table 2** the data for caffeine treatment at -65 mV were not combined with the other data and are presented in **Supplementary Figures 7–9**.

Calcium sparks detected on frog fibers were not symmetric in the spatial domain, their FWHM was smaller in the Y then in the X direction. Average FWHM in both directions was increasing with increased depolarization and further increased when caffeine was added (**Table 2**). The distribution histograms of spark parameters clearly demonstrate that both depolarization and caffeine increased the frequency of the larger sparks (**Figures 4B–D**), the effect was more pronounced for the latter. Since both depolarization and caffeine treatment elicit sparks with larger spatial widths, the calculated signal mass was also higher under these conditions (**Table 2**).

Representative images are shown for the three treatment groups in **Figure 5A** that display the cumulated number of sparks recorded in every 16 × 16 pixel regions of the fiber. Under control conditions only few active positions existed while during depolarization and in the presence of caffeine the events seemed to appear more equally spread along the fiber. The distribution of spark numbers among dedicated regions (16 × 16 pixel mesh) was compared to the Poisson distribution for all three treatments (**Figure 5B**). Since the theoretical Poisson functions calculated with the λ equal to the average of the event number was almost identical to the Poisson functions fitted to the measured values, our result suggests that both depolarization and caffeine treatment increased the frequency of the events evenly along the fiber without creating spatial clusters or 'hot spots' identified by concentrated activity specific to each conditions (**Figure 5A**).

Based on the spatial cluster analysis we hypothesized that sparks were randomly distributed within the cell, therefore the distance distribution of the center-to-center for each spark pair would follow a linear function. **Figure 6** presents the distances between all spark pairs on each frame for all images recorded. Only distances where one of the sparks was in the center of the respective fiber were considered in order to compensate for the finite size of the fiber. Furthermore, distances that were less than the radius of the given fiber were calculated. It should also be noted that events with centers closer than two FWHM could not be separated by the automated detection method (as their "contiguous areas" overlap and thus they are detected as a single, but large event; see Methods) thus only those sparks were considered where the centers were at least 15, 17, and 20 pixels (control, depolarization and caffeine, respectively) apart. Concentric squares (grid distance) were used instead of circles so as not to have any bias because of the grid pattern of pixels. Under control conditions (**Figure 6A**), on depolarized fibers (**Figure 6B**) and even in the presence of caffeine (**Figure 6C**) the data follow

TABLE 2 | Parameters of sparks in different conditions.

	0 mM Caffeine				1 mM Caffeine		
	NR	**−70 mV**	**−65 mV**	**−60 mV**	**NR**	**−70 mV**	**−65 mV**
Number of fibers	106	64	47	33	21	8	7
Number of events[§]	6164	55312	43326	21410	24942	16029	12391
Frequency (1/ms/mm^2)	1.47 ± 0.30	24.10 ± 3.80$^{*\#}$	37.15 ± 4.35*	38.15 ± 8.25*	91.54 ± 21.36$^{*\#}$	115.28 ± 40.34$^{*\#}$	147.77 ± 60.40$^{*\#}$
Amplitude (F/F_0)	0.188 ± 0.001	0.171 ± 0.001$^{*\#}$	0.164 ± 0.001*	0.173 ± 0.001$^{*\#}$	0.259 ± 0.001$^{*\#}$	0.305 ± 0.001$^{*\#}$	0.176 ± 0.001$^{*\#}$
FWHM-X (μm)	1.725 ± 0.005	1.836 ± 0.002$^{*\#}$	1.917 ± 0.003*	2.089 ± 0.004$^{*\#}$	2.342 ± 0.005$^{*\#}$	2.482 ± 0.005$^{*\#}$	2.150 ± 0.006$^{*\#}$
FWHM-Y (μm)	1.508 ± 0.004	1.587 ± 0.001$^{*\#}$	1.676 ± 0.002*	1.776 ± 0.004$^{*\#}$	2.081 ± 0.005$^{*\#}$	2.270 ± 0.006$^{*\#}$	1.845 ± 0.005$^{*\#}$
SM (μm^3)	1.024 ± 0.009	1.138 ± 0.004$^{*\#}$	1.335 ± 0.007*	1.776 ± 0.004$^{*\#}$	4.354 ± 0.034$^{*\#}$	6.464 ± 0.062$^{*\#}$	2.085 ± 0.021$^{*\#}$

[§]*All events with amplitude less than 0.1 and FWHM less than 1 and greater than 10 μm were discarded.*
**denotes significant difference from NR at $p < 0.001$.*
#denotes significant difference from −65 mV without caffeine treatment at $p < 0.001$.

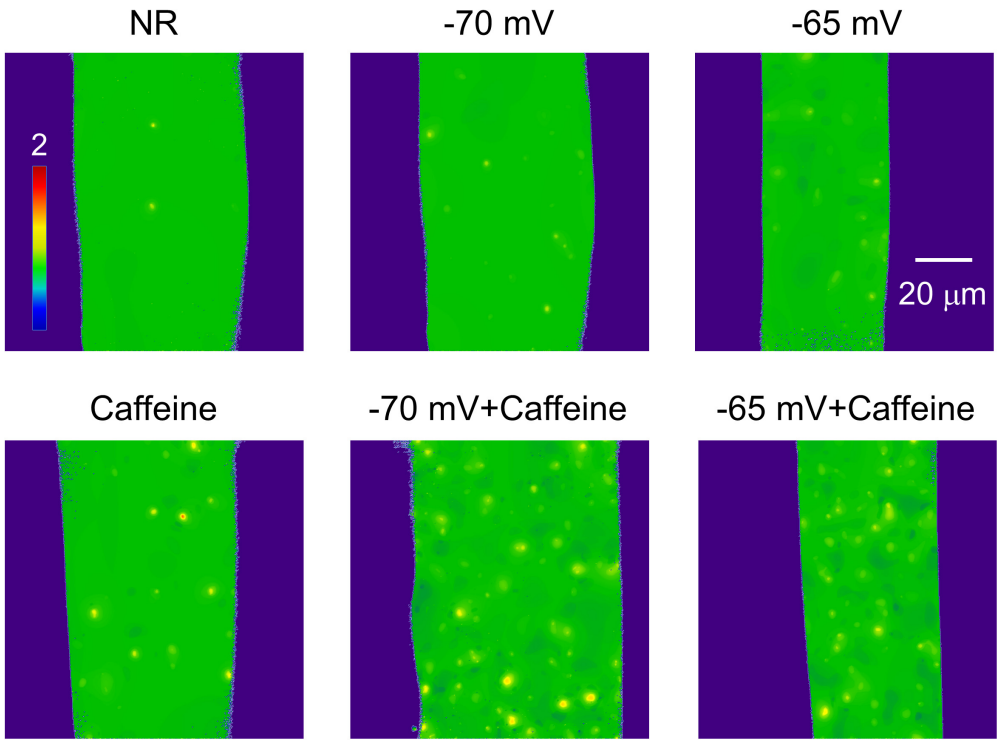

FIGURE 3 | Normalized (F/F_0) full size x-y images of intact frog skeletal muscle fibers bathed in Normal Ringer (NR), in the presence of 1 mM Caffeine (Caffeine), in depolarizing solutions corresponding to a calculated resting membrane potential of -70 and -65 mV, and supplemented with 1 mM Caffeine. All images were recorded with 30 FPS. Note how the number of sparks is changing with the different conditions.

a close to linear function, as demonstrated by the superimposed dashed lines, confirming the random distribution of the events.

Relative Position of Sparks to Z-Lines and Other Events

The determination of fiber structure during the analysis of images allowed us to examine the positions of sparks relative to the Z-lines. **Figure 7A** shows the position and orientation of Z-lines with superimposed sparks (the outlines of sparks are marked with white curves in the enlarged images). The histogram in **Figure 7B** presents the distribution of the distances of the position of the pixel with the highest intensity for each spark from the nearest Z-line. Under control conditions the average distance was calculated to be 0.311 ± 0.003 μm, which was increased significantly either by depolarization (0.401 ± 0.001 μm) or caffeine (0.391 ± 0.002 μm) treatment (**Figure 7C**).

Spatial Morphology of Sparks

To address the spatial orientation of sparks relative to the Z-lines FWHM-X and FWH-Y were measured under all experimental conditions and the modified eccentricity was calculated. As demonstrated in **Figure 8A**, the modified eccentricity showed

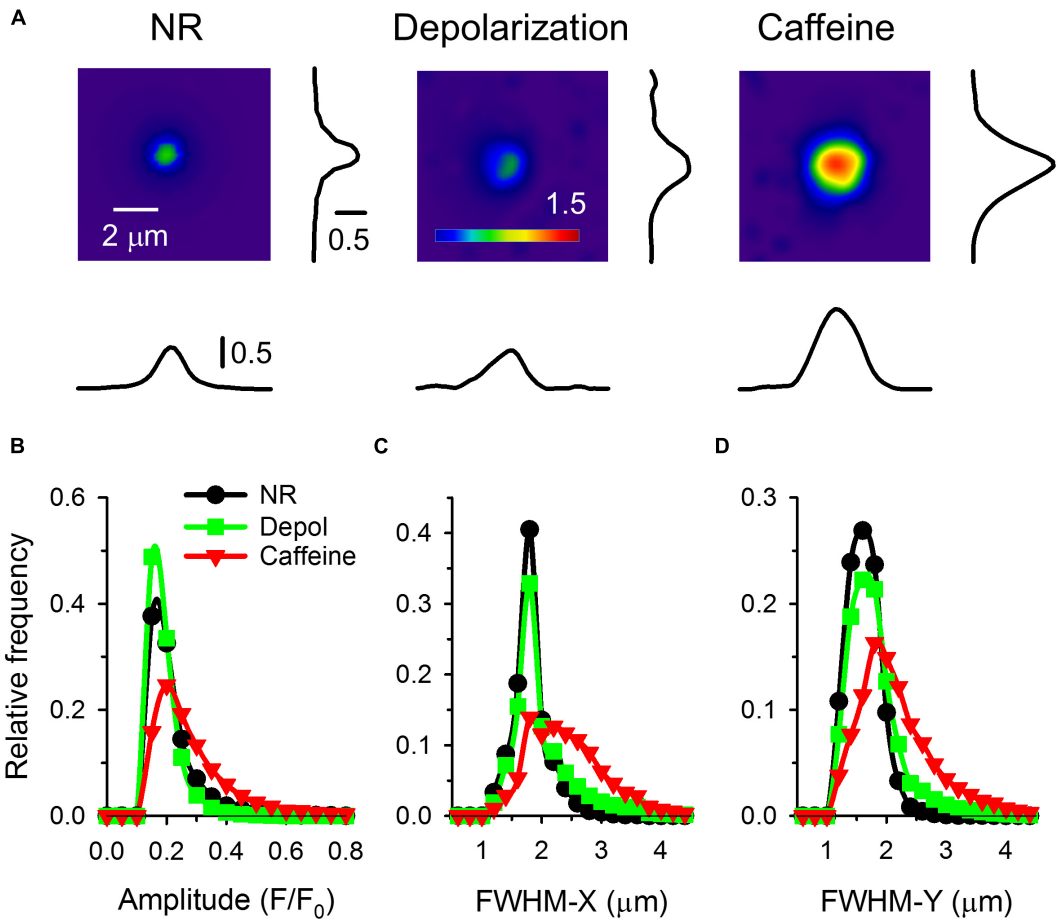

FIGURE 4 | (A) Individual sparks on a larger scale. All images were recorded with 30 FPS. Next to the spark the spatial profile of F/F_0 in X & Y direction (parallel and perpendicular to fiber axis) are presented. Panels **(B–D)** present the distribution histograms for the amplitude **(B)**, FWHM-X **(C)**, and FWHM-Y **(D)** under control conditions (black circles), on fibers depolarized to a calculated value of -65 mV (green squares), and in the presence of 1 mM caffeine (red triangles). Note how both depolarization and caffeine has shifted the distribution the higher values, especially visible in case of FWHM-X and FWHM-Y in the presence of caffeine from 2.5 μm to 4 μm.

an asymmetric distribution both under control conditions, on depolarized fibers, and in the presence of caffeine, indicating that FWHM-X was greater than FWHM-Y for most of the events detected. It is also clear from the histogram that the modified eccentricity was most frequent found between 0.30 and 0.42. This value is significantly greater than that expected to be introduced by scanning (see **Supplementary Figure 6**). Furthermore, larger modified eccentricity values appeared with greater frequency in depolarized as well as in caffeine treated cells. This is reflected in the mean values of modified eccentricity, as this mean was significantly greater for both the depolarized condition and the caffeine treatment (**Figure 8B**). Importantly, the asymmetric shape of the events suggests that either the source is extended or the diffusion is faster in the X direction, or both.

Travelling Sparks

Most sparks were visible only in one frame even when detected with high speed confocal microscopy. For sparks that were present in more than one consecutive frames (**Figure 9A**; **Supplementary Video 2**, **3**), the distance traveled by the center of the spark between two frames was calculated (**Figures 9B–D**). Note that a traveling spark indicates the presence of calcium-induced opening of RyR(s) that didn't get activated first at the beginning of the event.

While under control conditions only 1.5% of events appeared in two consecutive images, the probability was higher in depolarized fibers (9.8%) and even higher after caffeine treatment (29.7%). Sparks traveled significantly longer distances after caffeine treatment (1.66 ± 0.01 μm, n = 7416) than in depolarized fibers (0.95 ± 0.01 μm, n = 4247) which, nonetheless, was still significantly longer than under control conditions (0.52 ± 0.01 μm, n = 94; **Figure 9D**). While under control conditions and during depolarization the distance traveled by the events was the same in X and Y directions, in the caffeine-treated cells sparks traveled significantly longer distances especially in the Y direction ($p < 0.001$; **Figures 9B,C**). These results indicate that depolarization and caffeine treatment "primed" the release sites for subsequent activation by calcium.

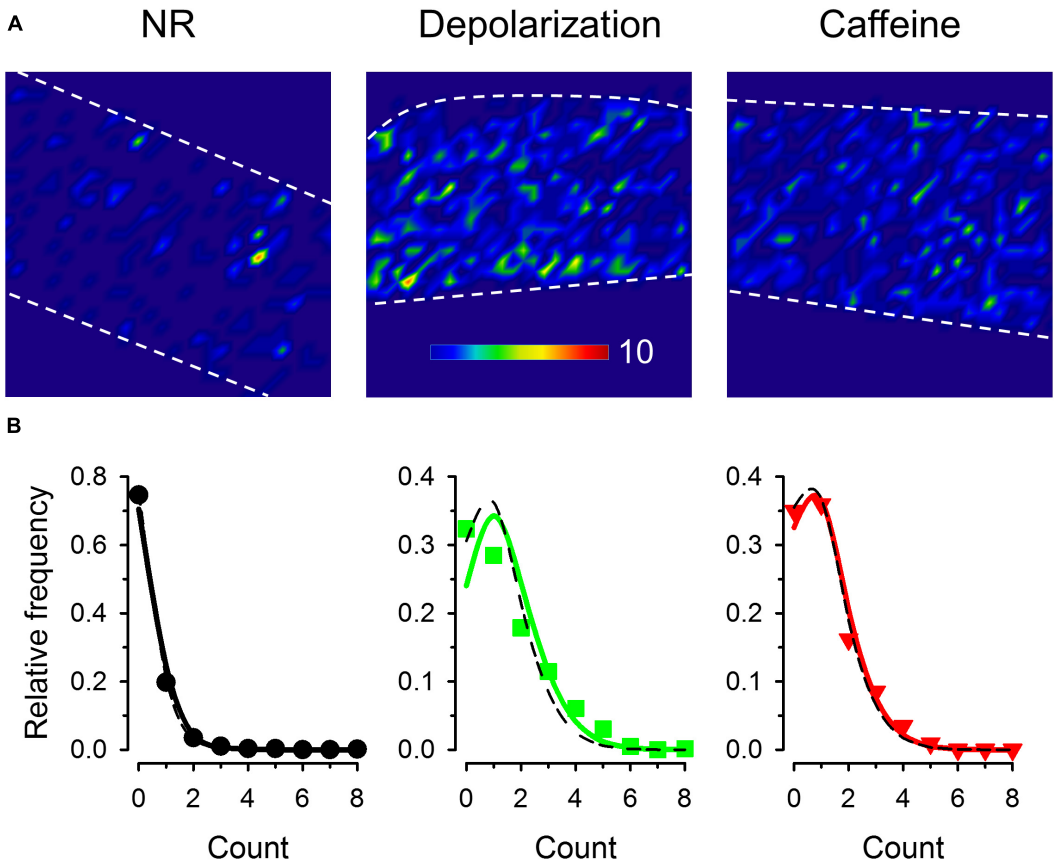

FIGURE 5 | Identifying positions of spark occurrence in images. **(A)** Mesh plot of frequencies of spark occurrence (i.e., the number of sparks in the given region) in a 16 × 16 pixel voxels (generated from 60 consecutive images). All images were recorded with 30 FPS. **(B)** Frequency distribution of regions with different number of sparks. Solid line superimposed is the fitted Poisson distribution, while dashed black curves show the Poisson distribution generated with λ being equal to the average event numbers. The values for λ used to generate the dashed curves were 0.349, 1.42, and 1.12 while those obtained from the fits were 0.281, 1.19, and 1.04 for control conditions, for depolarized fibers, and in the presence of caffeine, respectively.

DISCUSSION

In the past 15 years several automatic Ca^{2+} spark analyzer programs were developed. Some of them used Wavelet transformation methods (von Wegner et al., 2006; Szabo et al., 2010, Prada et al., 2018). Others employed noise thresholding (Picht et al., 2007), statistical analysis (Bányász et al., 2007), or pixel-by-pixel method (Illaste et al., 2019; Tian et al., 2019) to capture and analyze local calcium events.

In this study we showed that our Wavelet based automatic analysis method was suitable to reveal the spatial and temporal characteristics of calcium sparks detected via high-speed confocal microscopy. The program not only captured the calcium release events but was capable of identifying constant cell structures, like Z-lines, and calculate the distance between these structures and the detected sparks. Furthermore, it could calculate the distance between sparks and follow the movement of events appearing in consecutive images. These new features allowed us to describe the behavior of localized elementary calcium release more precisely, perform high throughput data analysis. It also gave us the opportunity to raise hypotheses on the role of the two types of RyRs present in frog skeletal muscle.

RyRα and RyRβ are present in nearly equal amounts in frog skeletal muscle, and are homologs of RyR1 and RyR3 of mammalian muscles (Ogawa et al., 2002). The depolarization-induced Ca^{2+} release is believed to be mediated by RyRα because of its similarity to RyR1 (Oyamada et al., 1994) and its location adjacent to DHPRs. While calcium-induced calcium release works with both types of RyRs in frog skeletal muscle, its activity on RyRα may have 20-fold lower than that on RyRβ (Murayama and Ogawa, 2001). From this, one can hypothesize that the two isoforms of RyR may have distinct roles in calcium release. We successfully showed that sparks detected on depolarized or caffeine treated frog muscle fibers have distinct spatiotemporal parameters and amplitude distribution in our experiments.

We found that sparks appeared at a higher frequency in both depolarized and caffeine treated fibers as compared to control. Importantly, although both the depolarization and caffeine increased both the signal mass of the sparks – i.e., the amount of calcium released during the event – and their frequency, this was not always the case when applied together. At greater

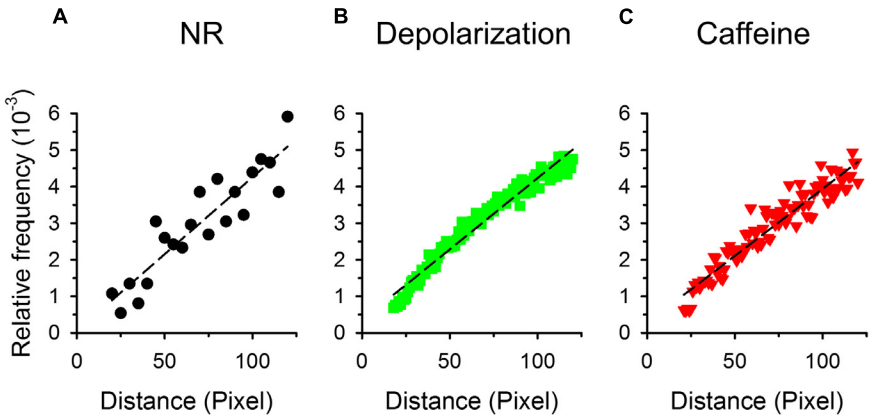

FIGURE 6 | Distribution of the distances between the centers of two sparks. For each spark concentric squares were constructed around the center of the selected spark. The number of sparks with centers falling onto the side of the given square were then counted. The relative frequency of these neighboring sparks are presented for control conditions **(A)**, for depolarized **(B)**, and caffeine-treated fibers **(C)**. Note that in this representation the number of pixels increases linearly with the length of the side of the square, thus if sparks appear randomly a linearly increasing distribution is expected. To avoid the problem of bringing pixels from outside of the fiber into the counting 1./only those sparks were selected that lay close to the center of the fiber and 2./the side of the square was restricted to being less the 120 pixels (appr. 25 μm). Thus in the panels **(A–C)** the ordinate is in pixels. Dashed lines represent least-squares fits of a straight line to the data points in each graph with R^2 being 0.829, 0.964, and 0.918, for panels **(A–C)**, respectively.

depolarizations albeit the frequency was further increased, the signal mass, due to a drop in both the amplitude and the spatial spread, decreased dramatically. This can be reconciled if one assumes that the large number of events leads to a partial depletion of calcium in the terminal cisternae of the SR. Indeed, if the rate of calcium release exceeds the uptake rate of the SR calcium pump one expects a depletion of calcium in the SR. However, in this case the cytosolic calcium concentration should increase as the released but not reuptake calcium should appear in the intracellular space. Although Fluo-4 is not suitable to allow a precise calculation of the exact calcium concentration, the overall increase in fluorescence seen at greater depolarizations supports this idea.

The analysis of FWHM on depolarized fibers treated with caffeine (**Supplementary Figure 7**) suggests that the two interventions exerted their effect independent of one another. We also observed widening of the spatial spread and shifting of the center of the spark further away from the Z-line (**Figure 7C** and **Supplementary Figure 9A**). In this framework under control conditions a small group of RyRα-s open under a strict control of DHPRs and depolarization recruits additional RyRα-s. The calcium thus released can then albeit to a small extent activate additional release channels via CICR. The addition of caffeine primes the release channels to the activating calcium making CICR more probable. As RyRβ-s are more sensitive to caffeine than RyRα (see e.g., Murayama and Ogawa, 2001; Kashiyama et al., 2010) calcium sparks in the presence of caffeine are likely to be generated more by RyRβ than by RyRα. This is reflected in our finding that sparks in the presence of caffeine appear with greater amplitude and frequency (**Table 2**). RyR-deficient myotubes expressing RyRα have uniform and sustained calcium release, whereas cells expressing RyRβ have regenerative Ca^{2+} release events (waves and oscillations; Kashiyama et al., 2010). Examining the distribution of amplitudes and FWHMs of the sparks revealed that under control conditions the spontaneously generated calcium sparks were initiated predominantly by RyRα since the distribution of their parameters was similar to those on depolarized fibers (**Figures 4B–D**). An important finding of our study was that the signal mass of sparks (representing the amount of calcium released) was only slightly increased by depolarization, but multiplied after caffeine treatment (**Table 2**).

The high number of events allowed us to statistically analyze the appearance of sparks macroscopically in a fiber. One important finding was that there were no "hot spots" where more sparks would develop than at other places in intact frog skeletal muscle fibers. The appearance of sparks in the whole fiber followed the Poison distribution in all cases examined (**Figure 5**). Similar results were found by Klein et al. (1996) during depolarization in also frog muscle fibers. This suggests that the events arose following a random process independently from depolarization and the presence of caffeine. The microscopic analysis of event position lead to the same conclusion. Interspark distances are close to linearly distributed on depolarized or caffeine treated muscle fibers indicating that sparks form independently from one another (**Figure 6**). Nevertheless, a slight deviation from this linearity can be observed at short distances on depolarized fibers and in the presence of caffeine. It was hypothesed by Stern et al. (2013) that calcium release from one couplon could influence its neighbors in several ways: (1) SR calcium can travel to other couplons by diffusion within the SR lumen; (2) cytosolic calcium can diffuse to activate or influence RyRs; and (3) SR calcium can be increased by SERCA uptake following the diffusion in the cytosol.

Calcium sparks were asymmetric and wider in the direction parallel to the axis of the muscle fibers. The events exhibited some eccentricity (**Figure 8**, **Supplementary Figures 6**, **9**B) comparable to that what was reported for the RyR cluster shape in cardiac myocytes (Galice et al., 2018). This behavior of sparks

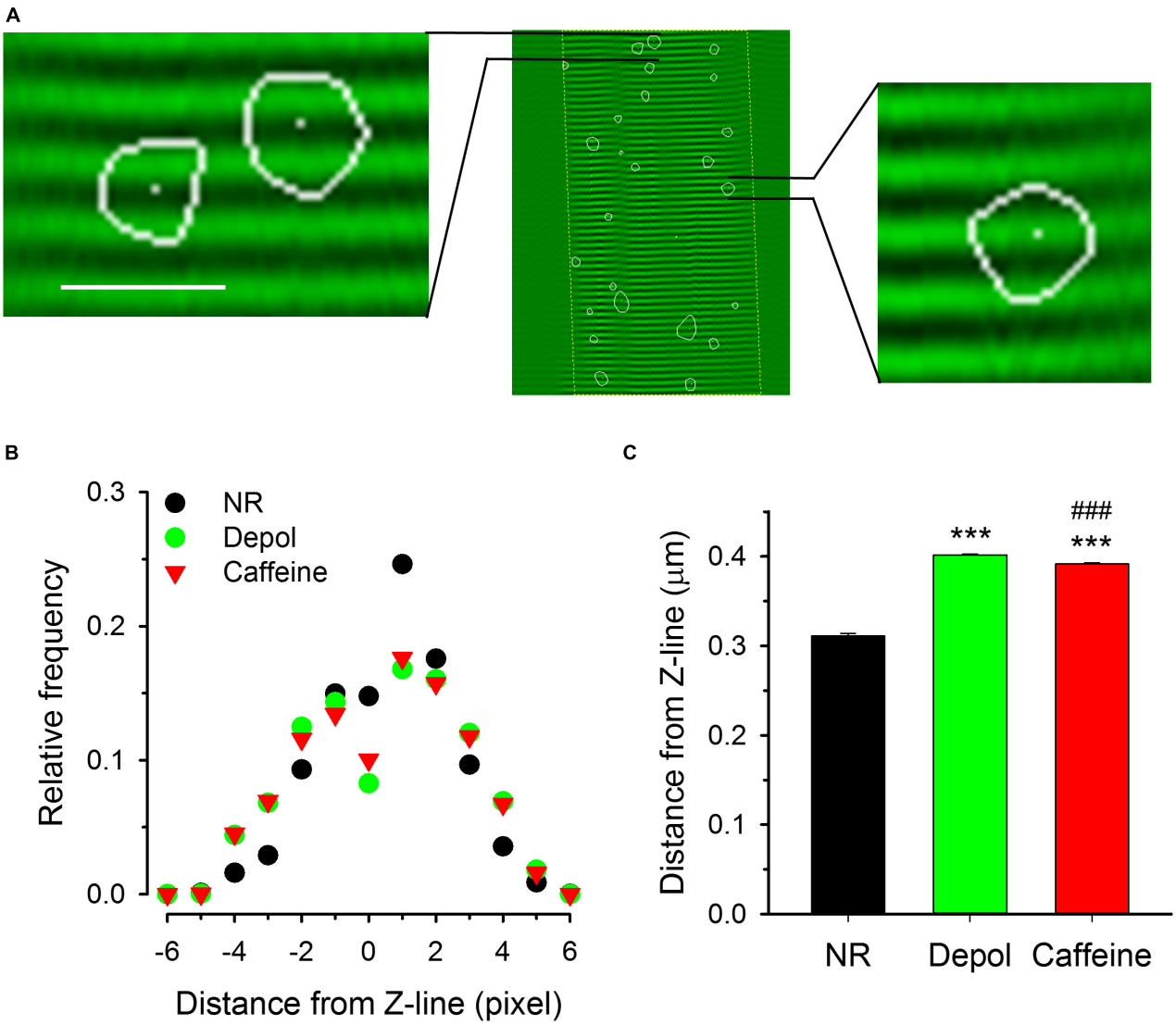

FIGURE 7 | Localization of spark centers relative to the Z-line. **(A)** Two samples from an image showing the fiber structure superimposed with sparks (indicated by the areas encircled by the white lines). White dots present the position of the center of the sparks. **(B)** Distribution histograms of the distance between center of sparks and the nearest Z-line for control conditions (NR, black circles), on depolarized fibers (green squares), and in the presence of caffeine (red triangles). Note that the distributions are essentially symmetric to the Z-line. **(C)** Mean distances of spark centers under the three conditions. Both the depolarization and the presence of caffeine shifted the center of the spark to positions further away from the Z-line as compared to the control conditions. Scale in panel A corresponds to 40 μm for the middle image and 4.3 μm for the enlarged images on left and right side. The middle image was recorded with 30 FPS. Here and in subsequent figures *** denotes significant difference versus NR at $p < 0.001$, ### denotes significant difference vs. Depol at $p < 0.001$.

was independent of the depolarization and caffeine treatment suggesting the idea that the size of RyR cluster creating a sparks was greater than in control but similar in the two investigated conditions. We have to underline that the difference between the FWHM values in the X and in the Y direction did not result from the non-instantaneous scanning of the frame (**Supplementary Figure 6A**). Taking the value for the speed of Ca^{2+} diffusion in the cytosol (0.73 μm/ms; Donahue and Abercrombie, 1987) and the speed of scanning (3.19 μm/ms, calculated as 106 μm/512/0.065 ms from 65 μs/line, 512 lines/frame, 106 μm/frame scanning parameters) one can conclude that the speed of diffusion is around one quarter of the scanning. This would result in a deformed spot of release (see **Supplementary Figure 6A**) and contribute to the eccentricity of events. The theoretical eccentricity calculated from the two speeds (diffusion divided by scanning) was 0.23 in our case. Eccentricity, however, did not take the orientation of the spark relative to that of the fiber into account. We have, thus introduced a modified eccentricity to keep this spatial information. From the calculations the eccentricity introduced by the scanning and represented by the value of the modified eccentricity was much smaller than those observed under either condition (see **Supplementary Figure 5**).

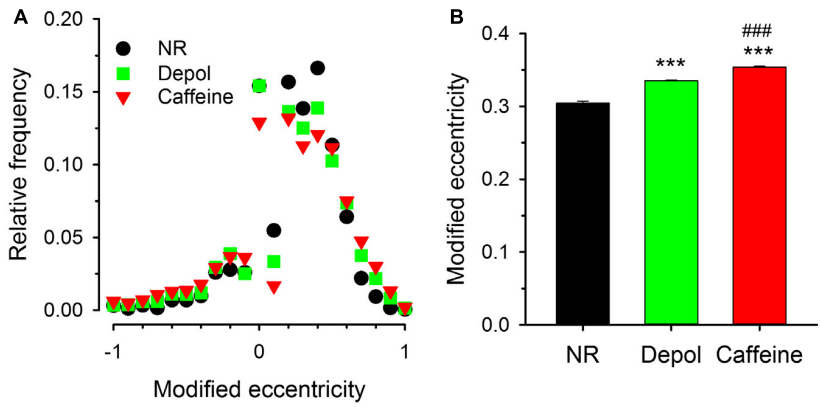

FIGURE 8 | Modified eccentricity of the sparks **(A)**. Distribution of the modified eccentricity calculated using Eqn. 2 for control conditions (NR, black circles), for depolarized fibers (green squares), and in the presence of caffeine (red triangles). Note that albeit negative values were present, the distribution is not symmetric, it is shifted toward positive values indicating that FWHM-X was, in most cases, greater than FWHM-Y. **(B)** Average modified eccentricity for the three experimental conditions calculated using only the positive values from panel **(A)**. Note that both the depolarization and caffeine treatment increased the modified eccentricity, and, furthermore, its value was far greater even under control conditions than what is expected from the skewing introduced by the scanning.

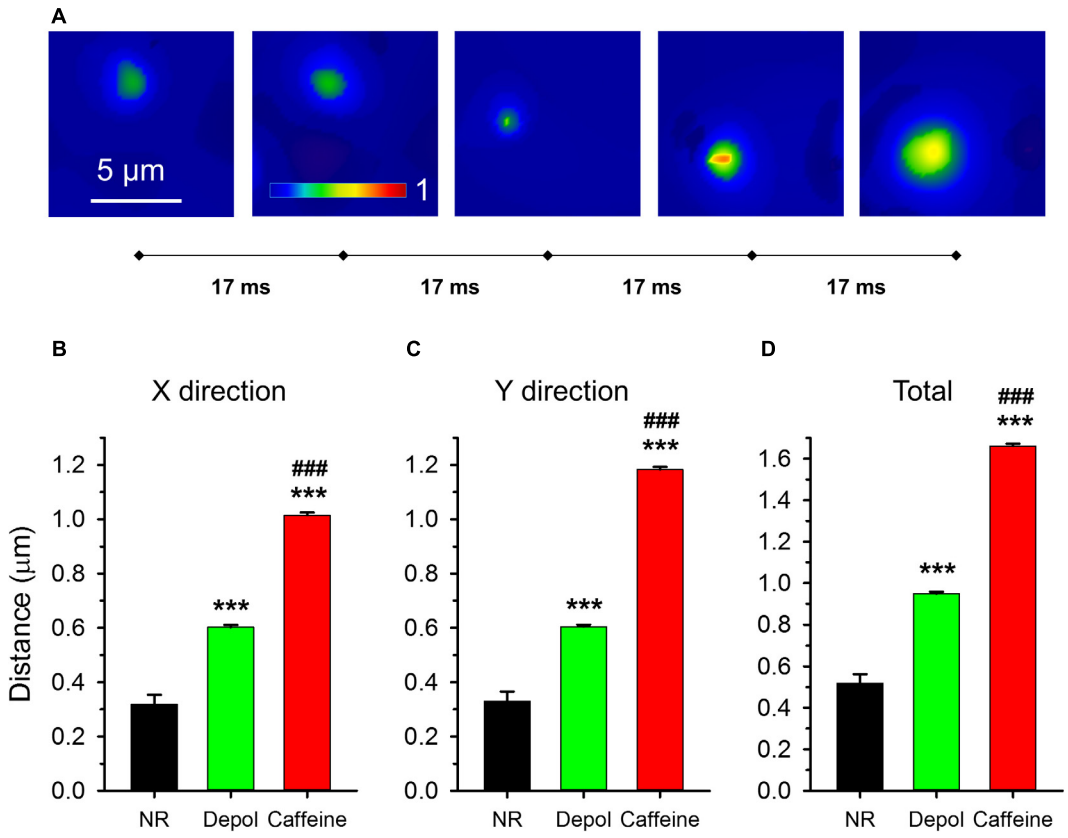

FIGURE 9 | Traveling events on consecutive x-y images. **(A)** Five consecutive F/F_0 images with the traveling sparks identified. The sampling rate was 17 ms/image (60 FPS). **(B–D)** Averages of distances traveled. **(B,C)** report distances in X and Y direction, respectively, while panel **(D)** presents the total distance traveled. The numbers of events analyzed are presented in **Table 2**.

This indicates that either the source was extended or the diffusion was not homogenous in all directions, or both. Furthermore, as both the depolarization and caffeine increased the value of modified eccentricity and neither is likely to alter the diffusion of calcium in the cytosol, one must conclude that they affected the size of the source. This is substantiated by the finding that

both interventions increased the signal mass, i.e., the amount of calcium released, in an event.

The detailed examination of consecutive images provided that only a minority (1.5%) of sparks could "travel" from their origin by around half μm under control conditions. Depolarization doubled and caffeine tripled this distance in average (**Figure 9D**) and the number of traveling sparks increased dramatically in both cases (∼10% and ∼30% of all events, respectively). Similar observation was obtained after the application of the special calcium chelator TPEN (Sztretye et al., 2009). All these interventions, depolarization and caffeine in this report and TPEN in that of Sztretye et al. (2009) have one feature in common. Namely, they prime RyRs for oncoming activating stimuli, in our case the calcium that diffuses from a neighboring release site. The observation that caffeine promoted longer distances of traveling than the depolarization did argue in favor of the hypothesis that the latter involved RyRs located further away from the original release site.

CONCLUSION

In this study we have analyzed a vast number of calcium sparks from intact frog skeletal muscles under control condition, during subthreshold depolarizations and in the presence of caffeine. We have introduced a method that enabled us to obtain spatial information of spark morphology and location relative to the orientation of the fiber axis and the Z-line. Understanding the role of CICR in the generation of spontaneous calcium sparks could help in revealing the mechanisms underlying the appearance of such events under pathological conditions and during regeneration in mammalian skeletal muscle. Furthermore, the role RyRα and RyRβ play in the generation of spontaneous calcium sparks should shed light on the interaction of RyR1 and RyR3 in those mammalian muscle fibers where RyR3 is expressed in greater amounts.

DATA AVAILABILITY STATEMENT

The raw data supporting the conclusions of this article will be made available by the authors, without undue reservation.

ETHICS STATEMENT

The animal study was reviewed and approved by University of Maryland Institutional Animal Care and Use Committee.

AUTHOR CONTRIBUTIONS

HC and MS designed the experiments. HC participated in the confocal microscopy spark experiments. JV wrote the image analyzer program. BD, HC, LC, and PS wrote the manuscript. DB, JV, and PS did the statistical analysis and prepared the figures. All authors contributed to discussion, and reviewed/edited the manuscript.

FUNDING

This work was supported by NIH grant 5R01NS023346 to MS. This work was supported by grant from the Hungarian National Research, Development and Innovation Office (EFOP-3.6.2-16-2017-0006 and GINOP-2.3.2-15-2016-00044). The project is co-financed by the European Union and the European Regional Development Fund.

SUPPLEMENTARY MATERIAL

The Supplementary Material for this article can be found online at: https://www.frontiersin.org/articles/10.3389/fphys.2020.599822/full#supplementary-material

REFERENCES

Bányász, T., Chen-Izu, Y., Balke, C. W., and Izu, L. T. (2007). A new approach to the detection and statistical classification of $Ca2^{+}$ sparks. *Biophys*. J. 92 4458–4465. doi: 10.1529/biophysj.106.103069

Brum, G., Gonzalez, A., Rengifo, J., Shirokova, N., and Rios, E. (2000). Fast imaging in two dimensions resolves extensive sources of Ca2+ sparks in frog skeletal muscle. *J. Physiol.* 528, 419–433. doi: 10.1111/j.1469-7793.2000.00419.x

Cheng, H., Lederer, W. J., and Cannell, M. B. (1993). Calcium sparks: elementary events underlying excitation-contraction coupling in heart muscle. *Science* 262, 740–744. doi: 10.1126/science.8235594

Cheng, H., Song, L. S., Shirokova, N., González, A., Lakatta, E. G., Ríos, E., et al. (1999). Amplitude distribution of calcium sparks in confocal images: theory and studies with an automatic detection method. *Biophys. J.* 76, 606–617. doi: 10.1016/S0006-3495(99)77229-2

Dayal, A., Schrötter, K., Pan, Y., Föhr, K., Melzer, W., and Grabner, M. (2017). The Ca2+ influx through the mammalian skeletal muscle dihydropyridine receptor is irrelevant for muscle performance. *Nat. Comm.* 8:475. doi: 10.1038/s41467-017-00629-x

Donahue, B. S., and Abercrombie, R. F. (1987). Free diffusion coefficient of ionic calcium in cytoplasm. *Cell Calcium* 8, 437–448. doi: 10.1016/0143-4160(87)90027-3

Felder, E., and Franzini-Armstrong, C. (2002). Type 3 ryanodine receptors of skeletal muscle are segregated in a parajunctional position. *Proc. Natl. Acad. Sci. U.S.A.* 99, 1695–1700. doi: 10.1073/pnas.032657599

Franzini-Armstrong, C. (2004). Functional implications of RyR-dHPR relationships in skeletal and cardiac muscles. *Biol. Res.* 37, 507–512. doi: 10.4067/s0716-97602004000400003

Franzini-Armstrong, C., and Protasi, F. (1997). Ryanodine receptors of striated muscles: a complex channel capable of multiple interactions. *Physiol. Rev.* 77, 699–729. doi: 10.1152/physrev.1997.77.3.699

Galice, S., Xie, Y., Yang, Y., Sato, D., and Bers, D. M. (2018). Size matters: ryanodine receptor cluster size affects arrhythmogenic sarcoplasmic reticulum calcium release. *Heart Assoc.* 7:e008724. doi: 10.1161/JAHA.118.008724

Gonzalez, A., Kirsch, W. G., Shirokova, N., Pizarro, G., Brum, G., Pessah, I. N., et al. (2000a). Involvement of multiple intracellular release channels in calcium sparks of skeletal muscle. *PNAS* 97, 4380–4385. doi: 10.1073/pnas.070056497

Gonzalez, A., Kirsch, W. G., Shirokova, N., Pizarro, G., Stern, M. D., and Rios, E. (2000b). The spark and its ember: separately gated local components of Ca2+

release in skeletal muscle. *J. Gen. Physiol.* 115, 139–157. doi: 10.1085/jgp.115.2.139

Hollingworth, S., Peet, J., Chandler, W. K., and Baylor, S. M. (2001). Calcium sparks in intact skeletal muscle fibers of the frog. *J. Gen. Physiol.* 118, 653–678. doi: 10.1085/jgp.118.6.653

Huang, C. L. (1996). Kinetic isoforms of intramembrane charge in intact amphibian striated muscle. *J. Gen. Physiol.* 107, 515–534. doi: 10.1085/jgp.107.4.515

Illaste, A., Wullschleger, M., Fernandez-Tenorio, M., Niggli, E., and Egger, M. (2019). Automatic detection and classification of Ca2+ release events in line- and frame-scan images. *Biophys. J.* 116, 383–394. doi: 10.1016/j.bpj.2018.12.013

Isaeva, E. V., Shkryl, V. M., and Shirokova, N. (2005). Mitochondrial redox state and Ca2+ sparks in permeabilized mammalian skeletal muscle. *J. Physiol.* 565, 855–872. doi: 10.1113/jphysiol.2005.086280

Kashiyama, T., Murayama, T., Suzuki, E., Allen, P. D., and Ogawa, Y. (2010). Frog alpha- and beta-ryanodine receptors provide distinct intracellular Ca2+ signals in a myogenic cell line. *PLoS One* 5:e11526. doi: 10.1371/journal.pone.0011526

Kirsch, W. G., Uttenweiler, D., and Fink, R. H. (2001). Spark- and ember-like elementary Ca2+ release events in skinned fibres of adult mammalian skeletal muscle. *J. Physiol.* 537, 379–389. doi: 10.1111/j.1469-7793.2001.00379.x

Klein, M. G., Cheng, H., Santana, L. F., Jiang, Y. H., Lederer, W. J., and Schneider, M. F. (1996). Two mechanisms of quantized calcium release in skeletal muscle. *Nature* 379, 455–458. doi: 10.1038/379455a0

Klein, M. G., Lacampagne, A., and Schneider, M. F. (1997). Voltage dependence of the pattern and frequency of discrete Ca2+ release events after brief repriming in frog skeletal muscle. *Proc. Natl. Acad. Sci. U.S.A.* 94, 11061–11066. doi: 10.1073/pnas.94.20.11061

Klein, M. G., and Schneider, M. F. (2006). Ca2+ sparks in skeletal muscle. *Prog. Biophys. Mol. Biol.* 92, 308–332. doi: 10.1016/j.pbiomolbio.2005.05.016

Murayama, T., and Ogawa, Y. (2001). Selectively suppressed Ca2+-induced Ca2+ release activity of alpha-ryanodine receptor (alpha-RyR) in frog skeletal muscle sarcoplasmic reticulum: potential distinct modes in Ca2+ release between alpha-and beta-RyR. *J. Biol. Chem.* 276, 2953–2960. doi: 10.1074/jbc.M005809200

Nelson, M. T., Cheng, H., Rubart, M., Santana, L. F., Bonev, A. D., Knot, H. J., et al. (1995). Relaxation of arterial smooth muscle by calcium sparks. *Science* 270, 633–637. doi: 10.1126/science.270.5236.633

Ogawa, Y., Kurebayashi, N., and Murayama, T. (1999). Ryanodine receptor isoforms in excitation-contraction coupling. *Adv. Biophys.* 36, 27–64. doi: 10.1016/s0065-227x(99)80004-5

Ogawa, Y., Murayama, T., and Kurebayashi, N. (2002). Ryanodine receptor isoforms of non-Mammalian skeletal muscle. *Front. Biosci.* 7, d1184–d1194.

Oyamada, H., Murayama, T., Takagi, T., Iino, M., Iwabe, N., Miyata, T., et al. (1994). Primary structure and distribution of ryanodine-binding protein isoforms of the bullfrog skeletal muscle. *J. Biol. Chem.* 269, 17206–17214.

Perez, C. F., Voss, A., Pessah, I. N., and Allen, P. D. (2003). RyR1/RyR3 Chimeras Reveal that multiple domains of RyR1 are involved in skeletal-type E-C coupling. *Biophys. J.* 84, 2655–2663.

Picht, E., Zima, A. V., Blatter, L. A., and Bers, D. M. (2007). SparkMaster: automated calcium spark analysis with ImageJ. *Am. J. Physiol. Cell Physiol.* 293, C1073–C1081. doi: 10.1152/ajpcell.00586.2006

Pouvreau, S., Royer, L., Yi, J., Brum, G., Meissner, G., Ríos, E., et al. (2007). Ca2+ sparks operated by membrane depolarization require isoform 3 ryanodine receptor channels in skeletal muscle. *Proc. Natl. Acad. Sci. U.S.A.* 104, 5235–5240. doi: 10.1073/pnas.0700748104

Prada, J., Sasi, M., Martin, C., Jablonka, S., Dandekar, T., and Blum, R. (2018). An open source tool for automatic spatiotemporal assessment of calcium transients and local 'signal-close-to-noise' activity in calcium imaging data. *PLoS Comput. Biol.* 14:e1006054. doi: 10.1371/journal.pcbi.1006054

Rios, E., and Pizarro, G. (1988). Voltage sensors and calcium channels of excitation-contraction coupling. *Physiology* 6, 223–227.

Rodney, G. G., and Schneider, M. F. (2003). Calmodulin modulates initiation but not termination of spontaneous Ca2+ sparks in frog skeletal muscle. *Biophys. J.* 85, 921–932. doi: 10.1016/S0006-3495(03)74531-7

Rossi, R., Bottinelli, R., Sorrentino, V., and Reggiani, C. (2001). Response to caffeine and ryanodine receptor isoforms in mouse skeletal muscles. *Am. J. Physiol. Cell Physiol.* 281, C585–C594.

Schneider, M. F., and Ward, C. W. (2002). Initiation and termination of calcium sparks in skeletal muscle. *Front. Biosci.* 7, d1212–d1222.

Stern, M. D., Ríos, E., and Maltsev, V. A. (2013). Life and death of a cardiac calcium spark. *J. Gen. Physiol.* 142, 257–274. doi: 10.1085/jgp.201311034

Sutko, J. L., and Airey, J. A. (1996). Ryanodine receptor Ca2+ release channels: does diversity in form equal diversity in function? *Physiol. Rev.* 76, 1027–1071. doi: 10.1152/physrev.1996.76.4.1027

Szabo, L. Z., Vincze, J., Csernoch, L., and Szentesi, P. (2010). Improved spark and ember detection using stationary wavelet transforms. *J. Theor. Biol.* 264, 1279–1292. doi: 10.1016/j.jtbi.2010.04.005

Szappanos, H., Smida-Rezgui, S., Cseri, J., Simut, C., Sabatier, J.-M., De Waard, M., et al. (2005). Differential effects of maurocalcine on Ca2+ release events and depolarization-induced Ca2+ release in rat skeletal muscle. *J. Physiol.* 565, 843–853. doi: 10.1113/jphysiol.2005.086074

Sztretye, M., Almássy, J., Deli, T., Szentesi, P., Jung, C., Dienes, B., et al. (2009). Altered sarcoplasmic reticulum calcium transport in the presence of the heavy metal chelator TPEN. *Cell Calcium* 46, 347–355. doi: 10.1016/j.ceca.2009.10.002

Tian, Q., Schröder, L., Schwarz, Y., Flockerzi, A., Kaestner, L., Zeug, A., et al. (2019). Large scale, unbiased analysis of elementary calcium signaling events in cardiac myocytes. *J. Mol. Cell Cardiol.* 135, 79–89. doi: 10.1016/j.yjmcc.2019.08.004

Tsugorka, A., Rios, E., and Blatter, L. A. (1995). Imaging elementary events of calcium release in skeletal muscle cells. *Science* 269, 1723–1726. doi: 10.1126/science.7569901

Vincze, J., Szabo, L. Z., Dienes, B., Szentesi, P., and Csernoch, L. (2013). Efficient automatic analysis of high-speed confocal images containing localized calcium release events. *Biophys. J.* 104:437a.

Vincze, J., Szabo, L. Z., Dienes, B., Szentesi, P., and Csernoch, L. (2014). Increased accuracy of calcium spark parameter detection using high-speed confocal microscopy. *Biophys. J.* 106:532a.

von Wegner, F., Both, M., and Fink, R. H. (2006). Automated detection of elementary calcium release events using the á trous wavelet transform. *Biophys. J.* 90, 2151–2163. doi: 10.1529/biophysj.105.069930

Wang, S. Q., Stern, M. D., Rios, E., and Cheng, H. (2004). The quantal nature of Ca2+ sparks and in situ operation of the ryanodine receptor array in cardiac cells. *Proc. Natl. Acad. Sci. U.S.A.* 101, 3979–3984. doi: 10.1073/pnas.0306157101

Zhou, J., Brum, G., Gonzalez, A., Launikonis, B. S., Stern, M. D., and Ríos, E. (2003). Ca2+ sparks and embers of mammalian muscle. Properties of the sources. *J. Gen. Physiol.* 122, 95–114. doi: 10.1085/jgp.200308796

Zhou, J., Launikonis, B. S., Rios, E., and Brum, G. (2004). Regulation of Ca2+ sparks by Ca2+ and Mg2+ in mammalian and amphibian muscle. An RyR isoform-specific role in excitation-contraction coupling? *J. Gen. Physiol.* 124, 409–428. doi: 10.1085/jgp.200409105

Conflict of Interest: The authors declare that the research was conducted in the absence of any commercial or financial relationships that could be construed as a potential conflict of interest.

frontiers in Physiology

REVIEW
published: 17 December 2020
doi: 10.3389/fphys.2020.615351

Disturbances in Calcium Homeostasis Promotes Skeletal Muscle Atrophy: Lessons From Ventilator-Induced Diaphragm Wasting

Hayden W. Hyatt and Scott K. Powers*

Department of Applied Physiology and Kinesiology, University of Florida, Gainesville, FL, United States

OPEN ACCESS

Edited by:
Matias Mosqueira, Heidelberg University Hospital, Germany

Reviewed by:
W. Bradley Nelson, Brigham Young University, United States
Susan Treves, University Hospital of Basel, Switzerland

***Correspondence:**
Hayden W. Hyatt
Haydenhyatt@ufl.edu

Specialty section:
This article was submitted to Striated Muscle Physiology, a section of the journal Frontiers in Physiology

Received: *08 October 2020*
Accepted: *19 November 2020*
Published: *17 December 2020*

Citation:
Hyatt HW and Powers SK (2020) Disturbances in Calcium Homeostasis Promotes Skeletal Muscle Atrophy: Lessons From Ventilator-Induced Diaphragm Wasting. Front. Physiol. 11:615351. doi: 10.3389/fphys.2020.615351

Mechanical ventilation (MV) is often a life-saving intervention for patients in respiratory failure. Unfortunately, a common and undesired consequence of prolonged MV is the development of diaphragmatic atrophy and contractile dysfunction. This MV-induced diaphragmatic weakness is commonly labeled "ventilator-induced diaphragm dysfunction" (VIDD). VIDD is an important clinical problem because diaphragmatic weakness is a major risk factor for the failure to wean patients from MV; this inability to remove patients from ventilator support results in prolonged hospitalization and increased morbidity and mortality. Although several processes contribute to the development of VIDD, it is clear that oxidative stress leading to the rapid activation of proteases is a primary contributor. While all major proteolytic systems likely contribute to VIDD, emerging evidence reveals that activation of the calcium-activated protease calpain plays a required role. This review highlights the signaling pathways leading to VIDD with a focus on the cellular events that promote increased cytosolic calcium levels and the subsequent activation of calpain within diaphragm muscle fibers. In particular, we discuss the emerging evidence that increased mitochondrial production of reactive oxygen species promotes oxidation of the ryanodine receptor/calcium release channel, resulting in calcium release from the sarcoplasmic reticulum, accelerated proteolysis, and VIDD. We conclude with a discussion of important and unanswered questions associated with disturbances in calcium homeostasis in diaphragm muscle fibers during prolonged MV.

Keywords: oxidative stress, reactive oxygen species, muscle atrophy, ryanodine receptors, calpain, proteolysis

Abbreviations: MV, Mechanical ventilation; VIDD, Ventilator-induced diaphragm dysfunction; ROS, Reactive oxygen species; SR, sarcoplasmic reticulum; CSA, cross-sectional area; EC, excitation-contraction; SOC, store-operated calcium channel; ROC, receptor-operated calcium channel; PMCA, plasma membrane Ca^{2+} ATPases; NCX, Na^{+}/Ca^{2+} exchanger; RyR, ryanodine receptor; DHPRs, dihydropyridine receptors; PKA, Protein Kinase A; MAMs, mitochondria associated membranes; VDAC, voltage dependent anion channel; MCU, mitochondrial uniporter.

INTRODUCTION

Mechanical ventilation (MV) is often a life-saving intervention for both critically ill patients and patients undergoing surgery. An unwanted side-effect of prolonged MV is the rapid development of inspiratory muscle weakness that occurs due to both diaphragmatic atrophy and contractile dysfunction. Collectively, this syndrome has been labeled ventilator-induced diaphragm dysfunction (VIDD) (Vassilakopoulos and Petrof, 2004). VIDD is a serious clinical problem because diaphragmatic weakness is a major risk factor contributing to the failure to wean patients from the ventilator (Petrof et al., 2010).

Abundant evidence confirms that MV-induced diaphragmatic atrophy occurs due to both a decrease in muscle protein synthesis and increased proteolysis with proteolysis playing a dominant role (Whidden et al., 1985b; Shanely et al., 2002, 2004; Agten et al., 2011; Powers et al., 2013; Smuder et al., 2014, 2018; Hudson et al., 2015). The MV-induced increase in proteolysis within diaphragm fibers is triggered by increases in mitochondrial production of reactive oxygen species (ROS); this redox imbalance contributes to the activation of the four major proteolytic systems in skeletal muscle (i.e., ubiquitin-proteasome, autophagy, calpain, and caspase-3) (Powers et al., 2011). Although all of these proteolytic systems contribute to MV-induced diaphragmatic atrophy, activation of the calcium (Ca^{2+})-activated protease, calpain, plays a central role in MV-induced diaphragmatic atrophy. Indeed, blockade of calpain activation in the diaphragm can markedly reduce both MV-induced diaphragmatic atrophy and contractile dysfunction (Maes et al., 2007; Nelson et al., 2012).

This review provides a summary of the cell signaling events leading to VIDD with a focus on the cellular processes that result in disturbed Ca^{2+} homeostasis and the subsequent activation of calpain within diaphragm muscle fibers. More specifically, we discuss the evidence that increased mitochondrial production of ROS results in modification of the ryanodine receptor/Ca^{2+} release channel in the sarcoplasmic reticulum (SR), resulting in the release of Ca^{2+} from the SR, calpain activation, and VIDD. In an effort to stimulate future research, we also highlight unanswered questions associated with signaling events.

THE PROBLEM: VENTILATOR-INDUCED DIAPHRAGMATIC WEAKNESS

The observation that prolonged MV results in diaphragmatic wasting was first reported in a retrospective study revealing that diaphragmatic atrophy was present in infants and neonates exposed to prolonged MV (Knisely et al., 1988). Direct evidence to support this conjecture was later provided by a preclinical study revealing that 48 h of MV results in marked diaphragmatic atrophy and contractile dysfunction (Le Bourdelles et al., 1996). Since these initial reports, numerous studies have confirmed that as few as 12–24 h of MV results in VIDD in both animals and humans [reviewed in Powers et al. (2013)].

Two primary modes of MV exist: (1) partial support and (2) full support MV. During partial support MV, the ventilator assists during inspiration, but the patients' inspiratory muscles remain engaged in breathing. During full support MV, the ventilator performs all of the work of breathing, resulting in inactivity of the diaphragm and other inspiratory muscles; compared to partial support, full support MV results in a more rapid rate of VIDD. Indeed, when contrasted with inactivity-induced limb muscle atrophy (e.g., prolonged bedrest), full support MV-induced diaphragmatic atrophy is a unique form of skeletal muscle atrophy that occurs extremely rapidly after the onset of MV. For instance, the cross-sectional area (CSA) of diaphragm muscle fibers is reduced by >15% within the first 12–18 h of MV in both rats and humans (Whidden et al., 1985a; Shanely et al., 2002; Levine et al., 2008; Nelson et al., 2012). In comparison with inactivity-induced atrophy in limb muscles, 5–7 days of inactivity would be required to achieve this magnitude of fiber atrophy in locomotor skeletal muscles (Powers et al., 2013). In this regard, the diaphragm muscle differs from limb muscle in several aspects. First, the diaphragm is chronically active, contracting several times per minute even during sleep (Lessa et al., 2016; Fogarty et al., 2018). Moreover, the diaphragm also contributes to several non-respiratory activities including swallowing and vocalization (Fogarty et al., 2018). Further, limb skeletal muscles exert force along the longitudinal axis of the fiber because diaphragm fibers are exposed to a pressure load both longitudinally and perpendicularly to the axis of the muscle (Lessa et al., 2016).

As mentioned previously, the diaphragmatic weakness associated with VIDD is a primary risk factor for the failure to wean patients from the ventilator. In this context, weaning is defined as the ability to remove patients from ventilator support and restore spontaneous breathing. The incidence of difficult weaning of patients from MV is variable but can reach >30% or higher in those ventilated for more than 3 days (Funk et al., 2010). The inability to wean patients from MV is a serious clinical problem that results in prolonged stays in the intensive care unit and significant increases in both morbidity and mortality (Funk et al., 2010). Developing a therapy to prevent VIDD and reduce the risk of weaning problems requires a thorough understanding of the signaling events that promote VIDD. The next segments provide a summary of our current knowledge of the cellular processes that promote MV-induced diaphragmatic weakness.

MV-INDUCED DIAPHRAGMATIC ATROPHY: PROTEOLYSIS VS DEPRESSED PROTEIN SYNTHESIS

The size of skeletal muscle fibers is controlled by the relative balance between rates of protein synthesis and protein breakdown. It is well established that prolonged MV results in a rapid increase in proteolysis and a decline in protein synthesis in the rodent diaphragm (Shanely et al., 2004). In regard to the rates of diaphragmatic protein synthesis, both mixed and myofibrillar protein synthesis rates decline within the first 6 h of MV (Shanely et al., 2004). While this MV-induced depression in protein synthesis rates clearly contributes

to diaphragmatic atrophy during prolonged MV (i.e., days to weeks), the rapid atrophy that occurs in the human or rat diaphragm (i.e., >15% reduction in diaphragm CSA) within the first 12–24 h of MV is largely driven by a swift increase in proteolysis (Powers et al., 2013). In reference to the proteolytic systems that contribute to MV-induced diaphragm atrophy, abundant evidence indicates that all four of the major proteolytic systems in skeletal muscle (i.e., calpains, caspase-3, ubiquitin-proteasome system, and autophagy) are active during prolonged MV (DeRuisseau et al., 1985; Kwon et al., 1985; Maes et al., 2007; McClung et al., 2007, 2008; Agten et al., 2011; Nelson et al., 2012; Smuder et al., 2018). Although each of these proteolytic systems contributes to MV-induced diaphragmatic wasting, evidence reveals that the calcium-activated protease calpain plays a key role. Because increases in cytosolic free Ca^{2+} are required to activate calpains, the next segment provides a brief overview of the regulation of cellular Ca^{2+} levels.

REGULATION OF Ca^{2+} HOMEOSTASIS IN SKLELETAL MUSCLE

Calcium ions play important roles in several signaling events in skeletal muscle fibers including excitation-contraction (E-C) coupling and a variety of cell signaling pathways. Importantly, high levels of free Ca^{2+} in the cytosol can be toxic to cells by promoting increased mitochondrial ROS production, protease activation, and myonuclear apoptosis (Bogeski et al., 2011; Vallejo-Illarramendi et al., 2014; Rossi et al., 2019). Therefore, it is not surprising that skeletal muscle fibers contain an intricate regulatory system that tightly manages the levels of free Ca^{2+} in the fiber. Indeed, Ca^{2+} concentration is controlled in muscle fibers via a network of voltage sensors, Ca^{2+} transporters, Ca^{2+} channels, Na^{+}/Ca^{2+} exchangers, Ca^{2+}-binding proteins, and ion pumps/exchangers. A detailed discussion of the regulation of Ca^{2+} homeostasis is beyond the scope of this review, and the reader is directed to comprehensive reviews on this topic for more details (Berridge et al., 2003; Bogeski et al., 2011; Vallejo-Illarramendi et al., 2014; Belosludtsev et al., 2019; Rossi et al., 2019). Nevertheless, prior to a discussion of the mechanisms responsible for MV-induced disturbances in Ca^{2+} homeostasis in diaphragm fibers, a brief introduction to some of the key checkpoints in cellular Ca^{2+} homeostasis is provided in the next segments.

Sarcolemma Regulation of Ca^{2+} Influx/Efflux

By design, the sarcolemma has a low permeability for Ca^{2+} as evidenced by the large difference (∼10,000-fold) between the extracellular and cytosolic Ca^{2+} concentration (Vallejo-Illarramendi et al., 2014). Because of this significant concentration gradient, Ca^{2+} movement from the extracellular fluid into the cytosol of muscle fibers is driven by the large electrochemical gradient across the sarcolemma. The major influx pathways for Ca^{2+} entry into the cytosol include voltage-gated channels, receptor operated channels (ROC), and store operated entry channels (SOC) (Vallejo-Illarramendi et al., 2014; **Figure 1**).

Because high cytosolic Ca^{2+} levels are toxic to muscle fibers, the sarcolemma is equipped with ATPases – e.g., plasma membrane Ca^{2+} ATPases (PMCA) – to pump Ca^{2+} from the cytosol across the sarcolemma (DeSantiago et al., 2007). Further, the Na^{+}/Ca^{2+} exchanger (NCX) also contributes to Ca^{2+} exchange across the sarcolemma (Burr et al., 2014). Compared to the PMCA, the NCX has a greater Ca^{2+} transport rate and therefore, can protect against Ca^{2+} overload in the cytosol over a wider range of Ca^{2+} transients (Brini and Carafoli, 2011). In healthy muscle fibers, the combined properties of these Ca^{2+} transport proteins are effective in maintaining cytosolic Ca^{2+} homeostasis.

Cytosolic Ca^{2+} Buffers

Cytosolic Ca^{2+} buffers are Ca^{2+} binding proteins that provide another means of regulating cytosolic levels of free Ca^{2+}. Indeed, the rapid binding of Ca^{2+} to cytosolic buffers make Ca^{2+} binding molecules an ideal strategy to regulate free Ca^{2+} levels in the cytosol (Schwaller, 2010). Important Ca^{2+} binding proteins in skeletal muscle fibers include troponin C, parvalbumin, and calmodulin (Kretsinger, 1976). Collectively, these Ca^{2+} binding proteins compose a network of molecules that modulate signaling (Yanez et al., 2012).

Ca^{2+}-Handling Within the Sarcoplasmic Reticulum

The SR, a highly specialized type of endoplasmic reticulum, is the primary reservoir for Ca^{2+} storage in muscle fibers (Pietrobon et al., 1990; Vallejo-Illarramendi et al., 2014). The SR is an organized tubular network that surrounds myofibrils with a dilated end sac labeled as the terminal cisternae (**Figure 1**). An extension of the sarcolemma forms the central T-tubule responsible for penetrating into the muscle cell and facilitating Ca^{2+} release. This structure is flanked on each side by terminal cisternae that form a region within the fiber called the triad; the triad serves as the anatomical structure responsible for triggering excitation-contraction coupling in skeletal muscle fibers.

The SR plays an essential role in the management of intracellular Ca^{2+} within skeletal muscle fibers. In particular, three major categories of Ca^{2+} handling proteins exist within the SR: (1) SR Ca^{2+} release channels; (2) SR Ca^{2+} binding proteins; and (3) Ca^{2+} ATPase pumps. A brief summary of these classes of SR handling proteins follows.

The primary Ca^{2+} release channel in the SR is the ryanodine receptor (RyR). Three isoforms of the RyR (i.e., RyR1, RyR2, and RyR3) exist in mammals, but RyR1 is the dominant isoform expressed in adult skeletal muscle and is crucial for muscular contraction (Capes et al., 2011; Vallejo-Illarramendi et al., 2014). RyR1 is the largest ion channel known (∼2.3 MDa) and is composed of four identical subunits; this organization forms a pore within the SR membrane that serves as the Ca^{2+} release channel (Hernandez-Ochoa et al., 2015). Importantly, the subunit structure of RyR1 is associated with

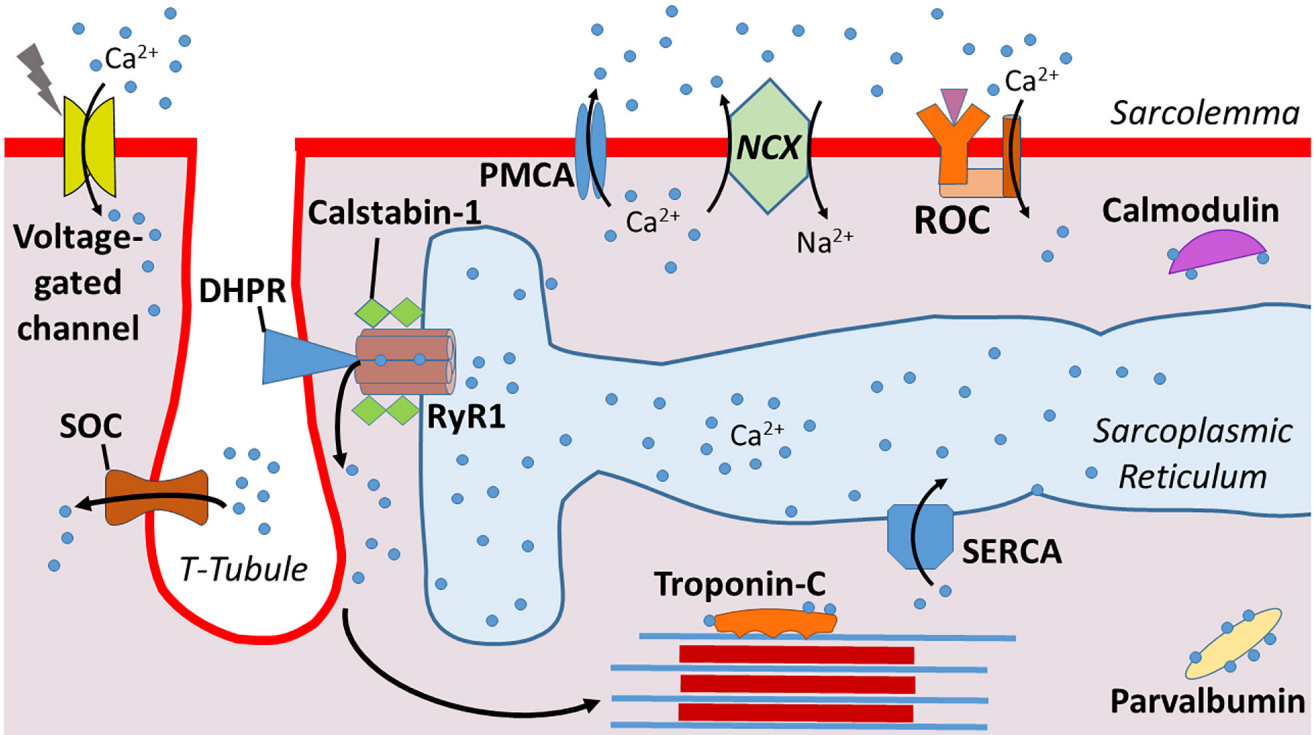

FIGURE 1 | Illustration of calcium (Ca^{2+}) regulation at the sarcolemma. Dihydropyridine receptors (DHPR) mediate Ca^{2+} release from the sarcoplasmic reticulum into the cytosol. Calstabin-1 is bound to RyR1 and stabilizes this complex to aid in maintaining a closed channel. Ca^{2+} is pumped back into the sarcoplasmic reticulum via sarcoplasmic reticulum Ca^{2+}-ATPase (SERCA). Ca^{2+} enters from the extracellular space via voltage-gated channels, store-operated channels (SOC), and receptor operated channels (ROC). Ca^{2+} is excreted from the cytosol via plasma membrane Ca^{2+} ATPases (PMCA) and Na^{+}/Ca^{2+} exchanger (NCX). Levels of cytosolic free Ca^{2+} are also regulated by Ca^{2+} binding proteins such as Troponin-C, parvalbumin, and calmodulin.

several accessory proteins including four calstabin-1 subunits (also known as FK506 binding protein 1A) (Wehrens et al., 2005). Calstabin is a key molecule regulating RyR1 function because, in a resting (non-contracting muscle), the binding of calstabin to RyR1 maintains the channel in a closed state to prevent leakage of Ca^{2+} from the SR into the cytoplasm (Brillantes et al., 1994).

Upon depolarization of the sarcolemma, the opening of the RyR1 is regulated by dihydropyridine receptors (DHPRs) (Capes et al., 2011; Vallejo-Illarramendi et al., 2014). DHPRs are mechanically linked to RyR1, and the voltage change induced by depolarization of the sarcolemma results in a conformational change in DHPR that opens the RyR1 (Protasi et al., 2002). This activation and opening of the RyR1 releases Ca^{2+} from the SR into the cytosol of muscle fibers, triggering E-C coupling and increased muscle force production. Notably, the magnitude of Ca^{2+} release from the SR into the cytosol is a primary determinant of the amount of force generated during muscular contraction (Wehrens et al., 2005).

In addition to the modulatory effects of DHPRs and calstabin-1, Ca^{2+} release through the RyR1 is also regulated by several post-translational events along with numerous proteins and small molecules. Cytosolic regulators of RyR1 include ATP, calmodulin II, and protein kinase A (PKA) (Vallejo-Illarramendi et al., 2014). RyR1 activity can also be regulated by oxidative stress, as oxidative modification of cysteine thiol residues such as S-nitrosylation, S-glutathionylation, and disulfide oxidation have been shown to modulate RyR1 function. In particular, oxidation, coupled with PKA-induced phosphorylation of RyR1, decreases the binding association between calstabin-1 and the RyR1 complex; this results in a leak of Ca^{2+} from the SR into the cytosol (Reiken et al., 2003; Ward et al., 2003).

Mitochondrial Ca^{2+} Handling

Along with their key role in muscle bioenergetics, mitochondria can also take up and store Ca^{2+} transiently (Rossi et al., 2019). Two subpopulations of mitochondria exist in skeletal muscle: (1) subsarcolemmal and (2) intermyofibrillar. As the names imply, subsarcolemmal mitochondria are located directly beneath the sarcolemma whereas intermyofibrillar mitochondria are found surrounding the myofibrillar contractile proteins. The adjacent locations of the subsarcolemmal mitochondria and the SR allow for significant interaction between these organelles; indeed, areas of adjacent SR and mitochondria form microdomains of contact that are described as mitochondria associated membranes (MAMs). MAMs describe the areas where SR proteins directly associate with components of the outer mitochondrial membrane (Csordas et al., 2006). This linkage facilitates efficient Ca^{2+} transfer between these two

organelles and therefore, mitochondria actively contribute to Ca^{2+} homeostasis in skeletal muscles.

The cytosolic Ca^{2+} fluxes that occur during muscular contraction result in a transient uptake of Ca^{2+} into the mitochondria (Rossi et al., 2019). This Ca^{2+} uptake at the outer mitochondrial membrane is facilitated by the voltage-dependent anion channel (VDAC), which allows for the exchange of molecules and ions between the cytosol and mitochondria. However, the mitochondrial inner membrane is impermeable to ions, and therefore, highly specialized channels are required for Ca^{2+} ions to enter the mitochondrial matrix (Vallejo-Illarramendi et al., 2014; Rossi et al., 2019). Ca^{2+} transport into the mitochondrial matrix is primarily facilitated by the mitochondrial uniporter (MCU) (Vallejo-Illarramendi et al., 2014; Belosludtsev et al., 2019; Rossi et al., 2019; **Figure 2**). This ruthenium-red-sensitive uniporter utilizes the negative membrane potential across the inner mitochondrial membrane to facilitate Ca^{2+} entry into the mitochondrial matrix. In particular, MAMs form junctures that facilitate microdomains of high Ca^{2+} levels due to their positioning near the SR, and these high Ca^{2+} levels induce the opening of the MCU pore, permitting Ca^{2+} entry into the matrix (Vallejo-Illarramendi et al., 2014; Rossi et al., 2019).

The discovery that mitochondria are capable of Ca^{2+} uptake led to studies revealing that Ca^{2+} is an important regulator of oxidative phosphorylation. For example, Ca^{2+} is a positive allosteric activator for several key enzymes that influence flux through the citric acid cycle (e.g., pyruvate dehydrogenase, isocitrate dehydrogenase, and 2-oxoglutarate dehydrogenase) (Denton et al., 1980; McCormack and Denton, 1980). Moreover, recent evidence shows that Ca^{2+} activates the entire oxidative phosphorylation cascade in skeletal muscle mitochondria (Glancy et al., 2013). In contrast to these metabolically beneficial effects of moderate Ca^{2+} uptake in mitochondria, excessive Ca^{2+} uptake resulting in a Ca^{2+} overload elevates mitochondrial ROS production and increases mitochondrial sensitivity to apoptotic stimuli (Pinton et al., 2008).

The primary means for extrusion of Ca^{2+} from the mitochondria in skeletal muscle is the Na^{+}/Ca^{2+} exchanger and the H^{+}/Ca^{2+} exchanger located within the inner mitochondrial membrane (Pizzo et al., 2012). Further, during Ca^{2+} overload in the mitochondria, a large conductance channel known as the mitochondrial permeability transition pore (mPTP) can be formed and operates as a conduit for release (Vallejo-Illarramendi et al., 2014). Nonetheless, at present, details about the role that the mPTP plays in regulating mitochondrial Ca^{2+} levels remains poorly understood (Giorgio et al., 2018).

DISTURBANCES IN DIAPHRAGMATIC Ca^{2+} HOMEOSTASIS IS REQUIRED FOR VIDD

Shanely et al. (2002) provided the earliest evidence that prolonged MV results in disturbances of Ca^{2+} homeostasis in rat diaphragm fibers. Although this study did not directly measure cytosolic

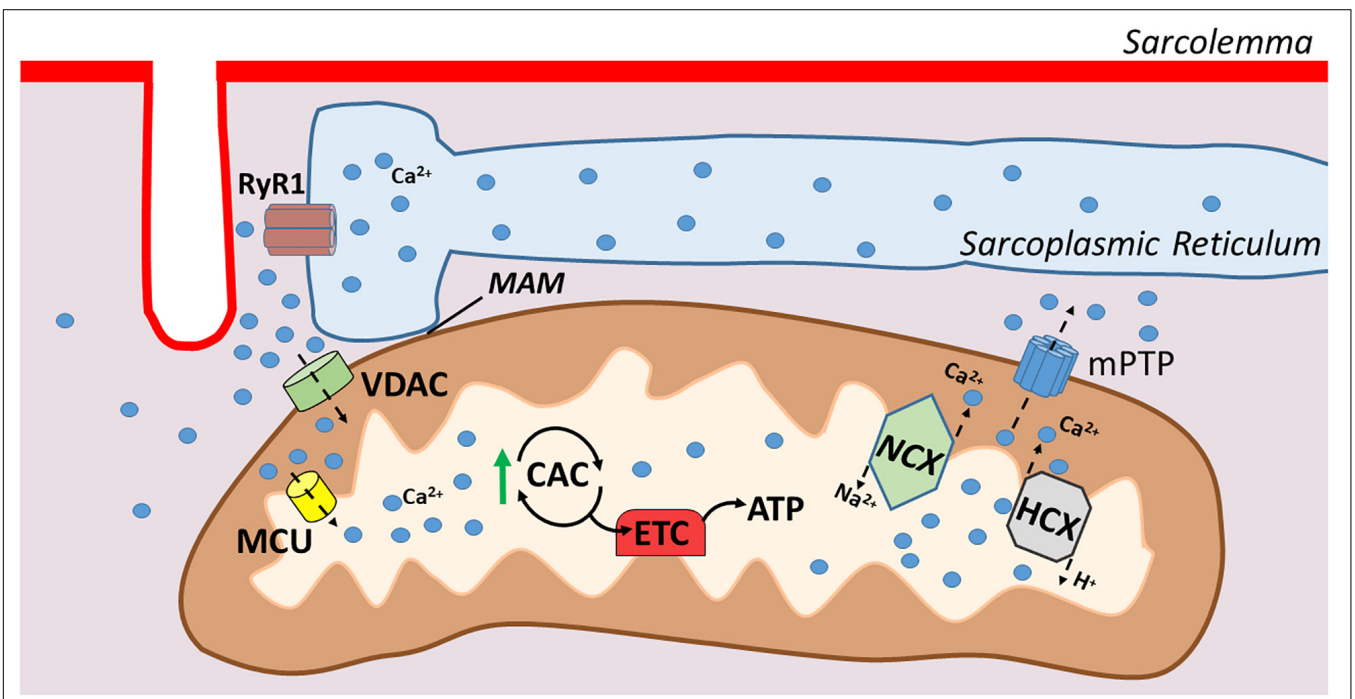

FIGURE 2 | Illustration of mitochondrial calcium transport. Mitochondrial associated membranes (MAMs) result in microdomains of high Ca^{2+} levels that facilitate Ca^{2+} entry through the outer mitochondrial membrane via voltage dependent anion channel (VDAC). Ca^{2+} crosses the inner mitochondrial membrane via the mitochondrial uniporter (MCU), which then stimulates respiration via increases in citric acid cycle enzymes. Ca^{2+} is extruded from the mitochondria via Na^{+}/Ca^{2+} exchanger (NCX) and H^{+}/Ca^{2+} exchanger (HCX) in the inner membrane and the outer membrane via the mitochondrial permeability transition pore (mPTP).

Ca^{2+} levels, the results revealed that prolonged MV activates calpain in diaphragm fibers and increased cytosolic levels of free Ca^{2+} is a requirement for calpain activation (Goll et al., 2003). MV-induced activation of calpains in diaphragm fibers has since been confirmed in many studies involving both humans and animals (Whidden et al., 1985b; Maes et al., 2007; Levine et al., 2008; McClung et al., 2008; Nelson et al., 2012; Dridi et al., 2020a). Moreover, two independent studies using calpain inhibitors have demonstrated that calpain is a major contributor to VIDD (Maes et al., 2007; Nelson et al., 2012). A brief overview of calpains and their activation in skeletal muscle follows.

Calpains are a family of Ca^{2+} activated proteases that cleave target substrates at specific sites (Goll et al., 2003). Three primary calpain isoforms exist in skeletal muscle (i.e., calpain1, calpain2, and calpain3); although evidence reveals that calpains 1 and 2 play an important role in promoting disuse muscle atrophy, it remains unknown as to whether calpain1 or calpain2 plays the dominant role in promoting fiber atrophy (Hyatt and Powers, 2020).

While activation of calpain involves several post-translational modifiers, it is established that calpain activation in muscle fibers requires increased cytosolic levels of free Ca^{2+}. Though the intracellular concentrations of free Ca^{2+} required to activate calpains in skeletal muscle *in vivo* remain unknown, it is clear that the proteolytic removal of the N-terminal domain of the calpain molecule allows for both calpain1 and calpain2 to be activated at significantly lower Ca^{2+} concentrations (Goll et al., 2003). For a detailed discussion of the factors regulating the activity of calpains see the classic review of Goll et al. (2003) and the recent review by Hyatt and Powers (2020).

To determine the source of increased free Ca^{2+} in the diaphragm during prolonged MV, Talbert et al. (2016) tested the hypothesis that leakage of Ca^{2+} from the RyR1 is required for MV-induced calpain activation in the diaphragm. Cause and effect were determined by treating ventilated animals with the RyR1 blocker, azumolene. Their results revealed that while azumolene did block stimulation-induced Ca^{2+} release from the RyR1, treatment with this RyR1 channel blocker was not sufficient to prevent MV-induced calpain activation or VIDD (Talbert et al., 2016). However, azumolene may not prevent all forms of Ca^{2+} release from RyR1s. For example, while it is established that azumolene prevents neural stimulation-induced Ca^{2+} release from the RyR1, it remains unknown if this compound blocks oxidation-induced release of Ca^{2+} from the RyR1. Hence, experiments using a different investigative approach are required to delineate the role that leaky RyR1s play in MV-induced disturbances in Ca^{2+} homeostasis in diaphragm fibers.

Matecki et al. (2016) performed the first study to directly evaluate the impact of prolonged MV on Ca^{2+} homeostasis in the diaphragm. This elegant study provided robust evidence that prolonged MV increases the opening of RyR1 in diaphragm muscle fibers (Matecki et al., 2016); this increased spontaneous opening of RyR1 results in increased Ca^{2+} release (i.e., Ca^{2+} sparks) and disrupts Ca^{2+} homeostasis (Matecki et al., 2016). Analysis of both human and mouse diaphragm fibers has established that prolonged MV results in oxidation, S-nitrosylation, and Ser-2844 phosphorylation of the RyR1. Importantly, these post-translational modifications of the RyR1 accompany the dissociation of calstabin1 (Matecki et al., 2016). The importance of calstabin-1 association with RyR1 for preventing RyR1 leak was confirmed by findings that treatment of animals with S107, a small molecule that stabilizes the RyR1-calstabin1 interaction, prevents MV-induced Ca^{2+} sparks in diaphragm fibers, and protects against VIDD (Matecki et al., 2016). Furthermore, animals treated with the antioxidant trolox do not experience MV-induced oxidation of RyR1 and RyR1-mediated Ca^{2+} leak in diaphragm fibers. Therefore, this landmark study demonstrates that RyR1 dysfunction is an early pathological event leading to VIDD in both mice and humans, and confirms that oxidative stress is a prerequisite for MV-induced RyR1 dysfunction (Matecki et al., 2016).

While the MV-induced increases in ROS production in the diaphragm is derived from several sources, mitochondrial ROS production is the dominant site of ROS emission in diaphragm fibers during prolonged MV (Falk et al., 1985, 2011; Whidden et al., 1985a; McClung et al., 2009; Powers et al., 2011). Recently, this supposition has gained additional support from a study concluding that MV-induced mitochondrial ROS production in the diaphragm is responsible for the oxidative remodeling of the RyR1 (Dridi et al., 2020b). Specifically, using the mitochondrial-targeted antioxidant SS-31 to prevent MV-induced increases in mitochondrial ROS production, Dridi et al. (2020a) provide further evidence that mitochondrial oxidative stress is responsible for oxidation of RyR1s resulting in SR Ca^{2+} leak, calpain activation, and VIDD (**Figure 3**). Moreover, prolonged MV is also associated with increased PKA activity, which is posited to play a role in the hyperphosphorylation of the RyR1 within diaphragm fibers (Dridi et al., 2020b). This MV-induced increase in PKA activity and hyperphosphorylation of RyR1 was abolished by treatment of animals with the mitochondrial-targeted antioxidant (SS-31). These findings are consistent with reports that oxidative stress increases PKA activity and decreases the activity of several phosphatases (Brennan et al., 2006; Steinberg, 2013). Collectively, these studies demonstrate that mitochondrial ROS emissions are key in the disruptions of Ca^{2+} homeostasis.

Investigations into the signaling pathways responsible for the MV-induced increases in mitochondrial ROS emission in the diaphragm have provided increased insight into the pathologic events underlying VIDD. Specifically, a growing number of studies suggest that MV-induced mitochondrial dysfunction is controlled by several interacting events including mechanical stimulation of angiotensin II type 1 receptors, along with activation of several signaling molecules including FoxO, STAT3, and Smad3 (Kwon et al., 1985; Smith et al., 2014; Smuder et al., 2015; Tang et al., 2015, 2017). Further, emerging evidence also suggests that accelerated autophagy and increased cytosolic levels of free Ca^{2+} are potential modulators of mitochondrial ROS production, acting as a positive feedback loop (Smuder et al., 2018; Tang and Shrager, 2018). Despite these recent advances

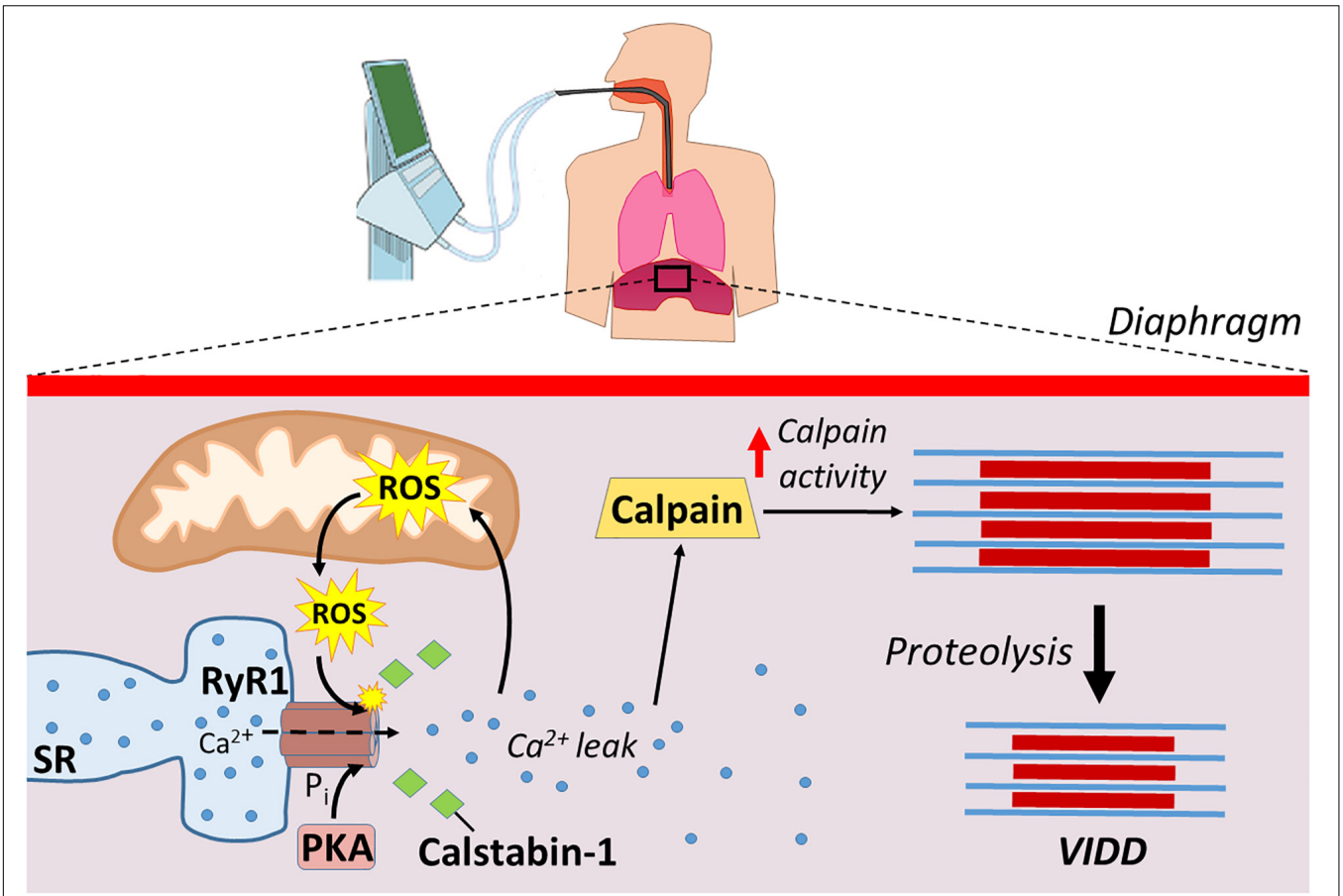

FIGURE 3 | Mechanical ventilation causes Ca^{2+} disruptions that lead to increased proteolysis. ROS production from mitochondria, along with increased protein kinase A (PKA) activity, modify ryanodine receptors (RyR1) leading to the disassociation of calstabin-1. Disassociation of calstabin-1 from RyR1 leads to Ca^{2+} leak, activation of calpains, and increased proteolysis that contributes to VIDD.

in our knowledge of the signaling network responsible for MV-induced increases in mitochondrial ROS production, numerous questions remain unanswered about the pathways responsible for MV-induced mitochondrial dysfunction.

DISCUSSION

Mechanical ventilation is a life-saving clinical intervention used to provide adequate alveolar ventilation in patients that are incapable of doing so on their own. Common applications of MV include patients suffering from chronic obstructive pulmonary disease, heart failure, acute myocardial infarction, and other critical illnesses. While MV is a life-saving intervention for many patients, prolonged MV promotes the rapid development of VIDD. VIDD is clinically significant because diaphragmatic weakness is a key risk factor contributing to problems in weaning patients from the ventilator. The inability to wean patients from the ventilator results in prolonged hospitalization and increased morbidity and mortality.

Mechanical ventilation-induced diaphragmatic atrophy results from both decreased protein synthesis and accelerated proteolysis. However, MV-induced activation of proteases in the diaphragm play a dominant role in the development of VIDD. Although all major proteolytic systems contribute to this MV-induced increase in proteolysis, evidence suggests that activation of the Ca^{2+}-activated protease, calpain, plays a required role in this process. The steps leading to MV-induced calpain activation begin with an increase in mitochondrial ROS emission resulting in redox disturbances in diaphragm fibers. This MV-induced oxidative stress in diaphragm fibers results in post-translation modifications of the RyR1 (e.g., phosphorylation and oxidation) leading to the disassociation of calstabin1 from RyR1 and Ca^{2+} leak from the SR. This disturbance in Ca^{2+} homeostasis provides a required stimulus for calpain activation in the diaphragm leading to accelerated proteolysis and VIDD (**Figure 3**).

Although significant progress has been made toward understanding the mechanisms responsible for the MV-induced disturbance in Ca^{2+} homeostasis in the diaphragm, several important unanswered questions remain. For example, although it is established that an increase in mitochondrial ROS production is a requirement for MV-induced RyR1 leak leading to increased cytosolic levels of free Ca^{2+}, the precise

mechanisms responsible for this increased oxidant production remain undefined.

Evidence also exists that accelerated autophagy also promotes an increase in mitochondrial ROS emission in the diaphragm during prolonged MV (Smuder et al., 2018). However, the signaling pathways that connect these two events remain unclear.

Finally, it is generally agreed that an uptake of cytosolic Ca^{2+} into mitochondria can produce a mitochondrial Ca^{2+} overload, resulting in significant increases in mitochondria ROS production (Brookes et al., 2004; Peng and Jou, 2010). Nonetheless, it is currently unknown as to whether the MV-induced increases in cytosolic levels of free Ca^{2+} in the diaphragm are sufficient to produce mitochondrial Ca^{2+} overload and stimulate additional mitochondrial ROS production. This is an important issue that warrants future study.

AUTHOR CONTRIBUTIONS

HH and SP formulated the outline of the review and contributed to writing and editing of the manuscript. Both authors approved the final submitted version.

FUNDING

This research was supported by the National Institutes of Health R21 AR073956.

REFERENCES

Agten, A., Maes, K., Smuder, A., Powers, S. K., Decramer, M., and Gayan-Ramirez, G. (2011). N-Acetylcysteine protects the rat diaphragm from the decreased contractility associated with controlled mechanical ventilation. *Crit. Care Med.* 39, 777–782. doi: 10.1097/ccm.0b013e318206cca9

Belosludtsev, K. N., Dubinin, M. V., Belosludtseva, N. V., and Mironova, G. D. (2019). Mitochondrial Ca2+ transport: mechanisms, molecular structures, and role in cells. *Biochemistry* 84, 593–607. doi: 10.1134/s0006297919060026

Berridge, M. J., Bootman, M. D., and Roderick, H. L. (2003). Calcium signalling: dynamics, homeostasis and remodelling. *Nat. Rev. Mol. Cell. Biol.* 4, 517–529. doi: 10.1038/nrm1155

Bogeski, I., Kappl, R., Kummerow, C., Gulaboski, R., Hoth, M., and Niemeyer, B. A. (2011). Redox regulation of calcium ion channels: chemical and physiological aspects. *Cell Calcium* 50, 407–423. doi: 10.1016/j.ceca.2011.07.006

Brennan, J. P., Bardswell, S. C., Burgoyne, J. R., Fuller, W., Schroder, E., Wait, R., et al. (2006). Oxidant-induced activation of type I protein kinase A is mediated by RI subunit interprotein disulfide bond formation. *J. Biol. Chem.* 281, 21827–21836. doi: 10.1074/jbc.m603952200

Brillantes, A. B., Ondrias, K., Scott, A., Kobrinsky, E., Ondriasova, E., Moschella, M. C., et al. (1994). Stabilization of calcium release channel (ryanodine receptor) function by FK506-binding protein. *Cell* 77, 513–523. doi: 10.1016/0092-8674(94)90214-3

Brini, M., and Carafoli, E. (2011). The plasma membrane Ca(2)+ ATPase and the plasma membrane sodium calcium exchanger cooperate in the regulation of cell calcium. *Cold Spring Harb. Perspect. Biol.* 3:a004168. doi: 10.1101/cshperspect.a004168

Brookes, P. S., Yoon, Y., Robotham, J. L., Anders, M. W., and Sheu, S. S. (2004). Calcium, ATP, and ROS: a mitochondrial love-hate triangle. *Am. J. Physiol. Cell Physiol.* 287, C817–C833.

Burr, A. R., Millay, D. P., Goonasekera, S. A., Park, K. H., Sargent, M. A., Collins, J., et al. (2014). Na+ dysregulation coupled with Ca2+ entry through NCX1 promotes muscular dystrophy in mice. *Mol. Cell Biol.* 34, 1991–2002. doi: 10.1128/mcb.00339-14

Capes, E. M., Loaiza, R., and Valdivia, H. H. (2011). Ryanodine receptors. *Skelet. Muscle* 1:18.

Csordas, G., Renken, C., Varnai, P., Walter, L., Weaver, D., Buttle, K. F., et al. (2006). Structural and functional features and significance of the physical linkage between ER and mitochondria. *J. Cell. Biol.* 174, 915–921. doi: 10.1083/jcb.200604016

Denton, R. M., McCormack, J. G., and Edgell, N. J. (1980). Role of calcium ions in the regulation of intramitochondrial metabolism. Effects of Na+, Mg2+ and ruthenium red on the Ca2+-stimulated oxidation of oxoglutarate and on pyruvate dehydrogenase activity in intact rat heart mitochondria. *Biochem. J.* 190, 107–117. doi: 10.1042/bj1900107

DeRuisseau, K. C., Kavazis, A. N., Deering, M. A., Falk, D. J., Van Gammeren, D., Yimlamai, T., et al. (1985). Mechanical ventilation induces alterations of the ubiquitin-proteasome pathway in the diaphragm. *J. Appl. Physiol.* 98, 1314–1321. doi: 10.1152/japplphysiol.00993.2004

DeSantiago, J., Batlle, D., Khilnani, M., Dedhia, S., Kulczyk, J., Duque, R., et al. (2007). Ca2+ /H+ exchange via the plasma membrane Ca2+ ATPase in skeletal muscle. *Front. Biosci.* 12, 4641–4660. doi: 10.2741/2414

Dridi, H., Liu, X., Yuan, Q., Reiken, S., Mohamad, Y., Sittenfeld, L. R., et al. (2020a). Role of defective calcium regulation in cardiorespiratory dysfunction in Huntington's disease. *JCI Insight* 5:e140614.

Dridi, H., Yehya, M., Barsotti, R., Reiken, S., Angebault, C., Jung, B., et al. (2020b). Mitochondrial oxidative stress induces leaky ryanodine receptor during mechanical ventilation. *Free Radic. Biol. Med.* 146, 383–391. doi: 10.1016/j.freeradbiomed.2019.11.019

Falk, D. J., Deruisseau, K. C., Van Gammeren, D. L., Deering, M. A., Kavazis, A. N., and Powers, S. K. (1985). Mechanical ventilation promotes redox status alterations in the diaphragm. *J. Appl. Physiol.* 101, 1017–1024. doi: 10.1152/japplphysiol.00104.2006

Falk, D. J., Kavazis, A. N., Whidden, M. A., Smuder, A. J., McClung, J. M., Hudson, M. B., et al. (2011). Mechanical ventilation-induced oxidative stress in the diaphragm: role of heme oxygenase-1. *Chest* 139, 816–824. doi: 10.1378/chest.09-2787

Fogarty, M. J., Mantilla, C. B., and Sieck, G. C. (2018). Breathing: motor control of diaphragm muscle. *Physiology* 33, 113–126. doi: 10.1152/physiol.00002.2018

Funk, G. C., Anders, S., Breyer, M. K., Burghuber, O. C., Edelmann, G., Heindl, W., et al. (2010). Incidence and outcome of weaning from mechanical ventilation according to new categories. *Eur. Respir. J.* 35, 88–94. doi: 10.1183/09031936.00056909

Giorgio, V., Guo, L., Bassot, C., Petronilli, V., and Bernardi, P. (2018). Calcium and regulation of the mitochondrial permeability transition. *Cell Calcium* 70, 56–63. doi: 10.1016/j.ceca.2017.05.004

Glancy, B., Willis, W. T., Chess, D. J., and Balaban, R. S. (2013). Effect of calcium on the oxidative phosphorylation cascade in skeletal muscle mitochondria. *Biochemistry* 52, 2793–2809. doi: 10.1021/bi3015983

Goll, D. E., Thompson, V. F., Li, H., Wei, W., and Cong, J. (2003). The calpain system. *Physiol. Rev.* 83, 731–801.

Hernandez-Ochoa, E. O., Pratt, S. J. P., Lovering, R. M., and Schneider, M. F. (2015). Critical role of intracellular RyR1 calcium release channels in skeletal muscle function and disease. *Front. Physiol.* 6:420. doi: 10.3389/fphys.2015.00420

Hudson, M. B., Smuder, A. J., Nelson, W. B., Wiggs, M. P., Shimkus, K. L., Fluckey, J. D., et al. (2015). Partial support ventilation and mitochondrial-targeted antioxidants protect against ventilator-induced decreases in diaphragm muscle protein synthesis. *PLoS One* 10:e0137693. doi: 10.1371/journal.pone.0137693

Hyatt, H. W., and Powers, S. K. (2020). The role of calpains in skeletal muscle remodeling with exercise and inactivity-induced atrophy. *Int. J. Sports Med.* [Epub ahead of print].

Knisely, A. S., Leal, S. M., and Singer, D. B. (1988). Abnormalities of diaphragmatic muscle in neonates with ventilated lungs. *J. Pediatr.* 113, 1074–1077. doi: 10.1016/s0022-3476(88)80585-7

Kretsinger, R. H. (1976). Calcium-binding proteins. *Annu. Rev. Biochem.* 45, 239–266.

Kwon, O. S., Smuder, A. J., Wiggs, M. P., Hall, S. E., Sollanek, K. J., Morton, A. B., et al. (1985). AT1 receptor blocker losartan protects against mechanical ventilation-induced diaphragmatic dysfunction. *J. Appl. Physiol.* 119, 1033–1041. doi: 10.1152/japplphysiol.00237.2015

Le Bourdelles, G., Mier, L., Fiquet, B., Djedaini, K., Saumon, G., Coste, F., et al. (1996). Comparison of the effects of heat and moisture exchangers and heated humidifiers on ventilation and gas exchange during weaning trials from mechanical ventilation. *Chest* 110, 1294–1298. doi: 10.1378/chest.110.5.1294

Lessa, T. B., de Abreu, D. K., Bertassoli, B. M., and Ambrosio, C. E. (2016). Diaphragm: a vital respiratory muscle in mammals. *Ann. Anat.* 205, 122–127. doi: 10.1016/j.aanat.2016.03.008

Levine, S., Nguyen, T., Taylor, N., Friscia, M. E., Budak, M. T., Rothenberg, P., et al. (2008). Rapid disuse atrophy of diaphragm fibers in mechanically ventilated humans. *N. Engl. J. Med.* 358, 1327–1335. doi: 10.1056/nejmoa070447

Maes, K., Testelmans, D., Powers, S., Decramer, M., and Gayan-Ramirez, G. (2007). Leupeptin inhibits ventilator-induced diaphragm dysfunction in rats. *Am. J. Respir. Crit. Care Med.* 175, 1134–1138. doi: 10.1164/rccm.200609-1342oc

Matecki, S., Dridi, H., Jung, B., Saint, N., Reiken, S. R., Scheuermann, V., et al. (2016). Leaky ryanodine receptors contribute to diaphragmatic weakness during mechanical ventilation. *Proc. Natl. Acad. Sci. U.S.A.* 113, 9069–9074. doi: 10.1073/pnas.1609707113

McClung, J. M., Kavazis, A. N., DeRuisseau, K. C., Falk, D. J., Deering, M. A., Lee, Y., et al. (2007). Caspase-3 regulation of diaphragm myonuclear domain during mechanical ventilation-induced atrophy. *Am. J. Respir. Crit. Care Med.* 175, 150–159. doi: 10.1164/rccm.200601-142oc

McClung, J. M., Van Gammeren, D., Whidden, M. A., Falk, D. J., Kavazis, A. N., Hudson, M. B., et al. (2009). Apocynin attenuates diaphragm oxidative stress and protease activation during prolonged mechanical ventilation. *Crit. Care Med.* 37, 1373–1379. doi: 10.1097/ccm.0b013e31819cef63

McClung, J. M., Whidden, M. A., Kavazis, A. N., Falk, D. J., Deruisseau, K. C., and Powers, S. K. (2008). Redox regulation of diaphragm proteolysis during mechanical ventilation. *Am. J. Physiol. Regul. Integr. Comp. Physiol.* 294, R1608–R1617.

McCormack, J. G., and Denton, R. M. (1980). Role of calcium ions in the regulation of intramitochondrial metabolism. Properties of the Ca2+-sensitive dehydrogenases within intact uncoupled mitochondria from the white and brown adipose tissue of the rat. *Biochem. J.* 190, 95–105. doi: 10.1042/bj19000095

Nelson, W. B., Smuder, A. J., Hudson, M. B., Talbert, E. E., and Powers, S. K. (2012). Cross-talk between the calpain and caspase-3 proteolytic systems in the diaphragm during prolonged mechanical ventilation. *Crit. Care Med.* 40, 1857–1863. doi: 10.1097/ccm.0b013e318246bb5d

Peng, T. I., and Jou, M. J. (2010). Oxidative stress caused by mitochondrial calcium overload. *Ann. N. Y. Acad. Sci.* 1201, 183–188. doi: 10.1111/j.1749-6632.2010.05634.x

Petrof, B. J., Jaber, S., and Matecki, S. (2010). Ventilator-induced diaphragmatic dysfunction. *Curr. Opin. Crit. Care* 16, 19–25.

Pietrobon, D., Di Virgilio, F., and Pozzan, T. (1990). Structural and functional aspects of calcium homeostasis in eukaryotic cells. *Eur. J. Biochem.* 193, 599–622. doi: 10.1111/j.1432-1033.1990.tb19378.x

Pinton, P., Giorgi, C., Siviero, R., Zecchini, E., and Rizzuto, R. (2008). Calcium and apoptosis: ER-mitochondria Ca2+ transfer in the control of apoptosis. *Oncogene* 27, 6407–6418. doi: 10.1038/onc.2008.308

Pizzo, P., Drago, I., Filadi, R., and Pozzan, T. (2012). Mitochondrial Ca(2)(+) homeostasis: mechanism, role, and tissue specificities. *Pflugers Arch.* 464, 3–17. doi: 10.1007/s00424-012-1122-y

Powers, S. K., Hudson, M. B., Nelson, W. B., Talbert, E. E., Min, K., Szeto, H. H., et al. (2011). Mitochondria-targeted antioxidants protect against mechanical ventilation-induced diaphragm weakness. *Crit. Care Med.* 39, 1749–1759. doi: 10.1097/ccm.0b013e3182190b62

Powers, S. K., Wiggs, M. P., Sollanek, K. J., and Smuder, A. J. (2013). Ventilator-induced diaphragm dysfunction: cause and effect. *Am. J. Physiol. Regul. Integr. Comp. Physiol.* 305, R464–R477.

Protasi, F., Paolini, C., Nakai, J., Beam, K. G., Franzini-Armstrong, C., and Allen, P. D. (2002). Multiple regions of RyR1 mediate functional and structural interactions with alpha(1S)-dihydropyridine receptors in skeletal muscle. *Biophys. J.* 83, 3230–3244. doi: 10.1016/s0006-3495(02)75325-3

Reiken, S., Lacampagne, A., Zhou, H., Kherani, A., Lehnart, S. E., Ward, C., et al. (2003). PKA phosphorylation activates the calcium release channel (ryanodine receptor) in skeletal muscle: defective regulation in heart failure. *J. Cell. Biol.* 160, 919–928. doi: 10.1083/jcb.200211012

Rossi, A., Pizzo, P., and Filadi, R. (2019). Calcium, mitochondria and cell metabolism: a functional triangle in bioenergetics. *Biochim. Biophys. Acta Mol. Cell. Res.* 1866, 1068–1078. doi: 10.1016/j.bbamcr.2018.10.016

Schwaller, B. (2010). Cytosolic Ca2+ buffers. *Cold Spring Harb. Perspect. Biol.* 2:a004051. doi: 10.1101/cshperspect.a004051

Shanely, R. A., Van Gammeren, D., Deruisseau, K. C., Zergeroglu, A. M., McKenzie, M. J., Yarasheski, K. E., et al. (2004). Mechanical ventilation depresses protein synthesis in the rat diaphragm. *Am. J. Respir. Crit. Care Med.* 170, 994–999. doi: 10.1164/rccm.200304-575oc

Shanely, R. A., Zergeroglu, M. A., Lennon, S. L., Sugiura, T., Yimlamai, T., Enns, D., et al. (2002). Mechanical ventilation-induced diaphragmatic atrophy is associated with oxidative injury and increased proteolytic activity. *Am. J. Respir. Crit. Care Med.* 166, 1369–1374. doi: 10.1164/rccm.200202-088oc

Smith, I. J., Godinez, G. L., Singh, B. K., McCaughey, K. M., Alcantara, R. R., Gururaja, T., et al. (2014). Inhibition of Janus kinase signaling during controlled mechanical ventilation prevents ventilation-induced diaphragm dysfunction. *FASEB J.* 28, 2790–2803.

Smuder, A. J., Nelson, W. B., Hudson, M. B., Kavazis, A. N., and Powers, S. K. (2014). Inhibition of the ubiquitin-proteasome pathway does not protect against ventilator-induced accelerated proteolysis or atrophy in the diaphragm. *Anesthesiology* 121, 115–126. doi: 10.1097/aln.0000000000000245

Smuder, A. J., Sollanek, K. J., Min, K., Nelson, W. B., and Powers, S. K. (2015). Inhibition of forkhead boxO-specific transcription prevents mechanical ventilation-induced diaphragm dysfunction. *Crit. Care Med.* 43, e133–e142.

Smuder, A. J., Sollanek, K. J., Nelson, W. B., Min, K., Talbert, E. E., Kavazis, A. N., et al. (2018). Crosstalk between autophagy and oxidative stress regulates proteolysis in the diaphragm during mechanical ventilation. *Free Radic. Biol. Med.* 115, 179–190. doi: 10.1016/j.freeradbiomed.2017.11.025

Steinberg, S. F. (2013). Oxidative stress and sarcomeric proteins. *Circ. Res.* 112, 393–405. doi: 10.1161/circresaha.111.300496

Talbert, E. E., Smuder, A. J., Kwon, O. S., Sollanek, K. J., Wiggs, M. P., and Powers, S. K. (2016). Blockage of the ryanodine receptor via azumolene does not prevent mechanical ventilation-induced diaphragm atrophy. *PLoS One* 11:e0148161. doi: 10.1371/journal.pone.0148161

Tang, H., Kennedy, C. L., Lee, M., Gao, Y., Xia, H., Olguin, F., et al. (2017). Smad3 initiates oxidative stress and proteolysis that underlies diaphragm dysfunction during mechanical ventilation. *Sci. Rep.* 7:14530.

Tang, H., and Shrager, J. B. (2018). The signaling network resulting in ventilator-induced diaphragm dysfunction. *Am. J. Respir. Cell. Mol. Biol.* 59, 417–427. doi: 10.1165/rcmb.2018-0022tr

Tang, H., Smith, I. J., Hussain, S. N., Goldberg, P., Lee, M., Sugiarto, S., et al. (2015). The JAK-STAT pathway is critical in ventilator-induced diaphragm dysfunction. *Mol. Med.* 20, 579–589. doi: 10.2119/molmed.2014.00049

Vallejo-Illarramendi, A., Toral-Ojeda, I., Aldanondo, G., and de Munain, A. Lopez (2014). Dysregulation of calcium homeostasis in muscular dystrophies. *Expert Rev. Mol. Med.* 16:e16.

Vassilakopoulos, T., and Petrof, B. J. (2004). Ventilator-induced diaphragmatic dysfunction. *Am. J. Respir. Crit. Care Med.* 169, 336–341.

Ward, C. W., Reiken, S., Marks, A. R., Marty, I., Vassort, G., and Lacampagne, A. (2003). Defects in ryanodine receptor calcium release in skeletal muscle from post-myocardial infarct rats. *FASEB J.* 17, 1517–1519.

Wehrens, X. H., Lehnart, S. E., Reiken, S., van der Nagel, R., Morales, R., Sun, J., et al. (2005). Enhancing calstabin binding to ryanodine receptors improves

cardiac and skeletal muscle function in heart failure. *Proc. Natl. Acad. Sci. U.S.A.* 102, 9607–9612. doi: 10.1073/pnas.0500353102

Whidden, M. A., McClung, J. M., Falk, D. J., Hudson, M. B., Smuder, A. J., Nelson, W. B., et al. (1985a). Xanthine oxidase contributes to mechanical ventilation-induced diaphragmatic oxidative stress and contractile dysfunction. *J. Appl. Physiol.* 106, 385–394. doi: 10.1152/japplphysiol.91106.2008

Whidden, M. A., Smuder, A. J., Wu, M., Hudson, M. B., Nelson, W. B., and Powers, S. K. (1985b). Oxidative stress is required for mechanical ventilation-induced protease activation in the diaphragm. *J. Appl. Physiol.* 108, 1376–1382. doi: 10.1152/japplphysiol.00098.2010

Yanez, M., Gil-Longo, J., and Campos-Toimil, M. (2012). Calcium binding proteins. *Adv. Exp. Med. Biol.* 740, 461–482.

Conflict of Interest: The authors declare that the research was conducted in the absence of any commercial or financial relationships that could be construed as a potential conflict of interest.

The reviewer WN declared a past co-authorship with one of the author SP to the handling editor.

frontiers in Physiology

ORIGINAL RESEARCH
published: 21 December 2020
doi: 10.3389/fphys.2020.601090

The Role of Orai1 in Regulating Sarcoplasmic Calcium Release, Mitochondrial Morphology and Function in Myostatin Deficient Skeletal Muscle

Mónika Sztretye[1], Zoltán Singlár[1], Norbert Balogh[1], Gréta Kis[2], Péter Szentesi[1], Ágnes Angyal[1], Ildikó Balatoni[1], László Csernoch[1] and Beatrix Dienes[1]*

[1] Department of Physiology, Faculty of Medicine, University of Debrecen, Debrecen, Hungary, [2] Department of Anatomy, Histology and Embryology, Faculty of Medicine, University of Debrecen, Debrecen, Hungary

OPEN ACCESS

Edited by:
Enrique Jaimovich, University of Chile, Chile

Reviewed by:
Gerolamo Lanfranchi, University of Padua, Italy
Xuexin Zhang,

***Correspondence:**
Mónika Sztretye
sztretye.monika@med.unideb.hu

Specialty section:
This article was submitted to Striated Muscle Physiology, a section of the journal Frontiers in Physiology

Received: *31 August 2020*
Accepted: *02 December 2020*
Published: *21 December 2020*

Citation:
Sztretye M, Singlár Z, Balogh N, Kis G, Szentesi P, Angyal Á, Balatoni I, Csernoch L and Dienes B (2020) The Role of Orai1 in Regulating Sarcoplasmic Calcium Release, Mitochondrial Morphology and Function in Myostatin Deficient Skeletal Muscle. Front. Physiol. 11:601090. doi: 10.3389/fphys.2020.601090

In mice a naturally occurring 12-bp deletion in the myostatin gene is considered responsible for the compact phenotype ($Mstn^{Cmpt-dl1Abc}$, Cmpt) labeled by a tremendous increase in body weight along with signs of muscle weakness, easier fatigability, decreased Orai1 expression and store operated calcium entry (SOCE). Here, on the one hand, Cmpt fibers were reconstructed with venus-Orai1 but this failed to restore SOCE. On the other hand, the endogenous Orai1 was silenced in fibers from wild type C57Bl6 mice which resulted in ∼70% of Orai1 being silenced in whole muscle homogenates as confirmed by Western blot, accompanied by an inhibitory effect on the voltage dependence of SR calcium release that manifested in a slight shift toward more positive potential values. This maneuver completely hampered SOCE. Our observations are consistent with the idea that Orai1 channels are present in distinct pools responsible for either a rapid refilling of the SR terminal cisternae connected to each voltage-activated calcium transient, or a slow SOCE associated with an overall depletion of calcium in the SR lumen. Furthermore, when Cmpt cells were loaded with the mitochondrial membrane potential sensitive dye TMRE, fiber segments with depolarized mitochondria were identified covering on average 26.5 ± 1.5% of the fiber area. These defective areas were located around the neuromuscular junction and displayed significantly smaller calcium transients. The ultrastructural analysis of the Cmpt fibers revealed changes in the mitochondrial morphology. In addition, the mitochondrial calcium uptake during repetitive stimulation was higher in the Cmpt fibers. Our results favor the idea that reduced function and/or expression of SOCE partners (in this study Orai1) and mitochondrial defects could play an important role in muscle weakness and degeneration associated with certain pathologies, perhaps including loss of function of the neuromuscular junction and aging.

Keywords: SOCE, myostatin deficiency, excitation contraction coupling, mithochondrial defect, mitochondrial calcium uptake

INTRODUCTION

Force generation, the main role of skeletal muscle is the result of muscle contraction and relaxation regulated by changes in the intracellular free Ca^{2+} level. The very low resting myoplasmic Ca^{2+} concentration from the nanomolar (nM) range rises rapidly into the micromolar (μM) range through the mechanism termed "excitation-contraction (EC) coupling" during which the action potential triggers Ca^{2+} release from the intracellular store (sarcoplasmic reticulum (SR)) mediated by coupling between the voltage sensor dihydropyridine receptor (DHPR) in the transverse tubule membrane and the ryanodine receptor (RyR1), Ca^{2+} release channel embedded in the SR membrane (Franzini-Armstrong, 2018). Released Ca^{2+} activates the contractile apparatus leading to contraction. During relaxation cytosolic [Ca^{2+}] returns to normal level by moving Ca^{2+} back to the SR via SERCA1, the Ca^{2+} pump located mainly in the longitudinal SR.

Depletion of SR calcium stores activate the process called store operated Ca^{2+} entry (SOCE) during which Ca^{2+} enters into the cytoplasm from the extracellular space to replenish the depleted intracellular stores. SOCE is coordinated by two key proteins: stromal interaction molecule 1 (STIM1) and Orai1. The former is the luminal Ca^{2+} level sensor in the SR membrane, while the latter is the Ca^{2+}-release activated calcium (CRAC) channel located in the surface membrane (Desai et al., 2015; Vaeth et al., 2017). Deficiency of either molecule impairs SOCE and leads to muscular abnormalities (McCarl et al., 2009; Cully et al., 2012; Li et al., 2012; Zhao et al., 2012; Böhm et al., 2013; Onopiuk et al., 2015; Carrell et al., 2016). The role of SOCE under physiological conditions in muscle is not yet completely determined. Its contribution to muscle development (Kurebayashi and Ogawa, 2001; Wei-Lapierre et al., 2013; Carrell et al., 2016) and myoblast fusion and differentiation (Darbellay et al., 2009) has already been demonstrated, however according to former opinions, because of its slower kinetics, SOCE has not been considered as a relevant process underlying muscle contraction. Recently, an increasing number of studies seem to contradict this idea presenting evidences on the role of SOCE in skeletal muscle contraction, development, fatigue reduction, replenishing SR stores during prolonged muscle contraction (Wei-Lapierre et al., 2013; Carrell et al., 2016; Boncompagni et al., 2017), in maintaining the SR calcium content during EC coupling (Sztretye et al., 2017; Koenig et al., 2018) even under conditions of sustained Ca^{2+} concentration in the SR (Koenig et al., 2019) and disease states (Stiber and Rosenberg, 2011).

Lately, the role of mitochondria in regulating the energy metabolism of muscle cells has been associated to the activity of SOCE (Malli and Graier, 2017) as well. Besides the refill of SR luminal store through SERCA pump, calcium ions can be taken up by mitochondria as well. Although mitochondrial uptake has limited impact on cytosolic [Ca^{2+}] regulation (it allots to around 10–18% of the total Ca^{2+} riddance, Yi et al., 2011), it is necessary for energy balance, i.e., to fulfill the high ATP demand of muscle contraction (Porter and Wall, 2012) and its role in governing the intracellular Ca^{2+} signaling in skeletal muscle during EC coupling has also been documented. On the other hand, mitochondrial Ca^{2+} overload can result in dysfunction of mitochondria and degeneration of muscle cells.

Mitochondria can control the ER/SR Ca^{2+} content in many ways and consequently affect the activation, maintenance, and deactivation of SOCE (Parekh, 2008). Also, they are known to have an effect on ER/SR Ca^{2+} release as mitochondrial Ca^{2+} withdrawal from ER/SR Ca^{2+} release channels impacts the degree of ER/SR Ca^{2+} depletion (Malli and Graier, 2017).

In our former studies a mouse strain with a naturally occurring mutation in the myostatin gene [Compact (*Cmpt*); Szabó et al., 1998] has been examined. These mice present a hypermuscular yet reduced muscle-force phenotype accompanied with reduced STIM1 and Orai1 expression, leading to lessened SOCE activity. The contribution of SOCE to the refilling of the SR has also been proven (Sztretye et al., 2017). These observations provided us with an obvious background and paved the rationale for the current study to analyze the role of SOCE partners and potential mitochondrial alterations in calcium release processes and muscle weakness.

Here, the role of Orai1 in the regulation of SR calcium release using either Cmpt muscle fibers reconstructed with venus-Orai1 and wild type fibers with silenced Orai1 expression were studied. Our results favor the idea that Orai1 channels are present in distinct pools responsible for either a rapid refilling of the SR terminal cisternae connected to each voltage-activated calcium transient, or a slow SOCE associated with an overall depletion of calcium in the SR lumen. In this framework, Orai1 channels in the former pool would be permanently associated with STIM partners while those in the latter would have to be recruited into calcium entry units (Protasi et al., 2020) once STIM molecules become activated.

MATERIALS AND METHODS

Animal Care and Experimental Design

Animal experiments conformed to the guidelines of the European Community (86/609/EEC). The experimental protocol was approved by the institutional Animal Care Committee of the University of Debrecen (3-1/2019/DEMAB). The mice were housed in plastic cages with mesh covers and were fed with pelleted standard mouse chow and had access to water *ad libitum*. Room illumination was an automated cycle of 12 h light and 12 h dark, and room temperature was maintained within the range of 22–25°C.

In vivo Electroporation

The mice were anesthetized with 2–4% isoflurane using a V1 Vet Equip tabletop anesthesia machine (Livermore, CA, United States). The O_2 flow was kept constant at 0.4 L/min. The FDB muscles were injected with 15 μl of 2 mg/ml hyaluronidase in sterile saline. One hour later 20 μg plasmid cDNA of interest was injected at the same location. Ten minutes later, two sterile gold-plated acupuncture needles were placed under the skin on adjacent sides of the muscle. Twenty 100 V/cm, 20-ms square-wave pulses of 1 Hz frequency were applied to the muscle for 1 sec

each using an ECM 830, BTX Harvard Apparatus electroporator (Holliston, MA, United States).

In vitro Experiments

Animals were anaesthetized and sacrificed following a protocol approved by the Animal Care Committee of the University of Debrecen (3-1/2019/DEMAB). After CO_2 overdose and manual cervical dislocation, the *m. flexor digitorum brevis* (FDB) from the hind limb were dissected manually in normal Tyrode's solution.

Isolation of Single Skeletal Muscle Fibers

The manual dissection of FDB muscle in normal Tyrode's solution was followed by an enzymatic dissociation in the presence of 0.2% Type I collagenase at 37°C for 50 min in a Ca^{2+} free Tyrode's solution. After the enzymatic treatment FDB muscles were placed in normal Tyrode's solution and stored in the refrigerator at 4 °C until use for up to 36 h. Single FDB fibers were obtained after gently triturating the muscle with a pipette (Szentesi et al., 1997; Fodor et al., 2008).

All calcium measurements were carried out on single skeletal muscle fibers from the FDB muscles of the mouse. SOCE measurement was performed similarly, as in our earlier report (Sztretye et al., 2017). Briefly, isolated single FDB fibers loaded with the green fluorescent calcium binding dye fluo-8AM (4 μM, 20 min at 20–22°C) were imaged with a laser scanning confocal microscope (5 Live, Carl Zeiss, Oberkochen, Germany) and subjected to multiple manual solution exchanges during which the fluorescence profile versus elapsed time was imaged and then plotted. The dye fluorescence showed a steady state followed by an initial increase (P1), then decrease as a consequence of the application of the releasing cocktail (see below) in a Ca^{2+} –free Tyrode's medium. This transient corresponded to the depletion of intracellular Ca^{2+} stores via RyR1s. When returning to the 1.8 mM Ca^{2+} in the external solution, another increase should be detected (P2), indicating perhaps SOCE activation and Ca^{2+}-influx through surface channels. After the manual delimitation of the cell border, the change of $[Ca^{2+}]_i$ was calculated as $\Delta F/F_0$, where ΔF is the fluorescence intensity change and was calculated over the cell, whereas F_0 is the background fluorescence and was calculated in a region next to the cell. The ratio of P2/P1 over time was then calculated and plotted.

Voltage Clamp

The experimental design was similar to the one described in our earlier study (Sztretye et al., 2017, 2020). Briefly, isolated FDB fibers were placed in the *external solution* and voltage clamped (Axoclamp 200B, Axon Instruments, Foster City, CA, United States). Changes in cytosolic Ca^{2+} were recorded, following the application of depolarizing voltages and simultaneously imaged using a confocal microscope (Zeiss 5 Live, Oberkochen, Germany). Fibers were dialyzed through the patch pipette with the rhod-2 or fluo-8 and 10 mM EGTA containing *internal solution* and the application of depolarizing pulses was started 15–20 min following the seal formation to assure enough loading time. The ambient temperature was set to 20–22°C. The holding potential was −80 mV and the pipette resistance varied between 2 and 4 MΩ. Correction for linear capacitive currents was performed by analog compensation.

The voltage dependence of activation was described by Boltzmann function:

$$Ca(V_m) = \frac{Ca_{max}}{1 + e^{\frac{-(V_m - V_{50})}{k}}} \quad (1)$$

to derive the transition voltage V_{50} and limiting logarithmic slope 1/k.

Voltage evoked Ca^{2+} transients were analyzed by an in-house custom-made program taking into account the dissociation constant for rhod-2 ($K_{d\ rhod-2}$ = 1.58 μM). The SR Ca^{2+} content was calculated taking into account the SERCA pump activity, the calcium binding to intracellular buffers as troponin-C, EGTA, parvalbumin and the dye as reported earlier (Sztretye et al., 2017, 2020).

Measurement of Mitochondrial Ca^{2+}-uptake

Activity-dependent changes in mitochondrial Ca^{2+} levels in single FDB fibers were monitored with rhod-2 as described in Sztretye et al., 2020. FDB fibers were loaded with 5 μM rhod-2-AM for 15 min at room temperature and then washed with dye free normal Tyrode's solution. Fibers were electrically stimulated (S88 Stimulator, Grass Technologies, Warwick, RI, United States) through a pair of platinum electrodes placed close to the fiber of interest. A single or a series of 5 consecutive tetani (500 ms duration, 100 Hz) were applied at supramaximal activating voltage for each cell. Time series x-y images (512 × 512 pixels, 0.5 ms/pixel) were taken at rest, following the 1st and 5th tetanus. Calculation of rhod-2 fluorescence values originating from the mitochondria (F_{mito}) were performed as follows: a line was drawn parallel to the longitudinal axis of the fiber and the fluorescence was calculated at the peaks (I-band fluorescence, representing mitochondria (F_{I-band})) and at troughs (A-band, non-mitochondrial fluorescence, baseline, F_{A-band}). Relative mitochondrial Ca^{2+} uptake expressed as F_{mito} was calculated as $F_{I-band} - F_{A-band}$ and then normalized to the baseline fluorescence.

Confocal Microscopy and Image Analysis

Images of rhod-2, fluo-8, TMRE and Alexa Fluor 488 α-bungarotoxin fluorescence were acquired with a laser scanning confocal microscope (Zeiss 5 Live, Oberkochen, Germany) equipped with a 20x air and a 40x oil objectives. Excitation of rhod-2 was done 543 nm, with emission collected above 550 nm with a long pass filter whereas for fluo-8 the excitation wavelength was 488 nm, the emission was at 520 nm. Line-scan image recordings were synchronized with the application of the depolarizing pulses via pClamp 11.0 (Molecular Devices, CA, United States) and the protocol used is always indicated on the figure. The time resolution was 0.5 ms per line whereas the spatial resolution was 0.24 μm/line. Peak F/F_0 values were obtained and plotted at close to maximal depolarizations. Single exponential functions were used to fit the time course of the

changes of the maximal F/F_0 values during the series of tetanic depolarizing pulses as described earlier (Sztretye et al., 2017, 2020). Peak F/F_0 values were then obtained by averaging the data points in the spatial domain and plotted at close to maximal depolarizations. When a series of tetanic depolarizing pulses were applied (200 ms long 8 consecutive pulses at +30 mV) single exponential functions were used to fit the time course of the changes of the maximal F/F_0:

$$y = y_0 + ae^{-bx} \quad (2)$$

This then enabled the estimation of SR calcium content as described in our earlier report (Sztretye et al., 2017). In the equation above x is the number of tetanic pulses applied, b is the time constant of SR calcium depletion, a is the remaining calcium in the SR following the last depolarizing pulse and y_0 is the difference between the total and the remaining SR calcium content following the 8th tetanic pulse.

Molecular Biology

Western Blot

The Western blot technique was applied to detect expression levels of Orai1. Protein samples were prepared from whole FDB muscle homogenates as well as homogenates of isolated single FDB muscle fibers using standard methods of BCA Protein Assay Kit (Thermo Fisher Scientific, Waltham, MA, United States). Protein samples were subjected to SDS-PAGE using 10% precast gels (Bio-Rad Laboratories, Hercules, CA, United States). 20 μg protein per lane was loaded in each case and separated proteins were transferred to 0.2 nitrocellulose membranes (Bio-Rad Laboratories). For immunological detection of Orai1 mouse monoclonal anti-Orai1 (Thermo Fisher Scientific, cat. No. MA5-15777) was used in 1:500 dilution as primary antibody. As for secondary antibody, horseradish peroxidase-conjugated goat anti-mouse IgG (Bio-Rad Laboratories, Hercules, CA, United States, cat. No. 170-6516) was used in a 1:1000 dilution and this was visualized by chemiluminescence reaction (Pierce Biotechnology, Waltham, MA, United States) using LAS-3000 Intelligent Dark Box (Fuji, Tokyo, Japan). For immunolabelling experiments on Cmpt fibers, we marked the endogenous Orai1 protein with Alexa-Fluor Plus 488 secondary antibody (Invitrogen cat. No. A11001) Densitometry of the signals was performed by using ImageJ software (NIH) and optical densities were calculated as normalized to control samples. To prove equal loading, membranes were re-probed with anti–β-actin antibody (Thermo Fisher Scientific, cat. No. MA1-140) or vinculin (Sigma Aldrich, cat. No. V4139) and visualized as described above.

Plasmid Preparation

The plasmid venus-Orai1 was kindly provided by R. Dirksen (Univ. of Rochester, NY, United States). The GFP tagged Orai1 shRNA and scrambled shRNA cassettes in pGFP-V-RS vector were purchased from Origene Technologies (cat. No. TG510804). The plasmids were amplified using bacterial cultures grown in the presence of selective antibiotics (kanamycin and ampicillin, respectively). Plasmid DNA preparations were obtained using Endofree Plasmid Kits (Qiagen Inc).

Electron-Microscopy

FDB muscles were fixed *in situ* with fixative solution (3% glutaraldehyde in Millonig's buffer) (Sztretye et al., 2017). Small bundles of fixed muscle fibers were then post fixed in 1% OsO4 in water. For rapid dehydration of the specimens, graded ethanol followed by propylene-oxide intermediate was used. Samples were then embedded in Durcupan epoxy resin (Sigma-Aldrich). Ultrathin sections were cut using a Leica Ultracut UCT (Leica Microsystems, Wien, Austria) ultra-microtome and stained with uranyl acetate and lead citrate. Sections were examined with a JEM1010 transmission electron microscope (JEOL, Tokyo, Japan) equipped with an Olympus camera.

Experimental Solutions

Kreb's solution (in mM): 135 NaCl, 5 KCl, 2.5 $CaCl_2$, 1 $MgSO_4$, 10 Hepes, 10 glucose, 10 $NaHCO_3$; pH 7.2.

Normal Tyrode's solution (in mM): 137 NaCl, 5.4 KCl, 1.8 mM $CaCl_2$, 0.5 $MgCl_2$, 11.8 HEPES; 1 gL^{-1} glucose; pH 7.4.

Ca^{2+} free Tyrode's solution: same as above except 5 mM EGTA was added and no $CaCl_2$ was present.

The "*cocktail*" consisted of 0.4mM 4-CmC, 0.004mM thapsigargin, and 0.05 mM N-benzyl-p-toluene sulphonamide.

External solution (in mM): 140 TEA-CH_3SO_3, 1 $CaCl_2$, 3.5 $MgCl_2$, 10 Hepes, 1 4-AP, 0.5 $CdCl_2$, 0.3 $LaCl_3$, 0.001 TTX (citrate), and 0.05 BTS (N-benzyl-p-toluene sulphonamide). pH was adjusted to 7.2 with TEA-OH and osmolality was adjusted to 320 mOsm with TEA methanesulfonate.

Internal solution (in mM): 110 N-methylglucamine, 110 L-glutamic acid, 10 EGTA, 10 Tris, 10 glucose, 5 Na_2 ATP, 5 PC Tris, 0.5 rhod-2, 3.56 $CaCl_2$, and 7.4 mM $MgCl_2$ were added for a nominal 1 mM [Mg^{2+}] and 100 nM [Ca^{2+}]. pH was set to 7.2 with NaOH and osmolality to 320 mOsm with N-methylglucamine.

Fluorescent dyes (rhod-2 tripotassium salt and AM, TMRE, α-bungarotoxin, Alexa Fluor 488 conjugate) were purchased from Invitrogen (Thermo Fischer, Waltham, MA, United States; cat. no. R14220; R1244; T669; B13422). Fluo-8 tripotassium salt was from AAT Bioquest (cat. no. 21087). All other chemicals were purchased from Sigma-Aldrich (St. Luise, MO, United States).

Statistical Analysis

Pooled data were expressed and plotted as mean ± standard error of the mean (SEM). Student's two-tailed *t*-test for two independent populations was used for calculating statistical significance ($p < 0.05$).

RESULTS

Functional Consequences of Manipulating Orai1 Protein Level by *in vivo* Plasmid Electroporation

In our earlier work (Sztretye et al., 2017) we have shown that endogenous Orai1 levels were reduced in the Cmpt FDB muscles which had direct functional consequences on SOCE activity. Here we decided to reconstruct the Cmpt muscles with

venus-Orai1 via *in vivo* electroporation. Five days after the procedure the rate of transfection efficiency was confirmed in FDB fibers by the green fluorescence of the venus-Orai construct (**Figure 1A**). We observed appropriate targeting of venus-Orai1 to the triad in Cmpt mice as supported by the fluorescence intensity profile plotted as a function of distance (**Figure 1B**). The correct targeting of the probe is further demonstrated by the representative immunolabelling image of a Cmpt FDB fiber probed with an Orai1 antibody where a similar double row pattern was observed (**Supplementary Figure 1A**).

Next, we evaluated the effects of silencing Orai1 in wild type C57Bl7 mice. For this, small-hairpin RNA (shRNA) tagged with GFP against Orai1 was introduced into FDB muscles via electroporation. Whole FDB muscles and ∼30 individual fibers identified via their green fluorescence from four different animals were collected and analyzed by Western blot. The representative immunoblot in **Figure 1C** shows a significant reduction in the Orai1 protein levels on the 5th day following the procedure both on whole muscle and fibers level. A scrambled non targeted shRNA probe (SCR) was used as control along with samples collected from the untreated WT mice. **Figure 1D** presents the quantitative densitometry analysis of four independent immunoblots. On average Orai1 silencing achieved ∼70% in the whole FDB muscle samples and ∼85% in single fibers. We also analyzed the extent of venus-Orai1 protein expression in whole FDB muscle homogenates by Western Blot (**Supplementary Figures 1B,C**). While the monoclonal antibody used in our study was excellent in detecting the endogenous Orai1 protein (∼50 kDa) it failed to reveal a band at the expected molecular weight of the venus-Orai1 fusion protein (∼75 kDa). We must clarify that the predicted molecular weight for Orai1 is 33 kDa, however, the observed value is generally between 50 and 60 kDa. In our hands, the Thermo Fisher monoclonal Orai1 antibody (cat. no. MA5-15777) recognizes the protein at ∼50 kDa. The difference is most likely due to post-translational modification of the protein. Based on the above, the quantification of the extent of venus-Orai1 expression was not carried out. Nevertheless, the endogenous Orai1 expression was essentially identical in the vehicle (physiological saline injected and electroporated) and venus-Orai1 electroporated Cmpt FDB muscles.

Store operated calcium entry measurement was performed as described in detail in our previous report (Sztretye et al., 2017). **Figure 1E** depicts a representative experiment done on an enzymatically dissociated single FDB fiber from a Cmpt mouse that was injected with 15 μl physiological saline solution (vehicle) and electroporated. First, the fiber loaded with rhod-2 AM was placed in the experimental chamber filled with normal Tyrode's solution (1.8 mM Ca^{2+}), which was exchanged manually to a Ca^{2+}-free Tyrode's solution (0 mM Ca^{2+}) while continuously imaging the fiber using a confocal microscope with the appropriate laser line. Application of a cocktail (see Materials and Methods, Experimental solutions section) lead to a rapid increase in dye fluorescence due to Ca^{2+} release via RyR1s from the SR (marked as P1). After washout and following the re-addition of 1.8 mM Ca^{2+} concentration in the external solution, a slowly activated secondary increase in fluorescence was observed after the SR store depletion as a result of Ca^{2+} influx via activated Orai1 channels (marked as P2; see also **Figure 1B** in Sztretye et al., 2017). This, however, was not the case in WT fibers silenced with shRNA-Orai1 (green, **Figure 1F** and **Supplementary Figure 2B**) as demonstrated by the lack of secondary peak P2, an indication that virtually no SOCE in these fibers can be detected (**Supplementary Table 1**). The pooled data of the peaks for the SOCE-associated Ca^{2+} transient (P2) normalized to RyR1-mediated Ca^{2+} transient induced by the depleting-cocktail (P1) revealed a slight increase of SOCE in Cmpt animals reconstructed with venus-Orai1 (blue, **Figure 1F**; red, **Supplementary Figure 2A**). This ratio (0.34 ± 0.12) remains, however, below the values we observed and published earlier for WT fibers (0.63 ± 0.09, black column on **Figure 1E** from Sztretye et al., 2017), suggesting that re-expression of Orai1 in these cells doesn't restore SOCE function. On Cmpt mice one leg was always injected with physiological saline (vehicle) and electroporated. The P2/P1 ratio for these cells (0.25 ± 0.07) was not statistically different from the untreated Cmpt cells (0.34 ± 0.07, red column on **Figure 1E** from Sztretye et al., 2017).

Assuming that the SR of the investigated cells are equally loaded, P1 will give a measure of the magnitude of depletion in the SR. Assuming that SOCE is proportional to the depletion, one expects greater SOCE if the depletion is greater. Therefore, although P2 (which is actually the difference between the peak and the baseline) reflects the actual SOCE in that particular fiber, P2/P1 would normalize the SOCE to SR depletion making comparisons across fibers more appropriate.

Voltage Activation of the FDB Muscles Following Orai1 Manipulation

We continued the functional studies by examining the possibility of altered coupling between the DHPR and RyR1 in single FDB fibers combining whole cell patch clamp and confocal imaging. **Figure 2A** shows a representative line-scan image of rhod-2 fluorescence from a WT fiber expressing the Orai1-shRNA construct. We have recorded with 10 mV increments calcium transients elicited by a series of 100-ms-long membrane depolarizations in the voltage range between of −60 and +30 mV.

Figure 2B compares the voltage dependence of the normalized maximal fluorescence at the given depolarization from nine WT+SCR (dark red), seven WT+shRNA Orai1 (green) and seven Cmpt fibers expressing the venus-Orai1 construct (blue). The voltage dependence of the normalized fluorescence followed a Boltzmann distribution (Eq. 1 in section "Materials and Methods"); these points were normalized to the obtained maximum for a given fiber and ultimately averaged over the fibers in each group. The solid lines represent the best fit of the Boltzmann function to the average values with the mean values of parameters given in **Table 1**. The Ca^{2+}-release activation in WT silenced fibers was found to be slightly shifted to more negative potentials as underlined by the V_{50} of release, however, this proved to be not different statistically.

Figure 2C illustrates the temporal profiles of the normalized fluorescence at individual depolarizing pulses with a length of 100 ms measured in single FDB fibers. The average peak

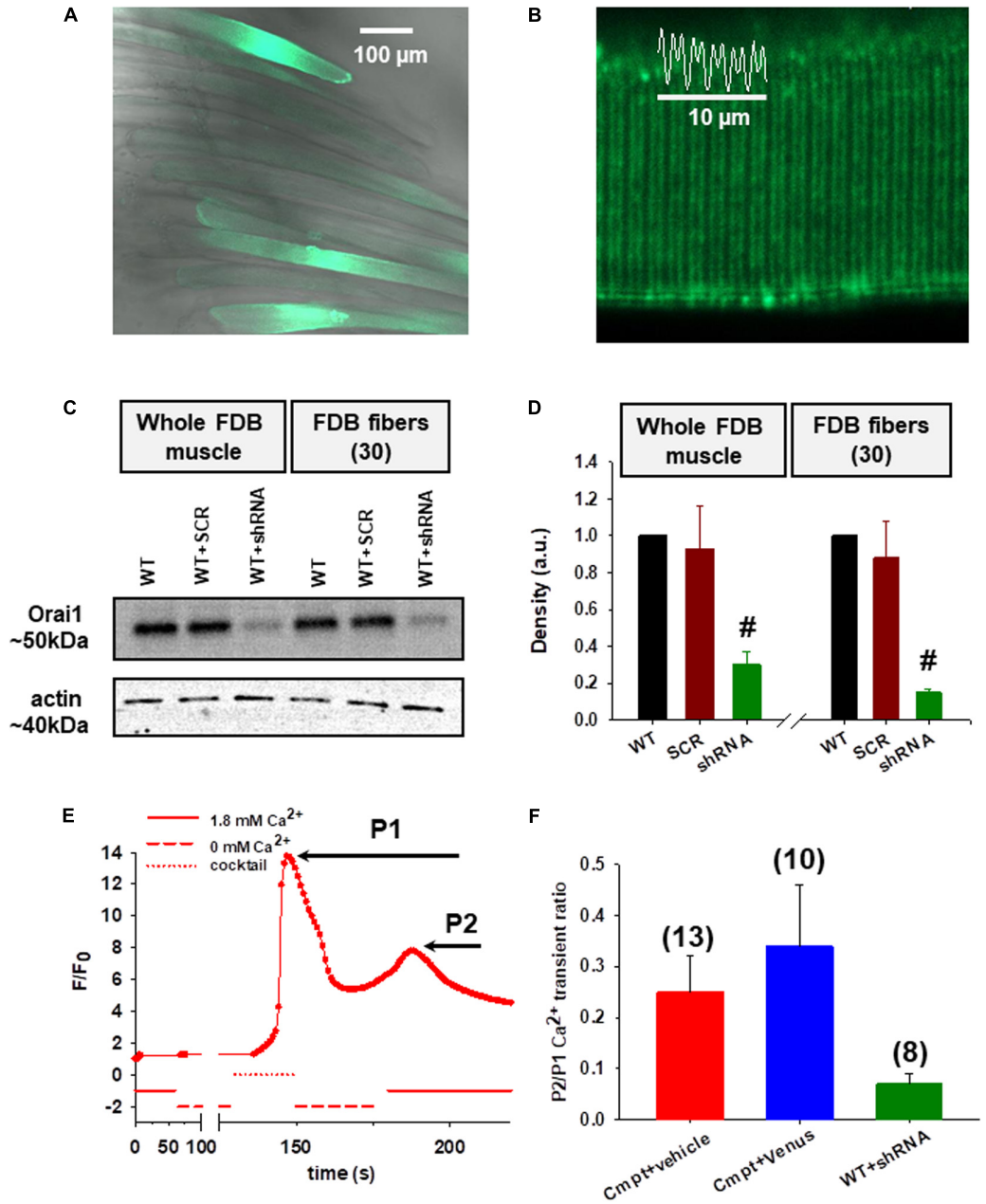

FIGURE 1 | Functional consequences of Orai1 protein level manipulation by *in vivo* plasmid electroporation. **(A)** Good efficiency of venus-Orai1 expression in Cmpt mice where a high percentage of the muscle fibers were transfected as illustrated by them displaying bright fluorescence signals. **(B)** Representative image showing correct targeting of venus-Orai1 to the triad in Cmpt mice as highlighted by the double-banded pattern of venus' fluorescence. The white trace illustrates the fluorescence intensity profile plotted as a function of distance along the white line for five successive triads. **(C)** Immunoblot analysis in WT mice 5-days after the small-hairpin RNA (shRNA) against Orai1 was introduced into FDB muscles using electroporation showed a significant reduction in the Orai1 protein levels. A scrambled non targeted shRNA probe was used as control along with samples collected from the untreated WT mice. The analysis was performed on whole FDB muscles and also using ~30 individual FDB fibers identified via the GFP signal and manually collected using a fluorescence microscope. Actin was used as internal control. **(D)** Quantitative densitometry analysis of four independent immunoblots revealed a significant decrease of Orai1 levels compared to WT taken as 100% in both whole FDB muscles and single fibers, respectively ($^{\#}p < 0.001$) **(E)** A representative SOCE measurement showing the fluorescence profile versus elapsed time following various solution exchanges performed on a Cmpt fiber injected with physiological saline solution (vehicle) and stained with rhod-2 AM. WT FDB fibers were silenced with shRNA-Orai1 5 days before dissection. Following the removal of calcium from the external solution the application of a releasing cocktail (see Materials and Methods and also Sztretye et al., 2017) caused a rapid and robust increase in fluorescence (P1) due to Ca^{2+} release from the SR via RyR1s. After returning to the 1.8 mM Ca^{2+} concentration in the external solution, a slowly activated secondary increase in fluorescence was detected corresponding to the consequent SOCE activation (P2). **(F)** The ratios of the peak of the slow Ca^{2+} transient (P2), representing the activation of SOCE, and that of the depleting-cocktail induced fast SR Ca^{2+} transient (P1). The numbers in parentheses indicate the numbers of individual cells studied. Note that reconstructing the Cmpt fibers with Orai1 does not restore SOCE, but silencing Orai1 in WT fibers does impede proper SOCE function.

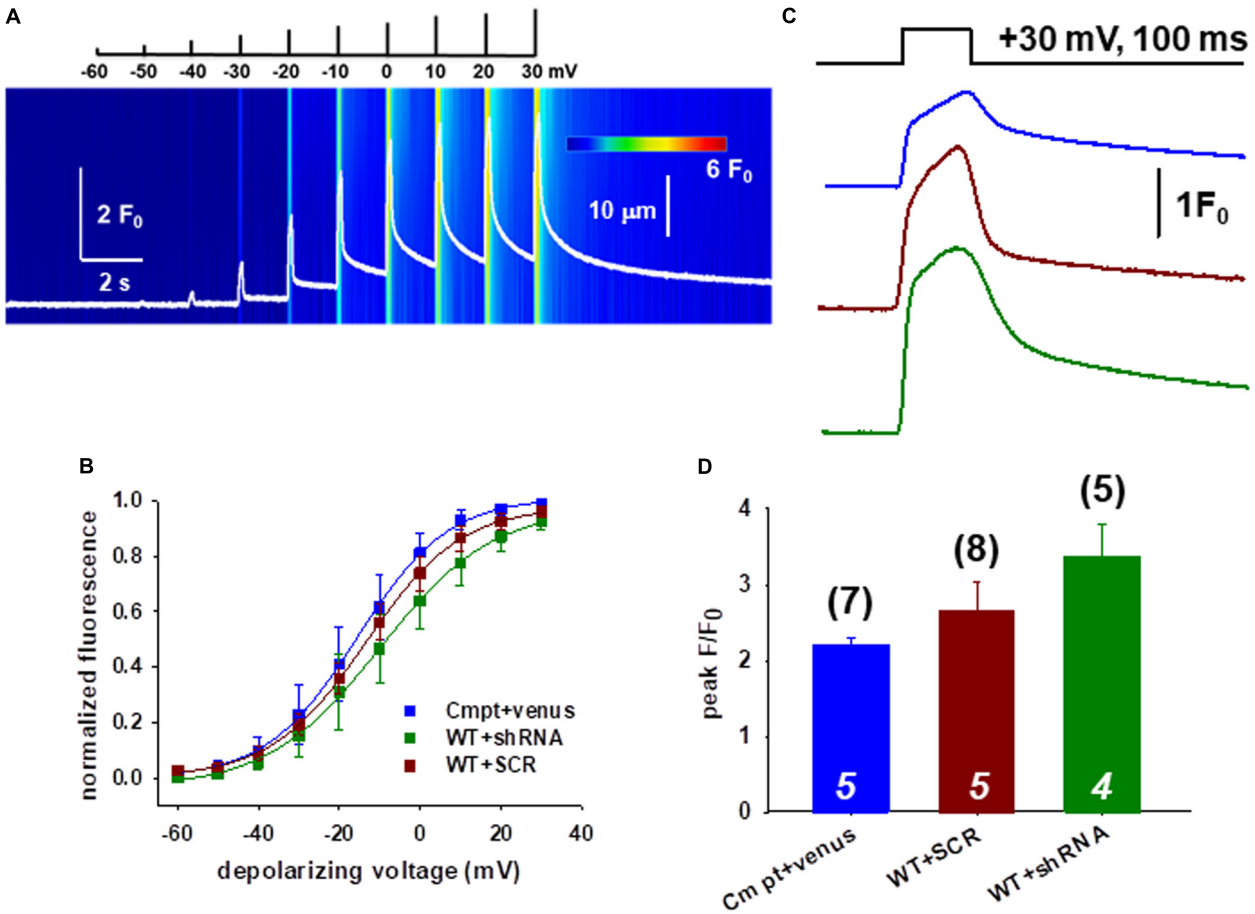

FIGURE 2 | Slight changes of the release channel sensibility to voltage activation in FDB muscles following Orai1 manipulation. **(A)** Representative line-scan image of rhod-2 fluorescence normalized to the baseline value $F_0(x)$ in a WT fiber expressing the shRNA construct. The cells were held at –80 mV and were subjected to successive depolarizing voltage steps (top) under whole-cell patch-clamp. The pulses lasted 100 ms and the delay between two pulses was 1100 ms. The cells were perfused with 10 mM EGTA via the patch pipette. **(B)** Voltage dependence of the calcium transients. The normalized F/F_0 values were fitted with a Boltzmann function (see Eq. 1 in section "Materials and Methods") and then normalized to the obtained maximum. The continuous lines represent the best fit of the Boltzmann function to the average values with the best fit parameters given in **Table 1**. **(C)** Representative fluorescence intensity profiles plotted for peak F/F_0 values obtained at maximal individual depolarizing pulses (+30 mV, 100 ms) for Cmpt fibers reconstructed with venus-Orai1 and the WT fibers transfected with SCR and shRNA-Orai1. **(D)** Pooled data for peak F/F_0 values show no significant changes. The numbers in parenthesis denote the number of individual fibers whereas the numbers in italics denote the number of animals studied.

F/F_0 values obtained at maximal depolarizing pulses (+30 mV) are presented in **Figure 2D**. When comparing the peak F/F_0 in WT+SCR (dark red) and silenced cells (green) we found slightly increased but statistically unaltered peak values (2.65 ± 0.38 vs. 3.38 ± 0.41) which suggests that the global voltage activated cytosolic Ca^{2+}-transients were not affected by the lack of Orai1.

TABLE 1 | The voltage dependence of the normalized fluorescence.

	V_{50} (mV)	k
Cmpt + venus-Orai1 (7)	−15.62 ± 1.55	11.27 ± 0.42
WT + SCR-Orai1 (9)	−13.34 ± 0.75	11.73 ± 0.65
WT + shRNA-Orai1 (7)	−9.89 ± 0.85	13.96 ± 0.75

V_{50} is the transition voltage and k is the slope of the Boltzmann fit. The mean values of parameters were not significantly different. Numbers in parenthesis are the number of fibers fitted.

Fatigability of Individual FDB Fibers Following Orai1 Manipulation

To assess the calcium fluxes and fatigability in individual FDB fibers under patch clamp a protocol to study the immediate refilling following repetitive stimulation that would also require the correct functioning of SOCE was used. To test this, a series of depolarizations with the arrangement illustrated in **Figure 3A** were applied. **Figure 3B** illustrates the change of SR Ca^{2+} content during repetitive stimulation in different fibers. The amount of calcium released decreased by the removal flux was used to calculate the decline in SR Ca^{2+} content, which covers the uptake of Ca^{2+} into the SR by the SERCA pump (Royer et al., 2010; Sztretye et al., 2011, 2017).

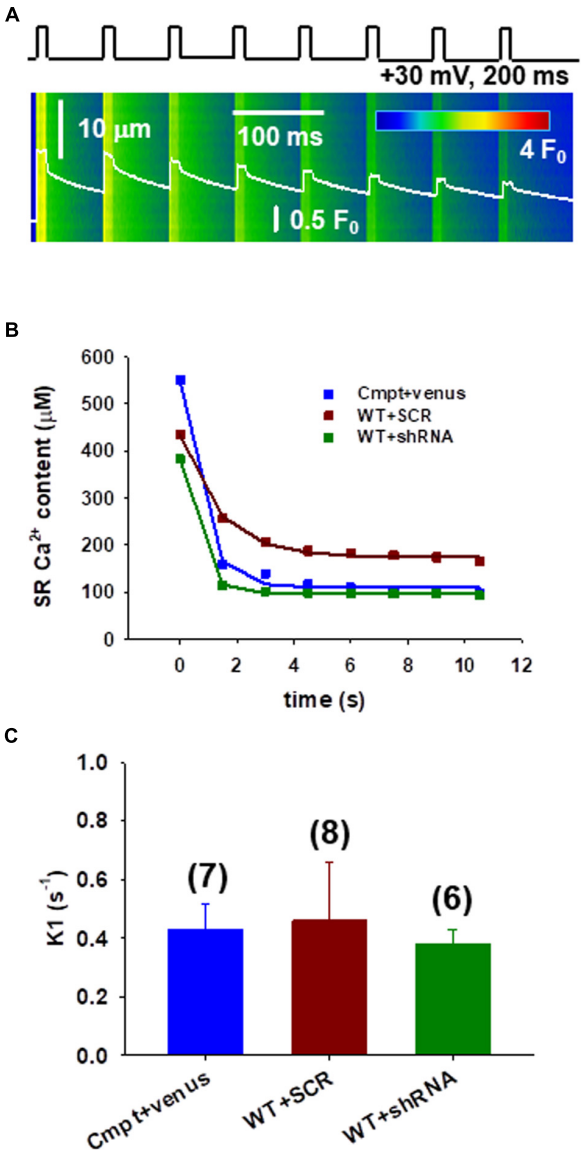

FIGURE 3 | Assessing the calcium fluxes of individual FDB fibers following Orai1 manipulation. **(A)** Line-scan image of the kinetic analysis of Ca^{2+}-release fluxes for transients elicited by a train of depolarizing pulses to +30 mV at 1 Hz frequency, lasting 200 ms each in Cmpt FDB fibers reconstructed with venus-Orai1. The white trace depicts the spatially averaged $F(t)/F_0$. **(B)** The SR Ca^{2+} content was estimated from the amount released minus the removal flux. A single-exponential function was fitted to the points (for further details please see Eq. A10 in Appendix A from Sztretye et al., 2017). Note that there is a sharp decrease of the SR calcium content following the first depolarizing pulse. **(C)** Pooled data of the calculated fluxes (K1) through Orai1 channels as predicted by our model (see Appendix A from Sztretye et al., 2017). Reconstructing the mutant fibers with venus-Orai1 restored the Ca^{2+} fluxes to the levels previously seen in WT fibers (consult Sztretye et al., 2017, Figure 4F). The numbers in parenthesis denote the number of cells studied.

Earlier a simple model including three compartments (extracellular, intracellular, and intra-SR spaces (Appendix A in Sztretye et al., 2017) was proposed that is in agreement with an exponential decay in the Ca^{2+} content of the SR under these conditions, where the rate constant of decay (a) is precisely related to the flux (K1) through Orai1 channels. The data points from **Figure 3B** were thus fitted with exponential functions (Eq.2 in Methods) and K1 values were calculated for each experiment. **Figure 3C** shows pooled data of K1 (fluxes through Orai1 channels) calculated using our model. The newly acquired data suggests that in the mutant fibers reconstructed with Orai1 (blue) we were able to restore the K1 values to those previously seen in WT (0.34 ± 0.21, black column in Figure 4F from Sztretye et al., 2017) while no significant changes in K1 for WT silenced fibers (green) were detected.

Activity Dependent Changes in Mitochondrial Calcium Uptake

Figure 4A presents a representative confocal image of rhod-2 fluorescence on a Cmpt FDB muscle fiber under resting condition. The method of measuring mitochondrial Ca^{2+}-uptake has been described in detail in our recent report (Sztretye et al., 2020). In brief, the average normalized fluorescence of mitochondria (F_{mito}) calculated as $(F_{I-band} - F_{A-band})/F_{A-band}$ was compared in WT and Cmpt FDB fibers at rest and following tetanic stimulation. The fluorescence was averaged over the spatial domain along a line (white trace) placed in parallel with the fiber's orientation. Typical traces are shown in **Figure 4C**. Images were recorded at rest (**Figure 4C**, panel c1), after the first (c2), and the fifth (c3) consecutive tetanic depolarizing pulses with supramaximal amplitude through platinum electrodes placed in the proximity of the cell studied. The analysis revealed that on average F_{mito} values were already higher at rest in the mutant when compared to WT (0.25 ± 0.03 vs 0.17 ± 0.02, $p > 0.05$) and significantly increased following the first and the fifth tetanic stimulation (0.28 ± 0.03 and 0.29 ± 0.04 in Cmpt vs 0.19 ± 0.02 and 0.18 ± 0.02 in WT, respectively, $p < 0.05$). The pooled data (**Figure 4B**) clearly indicate the activity dependent mitochondrial calcium uptake as being more pronounced in the mutant.

Structural Defects of Mitochondria in Cmpt Fibers

To investigate the mitochondrial morphology in a living muscle cell, FDB fibers from Cmpt mice were incubated with the voltage-sensitive fluorescent indicator TMRE indicating the mitochondrial transmembrane potential, $\Delta\Psi$. The distribution patterns of TMRE in the Cmpt muscle fiber displayed localized structural faults, as shown by the regions lacking TMRE staining (**Figure 5B**, panel b1). Out of 61 cells studied 17 showed defective zones, that is 28%. The areas of mitochondrial defects had uneven sizes but were always localized around the NMJ (**Figure 5B**, panel b2). The defective areas as revealed by TMRE staining occupied on average 26% of the fiber area (**Figure 5D**). To determine whether the observed mitochondrial defects in Cmpt fibers were associated with the NMJ, the mitochondrial lesion and the NMJ were imaged simultaneously by staining living Cmpt muscle fibers with TMRE (**Figure 5B**, b1) and Alexa Fluor 488 conjugated α-bungarotoxin (**Figure 5A**,

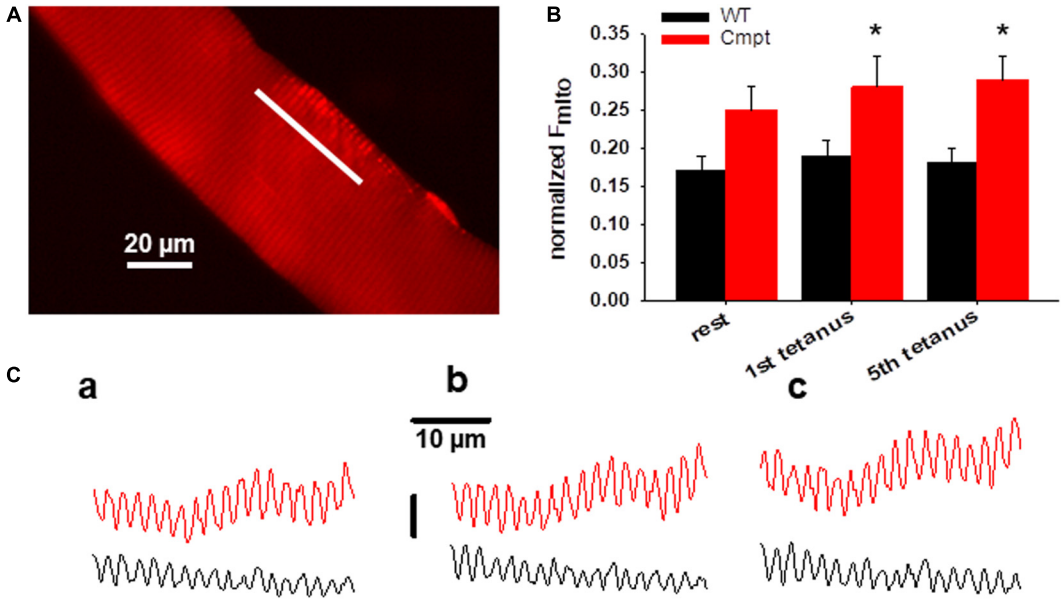

FIGURE 4 | Activity-dependent changes in mitochondrial calcium uptake in single FDB fibers from Cmpt mice. **(A)** Representative image of rhod-2 AM fluorescence in a live Cmpt FDB fiber at rest. **(B)** Average (± SEM) change of normalized mitochondrial fluorescence (F_{mito}) calculated as $(F_{I-band} - F_{A-band})/F_{A-band}$ in WT and Cmpt FDB fibers at rest, following 1, and 5 consecutive tetani (n = 8 cells, N = 3 mice). Note the tendency of mitochondrial calcium accumulation and the higher starting values of the normalized F_{mito} observed in Cmpt. **(C)** Mitochondrial fluorescence measured along the line arbitrarily drawn in parallel with the longitudinal axis of the WT (black) and Cmpt (red) fiber at rest **(a)**, following the first **(b)**, and the fifth consecutive tetanus **(c)**. * denotes significant difference between WT and Cmpt at $p < 0.05$.

a1), a ligand binding to the nicotinic acetylcholine receptors in postsynaptic membranes. Even if the size of area with depolarized mitochondria varied among fibers, this always included the muscle side of the NMJ (**Figure 5A** panel b2, white arrow). This phenotype was never found in the age-matched WT mice.

Individual FDB muscles isolated from WT and Cmpt mice were used for structural studies and explored in electronmicroscopy images. **Figure 5C** panel c1 shows the normal arrangement of triads flanked by mitochondria aligned within the sarcomeric I-band having uniform sizes (indicated by cyan arrows). In cross-section images from the Cmpt muscles (panel c2) enlarged mitochondria were identified invading the sarcomeric A-band (cyan arrows). The analysis of these structures revealed significantly increased perimeter (1.40 ± 0.01 vs 1.45 ± 0.003, $p < 0.05$, for WT and Cmpt, respectively, $n = 635$ vs. $n = 551$; **Figure 5F**) but no differences in the area of the organelles (**Figure 5E**).

Functional Defects of Mitochondria in Cmpt Fibers

Lastly, the functional consequences of the mitochondrial defects were studied applying in parallel confocal live cell imaging and the voltage-clamp technique. First, the cells were loaded with TMRE to identify the fiber segments with depolarized mitochondria (**Figure 6A**, panel a1) and then the cytosolic Ca^{2+} was simultaneously recorded in the normal (n) and defective (d) area (**Figure 6B**). **Figure 6A** panel a3 illustrates a representative image of a voltage-clamped FDB fiber that was loaded with the Ca^{2+}-sensitive dye fluo-8 AM through the glass pipette allowing the precise recording of Ca^{2+} transients in the cytosol. Line-scan images of voltage induced calcium transients were recorded in the two regions (**Figure 6B**) and a comparative analysis of the peak F/F_0 values was performed. Following the application of relatively brief maximal depolarizing pulses (100 ms, +30 mV) smaller calcium transients were observed in regions displaying loss of mitochondrial membrane potential (**Figure 6C**). On average the calculated F/F_0 values from ten cells in the normal and defective areas was 0.92 ± 0.18 vs. 0.74 ± 0.18, $p < 0.05$ (**Figure 6D**).

DISCUSSION

The role of SOCE in maintaining contractile function of skeletal muscle during sustained stimulation has been widely studied and its contribution to SR refilling required for maintained calcium release during prolonged activity, and to fatigue resistance is generally accepted (Allen et al., 2008; Wei-Lapierre et al., 2013; Pan et al., 2014; Boncompagni et al., 2017). In muscle, this type of SOCE occurs with rather slow kinetics (>1 s timescale), and highly depends on the decline of the SR calcium content. Our laboratory has shown earlier that SOCE plays role in maintaining and refilling the intracellular Ca^{2+} stores, not only during repetitive pronlonged tetanic stimulation, but also following fast activation (Sztretye et al., 2017). Recently, a so-called *phasic* mode of SOCE has been demonstrated directly

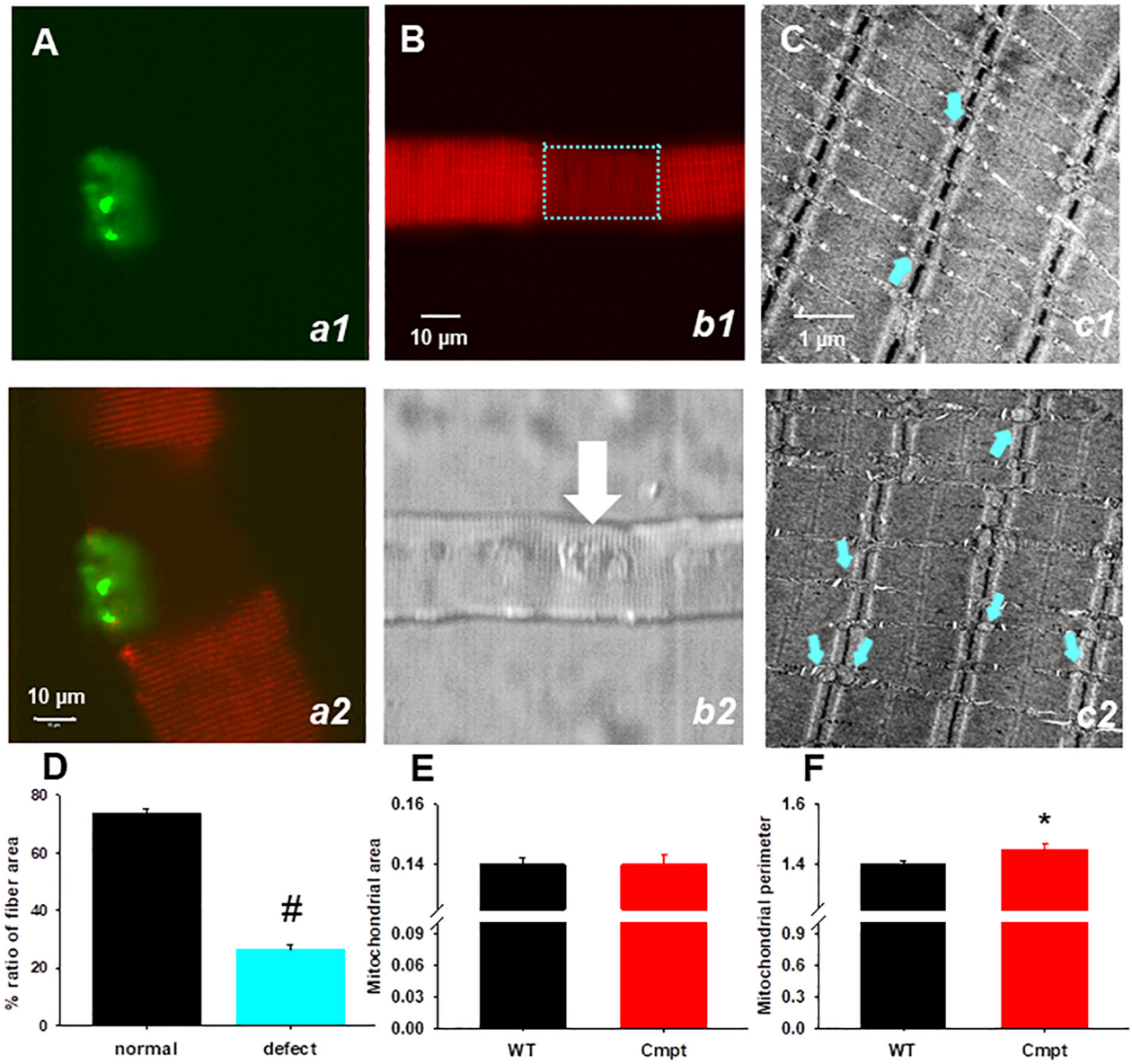

FIGURE 5 | Structural defects of mitochondria in Cmpt fibers. **(A)** FDB live muscle fiber probed with α-bungarotoxin (*panel a1).* Overlay of TMRE (*red*) and α-bungarotoxin images (*green*) of dually stained FDB fiber (*panel a2*). Note that the fiber segment with depolarized mitochondria is overlapped with the NMJ area. **(B)** A segment with depolarized mitochondria is identified in the Cmpt fiber (*panel b1 bracket*) with TMRE staining. The area of mitochondrial defect had variable sizes, but always faced the NMJ (arrow) as suggested by the transmitted light image (*panel b2*) **(C)** Representative electron microscopy images of FDB muscles from 4-month-old WT (*panel c1*) and Cmpt (*panel c2*) fibers. In the WT, mitochondria (*arrows*) aligned within the sarcomeric I band and had uniform sizes. In contrast, Cmpt muscles had enlarged mitochondria (arrows, *panel c2*). Horizontal field width was 4.9 µm, magnification was 30.000x. **(D)** Ratio of fiber area displaying mitochondrial defects (n = 28 fiber, N = 4 mice). # denotes significant difference at $p < 0.001$. **(E)** Mitochondrial area **(E)** and perimeter **(F)** analysis of electron microscopy images similar to those as presented in C revealed no changes in the area but significant increase in perimeter (n = 551 vs. 635, $^*p < 0.05$).

in skeletal muscle fibers, which is activated under physiological conditions, and this rapid activation of SOCE occurs at a millisecond timescale during each action potential (Koenig et al., 2018), requiring just a local depletion of Ca^{2+} in the SR terminal cisternae.

Orai1 is plentifully expressed in neonatal myotubes and mature muscle fibers as well (Stiber et al., 2008; Dirksen, 2009); it is necessary for the activation of SOCE in myotubes since the elimination of calcium influx through Orai1eradicate SOCE (Lyfenko and Dirksen, 2008; Wei-Lapierre et al., 2013). During the Ca^{2+} depletion of the SR endogenous Orai1 colocalizes with STIM1 or STIM1L at the triad junction to form STIM1/1L–Orai1 complexes making the activation of SOCE possible (Darbellay et al., 2011; Pan et al., 2014; Saüc et al., 2015). The colocalization of STIM1L and Orai1 might be a permanent physical pre-formation in the triad, a configuration which is independent of

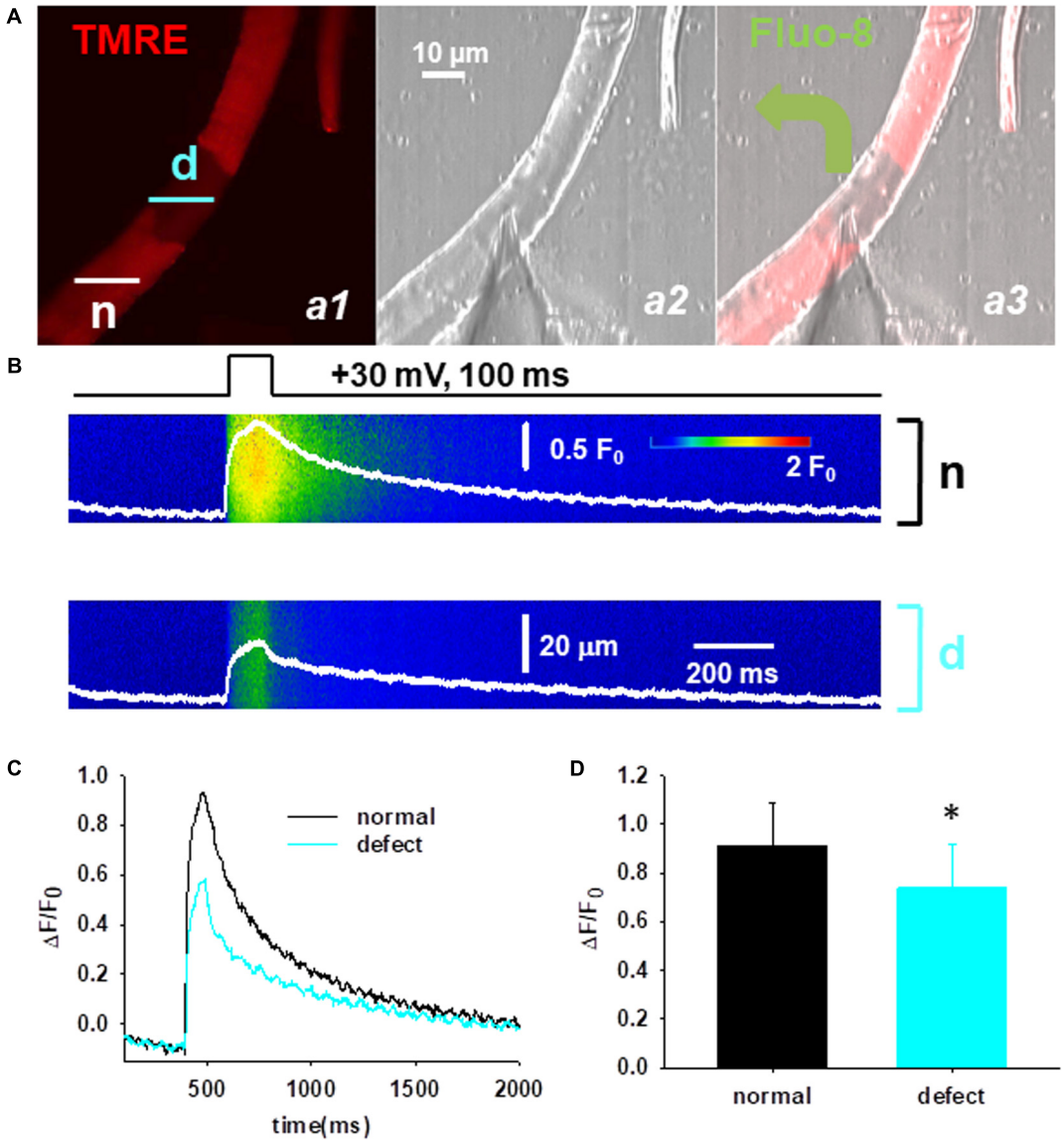

FIGURE 6 | Functional defects of mitochondria in Cmpt fibers. **(A)** Cmpt fibers were first loaded with TMRE to identify the fiber segment with depolarized mitochondria (*panel a1*). n denotes the fiber segment displaying normal mitochondrial membrane potential; d depicts the fiber segment with depolarized or defective mitochondria. The patch pipette was placed at the interface of the regions (*panel a2*). Fluo-8 diffused into the fiber through the pipette (*panel a3*). The pipette solution contained 10 mM EGTA. **(B)** Simultaneous imaging of Ca^{2+} transients of fluo-8 fluorescence in the normal (n) and defective (d) areas during a depolarizing pulse (top). **(C)** Ca^{2+} transients reported by normalized fluo-8 fluorescence changes (F/F_0), in the region with normal mitochondria (*black*), and in the region with depolarized mitochondria (*cyan*). Note the depressed Ca^{2+} transients in the area with defective mitochondria. **(D)** Averaged $\Delta F/F_0$ in the fiber region with or without defective mitochondria (n = 10 cells, N = 3 mice) *$p < 0.05$.

the SR Ca^{2+} content (Edwards et al., 2010; Darbellay et al., 2011; Koenig et al., 2018).

In this work muscle fibers of myostatin deficient Cmpt mice, where reduced expression of both STIM1 and Orai1 proteins has been previously observed, accompanied with lower SOCE activity, SR content and depolarization induced Ca^{2+} release (Sztretye et al., 2017) were examined.

The results presented here on the effects of manipulation of Orai1 expression in skeletal muscle fibers on SOCE activity might seem contradictory at first sight. The reconstruction of Orai1 with venus-Orai1 via *in vivo* electroporation in Cmpt fibers resulted in an expression level similar to wild type. Nevertheless, SOCE activity at a long timescale has not been affected by the increased levels of Orai1 in reconstructed fibers. The applied protocol for pharmacological depletion of SR did not reveal any significant difference between the magnitudes of the induced, slowly activated SOCE. The depolarization-induced calcium transients were also unaltered. At the same time, in the fibers where endogenous Orai1 has been silenced with shRNA, this type of SOCE has been hindered whereas the peak F/F_0 of

calcium transients evoked by membrane depolarization were not statistically different from WT. These latter observations are in accordance with data published on isolated fibers from inducible, muscle-specific Orai1 knockout mice (Carrell et al., 2016), where this mode of SOCE was absent. That is, the acute overexpression of Orai1 does not lead to assembly of functional STIM1/Orai1 complexes in Cmpt fibers.

On the other hand, reconstructing the Cmpt fibers with venus-Orai1 resettle the Ca^{2+} fluxes through Orai1 channels (more precisely, through the surface membrane Ca^{2+} channels, which we believe to be represented by Orai1 channels) to the levels measured in WT fibers, while in fibers, where Orai1 has been silenced, no significant alterations of Ca^{2+} fluxes have been detected. This phenomenon could be explained by the assumption of two pools of Orai1 channels (as in case of STIM1, however, no structural differences are presumed). One pool is located within the triad in a pre-assembled formation with STIM1L and is responsible for the rapid activation of SOCE in the nanodomain of the junctional membrane, adjacent to the RyR1s, during an action potential (*phasic* SOCE). Because of their occurrence in pairs with STIM1, we refer to this pool as "mated" Orai1 channels. The other pool is distributed along the t-tubule membrane randomly (not necessarily in the transverse t-tubules, where phasic SOCE takes place (Cully et al., 2017), but in longitudinal t-tubules as well). These channels are supposed to be devoid of STIM1 partners in a preset manner, thus we use the term "solitary" for these Orai1 channels. In case of different turnover of these two sets of Orai1 channels (for example because of the limited access to them in the crowded triadic junction, or the diverse composition of the neighboring membrane compartments), the manipulations targeting changes in Orai1 expression could have different impact on them. Our observations imply that electroporation of the venus-Orai1 in the Cmpt muscles has concerned mainly the "mated" pool, since the slowly activating SOCE activity induced by SR depletion in which the "solitary" Orai1 pool is involved remains essentially unaltered. That is, further functional STIM1/Orai1 complexes has not been formed via the slow rearrangement of "solitary" Orai1 to couple with STIM1, while the Ca^{2+} fluxes through the Orai1 channels (estimated by the K1 parameter) increased significantly as compared to untreated Cmpt fibers, denoting an increased number of "mated" Orai1 channels. Acute depletion of Orai1 channels in wild type muscles eventuates in a different response, indicating that the "solitary" pool of Orai1 has been concerned. In these fibers slow SOCE has been abolished almost completely which might reflect to a reduced "solitary" Orai1 pool, however, the K1 parameter has been found to be similar as in WT, that is, the "mated" Orai1 pool has been untouched.

Mitochondria are known to contribute to the activity of SOCE, thus having many roles in the activation, maintenance, and termination of this Ca^{2+} entry pathway (Parekh and Putney, 2005; Parekh, 2008; Demaurex et al., 2009). More recent data by Deak et al., 2014 clearly confirmed the importance of mitochondrial Ca^{2+} for proper SOCE activity. Although the mechanism termed *trans*-mitochondrial Ca^{2+} flux seems very important in regulating SOCE (Malli et al., 2003; Feldman et al., 2010), the precise molecular mechanisms by which mitochondria controls SOCE are still unclear (Malli and Graier, 2017).

At least two different but interrelated molecular mechanisms have been proposed to account for this interaction: i) mitochondria support SOCE activity through their ability to buffer and release Ca^{2+} (Abramov et al., 2007; Parekh, 2008; Demaurex et al., 2009), and ii) mitochondria control SOCE via small metabolites such as pyruvate or ATP, which can either assist the SR Ca^{2+} refilling or prevent the Ca^{2+}-dependent inactivation of I_{CRAC} (Montalvo et al., 2006; Demaurex et al., 2009). Although this study did not encompass the above mentioned second mechanism, the analysis of the activity-dependent calcium uptake of the mitochondrial network presented here suggests that the former mechanism in Cmpt fibers is not compromised; rather it is enhanced as underlined by our calcium uptake experiments (**Figure 4**). This could, partially, explain the lower global cytosolic calcium transients seen in Cmpt mice (see **Figure 2D** black and red columns).

Increased mitochondrial calcium uptake would then accelerate mitochondrial metabolism resulting in reactive oxygen species (ROS) production (Hempel and Trebak, 2017). While the low level of ROS in the mitochondria acts as an essential signaling molecule regulating several physiological process (D'Autréaux and Toledano, 2007), long term and uncontrolled production of ROS can place the cell under oxidative stress. In skeletal muscle, however, the anomalous ROS production is considered to initiate an intriguing interplay between ROS and Ca^{2+} signaling (Cully and Rodney, 2020). ROS promotes the release of Ca^{2+} from the SR via RyR1 (Marks et al., 2009). The released Ca^{2+} might further amplify the rate of ROS production, establishing a positive feed-back loop of Ca^{2+} and ROS signals leading finally, to disrupted calcium signaling. On the other hand, lower ROS production is associated with decreased RyR1 activity which again manifests in smaller depolarization-induced Ca^{2+} transients.

Altered mitochondrial dynamics are also connected to various neurodegenerative disorders (Zhou et al., 2019). Improper mitochondrial activity participates in neuromuscular relapse in a mouse model of amyotrophic lateral sclerosis (ALS) (Zhou et al., 2010). Mitochondria at the NMJ face display elevated local cytosolic [Ca^{2+}] and thereby become depolarized (Zhou et al., 2010). The elevated cytosolic [Ca^{2+}] may also decrease mitochondrial motility and promote mitochondrial fragmentation (Yi et al., 2004; Saotome et al., 2008), which could dampen the recovering capacity of damaged mitochondria. In contrast to our current observations on Cmpt mice, the reduced mitochondrial Ca^{2+} uptake led to cytosolic Ca^{2+} hyperactivity at the site of NMJ in muscle fibers of the G93A mouse model of ALS (Yi et al., 2011). The authors explained that the increased cytosolic amplitude of depolarization-induced Ca^{2+} transients could indicate reduced Ca^{2+} capacity of the depolarized mitochondrial region; hence the reduced Ca^{2+} uptake of the mitochondria led to hyperactive cytosolic Ca^{2+} transients.

Interestingly, it was shown that mitofusin 2 (an ER to mitochondria tethering protein) (De Brito and Scorrano, 2008;

Ainbinder et al., 2015), corrupts STIM1 trafficking upon ER Ca^{2+} depletion independently from mitochondrial Ca^{2+} handling when mitochondria are completely depolarized (Singaravelu et al., 2011). Filadi et al. (2015) showed that cells lacking mitofusin 2 have decreased expression levels of the mitochondrial calcium uniporter (MCU) which could explain the reduced mitochondrial Ca^{2+} signals they encountered. Albeit the role of mitofusin 2 and MCU were not explored in our study, this could be a possible explanation for the decrease in the amplitude of the calcium transients in the areas presenting local defects in mitochondrial $\Delta\Psi$. Another possibility that would explain this phenomenon could be due to alterations in ROS generation in the defective cell regions.

DATA AVAILABILITY STATEMENT

The raw data supporting the conclusions of this article will be made available by the authors, without undue reservation.

ETHICS STATEMENT

The animal study was reviewed and approved by Animal Care Committee of the University of Debrecen.

AUTHOR CONTRIBUTIONS

MS, BD, IB, PS, and LC wrote the manuscript, contributed to discussion and reviewed and edited the manuscript. MS, ZS, and BD did *in vitro* calcium experiments. NB did the Western Blot experiments. GK did the electron microscopy. MS, PS, ZS, ÁA, and NB analyzed the data. MS and PS did the statistical analysis. All authors contributed to discussion, laboratory support, and reviewed/edited the manuscript.

FUNDING

MS was a recipient of János Bolyai Research Scholarship of the Hungarian Academy of Sciences and was supported by NKFIH PD-108476 and PD-128370 grants of the Hungarian National Research, Development and Innovation Office (Hungary). The work was supported by the GINOP-2.3.2-15-2016-00044 project.

ACKNOWLEDGMENTS

We thank R. Őri for their excellent technical assistance.

SUPPLEMENTARY MATERIAL

The Supplementary Material for this article can be found online at: https://www.frontiersin.org/articles/10.3389/fphys.2020.601090/full#supplementary-material

Supplementary Figure1 | (A) Confocal image of an isolated Cmpt FDB fiber where endogenous Orai1 was labeled with an Alexa-Fluor-488 conjugated antibody. **(B)** Western blot analysis performed on whole FDB muscle homogenates obtained from two Cmpt mice injected with either vehicle or the venus-Orai1 construct. Vinculin was used as an internal control. **(C)** Densitometric analysis of the gel presented in panel B. Note that we were unable to detect an increase in the expression at the molecular weight where Orai1 protein is expected in control animals (∼50 kDa). In fact, we were unable to detect any band at the predicted molecular weight of the venus-Orai1 fusion protein (∼75 kDa). We can only reconcile these results if we assume that our monoclonal antibody is unable to recognize the venus-Orai1 fusion protein due to modification of the epitope that the antibody recognizes.

Supplementary Figure 2 | Representative SOCE measurements carried out on **(A)** Cmpt+venus-Orai1 and **(B)** WT+shRNA electroporated FDB fibers, respectively. Experimental protocol was identical as presented in **Figure 1E**.

Supplementary Table 1 | The compiled list of individual cells examined during the SOCE measurements. P1: cocktail induced SR calcium transient; P2: SR depletion activated SOCE transient. Highlighted data correspond to the traces presented in **Figure 1E** and **Supplementary Figures 2A,B**.

REFERENCES

Abramov, A. Y., Fraley, C., Diao, C. T., Winkfein, R., Colicos, M. A., Duchen, M. R., et al. (2007). Targeted polyphosphatase expression alters mitochondrial metabolism and inhibits calcium-dependent cell death. *Proc. Natl. Acad. Sci. U.S.A.* 104, 18091–18096. doi: 10.1073/pnas.0708959104

Ainbinder, A., Boncompagni, S., Protasi, F., and Dirksen, R. T. (2015). Role of Mitofusin-2 in mitochondrial localization and calcium uptake in skeletal muscle. *Cell Calcium* 57, 14–24. doi: 10.1016/j.ceca.2014.11.002

Allen, D. G., Lamb, G. D., and Westerblad, H. (2008). Skeletal muscle fatigue: cellular mechanisms. *Physiol. Rev.* 88, 287–332. doi: 10.1152/physrev.00015.2007

Böhm, J., Chevessier, F., De Paula, A. M., Koch, C., Attarian, S., Feger, C., et al. (2013). Constitutive activation of the calcium sensor STIM1 causes tubular-aggregate myopathy. *Am. J. Hum. Genet.* 92, 271–278. doi: 10.1016/j.ajhg.2012.12.007

Boncompagni, S., Michelucci, A., Pietrangelo, L., Dirksen, R. T., and Protasi, F. (2017). Exercise-dependent formation of new junctions that promote STIM1-Orai1 assembly in skeletal muscle. *Sci. Rep.* 7:14286. doi: 10.1038/s41598-017-14134-0

Carrell, E. M., Coppola, A. R., McBride, H. J., and Dirksen, R. T. (2016). Orai1 enhances muscle endurance by promoting fatigue-resistant type I fiber content but not through acute store-operated Ca2+ entry. *FASEB J.* 30, 4109–4119. doi: 10.1096/fj.201600621R

Cully, T. R., Edwards, J. N., Friedrich, O., George Stephenson, D., Murphy, R. M., and Launikonis, B. S. (2012). Changes in plasma membrane Ca-ATPase and stromal interacting molecule 1 expression levels for Ca2+ signaling in dystrophic mdx mouse muscle. *Am. J. Physiol. Cell Physiol.* 303, 567–576. doi: 10.1152/ajpcell.00144.2012

Cully, T. R., Murphy, R. M., Roberts, L., Raastad, T., Fassett, R. G., Coombes, J. S., et al. (2017). Human skeletal muscle plasmalemma alters its structure to change its Ca2+-handling following heavy-load resistance exercise. *Nat. Commun.* 8:14266. doi: 10.1038/ncomms14266

Cully, T. R., and Rodney, G. G. (2020). Nox4 – RyR1 – Nox2: regulators of micro-domain signaling in skeletal muscle. *Redox Biol.* 36:101557. doi: 10.1016/j.redox.2020.101557

Darbellay, B., Arnaudeau, S., Bader, C. R., Konig, S., and Bernheim, L. (2011). STIM1L is a new actin-binding splice variant involved in fast repetitive Ca 2+ release. *J. Cell Biol.* 194, 335–346. doi: 10.1083/jcb.201012157

Darbellay, B., Arnaudeau, S., König, S., Jousset, H., Bader, C., Demaurex, N., et al. (2009). STIM1- and Orai1-dependent store-operated calcium entry regulates

human myoblast differentiation. *J. Biol. Chem.* 284, 5370–5380. doi: 10.1074/jbc.M806726200

D'Autréaux, B., and Toledano, M. B. (2007). ROS as signalling molecules: mechanisms that generate specificity in ROS homeostasis. *Nat. Rev. Mol. Cell Biol.* 8, 813–824. doi: 10.1038/nrm2256

De Brito, O. M., and Scorrano, L. (2008). Mitofusin 2 tethers endoplasmic reticulum to mitochondria. *Nature* 456, 605–610. doi: 10.1038/nature07534

Deak, A. T., Blass, S., Khan, M. J., Groschner, L. N., Waldeck-Weiermair, M., Hallström, S., et al. (2014). IP3-mediated STIM1 oligomerization requires intact mitochondrial Ca2+ uptake. *J. Cell Sci.* 127, 2944–2955. doi: 10.1242/jcs.149807

Demaurex, N., Poburko, D., and Frieden, M. (2009). Regulation of plasma membrane calcium fluxes by mitochondria. *Biochim. Biophys. Acta Bioenerg.* 1787, 1383–1394. doi: 10.1016/j.bbabio.2008.12.012

Desai, P. N., Zhang, X., Wu, S., Janoshazi, A., Bolimuntha, S., Putney, J. W., et al. (2015). Multiple types of calcium channels arising from alternative translation initiation of the Orai1 message. *Sci. Signal.* 8:ra74. doi: 10.1126/scisignal.aaa8323

Dirksen, R. T. (2009). Checking your SOCCs and feet: the molecular mechanisms of Ca2+ entry in skeletal muscle. *J. Physiol.* 587, 3139–3147. doi: 10.1113/jphysiol.2009.172148

Edwards, J. N., Friedrich, O., Cully, T. R., Von Wegner, F., Murphy, R. M., and Launikonis, B. S. (2010). Upregulation of store-operated Ca2+ entry in dystrophic mdx mouse muscle. *Am. J. Physiol. Cell Physiol.* 299, 42–50. doi: 10.1152/ajpcell.00524.2009

Feldman, B., Fedida-Metula, S., Nita, J., Sekler, I., and Fishman, D. (2010). Coupling of mitochondria to store-operated Ca2+-signaling sustains constitutive activation of protein kinase B/Akt and augments survival of malignant melanoma cells. *Cell Calcium* 47, 525–537. doi: 10.1016/j.ceca.2010.05.002

Filadi, R., Greotti, E., Turacchio, G., Luini, A., Pozzan, T., and Pizzo, P. (2015). Mitofusin 2 ablation increases endoplasmic reticulum-mitochondria coupling. *Proc. Natl. Acad. Sci. U.S.A.* 112, E2174–E2181. doi: 10.1073/pnas.1504880112

Fodor, J., Gönczi, M., Sztretye, M., Dienes, B., Oláh, T., Szabó, L., et al. (2008). Altered expression of triadin 95 causes parallel changes in localized Ca2+ release events and global Ca2+ signals in skeletal muscle cells in culture. *J. Physiol.* 586, 5803–5818. doi: 10.1113/jphysiol.2008.160457

Franzini-Armstrong, C. (2018). The relationship between form and function throughout the history of excitation-contraction coupling. *J. Gen. Physiol.* 150:369. doi: 10.1085/jgp.20171188901162018c

Hempel, N., and Trebak, M. (2017). Crosstalk between calcium and reactive oxygen species signaling in cancer. *Cell Calcium* 63, 70–96. doi: 10.1016/j.ceca.2017.01.007

Koenig, X., Choi, R. H., and Launikonis, B. S. (2018). Store-operated Ca2+ entry is activated by every action potential in skeletal muscle. *Commun. Biol.* 1:31. doi: 10.1038/s42003-018-0033-7

Koenig, X., Choi, R. H., Schicker, K., Singh, D. P., Hilber, K., and Launikonis, B. S. (2019). Mechanistic insights into store-operated Ca 2+ entry during excitation-contraction coupling in skeletal muscle. *Biochim. Biophys. Acta Mol. Cell Res.* 1866, 1239–1248. doi: 10.1016/j.bbamcr.2019.02.014

Kurebayashi, N., and Ogawa, Y. (2001). Depletion of Ca2+ in the sarcoplasmic reticulum stimulates Ca2+ entry into mouse skeletal muscle fibres. *J. Physiol.* 533, 185–199. doi: 10.1111/j.1469-7793.2001.0185b.x

Li, T., Finch, E. A., Graham, V., Zhang, Z.-S., Ding, J.-D., Burch, J., et al. (2012). STIM1-Ca2+ signaling is required for the hypertrophic growth of skeletal muscle in mice. *Mol. Cell. Biol.* 32, 3009–3017. doi: 10.1128/mcb.06599-11

Lyfenko, A. D., and Dirksen, R. T. (2008). Differential dependence of store-operated and excitation-coupled Ca2+ entry in skeletal muscle on STIM1 and Orai1. *J. Physiol.* 586, 4815–4824. doi: 10.1113/jphysiol.2008.160481

Malli, R., Frieden, M., Osibow, K., Zoratti, C., Mayer, M., Demaurex, N., et al. (2003). Sustained Ca2+ transfer across mitochondria is essential for mitochondrial Ca2+ buffering. Store-operated Ca2+ entry, and Ca2+ store refilling. *J. Biol. Chem.* 278, 44769–44779. doi: 10.1074/jbc.M302511200

Malli, R., and Graier, W. F. (2017). *Store-Operated Ca^{2+} Entry (SOCE) Pathways*, Vol. 993. Cham: Springer International Publishing, 297–319. doi: 10.1007/978-3-319-57732-6

Marks, A., Vianna, D. M. L., and Carrive, P. (2009). Nonshivering thermogenesis without interscapular brown adipose tissue involvement during conditioned fear in the rat. *Am. J. Physiol. Regul. Integr. Comp. Physiol.* 296, 1239–1247. doi: 10.1152/ajpregu.90723.2008

McCarl, C. A., Picard, C., Khalil, S., Kawasaki, T., Röther, J., Papolos, A., et al. (2009). ORAI1 deficiency and lack of store-operated Ca2+ entry cause immunodeficiency, myopathy, and ectodermal dysplasia. *J. Allergy Clin. Immunol.* 124, 1311–1318. doi: 10.1016/j.jaci.2009.10.007

Montalvo, G. B., Artalejo, A. R., and Gilabert, J. A. (2006). ATP from subplasmalemmal mitochondria controls Ca2+-dependent inactivation of CRAC channels. *J. Biol. Chem.* 281, 35616–35623. doi: 10.1074/jbc.M603518200

Onopiuk, M., Brutkowski, W., Young, C., Krasowska, E., Róg, J., Ritso, M., et al. (2015). Store-operated calcium entry contributes to abnormal Ca2+ signalling in dystrophic mdx mouse myoblasts. *Arch. Biochem. Biophys.* 569, 1–9. doi: 10.1016/j.abb.2015.01.025

Pan, Z., Brotto, M., and Ma, J. (2014). Store-operated Ca2+ entry in muscle physiology and diseases. *BMB Rep.* 47, 69–79. doi: 10.5483/BMBRep.2014.47.2.015

Parekh, A. B. (2008). Ca2+ microdomains near plasma membrane Ca2+ channels: impact on cell function. *J. Physiol.* 586, 3043–3054. doi: 10.1113/jphysiol.2008.153460

Parekh, A. B., and Putney, J. W. (2005). Store-operated calcium channels. *Physiol. Rev.* 85, 757–810. doi: 10.1152/physrev.00057.2003

Porter, C., and Wall, B. T. (2012). Skeletal muscle mitochondrial function: is it quality or quantity that makes the difference in insulin resistance? *J. Physiol.* 590, 5935–5936. doi: 10.1113/jphysiol.2012.241083

Protasi, F., Pietrangelo, L., and Boncompagni, S. (2020). Calcium entry units (CEUs): perspectives in skeletal muscle function and disease. *J. Muscle Res. Cell Motil.* doi: 10.1007/s10974-020-09586-3 [Epub ahead of print].

Royer, L., Sztretye, M., Manno, C., Pouvreau, S., Zhou, J., Knollmann, B. C., et al. (2010). Paradoxical buffering of calcium by calsequestrin demonstrated for the calcium store of skeletal muscle. *J. Gen. Physiol.* 136, 325–338. doi: 10.1085/jgp.201010454

Saotome, M., Safiulina, D., Szabadkai, G., Das, S., Fransson, Å, Aspenstrom, P., et al. (2008). Bidirectional Ca2+-dependent control of mitochondrial dynamics by the Miro GTPase. *Proc. Natl. Acad. Sci. U.S.A.* 105, 20728–20733. doi: 10.1073/pnas.0808953105

Saüc, S., Bulla, M., Nunes, P., Orci, L., Marchetti, A., Antigny, F., et al. (2015). STIM1L traps and gates Orai1 channels without remodeling the cortical ER. *J. Cell Sci.* 128, 1568–1579. doi: 10.1242/jcs.164228

Singaravelu, K., Nelson, C., Bakowski, D., De Brito, O. M., Ng, S. W., Di Capite, J., et al. (2011). Mitofusin 2 regulates STIM1 migration from the Ca2+ store to the plasma membrane in cells with depolarized mitochondria. *J. Biol. Chem.* 286, 12189–12201. doi: 10.1074/jbc.M110.174029

Stiber, J., Hawkins, A., Zhang, Z. S., Wang, S., Burch, J., Graham, V., et al. (2008). STIM1 signalling controls store-operated calcium entry required for development and contractile function in skeletal muscle. *Nat. Cell Biol.* 10, 688–697. doi: 10.1038/ncb1731

Stiber, J. A., and Rosenberg, P. B. (2011). The role of store-operated calcium influx in skeletal muscle signaling. *Cell Calcium* 49, 341–349. doi: 10.1016/j.ceca.2010.11.012

Szabó, G., Dallmann, G., Müller, G., Patthy, L., Soller, M., and Varga, L. (1998). A deletion in the myostatin gene causes the compact (Cmpt) hypermuscular mutation in mice. *Mamm. Genome* 9, 671–672. doi: 10.1007/s003359900843

Szentesi, P., Jacquemond, V., Kovács, L., and Csernoch, L. (1997). Intramembrane charge movement and sarcoplasmic calcium release in enzymatically isolated mammalian skeletal muscle fibres. *J. Physiol.* 505, 371–384. doi: 10.1111/j.1469-7793.1997.371bb.x

Sztretye, M., Geyer, N., Vincze, J., Al-Gaadi, D., Oláh, T., Szentesi, P., et al. (2017). SOCE is important for maintaining sarcoplasmic calcium content and release in skeletal muscle fibers. *Biophys. J.* 113, 2496–2507. doi: 10.1016/j.bpj.2017.09.023

Sztretye, M., Singlár, Z., Szabó, L., Angyal, Á, Balogh, N., Vakilzadeh, F., et al. (2020). Improved tetanic force and mitochondrial calcium homeostasis by astaxanthin treatment in mouse skeletal muscle. *Antioxidants* 9:98. doi: 10.3390/antiox9020098

Sztretye, M., Yi, J., Figueroa, L., Zhou, J., Royer, L., and Ríos, E. (2011). D4cpv-calsequestrin: a sensitive ratiometric biosensor accurately targeted to the

calcium store of skeletal muscle. *J. Gen. Physiol.* 138, 211–229. doi: 10.1085/jgp.201010591

Vaeth, M., Maus, M., Klein-Hessling, S., Freinkman, E., Yang, J., Eckstein, M., et al. (2017). Store-operated Ca2+ entry controls clonal expansion of T cells through metabolic reprogramming. *Immunity* 47, 664–679.e6. doi: 10.1016/j.immuni.2017.09.003

Wei-Lapierre, L., Carrell, E. M., Boncompagni, S., Protasi, F., and Dirksen, R. T. (2013). Orai1-dependent calcium entry promotes skeletal muscle growth and limits fatigue. *Nat. Commun.* 4:2805. doi: 10.1038/ncomms3805

Yi, J., Ma, C., Li, Y., Weisleder, N., Ríos, E., Ma, J., et al. (2011). Mitochondrial calcium uptake regulates rapid calcium transients in skeletal muscle during excitation-contraction (E-C) coupling. *J. Biol. Chem.* 286, 32436–32443. doi: 10.1074/jbc.M110.217711

Yi, M., Weaver, D., and Hajnóczky, G. (2004). Control of mitochondrial motility and distribution by the calcium signal: a homeostatic circuit. *J. Cell Biol.* 167, 661–672. doi: 10.1083/jcb.200406038

Zhao, X., Moloughney, J. G., Zhang, S., Komazaki, S., and Weisleder, N. (2012). Orai1 mediates exacerbated Ca2+ entry in dystrophic skeletal muscle. *PLoS One* 7:e49862. doi: 10.1371/journal.pone.0049862

Zhou, J., Li, A., Li, X., and Yi, J. (2019). Dysregulated mitochondrial Ca 2+ and ROS signaling in skeletal muscle of ALS mouse model. *Arch. Biochem. Biophys.* 663, 249–258. doi: 10.1016/j.abb.2019.01.024

Zhou, J., Yi, J., Fu, R., Liu, E., Siddique, T., Rios, E., et al. (2010). Hyperactive intracellular calcium signaling associated with localized mitochondrial defects in skeletal muscle of an animal model of amyotrophic lateral sclerosis. *J. Biol. Chem.* 285, 705–712. doi: 10.1074/jbc.M109.041319

Conflict of Interest: The authors declare that the research was conducted in the absence of any commercial or financial relationships that could be construed as a potential conflict of interest.

frontiers in Physiology

ORIGINAL RESEARCH
published: 05 January 2021
doi: 10.3389/fphys.2020.601057

Long-Term Exercise Reduces Formation of Tubular Aggregates and Promotes Maintenance of Ca^{2+} Entry Units in Aged Muscle

Simona Boncompagni[1,2], Claudia Pecorai[1,3], Antonio Michelucci[1,3], Laura Pietrangelo[1,3] and Feliciano Protasi[1,3]*

[1] Center for Advanced Studies and Technology (CAST), University G. d'Annunzio (Ud'A) of Chieti-Pescara, Chieti, Italy, [2] Department of Neuroscience, Imaging and Clinical Sciences (DNICS), University G. d'Annunzio (Ud'A) of Chieti-Pescara, Chieti, Italy, [3] Department of Medicine and Aging Sciences (DMSI), University G. d'Annunzio (Ud'A) of Chieti-Pescara, Chieti, Italy

Tubular aggregates (TAs) in skeletal muscle fibers are unusual accumulation of sarcoplasmic reticulum (SR) tubes that are found in different disorders including TA myopathy (TAM). TAM is a muscular disease characterized by muscle pain, cramping, and weakness that has been recently linked to mutations in *STIM1* and *ORAI1.* STIM1 and ORAI1 are the two main proteins mediating store-operated Ca^{2+} entry (SOCE), a mechanism activated by depletion of intracellular Ca^{2+} stores (e.g., SR) that allows recovery of Ca^{2+} from the extracellular space during repetitive muscle activity. We have recently shown that exercise triggers the formation of unique intracellular junctions between SR and transverse tubules named *Ca^{2+} entry units* (CEUs). CEUs promote colocalization of STIM1 with ORAI1 and improve muscle function in presence of external Ca^{2+}. TAs virtually identical to those of TAM patients are also found in fast-twitch fibers of aging male mice. Here, we used a combination of electron and confocal microscopy, Western blotting, and *ex vivo* stimulation protocols (in presence or absence of external Ca^{2+}) to evaluate the presence of TAs, STIM1-ORAI1 localization and expression and fatigue resistance of intact extensor digitorum longus (EDL) muscles in wild-type male adult (4-month-old) and aged (24-month-old) mice and in mice trained in wheel cages for 15 months (from 9 to 24 months of age). The results collected indicate that (i) aging causes STIM1 and ORAI1 to accumulate in TAs and (ii) long-term exercise significantly reduced formation of TAs. In addition, (iii) EDL muscles from aged mice exhibited a faster decay of contractile force than adult muscles, likely caused by their inability to refill intracellular Ca^{2+} stores, and (iv) exercise in wheel cages restored the capability of aged EDL muscles to use external Ca^{2+} by promoting maintenance of CEUs. In conclusion, exercise prevented improper accumulation of STIM1 and ORAI1 in TAs during aging, maintaining the capability of aged muscle to refill intracellular Ca^{2+} stores *via* SOCE.

Keywords: sarcoplasmic reticulum, transverse tubule, excitation-contraction coupling, electron microscopy, store opereted calcium entry

Abbreviations: Ca^{2+}, calcium; CEU, Ca^{2+} entry unit; CM, confocal microscopy; CRU, Ca^{2+} release unit; EDL, extensor digitorum longus; EC coupling, excitation-contraction coupling; EM, electron microscopy; RYR1, ryanodine receptor type 1; SERCA, sarco/endoplasmic reticulum ATPase; SOCE, store-operated Ca^{2+} entry; SR, sarcoplasmic reticulum; STIM1, stromal interaction molecule-1; TA, tubular aggregate; TAM, TA myopathy; TT, transverse tubule; WT, wild type.

OPEN ACCESS

Edited by:
Enrique Jaimovich, University of Chile, Chile

Reviewed by:
Peter Szentesi, University of Debrecen, Hungary
Paul D. Allen, University of Leeds, United Kingdom

****Correspondence:***
Simona Boncompagni
simona.boncompagni@unich.it

Specialty section:
This article was submitted to Striated Muscle Physiology, a section of the journal Frontiers in Physiology

Received: *31 August 2020*
Accepted: *16 November 2020*
Published: *05 January 2021*

Citation:
Boncompagni S, Pecorai C, Michelucci A, Pietrangelo L and Protasi F (2021) Long-Term Exercise Reduces Formation of Tubular Aggregates and Promotes Maintenance of Ca^{2+} Entry Units in Aged Muscle. Front. Physiol. 11:601057. doi: 10.3389/fphys.2020.601057

INTRODUCTION

The sarcoplasmic reticulum (SR) is a highly organized system of membranes that functions as the main intracellular calcium (Ca^{2+}) storage of skeletal muscle (Franzini-Armstrong, 1980; Boncompagni et al., 2020). In adult muscle fibers, the SR is composed of two distinct compartments in direct continuity with each other: the SR terminal cisternae or junctional SR (jSR) and the longitudinal SR (lSR) (Franzini-Armstrong, 1984). Among other few important proteins, the jSR contains ryanodine receptors (RYRs), large proteins that constitute Ca^{2+} release channels (Franzini-Armstrong and Protasi, 1997) and calsequestrin (CASQ), a protein that accumulates Ca^{2+} in proximity of release sites (Saito et al., 1984; Franzini-Armstrong et al., 1987). The jSR is tightly associated with transverse tubules (TTs) to form triads, also known as Ca^{2+} release units (CRUs). In adult mammalian skeletal muscle fibers, CRUs are placed in proximity of the A-I band transition of relaxed sarcomeres and contain the macromolecular complex that mediates excitation–contraction (EC) coupling (Schneider and Chandler, 1973; Schneider, 1994; Franzini-Armstrong and Protasi, 1997). EC coupling is the mechanism that translates the action potential carried in the fiber interior by TTs into Ca^{2+} release through RYRs. On the other hand, the lSR membranes are enriched in sarco/endoplasmic reticulum Ca^{2+} ATPases (SERCAs), which rapidly remove cytosolic Ca^{2+} released by RYRs during EC coupling to replenish SR lumen after each contraction (Inui and Fleischer, 1988). lSR extends on both sides of the terminal cisternae and thus may be placed either next to A or to I bands.

Tubular aggregates (TAs) are abnormal and extensive accumulation of ordered and tightly packed SR tubes, first described in 1970 by Engel and colleagues in muscle biopsies from dyskalemic patients (Engel et al., 1970). TAs are also found in other human muscle disorders, such as periodic paralysis or myotonic disorders (De Groot and Arts, 1982; Pierobon-Bormioli et al., 1985; Rosenberg et al., 1985; Morgan-Hughes, 1998; Vissing et al., 1999) and constitute a constant histopathological feature in TA myopathy (TAM), a relatively rare disorder linked to gain-of-function mutations in both the stromal-interacting molecule-1 (STIM1) SR Ca^{2+} sensor and the ORAI1 Ca^{2+} release–activated Ca^{2+} channel of the plasma membrane (Bohm et al., 2013, 2014, 2017; Nesin et al., 2014; Endo et al., 2015; Walter et al., 2015; Lee and Noguchi, 2016; Okuma et al., 2016).

First discovered in non-excitable cells, STIM1 and ORAI1 are the two main players that coordinate store-operated Ca^{2+} entry (SOCE) (Liou et al., 2005; Roos et al., 2005; Feske et al., 2006; Vig et al., 2006). SOCE is a ubiquitous Ca^{2+} influx mechanism triggered by reduction of Ca^{2+} levels in the lumen of intracellular Ca^{2+} stores (Putney, 1986, 2011a,b; Parekh et al., 1997). Also expressed in skeletal muscle (Kurebayashi and Ogawa, 2001; Lyfenko and Dirksen, 2008), STIM1/ORAI1-dependent SOCE is important in limiting fatigue during repetitive high-frequency stimulation (Zhao et al., 2005; Wei-Lapierre et al., 2013; Boncompagni et al., 2017; Michelucci et al., 2019 and 2020). Altered SOCE has been associated to muscle dysfunction in various myopathies (Pan et al., 2014; Michelucci et al., 2018). Importantly, it has been reported that a reduction in SOCE activity contributes to altered muscle function during aging (Zhao et al., 2008; Brotto, 2011; Thornton et al., 2011).

Under resting conditions in muscle, ORAI1 is located within the TT system, whereas STIM1 is mainly positioned throughout the lSR at the I band region of the sarcomere (Wei-Lapierre et al., 2013; Carrell et al., 2016; Boncompagni et al., 2017). We have recently shown that, in extensor digitorum longus (EDL) muscle fibers from adult wild-type (WT) mice, acute exercise drives the formation of Ca^{2+} entry units (CEUs), new intracellular junctions between stacks of lSR membranes, and TT extensions within the I band that contain colocalized STIM1 and ORAI1 (Boncompagni et al., 2017, 2018; Protasi et al., 2020). Interestingly, CEUs are constitutively assembled in fibers of mice lacking CASQ1, which undergoes severe Ca^{2+} depletion during repetitive high-frequency stimulation (Michelucci et al., 2020). The presence of these junctions correlates to (a) enhanced resistance to fatigue in presence of extracellular Ca^{2+} (Boncompagni et al., 2017) and (b) increased Ca^{2+} influx *via* SOCE (Michelucci et al., 2019, 2020).

Besides being found in muscle disorders, TAs have been also described during aging in EDL muscles from male mice, where they preferentially assemble in fast-twitch fibers (Salviati et al., 1985; Chevessier et al., 2005; Boncompagni et al., 2012). To our knowledge, presence of TAs has not been confirmed in aged human muscles. Consistently with their SR origin, TA tubes stain negatively for mitochondrial proteins while positively for proteins resident in SR membranes such as CASQ1 and SERCA. Nevertheless, the interior of the aggregate does not contain RYRs (Salviati et al., 1985; Chevessier et al., 2005; Boncompagni et al., 2012). Schiaffino and collegues showed that formation of aggregates is induced by anoxia in isolated rat muscle (Schiaffino et al., 1977).

We have shown that inactive aging impairs structure, function, and architecture of EC coupling and metabolic (i.e., mitochondria) machineries in muscle of mice and human biopsies (Boncompagni et al., 2006; Pietrangelo et al., 2015), changes that were reduced/counteracted by regular/lifelong exercise, which successfully prevented improper remodeling of intracellular membranes (Zampieri et al., 2015; Pietrangelo et al., 2019). Lifelong training combined to selenium supplementation were recently shown to reduce the age-related loss of muscle force and to improve Ca^{2+} release from RYR1 (Fodor et al., 2020).

In the current study, we analyzed EDL muscles from adult (4-month-old), aged controls (24-month-old), and aged trained mice (24-month-old mice housed in wheel cages for a period of 15 months starting from the age of 9 months), using a combination of structural (electron and confocal microscopy) and functional (*ex vivo* muscle contractility) approaches to test the effect of prolonged voluntary exercise on the accrual of TAs in muscle of aging mice.

MATERIALS AND METHODS

Animals

All procedures and experiments in this study were conducted according to the National Committee for the protection of

animals used for scientific purposes (D. lgs n.26/2014). C57bl/6 WT animals were housed in microisolator cages at 20°C in a 12 h light–dark cycle and provided free access to standard chow and water. All surgeries were made to minimize animal suffering, and animals were euthanized by cervical dislocation as approved by the D. lgs n.26/2014.

In this study, we compared three groups of male WT mice: (a) adult mice, mice of 4–6 months of age ($n = 8$); (b) aged control mice, mice of 24 months of age housed in regular cages ($n = 10$); and (c) aged trained mice, mice of 24 months of age housed from 9 to 24 months of age in wheel cages ($n = 10$). All mice had free access to standard chow and water. Aged trained mice were housed for 15 months in wheel cages for voluntary running (16 Station Home Cage Running Wheel System with CMI Software, Columbus Instruments, Columbus, OH, United States) starting at 9 months of age. Voluntary running activity was monitored in all cages with a sensor connected to a personal computer. In this study, we included only mice that ran a distance of at least 30 km per month from 9 to 20 months of age. At 24 months of age, mice were euthanized by cervical dislocation and processed for different preparations.

Only for data in **Figure 2**, WT mice of 4 months of age ($n = 3$) were exposed to a single bout of exercise protocol using a running treadmill (Columbus Instruments) as described in Boncompagni et al. (2017). Briefly, a first step of warm-up at low speed (10 min at 5 m/min) was used to familiarize the mice with the apparatus and task. The experimental exercise protocol started immediately after the warm-up session and was designed as follows: at the beginning of the protocol, the speed was set to 10 m/min for 25 min, then to 15 m/min for 20 min, then to 20 m/min for 15 min, and finally the speed was increased for 1 m/min every 1 min until the final speed of 25 m/min was reached (and kept for maximum 1 min). Mice were then euthanized and processed for electron microscopy.

Preparation and Analysis of Samples for Histology and Electron Microscopy

Extensor digitorum longus muscles were quickly dissected from euthanized mice, pinned on a Sylgard dish, fixed at room temperature (RT) with 3.5% glutaraldehyde in 0.1 M NaCaCO buffer (pH 7.2), and stored in the fixative at 4°C before embedding. Fixed muscles were then postfixed, embedded, and stained *en bloc*, as described previously (Pietrangelo et al., 2015, 2019). For TT staining, specimens were postfixed in a mixture of 2% OsO_4 and 0.8% ferrocyanide $[K_3Fe(CN)_6]$ for 1–2 h followed by a rinse with 0.1 M NaCaCO buffer with 75 mM $CaCl_2$. For histological examination, 700-nm-thick sections were stained in a solution containing 1% toluidine blue-O and 1% sodium borate (tetra) in distilled water for 3 min on a hot plate at 55–60°C. After washing and drying, sections were mounted with mounting medium DPX Mountant for histology (Sigma–Aldrich, Milan, Italy) and observed with a Leica DMLB light microscope connected to a Leica DFC450 camera equipped with Leica Application Suite v 4.6 for Windows (Leica Microsystem, Vienna, Austria). For electron microscopy (EM), ultrathin sections (∼50 nm) were cut using a Leica Ultracut R microtome (Leica Microsystem, Vienna, Austria) with a Diatome diamond knife (Diatome, Biel, Switzerland) and double-stained with uranyl acetate replacement and lead citrate. Sections were viewed in an FP 505 Morgagni Series 268D electron microscope (FEI Company, Brno, Czechia), equipped with Megaview III digital camera and Soft Imaging System at 60 kV (Olympus Soft Imaging Solutions, Munster, Germany).

Immunofluorescence Labeling and Confocal Microscopy

Extensor digitorum longus muscles were dissected from euthanized animals, fixed with 2% paraformaldehyde in phosphate-buffered saline (PBS) for 20 min at RT, and stored at 4°C overnight. Small bundles of fixed EDL fibers were washed three times in PBS containing 1% [PBS/bovine serum albumin (BSA)] and incubated in blocking solution (PBS/BSA with 10% goat serum and 0.5% Triton X-100) for 1 h at RT, followed by an overnight incubation at 4°C with one of the following primary antibodies: (a) mouse monoclonal anti-RYR1 (34C antibody, 1:30, Developmental Studies Hybridoma Bank University of Iowa, Iowa City, Iowa); (b) rabbit polyclonal anti-STIM1 (1:100, Sigma–Aldrich, Milan, Italy); and (c) rabbit polyclonal anti-ORAI1 (1:20, Thermo Fisher Scientific, Waltham, MA, United States). Bundles of EDL muscles were then incubated for 1 h at RT with the following secondary antibodies (Jackson ImmunoResearch Laboratories, Lexington, KY, United States): Cy5-labeled goat anti–mouse immunoglobulin G (IgG) (1:100); and Cy3-labeled goat anti–rabbit IgG (1:200) for double labeling. Confocal images were acquired using a Zeiss LSM510 META laser-scanning confocal microscope system (Zeiss, Jena, Germany) equipped with a Zeiss Axiovert 200 inverted microscope and a Plan Neofluar oil-immersion objective (100 × /1.3 NA).

Quantitative Analysis in Histology and EM

For quantitative histological analyses, images of non-overlapping regions were randomly collected from transversal sections of internal areas of EDL fibers from adult ($n = 3$), aged ($n = 3$), and aged trained ($n = 3$) mice.

We evaluated the percentage of fibers containing TAs, the number of TAs per fiber, and the average size of TAs.

For quantitative EM analyses, micrographs of non-overlapping regions were randomly collected from transversal sections of internal areas of EDL fibers from adult ($n = 3$), aged ($n = 3$), and aged trained ($n = 3$) mice.

(1) The number of stacks in 100 μm^2 of EM section was determined from electron micrographs at 28,000 × magnification. In each fiber, five micrographs were taken.
(2) The extension of non-triadic TT network at the I band (TT length in microns) per 100 μm^2 of cross-sectional area was measured in electron micrographs at 28,000 × magnification and reported as length (micron)/100 μm^2. In each fiber, five micrographs were taken.
(3) The junctional gap covered by electron dense linkers between SR vesicles in adult control muscle fibers and SR

stacks in adult exercised mice was measured as previously reported (Boncompagni et al., 2017). Linkers between tubes of TAs in aged muscle were measured in electron micrographs at 56,000 × magnification; sample size: three mice, nine micrographs, and 50 measurements.

Ex vivo Fatigue Protocol

Ex vivo assessment of muscle force production during repetitive high-frequency stimulation was made in intact EDL muscles of adult ($n = 5$), aged ($n = 6$), and aged trained ($n = 6$) mice. Briefly, muscles were excised from hind limbs, placed in a dish containing a standard Krebs–Henseleit (KH) solution: (118 mM NaCl, 5 mM KCl, 2.5 mM $CaCl_2$, 1 mM KH_2PO_4, 1 mM $MgSO_4$, 25 mM $NaHCO_3$, and 11 mM glucose; pH 7.4) pinned and tied with fine silk sutures at each end. Muscles were then mounted vertically between two platinum electrodes immersed in an organ chamber filled with KH solution and attached to a servo motor and force transducer (model 1200 A; Aurora Scientific, Aurora, ON, Canada). Before starting the experimental protocol, stimulation level and optimal muscle length (L_0) were determined using a series of 80-Hz stimulus strains every 1 min in order to adjust the muscle to the length that generated maximal force (F_0) and avoid muscle fatigue. Twitch and tetanic contractile properties were then measured. Following these baseline measurements, EDL muscles were subjected to a repetitive high-frequency stimulation fatigue protocol consisting of 30 consecutive, 1 s duration, 60-Hz stimulus trains delivered every 5 s while being continuously perfused with KH solution. To assess the relative contribution of extracellular Ca^{2+} entry, other experiments were conducted under conditions designed to limit/block Ca^{2+} entry, including (i) nominally Ca^{2+}-free KH solution (where external Ca^{2+} was replaced with an equimolar amount of Mg^{2+}) and (ii) standard KH solution supplemented with 10 μM BTP-2, an established inhibitor of SOCE (Zitt et al., 2004). Before starting the repetitive high-frequency stimulation protocol, EDL muscles were equilibrated in either Ca^{2+}-free KH solution or standard KH solution plus BTP-2 for a period of at least 20 min. Muscle force was recorded using Dynamic Muscle Control software and analyzed using a combination of Dynamic Muscle Analysis (Aurora Scientific) software. Specific force (mN/mm^2) was calculated by normalizing the absolute force (mN) to the physiological cross-sectional area (mm^2) obtained as follows: wet weight (mg)/[L_0 (mm) × 1.06 (mg/mm^3) × 0.44] (Hakim et al., 2011; Michelucci et al., 2019, 2020). All experiments were carried out at RT.

Western Blot Analyses

Extensor digitorum longus muscles were dissected from adult ($n = 4$), aged ($n = 4$), and aged trained ($n = 4$) mice and homogenized in a lysing buffer containing 3% sodium dodecyl sulfate (Sigma–Aldrich, Milan, Italy) and 1 mM EGTA (Sigma–Aldrich, Milan, Italy) using a mechanical homogenizer and then centrifuged for 15 min at 900 × *g*, at RT. Protein concentration was determined spectrophotometrically using a modified Lowry method. Total protein (20–40 μg) was resolved in 10% polyacrylamide electrophoresis gels, transferred to nitrocellulose membrane, and blocked with 10% non-fat dry milk (EuroClone, Milan, Italy) in Tris-buffered saline and 0.1% Tween 20 (TBS-T) for 1 h. Membranes were then probed with primary antibodies diluted in 10% non-fat dry milk in TBS-T overnight, at 4°C: (a) rabbit polyclonal anti-STIM1 (1:5,000, Sigma–Aldrich, Milan, Italy); (b) rabbit polyclonal anti-ORAI1 (1:1,000, Santa Cruz Biotechnology, Dallas, TX, United States). The anti–glyceraldehyde-3-phosphate dehydrogenase antibody (mouse monoclonal, 1:15,000; OriGene Technologies, Rockville, MD, United States) was used as a loading control. Membranes were then incubated for 1 h at RT with mouse and rabbit secondary horseradish peroxidase–conjugated antibodies (1:10,000; Merck Millipore, Darmstadt, Germany), diluted in 10% non-fat dry milk in TBS-T. Proteins were detected by enhanced chemiluminescent liquid (Perkin-Elmer, Milan, Italy) and quantified using ImageJ software (National Institutes of Health, Bethesda, MD, United States).

Statistical Analyses

Statistical significance was determined using either two-tailed unpaired Student *t* test when comparing means between two groups or one-way analysis of variance (ANOVA) followed by *post hoc* Tukey test when comparing more than two groups. For *ex vivo* contractile experiments, significance was evaluated using repeated-measurements ANOVA followed by *post hoc* Tukey test. All data were presented as mean ± SEM. In all cases, differences were considered statistically significant at $^*p < 0.05$ (or $^*p < 0.01$ where indicated).

RESULTS

TAs Are STIM1 and ORAI1 Positive

To evaluate the presence of STIM1 and ORAI1 within TAs, we immunostained EDL muscles from aged and aged trained mice with antibodies for STIM1 and ORAI1 (**Figure 1** and **Supplementary Figure 1**). Fibers were double-labeled for RYR1 and STIM1 (**Figure 1A**) and for RYR1 and ORAI1 (**Figure 1B**): RYR1 staining (used to mark the position of CRUs/triads) produced the typical transverse cross striation corresponding to the position of CRUs at the A–I band junction, on both sides of Z-lines (**Figures 1A,B**; red staining). TAs in immunofluorescence images appear as elongated, spindle-shaped regions strongly positive to both STIM1 and ORAI1 antibodies (**Figures 1A,B** and **Supplementary Figures 1B,E**; green staining), whereas RYR1 staining is mainly excluded from the core of TAs, even if some positive spots of RYR1 are present.

STIM1 staining in TAs appears always very dense and quite uniform, whereas ORAI1 staining pattern was apparently less dense and more patchy (**Figures 1A,B**; insets) (see also **Supplementary Figure 1**). Note that the staining of STIM1 and ORAI1 within the aggregate did not overlap with the staining of RYR1 (marking the position of CRUs, which also contain TTs). As ORAI1 is a Ca^{2+}-permeable channel of the plasma membrane located in TTs in skeletal muscle (Wei-Lapierre et al., 2013; Boncompagni et al., 2017), the lack of colocalization with RYR1 suggests that part of ORAI1 may be trapped inside the SR membranes of TAs.

The presence of some RYR1-positive spots in TAs reflects the presence of few CRUs/triads at the interface between different

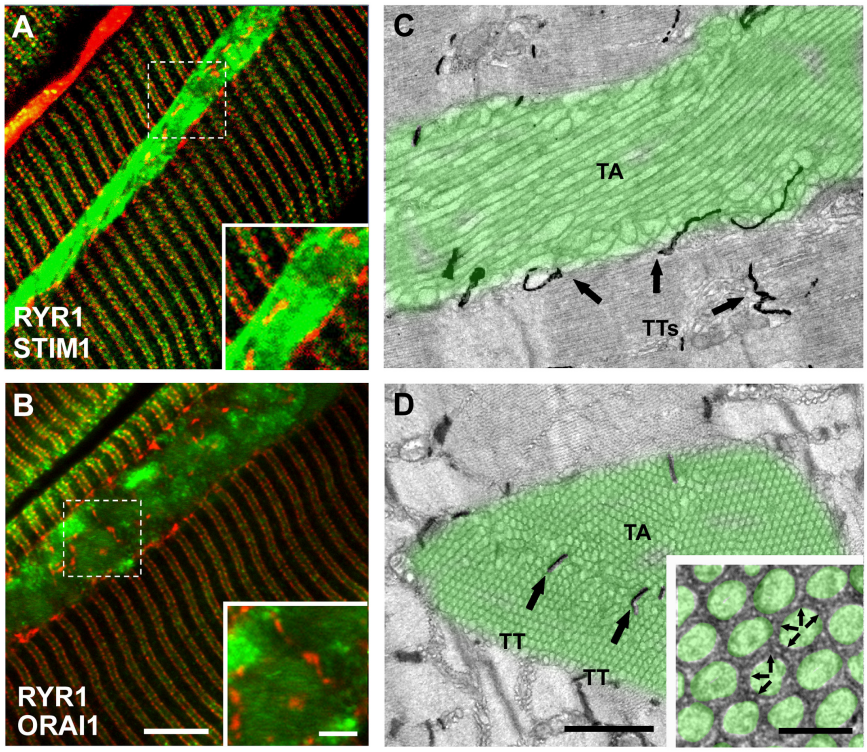

FIGURE 1 | Immunofluorescence and EM analysis of EDL fibers from aged-control mice. **(A,B)** Representative immunofluorescence images obtained from aged mice, double-labeled for RYR1 (red) and STIM1 (green) in panel **(A)** and RYR1 (red) and ORAI1 in panel **(B)**. Raw images for the individual fluorescence channel used to construct these overlays are shown in **Supplementary Figure 1**. **(C,D)** Representative EM images of longitudinal **(C)** and transversal **(D)** sections with TAs false-labeled in green (arrows point to TTs stained with ferrocyanide) and TTs stained with ferrocyanide (dark precipitate). Black arrows in panel **(C,D)** point to TTs within the interior of the TA. Inset in panel **(D)** small bridges, pointed by small arrows, are visible between membranes of adjacent cross-sectioned tubes. Scale bars: **(A,B)**, 5 μm (insets 2 μm); **(C,D)**, 1 μm (inset 0.1 μm).

SR domains that constitute large TAs. This was confirmed by ferrocyanide staining in EM, a technique that creates a dark precipitate inside the lumen of TTs (**Figures 1C,D**): TTs are mainly excluded from the aggregate core and confined at the edge of each TA (dark precipitate in **Figure 1C**). However, TTs were sometimes trapped between multiple smaller aggregates that fuse to form larger one (**Figure 1D**; arrows) [see Boncompagni et al. (2012) for additional detail].

Observation of TAs at high magnification revealed the presence of small electron-dense bridges between individual tubes (**Figure 1D**; arrows in inset). In **Figure 2**, we measured the length of these little bridges (that apparently keep the individual SR tubes together): their average size of 7.9 ± 0.1 nm is quite similar to that (i) of small linkers that are present between SR vesicles/tubes at the I band in adult control mice (8.4 ± 0.1 nm) and (ii) of linkers seen in SR stack of membranes forming CEUs that assemble during acute exercise in adult mice (7.4 ± 0.1 nm) (**Figure 2**) [see also Boncompagni et al. (2012, 2017)].

Exercise Prevents Formation of TAs

Using histological images taken from transversal sections of EDL muscles from aged and aged trained mice (**Figures 3A,B**), we evaluated: (i) the percentage of fibers presenting TAs (**Figure 3E**); (ii) the number of TAs per fiber (**Figure 3F**); and (iii) the average size of TAs (**Figure 3G**). As a visual example of TAs size, TA profiles were outlined in blue in the EM cross-sectional images of **Figures 3C,D**. We also performed similar analyses in muscles from adult mice, which do not contain TAs (**Figures 3E–G** and **Supplementary Figure 2**). Quantitative analysis of the percentage of fibers containing TAs indicated that exercise was quite effective in preventing their formation during aging. Specifically, the number of fibers containing TAs was reduced from ∼51% to only ∼8% following voluntary wheel running (**Figure 3E**). In addition, voluntary exercise was also effective in reducing (i) the average number of TAs per fiber from 6 to 3 (**Figure 3F**) and (ii) the average size of the few remaining TAs from 21 to 17 μm^2 (**Figure 3G**) (see also **Supplementary Table 1**).

Exercise Restores Resistance to Fatigue and Extracellular Ca^{2+} Dependence of EDL Muscles From Aged Mice

Intact EDL muscles dissected from adult, aged, and aged trained mice were subjected to fatigue protocols based on 30 consecutive 1-s-long, 60-Hz stimulus trains applied every 5 s. The experiments were carried out using a standard KH

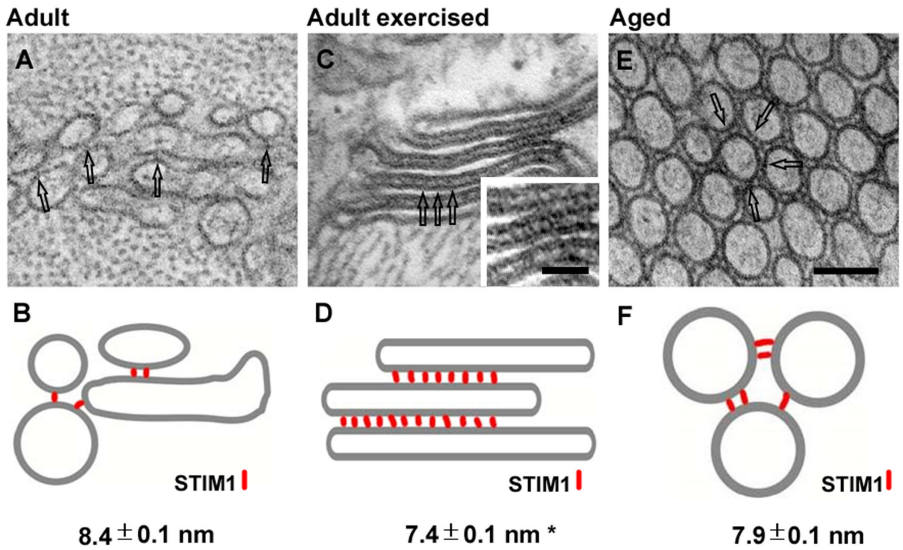

FIGURE 2 | Representative EM images and corresponding cartoons showing SR linkers. SR vesicles in adult control mice [**(A)**, and relative cartoon in panel **(B)**], SR stacks in adult exercised mice [**(C)**, and relative cartoon in panel **(D)**], and TA tubes in aged EDL muscle fibers [**(E)**, and relative cartoon in panel **(F)**]. SR linkers are pointed by empty arrows in EM images and represented as red rods in the cartoons. Image and numeric data in panels **(B,D)** originates from adult mice acutely exercised in Boncompagni et al. (2017). Data are shown as mean ± SEM; $*p < 0.01$ (adult vs. adult exercised). Scale bar: **(A,C,E)**, 0.1 μm; inset, 0.05 μm.

solution containing 2.5 mM Ca^{2+} (**Figure 4**) or under conditions designed to abolish Ca^{2+} entry, e.g., nominally Ca^{2+}-free KH solution or standard KH solution supplemented with 10 μM BTP-2 (**Figure 5**). In presence of the standard KH solution containing 2.5 mM Ca^{2+}, EDL muscles from aged mice exhibited both a reduced specific force during the first stimulus train and a more pronounced drop in either specific and relative force generation during repetitive high-frequency stimulation (e.g., accelerated fatigue) compared to that observed in muscles from adult mice (**Figures 4A,B**). The quantitative analysis of the force fold change relative to the force generated by muscles from adult mice (**Figure 4C**), evaluated at the 10th stimulus train (pointed by arrows in **Figures 4A,B**), indicated that the decrease of force in muscles from aged mice was about 20%. Interestingly, following 15 months of voluntary wheel running, EDL muscles from aged trained mice exhibited a completely recovered ability to maintain contractile force (**Figures 4A,B**), as the average force fold change displayed by muscles from aged trained mice was not significantly different from that of adult muscles (**Figure 4C**). Parallel measurements were also performed under conditions designed to limit/block Ca^{2+} entry (**Figure 5**): (a) in a first set of experiments, muscles were exposed to a nominally Ca^{2+}-free KH solution, where Ca^{2+} was replaced by an equimolar concentration of Mg^{2+}; (b) in a second set of experiments, muscles were exposed to a standard KH solution supplemented with 10 μM BTP-2. Consistent with previous studies (Boncompagni et al., 2017; Michelucci et al., 2019), these interventions exhibited a modest, but statistically significant, effect on force production during repetitive stimulation in EDL muscles from adult mice (**Figure 5A**), although in the absence of Ca^{2+} entry (e.g., when external Ca^{2+} is removed or in the presence of BTP-2) EDL muscles from aged mice did not show any significant reduction of force generation compared to the standard condition (**Figure 5B**), suggesting their impaired capability to use external Ca^{2+}. On the other hand, similarly to what was observed in muscles from adult mice, muscles from aged trained mice displayed a modest, but statistically significant, reduction in contractile force when Ca^{2+} influx was prevented (**Figure 5C**). The quantitative analysis of the fold force decay evaluated at the 10th stimulus train (pointed by arrows in **Figures 5A–C**) revealed that, in the absence of Ca^{2+} entry, EDL muscles from adult and aged trained mice exhibited a reduction in force of 15–20% compared to the condition in which Ca^{2+} entry was permitted (**Figures 5D,F**). Conversely, no significant difference of contractile force was reported in muscles of aged mice, in presence or absence of external Ca^{2+} (**Figure 5E**).

Exercise-Induced Remodeling of SR and TT Membranes (i.e., CEU Components) in Aged Trained Muscles

As EDL muscles from aged trained mice exhibited a recovered capability to use external Ca^{2+} during repetitive stimulation (**Figures 4**, **5**), we assessed and quantified the presence of the structural components needed for the assembly of Ca^{2+} entry units (CEUs): SR stacks (**Figures 6A–C**) and TT extension at the I band (**Figures 6D–F**).

Using EM, we quantified the number of SR stacks per area of cross section (**Figure 6G**) and the extent of the TT network at the I band following staining with ferrocyanide (**Figure 6H**). This analysis revealed that long-term voluntary running promoted (i) the formation of SR stacks in EDL muscles from aged trained mice, which were more numerous

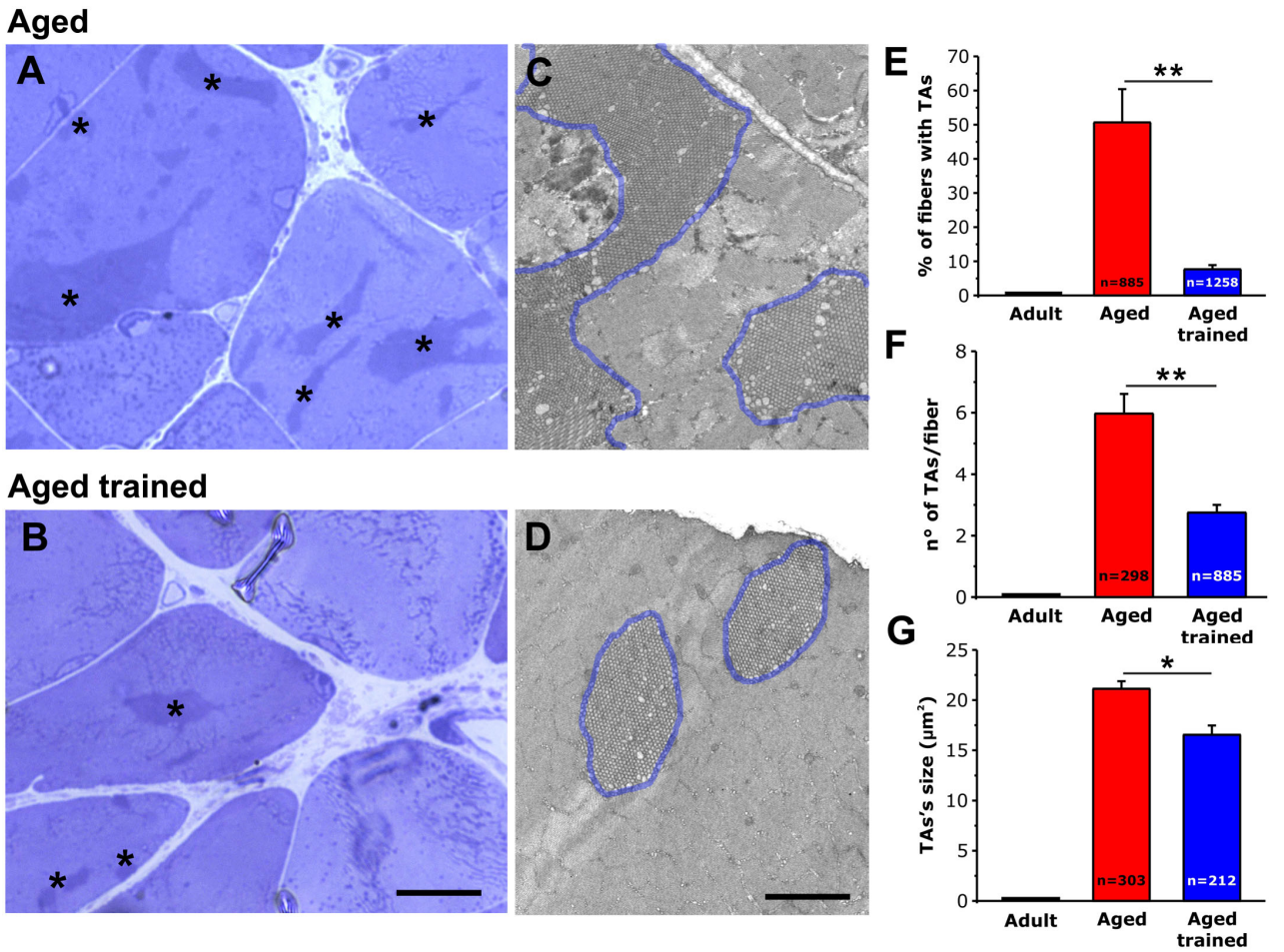

FIGURE 3 | Quantitative histological and EM analysis of TAs incidence in EDL fibers. **(A–D)** Representative histological **(A,B)** and EM **(C,D)** images from transversal sections of EDL muscles from aged **(A,C)** and aged trained **(B,D)** mice. TAs are marked with an asterisk in panels **(A,B)**, whereas TAs are outlined with a blue line in panels **(C,D)**. Representative histological and EM images of adult EDL muscle (which do not contain TAs) are shown in **Supplementary Figure 2**. **(E–G)** Bar plots showing the quantitative analysis of the percentage of EDL fibers containing TAs **(E)**, the number of TAs per fiber **(F)**, and finally the average size of TAs **(G)**. Data are shown as mean ± SEM; $^{**}p < 0.01$ in panels **(E,F)**; $^{*}p < 0.05$ in G; n = number of fibers analyzed. Scale bars: **(A,B)**, 10 μm; **(C,D)**, 2 μm.

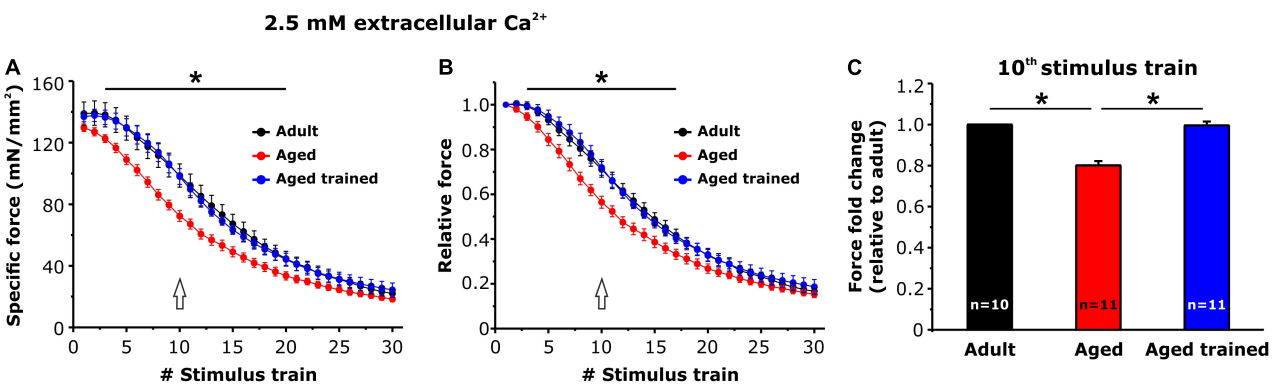

FIGURE 4 | *Ex vivo* fatigue protocols in EDL muscles. **(A,B)** Time course of specific **(A)** and relative **(B)** force decay (normalized to the first stimulus train) during 30 consecutive stimulus trains (60 Hz, 1-s duration, every 5 s) in presence of a standard KH solution containing 2.5 mM Ca^{2+}. The asterisks in panels **(A,B)** indicate the window in which there is a significant statistical difference between aged (control) and the other two groups of samples (adult and aged trained). **(C)** Bar plot showing the fold change of force, relative to adult mice, calculated at the 10th stimulus train [pointed by arrows in panels **(A,B)**]. Data are shown as mean ± SEM; $^{*}p < 0.05$; n = number of EDL muscles.

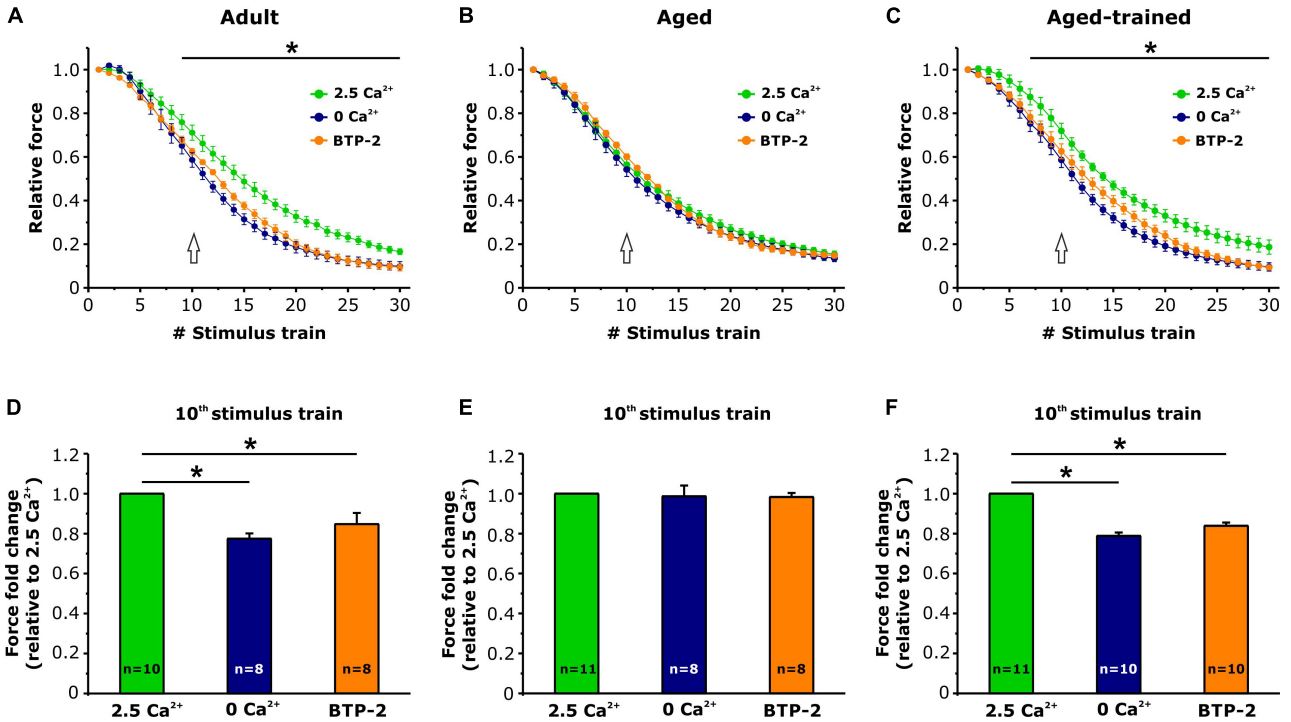

FIGURE 5 | *Ex vivo* fatigue protocols in EDL muscles in presence or absence of extracellular Ca^{2+}. **(A–C)** Time courses of relative force decay (normalized to the first stimulus train) during 30 consecutive stimuli (60 Hz, 1-s duration, every 5 s) in presence of standard KH solution either containing 2.5 mM Ca^{2+} (green), nominally Ca^{2+}-free solution (dark blue), or standard KH solution containing 2.5 mM Ca^{2+} and supplemented with 10 μM BTP-2 (orange). The asterisks in panels **(A,C)** indicate the window in which there is a significant statistical difference between presence of 2.5 mM Ca^{2+} and the other two conditions (0 Ca^{2+} and presence of BTP2). **(D–F)** Bar plots showing the fold change of the force, relative to the 2.5 mM Ca^{2+} condition, calculated at the 10th stimulus train [see arrows in panels **(A–C)**]. Data are shown as mean ± SEM; *$p < 0.05$; n = number of EDL muscles.

than those observed in muscles from both adult and aged mice (**Figure 6G**); (ii) elongation of TT at the I band, which is increased compared to aged mice, but not rescued to the levels of adult mice (**Figure 6H**) (see also **Supplementary Table 2**). As we previously showed that STIM1 and ORAI1 colocalize at SR-TT junctions formed by SR stacks and TT at the band (Boncompagni et al., 2017); here, we assessed the expression levels of the two proteins by performing Western blot experiments in EDL muscle homogenates (**Supplementary Figure 3**). The results of these experiments showed that expression of STIM1S and ORAI1 (but not STIM1L) is increased in muscles from aged trained compared to aged mice, even if only the STIM1S resulted statistically different.

DISCUSSION

Main Findings of the Study

In the present work, we showed that (i) STIM1 and ORAI1 are accumulated in TAs in muscle of aged mice (**Figure 1**); (ii) TAs, absent in fibers from adult mice while abundant in those from aged mice, are reduced in incidence and size following 15 months of voluntary running (**Figure 3**); (iii) the presence of TAs in EDL of aged mice correlates to a reduced ability to maintain contractile force during repetitive high-frequency stimulation, likely as the result of the lowered ability to refill internal Ca^{2+} stores *via* SOCE (**Figures 4**, **5**); and (iv) voluntary exercise improves the fatigue resistance during repetitive stimulation (**Figures 4**, **5**) and promotes the maintenance of SR and TT elements needed for the assembly of CEUs (**Figure 6**). Overall, our results suggest that (a) aging causes improper accumulation of STIM1 and ORAI1 in TAs and defective SOCE; and (b) long-term regular exercise strikingly reduces formation of TAs during aging, while promoting the maintenance of CEUs and improving the use of external Ca^{2+} during repetitive high-frequency stimulation.

SOCE Is Dysfunctional in Muscles Containing TAs

TAs in aging mice stain positively for both STIM1 and ORAI1. These results agree with the work of Endo and colleagues, showing that TAs of patients with TAM are immunopositive for both proteins (Endo et al., 2015). The staining pattern for STIM1 appears to be quite dense and uniform, whereas the staining of ORAI1 is not as uniform.

(1) We have previously shown (Boncompagni et al., 2012) that tubes of TAs appear linked together by many small bridges (Boncompagni et al., 2012). Although the molecular nature of these electron-dense strands

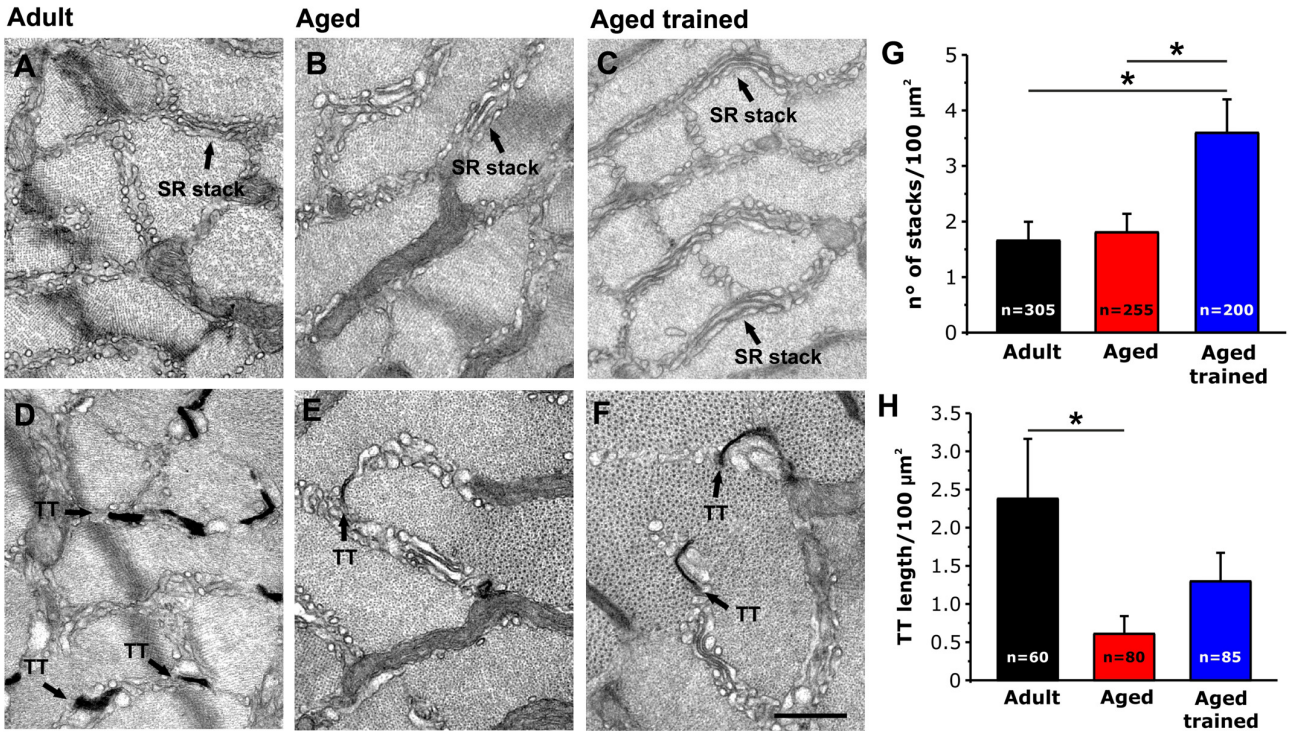

FIGURE 6 | Quantitative analysis by EM of SR stacks and TT length at the I band in EDL fibers. **(A–F)** Representative EM images of transversal sections of EDL fibers from adult **(A,D)**, aged **(B,E)** and aged trained **(C,F)** mice. In **(D–F)** panels, TTs are stained with ferrocyanide (dark precipitate). **(G,H)** Bar plots showing the incidence of SR stacks **(G)** and the TT length at the I band **(H)**. Arrows point to SR stacks in panels **(A–C)**; arrows point to TTs stained with ferrocyanide in panels **(D–F)**. Data are shown as mean ± SEM; $*p < 0.05$; n = number of measurements. Scale bar: **(A–F)**, 0.1 mm.

remains unknown, similar linkers are present between SR vesicles in fibers from control mice and between SR stack cisternae formed in muscle from mice subjected to acute exercise, both localized within the I band of the sarcomere [**Figure 2**; see also Boncompagni et al. (2017)]. Furthermore, electron-dense strands with similar length were reported between stacks of endoplasmic reticulum in HEK93 cells overexpressing STIM1 (Orci et al., 2009; Perni et al., 2015). Considering that STIM1 is localized throughout the I band in muscle fibers of control mice, we speculate that these little bridges could represent indeed aggregated STIM1 proteins, a hypothesis supported by immunogold staining in our previous studies (Boncompagni et al., 2017).

(2) ORAI1 is a Ca^{2+} release–activated Ca^{2+} channel of external membranes (Feske et al., 2006); hence, to be functional, it has to be localized either in the plasma membrane or in TTs. Our results show that ORAI1 also accumulated within TAs in muscles from aged mice. As TTs are mainly excluded from TAs [**Figure 1**; see also Boncompagni et al. (2012) for additional detail], and as Ca^{2+} entry is dysfunctional in aged muscles, it is plausible to argue that ORAI1 might be trapped in the SR tubes of TAs without being able to reach its functional destination in TTs. In line with this hypothesis, Thornton and colleagues showed that SOCE is significantly impaired in aged skeletal muscle, although the transcription levels of both STIM1 and ORAI1 were unchanged compared to young muscle (Thornton et al., 2011). Reduced SOCE activity could lead to impaired SR Ca^{2+} refilling upon repetitive contraction–relaxation cycles, and in turn, reduced availability of Ca^{2+} within the SR would underlie the lower ability to generate specific force during prolonged contraction (Zhao et al., 2008; Thornton et al., 2011; Michelucci et al., 2019). Consistent with these findings, we found that aged EDL muscles display a higher susceptibility to fatigue than adult muscles, during repetitive stimulation in presence of external Ca^{2+} (**Figure 4**). The lack of a further reduction of force in absence of extracellular Ca^{2+} influx in aged muscles (**Figure 5**) suggests that SOCE may be dysfunctional, possibly due to the accumulation of part of STIM1 and ORAI1 within TAs.

Exercise Prevents TAs Formation and Preserves Structural Elements of CEUs

We have recently provided evidence that exercise drives the formation of CEUs, new intracellular junctions representing sites of functional and dynamic STIM1-ORAI1 association that promote Ca^{2+} entry and limit muscle fatigue during repetitive stimulation (Boncompagni et al., 2017; Michelucci et al., 2019). While the formation of CEUs seems to be important for the

optimal coupling between STIM1 and ORAI1, the accrual of TAs might have the opposite effect of sequestering part of the two proteins in a way that they are no longer able to interact properly.

In this study, we found that regular exercise in wheel cages significantly reduces the accrual of TAs during aging and promotes the maintenance of the structural elements required for the assembly of functional CEUs, i.e., SR stacks and T tubules at the I band (**Figure 6**). Importantly, the exercise-induced maintenance of CEU elements is accompanied by recovered capability of EDL muscles to use external Ca^{2+} (**Figures 4**, **5**), suggesting that STIM1 and ORAI1 in aged trained mice are better available for functional activation of SOCE than in aged sedentary mice. Our results are supported by a recent article from Fodor and colleagues, showing that skeletal muscle Ca^{2+} homeostasis and force significantly improved in aged mice following voluntary wheel training (Fodor et al., 2020).

Stiber and colleagues proposed two functionally distinct pools of STIM1, one at the triad and another one within the lSR at the I band (Stiber et al., 2008). Recently, Darbellay and collegues provided a possible molecular explanation for these two STIM1 pools. Indeed, the authors identified a STIM1 splice variant highly expressed in skeletal muscle (STIM1L) proposed to be preassembled with ORAI1 at the triad to mediate rapid SOCE, while graded recruitment of additional SOCE during prolonged activity could be mediated by STIM1S (Darbellay et al., 2009, 2011; Michelucci et al., 2018). Being STIM1S distributed throughout the lSR at the I band, this isoform would indeed be in the right position to contribute to the assembly of CEUs during exercise. This idea is supported by our data showing a correlation between increased expression of STIM1S and maintenance of CEU elements in trained aged mice.

CONCLUSION

For a long time, the physiological role of extracellular Ca^{2+} in skeletal muscle function has been overlooked, as not required for mechanical EC coupling (Schneider and Chandler, 1973; Rios et al., 1991). Over the past two decades, though, the importance of SOCE in maintaining proper contractile function during prolonged activity has been taken into account (Pan et al., 2002, 2014; Putney, 2011b; Boncompagni et al., 2017; Michelucci et al., 2019). A deeper understanding of the molecular mechanisms that promote functional (and dysfunctional) interaction between STIM1 and ORAI1 in SOCE would be crucial for the development of safe/effective therapeutic interventions to limit susceptibility to fatigue and weakness in aging and in those muscle diseases caused by altered Ca^{2+} homeostasis. The results of the present work suggest that TAs could represent intracellular bins for dysfunctional accumulation of proteins, including STIM1 and ORAI1. The presence of TAs is accompanied by impaired ability to restore internal Ca^{2+} stores from extracellular space, which could contribute to both muscle weakness and increased susceptibility to fatigue during aging. Our hypothesis agrees with the work by Thornton and colleagues suggesting that SOCE contributes to normal contractility in young, but not in aged skeletal muscle (Thornton et al., 2011), although it is difficult to determine whether TAs form as a consequence of an altered Ca^{2+} handling, or else if they are the cause of muscle dysfunction. Undoubtedly, our experiments indicate that long-term regular exercise counteracts the formation of TAs and promotes the assembly of functional CEUs, which is accompanied by an improved capability of fibers to use extracellular Ca^{2+}.

DATA AVAILABILITY STATEMENT

The original contributions presented in the study are included in the article/**Supplementary Material**, further inquiries can be directed to the corresponding author/s.

ETHICS STATEMENT

The animal study was reviewed and approved by National Committee for the protection of animals used for scientific purposes (D. lgs n.26/2014), Italian Ministry of Health Viale Giorgio Ribotta, 5 – 00144 – Roma.

AUTHOR CONTRIBUTIONS

SB and FP conceived and directed the study. SB, CP, AM, and LP performed the experimental work and data analysis. In detail, CP, LP, and SB performed experiments and data analysis of **Figures 1–3**, **6** and **Supplementary Figures 1**, **2**. CP also performed the Western blot analysis (**Supplementary Figure 3**). AM performed functional experiments and analysis of **Figures 4**, **5**. Finally, SB, AM, and FP wrote and edited the manuscript. All authors contributed to the article and approved the submitted version.

FUNDING

This work was supported by grants: (1) GGP19231 from Italian Telethon ONLUS; (2) subcontract of AR059646 to FP from National Institutes of Health United States; (3) PRIN #2015ZZR4W3 to FP from Italian Ministry of University and Research; and (4) Italian Ministry of Health (Rome, Italy) no. GR-2011-02352681 to SB.

SUPPLEMENTARY MATERIAL

The Supplementary Material for this article can be found online at: https://www.frontiersin.org/articles/10.3389/fphys.2020.601057/full#supplementary-material

REFERENCES

Bohm, J., Bulla, M., Urquhart, J. E., Malfatti, E., Williams, S. G., O'sullivan, J., et al. (2017). ORAI1 mutations with distinct channel gating defects in tubular aggregate myopathy. *Hum. Mutat.* 38, 426–438. doi: 10.1038/s41598-017-14134-0

Bohm, J., Chevessier, F., Koch, C., Peche, G. A., Mora, M., Morandi, L., et al. (2014). Clinical, histological and genetic characterisation of patients with tubular aggregate myopathy caused by mutations in STIM1. *J. Med. Genet.* 51, 824–833. doi: 10.1136/jmedgenet-2014-102623

Bohm, J., Chevessier, F., Maues De Paula, A., Koch, C., Attarian, S., Feger, C., et al. (2013). Constitutive activation of the calcium sensor STIM1 causes tubular-aggregate myopathy. *Am. J. Hum. Genet.* 92, 271–278. doi: 10.1016/j.ajhg.2012.12.007

Boncompagni, S., d'Amelio, L., Fulle, S., Fanò, G., and Protasi, F. (2006). Progressive disorganization of the excitation-contraction coupling apparatus in aging human skeletal muscle as revealed by electron microscopy: a possible role in the decline of muscle performance. *J. Gerontol. A Biol. Sci. Med. Sci.* 61, 995–1008. doi: 10.1093/gerona/61.10.995

Boncompagni, S., Michelucci, A., Pietrangelo, L., Dirksen, R. T., and Protasi, F. (2017). Exercise-dependent formation of new junctions that promote STIM1-Orai1 assembly in skeletal muscle. *Sci. Rep.* 7:14286.

Boncompagni, S., Michelucci, A., Pietrangelo, L., Dirksen, R. T., and Protasi, F. (2018). Addendum: exercise-dependent formation of new junctions that promote STIM1-Orai1 assembly in skeletal muscle. *Sci. Rep.* 8:17463. doi: 10.1038/s41598-018-33063-0

Boncompagni, S., Pozzer, D., Viscomi, C., Ferreiro, A., and Zito, E. (2020). Physical and functional cross talk between endo-sarcoplasmic reticulum and mitochondria in skeletal muscle. *Antioxid. Redox Signal.* 32, 873–883. doi: 10.1089/ars.2019.7934

Boncompagni, S., Protasi, F., and Franzini-Armstrong, C. (2012). Sequential stages in the age-dependent gradual formation and accumulation of tubular aggregates in fast twitch muscle fibers: SERCA and calsequestrin involvement. *Age* 34, 27–41. doi: 10.1007/s11357-011-9211-y

Brotto, M. (2011). Ageing, sarcopenia and store-operated calcium entry: a common link? *Cell Cycle* 10, 4201–4202. doi: 10.4161/cc.10.24.18645

Carrell, E. M., Coppola, A. R., Mcbride, H. J., and Dirksen, R. T. (2016). Orai1 enhances muscle endurance by promoting fatigue-resistant type I fiber content but not through acute store-operated Ca2+ entry. *FASEB J.* 30, 4109–4119. doi: 10.1096/fj.201600621R

Chevessier, F., Bauche-Godard, S., Leroy, J. P., Koenig, J., Paturneau-Jouas, M., Eymard, B., et al. (2005). The origin of tubular aggregates in human myopathies. *J. Pathol.* 207, 313–323. doi: 10.1002/path.1832

Darbellay, B., Arnaudeau, S., Bader, C. R., Konig, S., and Bernheim, L. (2011). STIM1L is a new actin-binding splice variant involved in fast repetitive Ca2+ release. *J. Cell Biol.* 194, 335–346. doi: 10.1083/jcb.201012157

Darbellay, B., Arnaudeau, S., Konig, S., Jousset, H., Bader, C., Demaurex, N., et al. (2009). STIM1- and Orai1-dependent store-operated calcium entry regulates human myoblast differentiation. *J. Biol. Chem.* 284, 5370–5380. doi: 10.1074/jbc.M806726200

De Groot, J. G., and Arts, W. F. (1982). Familial myopathy with tubular aggregates. *J. Neurol.* 227, 35–41. doi: 10.1007/BF00313545

Endo, Y., Noguchi, S., Hara, Y., Hayashi, Y. K., Motomura, K., Miyatake, S., et al. (2015). Dominant mutations in ORAI1 cause tubular aggregate myopathy with hypocalcemia via constitutive activation of store-operated Ca(2)(+) channels. *Hum. Mol. Genet.* 24, 637–648. doi: 10.1093/hmg/ddu477

Engel, W. K., Bishop, D. W., and Cunningham, G. G. (1970). Tubular aggregates in type II muscle fibers: ultrastructural and histochemical correlation. *J. Ultrastruct. Res.* 31, 507–525. doi: 10.1016/s0022-5320(70)90166-8

Feske, S., Gwack, Y., Prakriya, M., Srikanth, S., Puppel, S. H., Tanasa, B., et al. (2006). A mutation in Orai1 causes immune deficiency by abrogating CRAC channel function. *Nature* 441, 179–185. doi: 10.1038/nature04702

Fodor, J., Al-Gaadi, D., Czirják, T., Oláh, T., Dienes, B., Csernoch, L., et al. (2020). Improved calcium homeostasis, and force by selenium treatment, and training in aged mouse skeletal muscle. *Sci. Rep.* 10:1707. doi: 10.1038/s41598-020-58500-x

Franzini-Armstrong, C. (1980). Structure of sarcoplasmic reticulum. *Fed. Proc.* 39, 2403–2409.

Franzini-Armstrong, C. (1984). Freeze-fracture of frog slow tonic fibers. Structure of surface and internal membranes. *Tissue Cell* 16, 647–664. doi: 10.1016/0040-8166(84)90038-7

Franzini-Armstrong, C., Kenney, L. J., and Varriano-Marston, E. (1987). The structure of calsequestrin in triads of vertebrate skeletal muscle: a deep-etch study. *J. Cell Biol.* 105, 49–56. doi: 10.1083/jcb.105.1.49

Franzini-Armstrong, C., and Protasi, F. (1997). Ryanodine receptors of striated muscles: a complex channel capable of multiple interactions. *Physiol. Rev.* 77, 699–729. doi: 10.1152/physrev.1997.77.3.699

Hakim, C. H., Li, D., and Duan, D. (2011). Monitoring murine skeletal muscle function for muscle gene therapy. *Methods Mol Biol.* 709, 75–89. doi: 10.1007/978-1-61737-982-65

Inui, M., and Fleischer, S. (1988). Reconstitution of calcium pumping of cardiac sarcoplasmic reticulum. *Methods Enzymol.* 157, 314–320. doi: 10.1016/0076-6879(88)57086-6

Kurebayashi, N., and Ogawa, Y. (2001). Depletion of Ca^{2+} in the sarcoplasmic reticulum stimulates Ca^{2+} entry into mouse skeletal muscle fibres. *J. Physiol.* 533, 185–199. doi: 10.1111/j.1469-7793.2001.0185b

Lee, J. M., and Noguchi, S. (2016). Calcium dyshomeostasis in tubular aggregate myopathy. *Int. J. Mol. Sci.* 17:1952. doi: 10.3390/ijms17111952

Liou, J., Kim, M. L., Heo, W. D., Jones, J. T., Myers, J. W., Ferrell, J. E., et al. (2005). STIM is a Ca2+ sensor essential for Ca2+-store-depletion-triggered Ca2+ influx. *Curr. Biol.* 15, 1235–1241. doi: 10.1016/j.cub.2005.05.055

Lyfenko, A. D., and Dirksen, R. T. (2008). Differential dependence of store-operated and excitation-coupled Ca2+ entry in skeletal muscle on STIM1 and Orai1. *J. Physiol.* 586, 4815–4824. doi: 10.1113/jphysiol.2008.160481

Michelucci, A., Boncompagni, S., Pietrangelo, L., Garcia-Castaneda, M., Takano, T., Malik, S., et al. (2019). Transverse tubule remodeling enhances Orai1-dependent Ca(2+) entry in skeletal muscle. *eLife* 8:e47576. doi: 10.7554/eLife.47576

Michelucci, A., Boncompagni, S., Pietrangelo, L., Takano, T., Protasi, F., and Dirksen, R. T. (2020). Pre-assembled Ca2+ entry units and constitutively active Ca2+ entry in skeletal muscle of calsequestrin-1 knockout mice. *J. Gen. Physiol.* 152:e202012617. doi: 10.1085/jgp.202012617

Michelucci, A., Garcia-Castaneda, M., Boncompagni, S., and Dirksen, R. T. (2018). Role of STIM1/ORAI1-mediated store-operated Ca(2+) entry in skeletal muscle physiology and disease. *Cell Calcium* 76, 101–115. doi: 10.1016/j.ceca.2018.10.004

Morgan-Hughes, J. A. (1998). Tubular aggregates in skeletal muscle: their functional significance and mechanisms of pathogenesis. *Curr. Opin. Neurol.* 11, 439–442. doi: 10.1097/00019052-199810000-00005

Nesin, V., Wiley, G., Kousi, M., Ong, E. C., Lehmann, T., Nicholl, D. J., et al. (2014). Activating mutations in STIM1 and ORAI1 cause overlapping syndromes of tubular myopathy and congenital miosis. *Proc. Natl. Acad. Sci. U.S.A.* 111, 4197–4202. doi: 10.1073/pnas.1312520111

Okuma, H., Saito, F., Mitsui, J., Hara, Y., Hatanaka, Y., Ikeda, M., et al. (2016). Tubular aggregate myopathy caused by a novel mutation in the cytoplasmic domain of STIM1. *Neurol. Genet.* 2:e50. doi: 10.1212/NXG.0000000000000050

Orci, L., Ravazzola, M., Le Coadic, M., Shen, W. W., Demaurex, N., and Cosson, P. (2009). From the Cover: STIM1-induced precortical and cortical subdomains of the endoplasmic reticulum. *Proc. Natl. Acad. Sci. U.S.A.* 106, 19358–19362. doi: 10.1073/pnas.0911280106

Pan, Z., Brotto, M., and Ma, J. (2014). Store-operated Ca2+ entry in muscle physiology and diseases. *BMB Rep.* 47, 69–79. doi: 10.5483/bmbrep.2014.47.2.015

Pan, Z., Yang, D., Nagaraj, R. Y., Nosek, T. A., Nishi, M., Takeshima, H., et al. (2002). Dysfunction of store-operated calcium channel in muscle cells lacking mg29. *Nat. Cell Biol.* 4, 379–383. doi: 10.1038/ncb788

Parekh, H., Pillarisetti, K., Kunapuli, S., and Simpkins, H. (1997). Isolation of a hamster cDNA homologous to the mouse and human cyclin kinase inhibitory protein p27Kip1. *Somat. Cell. Mol. Genet.* 23, 147–151. doi: 10.1007/BF02679973

Perni, S., Dynes, J. L., Yeromin, A. V., Cahalan, M. D., and Franzini-Armstrong, C. (2015). Nanoscale patterning of STIM1 and Orai1 during store-operated Ca2+ entry. *Proc. Natl. Acad. Sci. U.S.A.* 112, E5533–E5542. doi: 10.1073/pnas.1515606112

Pierobon-Bormioli, S., Armani, M., Ringel, S. P., Angelini, C., Vergani, L., Betto, R., et al. (1985). Familial neuromuscular disease with tubular aggregates. *Muscle Nerve* 8, 291–298. doi: 10.1002/mus.880080405

Pietrangelo, L., D'incecco, A., Ainbinder, A., Michelucci, A., Kern, H., Dirksen, R. T., et al. (2015). Age-dependent uncoupling of mitochondria from Ca2(+) release units in skeletal muscle. *Oncotarget* 6, 35358–35371. doi: 10.18632/oncotarget.6139

Pietrangelo, L., Michelucci, A., Ambrogini, P., Sartini, S., Guarnier, F. A., Fusella, A., et al. (2019). Muscle activity prevents the uncoupling of mitochondria from Ca(2+) Release Units induced by ageing and disuse. *Arch. Biochem. Biophys.* 663, 22–33. doi: 10.1016/j.abb.2018.12.017

Protasi, F., Pietrangelo, L., and Boncompagni, S. (2020). Calcium entry units (CEUs): perspectives in skeletal muscle function and disease. *J. Muscle Res. Cell. Motil.* [Epub ahead of print]. doi: 10.1007/s10974-020-09586-3

Putney, J. W. Jr. (1986). A model for receptor-regulated calcium entry. *Cell Calcium* 7, 1–12. doi: 10.1016/0143-4160(86)90026-6

Putney, J. W. (2011a). Origins of the concept of store-operated calcium entry. *Front. Biosci.* 3, 980–984. doi: 10.2741/202

Putney, J. W. (2011b). The physiological function of store-operated calcium entry. *Neurochem. Res.* 36, 1157–1165. doi: 10.1007/s11064-010-0383-0

Rios, E., Ma, J. J., and Gonzalez, A. (1991). The mechanical hypothesis of excitation-contraction (EC) coupling in skeletal muscle. *J. Muscle Res. Cell Motil.* 12, 127–135. doi: 10.1007/BF01774031

Roos, J., Digregorio, P. J., Yeromin, A. V., Ohlsen, K., Lioudyno, M., Zhang, S., et al. (2005). STIM1, an essential and conserved component of store-operated Ca2+ channel function. *J. Cell Biol.* 169, 435–445. doi: 10.1083/jcb.200502019

Rosenberg, N. L., Neville, H. E., and Ringel, S. P. (1985). Tubular aggregates. Their association with neuromuscular diseases, including the syndrome of myalgias/cramps. *Arch. Neurol.* 42, 973–976. doi: 10.1001/archneur.1985.04060090055014

Saito, A., Seiler, S., Chu, A., and Fleischer, S. (1984). Preparation and morphology of sarcoplasmic reticulum terminal cisternae from rabbit skeletal muscle. *J. Cell Biol.* 99, 875–885. doi: 10.1083/jcb.99.3.875

Salviati, G., Pierobon-Bormioli, S., Betto, R., Damiani, E., Angelini, C., Ringel, S. P., et al. (1985). Tubular aggregates: sarcoplasmic reticulum origin, calcium storage ability, and functional implications. *Muscle Nerve* 8, 299–306. doi: 10.1002/mus.880080406

Schiaffino, S., Severin, E., Cantini, M., and Sartore, S. (1977). Tubular aggregates induced by anoxia in isolated rat skeletal muscle. *Lab. Invest.* 37, 223–228.

Schneider, M. F. (1994). Control of calcium release in functioning skeletal muscle fibers. *Annu. Rev. Physiol.* 56, 463–484. doi: 10.1146/annurev.ph.56.030194.002335

Schneider, M. F., and Chandler, W. K. (1973). Voltage dependent charge movement of skeletal muscle: a possible step in excitation-contraction coupling. *Nature* 242, 244–246. doi: 10.1038/242244a0

Stiber, J., Hawkins, A., Zhang, Z. S., Wang, S., Burch, J., Graham, V., et al. (2008). STIM1 signalling controls store-operated calcium entry required for development and contractile function in skeletal muscle. *Nat. Cell Biol.* 10, 688–697. doi: 10.1038/ncb1731

Thornton, A. M., Zhao, X., Weisleder, N., Brotto, L. S., Bougoin, S., Nosek, T. M., et al. (2011). Store-operated Ca(2+) entry (SOCE) contributes to normal skeletal muscle contractility in young but not in aged skeletal muscle. *Aging* 3, 621–634. doi: 10.18632/aging.100335

Vig, M., Peinelt, C., Beck, A., Koomoa, D. L., Rabah, D., Koblan-Huberson, M., et al. (2006). CRACM1 is a plasma membrane protein essential for store-operated Ca2+ entry. *Science* 312, 1220–1223. doi: 10.1126/science.1127883

Vissing, J., Schmalbruch, H., Haller, R. G., and Clausen, T. (1999). Muscle phosphoglycerate mutase deficiency with tubular aggregates: effect of dantrolene. *Ann. Neurol.* 46, 274–277. doi: 10.1002/1531-8249(199908)46:2<274::aid-ana22>3.0.co;2-g

Walter, M. C., Rossius, M., Zitzelsberger, M., Vorgerd, M., Muller-Felber, W., Ertl-Wagner, B., et al. (2015). 50 years to diagnosis: autosomal dominant tubular aggregate myopathy caused by a novel STIM1 mutation. *Neuromuscul. Disord.* 25, 577–584. doi: 10.1016/j.nmd.2015.04.005

Wei-Lapierre, L., Carrell, E. M., Boncompagni, S., Protasi, F., and Dirksen, R. T. (2013). Orai1-dependent calcium entry promotes skeletal muscle growth and limits fatigue. *Nat. Commun.* 4:2805. doi: 10.1038/ncomms3805

Zampieri, S., Mammucari, C., Romanello, V., Barberi, L., Pietrangelo, L., Fusella, A., et al. (2015). Physical exercise in aging human skeletal muscle increases mitochondrial calcium uniporter expression levels and affects mitochondria dynamics. *Physiol. Rep.* 4:e13005. doi: 10.14814/phy2.13005

Zhao, X., Weisleder, N., Thornton, A., Oppong, Y., Campbell, R., Ma, J., et al. (2008). Compromised store-operated Ca2+ entry in aged skeletal muscle. *Cell* 7, 561–568. doi: 10.1111/j.1474-9726.2008.00408.x

Zhao, X., Yoshida, M., Brotto, L., Takeshima, H., Weisleder, N., Hirata, Y., et al. (2005). Enhanced resistance to fatigue and altered calcium handling properties of sarcalumenin knockout mice. *Physiol. Genomics* 23, 72–78. doi: 10.1152/physiolgenomics.00020.2005

Zitt, C., Strauss, B., Schwarz, E. C., Spaeth, N., Rast, G., Hatzelmann, A., et al. (2004). Potent inhibition of Ca2+ release–activated Ca2+ channels and T-lymphocyte activation by the pyrazole derivative BTP2. *J. Biol. Chem.* 279, 12427–12437. doi: 10.1074/jbc.M309297200

Conflict of Interest: The authors declare that the research was conducted in the absence of any commercial or financial relationships that could be construed as a potential conflict of interest.

frontiers in Physiology

ORIGINAL RESEARCH
published: 12 January 2021
doi: 10.3389/fphys.2020.601189

Senescence Is Associated With Elevated Intracellular Resting [Ca^{2+}] in Mice Skeletal Muscle Fibers. An *in vivo* Study

Alfredo Mijares[1], Paul D. Allen[2] and Jose R. Lopez[3]*

[1] Centro de Biofísica y Bioquímica, Instituto Venezolano de Investigaciones Científicas, Caracas, Venezuela, [2] Malignant Hyperthermia Investigation Unit, St James' University Hospital, University of Leeds, Leeds, United Kingdom, [3] Department of Research, Mount Sinai Medical Center, Miami, FL, United states

Aging causes skeletal muscles to become atrophied, weak, and easily fatigued. Here, we have tested the hypothesis that normal aging in skeletal muscle cells is associated with Ca^{2+} intracellular dyshomeostasis and oxidative stress. Intracellular Ca^{2+} concentration ($[Ca^{2+}]_i$), resting intracellular Na^+ concentration ($[Na^+]_i$) and reactive oxygen species (ROS) production were measured *in vivo* (superficial gastrocnemius fibers) using double-barreled ion-selective microelectrodes, and *in vitro* [isolated single flexor digitorum brevis fibers] using fluorescent ROS sensor CM-H2DCFDA in young (3 months of age), middle-aged (12 months of age), and aged (24 months of age) mice. We found an age-related increase in $[Ca^{2+}]_i$ from 121 ± 4 nM in young muscle cells which rose to 255 ± 36 nM in middle-aged and to 409 ± 25 nM in aged cells. $[Na^+]_i$ also showed an age-dependent elevation, increasing from 8 ± 0.5 mM in young muscle fibers, to 12 ± 1 mM in middle-aged and to 17 ± 1 mM in old muscle fibers. Using the fluorescent ROS sensor CM-H2DCFDA we found that these increases in intracellular cation concentrations were associated with significantly increased basal ROS production as demonstrated by age related increases in the rate of dichlorodihydrofluorescein fluorescence. To determine is this could be modified by reducing ROS and/or blocking sarcolemmal Ca^{2+} influx we administered flufenamic acid (FFA), a non-steroidal anti-inflammatory drug which is also a non-selective blocker of the transient receptor potential canonical channels (TRPCs), for 4 weeks to determine if this would have a beneficial effect. FFA treatment reduced both basal ROS production and muscle $[Ca^{2+}]_i$ and $[Na^+]_i$ in middle-aged and aged muscle fibers compared to fibers and muscles of untreated 12 and 24-months old mice. $[Ca^{2+}]_i$ was reduced to 134 ± 8 nM in middle-aged muscle and to 246 ± 40 nM in muscle from aged mice. Likewise $[Na^+]_i$ was reduced to 9 ± 0.7 mM in middle-aged muscles and to 13 ± 1 mM in muscle from aged mice. FFA treatment also reduced age associated increases in plasma interleukin 6 and tumor necrosis factor-alpha (TNF-α) concentrations which were elevated in 12 and 24-months old mice compared to young mice and decreased age-related muscle damage as indicated by a reduction in serum creatine kinase (CK)

OPEN ACCESS

Edited by:
Enrique Jaimovich, University of Chile, Chile

Reviewed by:
Noah Lucas Weisleder, The Ohio State University, United States
Erick Omar Hernandez-Ochoa, University of Maryland, Baltimore, United States

***Correspondence:**
Paul D. Allen
paul_allen@hms.harvard.edu

Specialty section:
This article was submitted to Striated Muscle Physiology, a section of the journal Frontiers in Physiology

Received: *31 August 2020*
Accepted: *23 November 2020*
Published: *12 January 2021*

Citation:
Mijares A, Allen PD and Lopez JR (2021) Senescence Is Associated With Elevated Intracellular Resting [Ca^{2+}] in Mice Skeletal Muscle Fibers. An in vivo Study. Front. Physiol. 11:601189. doi: 10.3389/fphys.2020.601189

activity. Our data provides a direct demonstration that normal aging is associated with a significant elevation $[Ca^{2+}]_i$, $[Na^+]_i$, and intracellular ROS production in skeletal muscle fibers. Furthermore, the fact that FFA reduced the intracellular $[Ca^{2+}]$, $[Na^+]$, and ROS production as well as the elevated IL6, TNF-α, and CK levels, led us to suggest that its pharmacological effect may be related to its action both as a TRPC channel blocker and as an anti-inflammatory.

Keywords: aging, calcium, TRPC, skeletal muscle, inflammation

INTRODUCTION

Aging is associated with a concomitant reduction in skeletal mass and muscle strength with a lack of causal disease (Rolland et al., 2008; Tieland et al., 2018). The etiology of muscle aging is complex and still is not fully elucidated. Diverse alterations in muscle have been described, e.g., a significant decrease in myofiber size and number, improper protein synthesis–degradation, and a reduction in the magnitude of motor neurons innervating muscle cells (Doherty, 2003; Mosole et al., 2014). The reduction in muscle mass and strength observed during senescence compromises physical activity promoting a sedentary lifestyle that predisposes the individual to the risk of falling and even death (Visser and Schaap, 2011). Dysfunctional excitation–contraction coupling (Delbono et al., 1995), reduced density of calcium release units (Boncompagni et al., 2006), increased oxidative stress, and alterations of mitochondrial function appears to play a role in age-related changes in muscle (Pietrangelo et al., 2015).

Although abnormalities in intracellular calcium regulatory mechanisms in skeletal muscle with aging have been suggested, no systematic study has been conducted. To our knowledge, the present study represents the first attempt to determine the impact of senescence on intracellular Ca^{2+} concentration ($[Ca^{2+}]_i$) in skeletal muscle, and the role of Ca^{2+} influx mediated by the transient receptor potential canonical (TRPC channels) observed with aging. In addition, we also probed the contribution of oxidative stress and the inflammatory cytokines interleukin (IL-6) and tumor necrosis factor-alpha (TNF-α). We hypothesized that senescence is associated with a chronic increase in $[Ca^{2+}]_i$ and resting intracellular Na^+ ($[Na^+]_i$) in skeletal muscle cells that could be modified or normalized with pharmacological intervention with flufenamic acid (FFA), which is both a non-steroidal anti-inflammatory (NSAID) drug and a non-selective blocker of TRPC channels (Foster et al., 2009; Suzuki et al., 2011; Jiang et al., 2012). We found that treatment with FFA reduced $[Ca^{2+}]_i$ and $[Na^+]_i$, decreased production of reactive oxygen species (ROS), lowered cytokine release, and diminished muscle damage as indicated by a reduction of plasma creatine kinase (CK) activity.

MATERIALS AND METHODS

Animals and Experimental Groups

Young – 3 months; middle-aged – 12 months, and aged – 24 months old C57BL/6J male mice were maintained in the Mount Sinai Medical Center, United States vivarium under constant temperature (21–22°C) on a 12-h light/12-h dark cycle with free access to food and water. All experimental procedures were approved by the Institutional Animal Care and Use Committee at Mount Sinai Hospital.

The first cohort of mice was used for *in vivo* intracellular ion measurements in muscle and consisted of five groups of mice: (A) Control group: Mice ($N = 6$) that did not receive any treatment for the 24 months study and had *in vivo* intracellular Ca^{2+} and Na^+ determinations performed serially at 3, 12, and 24 months. (B) Experimental group 1: 8-week old mice ($N = 7$) were treated for 4 weeks with flufenamic acid (FFA-an anti-inflammatory and non-selective blocker of TRPC channels) injected intraperitoneally (IP) (12.5 mg/kg) once per day for 4 weeks and *in vivo* intracellular Ca^{2+} and Na^+ determinations were carried out at the age of 3-months. (C) Experimental group 2: 44-week old mice ($N = 6$) were treated with FFA for 4 weeks, and *in vivo* intracellular Ca^{2+} and Na^+ determinations were carried out at the age of 12-months. (D) Experimental group 3: 92-week-old mice ($N = 5$) were treated with FFA for 4 weeks, and *in vivo* intracellular Ca^{2+} and Na^+ determinations were carried out at the age of 24-months.

The second cohort of 24 mice were randomly divided into six groups (three treatment and three control, $N = 4$ mice per group) and given the same treatment that was used in the first cohort at 8, 44, and 92 weeks and the studies carried out at 3, 12, and 24 months of age. In this cohort, enzymatically dissociated isolated single flexor digitorum brevis (FDB) muscle cells were used to determine ROS production rate using a fluorescence assay. Unlike the first group, where it was possible to make serial measurements in the control group, separate control groups were used for each time point.

The third cohort of 36 mice of each age were randomly divided into six groups (three treatment and three controls, $N = 6$ mice per group) and given the same treatment given as in the first cohort at 8, 44, and 92 weeks and the studies carried out at 3-, 12- and 24-months of age. At that time, the mice blood was collected from the tail vein for measurements of plasma IL-6, TNF-α, and CK concentrations, and the animals were then euthanized by cervical dislocation.

Ca^{2+}- and Na^+-ion Selective Microelectrodes

Double-barreled, Ca^{2+}- or Na^+-selective microelectrodes were prepared from thin-walled 1.2- and 1.5-mm outside diameter (OD) borosilicate HCl-washed glass capillaries (PB150F-4,

World Precision Instruments, FL, United States). They were heat sterilized (UX-10776-00, Cole Palmer, IL, United States) stretched in a pipette puller (P-97 Flaming/Brown, Automate Scientific, Berkeley, CA, United States) to obtain small-tipped microelectrodes ($\leq$1 μM). The ions-selective barrel (1.5-mm OD) was silanized by exposing it to dimethyldichlorosilane vapor. The tip was then back-filled with either the Ca^{2+} ionophore II (ETH 129, Sigma-Aldrich, MO, United States) or Na^{+} ionophore (ETH 227, Sigma-Aldrich, MO, United States). The barrel's remainder was back-filled with pCa7 for the Ca^{2+} selective microelectrode or 8 mM NaCl solution for the Na^{+} selective as described previously (Eltit et al., 2013). The membrane potential barrel (1.2-mm OD) was back-filled with 3 M KCl just before the measurements were performed. The tip resistances were measured by passing a current pulse of 1 pA through an individual barrel while the electrode tip was in the Ringer bathing solution (Eltit et al., 2013). For the Ca^{2+} and Na^{+}-selective microelectrodes, the resistances ranged from 8 to 10×10^{10} Ω, and for the membrane potential microelectrodes (Vm), the resistances ranged from 10 to 15 MΩ with a tip potential less than 5 mV. The double-barreled ion-selective microelectrode was mounted in a modified plastic holder containing Ag/AgCl wires. It was attached to a miniature head stage (probe input impedance $> 10^{11}$Ω), which was connected to a Duo 773 electrometer (World Precision Instruments, FL, United States). The Vm and ions specific potentials were acquired at a frequency of 1,000 Hz with AxoGraph software (version 4.6; Axon Instruments, CA, United States) and stored in a computer for further analysis. Each ion-selective microelectrode was individually calibrated before and after the measurement by exposure of the tip to a series of calibrating solutions, as described previously, and if the two calibration curves did not agree within 3 mV, data from that microelectrode were discarded (Lopez et al., 1983; Eltit et al., 2013). The bath's reference electrode was either an Ag–AgCl pellet or an agar bridge made of a polythene tube containing 3 M KCl gelled in agar. Muscle cells were impaled with the double-barreled ion-microelectrode and Vm and Ca^{2+} or Vm and Na^{+} potentials were measured. After both potentials were stable for at least 1 min, the microelectrode was withdrawn.

Recording of Intracellular [Ca^{2+}] and [Na^{+}] in Muscle Fibers *in vivo*

Intracellular Ca^{2+} and Na^{+} determinations were carried out *in vivo* using Ca^{2+}- and Na^{+}-selective microelectrodes (Eltit et al., 2013) under aseptic conditions. After the mice were anesthetized, the hair on the leg was removed, the skin was cleaned with an antiseptic solution, and a small incision was made. The gastrocnemius muscle was identified, the muscle fascia was partially removed, and the superficial fibers were exposed. Warm sterile Ringer's solution was perfused onto the superficial muscle fibers to preserve moisture. The mice were kept euthermic (37°C) with the aid of a low noise heating system (ATC1000, World Precision Instruments, FL, United States). Through the aid of a stereomicroscope (233445 Olympus, MA, United States), individual muscle fibers were impaled with either Ca^{2+} or Na^{+} double-barreled microelectrodes. Examples of actual recordings from these electrodes can be found in our previous publications (Lopez et al., 1983, 2000, 2011, 2020).

In the control group, $[Ca^{2+}]_i$ and $[Na^{+}]_i$ measurements were repeated in the same animal at all three-time points (3, 12, and 24-months). In this group, after the measurements of $[Ca^{2+}]_i$ and $[Na^{+}]_i$ were made, the area around the wound was washed with streptomycin solution (10 mg/L), and the skin was sutured. Topical local anesthetic (bupivacaine) was applied every 12 h for 48 h to the wound area to relieve minor pain (type A – wound suturing) produced by survival surgery according to the Guide for the Care and Use of Laboratory Animals. In the treated groups and the control group at 24 months, after completing measurements of $[Ca^{2+}]_i$ and $[Na^{+}]_i$, mice were euthanized by cervical dislocation. Before making measurements, all mice were kept in individual cages to avoid potential damage by other mice.

Determination of Reactive Oxygen Species in Muscle Cells

Intracellular ROS levels were determined in enzymatically isolated FDB muscle cells from treated and untreated 3, 12, and 24 month-old mice using the dichlorodihydrofluorescein diacetate (DCFHDA) assay (Luis, MO, United States) as previously described (Lopez et al., 2018b). The fluorescence intensity of dichlorodihydrofluorescein (DCF) was detected by a fluorescence microplate reader (Molecular Device, Sunnyvale, CA, United States) at an excitation wavelength of 488 nm and an emission wavelength 525 nm. All measurements were performed in triplicate, and the results reported as the percentage of ROS production relative to untreated 3-month muscle cells.

Determination of Plasma IL6 and TNF-α Concentrations and CK Activity

Plasma IL-6 concentrations were measured in plasma samples from blood collected from the tail vein in treated and untreated 3, 12, and 24 months-old animals using a Milliplex Mouse Cytokine/Chemokine Panel (EMD Millipore, MA, United States) with a Bio-Plex Suspension Array System (Bio-Rad Laboratories, CA, United States). Similarly, TNF-α content was measured in plasma samples from untreated and treated 3, 12, and 24 months-old animals using a mouse TNF-α ELISA kit (Invitrogen, CA, United States). The values were normalized to muscle protein concentration determined by BCA protein assay (Thermo Scientific, MA, United States). Plasma CK activity was determined using a creatine kinase assay kit (Sekisui Diagnostics, MA, United States) according to manufacturer's instructions. CK activity was determined in triplicate from each sample and expressed as units per liter (U/L). All measurements were carried out on triplicate blood samples obtained from the same animal at three different times on the same day (8 am, 12 pm, and 4 pm). Despite the small blood volume withdrawn, oral fluid replacement was provided between each endpoint.

Statistics

Data are reported as mean ± standard deviation (SD). For $[Ca^{2+}]_i$ and $[Na^{+}]_i$ determinations, each successful impalement

was considered one experimental *n*. We excluded all data from muscle fibers showing a resting membrane potential of less than −80 mV from the final analysis (22% of the total fibers measured). In the biochemical assay, each animal represented one experimental *N* and *n* the number of measurements. We used the D'Agostino and Pearson test to determine whether the samples were normally distributed. We compared the experimental values using a one-way analysis of variance (ANOVA) and Tukey *post hoc* test. A *p*-value <0.05 was set as statistically significant level. All statistical analyses were carried out with GraphPad Prism 9.0 (GraphPad Software, CA, United States).

RESULTS

Muscle Intracellular [Ca^{2+}] and [Na^{+}] and Aging. Effects of FFA

We examined muscle $[Ca^{2+}]_i$ and $[Na^{+}]_i$ *in vivo* in young, middle-aged, and aged mice to explore the changes associated with normal aging in mice. Compared to young muscle fibers $[Ca^{2+}]_i$ from middle-aged and aged mice was significantly elevated. In young mice, muscle $[Ca^{2+}]_i$ was 121 ± 4 nM (N = 6, n = 15). In middle-aged mice muscle $[Ca^{2+}]_i$ increased to 255 ± 36 nM (N = 6, n = 16, $p \leq 0.001$ compared to young mice), and in aged mice it rose to 409 ± 35 nM (N = 6, n = 14, $p \leq 0.001$ compared to young mice; **Figure 1** left panel). We also found that muscle $[Na^{+}]_i$ is also significantly elevated in middle-aged and aged muscle compared to young mice. In muscle fibers from young mice $[Na^{+}]_i$ was 8 ± 0.5 mM, (N = 6, n = 11), from middle-aged mice $[Na^{+}]_i$ was 12 ± 1 mM (N = 6, n = 13, $p \leq 0.001$ compared to young mice) and from aged mice [Na+]$_i$ was 17 ± 1 mM (N = 6, n = 12, $p \leq 0.001$ compared to young mice; **Figure 2** left panel).

Treatment with FFA (12.5 mg/kg IP once per day for 4 weeks; see section "Materials and Methods" for more details) normalized $[Ca^{2+}]_i$ in muscle fibers from middle-aged mice (134 ± 8 nM, N = 6, n = 16, $p \geq 0.65$ compared to young muscle cells) and significantly reduced $[Ca^{2+}]_i$ in muscle cells from aged mice (246 ± 40 nM, N = 5, n = 18, $p \leq 0.001$ compared to untreated aged mice). No effect of FFA treatment on $[Ca^{2+}]_i$ was observed in muscle fibers from young mice (**Figure 1** right panel). Similarly, FFA treatment normalized $[Na^{+}]_i$ in muscle cells from middle-aged mice (9 ± 0.7 mM. N = 6, n = 11, $p \geq 0.52$ compared to young muscle fibers) and significantly reduced $[Na^{+}]_i$ in muscle from aged mice (13 ± 1 mM, N = 5, n = 12, $p \leq 0.001$ compared to muscle from untreated aged mice). FFA did not modify $[Na^{+}]_i$ in young muscle cells (**Figure 2** right panel).

Increased Oxidative Stress With Aging

We measured ROS production in isolated FDB muscle cells from young, middle-aged, and aged mice. FDB muscle fibers loaded with the fluorescent ROS sensor CM-H2DCFDA in middle-aged and aged mice showed significantly increased rates of DCF fluorescence increase compared to FDB muscle fibers isolated from young mice ($p \leq 0.001$ for both middle-aged and aged fibers compared to muscle from young mice; **Figure 3** left panel). Evidence has been presented suggesting

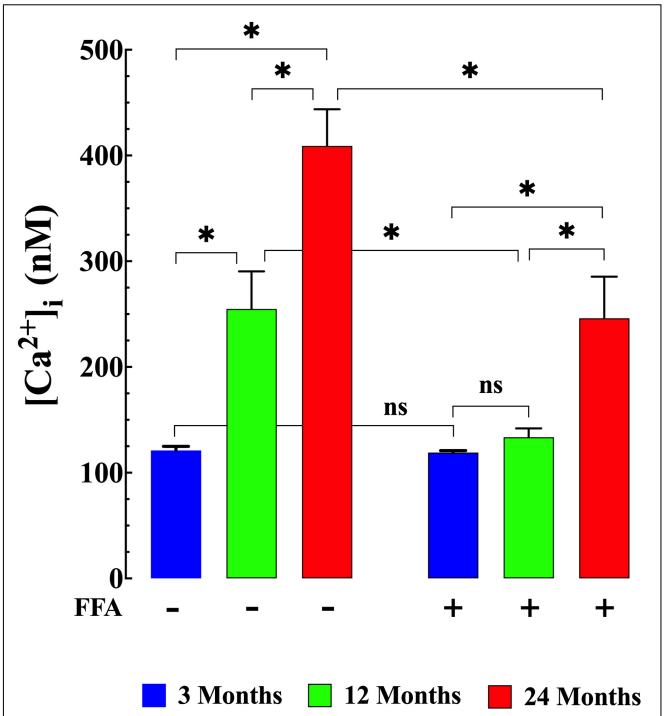

FIGURE 1 | Augmented $[Ca^{2+}]_i$ in aged muscle fibers. Effect of flufenamic acid (FFA). Middle-aged (12-month) and aged (24-month) muscles have higher $[Ca^{2+}]_i$ than muscles in young animals ($p \leq 0.001$ compared to young mice) **(left panel)**. FFA (12.5 mg/kg IP once per day for 4 weeks) normalized $[Ca^{2+}]_i$ in muscle cells from middle-aged animals compared to young animals ($p > 0.65$) and significantly decreased $[Ca^{2+}]_i$ in muscle from aged mice compared to untreated aged mice ($p \leq 0.001$) **(right panel)**. $[Ca^{2+}]_i$ measurements in untreated mice were obtained from: N = 6 mice/age group, n_{cell} = 14–16/age group; $[Ca^{2+}]_i$ measurements in FFA-treated mice were obtained from: N = 6 mice/per age group, n_{cell} = 15–18/age group. Values are expressed as means ± SD. 1-Way ANOVA followed by Tukey's *post hoc* comparisons, *$p < 0.05$.

that $[Ca^{2+}]_i$ could modulate either ROS production and/or clearance in excitable cells (Gorlach et al., 2015). Thus, we reasoned that reducing muscle $[Ca^{2+}]_i$ by treatment with FFA (see **Figure 1** right panel) should decrease intracellular ROS production. Pre-treatment with FFA (12.5 mg/kg IP once per day for four weeks) significantly reduced ROS production in middle-aged and aged muscle cells ($p \leq 0.001$ compared to muscle cells from untreated middle-aged and aged mice; **Figure 3** right panel). No effect of FFA treatment on ROS production was detected in muscle cells from young mice ($p \geq 0.98$ compared to muscle cells from untreated mice; **Figure 3** right panel).

Plasma IL-6 and TNF-α Concentrations and Aging

Senescence has been shown to be associated with an increase in inflammatory markers such as IL6 and TNF-α (Wei et al., 1992; Garner et al., 2018). Therefore, we measured IL-6 levels and TNF-α levels in plasma from young, middle-aged, and aged mice. We found that plasma IL-6 concentration increased

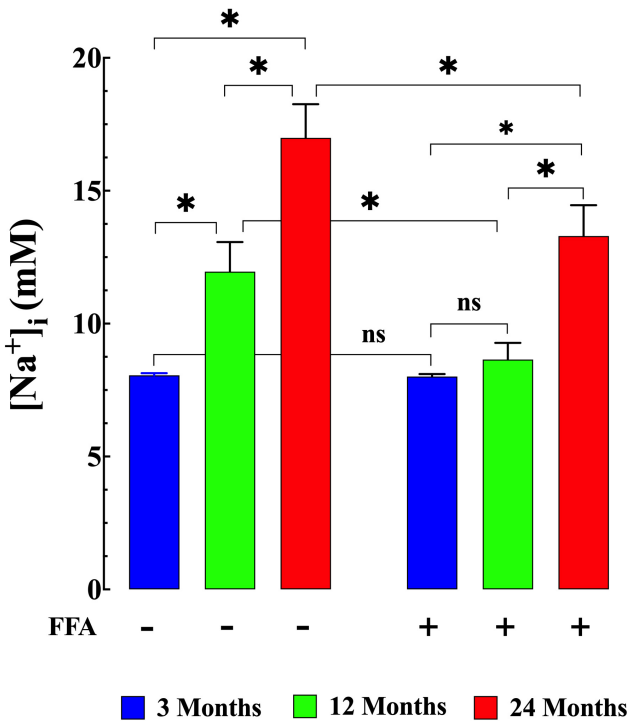

FIGURE 2 | Augmented $[Na^+]_i$ in aged muscle fibers. Effect of flufenamic acid (FFA). Muscle cells from middle-aged (12-months) and aged (24-months) old mice have a higher $[Na^+]_i$ than muscle cells from young animals ($p \leq 0.001$ compared young mice) **(left panel)**. FFA normalized $[Na^+]_i$ in middle-aged compared to young muscle ($p \geq 0.62$) and significantly decreased in aged compared to untreated aged muscle cells ($p \leq 0.001$) **(right panel)**. No effect of FFA treatment on $[Na^+]_i$ was observed in muscle from young mice ($p \geq 0.99$ compared to muscle from untreated young mice). $[Na^+]_i$ measurements in untreated mice were obtained from: $N = 6$ mice/age group, $n_{cell} = 11–13$/age group; $[Na^+]_i$ measurements in FFA-treated mice were obtained from: $N = 6$ mice/per age group, $n_{cell} = 11–12$/age group. Values are expressed as means ± SD. 1-Way ANOVA followed by Tukey's *post hoc* comparisons, $^*p < 0.05$.

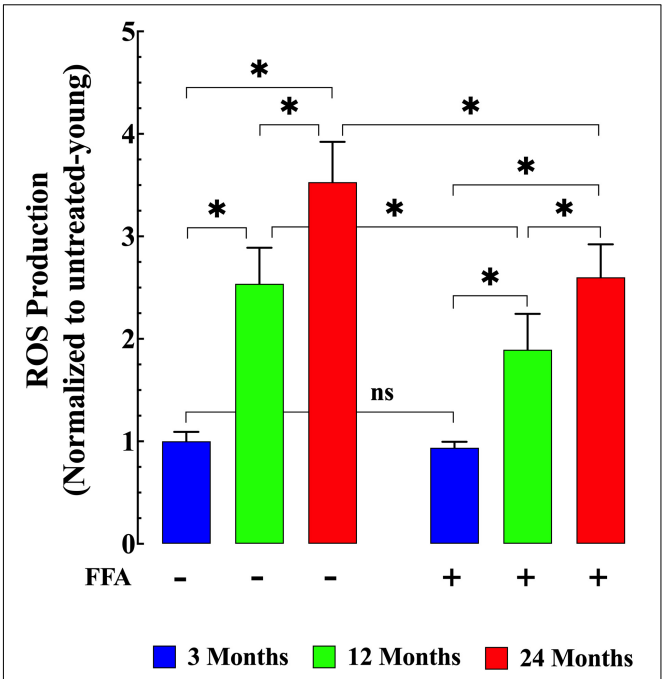

FIGURE 3 | Age-related changes in skeletal muscle reactive oxygen (ROS) production. ROS production in isolated FDB fibers was significantly increased in middle-aged ($p \leq 0.001$ compared to muscle cells from young mice) and aged fibers ($p \leq 0.001$ compared to muscle cells from young mice) **(left panel)**. While treatment with FFA significantly reduced ROS production in middle-aged and aged muscle fibers ($p \leq 0.001$ compared to muscle cells from untreated age-matched mice) no effect was observed in young muscle cells ($p \geq 0.98$ compared to muscle cells from untreated young mice) **(right panel)**. ROS measurements in untreated mice were obtained from $N = 4$ mice/age group, $n_{cell} = 22–25$/age group; ROS measurements in FFA-treated mice were obtained from $N = 4$ per age group, $n_{cell} = 19–25$/age group. Values are expressed as means ± SD. 1-Way ANOVA followed by Tukey's *post hoc* comparisons, $^*p < 0.05$.

from 19 ± 2 pg/mL (N = 6 mice, n = 13) in young mice, to 30 ± 3 pg/mL in middle-aged mice (N = 6 mice, n = 14, $p \leq 0.001$ compared to young mice), and to 50 ± 6 pg/mL in aged mice (N = 6 mice, n = 16, $p \leq 0.001$ compared to young mice), (**Figure 4** left panel). Similarly, we found that there was an age-dependent elevation of plasma TNF-α concentration from 5.9 ± 1.1 pg/mg^{-1} protein (N = 6 mice, n = 15) in young mice to 9.6 ± 1.6 pg/mg protein middle-aged mice (N = 6 mice, n = 16, $p \leq 0.001$ compared to young mice) and to 15.9 ± 2.1 pg/mg protein in aged mice (N = 6 mice, n = 18, $p \leq 0.001$ compared to young mice; **Figure 5** left panel). Treatment with FFA (12.5 mg/kg IP once per day for four weeks) normalized plasma IL-6 levels in middle-aged mice (22 ± 3 pg/mL, N = 6 mice, n = 16, $p \geq 0.31$ compared to plasma levels from young mice and $p \leq 0.001$ compared to plasma IL-6 levels from untreated middle-aged mice). In aged mice FFA reduced plasma IL-6 levels to 36 ± 4 pg/mL (N = 6 mice, n = 15, $p \leq 0.001$ compared to plasma IL-6 levels from untreated aged mice; **Figure 4** right panel). Likewise FFA treatment significantly reduced TNF-α levels in both middle-aged mice group where it was normalized to the levels of untreated young mice (6 ± 1.3 pg/mg protein, N = 6 mice, n = 15, $p \geq 0.99$ compared to plasma levels from young mice) and in the aged group it was reduced to 10.7 ± 1.9 pg/mg protein, N = 6 mice, n = 18, $p \leq 0.001$ compared to plasma concentrations from untreated aged-mice; **Figure 5** right panel) In young mice, FFA did not change the IL-6 plasma level (20 ± 3 pg/mL, N = 6 mice, n = 14, $p \geq 0.99$ compared to plasma IL-6 levels from untreated young mice; **Figure 4** right panel) or TNF-α levels (5.6 ± 1.2 pg/mg protein, N = 6 mice, n = 16, $p \geq 0.98$ compared to plasma concentration from untreated aged-mice; **Figure 5** right panel).

Muscle Damage and Aging

Although an increase in plasma CK can indicate acute cardiac muscle damage, levels which remain increased over time are more likely to be an indication of skeletal muscle damage which has previously been shown to be associated with aging (Kim et al., 2018). Here we found that plasma CK activity was significantly elevated in both middle-aged mice (141 ± 13 IU/L,

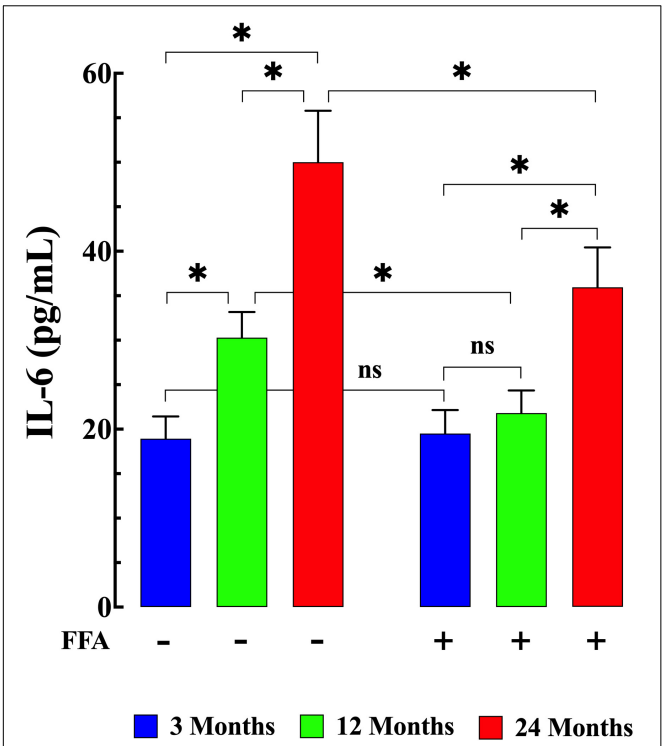

FIGURE 4 | Age-associated increases in interleukin-6 (IL-6). Plasma IL6 levels were significantly increased in middle-aged and aged mice ($p \leq 0.001$ for both) compared to plasma levels from young mice **(left panel)**. FFA treatment normalized plasma IL6 levels in middle-aged animals ($p \geq 0.31$ compared to plasma levels from young mice), and significantly reduced plasma IL-6 in aged mice ($p \leq 0.001$ compared to untreated aged mice). No effect on basal IL-6 levels were observed in young mice ($p \geq 0.99$ compared to plasma levels from untreated young mice) **(right panel)**. IL-6 measurements in untreated mice were obtained from $N = 6$ mice/age group, n determinations = 13–16/age group; IL-6 measurements in FFA-treated mice were obtained from $N = 6$ per age group, n determinations = 14–16/age group. Values are expressed as means ± SD. 1-Way ANOVA followed by Tukey's *post hoc* comparisons, $^*p < 0.05$.

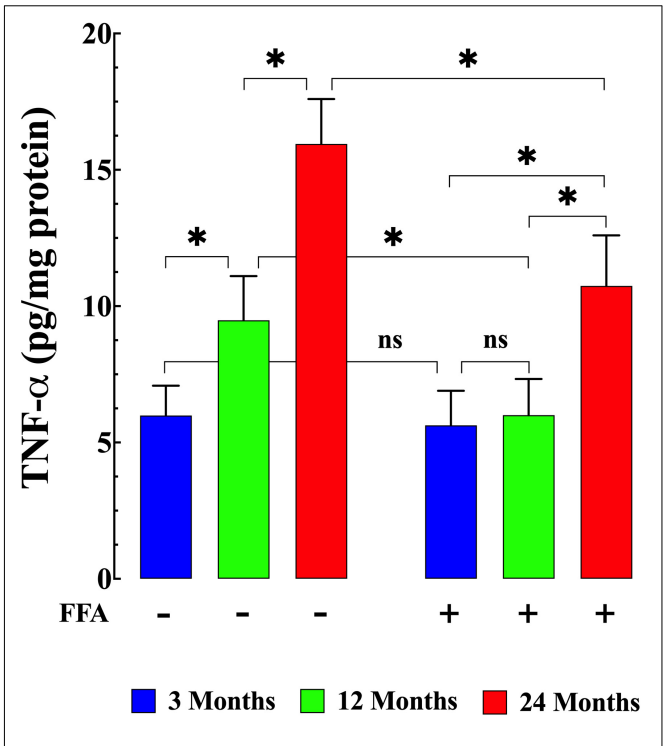

FIGURE 5 | Increased TNF-α plasma level and aging. Middle-aged and aged mice had significantly TNF-α higher levels than young mice ($p \leq 0.001$) **(left panel)**. FFA treatment normalized plasma TNF-α in middle-aged animals ($p \geq 0.99$ compared to plasma levels from young mice), and although it did not normalize plasma TNF-α in aged mice, it significantly reduced plasma TNF-α levels compared to untreated aged mice **(right panel)** ($p \leq 0.001$). FFA treatment had no effect on basal TNF-a levels in young animals ($p \geq 0.98$ compared to untreated young mice) **(right panel)**. TNF-α measurements in untreated mice were obtained from $N = 6$ mice/age group, n determinations = 15–18/age group; TNF-α measurements in FFA-treated mice were obtained from $N = 6$ per age group, n determinations = 16–18/age group. Values are expressed as means ± SD. 1-Way ANOVA followed by Tukey's *post hoc* comparisons, $^*p < 0.05$.

$N = 6$ mice, $n = 18$) and aged mice (213 ± 27 IU/L, $N = 6$, $n = 20$) compared to young mice (95 ± 11 IU/L $N = 6$ mice, $n = 20$ $p \leq 0.001$ compared to middle-aged and aged mice; **Figure 6** left panel). FFA treatment significantly lowered CK levels in middle-aged (117 ± 13 IU/L $N = 6$, $n = 17$, $p \leq 0.001$ compared to untreated middle aged-mice) and in aged mice (162 ± 23 IU/L $N = 6$, $n = 18$, $p \leq 0.001$ compared to untreated aged-mice; **Figure 6** right panel). As seen with the increase in inflammatory markers, FFA had no effect on plasma CK levels in young animals (96 ± 12 IU/L ($N = 6$, $n = 16$, $p \geq 0.99$ compared to untreated mice; **Figure 6** right panel).

DISCUSSION

In this study we directly examined changes in resting intracellular Ca^{2+} and Na^+ homeostasis in skeletal muscle during normal aging. The major findings of the present study are an age-dependent increase of skeletal muscle $[Ca^{2+}]_i$, $[Na^+]_i$, increased ROS generation and elevation of plasma IL-6, TNF-α and CK concentrations (aged > middle-aged > young). Treatment with FFA, reduced muscle levels of $[Ca^{2+}]_i$, $[Na^+]_i$, reduced ROS production and reduced plasma levels of IL-6, TNF-α and CK in middle aged and aged mice (12 and 24-months) but had no effect in young mice (3-months).

Regulation of resting intracellular calcium $[Ca^{2+}]$ is critical in muscle cells. While extracellular Ca^{2+} concentration ranges within 1–2 mM in quiescent and healthy muscle cells resting free cytosolic $[Ca^{2+}]$ is remarkably low (10^{-7} M) (Marban et al., 1980; Lopez et al., 1983, 2018a). Several intracellular regulatory mechanisms have been proposed in muscle cells to preserve this low resting $[Ca^{2+}]_i$. ATP-driven Ca^{2+} pumps pump out Ca^{2+} from the cytoplasm, including the sarcoplasmic reticulum (SR) Ca^{2+}ATPase that pumps it back into the SR and the plasma membrane Ca^{2+}-ATPase (Brini and Carafoli, 2009) that pumps it out of the cytoplasm into the extracellular space. Furthermore $[Ca^{2+}]_i$ is also regulated by Ca^{2+} influx

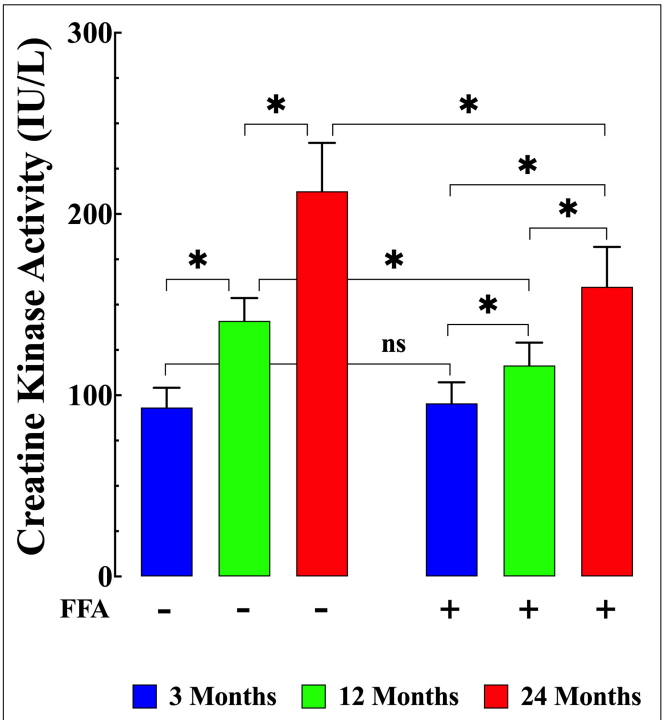

FIGURE 6 | Variation of creatine kinase (CK) levels with aging. CK levels were significantly higher in middle-aged and aged mice ($p \leq 0.001$) compared to plasma levels young mice **(left panel)**. FFA treatment normalized plasma CK levels in middle-aged animals compared to young animals ($p \geq 0.99$ compared to plasma levels from young mice) and FFA significantly reduced plasma CK concentrations in aged mice compared to untreated aged mice ($p \leq 0.001$). FFA did not modify basal CK levels in young animals ($p \geq 0.99$ compared to plasma levels from untreated young mice). CK measurements in untreated mice were obtained from $N = 6$ mice/age group, n determinations = 19–20/age group; CK measurements in FFA-treated mice were obtained from $N = 6$ per age group, n determinations = 16–17/age group. Values are expressed as means ± SD. 1-Way ANOVA followed by Tukey's *post hoc* comparisons, $^*p < 0.05$.

through TRPC channels (Choi et al., 2020), store-operated Ca^{2+} channels (Lyfenko and Dirksen, 2008), the bidirectional and electrogenic Na^+/Ca^{2+} exchanger in the plasma membrane (Cifuentes et al., 2000; Fraysse et al., 2001; Blaustein, 2013) and by passive leak from the SR through the ryanodine receptor (Yang et al., 2007; Eltit et al., 2010; Andersson et al., 2011; Lamboley et al., 2016).

Transient receptor potential canonical channels are non-selective cation channels localized in mammalian cells' plasma membrane. Among the TRPCs, in skeletal muscle, TRPC3 is the most expressed, followed by TRPC1 and TRPC6 (Kunert-Keil et al., 2006). TRPC channels have been implicated in the pathogenesis of diverse muscle diseases, in particular muscle dystrophies and myasthenia gravis (Kruger et al., 2008; Gailly, 2012; Mijares et al., 2014; Sauc and Frieden, 2017; Lopez et al., 2020). Furthermore, overexpression of a dominant-negative form of TRPC6 (dnTRPC6) in this TRPC3 overexpression background reverted its dystrophic phenotype as well as reverting the dystrophic phenotype both in mdx and in Scgd mouse (Millay et al., 2009; Burr et al., 2014).

Our data show that muscle fibers from aged mice have an elevated resting intracellular $[Ca^{2+}]_i$ and $[Na^+]_i$ compared with young muscle cells. The elevated resting $[Ca^{2+}]_i$ and $[Na^+]_i$ found in aged muscle cells is consistent with our recent report showing that $[Ca^{2+}]_i$ is increased in aged neurons compared to young neurons (Uryash et al., 2020). The failure to maintain a low resting $[Ca^{2+}]_i$ in muscle cells can activate enzymes such as proteases, nucleases, and lipases that impair energy production, compromise muscle function and provokes cell death (Nicotera and Orrenius, 1998; Altamirano et al., 2014a). The underlying mechanisms related to the observed dysfunction of $[Ca^{2+}]_i$ in aging muscle is complicated. However, an increase in RyR1 leak has been reported in aged muscle (Andersson et al., 2011; Lamboley et al., 2016). This leak then provokes a chronic partial depletion of SR Ca^{2+} which induces an increased influx of extracellular Ca^{2+} that is independent of the L-type Ca^{2+} channel mediated Ca^{2+} entry (Launikonis and Rios, 2007; Lyfenko and Dirksen, 2008). This pathway's identity is not fully understood; however, the involvement of TRPCs, which are highly expressed in skeletal muscle cells, has been suggested (Vandebrouck et al., 2002; Millay et al., 2009). A similar aberrant elevation in $[Ca^{2+}]_i$ and $[Na^+]_i$ have been observed in muscle cells from patients with Duchene's muscular dystrophy and mdx mice (Lopez et al., 1987; Altamirano et al., 2014b; Lopez et al., 2017, 2020) where an abnormal Ca^{2+} influx has also been reported (Tutdibi et al., 1999; Kruger et al., 2008; Millay et al., 2009). Thus, if it were possible to prevent this chronic elevation of $[Ca^{2+}]_i$ during aging, it may exert a myo-protective effect and potentially prevent the muscle wasting and dysfunction observed in the aging muscle.

We show here that there is a significant increase in ROS generation in aging muscles (old > middle-aged > young). Physiological concentrations of ROS play essential roles in diverse muscle signaling pathways. However, elevated ROS production harms muscle function (Wanagat et al., 2001; Calvani et al., 2013; Le Moal et al., 2017). ROS and lipid peroxidation levels are abnormal in senescent muscle cells (Ryan et al., 2010). However, there is a large body of evidence showing mitochondrial dysfunction is associated with aging, and it is well known that the mitochondria are a primary source of cells ROS production (Boengler et al., 2017). Intracellular ROS dyshomeostasis has been suggested to decrease protein synthesis and increase protein degradation, provoking muscle atrophy (Kinugawa et al., 2015) and microdamage of the muscle membrane allowing release of intracellular components such as CK (Kim et al., 2018). One of the results of increased ROS production is an increase in the plasma levels inflammatory markers such as IL-6 and TNF-α such as we found here. The above-described results suggest that increased ROS production in senescent skeletal muscle might be linked with age-dependent intracellular Ca^{2+} imbalance observed in aging mice (Kinugawa et al., 2015).

To further explore the mechanism involved in the changes of $[Ca^{2+}]_i$, $[Na^+]_i$, ROS, IL-6, TNF-α with aging we treated mice

with FFA, a NSAID drug which also blocks TRPCs which are non-selective plasmalemmal cation channels (Chen et al., 1993; Hescheler and Schultz, 1993). The FFA anti-inflammatory effect appears to be mediated by reduction of prostaglandin synthesis by inhibiting the cyclo-oxygenases (Flower, 1974). Clinically FFA has been used locally for analgesia against pain and inflammation associated with musculoskeletal and joint disorders, peri-articular, and soft tissue disorders (Flower, 1974). In addition, FFA has been used as a non-selective plasmalemmal cation entry channel blocker and has been shown to inhibit the spontaneous active tone of carotid artery (Shimamura et al., 2002) and to attenuate the K^+-induced contraction in endothelium-denuded small and large arteries (Bencze et al., 2015). In this study, we demonstrated that administration of FFA reduced intracellular Ca^{2+} and Na^+ overload, decreased the rate of ROS production, and lowered the high plasma concentration levels of IL-6 and TNF-α and CK activity in aging mice. Due to FFA's lack of pharmacological specificity (anti-inflammatory and TRPC channel blocker), we are unable to dissect which of these is the primary mechanism of action and which is the result of the primary action.

CONCLUSION

In this study we present direct evidence of abnormal regulation of $[Ca^{2+}]_i$, $[Na^+]_i$, and increased ROS production in aging muscles. Furthermore, we show that aging is associated with elevated plasma levels of the inflammatory markers, IL6, TNF-α, and CK which is an indicator of chronic muscle damage. Treatment with FFA significantly decreased elevated $[Ca^{2+}]_i$, $[Na^+]_I$, and reduced ROS overload, which was accompanied by decreases in plasma IL6, TNF-α, and CK levels. The mechanism of FFA's action in correcting these age related defects may be related either to its action as a TRPC channel blocker and/or its direct anti-inflammatory effect on ROS production.

DATA AVAILABILITY STATEMENT

The raw data supporting the conclusions of this article will be made available by the authors, without undue reservation.

ETHICS STATEMENT

All protocols used in the study were performed following the recommendations in the Guide for the Care and Use of Laboratory Animals of the National Institutes of Health and approved by the IACUC of the Mount Sinai Medical Center, United States.

AUTHOR CONTRIBUTIONS

AM and JL performed the research and analyzed the data. AM, JL, and PA wrote the manuscript. All authors contributed to the manuscript revision and read and approved the submitted version.

FUNDING

This work was supported by the AFM-Téléthon-France (Grant No. 21543) and Florida Heart Research Foundation, United States to JL, and the NIH National Institute of Arthritis, Musculoskeletal, and Skin diseases R01AR068897 to PA and JL.

REFERENCES

Altamirano, F., Eltit, J. M., Robin, G., Linares, N., Ding, X., Pessah, I. N., et al. (2014a). Ca2+ influx via the Na+/Ca2+ exchanger is enhanced in malignant hyperthermia skeletal muscle. *J Biol Chem* 289, 19180–19190. doi: 10.1074/jbc.m114.550764

Altamirano, F., Perez, C. F., Liu, M., Widrick, J., Barton, E. R., Allen, P. D., et al. (2014b). Whole body periodic acceleration is an effective therapy to ameliorate muscular dystrophy in mdx mice. *PLoS One* 9:e106590. doi: 10.1371/journal.pone.0106590

Andersson, D. C., Betzenhauser, M. J., Reiken, S., Meli, A. C., Umanskaya, A., Xie, W., et al. (2011). Ryanodine receptor oxidation causes intracellular calcium leak and muscle weakness in aging. *Cell Metab* 14, 196–207. doi: 10.1016/j.cmet.2011.05.014

Bencze, M., Behuliak, M., Vavrinova, A., and Zicha, J. (2015). Broad-range TRP channel inhibitors (2-APB, flufenamic acid, SKF-96365) affect differently contraction of resistance and conduit femoral arteries of rat. *Eur J Pharmacol* 765, 533–540. doi: 10.1016/j.ejphar.2015.09.014

Blaustein, M. P. (2013). Livin' with NCX and lovin' it: a 45 year romance. *Adv Exp Med Biol* 961, 3–15. doi: 10.1007/978-1-4614-4756-6_1

Boengler, K., Kosiol, M., Mayr, M., Schulz, R., and Rohrbach, S. (2017). Mitochondria and ageing: role in heart, skeletal muscle and adipose tissue. *J Cachexia Sarcopenia Muscle* 8, 349–369. doi: 10.1002/jcsm.12178

Boncompagni, S., D'amelio, L., Fulle, S., Fano, G., and Protasi, F. (2006). Progressive disorganization of the excitation-contraction coupling apparatus in aging human skeletal muscle as revealed by electron microscopy: a possible role in the decline of muscle performance. *J Gerontol A Biol Sci Med Sci* 61, 995–1008. doi: 10.1093/gerona/61.10.995

Brini, M., and Carafoli, E. (2009). Calcium pumps in health and disease. *Physiol Rev* 89, 1341–1378. doi: 10.1152/physrev.00032.2008

Burr, A. R., Millay, D. P., Goonasekera, S. A., Park, K. H., Sargent, M. A., Collins, J., et al. (2014). Na+ dysregulation coupled with Ca2+ entry through NCX1 promotes muscular dystrophy in mice. *Mol Cell Biol* 34, 1991–2002. doi: 10.1128/mcb.00339-14

Calvani, R., Joseph, A. M., Adhihetty, P. J., Miccheli, A., Bossola, M., Leeuwenburgh, C., et al. (2013). Mitochondrial pathways in sarcopenia of aging and disuse muscle atrophy. *Biol Chem* 394, 393–414. doi: 10.1515/hsz-2012-0247

Chen, S., Inoue, R., and Ito, Y. (1993). Pharmacological characterization of muscarinic receptor-activated cation channels in guinea-pig ileum. *Br J Pharmacol* 109, 793–801. doi: 10.1111/j.1476-5381.1993.tb13644.x

Choi, J. H., Jeong, S. Y., Oh, M. R., Allen, P. D., and Lee, E. H. (2020). TRPCs: Influential Mediators in Skeletal Muscle. *Cells* 9, 850. doi: 10.3390/cells9040850

Cifuentes, F., Vergara, J., and Hidalgo, C. (2000). Sodium/calcium exchange in amphibian skeletal muscle fibers and isolated transverse tubules. *Am J Physiol Cell Physiol* 279, C89–C97.

Delbono, O., O'rourke, K. S., and Ettinger, W. H. (1995). Excitation-calcium release uncoupling in aged single human skeletal muscle fibers. *J Membr Biol* 148, 211–222.

Doherty, T. J. (2003). Invited review: Aging and sarcopenia. *J Appl Physiol (1985)* 95, 1717–1727. doi: 10.1152/japplphysiol.00347.2003

Eltit, J. M., Ding, X., Pessah, I. N., Allen, P. D., and Lopez, J. R. (2013). Nonspecific sarcolemmal cation channels are critical for the pathogenesis of malignant hyperthermia. *FASEB J* 27, 991–1000. doi: 10.1096/fj.12-218354

Eltit, J. M., Yang, T., Li, H., Molinski, T. F., Pessah, I. N., Allen, P. D., et al. (2010). RyR1-mediated Ca2+ leak and Ca2+ entry determine resting intracellular Ca2+ in skeletal myotubes. *J Biol Chem* 285, 13781–13787. doi: 10.1074/jbc.m110.107300

Flower, R. J. (1974). Drugs which inhibit prostaglandin biosynthesis. *Pharmacol Rev* 26, 33–67.

Foster, R. R., Zadeh, M. A., Welsh, G. I., Satchell, S. C., Ye, Y., Mathieson, P. W., et al. (2009). Flufenamic acid is a tool for investigating TRPC6-mediated calcium signalling in human conditionally immortalised podocytes and HEK293 cells. *Cell Calcium* 45, 384–390. doi: 10.1016/j.ceca.2009.01.003

Fraysse, B., Rouaud, T., Millour, M., Fontaine-Perus, J., Gardahaut, M. F., and Levitsky, D. O. (2001). Expression of the Na(+)/Ca(2+) exchanger in skeletal muscle. *Am J Physiol Cell Physiol* 280, C146–C154.

Gailly, P. (2012). TRP channels in normal and dystrophic skeletal muscle. *Curr Opin Pharmacol* 12, 326–334. doi: 10.1016/j.coph.2012.01.018

Garner, K. M., Amin, R., Johnson, R. W., Scarlett, E. J., and Burton, M. D. (2018). Microglia priming by interleukin-6 signaling is enhanced in aged mice. *J Neuroimmunol* 324, 90–99. doi: 10.1016/j.jneuroim.2018.09.002

Gorlach, A., Bertram, K., Hudecova, S., and Krizanova, O. (2015). Calcium and ROS: A mutual interplay. *Redox Biol* 6, 260–271. doi: 10.1016/j.redox.2015.08.010

Hescheler, J., and Schultz, G. (1993). Nonselective cation channels: physiological and pharmacological modulations of channel activity. *EXS* 66, 27–43. doi: 10.1007/978-3-0348-7327-7_2

Jiang, H., Zeng, B., Chen, G. L., Bot, D., Eastmond, S., Elsenussi, S. E., et al. (2012). Effect of non-steroidal anti-inflammatory drugs and new fenamate analogues on TRPC4 and TRPC5 channels. *Biochem Pharmacol* 83, 923–931. doi: 10.1016/j.bcp.2012.01.014

Kim, K. Y., Ku, S. K., Lee, K. W., Song, C. H., and An, W. G. (2018). Muscle-protective effects of Schisandrae Fructus extracts in old mice after chronic forced exercise. *J Ethnopharmacol* 212, 175–187. doi: 10.1016/j.jep.2017.10.022

Kinugawa, S., Takada, S., Matsushima, S., Okita, K., and Tsutsui, H. (2015). Skeletal Muscle Abnormalities in Heart Failure. *Int Heart J* 56, 475–484. doi: 10.1536/ihj.15-108

Kruger, J., Kunert-Keil, C., Bisping, F., and Brinkmeier, H. (2008). Transient receptor potential cation channels in normal and dystrophic mdx muscle. *Neuromuscul Disord* 18, 501–513. doi: 10.1016/j.nmd.2008.04.003

Kunert-Keil, C., Bisping, F., Kruger, J., and Brinkmeier, H. (2006). Tissue-specific expression of TRP channel genes in the mouse and its variation in three different mouse strains. *BMC Genomics* 7:159.

Lamboley, C. R., Wyckelsma, V. L., Mckenna, M. J., Murphy, R. M., and Lamb, G. D. (2016). Ca(2+) leakage out of the sarcoplasmic reticulum is increased in type I skeletal muscle fibres in aged humans. *J Physiol* 594, 469–481. doi: 10.1113/jp271382

Launikonis, B. S., and Rios, E. (2007). Store-operated Ca2+ entry during intracellular Ca2+ release in mammalian skeletal muscle. *J Physiol* 583, 81–97. doi: 10.1113/jphysiol.2007.135046

Le Moal, E., Pialoux, V., Juban, G., Groussard, C., Zouhal, H., Chazaud, B., et al. (2017). Redox Control of Skeletal Muscle Regeneration. *Antioxid Redox Signal* 27, 276–310. doi: 10.1089/ars.2016.6782

Lopez, J. R., Alamo, L., Caputo, C., Dipolo, R., and Vergara, S. (1983). Determination of ionic calcium in frog skeletal muscle fibers. *Biophys J* 43, 1–4. doi: 10.1016/s0006-3495(83)84316-1

Lopez, J. R., Briceno, L. E., Sanchez, V., and Horvart, D. (1987). Myoplasmic (Ca2+) in Duchenne muscular dystrophy patients. *Acta Cient Venez* 38, 503–504.

Lopez, J. R., Contreras, J., Linares, N., and Allen, P. D. (2000). Hypersensitivity of malignant hyperthermia-susceptible swine skeletal muscle to caffeine is mediated by high resting myoplasmic [Ca2+]. *Anesthesiology* 92, 1799–1806. doi: 10.1097/00000542-200006000-00040

Lopez, J. R., Espinosa, R., Landazuru, P., Linares, N., Allen, P., and Mijares, A. (2011). [Dysfunction of diastolic [Ca(2)(+)] in cardiomyocytes isolated from chagasic patients]. *Rev Esp Cardiol* 64, 456–462. doi: 10.1016/j.rec.2011.01.008

Lopez, J. R., Kaura, V., Diggle, C. P., Hopkins, P. M., and Allen, P. D. (2018a). Malignant hyperthermia, environmental heat stress, and intracellular calcium dysregulation in a mouse model expressing the p.G2435R variant of RYR1. *Br J Anaesth* 121, 953–961. doi: 10.1016/j.bja.2018.07.008

Lopez, J. R., Kolster, J., Zhang, R., and Adams, J. (2017). Increased constitutive nitric oxide production by whole body periodic acceleration ameliorates alterations in cardiomyocytes associated with utrophin/dystrophin deficiency. *J Mol Cell Cardiol* 108, 149–157. doi: 10.1016/j.yjmcc.2017.06.004

Lopez, J. R., Uryash, A., Faury, G., Esteve, E., and Adams, J. A. (2020). Contribution of TRPC Channels to Intracellular Ca(2 +) Dyshomeostasis in Smooth Muscle From mdx Mice. *Front Physiol* 11:126.

Lopez, J. R., Uryash, A., Kolster, J., Esteve, E., Zhang, R., and Adams, J. A. (2018b). Enhancing Endogenous Nitric Oxide by Whole Body Periodic Acceleration Elicits Neuroprotective Effects in Dystrophic Neurons. *Mol Neurobiol* 55, 8680–8694. doi: 10.1007/s12035-018-1018-8

Lyfenko, A. D., and Dirksen, R. T. (2008). Differential dependence of store-operated and excitation-coupled Ca2+ entry in skeletal muscle on STIM1 and Orai1. *J Physiol* 586, 4815–4824. doi: 10.1113/jphysiol.2008.160481

Marban, E., Rink, T. J., Tsien, R. W., and Tsien, R. Y. (1980). Free calcium in heart muscle at rest and during contraction measured with Ca2+ -sensitive microelectrodes. *Nature* 286, 845–850. doi: 10.1038/286845a0

Mijares, A., Altamirano, F., Kolster, J., Adams, J. A., and Lopez, J. R. (2014). Age-dependent changes in diastolic Ca(2+) and Na(+) concentrations in dystrophic cardiomyopathy: Role of Ca(2+) entry and IP3. *Biochem Biophys Res Commun* 452, 1054–1059. doi: 10.1016/j.bbrc.2014.09.045

Millay, D. P., Goonasekera, S. A., Sargent, M. A., Maillet, M., Aronow, B. J., and Molkentin, J. D. (2009). Calcium influx is sufficient to induce muscular dystrophy through a TRPC-dependent mechanism. *Proc Natl Acad Sci U S A* 106, 19023–19028. doi: 10.1073/pnas.0906591106

Mosole, S., Carraro, U., Kern, H., Loefler, S., Fruhmann, H., Vogelauer, M., et al. (2014). Long-term high-level exercise promotes muscle reinnervation with age. *J Neuropathol Exp Neurol* 73, 284–294. doi: 10.1097/nen.0000000000000032

Nicotera, P., and Orrenius, S. (1998). The role of calcium in apoptosis. *Cell Calcium* 23, 173–180. doi: 10.1016/s0143-4160(98)90116-6

Pietrangelo, L., D'incecco, A., Ainbinder, A., Michelucci, A., Kern, H., Dirksen, R. T., et al. (2015). Age-dependent uncoupling of mitochondria from Ca2(+) release units in skeletal muscle. *Oncotarget* 6, 35358–35371. doi: 10.18632/oncotarget.6139

Rolland, Y., Czerwinski, S., Abellan Van Kan, G., Morley, J. E., Cesari, M., Onder, G., et al. (2008). Sarcopenia: its assessment, etiology, pathogenesis, consequences and future perspectives. *J Nutr Health Aging* 12, 433–450. doi: 10.1007/bf02982704

Ryan, M. J., Jackson, J. R., Hao, Y., Williamson, C. L., Dabkowski, E. R., Hollander, J. M., et al. (2010). Suppression of oxidative stress by resveratrol after isometric contractions in gastrocnemius muscles of aged mice. *J Gerontol A Biol Sci Med Sci* 65, 815–831. doi: 10.1093/gerona/glq080

Sauc, S., and Frieden, M. (2017). Neurological and Motor Disorders: TRPC in the Skeletal Muscle. *Adv Exp Med Biol* 993, 557–575. doi: 10.1007/978-3-319-57732-6_28

Shimamura, K., Zhou, M., Ito, Y., Kimura, S., Zou, L. B., Sekiguchi, F., et al. (2002). Effects of flufenamic acid on smooth muscle of the carotid artery isolated from spontaneously hypertensive rats. *J Smooth Muscle Res* 38, 39–50. doi: 10.1540/jsmr.38.39

Suzuki, Y., Kodama, D., Goto, S., and Togari, A. (2011). Involvement of TRP channels in the signal transduction of bradykinin in human osteoblasts. *Biochem Biophys Res Commun* 410, 317–321. doi: 10.1016/j.bbrc.2011.05.140

Tieland, M., Trouwborst, I., and Clark, B. C. (2018). Skeletal muscle performance and ageing. *J Cachexia Sarcopenia Muscle* 9, 3–19. doi: 10.1002/jcsm.12238

Tutdibi, O., Brinkmeier, H., Rudel, R., and Fohr, K. J. (1999). Increased calcium entry into dystrophin-deficient muscle fibres of MDX and ADR-MDX mice is reduced by ion channel blockers. *J Physiol* 515(Pt 3), 859–868. doi: 10.1111/j.1469-7793.1999.859ab.x

Uryash, A., Flores, V., Adams, J. A., Allen, P. D., and Lopez, J. R. (2020). Memory and Learning Deficits Are Associated With Ca(2+) Dyshomeostasis in Normal Aging. *Front Aging Neurosci* 12:224.

Vandebrouck, C., Martin, D., Colson-Van Schoor, M., Debaix, H., and Gailly, P. (2002). Involvement of TRPC in the abnormal calcium influx observed in

dystrophic (mdx) mouse skeletal muscle fibers. *J Cell Biol* 158, 1089–1096. doi: 10.1083/jcb.200203091

Visser, M., and Schaap, L. A. (2011). Consequences of sarcopenia. *Clin Geriatr Med* 27, 387–399. doi: 10.1016/j.cger.2011.03.006

Wanagat, J., Cao, Z., Pathare, P., and Aiken, J. M. (2001). Mitochondrial DNA deletion mutations colocalize with segmental electron transport system abnormalities, muscle fiber atrophy, fiber splitting, and oxidative damage in sarcopenia. *FASEB J* 15, 322–332. doi: 10.1096/fj.00-0320com

Wei, J., Xu, H., Davies, J. L., and Hemmings, G. P. (1992). Increase of plasma IL-6 concentration with age in healthy subjects. *Life Sci* 51, 1953–1956. doi: 10.1016/0024-3205(92)90112-3

Yang, T., Esteve, E., Pessah, I. N., Molinski, T. F., Allen, P. D., and Lopez, J. R. (2007). Elevated resting [Ca(2+)](i) in myotubes expressing malignant hyperthermia RyR1 cDNAs is partially restored by modulation of passive calcium leak from the SR. *Am J Physiol Cell Physiol* 292, C1591–C1598.

Conflict of Interest: The authors declare that the research was conducted in the absence of any commercial or financial relationships that could be construed as a potential conflict of interest.

frontiers in Physiology

ORIGINAL RESEARCH
published: 26 January 2021
doi: 10.3389/fphys.2020.601313

Changes in Gene Expression of the MCU Complex Are Induced by Electrical Stimulation in Adult Skeletal Muscle

*Esteban R. Quezada, Alexis Díaz-Vegas, Enrique Jaimovich and Mariana Casas**

Center for Exercise, Metabolism, and Cancer, Physiology and Biophysics Program, Biomedical Sciences Institute (ICBM), Faculty of Medicine, University of Chile, Santiago, Chile

The slow calcium transient triggered by low-frequency electrical stimulation (ES) in adult muscle fibers and regulated by the extracellular ATP/IP3/IP3R pathway has been related to muscle plasticity. A regulation of muscular tropism associated with the MCU has also been described. However, the role of transient cytosolic calcium signals and signaling pathways related to muscle plasticity over the regulation of gene expression of the MCU complex (MCU, MICU1, MICU2, and EMRE) in adult skeletal muscle is completely unknown. In the present work, we show that 270 0.3-ms-long pulses at 20-Hz ES (and not at 90 Hz) transiently decreased the mRNA levels of the MCU complex in mice flexor digitorum brevis isolated muscle fibers. Importantly, when ATP released after 20-Hz ES is hydrolyzed by the enzyme apyrase, the repressor effect of 20 Hz on mRNA levels of the MCU complex is lost. Accordingly, the exposure of muscle fibers to 30 μM exogenous ATP produces the same effect as 20-Hz ES. Moreover, the use of apyrase in resting conditions (without ES) increased mRNA levels of MCU, pointing out the importance of extracellular ATP concentration over MCU mRNA levels. The use of xestospongin B (inhibitor of IP3 receptors) also prevented the decrease of mRNA levels of MCU, MICU1, MICU2, and EMRE mediated by a low-frequency ES. Our results show that the MCU complex can be regulated by electrical stimuli in a frequency-dependent manner. The changes observed in mRNA levels may be related to changes in the mitochondria, associated with the phenotypic transition from a fast- to a slow-type muscle, according to the described effect of this stimulation frequency on muscle phenotype. The decrease in mRNA levels of the MCU complex by exogenous ATP and the increase in MCU levels when basal ATP is reduced with the enzyme apyrase indicate that extracellular ATP may be a regulator of the MCU complex. Moreover, our results suggest that this regulation is part of the axes linking low-frequency stimulation with ATP/IP3/IP3R.

Keywords: mitochondria, calcium handling, muscle plasticity, ATP release, IP3R

OPEN ACCESS

Edited by:
Bruno Bastide, Lille University of Science and Technology, France

Reviewed by:
Kevin Foskett, University of Pennsylvania, United States
Roland Malli, Medical University of Graz, Austria

****Correspondence:***
Mariana Casas
mcasas@med.uchile.cl

Specialty section:
This article was submitted to Striated Muscle Physiology, a section of the journal Frontiers in Physiology

Received: *31 August 2020*
Accepted: *27 November 2020*
Published: *26 January 2021*

Citation:
Quezada ER, Díaz-Vegas A, Jaimovich E and Casas M (2021) Changes in Gene Expression of the MCU Complex Are Induced by Electrical Stimulation in Adult Skeletal Muscle. Front. Physiol. 11:601313. doi: 10.3389/fphys.2020.601313

INTRODUCTION

Skeletal muscle can modify its phenotype to adapt to different external stimuli, such as disuse (Goldspink et al., 1986; Kneppers et al., 2019), hypoxia (Baresic et al., 2014; Nguyen et al., 2016), physical exercise (Yan et al., 2012; Joseph et al., 2016), among others (Gundersen, 2011), in a process known as muscle plasticity. According to this, different muscles of the body

differ in their phenotype depending on the function they perform, expressing different isoforms of contractile proteins and metabolic enzymes. Accordingly, muscles (and, in a more general manner, motor units) have been broadly classified into three groups: slow-fatigue resistance, fast-fatigue resistance, and fast-fatigable. The model of muscle phenotype adaptation to different types of exercise is intimately linked to patterned electrical stimulation (ES) from the motoneurons innervating them. The first evidence involving frequency of ES in triggering molecular events associated with muscle plasticity was originated on *in vivo* models of cross-innervation, where a transition from fast to slow phenotype was observed in fast muscles innervated with α-motoneurons belonging to slow motor units presenting a low-frequency, long-lasting firing pattern (Eccles et al., 1962; Salmons and Vrbova, 1969). We have demonstrated that the inositol triphosphate receptor (IP_3R) mediates the frequency-dependent induced changes (excitation–transcription coupling process) in gene expression involved in muscle plasticity of adult skeletal muscle. In particular, our results show that IP_3R (and associated calcium signals) has a role in the activation of transcriptional programs associated with a slow phenotype that are activated at low frequencies of stimulation (Jorquera et al., 2013), partially emulating muscle changes induced by aerobic training (Klitgaard et al., 1990; Casas et al., 2010; Jorquera et al., 2013).

Excitation–transcription coupling is a process linking patterned depolarization of the muscle fibers with the activation of specific signaling pathways downstream. After a train of electrical stimuli, the process is triggered by the activation of the voltage-dependent L-type calcium channel Cav1.1 or dihydropyridine receptor (DHPR) (Jaimovich et al., 2000; Araya et al., 2003). At low frequencies of stimulation, DHPR activates the release of adenosine triphosphate (ATP), from the inside of the muscle fiber to the extracellular medium, through type 1 pannexin channels (Panx1). Extracellular ATP and its metabolites can thus act in an autocrine and paracrine manner, activating purinergic receptors, which, in turn, activate phosphatidylinositol 3-kinase (PI3K) and downstream pathway that favors the production of the second messenger 1,4,5 triphosphate (IP_3) (Araya et al., 2003; Buvinic et al., 2009; Jorquera et al., 2013). Subsequently, IP_3 binds to the membrane receptor of the sarcoplasmic reticulum (SR) and the nuclear envelope, causing Ca^{2+} release from the SR and the consequent increase in the cytosolic and nuclear Ca^{2+} concentration, which modulates the activity of several transcription factors to foster transcription (Carrasco et al., 2003).

During muscle contraction, the energy requirements of the muscle fiber are increased several times compared to rest (Weibel and Hoppeler, 2005). In muscle cells, mitochondria are the main source of ATP, and its function can be stimulated by various molecules, such as adenosine diphosphate (ADP), adenosine monophosphate (AMP), and Ca^{2+} (Lazarowski et al., 2003; Yi et al., 2011). In the mitochondrial matrix, different enzymes, such as isocitrate dehydrogenase and α-ketoglutarate dehydrogenase, have Ca^{2+} as a co-factor (Cortassa et al., 2003). Consequently, increases in the intramitochondrial concentration of Ca^{2+} increase the activity of these enzymes, increasing the speed of the Krebs cycle as well as the production of reduced compounds (NADH and $FADH_2$) that feed the electron transport chain and ATP synthesis (Diaz-Vegas et al., 2019). Therefore, Ca^{2+} entry into the mitochondria is key to maintain the balance between the metabolic requirements and the synthesis of ATP in the skeletal muscle (Baughman et al., 2011; Tarasov et al., 2012; Diaz-Vegas et al., 2019).

The mitochondrial calcium uniporter (MCU) is a highly selective Ca^{2+} channel located in the inner mitochondrial membrane. MCU mediates an electrogenic Ca^{2+} influx from the intermembrane space to the mitochondrial matrix (Wan et al., 1989; O'Donnell et al., 1998; Carafoli, 2010). Furthermore, MCU is associated with different regulatory proteins that modulate their affinity for Ca^{2+} (Fan et al., 2020). MCU and its regulatory proteins are collectively known as the MCU complex, where MCU is the protein forming the pore of the channel (Chaudhuri et al., 2013; Shanmughapriya et al., 2015). The main components of the MCU complex expressed in adult skeletal muscle are MCU, essential MCU regulator (EMRE), mitochondrial Ca^{2+} uptake 1 (MICU1), and mitochondrial Ca^{2+} uptake 2 (MICU2) (Murgia and Rizzuto, 2015). Among these, the MICU1/MCU ratio appears to be particularly important for the regulation of mitochondrial Ca^{2+} uptake (Paillard et al., 2017). Increases in cytosolic Ca^{2+} levels generate an increase in mitochondrial Ca^{2+} through MCU. This process takes place after depolarization of the muscle fiber, where a high increase in intracellular Ca^{2+} concentration occurs. The consequent rise in mitochondrial Ca^{2+} depends on the activation of ryanodine receptor 1 (RyR1) (a fast component of Ca^{2+} release) as well as IP_3R (a slow component of calcium release) (Diaz-Vegas et al., 2018).

There is evidence pointing to a possible role of MCU in muscle plasticity. Indeed, the silencing of MCU has been suggested to induce muscular atrophy, and its overexpression generates muscular hypertrophy in murine models (Mammucari et al., 2015), although these results are somehow controversial (Kwong et al., 2018). Also, 9 weeks of strength training or high-frequency EE (60 Hz) in humans induces hypertrophy and increases MCU protein levels in skeletal muscle (Zampieri et al., 2016). Interestingly, microarray analysis of muscles overexpressing MCU or underexpressing MCU showed differential changes in expression of genes related to sarcomere organization, calcium regulation, differentiation, and development. Notably, when MCU was overexpressed, an increase in expression of genes related to Ca^{2+} homeostasis was observed (Chemello et al., 2015).

Recently, the role of Ca^{2+} in the control of expression of MCU has been studied using the Ca^{2+} ionophore ionomycin to increase intracellular calcium concentration (Shanmughapriya et al., 2015). The results showed that CREB binds to the MCU promoter and alterations in cytosolic Ca^{2+} levels induced changes in MCU levels. Interestingly, these results suggest the existence of a crosstalk between cytosolic Ca^{2+} levels and the control of mitochondrial Ca^{2+} buffering capacity mechanisms (Shanmughapriya et al., 2015). Studies using more physiological stimuli are thus needed to further explore this mechanism. Furthermore, in hippocampal and cortical neurons,

a reduction of MCU levels after increases in cytosolic Ca^{2+} through activation of NMDA receptor has been described (Qiu et al., 2013).

These works reveal the importance of understanding the role that transient changes in cytosolic Ca^{2+} levels (induced by a physiological stimulus) play in the regulation of gene expression of MCU, MICU1.1, MICU2, and EMRE in a tissue such as skeletal muscle where Ca^{2+} is a key factor. Such regulation could modulate the Ca^{2+} buffering efficiency of mitochondria, generating a physiological control loop of intracellular Ca^{2+} signals. In the case of adult skeletal muscle, a phenotypic change is observed under low-frequency ES, with modifications, among others, in the expression of oxidative related metabolic enzymes and an increase in mitochondria content (Hood et al., 1989; Putman et al., 2004; Petrie et al., 2015). The possible changes in mitochondrial proteins related to its Ca^{2+} buffering capacity is a subject that remains poorly studied until now.

In this work, we show a decrease in mRNA levels of MCU, MICU1, MICU2, and EMRE specifically after low-frequency ES. Moreover, the changes observed appear in line with an asymmetric distribution of some of these proteins between fast and slow phenotype muscle fibers.

RESULTS

20-Hz ES Produces a Decrease in mRNA Levels of the MCU Complex

We have previously demonstrated that ES of muscle fibers with 270 pulses, 0.3 ms long, at 20 Hz, induces changes in mRNA levels related to a slow-to-fast phenotypic transition, whereas the same amount of pulses at 90 Hz induces the inverse effect (Jorquera et al., 2013). We evaluated the effect of ES on mRNA levels of the MCU complex finding a significant decrease in MCU

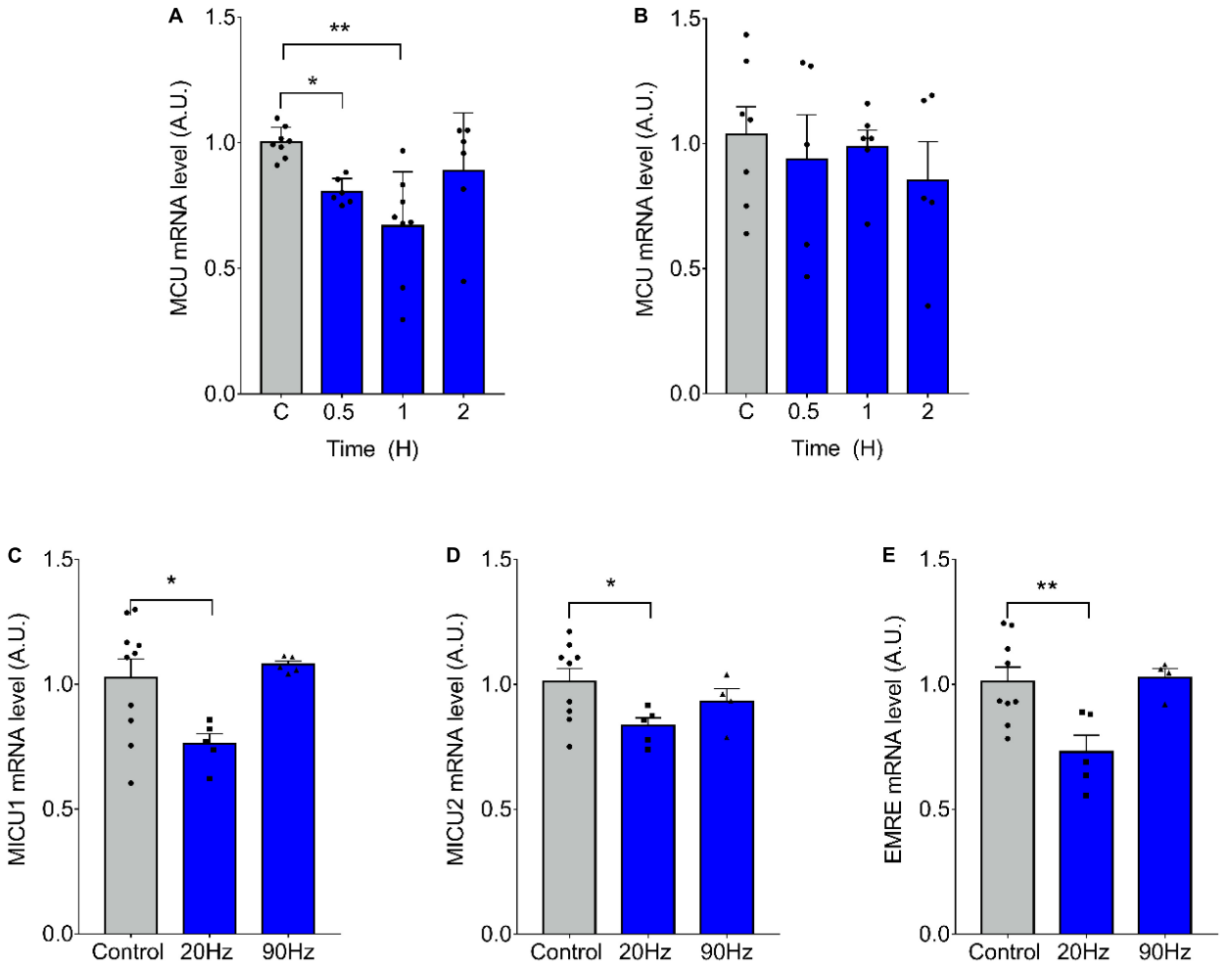

FIGURE 1 | Low-frequency electrical stimulation (ES) transiently reduces mRNA levels of MCU complex in skeletal muscle fibers. Muscle fibers isolated from the *Flexor Digitorium Brevis* (*fdb*) muscle were stimulated with 270 pulses, 0.3 ms each **(A)** at 20 Hz (n = 6–8 per condition) or **(B)** 90 Hz (n = 5–7 per condition). mRNA levels of MCU decreased 1h post-ES **(A)**; while high-frequency stimulation produced no change **(B)**. The low frequency stimulation also decreased mRNA levels of MICU1 (n = 5–10 per condition) **(C)**, MICU2 (n = 4–9 per condition) **(D)** and EMRE (n = 4–9 per condition) **(E)** 1 h post ES. For **(A)** using the Kruskal–Wallis test with *post hoc* Dunn's was applied. Values are presented as mean ± SEM. 18S was used as normalizer. *$p < 0.05$; **$p < 0.01$; ***$p < 0.001$.

mRNA levels 30 min (1.00 ± 0.06 vs 0.81 ± 0.05 at 30 min) and 1 h (1.002 ± 0.061 vs 0.669 ± 0.216 at 1 h) after 20-Hz ES of isolated *fdb* muscle fibers (**Figure 1A**). High-frequency, 90-Hz ES did not produce changes in MCU mRNA levels (**Figure 1B**). Moreover, a decrease in the mRNA levels of MICU1 (1.03 ± 0.23; vs 0.761 ± 0.091 at 20 Hz), MICU2 (1.01 ± 0.16; vs 0.83 ± 0.07 at 20 Hz), and EMRE (1.01 ± 0.17 vs 0.73 ± 0.15 at 20 Hz) was also observed 1 h after 20-Hz ES, whereas 90-Hz ES did not generate any changes in mRNA levels of these genes (**Figures 1C–E**).

Changes in mRNA Levels of the MCU Complex Are Dependent on Extracellular ATP and IP_3R

To evaluate the downstream signaling after low-frequency ES, responsible for the observed changes in mRNA levels of MCU complex genes, we searched to determine the role of extracellular ATP. We have demonstrated that 20-Hz ES induces a release of ATP to the extracellular milieu trough Pannexin-1 channels (Jorquera et al., 2013). The ATP released acts over purinergic receptors to activate signaling cascades that activate, among others, the production of IP_3 and the release of Ca^{2+} through IP_3R, inducing changes in transcriptional activity of several genes (Casas et al., 2010). **Figure 2** shows changes in MCU mRNA level in *fdb* muscle fibers pre-incubated with 2 U/ml of the ecto-nucleotidase apyrase to reduce extracellular ATP levels. The decrease observed in mRNA levels of MCU, MICU1, MICU2, and EMRE after a 20-Hz ES was absent when fibers were pre-incubated with apyrase (**Figures 2A–E**), when compared to control fibers. A significant increase in MCU mRNA levels (C = 1.02 ± 0.14; Apy = 1.32 ± 0.19) was also observed after incubation with apyrase (**Figure 2A**) in basal conditions (without ES). This effect of apyrase was not observed in MICU1, MICU2, and EMRE mRNA levels.

To evaluate if ATP alone (in absence of ES) can induce the observed changes in mRNA levels after 20-Hz ES, we stimulated *fdb* muscle fibers with 30 μM of exogenous ATP and measured mRNA levels of the MCU complex. We observed that ATP exposure resulted in a significant decrease (C = 1.02 ± 0.20; 0.5 h = 0.74 ± 0.20) in mRNA levels of MCU after 30 min (**Figure 3A**). The same was observed at 30 min for mRNA levels of MICU1 (Control = 1.01 ± 0.17; 30 μM = 0.78 ± 0.17), MICU2 (Control = 1.02 ± 0.15; 30 μM = 0.79 ± 0.25), and EMRE (Control = 1.01 ± 0.13; 30 μM = 0.74 ± 0.15) after (**Figures 3B–D**). Similar effects were produced by extracellular ATP in an *ex vivo* model of complete *fdb* muscle (**Supplementary Figure 1**).

As it was previously mentioned, signaling downstream ATP release and purinergic receptors activation can be mediated by the production of IP_3 and Ca^{2+} released through IP_3R. To test the role of IP_3R, we blocked this intracellular Ca^{2+} channel using xestospongin B. No changes in MCU, MICU1, 0.MICU2, and EMRE mRNA levels after 20 Hz ES were observed when fibers were pre-incubated with 10 μM of xestospongin B (**Figures 4A–D**), suggesting a role of Ca^{2+} released through IP_3R in the regulation of mRNA levels of the MCU complex.

Mitochondria From Fast Muscles Have a Higher Content of MCU Complex Proteins

We found a decrease in mRNA levels of the MCU complex after low-frequency ES. Considering that low-frequency ES is appropriate for slow-type motor units and that this type of ES can trigger transcriptional changes related to muscle fast-to-slow phenotype transitions, we hypothesized that proteins of the MCU complex could be differentially expressed in slow compared with fast phenotype adult muscles. We evaluated the levels of MCU and MICU1 proteins in a fast (*fdb*) and a slow (soleus) muscle by Western blot. We found a smaller amount of MCU (*fdb* = 1.00 ± 0.18; sol = 0.47 ± 0.13) (**Figure 5A**) and MICU1 (*fdb* = 1.00 ± 0.32; sol = 0.55 ± 0.24) (**Figure 6A**) in soleus muscle compared with *fdb* muscles. The protein content was normalized by TOM20, indicating that the relative amount of the MCU

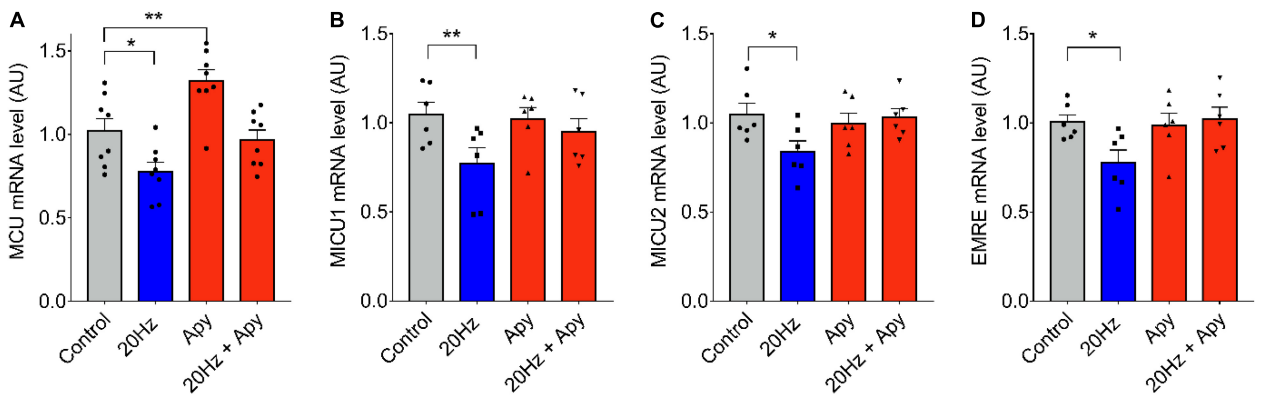

FIGURE 2 | Low-frequency ES-dependent reduction in mRNA levels of MCU complex is dependent on extracellular ATP. Muscle fibers isolated from the *fdb* muscle were pre-incubated 30 min with apyrase (2 U/ml) before ES (as in **Figure 1**). The mRNA was extracted 1 h after the ES. MCU mRNA levels increased with pre-incubation with apyrase in the absence of ES **(A)**. Preincubation with apyrase prevented the low frequency-dependent reduction in mRNA levels of MCU (n = 8) **(A)**, MICU1 (n = 6) **(B)**, MICU2 (n = 6) **(C)**, and EMRE (n = 6) **(D)**. Values are presented as mean ± SEM. 18s was used as normalizer. $^*p < 0.05$; $^{**}p < 0.01$; $^{***}p < 0.001$.

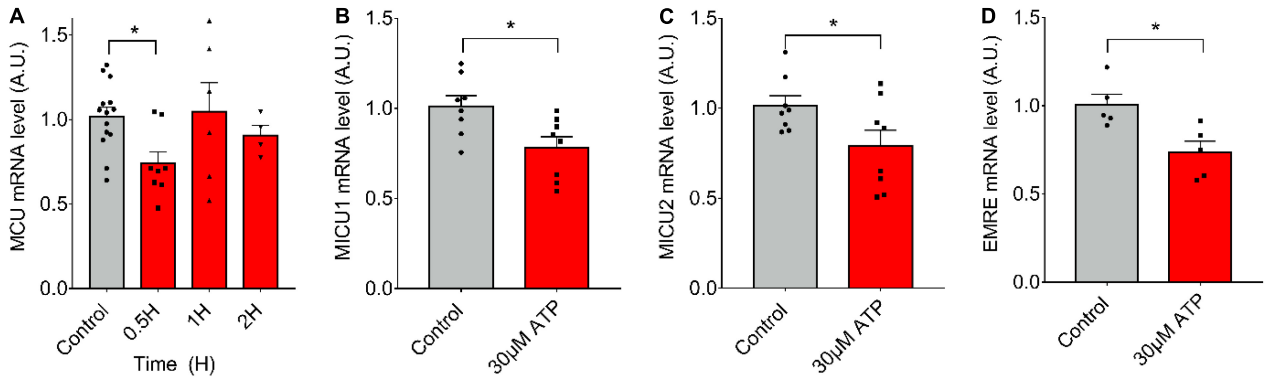

FIGURE 3 | Extracellular ATP is sufficient to reduce mRNA levels of the MCU complex in skeletal muscle fibers. Muscle fibers *fdb* muscle and stimulated with exogenous ATP (30 μM). A decrease in mRNA levels of all the MCU complex components after 30 min of stimulation is observed. mRNA levels are shown normalized by mRNA level of control fibers. mRNA levels for MCU (n = 4–14) **(A)**, MICU1 (n = 8) **(B)**, MICU2 (n = 8) **(C)**, and EMRE (n = 5) **(D)** were measured. Values are presented as mean ± SEM. 18S was used as normalizer. *$p < 0.05$; **$p < 0.01$; ***$p < 0.001$.

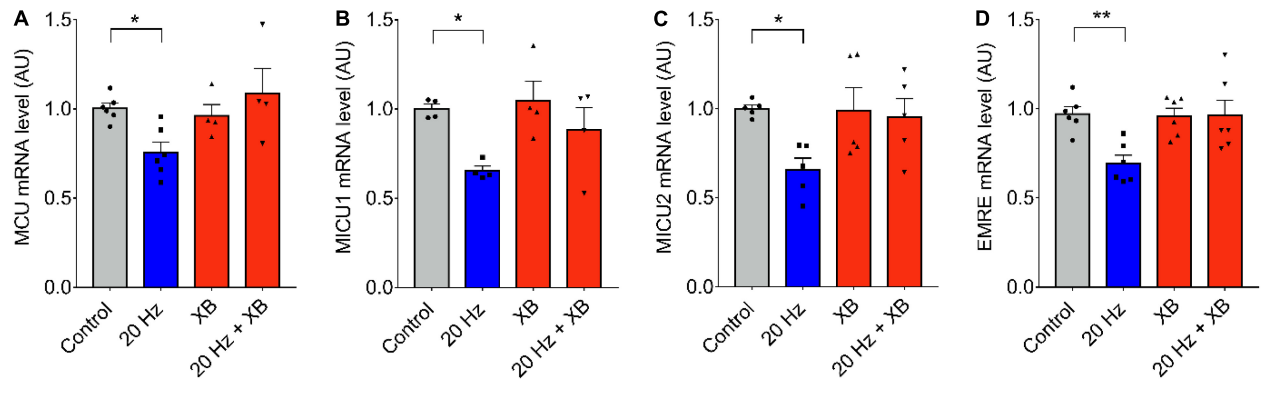

FIGURE 4 | IP3R is involved in low-frequency ES-dependent reduction of mRNA levels of MCU complex. Muscle fibers *fdb* muscle were pretreated with the IP3R blocker, XB (10 μM) by 30 min before being electrically stimulated (as in **Figure 1**). The mRNA was extracted 1 h after electrical stimulation. Preincubation with XB prevented the low frequency-dependent reduction in mRNA levels of MCU (n = 6) **(A)**, MICU1 (n = 5) **(B)**, MICU2 (n = 5) **(C)**, and EMRE (n = 6) **(D)**. For **(C)** using the Kruskal–Wallis test with *post hoc* Dunn's was applied. Values are presented as mean ± SEM. 18S was used as normalizer. *$p < 0.05$; **$p < 0.01$; ***$p < 0.001$.

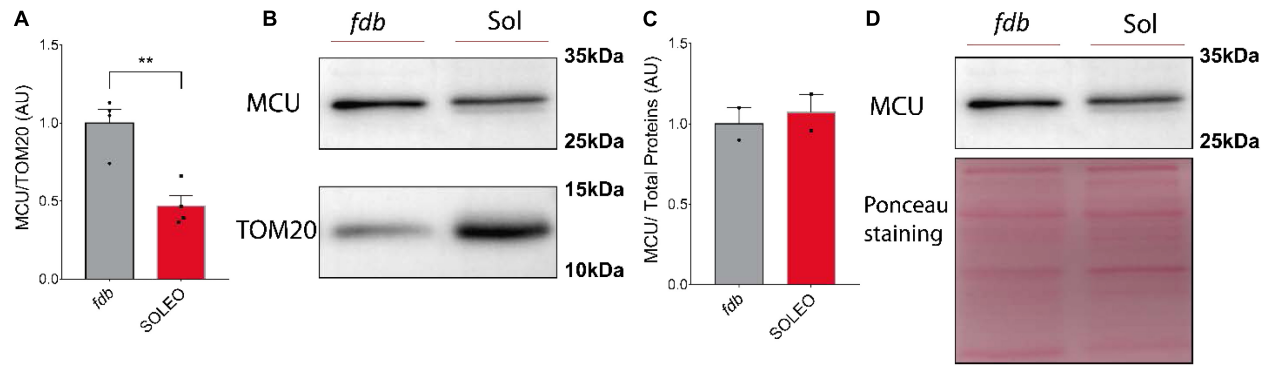

FIGURE 5 | Mitochondria from *Flexor Digitorium Brevis* (*fdb*) muscle presented a higher content of MCU protein than soleus (sol) muscle. Representative Western Blot and quantification show the levels of the MCU protein in homogenates of *fdb* and Sol normalized by mitochondrial content using TOM20 as a normalizing protein (n = 4) **(A,B)**. When MCU content was normalized by total protein content, no differences between these two muscles were observed (n = 2) **(C,D)**. Values are presented as mean ± S.E.M. Values are presented as mean ± SEM. *$p < 0.05$; **$p < 0.01$; ***$p < 0.001$.

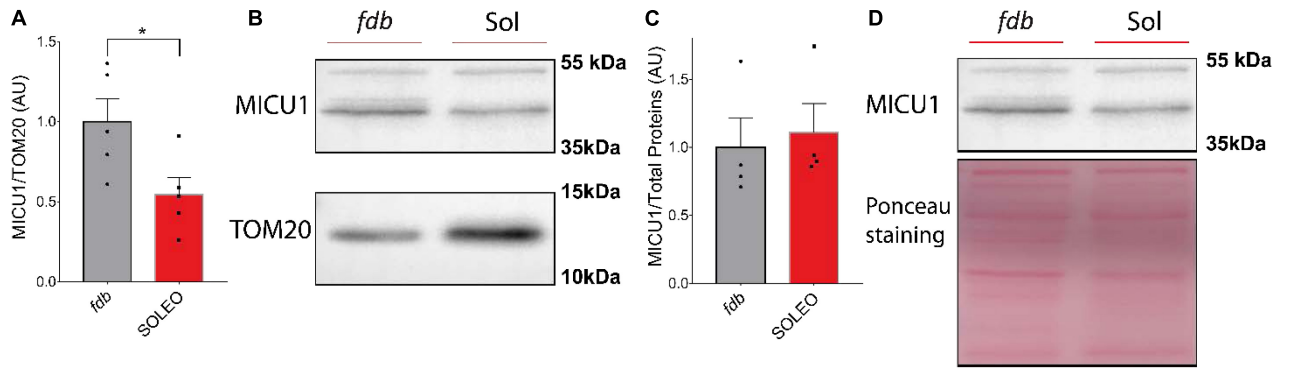

FIGURE 6 | Mitochondria from *Flexor Digitorium Brevis* (*fdb*) muscle presented a higher content of MICU1 protein than mitochondria from soleus (sol) muscle. Representative Western Blot and quantification show the levels of the MICU1 protein in homogenates of *fdb* and sol, normalized by a mitochondrial marker ($n = 5$) **(A,B)** and total protein ($n = 4$) **(C,D)**. For **(C)** using the Mann-Whitney test was applied. Values are presented as mean ± SEM. $^{*}p < 0.05$; $^{**}p < 0.01$; $^{***}p < 0.001$.

complex is lower in mitochondria from soleus muscle compared to *fdb*. This difference is not significant when normalized by total proteins (**Figures 5C**, **6C**). This is probably due to the intrinsic difference in mitochondria content between these muscles, a difference that is compensated by the normalization of MCU protein content with a marker of mitochondria such as TOM20. MCU, MICU1, and TOM20 membranes are shown (**Supplementary Figures 2**, **3**).

DISCUSSION

We have demonstrated that low-frequency ES results in a decrease in the mRNA levels of MCU, MICU1, MICU2, and EMRE, while high-frequency ES does not generate modifications. Our laboratory has described a fine-tuned mechanism that relates the decoding of the frequency of stimulation by Cav1.1, ATP release, IP_3R activation, and transcription changes related to fast-to-slow muscle phenotype transition (Jorquera et al., 2013). Therefore, if there is a differential calcium management between different types of muscle fibers (Carroll et al., 1997), it is to be expected that genes that regulate mitochondrial calcium uptake could be regulated by different stimulation frequencies. In the present work, we showed that mRNA levels of MCU, MICU1, MICU2, and EMRE are also regulated in a frequency-dependent manner, being affected only by low-frequency ES. We have pooled the data from all controls and 20 Hz from the different experiments (**Supplementary Figure 4**). The observed changes suggest a new process related to the phenotypic transition of a fast to slow muscle fiber, in this case, related to mitochondrial proteins other than those related to oxidative metabolism, classically described before in the plasticity process from fast to slow muscle phenotype transition.

Our results showed that in fibers stimulated at 20 Hz after pre-incubation with apyrase, mRNA of the MCU complex did not decrease (as it does when they are only ES at 20 Hz), showing no significant statistical difference between control and 20 Hz + Apy conditions, indicating that the effect of 20-Hz ES in the decrease of MCU complex mRNAs is lost when fibers are pre-incubated with apyrase. The same is observed when fibers are pre-incubated with xestospongin B (IP_3R blocker). No statistical difference was found between mRNA levels of the MCU complex from fibers electrically stimulated at 20 Hz compared to those electrically stimulated at 20 Hz and pre-incubated with apyrase or xestospongin B. However, these results, together with those showing an increase in mRNA levels of the MCU complex after stimulation with exogenous ATP, although not conclusive, are consistent with the idea that the transcriptional effects observed on MCU, MICU1, MICU2, and EMRE after low-frequency ES would be mediated by slow calcium transients activated by the extracellular ATP/IP_3 production/IP_3R signaling pathway (Buvinic et al., 2009; Jorquera et al., 2013). The role of mitochondrial Ca^{2+} uptake over cytosolic Ca^{2+} signals after muscle fiber depolarization has been shown previously to play a role in excitation–contraction coupling (Yi et al., 2011). Moreover, there is also evidence that protein levels of MCU are susceptible to change after exercise and to ES in humans (Zampieri et al., 2016). Interestingly, it has been postulated that protective synaptic activity is related to a decrease in MCU protein levels, which is lost in the presence of a CaM kinase inhibitor, suggesting a role of cytoplasmic Ca^{2+} in MCU regulation (Qiu et al., 2013). On the other hand, the reduction in mRNA levels of the MCU complex is observed at shorter times (30 min compared to 60 min for ES) when fibers are stimulated with exogenous ATP; this phenomenon could be related to the final concentration of ATP reached in the T-tubules and their affinity for purinergic receptors (Lazarowski et al., 2003) or the activation of these receptors without the process involving depolarization sensing by Cav1.1 and triggering of ATP release through pannexin-1 channels.

The results showing an increase in mRNA levels of MCU in the presence of apyrase, in the absence of further stimulus, suggest that basal levels of ATP present in the extracellular medium would be inhibiting or repressing the transcription of this gene.

Our data provide new information on the relative amount of MCU and MICU1 in muscle of different phenotypes, showing the existence of higher protein levels of MCU and MICU1

per mitochondria in *fdb* than those belonging to the soleus. Therefore, the decrease in mRNA of the MCU complex after low-frequency ES of isolated fibers of the *fdb* muscle would favor a lower level of the MCU and MICU1 per mitochondrion, such as that present in a slow muscle. This could be considered an early metabolic response to the phenotypic shift from fast to slow muscle fiber (Loucif et al., 2020). The gradual increase in the number of mitochondria, together with a decrease in MCU complex content in response to a low-frequency stimulus, will allow adapting mitochondrial Ca^{2+} homeostasis to finally reach that of a slow muscle. Besides, the higher levels of TOM20 in slow muscle compared to fast muscle are consistent with that described with other mitochondrial proteins, such as ATP synthase and succinate dehydrogenase (Schiaffino and Reggiani, 2011; Khodabukus and Baar, 2015). Moreover, the kinetics of Ca^{2+} entry to the mitochondria have also been reported to be different between different fiber types (Sembrowich et al., 1985; Picard et al., 2008). Interestingly, it has been described that MCU overexpression causes neuronal death (Granatiero et al., 2019). On the other hand, stimulation of cortical and hippocampal neurons results in a decrease in mRNA and protein levels of MCU (Qiu et al., 2013), which have been associated with a protective effect preventing mitochondrial Ca^{2+} overload, thus preventing cytochrome C from triggering cell death. Likewise, it has been observed that the decrease in MCU in a model of cells from colon cancer results in a resistance to apoptosis (Marchi et al., 2013; Nemani et al., 2018). It appears then that a fine regulation of the MCU protein complex is needed to balance protection and cell death after different stimuli. In this sense, it has been proposed that the concentration of mitochondrial Ca^{2+} necessary to exceed the threshold to trigger the opening of the mitochondrial permeability transition pore (mPTP) is lower in a slow fiber compared to a fast fiber (Picard et al., 2008, 2012). Therefore, since the muscle contraction of a slow phenotype fiber results in regular and prolonged elevations in cytosolic (and possibly mitochondrial) (Ca^{2+}), we can hypothesize that low-frequency ES appropriate for slow-type muscles could induce a decrease in the MCU complex to regulate the entry of Ca^{2+} to the mitochondria and to prevent mPTP opening and thus protect the muscle fiber from triggering cell death. Even if muscle contraction in slow phenotype muscle relies strongly on mitochondrial production of ATP, which depends on mitochondrial Ca^{2+}, the lower protein abundance of MCU and MICU1 per mitochondria in the soleus muscle could be compensated in the first place by the higher mitochondrial content in slow phenotype muscle and also by phenotypic adaptations of the slow muscle, such as an increase in sensitivity to Ca^{2+} by the enzymes isocitrate dehydrogenase and α-ketoglutarate dehydrogenase, maintaining the metabolism according to energy requirements (McCormack and Denton, 1989; Hurst et al., 2017). Not only has the protein level been described as a regulator of mitochondrial calcium uptake (Qiu et al., 2013), the stoichiometry of MCU/MICU1 (Paillard et al., 2017), mitochondrial endoplasmic reticulum interaction (Ainbinder et al., 2015), calcium release from the IP3R (Diaz-Vegas et al., 2018), and mitochondrial membrane potential (Diaz-Vegas et al., 2018) have also been described. Also, it has been described that an adaptive process of a cell is supported by a previous metabolic change, such as the case of metabolic changes associated with the activation of T-cell (Loucif et al., 2020). Exercise increases transcription factors of mitochondrial biogenesis and muscle hypertrophy in humans (Ruas et al., 2012). Deletion of PGC-1α (regulator of mitochondrial biogenesis) decreases the number and size of the mitochondria and the mass of the soleus and affects muscle performance (Leone et al., 2005). Thus, the changes observed at the level of the MCU complex in *fdb* could signify a prior process for the regulation of cytoplasmic Ca^{2+} signals mediated by the mitochondria, changing the regulation of genes related to contractility and favoring muscle plasticity. Therefore, future research is required to evaluate changes induced by ES in protein expression of the MCU complex and the consequences of a reduction of the MCU complex in the different functions of a skeletal muscle fiber, in the muscle plasticity process.

MATERIALS AND METHODS

Animals

This study was carried out following the guidelines of the Bioethics Committee of the Faculty Medicine, University of Chile (FONDECYT #1151293). Eight- to 10-week-old male C57/BL6J mice were obtained from the Central Animal Facility of the Faculty of Medicine, University of Chile. Mice were kept in a room with controlled temperature in a light–dark cycle of 12 h and fed *ad libitum*.

Adult FBD Fiber Isolation

The isolated adult muscle fibers were obtained from the *fdb* muscle by enzymatic digestion of the whole muscle with 450–500 units/ml of collagenase type II (Worthington) for 90 min, followed by mechanical dissociation with Pasteur pipettes of different diameters as described previously (Casas et al., 2010). Fibers were plated in ECM (Sigma)-covered 35-mm plates in culture medium [Dulbecco's modified Eagle's medium (DMEM), 10% horse serum, and 1% penicillin/streptomycin]. Fibers were used for analysis 20 h after seeding.

Electrical Stimulation

The skeletal muscle fibers were electrically stimulated by field stimulation with a device consisting of parallel platinum wires with alternate polarity, as described previously (Casas et al., 2010). The protocol consisted of 270 pulses, 0.3 ms each at 20 Hz or 90 Hz (Jorquera et al., 2013).

mRNA Isolation, cDNA, and Real-Time qPCR

Total mRNA was isolated from the muscle complete of the *fdb* by using TRIzol® reagent (Invitrogen) according to the manufacturer's protocol. The same extraction protocol was used to obtain total RNA from isolated fibers after ES. The cDNA was obtained by reverse transcription reaction of 1 μg of total RNA using random primer and polyDT primers. Real-time qPCR was performed according to the recommendations of

EvaGreen® qPCR Mix Plus (ROX) using the following primers: MCU-fw: 5′-GTGCGCCTGTTTGTAACTCA-3′ and MCU-rv: 5′-CAAGACTCGCTAAGCCCTTT-3′, MICU1.1-fw: 5′-CTTTG ATGGAAAGGAGTTCTGGC-3′ and MICU1.1-rv: 5′-CCTCCA TGTCTACCTCTCCGT-3′, MICU2-fw: 5′-TGGAGCACGACG GAGAGTAT-3′ and MICU2-rv: 5′-GCCAGCTTCTTGACCA GTGT-3′, EMRE-fw: 5′-AACTTCGCTGCTCTGCTTGA-3′ and EMRE-rv: 5′-TGAGGCTGAGGGCTTTCCTT-3′, 18 s. The design of primers was performed using the AmplifX program and validated by Primer-BLAST.

Western Blot

The *fdb* and soleus samples were homogenized with an electric homogenizer (Fluko, Shanghai, China) in a lysis buffer containing 20 mM Tris–HCl (pH 7.5), 1% Triton X-100, 2 mM EDTA, 20 mM NaF, 1 mM $Na_2P_2O_7$, 10% glycerol, 150 mM NaCl, 10 mM Na_3VO_4, 1 mM PMSF, and protease inhibitors (Complete™, Roche Applied Science). Proteins were separated using SDS-PAGE and transferred to PVDF membranes. The following antibodies and their dilutions were used: MCU (1:2,000; HPA016480, Sigma), MICU1 (1:2,000; HPA037480, Sigma), and TOM20 (1:10,000; ab186735, ABCAM). The protein bands in the blots were visualized using a WESTAR Supernova detection kit (Cyanagen, Bologna, Italy), super-resolution, and, further, ChemiDoc™ MP System (Bio-Rad, United States). The intensity of the bands was determined with ImageJ densitometry analysis.

Statistical analysis

The results were expressed as mean ± standard error (±SEM). For the difference between data groups, the two-tailed paired *t* test was used. For comparison of more than two groups, the one-tailed one-way ANOVA was used followed by Dunnett's multiple comparisons test. In cases where the data could not pass Levene's equal variance test and Shapiro–Wilk test, Mann–Whitney test, and Kruskal–Wallis test with *post hoc* Dunn's, a non-parametric test, as indicated in the figure legend, was applied. The level of significance was set at $p < 0.05$. All statistical analyses were performed in GraphPad Prism 7 and SPSS25.

DATA AVAILABILITY STATEMENT

The original contributions presented in the study are included in the article/**Supplementary Material**, further inquiries can be directed to the corresponding author/s.

ETHICS STATEMENT

The animal study was reviewed and approved by Comité Institucional de Cuidado y Uso de Animales (CICUA).

AUTHOR CONTRIBUTIONS

EQ performed experiments, analyzed results, and contributed to write the manuscript. AD-V analyzed results and contributed to design experiments. EJ planned experiments, discussed results, and contributed to wrote the manuscript. MC design the project, planned experiments, analyzed and discussed results, and wrote the manuscript. All authors contributed to the article and approved the submitted version.

FUNDING

Financed by Fondecyt 1151293, VID-Enl09, Líneas de apoyo a la investigación financiadas por ICBM 2020.

SUPPLEMENTARY MATERIAL

The Supplementary Material for this article can be found online at: https://www.frontiersin.org/articles/10.3389/fphys.2020.601313/full#supplementary-material

REFERENCES

Ainbinder, A., Boncompagni, S., Protasi, F., and Dirksen, R. T. (2015). Role of Mitofusin-2 in mitochondrial localization and calcium uptake in skeletal muscle. *Cell Calc.* 57, 14–24. doi: 10.1016/j.ceca.2014.11.002

Araya, R., Liberona, J. L., Cardenas, J. C., Riveros, N., Estrada, M., Powell, J. A., et al. (2003). Dihydropyridine receptors as voltage sensors for a depolarization-evoked, IP3R-mediated, slow calcium signal in skeletal muscle cells. *J. Gen. Physiol.* 121, 3–16. doi: 10.1085/jgp.20028671

Baresic, M., Salatino, S., Kupr, B., van Nimwegen, E., and Handschin, C. (2014). Transcriptional network analysis in muscle reveals AP-1 as a partner of PGC-1alpha in the regulation of the hypoxic gene program. *Mol. Cell. Biol.* 34, 2996–3012. doi: 10.1128/mcb.01710-13

Baughman, J. M., Perocchi, F., Girgis, H. S., Plovanich, M., Belcher-Timme, C. A., Sancak, Y., et al. (2011). Integrative genomics identifies MCU as an essential component of the mitochondrial calcium uniporter. *Nature* 476, 341–345. doi: 10.1038/nature10234

Buvinic, S., Almarza, G., Bustamante, M., Casas, M., Lopez, J., Riquelme, M., et al. (2009). ATP released by electrical stimuli elicits calcium transients and gene expression in skeletal muscle. *J. Biol. Chem.* 284, 34490–34505. doi: 10.1074/jbc.m109.057315

Carafoli, E. (2010). The fateful encounter of mitochondria with calcium: how did it happen? *Biochim. Biophys. Acta* 1797, 595–606. doi: 10.1016/j.bbabio.2010.03.024

Carrasco, M. A., Riveros, N., Rios, J., Muller, M., Torres, F., Pineda, J., et al. (2003). Depolarization-induced slow calcium transients activate early genes in skeletal muscle cells. *Am. J. Physiol. Cell Physiol.* 284, C1438–C1447.

Carroll, S. L., Klein, M. G., and Schneider, M. F. (1997). Decay of calcium transients after electrical stimulation in rat fast- and slow-twitch skeletal muscle fibres. *J. Physiol.* 501(Pt 3), 573–588. doi: 10.1111/j.1469-7793.1997.573bm.x

Casas, M., Figueroa, R., Jorquera, G., Escobar, M., Molgo, J., and Jaimovich, E. (2010). IP(3)-dependent, post-tetanic calcium transients induced by electrostimulation of adult skeletal muscle fibers. *J. Gen. Physiol.* 136, 455–467. doi: 10.1085/jgp.200910397

Chaudhuri, D., Sancak, Y., Mootha, V. K., and Clapham, D. E. (2013). MCU encodes the pore conducting mitochondrial calcium currents. *eLife* 2:e00704.

Chemello, F., Mammucari, C., Gherardi, G., Rizzuto, R., Lanfranchi, G., and Cagnin, S. (2015). Gene expression changes of single skeletal muscle fibers

in response to modulation of the mitochondrial calcium uniporter (MCU). *Genom. Data* 5, 64–67. doi: 10.1016/j.gdata.2015.05.023

Cortassa, S., Aon, M. A., Marban, E., Winslow, R. L., and O'Rourke, B. (2003). An integrated model of cardiac mitochondrial energy metabolism and calcium dynamics. *Biophys. J.* 84, 2734–2755. doi: 10.1016/s0006-3495(03)75079-6

Diaz-Vegas, A., Eisner, V., and Jaimovich, E. (2019). Skeletal muscle excitation-metabolism coupling. *Arch. Biochem. Biophys.* 664, 89–94.

Diaz-Vegas, A. R., Cordova, A., Valladares, D., Llanos, P., Hidalgo, C., Gherardi, G., et al. (2018). Mitochondrial calcium increase induced by RyR1 and IP3R channel activation after membrane depolarization regulates skeletal muscle metabolism. *Front. Physiol.* 9:791. doi: 10.3389/fphys.2018.00791

Eccles, J. C., Eccles, R. M., and Kozak, W. (1962). Further investigations on the influence of motoneurones on the speed of muscle contraction. *J. Physiol.* 163, 324–339. doi: 10.1113/jphysiol.1962.sp006978

Fan, M., Zhang, J., Tsai, C.-W., Orlando, B. J., Rodriguez, M., Xu, Y., et al. (2020). Structure and mechanism of the mitochondrial Ca2+ uniporter holocomplex. *Nature* 582, 129–133. doi: 10.1038/s41586-020-2309-6

Goldspink, D. F., Morton, A. J., Loughna, P., and Goldspink, G. (1986). The effect of hypokinesia and hypodynamia on protein turnover and the growth of four skeletal muscles of the rat. *Pfluger. Archiv.* 407, 333–340. doi: 10.1007/bf00585311

Granatiero, V., Pacifici, M., Raffaello, A., De Stefani, D., and Rizzuto, R. (2019). Overexpression of mitochondrial calcium uniporter causes neuronal death. *Oxid. Med. Cell Longev.* 2019:1681254.

Gundersen, K. (2011). Excitation-transcription coupling in skeletal muscle: the molecular pathways of exercise. *Biol. Rev. Cambr. Philos. Soc.* 86, 564–600. doi: 10.1111/j.1469-185x.2010.00161.x

Hood, D. A., Zak, R., and Pette, D. (1989). Chronic stimulation of rat skeletal muscle induces coordinate increases in mitochondrial and nuclear mRNAs of cytochrome-c-oxidase subunits. *Eur. J. Biochem.* 179, 275–280. doi: 10.1111/j.1432-1033.1989.tb14551.x

Hurst, S., Hoek, J., and Sheu, S. S. (2017). Mitochondrial Ca(2+) and regulation of the permeability transition pore. *J. Bioenerget. Biomembr.* 49, 27–47.

Jaimovich, E., Reyes, R., Liberona, J. L., and Powell, J. A. (2000). IP(3) receptors, IP(3) transients, and nucleus-associated Ca(2+) signals in cultured skeletal muscle. *Am. J. Physiol. Cell Physiol.* 278, C998–C1010.

Jorquera, G., Altamirano, F., Contreras-Ferrat, A., Almarza, G., Buvinic, S., Jacquemond, V., et al. (2013). Cav1.1 controls frequency-dependent events regulating adult skeletal muscle plasticity. *J. Cell Sci.* 126(Pt 5), 1189–1198. doi: 10.1242/jcs.116855

Joseph, A. M., Adhihetty, P. J., and Leeuwenburgh, C. (2016). Beneficial effects of exercise on age-related mitochondrial dysfunction and oxidative stress in skeletal muscle. *J. Physiol.* 594, 5105–5123. doi: 10.1113/jp270659

Khodabukus, A., and Baar, K. (2015). Contractile and metabolic properties of engineered skeletal muscle derived from slow and fast phenotype mouse muscle. *J. Cell. Physiol.* 230, 1750–1757. doi: 10.1002/jcp.24848

Klitgaard, H., Mantoni, M., Schiaffino, S., Ausoni, S., Gorza, L., Laurent-Winter, C., et al. (1990). Function, morphology and protein expression of ageing skeletal muscle: a cross-sectional study of elderly men with different training backgrounds. *Acta Physiol. Scand.* 140, 41–54. doi: 10.1111/j.1748-1716.1990.tb08974.x

Kneppers, A., Leermakers, P., Pansters, N., Backx, E., Gosker, H., van Loon, L., et al. (2019). Coordinated regulation of skeletal muscle mass and metabolic plasticity during recovery from disuse. *FASEB J.* 33, 1288–1298. doi: 10.1096/fj.201701403rrr

Kwong, J. Q., Huo, J., Bround, M. J., Boyer, J. G., Schwanekamp, J. A., Ghazal, N., et al. (2018). The mitochondrial calcium uniporter underlies metabolic fuel preference in skeletal muscle. *JCI Insight.* 3:e121689.

Lazarowski, E. R., Boucher, R. C., and Harden, T. K. (2003). Mechanisms of release of nucleotides and integration of their action as P2X- and P2Y-receptor activating molecules. *Mol. Pharmacol.* 64, 785–795. doi: 10.1124/mol.64.4.785

Leone, T. C., Lehman, J. J., Finck, B. N., Schaeffer, P. J., Wende, A. R., Boudina, S., et al. (2005). PGC-1alpha deficiency causes multi-system energy metabolic derangements: muscle dysfunction, abnormal weight control and hepatic steatosis. *PLoS Biol.* 3:e101. doi: 10.1371/journal.pbio.0030101

Loucif, H., Dagenais-Lussier, X., Beji, C., Telittchenko, R., Routy, J. P., and van Grevenynghe, J. (2020). Plasticity in T-cell mitochondrial metabolism: a necessary peacekeeper during the troubled times of persistent HIV-1 infection. *Cytok. Growth Fact. Rev.* 55, 26–36. doi: 10.1016/j.cytogfr.2020.02.004

Mammucari, C., Gherardi, G., Zamparo, I., Raffaello, A., Boncompagni, S., Chemello, F., et al. (2015). The mitochondrial calcium uniporter controls skeletal muscle trophism in vivo. *Cell Rep.* 10, 1269–1279. doi: 10.1016/j.celrep.2015.01.056

Marchi, S., Lupini, L., Patergnani, S., Rimessi, A., Missiroli, S., Bonora, M., et al. (2013). Downregulation of the mitochondrial calcium uniporter by cancer-related miR-25. *Curr. Biol.* 23, 58–63. doi: 10.1016/j.cub.2012.11.026

McCormack, J. G., and Denton, R. M. (1989). The role of Ca2+ ions in the regulation of intramitochondrial metabolism and energy production in rat heart. *Mol. Cell. Biochem.* 89, 121–125.

Murgia, M., and Rizzuto, R. (2015). Molecular diversity and pleiotropic role of the mitochondrial calcium uniporter. *Cell Calc.* 58, 11–17. doi: 10.1016/j.ceca.2014.11.001

Nemani, N., Shanmughapriya, S., and Madesh, M. (2018). Molecular regulation of MCU: Implications in physiology and disease. *Cell Calc.* 74, 86–93. doi: 10.1016/j.ceca.2018.06.006

Nguyen, D. D., Kim, G., and Pae, E. K. (2016). Modulation of muscle fiber compositions in response to hypoxia via pyruvate dehydrogenase kinase-1. *Front. Physiol.* 7:e604. doi: 10.3389/fphys.2016.00604

O'Donnell, J. M., Doumen, C., LaNoue, K. F., White, L. T., Yu, X., Alpert, N. M., et al. (1998). Dehydrogenase regulation of metabolite oxidation and efflux from mitochondria in intact hearts. *Am. J. Physiol.* 274(2 Pt 2), H467–H476.

Paillard, M., Csordas, G., Szanda, G., Golenar, T., Debattisti, V., Bartok, A., et al. (2017). Tissue-specific mitochondrial decoding of cytoplasmic Ca2+ signals is controlled by the stoichiometry of MICU1/2 and MCU. *Cell Rep.* 18, 2291–2300. doi: 10.1016/j.celrep.2017.02.032

Petrie, M., Suneja, M., and Shields, R. K. (2015). Low-frequency stimulation regulates metabolic gene expression in paralyzed muscle. *J. Appl. Physiol.* 118, 723–731. doi: 10.1152/japplphysiol.00628.2014

Picard, M., Csukly, K., Robillard, M. E., Godin, R., Ascah, A., Bourcier-Lucas, C., et al. (2008). Resistance to Ca2+-induced opening of the permeability transition pore differs in mitochondria from glycolytic and oxidative muscles. *Am. J. Physiol. Regul. Integr. Comp. Physiol.* 295, R659–R668.

Picard, M., Hepple, R. T., and Burelle, Y. (2012). Mitochondrial functional specialization in glycolytic and oxidative muscle fibers: tailoring the organelle for optimal function. *Am. J. Physiol. Cell Physiol.* 302, C629–C641.

Putman, C. T., Dixon, W. T., Pearcey, J. A., Maclean, I. M., Jendral, M. J., Kiricsi, M., et al. (2004). Chronic low-frequency stimulation upregulates uncoupling protein-3 in transforming rat fast-twitch skeletal muscle. *Am. J. Physiol. Regul. Integr. Comp. Physiol.* 287, R1419–R1426.

Qiu, J., Tan, Y. W., Hagenston, A. M., Martel, M. A., Kneisel, N., Skehel, P. A., et al. (2013). Mitochondrial calcium uniporter Mcu controls excitotoxicity and is transcriptionally repressed by neuroprotective nuclear calcium signals. *Nat. Commun.* 4:2034.

Ruas, J. L., White, J. P., Rao, R. R., Kleiner, S., Brannan, K. T., Harrison, B. C., et al. (2012). A PGC-1alpha isoform induced by resistance training regulates skeletal muscle hypertrophy. *Cell* 151, 1319–1331. doi: 10.1016/j.cell.2012.10.050

Salmons, S., and Vrbova, G. (1969). The influence of activity on some contractile characteristics of mammalian fast and slow muscles. *J. Physiol.* 201, 535–549. doi: 10.1113/jphysiol.1969.sp008771

Schiaffino, S., and Reggiani, C. (2011). Fiber types in mammalian skeletal muscles. *Physiol. Rev.* 91, 1447–1531. doi: 10.1152/physrev.00031.2010

Sembrowich, W. L., Quintinskie, J. J., and Li, G. (1985). Calcium uptake in mitochondria from different skeletal muscle types. *J. Appl. Physiol.* 59, 137–141. doi: 10.1152/jappl.1985.59.1.137

Shanmughapriya, S., Rajan, S., Hoffman, N. E., Zhang, X., Guo, S., Kolesar, J. E., et al. (2015). Ca2+ signals regulate mitochondrial metabolism by stimulating CREB-mediated expression of the mitochondrial Ca2+ uniporter gene MCU. *Sci. Signal.* 8:ra23. doi: 10.1126/scisignal.2005673

Tarasov, A. I., Semplici, F., Ravier, M. A., Bellomo, E. A., Pullen, T. J., Gilon, P., et al. (2012). The mitochondrial Ca2+ uniporter MCU is essential for glucose-induced ATP increases in pancreatic beta-cells. *PLoS One* 7:e39722. doi: 10.1371/journal.pone.0039722

Wan, B., LaNoue, K. F., Cheung, J. Y., and Scaduto, R. C. Jr. (1989). Regulation of citric acid cycle by calcium. *J. Biol. Chem.* 264, 13430–13439.

Weibel, E. R., and Hoppeler, H. (2005). Exercise-induced maximal metabolic rate scales with muscle aerobic capacity. *J. Exper. Biol.* 208(Pt 9), 1635–1644. doi: 10.1242/jeb.01548

Yan, Z., Lira, V. A., and Greene, N. P. (2012). Exercise training-induced regulation of mitochondrial quality. *Exerc. Sport Sci. Rev.* 40, 159–164. doi: 10.1097/jes.0b013e3182575599

Yi, J., Ma, C., Li, Y., Weisleder, N., Rios, E., Ma, J., et al. (2011). Mitochondrial calcium uptake regulates rapid calcium transients in skeletal muscle during excitation-contraction (E-C) coupling. *J. Biol. Chem.* 286, 32436–32443. doi: 10.1074/jbc.m110.217711

Zampieri, S., Mammucari, C., Romanello, V., Barberi, L., Pietrangelo, L., Fusella, A., et al. (2016). Physical exercise in aging human skeletal muscle increases mitochondrial calcium uniporter expression levels and affects mitochondria dynamics. *Physiol. Rep.* 4:e13005. doi: 10.14814/phy2.13005

Conflict of Interest: The authors declare that the research was conducted in the absence of any commercial or financial relationships that could be construed as a potential conflict of interest.

frontiers in Physiology

REVIEW
published: 26 February 2021
doi: 10.3389/fphys.2021.619710

Tissue-Engineered Skeletal Muscle Models to Study Muscle Function, Plasticity, and Disease

*Alastair Khodabukus**

Department of Biomedical Engineering, Duke University, Durham, NC, United States

Skeletal muscle possesses remarkable plasticity that permits functional adaptations to a wide range of signals such as motor input, exercise, and disease. Small animal models have been pivotal in elucidating the molecular mechanisms regulating skeletal muscle adaptation and plasticity. However, these small animal models fail to accurately model human muscle disease resulting in poor clinical success of therapies. Here, we review the potential of *in vitro* three-dimensional tissue-engineered skeletal muscle models to study muscle function, plasticity, and disease. First, we discuss the generation and function of *in vitro* skeletal muscle models. We then discuss the genetic, neural, and hormonal factors regulating skeletal muscle fiber-type *in vivo* and the ability of current *in vitro* models to study muscle fiber-type regulation. We also evaluate the potential of these systems to be utilized in a patient-specific manner to accurately model and gain novel insights into diseases such as Duchenne muscular dystrophy (DMD) and volumetric muscle loss. We conclude with a discussion on future developments required for tissue-engineered skeletal muscle models to become more mature, biomimetic, and widely utilized for studying muscle physiology, disease, and clinical use.

Keywords: skeletal muscle, tissue engineering, fiber-type, satellite cell, disease modeling, Duchenne Muscle dystrophy, innervation, myosin heavy chain

OPEN ACCESS

Edited by:
Enrique Jaimovich, University of Chile, Chile

Reviewed by:
Mariana Casas, University of Chile, Chile
Morayma Reyes, Montefiore Medical Center, United States

***Correspondence:**
Alastair Khodabukus
aik12@duke.edu

Specialty section:
This article was submitted to Striated Muscle Physiology, a section of the journal Frontiers in Physiology

Received: *20 October 2020*
Accepted: *25 January 2021*
Published: *26 February 2021*

Citation:
Khodabukus A (2021) Tissue-Engineered Skeletal Muscle Models to Study Muscle Function, Plasticity, and Disease. Front. Physiol. 12:619710. doi: 10.3389/fphys.2021.619710

INTRODUCTION

Skeletal muscle is the largest organ in the body by mass and is essential for respiration, locomotion, posture, and whole-body energy homeostasis. To attain maximal performance and efficiency for these diverse roles, skeletal muscle displays a remarkable level of plasticity. Specifically, multiple isoforms of contractile, calcium-handling, metabolic, and structural proteins have evolved to meet the broad demands placed upon skeletal muscle (Schiaffino and Reggiani, 2011). Skeletal muscle dysfunction due to genetic mutations, aging, volumetric muscle loss, or acquired diseases significantly impair quality of life and can even be lethal. The foundation of our mechanistic understanding of skeletal muscle function, plasticity, and disease is derived predominantly from *in vivo* animal experiments and two-dimensional (2D) *in vitro* cell culture studies. Small animal studies, particularly comparative biology and genetic manipulations, have been pivotal in elucidating the molecular mechanisms regulating skeletal muscle function and plasticity (Schiaffino and Reggiani, 2011; Hoppeler, 2016). However, small animal models require additional translational and validation models to increase the successful translation of identified therapies to the clinic (Hay et al., 2014). The *in vitro* culture of human cells has the potential to generate experimental models with increased translational relevance. However, traditional skeletal muscle

cell culture systems have limited longevity due to cellular detachment resulting in developmentally immature tissues with limited translational relevance. Over the past 30 years, three-dimensional (3D) tissue engineered skeletal muscle culture systems have been developed that better mimic the native muscle microenvironment, permit functional testing, and enable prolonged culture durations (Khodabukus et al., 2018; Wang J. et al., 2019). In this review, we discuss methods to generate three-dimensional tissues and factors that regulate their functionality. We then discuss multiple factors regulating skeletal muscle fiber-type *in vivo* and the ability to study these factors *in vitro*. Lastly, we discuss further developments regulated for engineered muscle tissues to become more widely utilized and to better model adult skeletal muscle.

SKELETAL MUSCLE STRUCTURE AND FUNCTION

Skeletal Muscle Structure

Skeletal muscle is comprised of a hierarchical architectural structure that permits efficient force generation. Ultra-structurally, the most basic units of a myofibers are sarcomeres that contain myosin and actin which form overlaps to permits muscle contraction in a calcium-dependent manner. Efficient muscle contraction is coordinated by the transverse tubule system, a branched membrane network that runs along the entire length of the myofiber to the junction of the A and I bands of the sarcomere. The calcium required for contraction is stored in the sarcoplasmic reticulum (SR) which connects to the t-tubule at the specialized terminal cisternae. The SR stores calcium at a significantly higher concentration than seen in the sarcoplasm due to the calcium-binding protein calsequestrin (CSQ) (Murphy et al., 2009; Lamboley et al., 2013). Calcium is released from SR by the ryanodine receptor 1 (RyR1) into the myofibrils and binds to troponin C inducing a conformational change which results in removal of tropomyosin from myosin which enables actin to bind to myosin. Actin binding to myosin results in adenosine triphosphate (ATP) hydrolysis that causes actin to pull along myosin, shortening the sarcomere and generating muscle contraction (Sellers, 2004). Skeletal muscle relaxation is an active process that requires removal of calcium from the myofibrils to reestablish tropomyosin blocking of myosin actin-binding sites. Calcium removal is regulated by the sarcoplasmic-endoplasmic reticulum Ca^{2+} ATPase pumps (SERCA) that pump calcium back to the SR and the high affinity calcium binding protein parvalbumin found in fast skeletal muscle that quickens relaxation rate (Muntener et al., 1985; Schwaller et al., 1999).

SKELETAL MUSCLE CULTURE MODELS

Skeletal Muscle Explants and Single Fiber Cultures

Due to the high metabolic demands of skeletal muscle, long-term *in vitro* culture of whole skeletal muscles is impossible due to hypoxia and resultant loss of viability. To minimize hypoxic stress, muscles such as the extensor digitorum longus (EDL) and soleus (SOL) can be dissected to generate muscle strips that can be cultured for up to 12 h in highly oxygenated media (Park et al., 2012). These tissues can be utilized to measure contractile function (Brooks and Faulkner, 1988) and assess insulin-stimulated glucose uptake (Hansen et al., 1994). To overcome the short-term culture duration of intact muscle explants, single myofibers can be carefully dissected and isolated from the muscle belly and cultured for up to 7 days (Renzini et al., 2018), though most studies utilize 48–96 h time points. The single myofiber model is the gold-standard model to study satellite cell activation *in vitro*, due to SCs being retained within their niche and the ability to study SC dynamics with multiple modalities (Pasut et al., 2013; Wang Y. X. et al., 2019). Single fiber studies utilizing transgenic mice have been used to help unravel the transcription factors and molecular mechanisms regulating SC activation (Beauchamp et al., 2000; Kuang et al., 2007), polarity (Le Grand et al., 2009; Dumont et al., 2015), and symmetric divisions (Wang Y. X. et al., 2019). Intact single fiber studies have also enabled role of MyHC isoform on contractile properties (Bottinelli et al., 1996; Harridge et al., 1996) and the factors regulating muscle fatigue to be assessed (Westerblad and Allen, 1991; Westerblad et al., 1993). Single myofibers can also be used to assess multiple aspects of muscle physiology includingfactors regulating excitation-coupling (Allen et al., 1997; Prosser et al., 2010), genetic regulators of calcium-handling and t-tubule stability (Al-Qusairi et al., 2009; Kerr et al., 2013), membrane resealing in response to injury (Bansal et al., 2003; Sreetama et al., 2018), glucose uptake in response to electrical stimulation (Castorena et al., 2015) and insulin (Lanner et al., 2006), and to study mitochondrial function (Schuh et al., 2012). Single fiber studies have been pivotal to increasing our understanding of muscle physiology and permit *in vitro* testing of muscle fibers with adult ultrastructure and function. Importantly, the described 2D and 3D studies below are yet to replicate the developmental maturation and contractile function of the single fiber system. However, both explant and single fiber preparations are technically challenging, have limited experimental duration, are difficult to scale up for high throughput screening, and require continual new samples – making large-scale experiments in human tissues infeasible.

Traditional Two-Dimensional Models

The alternative method to single fiber culture models is to liberate satellite cells from their niche by enzymatic dissociation or permitting them to "outgrow" from partially minced muscle tissue. This method results in heterogenous cell populations found within skeletal muscles that can be further purified by cell surface marker expression (Maesner et al., 2016; Uezumi et al., 2016) by taking advantage of the faster adhesion kinetics of fibroblasts to enrich for muscle progenitor cells by pre-plating (Gharaibeh et al., 2008). Satellite cells isolated by this method rapidly activate and become myoblasts or muscle precursor cells (MPCs) characterized by increased expression of MyoD, and decreased expression of Pax7 (Ryall et al., 2015). The functional impact of this SC activation is the

dramatically impaired ability of these cultured cells to engraft in skeletal muscle upon transplantation, with just 72 h in culture decreasing engraftment efficiency threefold (Montarras et al., 2005). To minimize activation of these cells, small molecules (Charville et al., 2015), culture substratum stiffness (Gilbert et al., 2010), and regulating metabolic fuel source (Ryall et al., 2015) have been described to maintain MPCs in a more stem-like state. Alternatively, a quiescence media and culture system has been developed that can maintain SCs in a quiescent-like state but cannot reverse activated cells into a quiescent state (Quarta et al., 2016).

After expansion, MPCs can be induced to differentiate by reduction of serum content that induces cell cycle withdrawal, upregulation of differentiation genes, and ultimately fusion into multi-nucleated myotubes. Due to the rapid rate (48–96 h) of fusion and ease of the system, this model is the most frequently used system to assess the impact of genetic manipulations, growth factors, or small molecules on muscle differentiation and fusion. However, the assessment of longer-term (<7 days) experimental interventions are often prevented due to the detachment of myotubes due to spontaneous contractions of developing myotubes (Cooper et al., 2004). Furthermore, this detachment limits the developmental maturation of the tissue cultures, limiting the translation relevance of experimental findings (Rao et al., 2018). Lastly, the assessment of contractile function, the primary measure for therapeutic efficacy, is not permitted by traditional two-dimensional culture preventing functional assessments.

Engineered Skeletal Muscle Models

To overcome the limitations of 2D cell culture, several 3D skeletal muscle culture models have been developed over the past 30 years (Khodabukus et al., 2018; Wang J. et al., 2019). Two culture methods have been predominantly utilized: (1) hydrogel and (2) self-organized/assembled tissues (**Figure 1**). Both methods aim to create a biomimetic muscle microenvironment that provides cells with the appropriate extracellular matrix (ECM) and the biological and mechanical signals to promote rapid muscle development, maturation, and function.

Hydrogels

The majority of engineered tissues are generated from three-dimensional hydrogels derived from natural ECM proteins such as collagen and fibrin. Hydrogels should: (1) provide a high surface area for cell adhesion, (2) provide mechanical support and/or topical guidance to maximize, (3) minimize diffusion distances, and (4) fully degrade once sufficient cell-derived ECM is deposited to generate densely packed muscle tissue supported by its own ECM. Hydrogel based tissues are typically formed from expanded MPCs that are embedded at high density within or on top of these hydrogels. The hydrogels are cast between two fixed anchor points that enable cellular forces to remodel the hydrogel and maintain the tissues under tension that promotes tissue alignment, rapid fusion, and muscle hypertrophy (Vandenburgh et al., 1988; Khodabukus et al., 2018; Wang J. et al., 2019).

Collagen

The first 3D engineered tissues utilized Type I collagen hydrogels (Vandenburgh et al., 1988; Okano and Matsuda, 1997, 1998; Shansky et al., 1997; Powell et al., 2002), due to Type I collagen being the most abundant ECM protein in skeletal muscle (Kjaer, 2004). Whilst these studies initially utilized the C2C12 cell line, this method has successfully generated tissues from primary rodent (Vandenburgh et al., 2008; Lee and Vandenburgh, 2013) and human (Powell et al., 2002; Brady et al., 2008; Gholobova et al., 2015) cells. While collagen I is the most abundant ECM in skeletal muscle, excessive collagen levels are associated with poor regeneration and function of native muscle (Stearns-Reider et al., 2017). In native muscle, myofibers directly interact with the basal lamina which is rich in collagen IV and laminin but not type I collagen (Thorsteinsdottir et al., 2011). To better model native muscle structure, collagen hydrogels can be combined with Matrigel^{TM}, a commercially available basal lamina extract isolated from murine Engelbreth-Holm-Swarm tumors, at the time of tissue formation. Collagen-matrigel hydrogels improve muscle structure but still generate lower contractile forces than fibrin based tissues and consequently are being used less frequently for studies measuring contractile function (Hinds et al., 2011; Sato et al., 2011).

Fibrin

Fibrin is the major structural component of blood clots that functions to first prevent bleeding and then be completely remodeled, resorbed, and replaced over time making it an ideal substrate for tissue engineering (Ahmed et al., 2008). The main disadvantage of fibrin is the significant lot-to-lot variability in tissue function and gel degradation rate which can be overcome by lot testing and regulation of fibrinolysis with cross-linkers and anti-fibrinolytics, respectively (Khodabukus and Baar, 2009). Tissues engineered from fibrin alone have specific contractile force generation significantly higher than collagen-matrigel tissues (Huang et al., 2005, 2006) and can be further enhanced by the addition of matrigel to generate engineered muscle tissues with the highest reported contractile function (Hinds et al., 2011; Juhas et al., 2014; Madden et al., 2015; Khodabukus et al., 2019). The increase in force generation is due in part to fibrin being several orders of magnitude less stiff than collagen (Collet et al., 2005; Yang et al., 2007) and fibrin gels having muscle-like stiffness (Chiron et al., 2012). Substrate stiffness is a key regulator of tissue dependent gene transcription programs (Engler et al., 2006), with muscle-like stiffness increasing myogenic gene expression and promoting muscle maturation (Engler et al., 2004).

Scaffold-Free/Self-Assembled Muscle Tissues

An alternative approach to the use of hydrogels/scaffolds is to allow cells to secrete their own ECM and self-organize into a 3D tissue. The first self-organized engineered muscle used saran wrap substratum upon which MPCs were seeded with fibroblasts to ensure sufficient ECM deposition to enable tissue self-assembly (Strohman et al., 1990; Li et al., 2011). This model was then improved by seeding cells onto a PDMS substratum coated with

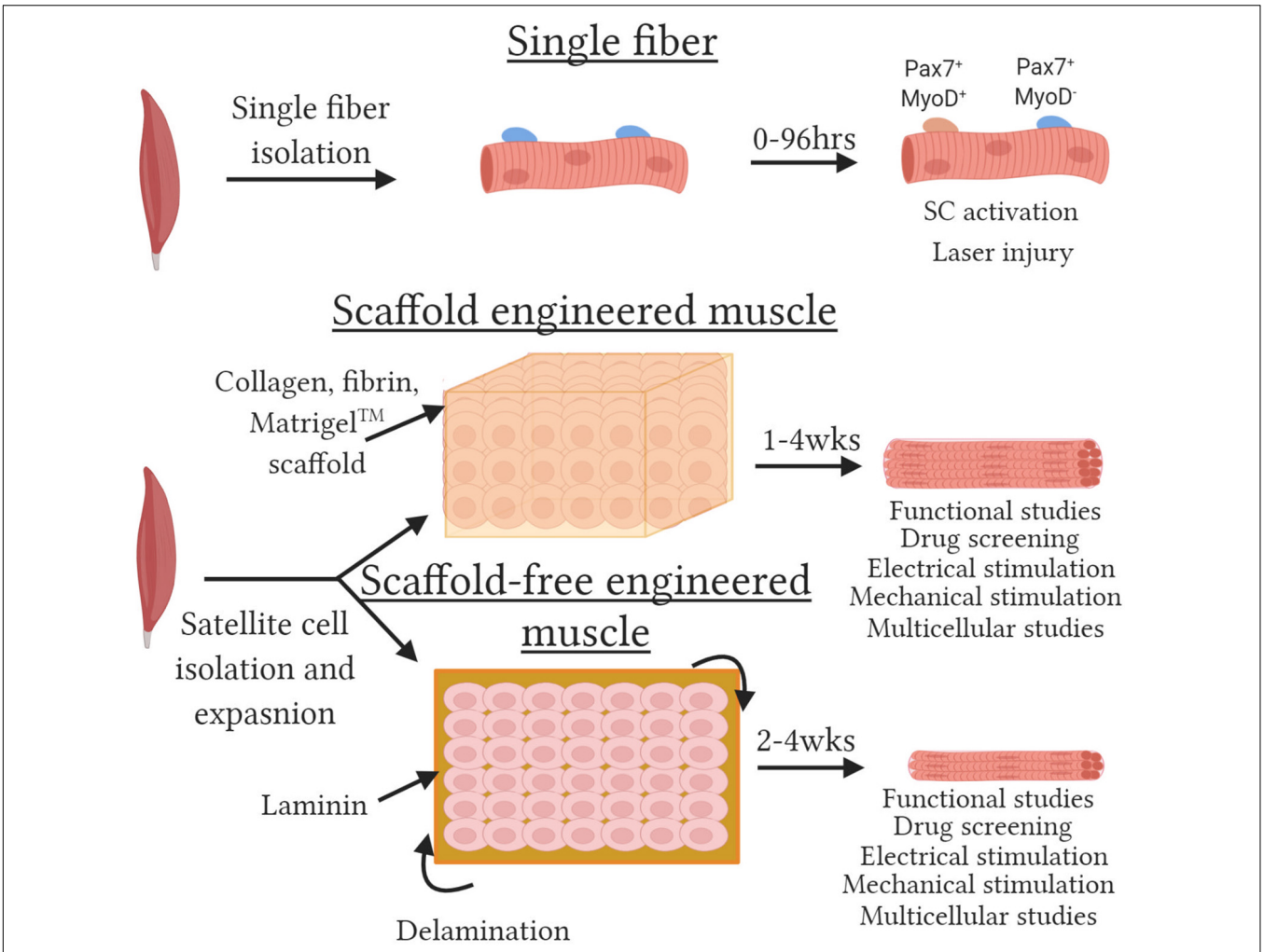

FIGURE 1 | Methods to engineered functional skeletal muscle. Schematic depicting various skeletal muscle models. **(Top)** Single fibers with satellite cells retained within their niche are isolated by enzymatic and mechanical dissociation. Single fibers can be cultured for up to 120 h and satellite cell activation assessed by evaluating Pax7 and MyoD expression or resistance to injury susceptibility assessed with laser-induced membrane damage. **(Middle)** Scaffold engineered muscles are created by embedding muscle progenitor cells at high density in a hydrogel. Cells remodel the hydrogel to generate 3D tissues packed with aligned functional myotubes. **(Bottom)** Scaffold-free engineered muscles created by seeding a monolayer of cells on laminin coated plates. The cells secrete sufficient ECM and progressive lift off the plate or "delaminate" and roll up to generate small 3D tissues. Both scaffold and scaffold-free tissues can be utilized for multiple assays with multiple functional output for up to 4 weeks.

laminin to support cell adhesion and reduce the number of fibroblasts required to generate sufficient ECM to support tissue formation (Dennis and Kosnik, 2000; Dennis et al., 2001; Kosnik et al., 2001; Larkin et al., 2006a,b). Further improvements to this model by utilizing aligned micropatterned surfaces to both quicken myoblast fusion and myotube alignment resulted in greater muscle differentiation (Lam et al., 2009). More recently, self-organized muscle cell sheets have been generated using the thermoresponsive polymer poly(N-isopropylacrylamide) (Takahashi and Okano, 2015; Takahashi et al., 2018). The cell sheets can be detached from culture plates by lowering temperature and used to engineer multi-layered tissue sheets comprised of muscle, vascular, or neuronal cells (Nagamori et al., 2013; Ngo et al., 2013; Takahashi et al., 2013). The benefits of these self-organized models are the tissues being encased entirely in cell secreted ECM and circumventing the lot variability of commercially available ECM proteins. However, the longer time to tissue formation and the inability of this model to easily be automated have resulted in hydrogel methods being more frequently used. A further limitation of self-assembled tissues is the small tissue size which hinders translational studies, though the ability to stack cell sheets or engraft multiple tissues together may overcome this issue.

Tissue-Engineered Muscle Function

Tissue engineered muscles replicate basic muscle contractile physiology such as force-length relationships and positive force-frequency relationships (Dennis and Kosnik, 2000; Huang et al., 2005; Hinds et al., 2011). However, their twitch:tetanus ratio, contractile kinetics (i.e., time to peak tension and half-relaxation

time), and specific force generation are more consistent with embryonic and neonatal skeletal muscle values (Close, 1972). The developmentally immature contractile properties reflect the developmentally immature transcriptome and protein isoform expression seen in engineered tissues. While myotubes with engineered tissues have more mature gene expression and greater hypertrophy than myotubes cultured in 2D and undergo progressive hypertrophy in culture (Rao et al., 2018), even after 4 weeks of culture myotubes resemble developmentally immature or long-term denervated fibers (Kern et al., 2004). As discussed below, the incorporation of additional cell types and electro-mechanical stimulation can further increase muscle hypertrophy and contractile function. However, significant advances are required to generate adult-like engineered muscles within the shortened timeframe that would be most attractive to researchers.

SKELETAL MUSCLE MODELS FOR STUDYING MUSCLE GROWTH AND PLASTICITY

Skeletal muscle has a remarkable level of plasticity that enables muscle to adapt to several physiological stressors such as changes in contractile activity, mechanical load, nutritional state, and hypoxia. Studying these processes in isolation *in vivo* is extremely difficult and confounding factors can hinder interpretation of the results. As discussed below, tissue-engineered skeletal muscle models have the potential to study many of these factors in isolation to not only better understand these mechanistic processes but to further enhance the maturation of engineered muscle tissues.

Skeletal Muscle Fiber-Types

Skeletal muscle can be classified as type 1 slow-twitch (ST) or type 2 fast-twitch (FT) fiber types based on myosin heavy chain (MYH) isoform expression. While ST fibers express type I myosin (MYH7), FT fibers can be further classified into three subtypes, IIa (MYH1), IIx (MYH2), and IIb (MYH4), resulting in four fiber-type classifications. However, Type IIb fibers which possess the fastest contractile phenotype, are absent in human skeletal muscle resulting in humans only possessing three fiber-types (Schiaffino, 2010). During development and muscle regeneration, the embryonic (MYH3) and neonatal (MYH8) MYH isoforms are sequentially expressed before being down regulated and replaced by the adult MYH isoforms (Chargé and Rudnicki, 2004). Importantly, approximately 25% of muscle fibers are "hybrid" and express two or more MYH isoforms that arise to provide a functional continuum for optimal contractile performance or reflect transitionary states during development and regeneration (Medler, 2019). In addition to MYH isoform, slow and fast isoforms of multiple sarcomeric and calcium-handling proteins are found in a graded fashion in fiber-types to regulate speed of contraction. Functionally, slow contractile and calcium-handling isoforms result in slower contractile kinetics and importantly permit more energy efficient contraction by utilizing less ATP to generate equivalent contractile forces than fast muscle fibers (Bottinelli et al., 1994; Stienen et al., 1996). Additionally, ST fibers possess sarcomeric isoforms of titin, nebulin, and myomesin that contribute to the increased width of the z-disk and help to stabilize muscles during muscle contraction (Yamaguchi et al., 1985; Agarkova et al., 2004; Prado et al., 2005) (**Figure 2**). Functionally, these adaptations result in ST fibers being less prone to contraction-induced muscle damage (Choi and Widrick, 2010) and contribute to the increased disease severity of FT fibers seen in Duchenne muscle dystrophy (Webster et al., 1988). Lastly, type I and IIa fibers are characterized by high mitochondrial content, increased myoglobin levels, and high capillary density to maximize oxygen delivery to support more oxidative metabolism. Importantly, mitochondrial specialization occurs between fiber-types with mitochondria in ST fibers adapted to maximize fatty acid oxidization and reduced mitochondrial transition pore opening to prevent cell death due to the chronically elevated calcium levels in ST fibers (Picard et al., 2012). In contrast, mitochondria in FT fibers have a 10-fold greater ability to oxidize of glycerol-3-phosphate to help maintain a balanced redox state (Picard et al., 2012). ST fibers also have increased reactive oxygen species scavenging capacity due in part to increased antioxidant enzyme levels (Loureiro et al., 2016) and increased NADPH generation due to increased isocitrate dehydrogenase two expression and consequent regulation of the tricarboxylic acid cycle (Murgia et al., 2015).

Over the past 30 years, significant advances in elucidating the complex molecular and transcriptomic regulation of fiber-type have been achieved. A combination of epigenetic imprinting, neuronal activity, oxygen tension, environmental factors, and metabolic and hormonal influences regulate signaling pathway cascades and transcription factor activity (Hoppeler, 2016). A key regulator of fiber-type specification is intracellular calcium concentrations, with slow tonic motor neuron activity promoting sustained elevated calcium levels that activate calcineurin and calmodulin kinase (Meissner et al., 2001; Kubis et al., 2003). This activation then results in increased activity of NFAT (Swoap et al., 2000; Kubis et al., 2002, 2003; Mccullagh et al., 2004; Calabria et al., 2009; Ehlers et al., 2014) and MEF2 (Wu et al., 2000), and decreased class II HDAC activity (Potthoff et al., 2007) to promote slow sarcomeric and oxidative metabolism gene expression. The four isoforms of NFAT contribute to muscle fiber-type with NFATc1-4 expressed in ST fibers, NFATc2-4 expressed in type IIa fibers, and IIb fibers only expressing NFATc4 (Calabria et al., 2009). In addition to regulation by calcineurin, the transcription factor Prox1 increases expression of NFATc1-3 (Kivela et al., 2016), represses multiple members of the fast transcription program (Petchey et al., 2014), and is required for typical slow fiber distribution. Elevated calcium levels also promote mitochondrial biogenesis and oxidative phosphorylation via activation of the transcription factors PGC1α, PGC1β, PPARβ, and PPARδ (Jornayvaz and Shulman, 2010; Phua et al., 2018). Overexpression of PGC1α (Handschin et al., 2007; Rasbach et al., 2010; Summermatter et al., 2012), PPARβ (Schuler et al., 2006), and PPARδ (Wang et al., 2004) result in fast-slow fiber type and alter sarcomeric and calcium-handling gene expression demonstrating the interrelationship between metabolism, calcium-handling, and sarcomeric transcriptome.

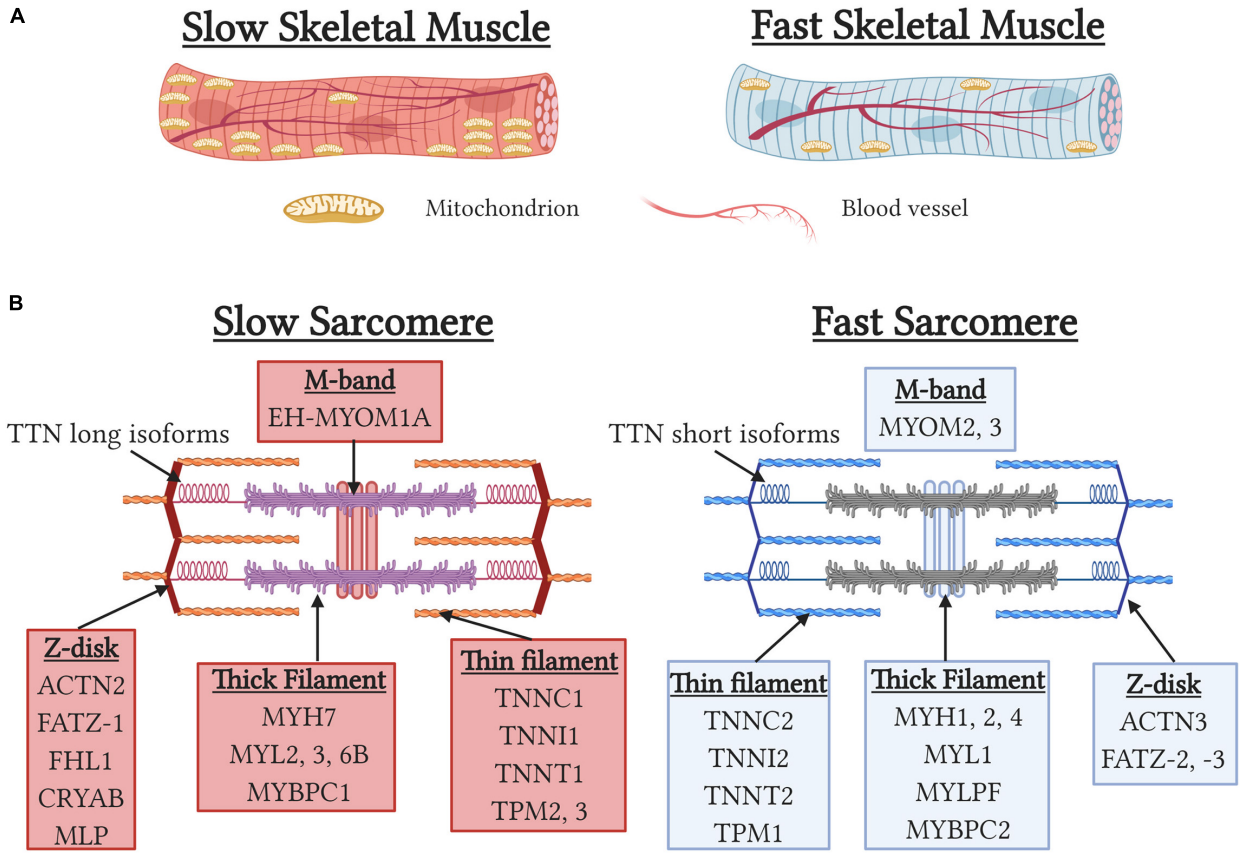

FIGURE 2 | Structural differences between slow and fast-fiber type muscles. **(A)** Schematic depicting gross morphological differences between slow and fast skeletal muscles. Note the higher levels of mitochondria and capillary density associated with slow skeletal muscles. **(B)** Sarcomeric gene specialization and enrichment in slow and fast myofibers.

Additionally, overexpression of TEAD1, a member of the Hippo pathway, induces fast-to-slow fiber type conversions (Tsika et al., 2008). Conversely, a slow-to-fast transition occurs in the presence of thyroid hormone (Zhang et al., 2014) or deletion of VGLL2 (Honda et al., 2017) by disruption of TEAD1. Whilst the molecular transduction pathways leading to fast muscle fiber-types are less well characterized, genetic regulation of fast muscle fiber-type is well established. Fast muscle fiber neural input is linked to increased HIF1α content (Lunde et al., 2011), which is known to increase glycolytic gene expression, and decreased MyoD phosphorylation (Ekmark et al., 2007). MyoD is enriched in fast muscle fibers (Hughes et al., 1997) and repressed by the key slow-fiber type regulator NFATc1 (Ehlers et al., 2014) but its deletion only results in mild fiber-type switching suggesting that, whilst important, MyoD is not a master regulator of fast-fiber transcription. The master regulators of the fast muscle program are the Six1, Six4, Eya1 transcription factor complex which promote fast muscle gene expression (Grifone et al., 2004; Niro et al., 2010) and the transcriptional repressor Sox6 which inhibit slow muscle gene expression and increases fast muscle gene expression (Hagiwara et al., 2005, 2007; An et al., 2011; Quiat et al., 2011; Wang et al., 2011; Sakakibara et al., 2014). In humans, increases in fast muscle fiber-types are seen in donors with polymorphisms in HIF1α that increase HIF1α transcriptional activity (Ahmetov et al., 2008). Similarly, polymorphisms that decrease levels of the fast-fiber specific z-disk protein α-actinin3 are associated with increased calcineurin activity and endurance performance indicating that regulators of muscle fiber type can regulate human muscle performance (Yang et al., 2003; Eynon et al., 2012; Seto et al., 2013).

Role of Neural Input on Muscle Fiber Type *in vivo*

Complete muscle development and maintenance of adult muscle mass and fiber-type requires functional innervation. A key difference between slow and fast fiber-types is the motor input received with the frequency neural impulses differing between slow (10–30 Hz) and fast (50–100 Hz) muscle fibers (Hennig and Lomo, 1985; Eken et al., 2008). Additionally, slow fibers are active for greater periods of time and receive a far higher number of neural impulses per day than fast muscle fibers. The predominant role of neural input in regulating muscle fiber-type was first described in 1960 (Buller et al., 1960) and

detailed in multiple elegant studies in the 1960s and 1970s (Close, 1969; Barany and Close, 1971; Hoh, 1975). Specifically, the contractile properties of slow muscles become faster when reinnervated by a fast nerve and fast muscles become slower when reinnervated by a slow nerve. The second series of studies used implanted electrodes to determine the role of stimulation frequency, work:rest ratio, and contractile impulse numbers in directing contractile kinetics and fiber-type shifts (Salmons and Sreter, 1976; Eberstein and Pachter, 1986; Eken and Gundersen, 1988; Gorza et al., 1988; Westgaard and Lomo, 1988; Windisch et al., 1998). The seminal finding of these studies is that neural input firing pattern is the predominant neural factor regulating muscle fiber-type and not secreted neurotrophic factors (Salmons and Sreter, 1976). Overall, these studies showed that increasing stimulation frequency, decreasing the work:rest ratio, and decreasing the total number of delivered impulses resulted in shifts to a faster-fiber type. Critically, both experimental models revealed that each individual muscle has an "adaptive range", the degree of plasticity is species dependent, and long time periods (>3 months) are required for more definitive fiber-type changes. This adaptative range can be expanded by thyroid levels, with hypothyroidism and hyperthyroidism promoting greater slow and fast fiber-type shifts respectively (Kirschbaum et al., 1990; Caiozzo et al., 1998, 2000; Di Maso et al., 2000; Zhou et al., 2019). Overall, the typical adaptive ranges of mouse ST fibers permit expression of type I, IIa, and IIx but not IIB fibers, while mouse FT fibers can express Type IIa, IIx, and IIB fibers but not type I fibers.

Role of Neural Input on Muscle Fiber Type *in vitro*

The role of distinct neural inputs can be studied in culture by field electrical stimulation without potential confounding effects such as regenerative ability, compensatory hypertrophy, and animal locomotion. In 2D cultures, these studies have demonstrated that slow or fast-like stimulation patterns can increase isoform specific sarcomeric and calcium-handling proteins, and induce muscle hypertrophy (Wehrle et al., 1994; Hamalainen and Pette, 1997). The number of impulses and period of contractile activity must be regulated to prevent detachment of contracting myotubes in 2D culture. In contrast, in engineered muscle tissues the 3D environment supports tissue contraction and permits long-term electrical stimulation. However, long-term field electrical stimulation can induce electrochemical damage resulting in tissue damage and ultimately cell death. Electrochemical damage can be minimized by utilizing bipolar impulses and optimizing impulse parameters (i.e., electric field and pulse width) based on tissue excitability to enable adult-like long-term, chronic electrical stimulation without electrochemical damage for at least 2 weeks (Donnelly et al., 2010; Khodabukus and Baar, 2012, 2015c). Clinically, rheobase and chronaxie have been utilized to prevent tissue damaged in chronically denervated patients undergoing neuromuscular electrical stimulation (NMES) therapy (Pieber et al., 2015). The excitability of engineered tissues are similar to that of long-term denervated muscle and thus have potential to be used as an *in vitro* model to study factors regulating excitability and to screen factors that promote muscle excitability (Dennis and Dow, 2007; Khodabukus and Baar, 2012). In patients, NMES results in increased muscle cross-sectional area and tissue functionality in long-term denervated tissue (Boncompagni et al., 2007; Kern et al., 2010; Kern and Carraro, 2014; Carraro et al., 2015). In engineered muscle tissues, electrical stimulation increases force generation, muscle hypertrophy, and MHC and dystrophin protein levels in engineered tissues (Huang et al., 2006; Khodabukus and Baar, 2012, 2015c; Ito et al., 2014; Khodabukus et al., 2015, 2019). Like native muscle (Baar and Esser, 1999; Terzis et al., 2008; Drummond et al., 2009), these increases in muscle hypertrophy are associated with increased mTORC1 activity and can be inhibited by the mTOR inhibitor rapamycin. These studies also show that electrical stimulation of engineered muscle tissues for 1 or 2 weeks does not induce transformative changes in muscle size and that additional factors and/or time are required to attain adult muscle size.

To date, relatively few studies have determined the fiber-type impacts of different electrical stimulation protocols on engineered tissue function. The first study showed differential functional responses between muscles engineered from cells isolated from fast and slow muscles when electrically stimulated with biomimetic fiber-type neural input protocols (Huang et al., 2006). Specifically, engineered slow tissues increased force generation but did not alter their contractile kinetics in response to slow-fiber mimetic electrical stimulation. In contrast, slow-fiber mimetic stimulation in TA tissues did not increase force generation but did slow contractile kinetics. The fast fiber-type protocol did not change any parameters in either slow or fast engineered tissues, potentially due to the number of contractions being insufficient to induce functional changes or the lack of factors such as T3 which are critical for the fast-fiber type program. Human engineered tissues increase force generation and hypertrophy when subjected to a fast-like periodic intermittent electrical stimulation protocol with slow-like 1 or 10 Hz frequencies (Khodabukus et al., 2019). The 10 Hz but not the non-physiological 1 Hz protocol induced a quickening of half-relaxation time which was associated with increased fast CSQ and SERCA gene expression indicating that initial fiber-type shifts can be studied in human tissues. To date, the greatest fiber-type shift has been shown in C2C12 tissues where the role of contraction duration in inducing a slow fiber-type transition was defined (Khodabukus et al., 2015). When keeping the stimulation frequency, work:rest ratio, and total number of impulses received per day consistent, contraction lengths of greater than 6 s were required to induce more complete fast-to-slow MYH shifts. Fast-to-slow isoform switching of each troponin isoform, CSQ, and SERCA were independent of contraction length changes, suggesting differential regulation of MYH and other contractile proteins. These changes in protein abundance correlated to functional changes, with the slow electrical stimulation paradigm inducing slowing of contractile kinetics and increased fatigue resistance. Overall, these studies demonstrate the ability of engineered muscle tissues to study the fiber-type changes induced by electrical stimulation. However, while generation of slow fiber-types has been demonstrated, further optimization of the culture

conditions and electrical stimulation protocols are required to generate fast fiber-type tissues.

Motor Innervation of Engineered Muscle Tissues

While field electrical stimulation can mimic neural input, it does not faithfully recapitulate EC-coupling or model the complex physical and chemical interactions between muscle and nerves. Motor innervation is essential for complete muscle development and maintenance of muscle mass and defects in the neuromuscular junction (NMJ) result in multiple neuromuscular diseases such as myasthenia gravis (MG) and amyotrophic lateral sclerosis (ALS) (Rudolf et al., 2016; Cappello and Francolini, 2017). The first reports of NMJ formation were reported over 40 years in co-cultures of Xenopus myoblasts and embryonic neurons (Anderson and Cohen, 1977; Anderson et al., 1977). Similar studies utilizing rodent cells show markers of muscle maturation such as fetal to neonatal MHC isoform transitions, increased sarcomere structural maturation, and acetylcholine receptor (AchR) clustering (Das et al., 2007, 2010; Guo et al., 2010). However, in these studies AchR clustering does not co-localize with nerve terminals, as seen in embryonic development (Witzemann, 2006), the NMJs fail to replicate mature pretzel-like morphology, and no definitive evidence of electrical transmission provided suggesting incomplete NMJ development and maturation. In the past decade, substantial progress has been made in generating motor neuron-like progenitors from hiPSCs to permit studies utilizing human cells (Patani et al., 2011; Amoroso et al., 2013; Faravelli et al., 2014; Sances et al., 2016). These cells when co-cultured with primary or hiPSC-derived myotubes demonstrate AchR clustering but more importantly show functional NMJ formation (Demestre et al., 2015; Puttonen et al., 2015; Toli et al., 2015). Specifically, motor neuron-induced muscle contraction can be induced by specific motor neuron glutamatergic excitation by glutamate or N-Methyl-D-aspartate or inhibited by tubocurarine, an anti-cholinergic drug that prevents neural transmission (**Figure 3E**). Alternatively, muscle contraction can be induced optically by transduction of motor neurons with the light-sensitive ion channel channelrhodopsin2 (ChR2) (Steinbeck et al., 2016). Expression of ChR2 permits specific optical activation of motor neurons with blue light and subsequent myotube contraction if functional NMJs are present. Importantly, the use of hiPSCs allows the modeling of multiple human neuromuscular disease such as MG, spinal muscular atrophy (SMA), and ALS which would not be possible due to the post-mitotic state of adult motor neurons (Dimos et al., 2008; Ebert et al., 2009; Sances et al., 2016).

The first 3D tissue engineered muscle motor-neuron co-cultures utilized neonatal rat MPCs and embryonic spinal cord explants (Larkin et al., 2006b). Neural projections from the explants extended into the engineered muscle and preserved their structure to enable neural specific stimulation of the resulting tissue. Spinal explants increased force generation, ∼25% of which could be achieved by direct neural stimulation, indicating incomplete innervation of all myotubes and/or the presence of non-functional NMJs. Mixing of rat motor neurons with rat MPCs at time of tissue formation also results in improved contractile force and muscle structure, though the level of functional NMJ generation was not tested (Martin et al., 2015). Incorporation of hiPSC-derived neurospheres, that contain motor neurons and other supporting cell types, into primary human engineered muscle tissues results in successful generation of innervated myotubes as assessed by glutamate stimulation (Afshar Bakooshli et al., 2019) (**Figures 3A,B**). Neurosphere co-culture also resulted in shifts to more developmentally mature AchR subunit expression and more adult-like AchR structure then that seen in 2D cultures. While motor neuron-muscle co-cultures clearly increase functionality and muscle structure, it is still unclear what effects are due to increased contractile activity and secreted neurotrophic factors. The synaptogenic factor agrin can induce AchR formation, AchR clustering, and increase force generation almost 2-fold (Bian and Bursac, 2012). Similarly, the neurotrophic factor neuregulin-1 induced AchR subunit isoform maturation though its role in regulating muscle function unknown (Afshar Bakooshli et al., 2019). The most recent models to study NMJ formation in 3D tissues utilize neural cells and engineered muscle tissues in two distinct modular compartments (**Figures 3C,D**). These compartments are then attached by a collagen gel bridge that supports and guides neural cell migration and neurite extension into the engineered muscle tissue. Importantly, specific activation of the neural compartment can induced optogenetically by overexpression of ChR2 and engineered muscle contractile function assessed by pillar deformation (Uzel et al., 2016; Osaki et al., 2018b; Vila et al., 2019). Thus in the presence of functional NMJ formation, optical stimulation of the neural compartment induces contraction of the engineered muscle compartment. These models have been used to successfully model impaired NMJ function in ALS and MG (Osaki et al., 2018b; Afshar Bakooshli et al., 2019; Vila et al., 2019) and to identify and validate prospective clinical drug candidates such as rapamycin and bosutinib for ALS (Osaki et al., 2018b). Overall, significant progress has been made with innervation of engineered muscle tissues over the past 5 years and they possess great potential as more biomimetic models for muscle disease and development. However, significant improvements in NMJ maturation are still required as well as more detailed assessment of NMJ electrophysiology, structure, and function.

Effect of Cell Source on Fiber-Type

A fundamental question underlying muscle plasticity is if the satellite cells that make typically slow (e.g., SOL) or fast (e.g., tibialis anterior) muscle fibers are distinct and predisposed to generate a specific fiber-type. As discussed above, the adaptive ranges of muscle fibers suggest that fiber-type is predetermined. Slow fiber-type muscles contain a higher level of satellite cells than fast fiber type tissues (Gibson and Schultz, 1982; Putman et al., 2001; Mackey et al., 2009). This difference is further exacerbated with aging due to a greater loss of SCs in fast muscle fibers (Verdijk et al., 2007, 2014), which correlates to the greater loss of function seen in fast muscles in sarcopenia (Deschenes et al., 2013; Purves-Smith et al., 2014). Satellite cells isolated from slow-fiber type muscles have increased transplantation efficiency and thus are likely more translationally relevant for

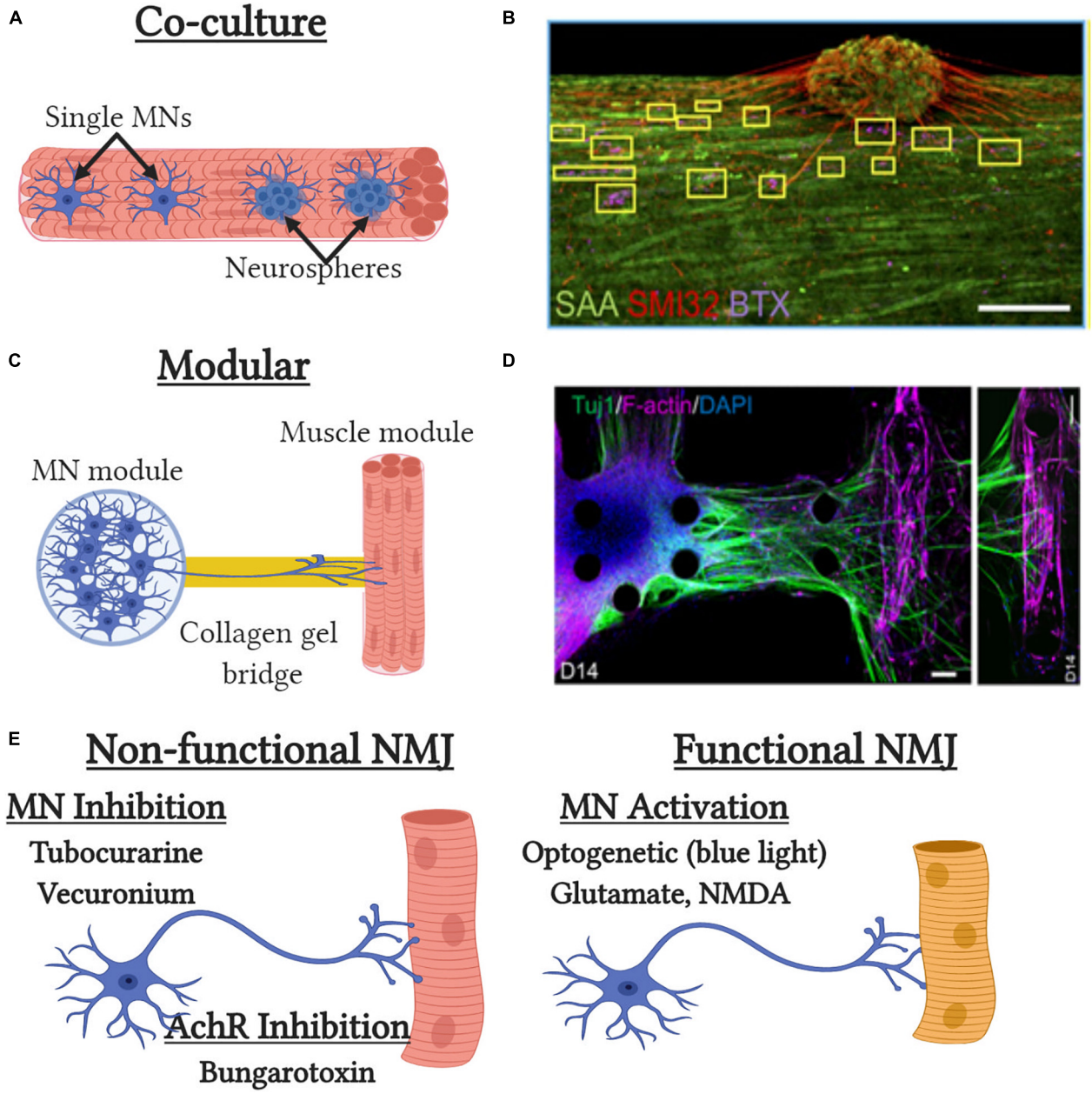

FIGURE 3 | Tissue-engineered neuromuscular junction (NMJ) models. **(A)** Traditional co-culture NMJ models where single MNs or neurospheres are embedded with muscle cells at the time of tissue formation. **(B)** Representative image of the co-culture NMJ model (Afshar Bakooshli et al., 2019) with immunofluorescent staining of neurite extensions (SMI32), acetylcholine receptors [α-bungarotoxin (BTX)] and muscle sarcomeres [sarcomeric α-actinin (SAA)]. Scale bar, 200μm. **(C)** Modular NMJ muscle model where motor neurons (MNs) and engineered muscle tissues are cultured in separate compartments and connected by a collagen gel which supports neurite extension. **(D)** Representative image of the modular NMJ model (Osaki et al., 2018b) with immunofluorescent staining of neurite extensions (TUJ1) and myotubes [filamentous(f)-actin]. Scale bars, 100 μm. **(E)** Schematic depicting pharmacological and genetic methods to assess neuromuscular junction (NMJ) functionality *in vitro*.

future SC transplantation therapies (Collins et al., 2005). The existence of intrinsic differences between satellite cells from fast and slow muscles is further suggested by the finding that electrical stimulation of regenerating slow SOL and fast EDL muscles with the same slow stimulus pattern in the absence of innervation leads to widespread slow MYH expression in regenerated SOL but only limited expression of slow MYH in regenerated EDL (Kalhovde et al., 2005). Additionally, the altered MYH isoform profile of single fibers isolated from long-term denervated slow and fast-fiber type muscles remain distinct and do not converge to similar MYH isoform expression (Patterson et al., 2006). Traditional 2D cell cultures of cells

isolated from slow and fast muscles show preferential expression of fiber-type MYH expression and displayed expected adaptive ranges to fiber-like electrical stimulation (Wehrle et al., 1994; Rosenblatt et al., 1996; DiMario and Stockdale, 1997). In 3D culture, muscles engineered from MPCs isolated from rats (Huang et al., 2006) or mice (Khodabukus and Baar, 2015a) retain the contractile and metabolic properties of the muscles from which they were derived. Specifically, expected isoform shifts in multiple sarcomeric, calcium-handling, and metabolic proteins are seen. However, due to the lack of neural input these shifts are less distinct than seen in innervated adult muscle fibers and more closely resemble long-term denervated myofibers. Interestingly, these changes are linked to changes in transcriptional master regulators such as Sox6 which is more abundant in myotubes derived from fast muscles (Khodabukus and Baar, 2015a). Overall, these studies demonstrate that the satellite cells generating fast and slow muscles are distinct and result in long-term differences in metabolism and function both *in vitro* and *in vivo*.

Role of Mechanical Load on Engineered Muscle Size and Function

Skeletal muscle function and size is dependent upon the load placed upon it as evidenced by loss of muscle mass and strength following immobilization, bed rest, spaceflight (Haddad et al., 2006; Baldwin et al., 2013), and gain of muscle mass and function with resistance exercise (Hughes et al., 2018; Jorgenson et al., 2020). Mechanical load is modeled *in vitro* by the application of stretch to tissue cultures using deformable membranes (Sim et al., 2007; Pavesi et al., 2015) or custom-made bioreactors (Dennis et al., 2009; Rangarajan et al., 2014) to induce programmable levels of stretch in custom-made regimes. Most studies utilize custom-made systems and unique stimulation protocols that hinder comparisons between studies. To date, *in vitro* mechanical stimulations of engineered muscle have aimed to replicate: (1) the continual increase in muscle length seen during development (ramp stretch/stimulation); and; (2) muscle strain that occurs during locomotion and exercise (cyclic stretch/stimulation). Ramp stretch results in concomitant proliferation and differentiation of MPCs (Vandenburgh and Karlisch, 1989) which may be due in part to the secretion of the IGF-1 splice variant mechanogrowth factor (Cheema et al., 2005). Application of ramp stretch for only 45 h induces significant muscle hypertrophy and increases in contractile force generation in C2C12 engineered tissues (Aguilar-Agon et al., 2019). Applying both ramp and cyclic stretch induced significant myotube hypertrophy in engineered human tissues (Powell et al., 2002) and increased glucose uptake in avian tissues (Hatfaludy et al., 1989). The seminal *in vitro* work of Vandenburgh showed that cyclical stretch induces muscle hypertrophy and increases protein and DNA content (Vandenburgh and Kaufman, 1979, 1981; Vandenburgh, 1982, 1988; Vandenburgh et al., 1989, 1991). Like native muscle following resistance exercise or altered mechanical load (Baar and Esser, 1999; Terzis et al., 2008; Marabita et al., 2016), mechanical stimulation induced hypertrophy of *in vitro* cultures is associated with mTORC1 activation (Baar et al., 2000; Khodabukus et al., 2007; Aguilar-Agon et al., 2019). Conversely, muscle atrophy can be modeled by decreasing engineered tissue length to induce decreases in myotube size and loss of contractile force (Lee and Vandenburgh, 2013). Together, these studies demonstrate that mechanical loading/unloading can model aspects of muscle hypertrophy/atrophy and be used a model system to study these processes. Similar to electrical stimulation studies, no transformative breakthroughs in generating engineered tissues with native-like muscle size or strength have been reported with use of mechanical stimulation alone or in combination with electrical stimulation (Liao et al., 2008).

Metabolic and Hormonal Control of Muscle Fiber-Type *in vitro*

A key difference between fiber-types is the greater reliance of fast-fiber type muscles on glycolysis and slow-fiber-type muscle on oxidative phosphorylation to meet energy needs. Muscles engineered from fast twitch muscle fibers have increased levels of glycolytic enzymes and fatigue at a greater rate than tissues generated from slow twitch muscle fibers (Khodabukus and Baar, 2015a). Engineered C2C12 tissues cultured with supraphysiological glucose levels promotes a fast fiber-type contractile and metabolic phenotype, permits detectable levels of the fast-fiber specific protein parvalbumin, and increased levels of glycolytic proteins (Khodabukus and Baar, 2015b). Whilst promising, accurate modeling and studying of oxidative metabolism *in vitro* is hindered by the Crabtree effect where *in vitro* cultured cells typically utilize glycolysis to generate ATP despite the presence of abundant oxygen and functional mitochondria (Crabtree, 1929; Marroquin et al., 2007). The Crabtree effect can be circumvented by replacing glucose in the cell culture media with galactose which forces cells to rely on oxidative phosphorylation to meet their energy demands due to galactose requiring 2 molecules of ATP to generate pyruvate and thus producing 0 net ATP from anaerobic glycolysis (Marroquin et al., 2007; Ryall et al., 2015). Galactose culture of primary human myotubes increases mitochondrial enzyme levels, increases basal and maximal oxygen consumption, and increased phosphorylation of AMPK (Aguer et al., 2011) – which when chronically activated results in a fast-to-slow fiber-type transition (Ljubicic et al., 2011). Importantly, these adaptations to galactose culture conditions were not seen in myotubes derived from type II diabetics suggesting that true assessment of metabolic dysfunction in diabetic myotubes may require novel culture conditions (Aguer et al., 2011). In contrast, C2C12 cells do not respond to galactose culture conditions indicating that modeling metabolism in immortalized cell lines should be treated with caution (Elkalaf et al., 2013). Alternatively, supplementing culture media with fatty acids has the potential to promote oxidative metabolism and potentially promote a slow fiber-type phenotype. However, *in vitro* cultures are prone to lipotoxicity due to the low reliance on oxidative phosphorylation and β-oxidation to meet energy demands. In agreement with this, the saturated fatty acid palmitate is known to induce atrophy (Bryner et al., 2012), insulin resistance (Yuzefovych et al., 2010),

and cell death (Patkova et al., 2014) in myotubes. Addition of polyunsaturated fatty acids (PUFAs) such as oleic, linoleic, docosahexaenoic, and eicosapentaenoic acid can reduce or prevent these negative cellular effects of palmitate (Bryner et al., 2012; Yuzefovych et al., 2012; Lee et al., 2017; Woodworth-Hobbs et al., 2017). Recently, oleic acid alone was shown to increase MYH7 protein levels, mitochondrial mass, and increase maximal respiration rate in human myotubes supporting the potential role of fatty acids in promoting fiber-type shifts (Watanabe et al., 2020). In contrast, promoting a fast fiber-type *in vitro* has proven to be more difficult due in part to the fact that fast MYH expression occurs in more mature muscles cultures (Cooper et al., 2004). Lactate can increase fast MYH (MYH 1 and 4) gene expression (Tsukamoto et al., 2018) and thyroid hormone upregulates fast SERCA isoform expression (Thelen et al., 1997). Overall, these studies show that fiber-type shifts can be studied *in vitro* by modulation of fuel source and hormone availability but advances in generating fast fiber-type changes are still required.

VASCULARIZATION OF ENGINEERED MUSCLE TISSUES

Native skeletal muscle is highly vascularized to provide the oxygen and nutrient supply required to support the high metabolic demands induced by muscle contraction. Hypoxia and impaired cell survival typically occur at a diffusion distance of 150–200μm from blood vessels or in culture media and limits tissue-engineered muscle size (Gholobova et al., 2020a). Satellite cell fate and muscle regeneration is also regulated by vasculature (Abou-Khalil et al., 2009, 2010; Fu et al., 2015), with 50-80% of satellite cells are in near or direct contact with capillaries (Verma et al., 2018). Therefore, vascularized tissue-engineered skeletal muscles are required for accurate modeling of native skeletal muscle *in vitro* and effective cellular therapies *in vivo*.

Vascularization of tissue-engineered skeletal muscles has typically been performed by the incorporation of vascular cells at the time of tissue formation. A key technical limitation with vascularized engineered muscle tissues are the incompatible media requirements of muscle and vascular cells (Gholobova et al., 2015). This has led to compromised media conditions that result in suboptimal differentiation of muscle and/or vascular cells than if cultured in isolation. A second technical limitation of co-culturing muscle and vascular cells is the potential for vascular cells to impede myoblast fusion. This issue can be overcome by 3D bioprinting techniques (Choi et al., 2019), the stacking of muscle-only and vascular-only cell sheets (Nagamori et al., 2013), culturing vascular and muscle cells in distinct compartments (Osaki et al., 2018a), or the coating of vascular cells to differentiated mature muscle tissues (Gholobova et al., 2020b). The formation of stable vasculature requires the inclusion of supporting cell types such as fibroblasts, pericytes, and/or smooth muscle cells (Levenberg et al., 2005; Koffler et al., 2011; Perry et al., 2017). Implantation of pre-vascularized engineered muscle tissues with these supporting cell types accelerates vascular anastomosis, increases blood vessel density, and tissue survival compared to co-cultures alone. While the benefit of forming vascular networks for implantation survival is well established, to date no studies have shown increased muscle function, increased muscle maturation, or enhanced SC quiescence in co-cultured tissues *in vitro*. Additionally, the ability of these vascular networks to enhance nutrient delivery and increase engineered muscle size *in vitro* have yet to be shown.

MODELING AND TREATING MUSCLE DISEASE

Over the last century, small animal models have been the predominant experimental platform to study disease by genetic manipulations, surgical procedures, or other interventions such as changes made to diet and aging. These studies have given us the majority of the insight we have into the underlying mechanisms of disease and for identifying and pre-clinical validation of novel therapeutics. When assessing all drugs entering clinical trials for all diseases, the successful clinical translation is alarmingly low – with less than 1% of identified drugs making it to the clinic resulting in an estimated cost of $1 billion dollars per drug (Hay et al., 2014). The underlying reasons for this low level of success are multifactorial but include species-specific differences in drug metabolism and toxicity (Dykens and Will, 2007; Shen et al., 2011), animal models not fully recapitulating disease severity in humans (Yucel et al., 2018), animals not accurately modeling human pharmacogenomics (Weinshilboum and Wang, 2017), and epigenetic regulation of disease severity (Lamar and Mcnally, 2014). The ability to generate functional human tissue-engineered organs has potential to address some of the limitations of animal studies and provide complementary methods to improve successful drug clinical translation.

Duchenne Muscular Dystrophy

Duchenne muscular dystrophy (DMD) is a fatal X-linked recessive disorder that affects approximately 1 in 5000 male births due to mutations in the dystrophin gene. Dystrophin is part of the dystrophin-glycoprotein complex (DGC) that functions to efficiently transmit contractile force to the ECM and stabilize the sarcolemmal membrane during contraction to prevent muscle damage. The increased susceptibility to muscle injury due to compromised membrane stability and impaired regenerative response of satellite cells results in constant cycles of muscle degeneration and regeneration. Ultimately, this leads to progressive muscle weakness, loss of ambulation, and fatal respiratory failure by the age of 20. Currently, there is no curative treatment with standard-of-care corticosteroid (prednisone and deflazacort) therapy extending life expectancy up to the fourth decade by delaying disease progression (Bushby et al., 2010).

The most widespread animal model of DMD, the mdx mouse model, arose due to spontaneous mutation in exon 23 on the dystrophin gene in C57/BL10 mice. Like DMD patients, mdx muscles undergo consistent rounds of degeneration and regeneration, display increased susceptibility to eccentric contractions, and display abnormalities in SC function. However, these mice do not show more severe disease phenotypes such as severe muscle weakness, early mortality, cardiac dysfunction

and only display significant fat and fibrotic replacement at old age (20–24 months) (Yucel et al., 2018; Aartsma-Rus and Van Putten, 2019). In the past two decades, additional dystrophin-deficient mice have been generated on the C57/BL6 (e.g., mdx^{cv2-5}) and on the DBA/2J backgrounds (Yucel et al., 2018; Aartsma-Rus and Van Putten, 2019). The mdx^{cv2-5} mice have mutations in a range of exons but still demonstrate the lack of functional weakness seen in traditional mdx model. In contrast, the hDMDdel45D2/mdx mouse displays a stronger dystrophic phenotype and displays contractile weakness potentially improving the efficacy of pharmacological therapeutic validation studies (Coley et al., 2016; Young et al., 2017; Van Putten et al., 2019). Mouse models that more accurately replicate human disease severity have required knockout of both dystrophin and utrophin (Deconinck et al., 1997; Grady et al., 1997). These double knockout mice show severe functional and regenerative defects in skeletal muscle, cardiac, and bone tissues. Alternatively, knocking out the telomerase gene in mdx mice (mdx/mTR) induces a more severe muscle (Sacco et al., 2010) and cardiac (Mourkioti et al., 2013) disease phenotype. Together, these double knockout mice provide more severe disease models with which to study dystrophin deficiency and the efficacy of novel therapeutics. Advances in genome editing have permitted the generation of transgenic mice that model disease mutations in human hotspots and allow the testing of gene therapies *in vivo*. However, these mice do not replicate the significant role that disease modifiers play in disease severity for DMD. Multiple genetic and epigenetic modifiers have been shown to significantly influence disease severity and corticosteroid efficacy (Pegoraro et al., 2011; Flanigan et al., 2013; Lamar and Mcnally, 2014; Bello et al., 2015). For example, latent TGF-β binding protein 4 (LTBP4) and osteopontin, which modulate TGF-β signaling, significantly impact disease progression and efficacy of corticosteroid treatment (Bello et al., 2015), and inhibition of TGF-β signaling reversing disease phenotypes *in vitro* and *in vivo* (Choi et al., 2016). Therefore, high throughput personalized *in vitro* muscle platforms that accurately model pharmacogenomic responses will be required to generate high fidelity and clinically predictive drug screens. The mdx mouse model was used as the preclinical system to validate the current standard of care drugs prednisolone (Hudecki et al., 1993) and deflazacort (Anderson et al., 1996). More recently, these models have been used to validate the antisense oligonucleotide treatments eteplirsen (Mendell et al., 2013) which was approved by the FDA in 2016 (Mendell et al., 2013; Stein, 2016; Khan et al., 2019). The use of more severe mdx models in combination with high fidelity human *in vitro* models may lead to more successful clinical translation and drug discovery efforts.

To date, two 3D *in vitro* skeletal muscle models of DMD have been reported using primary cells. The first utilized immortalized dystrophic mouse myoblasts and identified 11 compounds that increased contractile force generation (Vandenburgh et al., 2008). More recently, engineered muscle sheets derived from human primary DMD myoblasts demonstrated decreased fusion ability, decreased myotube size, and produced less force compared to healthy controls after 6 days in differentiation media (Nesmith et al., 2016). Whilst promising, these studies did not describe more mature disease markers such as evidence of degeneration/regeneration, fibrosis or fat replacement or increased susceptibility to contraction-induced injury that will be critical to study DMD pathology and treatment efficacy *in vitro*. Widespread *in vitro* personalized medicine models of DMD or any other myopathy will require the use of hiPSC-derived muscle due to the ethical considerations and proliferative limitations of taking muscle biopsies from myopathic patients. To date, the majority of hiPSC studies of DMD have been performed in 2D cell culture. These studies have demonstrated disease phenotypes such as calcium overload (Shoji et al., 2015), fusion deficits, increased creatine kinase release (Young et al., 2016), and elevated BMP/TGF-β signaling (Choi et al., 2016). Interestingly, fusion deficits are not always seen in hiPSC cultures and appear to be dependent upon media conditions or cell surface marker selection that potentially prevent fusion deficits (Hicks et al., 2018). Recently, a high throughput drug screen in 2D iPSC-derived myotubes identified ginsenoside and fenofibrate as factors that improved hiPSC myoblast fusion *in vitro* and improved mdx morphology and function *in vitro* (Sun et al., 2020). In addition to pharmaceutical screening, engineered tissues can be used to optimize guide RNA design for highly efficient and maximal functional return for CRISPR-Cas9 mediated exon skipping in engineered DMD hiPSC-derived cardiac tissues (Long et al., 2018). A further advantage of hiPSC cell models is the ability to generate increasingly complex disease models by the addition of multiple cell types. In particular, the NMJ pathophysiology in DMD is poorly studied and has the potential to be studied in hiPSC-derived tissues. The generation of multi-cellular 3D muscle tissues holds promise for studying complex tissue interactions in healthy and diseased states (Maffioletti et al., 2018; Mazaleyrat et al., 2020). Overall, the iPSC-derived disease models have significant potential for generating personalized medicine platforms, disease specific drug screening, and studying pathogenic cellular or organ-organ crosstalk in a modular fashion.

Volumetric Muscle Loss

Skeletal muscle regenerative capacity can be overwhelmed by extensive muscle loss seen with trauma, blast injuries, and surgical resection. In animal models, this is typically modeled by the surgical removal of 20-40% of muscle mass (Sicari et al., 2014; Corona et al., 2017; Quarta et al., 2017). This level of muscle loss results in irrecoverable loss of muscle function and mass with fibrotic replacement of the lost muscle tissue (Corona et al., 2016). In contrast, other injury models such as snake venom, ischemia-reperfusion, crush, and repeated eccentric contractions in healthy skeletal muscle typically result in return of function 1–2 months post injury. The incomplete muscle regeneration in VML injuries is likely due to the ablation of muscle fibers and their associated SCs, the loss of ECM and associated biochemical and mechanical guidance cues, and the extensive and prolonged inflammatory response to VML injury (Greising et al., 2017; Aguilar et al., 2018; Corona et al., 2018; Larouche et al., 2018). The only current clinical option for VML, autologous tissue transfer, is ineffective due to high donor site morbidity and graft failure. Recent clinical trials utilizing decellularized ECM,

which promote vascularization and an anti-inflammatory healing response, have shown limited therapeutic efficacy due to the lack of significant *de novo* muscle formation necessitating novel therapeutic approaches (Sicari et al., 2014).

Injection of satellite cells alone into VML injury models does not support muscle regeneration, highlighting the need for a satellite cell niche and myofiber guidance for successful regenerative outcomes (Quarta et al., 2017). In non-VML injury models, successful transplantation of SCs is increased by delivering SCs within a native-like niche such as native myofiber fragments (Marg et al., 2014) or tissue engineered muscle constructs (Juhas et al., 2014). In VML injury models, injection of satellite cells in combination with muscle resident cells (which include endothelial cells and mesenchymal progenitors) attached to artificially engineered muscle fiber scaffold results in retention of SCs and functional regeneration of the injured muscle (Quarta et al., 2017). Incorporating additional cell types such as endothelial (Levenberg et al., 2005; Koffler et al., 2011; Perry et al., 2017; Choi et al., 2019), neuronal (Das et al., 2020; Kim et al., 2020), and immune (Juhas et al., 2018) cells improves the survival of transplanted 3D engineered tissues due a combination of cellular recruitment and paracrine signaling to promote vascular and neural integration. The key limitation in the clinical use of the engineered tissue replacements is neural integration with the host. Implantation of engineered muscle tissues and incorporation of the host nerve into the implant increases implant contractile function and maturation compared to time-matched *in vitro* controls (Borschel et al., 2006; Dhawan et al., 2007; Williams et al., 2013; VanDusen et al., 2014; Adams et al., 2017). In these studies, AchR clustering and primitive NMJ synaptogenesis can occur in as little as 7 days post-implantation but functional integration with the host system was only seen 3 months post-implantation (Urbanchek et al., 2016). Encouragingly, muscle innervation after VML injury treated with satellite cell-containing construct was significantly enhanced with exercise (Quarta et al., 2017), suggesting a possibility that engineered muscle innervation could be optimized through physical therapy. Importantly, the incorporation of exercise following implantation of these tissues promotes improved muscle recovery and host innervation of the resulting muscle fibers (Quarta et al., 2017) – the key limitation in translating engineered muscle to the clinic. Transplantation of engineered muscle tissues results in their initial degeneration due to the loss of nutrients and hypoxia. Generation of tissues that regenerate *in vitro* not only enables the study of muscle regeneration in controlled conditions but also correlates to tissue survival upon implantation (Juhas et al., 2014, 2018). Tissues generated from adult rat MPCs fail to regenerate *in vitro* but the addition of macrophages supports *in vitro* regeneration and increased regenerative ability and functionality upon implantation *in vivo* (Juhas et al., 2018).

DISCUSSION

The recent advances and progress made in tissue engineering more biomimetic muscle tissues has provided researchers a novel model to complement traditional 2D cell culture and animal models. Here, we have discussed the utility of these engineered tissues to study muscle physiology, regeneration, exercise, and disease. However, the highest functioning engineered muscle tissues have the functionality of neonatal muscle tissue and do not possess the developmental maturity of adult skeletal muscle (Juhas et al., 2014; Khodabukus et al., 2019). Given that full mouse and human muscle maturation requires 3 months and 18 years respectively, methods to rapidly mature engineered muscle tissues are required. Supraphysiological electrical stimulation of engineered hiPSC cardiac tissues accelerates development to achieve adult-like transcriptomic signatures and mitochondrial levels in 4 weeks (Ronaldson-Bouchard et al., 2018). However, the resulting contractile function was inferior to the highest reported in the field demonstrating incomplete tissue maturation and that paradoxically high tissue function does not always equate to greater maturation. For skeletal muscle, the combined use of electrical and mechanical stimulation, functional innervation, small molecules, and appropriately timed biochemical signals will be required to generate more developmentally mature tissues.

For engineered muscle tissues to be more widely utilized, a shift to serum-free culture conditions is also required to increase reproducibility and permit clinical translation of cellular therapies. This is highlighted by the fact that geographical origin of serum can impact the contractile kinetics and isoform expression of calcium-handling proteins in engineered tissues (Khodabukus and Baar, 2014). Furthermore, batch variations in serum, matrigel, and fibrinogen induce significant functional variations, further adding to reproducibility issues in and between laboratories (Khodabukus and Baar, 2009). The use of serum-free differentiation media utilizing commercially available serum-free supplements such as Ultroser-G (Gawlitta et al., 2007; Fujita et al., 2010) or N-2 (Rao et al., 2018; Khodabukus et al., 2020) have demonstrated the muscle function and structure can be maintained or even improved with serum-free supplements. Further advances will also be required in the generation of more physiologically relevant basal media to provide physiologically relevant levels of saccharides, TCA derivatives, metabolites, and hormones (Cantor et al., 2017). Similarly, the use of synthetic or recombinant extracellular matrices will also be required to improve reproducibility, improve toxicity studies, and for successful clinical translation of cellular or engineered tissue therapies (Nguyen et al., 2017). Lastly, the combinatorial use of small molecules can also be used to enhance muscle function (Selvaraj et al., 2019) but the ability to use these tissues for additional drug screening may be limited due to toxicity issues related to high concentrations organic solvents often used as solvent vehicles.

The majority of studies on engineered muscle tissue function are derived of cultures only containing muscle and contaminating or added fibroblasts. While this enables the ability to isolate muscle-specific effects, native muscle tissue is comprised of multiple cell types that are required for complete muscle development and function. The incorporation of motor neurons (Osaki et al., 2018b; Afshar Bakooshli et al., 2019; Vila et al., 2019), sensory neuron (Colon et al., 2017; Guo et al., 2017), vascular (Levenberg et al., 2005; Perry et al., 2017), immune

(Juhas et al., 2018), and other supporting cell types will be required to generate more biomimetic engineered muscles. Furthermore, the ability to generate multiple tissue types and to couple them together will enable researchers to study organ-organ crosstalk in a highly controlled and regulated environment. These multi-organ or human-on-a-chip systems are required for more physiologically relevant drug screens and the identification of unexpected drug toxicity (Maschmeyer et al., 2015; Oleaga et al., 2016; Skardal et al., 2017; Vernetti et al., 2017). For drug screening purposes, more high throughput systems such as 96 well plate platforms using pillar deflection methods to record force generation are required (Vandenburgh et al., 2008; Mills et al., 2019). Additionally, identifying culture conditions that prevent the Crabtree effect and promote the use of oxidative phosphorylation to meet energy demands are required to improve tissue maturation and better assay mitochondrial toxicity – the most common factor for drug toxicity (Dykens and Will, 2007; Marroquin et al., 2007). Lastly, generation of clinically relevant muscle tissues for VML injuries will require the combination of all factors discussed above and novel approaches to promote rapid neuronal and vascular host integration. Specifically, the use of small molecules (Ko et al., 2013; Quarta et al., 2016), innovative engineering and/or surgical techniques (Borschel et al., 2006; Kim et al., 2015; Al-Himdani et al., 2017), and physical rehabilitation therapy (Quarta et al., 2017) in conjunction with novel methods to generate viable human size tissues are essential for VML therapies.

Overall, tissue engineered muscle systems are a powerful tool to study skeletal muscle function, development, plasticity, and disease. These systems can be used for stand-alone studies, add functional translational components, or be used to supplement *in vivo* studies as 2D systems have been for decades. Future advances in tissue maturation, generation of more complex heterocellular tissues, and coupling to other organ systems will generate improved models to study muscle disease and increase the chance of identifying novel biological and pharmaceutical therapeutics.

AUTHOR CONTRIBUTIONS

AK wrote, edited, and generated figures for the entire manuscript.

FUNDING

This work was supported by the NIH Grants AR055226 and AR065873 from National Institute of Arthritis and Musculoskeletal and Skin Disease, grant UG3TR002142 from the NIH Common Fund for the Microphysiological Systems Initiative, the Jain foundation, and Duke COPE funding.

ACKNOWLEDGMENTS

Figures were created with Biorender.com.

REFERENCES

Aartsma-Rus, A., and Van Putten, M. (2019). The use of genetically humanized animal models for personalized medicine approaches. *Dis. Model Mech.* 13:dmm041673. doi: 10.1242/dmm.041673

Abou-Khalil, R., Le Grand, F., Pallafacchina, G., Valable, S., Authier, F. J., Rudnicki, M. A., et al. (2009). Autocrine and paracrine angiopoietin 1/Tie-2 signaling promotes muscle satellite cell self-renewal. *Cell Stem. Cell* 5, 298–309. doi: 10.1016/j.stem.2009.06.001

Abou-Khalil, R., Mounier, R., and Chazaud, B. (2010). Regulation of myogenic stem cell behavior by vessel cells: the "menage a trois" of satellite cells, periendothelial cells and endothelial cells. *Cell Cycle* 9, 892–896. doi: 10.4161/cc.9.5.10851

Adams, A. M., Vandusen, K. W., Kostrominova, T. Y., Mertens, J. P., and Larkin, L. M. (2017). Scaffoldless tissue-engineered nerve conduit promotes peripheral nerve regeneration and functional recovery after tibial nerve injury in rats. *Neural. Regen. Res.* 12, 1529–1537. doi: 10.4103/1673-5374.215265

Afshar Bakooshli, M., Lippmann, E. S., Mulcahy, B., Iyer, N., Nguyen, C. T., Tung, K., et al. (2019). A 3D culture model of innervated human skeletal muscle enables studies of the adult neuromuscular junction. *Elife* 8:e44530.

Agarkova, I., Schoenauer, R., Ehler, E., Carlsson, L., Carlsson, E., Thornell, L. E., et al. (2004). The molecular composition of the sarcomeric M-band correlates with muscle fiber type. *Eur. J. Cell Biol.* 83, 193–204. doi: 10.1078/0171-9335-00383

Aguer, C., Gambarotta, D., Mailloux, R. J., Moffat, C., Dent, R., Mcpherson, R., et al. (2011). Galactose enhances oxidative metabolism and reveals mitochondrial dysfunction in human primary muscle cells. *PLoS One* 6:e28536. doi: 10.1371/journal.pone.0028536

Aguilar, C. A., Greising, S. M., Watts, A., Goldman, S. M., Peragallo, C., Zook, C., et al. (2018). Multiscale analysis of a regenerative therapy for treatment of volumetric muscle loss injury. *Cell Death Discov.* 4:33.

Aguilar-Agon, K. W., Capel, A. J., Martin, N. R. W., Player, D. J., and Lewis, M. P. (2019). Mechanical loading stimulates hypertrophy in tissue-engineered skeletal muscle: Molecular and phenotypic responses. *J. Cell Physiol.* 234, 23547–23558. doi: 10.1002/jcp.28923

Ahmed, T. A., Dare, E. V., and Hincke, M. (2008). Fibrin: a versatile scaffold for tissue engineering applications. *Tissue Eng. Part B. Rev.* 14, 199–215. doi: 10.1089/ten.teb.2007.0435

Ahmetov, I. I., Hakimullina, A. M., Lyubaeva, E. V., Vinogradova, O. L., and Rogozkin, V. A. (2008). Effect of HIF1A gene polymorphism on human muscle performance. *Bull. Exp. Biol. Med.* 146, 351–353. doi: 10.1007/s10517-008-0291-3

Al-Himdani, S., Jessop, Z. M., Al-Sabah, A., Combellack, E., Ibrahim, A., Doak, S. H., et al. (2017). Tissue-engineered solutions in plastic and reconstructive surgery: principles and practice. *Front. Surg.* 4:4.

Allen, D. G., Lannergren, J., and Westerblad, H. (1997). The role of ATP in the regulation of intracellular Ca2+ release in single fibres of mouse skeletal muscle. *J. Physiol.* 498(Pt 3), 587–600. doi: 10.1113/jphysiol.1997.sp021885

Al-Qusairi, L., Weiss, N., Toussaint, A., Berbey, C., Messaddeq, N., Kretz, C., et al. (2009). T-tubule disorganization and defective excitation-contraction coupling in muscle fibers lacking myotubularin lipid phosphatase. *Proc. Natl. Acad. Sci. U.S.A.* 106, 18763–18768. doi: 10.1073/pnas.0900705106

Amoroso, M. W., Croft, G. F., Williams, D. J., Keeffe, S., Carrasco, M. A., Davis, A. R., et al. (2013). Accelerated high-yield generation of limb-innervating motor neurons from human stem cells. *J. Neurosci.* 33:574. doi: 10.1523/jneurosci.0906-12.2013

An, C. I., Dong, Y., and Hagiwara, N. (2011). Genome-wide mapping of Sox6 binding sites in skeletal muscle reveals both direct and indirect regulation of muscle terminal differentiation by Sox6. *BMC Dev. Biol.* 11:59. doi: 10.1186/1471-213x-11-59

Anderson, J. E., Mcintosh, L. M., and Poettcker, R. (1996). Deflazacort but not prednisone improves both muscle repair and fiber growth in diaphragm and

limb muscle in vivo in the mdx dystrophic mouse. *Muscle Nerve* 19, 1576–1585. doi: 10.1002/(sici)1097-4598(199612)19:12<1576::aid-mus7>3.0.co;2-7

Anderson, M. J., and Cohen, M. W. (1977). Nerve-induced and spontaneous redistribution of acetylcholine receptors on cultured muscle cells. *J. Physiol.* 268, 757–773. doi: 10.1113/jphysiol.1977.sp011880

Anderson, M. J., Cohen, M. W., and Zorychta, E. (1977). Effects of innervation on the distribution of acetylcholine receptors on cultured muscle cells. *J. Physiol.* 268, 731–756. doi: 10.1113/jphysiol.1977.sp011879

Baar, K., and Esser, K. (1999). Phosphorylation of p70(S6k) correlates with increased skeletal muscle mass following resistance exercise. *Am. J. Physiol.* 276, C120–C127.

Baar, K., Torgan, C. E., Kraus, W. E., and Esser, K. (2000). Autocrine phosphorylation of p70(S6k) in response to acute stretch in myotubes. *Mol. Cell Biol. Res. Commun.* 4, 76–80. doi: 10.1006/mcbr.2000.0257

Baldwin, K. M., Haddad, F., Pandorf, C. E., Roy, R. R., and Edgerton, V. R. (2013). Alterations in muscle mass and contractile phenotype in response to unloading models: role of transcriptional/pretranslational mechanisms. *Front. Physiol.* 4:284.

Bansal, D., Miyake, K., Vogel, S. S., Groh, S., Chen, C. C., Williamson, R., et al. (2003). Defective membrane repair in dysferlin-deficient muscular dystrophy. *Nature* 423, 168–172. doi: 10.1038/nature01573

Barany, M., and Close, R. I. (1971). The transformation of myosin in cross-innervated rat muscles. *J. Physiol.* 213, 455–474. doi: 10.1113/jphysiol.1971.sp009393

Beauchamp, J. R., Heslop, L., Yu, D. S., Tajbakhsh, S., Kelly, R. G., Wernig, A., et al. (2000). Expression of CD34 and Myf5 defines the majority of quiescent adult skeletal muscle satellite cells. *J. Cell Biol.* 151, 1221–1234. doi: 10.1083/jcb.151.6.1221

Bello, L., Kesari, A., Gordish-Dressman, H., Cnaan, A., Morgenroth, L. P., Punetha, J., et al. (2015). Genetic modifiers of ambulation in the cooperative international neuromuscular research group duchenne natural history study. *Ann. Neurol.* 77, 684–696. doi: 10.1002/ana.24370

Bian, W., and Bursac, N. (2012). Soluble miniagrin enhances contractile function of engineered skeletal muscle. *FASEB J.* 26, 955–965. doi: 10.1096/fj.11-187575

Boncompagni, S., Kern, H., Rossini, K., Hofer, C., Mayr, W., Carraro, U., et al. (2007). Structural differentiation of skeletal muscle fibers in the absence of innervation in humans. *Proc. Natl. Acad. Sci. U.S.A.* 104, 19339–19344. doi: 10.1073/pnas.0709061104

Borschel, G. H., Dow, D. E., Dennis, R. G., and Brown, D. L. (2006). Tissue-engineered axially vascularized contractile skeletal muscle. *Plast. Reconstr. Surg.* 117, 2235–2242. doi: 10.1097/01.prs.0000224295.54073.49

Bottinelli, R., Canepari, M., Pellegrino, M. A., and Reggiani, C. (1996). Force-velocity properties of human skeletal muscle fibres: myosin heavy chain isoform and temperature dependence. *J. Physiol.* 495, 573–586. doi: 10.1113/jphysiol.1996.sp021617

Bottinelli, R., Canepari, M., Reggiani, C., and Stienen, G. J. (1994). Myofibrillar ATPase activity during isometric contraction and isomyosin composition in rat single skinned muscle fibres. *J. Physiol.* 481(Pt 3), 663–675. doi: 10.1113/jphysiol.1994.sp020472

Brady, M. A., Lewis, M. P., and Mudera, V. (2008). Synergy between myogenic and non-myogenic cells in a 3D tissue-engineered craniofacial skeletal muscle construct. *J. Tissue Eng. Regen. Med.* 2, 408–417. doi: 10.1002/term.112

Brooks, S. V., and Faulkner, J. A. (1988). Contractile properties of skeletal muscles from young, adult and aged mice. *J. Physiol.* 404, 71–82. doi: 10.1113/jphysiol.1988.sp017279

Bryner, R. W., Woodworth-Hobbs, M. E., Williamson, D. L., and Alway, S. E. (2012). Docosahexaenoic acid protects muscle cells from palmitate-induced atrophy. *ISRN Obes* 2012:647348.

Buller, A. J., Eccles, J. C., and Eccles, R. M. (1960). Interactions between motoneurones and muscles in respect of the characteristic speeds of their responses. *J. Physiol.* 150, 417–439. doi: 10.1113/jphysiol.1960.sp006395

Bushby, K., Finkel, R., Birnkrant, D. J., Case, L. E., Clemens, P. R., Cripe, L., et al. (2010). Diagnosis and management of Duchenne muscular dystrophy, part 1: diagnosis, and pharmacological and psychosocial management. *Lancet Neurol.* 9, 77–93. doi: 10.1016/s1474-4422(09)70271-6

Caiozzo, V. J., Baker, M. J., and Baldwin, K. M. (1998). Novel transitions in MHC isoforms: separate and combined effects of thyroid hormone and mechanical unloading. *J. Appl. Physiol. (1985)* 85, 2237–2248. doi: 10.1152/jappl.1998.85.6.2237

Caiozzo, V. J., Haddad, F., Baker, M., Mccue, S., and Baldwin, K. M. (2000). MHC polymorphism in rodent plantaris muscle: effects of mechanical overload and hypothyroidism. *Am. J. Physiol. Cell Physiol.* 278, C709–C717.

Calabria, E., Ciciliot, S., Moretti, I., Garcia, M., Picard, A., Dyar, K. A., et al. (2009). NFAT isoforms control activity-dependent muscle fiber type specification. *Proc. Natl. Acad. Sci. U.S.A.* 106, 13335–13340. doi: 10.1073/pnas.0812911106

Cantor, J. R., Abu-Remaileh, M., Kanarek, N., Freinkman, E., Gao, X., Louissaint, A. Jr., et al. (2017). Physiologic medium rewires cellular metabolism and reveals uric acid as an endogenous inhibitor of UMP synthase. *Cell* 169:e217.

Cappello, V., and Francolini, M. (2017). Neuromuscular junction dismantling in amyotrophic lateral sclerosis. *Int. J. Mol. Sci.* 18:2092. doi: 10.3390/ijms18102092

Carraro, U., Boncompagni, S., Gobbo, V., Rossini, K., Zampieri, S., Mosole, S., et al. (2015). Persistent muscle fiber regeneration in long term denervation. Past, Present, Future. *Eur. J. Transl. Myol.* 25:4832.

Castorena, C. M., Arias, E. B., Sharma, N., Bogan, J. S., and Cartee, G. D. (2015). Fiber type effects on contraction-stimulated glucose uptake and GLUT4 abundance in single fibers from rat skeletal muscle. *Am. J. Physiol. Endocrinol. Metab.* 308, E223–E230.

Chargé, S. B. P., and Rudnicki, M. A. (2004). Cellular and molecular regulation of muscle regeneration. *Physiol. Rev.* 84, 209–238. doi: 10.1152/physrev.00019.2003

Charville, G. W., Cheung, T. H., Yoo, B., Santos, P. J., Lee, G. K., Shrager, J. B., et al. (2015). Ex vivo expansion and in vivo self-renewal of human muscle stem cells. *Stem. Cell Rep.* 5, 621–632. doi: 10.1016/j.stemcr.2015.08.004

Cheema, U., Brown, R., Mudera, V., Yang, S. Y., Mcgrouther, G., and Goldspink, G. (2005). Mechanical signals and IGF-I gene splicing in vitro in relation to development of skeletal muscle. *J. Cell Physiol.* 202, 67–75. doi: 10.1002/jcp.20107

Chiron, S., Tomczak, C., Duperray, A., Laine, J., Bonne, G., Eder, A., et al. (2012). Complex interactions between human myoblasts and the surrounding 3D fibrin-based matrix. *PLoS One* 7:e36173. doi: 10.1371/journal.pone.0036173

Choi, I. Y., Lim, H., Estrellas, K., Mula, J., Cohen, T. V., Zhang, Y., et al. (2016). Concordant but varied phenotypes among duchenne muscular dystrophy patient-specific myoblasts derived using a human iPSC-based model. *Cell Rep.* 15, 2301–2312. doi: 10.1016/j.celrep.2016.05.016

Choi, S. J., and Widrick, J. J. (2010). Calcium-activated force of human muscle fibers following a standardized eccentric contraction. *Am. J. Physiol. Cell Physiol.* 299, C1409–C1417.

Choi, Y. J., Jun, Y. J., Kim, D. Y., Yi, H. G., Chae, S. H., Kang, J., et al. (2019). A 3D cell printed muscle construct with tissue-derived bioink for the treatment of volumetric muscle loss. *Biomaterials* 206, 160–169. doi: 10.1016/j.biomaterials.2019.03.036

Close, R. (1969). Dynamic properties of fast and slow skeletal muscles of the rat after nerve cross-union. *J. Physiol.* 204, 331–346. doi: 10.1113/jphysiol.1969.sp008916

Close, R. I. (1972). Dynamic properties of mammalian skeletal muscles. *Physiol. Rev.* 52, 129–197. doi: 10.1152/physrev.1972.52.1.129

Coley, W. D., Bogdanik, L., Vila, M. C., Yu, Q., Van Der Meulen, J. H., Rayavarapu, S., et al. (2016). Effect of genetic background on the dystrophic phenotype in mdx mice. *Hum. Mol. Genet.* 25, 130–145.

Collet, J. P., Shuman, H., Ledger, R. E., Lee, S., and Weisel, J. W. (2005). The elasticity of an individual fibrin fiber in a clot. *Proc. Natl. Acad. Sci. U.S.A.* 102, 9133–9137. doi: 10.1073/pnas.0504120102

Collins, C. A., Olsen, I., Zammit, P. S., Heslop, L., Petrie, A., Partridge, T. A., et al. (2005). Stem cell function, self-renewal, and behavioral heterogeneity of cells from the adult muscle satellite cell niche. *Cell* 122, 289–301. doi: 10.1016/j.cell.2005.05.010

Colon, A., Guo, X., Akanda, N., Cai, Y., and Hickman, J. J. (2017). Functional analysis of human intrafusal fiber innervation by human gamma-motoneurons. *Sci. Rep.* 7:17202.

Cooper, S. T., Maxwell, A. L., Kizana, E., Ghoddusi, M., Hardeman, E. C., Alexander, I. E., et al. (2004). C2C12 co-culture on a fibroblast substratum enables sustained survival of contractile, highly differentiated myotubes with

peripheral nuclei and adult fast myosin expression. *Cell Motil. Cytoskeleton* 58, 200–211. doi: 10.1002/cm.20010

Corona, B. T., Henderson, B. E., Ward, C. L., and Greising, S. M. (2017). Contribution of minced muscle graft progenitor cells to muscle fiber formation after volumetric muscle loss injury in wild-type and immune deficient mice. *Physiol. Rep.* 5:e13249. doi: 10.14814/phy2.13249

Corona, B. T., Rivera, J. C., and Greising, S. M. (2018). Inflammatory and physiological consequences of debridement of fibrous tissue after volumetric muscle loss injury. *Clin. Transl. Sci.* 11, 208–217. doi: 10.1111/cts.12519

Corona, B. T., Wenke, J. C., and Ward, C. L. (2016). Pathophysiology of Volumetric muscle loss injury. *Cells Tissues Organs* 202, 180–188. doi: 10.1159/000443925

Crabtree, H. G. (1929). Observations on the carbohydrate metabolism of tumours. *Biochem. J.* 23, 536–545. doi: 10.1042/bj0230536

Das, M., Rumsey, J. W., Bhargava, N., Stancescu, M., and Hickman, J. J. (2010). A defined long-term in vitro tissue engineered model of neuromuscular junctions. *Biomaterials* 31, 4880–4888. doi: 10.1016/j.biomaterials.2010.02.055

Das, M., Rumsey, J. W., Gregory, C. A., Bhargava, N., Kang, J. F., Molnar, P., et al. (2007). Embryonic motoneuron-skeletal muscle co-culture in a defined system. *Neuroscience* 146, 481–488. doi: 10.1016/j.neuroscience.2007.01.068

Das, S., Browne, K. D., Laimo, F. A., Maggiore, J. C., Hilman, M. C., Kaisaier, H., et al. (2020). Pre-innervated tissue-engineered muscle promotes a pro-regenerative microenvironment following volumetric muscle loss. *Commun. Biol.* 3:330.

Deconinck, A. E., Rafael, J. A., Skinner, J. A., Brown, S. C., Potter, A. C., Metzinger, L., et al. (1997). Utrophin-dystrophin-deficient mice as a model for Duchenne muscular dystrophy. *Cell* 90, 717–727. doi: 10.1016/s0092-8674(00)80532-2

Demestre, M., Orth, M., Fohr, K. J., Achberger, K., Ludolph, A. C., Liebau, S., et al. (2015). Formation and characterisation of neuromuscular junctions between hiPSC derived motoneurons and myotubes. *Stem. Cell Res.* 15, 328–336. doi: 10.1016/j.scr.2015.07.005

Dennis, R. G., and Dow, D. E. (2007). Excitability of skeletal muscle during development, denervation, and tissue culture. *Tissue Eng.* 13, 2395–2404. doi: 10.1089/ten.2006.0367

Dennis, R. G., and Kosnik, P. E. II (2000). Excitability and isometric contractile properties of mammalian skeletal muscle constructs engineered in vitro. *In Vitro Cell Dev. Biol. Anim.* 36, 327–335.

Dennis, R. G., Kosnik, P. E. II, Gilbert, M. E., and Faulkner, J. A. (2001). Excitability and contractility of skeletal muscle engineered from primary cultures and cell lines. *Am. J. Physiol. Cell Physiol.* 280, C288–C295. doi: 10.1290/1071-2690(2000)036<0327:eaicpo>2.0.co;2

Dennis, R. G., Smith, B., Philp, A., Donnelly, K., and Baar, K. (2009). Bioreactors for guiding muscle tissue growth and development. *Adv. Biochem. Eng. Biotechnol.* 112, 39–79. doi: 10.1007/978-3-540-69357-4_3

Deschenes, M. R., Gaertner, J. R., and O'reilly, S. (2013). The effects of sarcopenia on muscles with different recruitment patterns and myofiber profiles. *Curr. Aging Sci.* 6, 266–272. doi: 10.2174/1874609813066660035

Dhawan, V., Lytle, I. F., Dow, D. E., Huang, Y. C., and Brown, D. L. (2007). Neurotization improves contractile forces of tissue-engineered skeletal muscle. *Tissue Eng.* 13, 2813–2821. doi: 10.1089/ten.2007.0003

Di Maso, N. A., Caiozzo, V. J., and Baldwin, K. M. (2000). Single-fiber myosin heavy chain polymorphism during postnatal development: modulation by hypothyroidism. *Am. J. Physiol. Regul. Integr. Comp. Physiol.* 278, R1099–R1106.

DiMario, J. X., and Stockdale, F. E. (1997). Both myoblast lineage and innervation determine fiber type and are required for expression of the slow myosin heavy chain 2 gene. *Dev. Biol.* 188, 167–180. doi: 10.1006/dbio.1997.8619

Dimos, J. T., Rodolfa, K. T., Niakan, K. K., Weisenthal, L. M., Mitsumoto, H., Chung, W., et al. (2008). Induced pluripotent stem cells generated from patients with ALS can be differentiated into motor neurons. *Science* 321, 1218–1221. doi: 10.1126/science.1158799

Donnelly, K., Khodabukus, A., Philp, A., Deldicque, L., Dennis, R. G., and Baar, K. (2010). A novel bioreactor for stimulating skeletal muscle in vitro. *Tissue Eng. Part C Methods* 16, 711–718. doi: 10.1089/ten.tec.2009.0125

Drummond, M. J., Fry, C. S., Glynn, E. L., Dreyer, H. C., Dhanani, S., Timmerman, K. L., et al. (2009). Rapamycin administration in humans blocks the contraction-induced increase in skeletal muscle protein synthesis. *J. Physiol.* 587, 1535–1546. doi: 10.1113/jphysiol.2008.163816

Dumont, N. A., Wang, Y. X., Von Maltzahn, J., Pasut, A., Bentzinger, C. F., Brun, C. E., et al. (2015). Dystrophin expression in muscle stem cells regulates their polarity and asymmetric division. *Nat. Med.* 21, 1455–1463. doi: 10.1038/nm.3990

Dykens, J. A., and Will, Y. (2007). The significance of mitochondrial toxicity testing in drug development. *Drug Discov. Today* 12, 777–785. doi: 10.1016/j.drudis.2007.07.013

Eberstein, A., and Pachter, B. R. (1986). The effect of electrical stimulation on reinnervation of rat muscle: contractile properties and endplate morphometry. *Brain Res.* 384, 304–310. doi: 10.1016/0006-8993(86)91166-2

Ebert, A. D., Yu, J., Rose, F. F. Jr., Mattis, V. B., Lorson, C. L., Thomson, J. A., et al. (2009). Induced pluripotent stem cells from a spinal muscular atrophy patient. *Nature* 457, 277–280. doi: 10.1038/nature07677

Ehlers, M. L., Celona, B., and Black, B. L. (2014). NFATc1 controls skeletal muscle fiber type and is a negative regulator of MyoD activity. *Cell Rep.* 8, 1639–1648. doi: 10.1016/j.celrep.2014.08.035

Eken, T., Elder, G. C., and Lomo, T. (2008). Development of tonic firing behavior in rat soleus muscle. *J. Neurophysiol.* 99, 1899–1905. doi: 10.1152/jn.00834.2007

Eken, T., and Gundersen, K. (1988). Electrical stimulation resembling normal motor-unit activity: effects on denervated fast and slow rat muscles. *J. Physiol.* 402, 651–669. doi: 10.1113/jphysiol.1988.sp017227

Ekmark, M., Rana, Z. A., Stewart, G., Hardie, D. G., and Gundersen, K. (2007). De-phosphorylation of MyoD is linking nerve-evoked activity to fast myosin heavy chain expression in rodent adult skeletal muscle. *J. Physiol.* 584, 637–650. doi: 10.1113/jphysiol.2007.141457

Elkalaf, M., Andel, M., and Trnka, J. (2013). Low glucose but not galactose enhances oxidative mitochondrial metabolism in C2C12 myoblasts and myotubes. *PLoS One* 8:e70772. doi: 10.1371/journal.pone.0070772

Engler, A. J., Griffin, M. A., Sen, S., Bonnemann, C. G., Sweeney, H. L., and Discher, D. E. (2004). Myotubes differentiate optimally on substrates with tissue-like stiffness: pathological implications for soft or stiff microenvironments. *J. Cell Biol.* 166, 877–887. doi: 10.1083/jcb.200405004

Engler, A. J., Sen, S., Sweeney, H. L., and Discher, D. E. (2006). Matrix elasticity directs stem cell lineage specification. *Cell* 126, 677–689. doi: 10.1016/j.cell.2006.06.044

Eynon, N., Ruiz, J. R., Femia, P., Pushkarev, V. P., Cieszczyk, P., Maciejewska-Karlowska, A., et al. (2012). The ACTN3 R577X polymorphism across three groups of elite male European athletes. *PLoS One* 7:e43132. doi: 10.1371/journal.pone.0043132

Faravelli, I., Bucchia, M., Rinchetti, P., Nizzardo, M., Simone, C., Frattini, E., et al. (2014). Motor neuron derivation from human embryonic and induced pluripotent stem cells: experimental approaches and clinical perspectives. *Stem Cell Res. Ther.* 5:87. doi: 10.1186/scrt476

Flanigan, K. M., Ceco, E., Lamar, K. M., Kaminoh, Y., Dunn, D. M., Mendell, J. R., et al. (2013). LTBP4 genotype predicts age of ambulatory loss in Duchenne muscular dystrophy. *Ann. Neurol.* 73, 481–488.

Fu, X., Wang, H., and Hu, P. (2015). Stem cell activation in skeletal muscle regeneration. *Cell Mol. Life Sci.* 72, 1663–1677. doi: 10.1007/s00018-014-1819-5

Fujita, H., Endo, A., Shimizu, K., and Nagamori, E. (2010). Evaluation of serum-free differentiation conditions for C2C12 myoblast cells assessed as to active tension generation capability. *Biotechnol. Bioeng.* 107, 894–901. doi: 10.1002/bit.22865

Gawlitta, D., Boonen, K. J., Oomens, C. W., Baaijens, F. P., and Bouten, C. V. (2007). The influence of serum-free culture conditions on skeletal muscle differentiation in a tissue-engineered model. *Tissue Eng.* 14, 161–171. doi: 10.1089/ten.2007.0095

Gharaibeh, B., Lu, A., Tebbets, J., Zheng, B., Feduska, J., Crisan, M., et al. (2008). Isolation of a slowly adhering cell fraction containing stem cells from murine skeletal muscle by the preplate technique. *Nat. Protoc.* 3, 1501–1509. doi: 10.1038/nprot.2008.142

Gholobova, D., Decroix, L., Van Muylder, V., Desender, L., Gerard, M., Carpentier, G., et al. (2015). Endothelial network formation within human tissue-engineered skeletal muscle. *Tissue Eng. Part A* 21, 2548–2558. doi: 10.1089/ten.tea.2015.0093

Gholobova, D., Terrie, L., Gerard, M., Declercq, H., and Thorrez, L. (2020a). Vascularization of tissue-engineered skeletal muscle constructs. *Biomaterials* 235:119708. doi: 10.1016/j.biomaterials.2019.119708

Gholobova, D., Terrie, L., Mackova, K., Desender, L., Carpentier, G., Gerard, M., et al. (2020b). Functional evaluation of prevascularization in one-stage versus two-stage tissue engineering approach of human bio-artificial muscle. *Biofabrication* 12:035021. doi: 10.1088/1758-5090/ab8f36

Gibson, M. C., and Schultz, E. (1982). The distribution of satellite cells and their relationship to specific fiber types in soleus and extensor digitorum longus muscles. *Anat. Rec.* 202, 329–337. doi: 10.1002/ar.1092020305

Gilbert, P. M., Havenstrite, K. L., Magnusson, K. E., Sacco, A., Leonardi, N. A., Kraft, P., et al. (2010). Substrate elasticity regulates skeletal muscle stem cell self-renewal in culture. *Science* 329, 1078–1081. doi: 10.1126/science.1191035

Gorza, L., Gundersen, K., Lomo, T., Schiaffino, S., and Westgaard, R. H. (1988). Slow-to-fast transformation of denervated soleus muscles by chronic high-frequency stimulation in the rat. *J. Physiol.* 402, 627–649. doi: 10.1113/jphysiol.1988.sp017226

Grady, R. M., Teng, H., Nichol, M. C., Cunningham, J. C., Wilkinson, R. S., and Sanes, J. R. (1997). Skeletal and cardiac myopathies in mice lacking utrophin and dystrophin: a model for Duchenne muscular dystrophy. *Cell* 90, 729–738. doi: 10.1016/s0092-8674(00)80533-4

Greising, S. M., Rivera, J. C., Goldman, S. M., Watts, A., Aguilar, C. A., and Corona, B. T. (2017). Unwavering pathobiology of volumetric muscle loss injury. *Sci. Rep.* 7:13179.

Grifone, R., Laclef, C., Spitz, F., Lopez, S., Demignon, J., Guidotti, J. E., et al. (2004). Six1 and Eya1 expression can reprogram adult muscle from the slow-twitch phenotype into the fast-twitch phenotype. *Mol. Cell Biol.* 24, 6253–6267. doi: 10.1128/mcb.24.14.6253-6267.2004

Guo, X., Colon, A., Akanda, N., Spradling, S., Stancescu, M., Martin, C., et al. (2017). Tissue engineering the mechanosensory circuit of the stretch reflex arc with human stem cells: Sensory neuron innervation of intrafusal muscle fibers. *Biomaterials* 122, 179–187. doi: 10.1016/j.biomaterials.2017.01.005

Guo, X., Das, M., Rumsey, J., Gonzalez, M., Stancescu, M., and Hickman, J. (2010). Neuromuscular junction formation between human stem-cell-derived motoneurons and rat skeletal muscle in a defined system. *Tissue Eng. Part C Methods* 16, 1347–1355. doi: 10.1089/ten.tec.2010.0040

Haddad, F., Adams, G. R., Bodell, P. W., and Baldwin, K. M. (2006). Isometric resistance exercise fails to counteract skeletal muscle atrophy processes during the initial stages of unloading. *J. Appl. Physiol.* 100, 433–441. doi: 10.1152/japplphysiol.01203.2005

Hagiwara, N., Ma, B., and Ly, A. (2005). Slow and fast fiber isoform gene expression is systematically altered in skeletal muscle of the Sox6 mutant, p100H. *Dev. Dyn.* 234, 301–311. doi: 10.1002/dvdy.20535

Hagiwara, N., Yeh, M., and Liu, A. (2007). Sox6 is required for normal fiber type differentiation of fetal skeletal muscle in mice. *Dev. Dyn.* 236, 2062–2076. doi: 10.1002/dvdy.21223

Hamalainen, N., and Pette, D. (1997). Coordinated fast-to-slow transitions of myosin and SERCA isoforms in chronically stimulated muscles of euthyroid and hyperthyroid rabbits. *J. Muscle Res. Cell Motil.* 18, 545–554.

Handschin, C., Chin, S., Li, P., Liu, F., Maratos-Flier, E., Lebrasseur, N. K., et al. (2007). Skeletal muscle fiber-type switching, exercise intolerance, and myopathy in PGC-1alpha muscle-specific knock-out animals. *J. Biol. Chem.* 282, 30014–30021. doi: 10.1074/jbc.m704817200

Hansen, P. A., Gulve, E. A., and Holloszy, J. O. (1994). Suitability of 2-deoxyglucose for in vitro measurement of glucose transport activity in skeletal muscle. *J. Appl. Physiol. (1985)* 76, 979–985. doi: 10.1152/jappl.1994.76.2.979

Harridge, S. D., Bottinelli, R., Canepari, M., Pellegrino, M. A., Reggiani, C., Esbjornsson, M., et al. (1996). Whole-muscle and single-fibre contractile properties and myosin heavy chain isoforms in humans. *Pflugers Arch.* 432, 913–920. doi: 10.1007/s004240050215

Hatfaludy, S., Shansky, J., and Vandenburgh, H. H. (1989). Metabolic alterations induced in cultured skeletal muscle by stretch-relaxation activity. *Am. J. Physiol.* 256, C175–C181.

Hay, M., Thomas, D. W., Craighead, J. L., Economides, C., and Rosenthal, J. (2014). Clinical development success rates for investigational drugs. *Nat. Biotechnol.* 32, 40–51. doi: 10.1038/nbt.2786

Hennig, R., and Lomo, T. (1985). Firing patterns of motor units in normal rats. *Nature* 314, 164–166. doi: 10.1038/314164a0

Hicks, M. R., Hiserodt, J., Paras, K., Fujiwara, W., Eskin, A., Jan, M., et al. (2018). ERBB3 and NGFR mark a distinct skeletal muscle progenitor cell in human development and hPSCs. *Nat. Cell Biol.* 20, 46–57. doi: 10.1038/s41556-017-0010-2

Hinds, S., Bian, W., Dennis, R. G., and Bursac, N. (2011). The role of extracellular matrix composition in structure and function of bioengineered skeletal muscle. *Biomaterials* 32, 3575–3583. doi: 10.1016/j.biomaterials.2011.01.062

Hoh, J. F. (1975). Selective and non-selective reinnervation of fast-twitch and slow-twitch rat skeletal muscle. *J. Physiol.* 251, 791–801. doi: 10.1113/jphysiol.1975.sp011122

Honda, M., Hidaka, K., Fukada, S. I., Sugawa, R., Shirai, M., Ikawa, M., et al. (2017). Vestigial-like 2 contributes to normal muscle fiber type distribution in mice. *Sci. Rep.* 7:7168.

Hoppeler, H. (2016). Molecular networks in skeletal muscle plasticity. *J. Exp. Biol.* 219, 205–213. doi: 10.1242/jeb.128207

Huang, Y. C., Dennis, R. G., and Baar, K. (2006). Cultured slow vs. fast skeletal muscle cells differ in physiology and responsiveness to stimulation. *Am. J. Physiol. Cell Physiol.* 291, C11–C17.

Huang, Y. C., Dennis, R. G., Larkin, L., and Baar, K. (2005). Rapid formation of functional muscle in vitro using fibrin gels. *J. Appl. Physiol.* 98, 706–713. doi: 10.1152/japplphysiol.00273.2004

Hudecki, M. S., Pollina, C. M., Granchelli, J. A., Daly, M. K., Byrnes, T., Wang, J. C., et al. (1993). Strength and endurance in the therapeutic evaluation of prednisolone-treated MDX mice. *Res. Commun. Chem. Pathol Pharmacol.* 79, 45–60.

Hughes, D. C., Ellefsen, S., and Baar, K. (2018). Adaptations to endurance and strength training. *Cold Spring Harb. Perspect. Med.* 8:a029769.

Hughes, S. M., Koishi, K., Rudnicki, M., and Maggs, A. M. (1997). MyoD protein is differentially accumulated in fast and slow skeletal muscle fibres and required for normal fibre type balance in rodents. *Mech. Dev.* 61, 151–163. doi: 10.1016/s0925-4773(96)00631-4

Ito, A., Yamamoto, Y., Sato, M., Ikeda, K., Yamamoto, M., Fujita, H., et al. (2014). Induction of functional tissue-engineered skeletal muscle constructs by defined electrical stimulation. *Sci. Rep.* 4:4781.

Jorgenson, K. W., Phillips, S. M., and Hornberger, T. A. (2020). Identifying the structural adaptations that drive the mechanical load-induced growth of skeletal muscle: a scoping review. *Cells* 9:1658. doi: 10.3390/cells9071658

Jornayvaz, F. R., and Shulman, G. I. (2010). Regulation of mitochondrial biogenesis. *Essays Biochem.* 47, 69–84.

Juhas, M., Abutaleb, N., Wang, J. T., Ye, J., Shaikh, Z., Sriworarat, C., et al. (2018). Incorporation of macrophages into engineered skeletal muscle enables enhanced muscle regeneration. *Nat. Biomed. Eng.* 2, 942–954. doi: 10.1038/s41551-018-0290-2

Juhas, M., Engelmayr, G. C. Jr., Fontanella, A. N., Palmer, G. M., and Bursac, N. (2014). Biomimetic engineered muscle with capacity for vascular integration and functional maturation in vivo. *Proc. Natl. Acad. Sci. U.S.A.* 111, 5508–5513. doi: 10.1073/pnas.1402723111

Kalhovde, J. M., Jerkovic, R., Sefland, I., Cordonnier, C., Calabria, E., Schiaffino, S., et al. (2005). "Fast" and "slow" muscle fibres in hindlimb muscles of adult rats regenerate from intrinsically different satellite cells. *J. Physiol.* 562, 847–857. doi: 10.1113/jphysiol.2004.073684

Kern, H., Boncompagni, S., Rossini, K., Mayr, W., Fano, G., Zanin, M. E., et al. (2004). Long-term denervation in humans causes degeneration of both contractile and excitation-contraction coupling apparatus, which is reversible by functional electrical stimulation (FES): a role for myofiber regeneration? *J. Neuropathol. Exp. Neurol.* 63, 919–931. doi: 10.1093/jnen/63.9.919

Kern, H., and Carraro, U. (2014). Home-based functional electrical stimulation for long-term denervated human muscle: history, basics, results and perspectives of the vienna rehabilitation strategy. *Eur. J. Transl. Myol.* 24:3296.

Kern, H., Carraro, U., Adami, N., Biral, D., Hofer, C., Forstner, C., et al. (2010). Home-based functional electrical stimulation rescues permanently denervated muscles in paraplegic patients with complete lower motor neuron lesion. *Neurorehabil. Neural. Repair.* 24, 709–721. doi: 10.1177/1545968310366129

Kerr, J. P., Ziman, A. P., Mueller, A. L., Muriel, J. M., Kleinhans-Welte, E., Gumerson, J. D., et al. (2013). Dysferlin stabilizes stress-induced Ca2+ signaling in the transverse tubule membrane. *Proc. Natl. Acad. Sci. U.S.A.* 110, 20831–20836. doi: 10.1073/pnas.1307960110

Khan, N., Eliopoulos, H., Han, L., Kinane, T. B., Lowes, L. P., Mendell, J. R., et al. (2019). Eteplirsen treatment attenuates respiratory decline in ambulatory and

non-ambulatory patients with duchenne muscular dystrophy. *J. Neuromuscul. Dis.* 6, 213–225. doi: 10.3233/jnd-180351

Khodabukus, A., and Baar, K. (2009). Regulating fibrinolysis to engineer skeletal muscle from the C2C12 Cell Line. *Tissue Eng. Part C Methods* 15, 501–511. doi: 10.1089/ten.tec.2008.0286

Khodabukus, A., and Baar, K. (2012). Defined electrical stimulation emphasizing excitability for the development and testing of engineered skeletal muscle. *Tissue Eng. Part C Methods* 18, 349–357. doi: 10.1089/ten.tec.2011.0364

Khodabukus, A., and Baar, K. (2014). The effect of serum origin on tissue engineered skeletal muscle function. *J. Cell Biochem.* 115, 2198–2207. doi: 10.1002/jcb.24938

Khodabukus, A., and Baar, K. (2015a). Contractile and metabolic properties of engineered skeletal muscle derived from slow and fast phenotype mouse muscle. *J. Cell Physiol.* 230, 1750–1757. doi: 10.1002/jcp.24848

Khodabukus, A., and Baar, K. (2015b). Glucose concentration and streptomycin alter in vitro muscle function and metabolism. *J. Cell Physiol.* 230, 1226–1234. doi: 10.1002/jcp.24857

Khodabukus, A., and Baar, K. (2015c). Streptomycin decreases the functional shift to a slow phenotype induced by electrical stimulation in engineered muscle. *Tissue Eng. Part A* 21, 1003–1012. doi: 10.1089/ten.tea.2014.0462

Khodabukus, A., Baehr, L. M., Bodine, S. C., and Baar, K. (2015). Role of contraction duration in inducing fast-to-slow contractile and metabolic protein and functional changes in engineered muscle. *J. Cell Physiol.* 230, 2489–2497. doi: 10.1002/jcp.24985

Khodabukus, A., Kaza, A., Wang, J., Prabhu, N., Goldstein, R., Vaidya, V. S., et al. (2020). Tissue-engineered human myobundle system as a platform for evaluation of skeletal muscle injury biomarkers. *Toxicol. Sci.* 176, 124–136. doi: 10.1093/toxsci/kfaa049

Khodabukus, A., Madden, L., Prabhu, N. K., Koves, T. R., Jackman, C. P., Muoio, D. M., et al. (2019). Electrical stimulation increases hypertrophy and metabolic flux in tissue-engineered human skeletal muscle. *Biomaterials* 198, 259–269. doi: 10.1016/j.biomaterials.2018.08.058

Khodabukus, A., Paxton, J. Z., Donnelly, K., and Baar, K. (2007). Engineered muscle: a tool for studying muscle physiology and function. *Exerc. Sport Sci. Rev.* 35, 186–191. doi: 10.1097/jes.0b013e318156df01

Khodabukus, A., Prabhu, N., Wang, J., and Bursac, N. (2018). In vitro tissue-engineered skeletal muscle models for studying muscle physiology and disease. *Adv. Healthc Mater.* 7:e1701498.

Kim, J. H., Kim, I., Seol, Y. J., Ko, I. K., Yoo, J. J., Atala, A., et al. (2020). Neural cell integration into 3D bioprinted skeletal muscle constructs accelerates restoration of muscle function. *Nat. Commun.* 11:1025.

Kim, S. H., Lee, H. R., Yu, S. J., Han, M. E., Lee, D. Y., Kim, S. Y., et al. (2015). Hydrogel-laden paper scaffold system for origami-based tissue engineering. *Proc. Natl. Acad. Sci. U.S.A.* 112, 15426–15431. doi: 10.1073/pnas.1504745112

Kirschbaum, B. J., Kucher, H. B., Termin, A., Kelly, A. M., and Pette, D. (1990). Antagonistic effects of chronic low frequency stimulation and thyroid hormone on myosin expression in rat fast-twitch muscle. *J. Biol. Chem.* 265, 13974–13980. doi: 10.1016/s0021-9258(18)77444-9

Kivela, R., Salmela, I., Nguyen, Y. H., Petrova, T. V., Koistinen, H. A., Wiener, Z., et al. (2016). The transcription factor Prox1 is essential for satellite cell differentiation and muscle fibre-type regulation. *Nat. Commun.* 7:13124.

Kjaer, M. (2004). Role of extracellular matrix in adaptation of tendon and skeletal muscle to mechanical loading. *Physiol. Rev.* 84, 649–698. doi: 10.1152/physrev.00031.2003

Ko, I. K., Lee, B. K., Lee, S. J., Andersson, K. E., Atala, A., and Yoo, J. J. (2013). The effect of in vitro formation of acetylcholine receptor (AChR) clusters in engineered muscle fibers on subsequent innervation of constructs in vivo. *Biomaterials* 34, 3246–3255. doi: 10.1016/j.biomaterials.2013.01.029

Koffler, J., Kaufman-Francis, K., Shandalov, Y., Egozi, D., Pavlov, D. A., Landesberg, A., et al. (2011). Improved vascular organization enhances functional integration of engineered skeletal muscle grafts. *Proc. Natl. Acad. Sci. U.S.A.* 108, 14789–14794. doi: 10.1073/pnas.1017825108

Kosnik, P. E., Faulkner, J. A., and Dennis, R. G. (2001). Functional development of engineered skeletal muscle from adult and neonatal rats. *Tissue Eng.* 7, 573–584. doi: 10.1089/107632701753213192

Kuang, S., Kuroda, K., Le Grand, F., and Rudnicki, M. A. (2007). Asymmetric self-renewal and commitment of satellite stem cells in muscle. *Cell* 129, 999–1010. doi: 10.1016/j.cell.2007.03.044

Kubis, H. P., Hanke, N., Scheibe, R. J., Meissner, J. D., and Gros, G. (2003). Ca2+ transients activate calcineurin/NFATc1 and initiate fast-to-slow transformation in a primary skeletal muscle culture. *Am. J. Physiol. Cell Physiol.* 285, C56–C63.

Kubis, H. P., Scheibe, R. J., Meissner, J. D., Hornung, G., and Gros, G. (2002). Fast-to-slow transformation and nuclear import/export kinetics of the transcription factor NFATc1 during electrostimulation of rabbit muscle cells in culture. *J. Physiol.* 541, 835–847. doi: 10.1113/jphysiol.2002.017574

Lam, M. T., Huang, Y. C., Birla, R. K., and Takayama, S. (2009). Microfeature guided skeletal muscle tissue engineering for highly organized 3-dimensional free-standing constructs. *Biomaterials* 30, 1150–1155. doi: 10.1016/j.biomaterials.2008.11.014

Lamar, K. M., and Mcnally, E. M. (2014). Genetic modifiers for neuromuscular diseases. *J. Neuromuscul. Dis.* 1, 3–13. doi: 10.3233/jnd-140023

Lamboley, C. R., Murphy, R. M., Mckenna, M. J., and Lamb, G. D. (2013). Endogenous and maximal sarcoplasmic reticulum calcium content and calsequestrin expression in type I and type II human skeletal muscle fibres. *J. Physiol.* 591, 6053–6068. doi: 10.1113/jphysiol.2013.265900

Lanner, J. T., Katz, A., Tavi, P., Sandstrom, M. E., Zhang, S. J., Wretman, C., et al. (2006). The role of Ca2+ influx for insulin-mediated glucose uptake in skeletal muscle. *Diabetes* 55, 2077–2083. doi: 10.2337/db05-1613

Larkin, L. M., Calve, S., Kostrominova, T. Y., and Arruda, E. M. (2006a). Structure and functional evaluation of tendon-skeletal muscle constructs engineered in vitro. *Tissue Eng.* 12, 3149–3158. doi: 10.1089/ten.2006.12.3149

Larkin, L. M., Van Der Meulen, J. H., Dennis, R. G., and Kennedy, J. B. (2006b). Functional evaluation of nerve-skeletal muscle constructs engineered in vitro. *In Vitro Cell Dev. Biol. Anim.* 42, 75–82. doi: 10.1290/0509064.1

Larouche, J., Greising, S. M., Corona, B. T., and Aguilar, C. A. (2018). Robust inflammatory and fibrotic signaling following volumetric muscle loss: a barrier to muscle regeneration. *Cell Death Dis.* 9:409.

Le Grand, F., Jones, A. E., Seale, V., Scime, A., and Rudnicki, M. A. (2009). Wnt7a activates the planar cell polarity pathway to drive the symmetric expansion of satellite stem cells. *Cell Stem. Cell* 4, 535–547. doi: 10.1016/j.stem.2009.03.013

Lee, H., Lim, J. Y., and Choi, S. J. (2017). Oleate prevents palmitate-induced atrophy via modulation of mitochondrial ROS production in skeletal myotubes. *Oxid. Med. Cell Longev.* 2017:2739721.

Lee, P. H., and Vandenburgh, H. H. (2013). Skeletal muscle atrophy in bioengineered skeletal muscle: a new model system. *Tissue Eng. Part A* 19, 2147–2155. doi: 10.1089/ten.tea.2012.0597

Levenberg, S., Rouwkema, J., Macdonald, M., Garfein, E. S., Kohane, D. S., Darland, D. C., et al. (2005). Engineering vascularized skeletal muscle tissue. *Nat. Biotechnol.* 23, 879–884.

Li, M., Dickinson, C. E., Finkelstein, E. B., Neville, C. M., and Sundback, C. A. (2011). The role of fibroblasts in self-assembled skeletal muscle. *Tissue Eng. Part A* 17, 2641–2650. doi: 10.1089/ten.tea.2010.0700

Liao, I. C., Liu, J. B., Bursac, N., and Leong, K. W. (2008). Effect of electromechanical stimulation on the maturation of myotubes on aligned electrospun fibers. *Cell Mol. Bioeng.* 1, 133–145. doi: 10.1007/s12195-008-0021-y

Ljubicic, V., Miura, P., Burt, M., Boudreault, L., Khogali, S., Lunde, J. A., et al. (2011). Chronic AMPK activation evokes the slow, oxidative myogenic program and triggers beneficial adaptations in mdx mouse skeletal muscle. *Hum. Mol. Genet.* 20, 3478–3493. doi: 10.1093/hmg/ddr265

Long, C., Li, H., Tiburcy, M., Rodriguez-Caycedo, C., Kyrychenko, V., Zhou, H., et al. (2018). Correction of diverse muscular dystrophy mutations in human engineered heart muscle by single-site genome editing. *Sci. Adv.* 4:eaa9004.

Loureiro, A. C., Do Rego-Monteiro, I. C., Louzada, R. A., Ortenzi, V. H., De Aguiar, A. P., De Abreu, E. S., et al. (2016). Differential expression of NADPH oxidases depends on skeletal muscle fiber type in rats. *Oxid. Med. Cell Longev.* 2016:6738701.

Lunde, I. G., Anton, S. L., Bruusgaard, J. C., Rana, Z. A., Ellefsen, S., and Gundersen, K. (2011). Hypoxia inducible factor 1 links fast-patterned muscle activity and fast muscle phenotype in rats. *J. Physiol.* 589, 1443–1454. doi: 10.1113/jphysiol.2010.202762

Mackey, A. L., Kjaer, M., Charifi, N., Henriksson, J., Bojsen-Moller, J., Holm, L., et al. (2009). Assessment of satellite cell number and activity status in human skeletal muscle biopsies. *Muscle Nerve.* 40, 455–465. doi: 10.1002/mus.21369

Madden, L., Juhas, M., Kraus, W. E., Truskey, G. A., and Bursac, N. (2015). Bioengineered human myobundles mimic clinical responses of skeletal muscle to drugs. *Elife* 4:e04885.

Maesner, C. C., Almada, A. E., and Wagers, A. J. (2016). Established cell surface markers efficiently isolate highly overlapping populations of skeletal muscle satellite cells by fluorescence-activated cell sorting. *Skelet Muscle* 6:35.

Maffioletti, S. M., Sarcar, S., Henderson, A. B. H., Mannhardt, I., Pinton, L., Moyle, L. A., et al. (2018). Three-dimensional human iPSC-derived artificial skeletal muscles model muscular dystrophies and enable multilineage tissue engineering. *Cell Rep.* 23, 899–908. doi: 10.1016/j.celrep.2018.03.091

Marabita, M., Baraldo, M., Solagna, F., Ceelen, J. J. M., Sartori, R., Nolte, H., et al. (2016). S6K1 is required for increasing skeletal muscle force during hypertrophy. *Cell Rep.* 17, 501–513. doi: 10.1016/j.celrep.2016.09.020

Marg, A., Escobar, H., Gloy, S., Kufeld, M., Zacher, J., Spuler, A., et al. (2014). Human satellite cells have regenerative capacity and are genetically manipulable. *J. Clin. Invest.* 124, 4257–4265. doi: 10.1172/jci63992

Marroquin, L. D., Hynes, J., Dykens, J. A., Jamieson, J. D., and Will, Y. (2007). Circumventing the Crabtree effect: replacing media glucose with galactose increases susceptibility of HepG2 cells to mitochondrial toxicants. *Toxicol. Sci.* 97, 539–547. doi: 10.1093/toxsci/kfm052

Martin, N. R., Passey, S. L., Player, D. J., Mudera, V., Baar, K., Greensmith, L., et al. (2015). Neuromuscular junction formation in tissue-engineered skeletal muscle augments contractile function and improves cytoskeletal organization. *Tissue Eng. Part A* 21, 2595–2604. doi: 10.1089/ten.tea.2015.0146

Maschmeyer, I., Lorenz, A. K., Schimek, K., Hasenberg, T., Ramme, A. P., Hubner, J., et al. (2015). A four-organ-chip for interconnected long-term co-culture of human intestine, liver, skin and kidney equivalents. *Lab. Chip.* 15, 2688–2699. doi: 10.1039/c5lc00392j

Mazaleyrat, K., Badja, C., Broucqsault, N., Chevalier, R., Laberthonniere, C., Dion, C., et al. (2020). Multilineage differentiation for formation of innervated skeletal muscle fibers from healthy and diseased human pluripotent stem cells. *Cells* 9:1531. doi: 10.3390/cells9061531

Mccullagh, K. J., Calabria, E., Pallafacchina, G., Ciciliot, S., Serrano, A. L., Argentini, C., et al. (2004). NFAT is a nerve activity sensor in skeletal muscle and controls activity-dependent myosin switching. *Proc. Natl. Acad. Sci. U.S.A.* 101, 10590–10595. doi: 10.1073/pnas.0308035101

Medler, S. (2019). Mixing it up: the biological significance of hybrid skeletal muscle fibers. *J. Exp. Biol.* 222(Pt 23):jeb200832. doi: 10.1242/jeb.200832

Meissner, J. D., Gros, G., Scheibe, R. J., Scholz, M., and Kubis, H. P. (2001). Calcineurin regulates slow myosin, but not fast myosin or metabolic enzymes, during fast-to-slow transformation in rabbit skeletal muscle cell culture. *J. Physiol.* 533, 215–226. doi: 10.1111/j.1469-7793.2001.0215b.x

Mendell, J. R., Rodino-Klapac, L. R., Sahenk, Z., Roush, K., Bird, L., Lowes, L. P., et al. (2013). Eteplirsen for the treatment of Duchenne muscular dystrophy. *Ann. Neurol.* 74, 637–647.

Mills, R. J., Parker, B. L., Monnot, P., Needham, E. J., Vivien, C. J., Ferguson, C., et al. (2019). Development of a human skeletal micro muscle platform with pacing capabilities. *Biomaterials* 198, 217–227. doi: 10.1016/j.biomaterials.2018.11.030

Montarras, D., Morgan, J., Collins, C., Relaix, F., Zaffran, S., Cumano, A., et al. (2005). Direct isolation of satellite cells for skeletal muscle regeneration. *Science* 309, 2064–2067. doi: 10.1126/science.1114758

Mourkioti, F., Kustan, J., Kraft, P., Day, J. W., Zhao, M. M., Kost-Alimova, M., et al. (2013). Role of telomere dysfunction in cardiac failure in Duchenne muscular dystrophy. *Nat. Cell Biol.* 15, 895–904. doi: 10.1038/ncb2790

Muntener, M., Berchtold, M. W., and Heizmann, C. W. (1985). Parvalbumin in cross-reinnervated and denervated muscles. *Muscle Nerve* 8, 132–137. doi: 10.1002/mus.880080209

Murgia, M., Nagaraj, N., Deshmukh, A. S., Zeiler, M., Cancellara, P., Moretti, I., et al. (2015). Single muscle fiber proteomics reveals unexpected mitochondrial specialization. *EMBO Rep.* 16, 387–395. doi: 10.15252/embr.201439757

Murphy, R. M., Larkins, N. T., Mollica, J. P., Beard, N. A., and Lamb, G. D. (2009). Calsequestrin content and SERCA determine normal and maximal Ca^{2+} storage levels in sarcoplasmic reticulum of fast- and slow-twitch fibres of rat. *J. Physiol.* 587, 443–460. doi: 10.1113/jphysiol.2008.163162

Nagamori, E., Ngo, T. X., Takezawa, Y., Saito, A., Sawa, Y., Shimizu, T., et al. (2013). Network formation through active migration of human vascular endothelial cells in a multilayered skeletal myoblast sheet. *Biomaterials* 34, 662–668. doi: 10.1016/j.biomaterials.2012.08.055

Nesmith, A. P., Wagner, M. A., Pasqualini, F. S., O'connor, B. B., Pincus, M. J., August, P. R., et al. (2016). A human in vitro model of Duchenne muscular dystrophy muscle formation and contractility. *J. Cell Biol.* 215, 47–56. doi: 10.1083/jcb.201603111

Ngo, T. X., Nagamori, E., Kikuchi, T., Shimizu, T., Okano, T., Taya, M., et al. (2013). Endothelial cell behavior inside myoblast sheets with different thickness. *Biotechnol. Lett.* 35, 1001–1008. doi: 10.1007/s10529-013-1174-x

Nguyen, E. H., Daly, W. T., Le, N. N. T., Farnoodian, M., Belair, D. G., Schwartz, M. P., et al. (2017). Versatile synthetic alternatives to Matrigel for vascular toxicity screening and stem cell expansion. *Nat. Biomed. Eng.* 1:0096.

Niro, C., Demignon, J., Vincent, S., Liu, Y., Giordani, J., Sgarioto, N., et al. (2010). Six1 and Six4 gene expression is necessary to activate the fast-type muscle gene program in the mouse primary myotome. *Dev. Biol.* 338, 168–182. doi: 10.1016/j.ydbio.2009.11.031

Okano, T., and Matsuda, T. (1997). Hybrid muscular tissues: preparation of skeletal muscle cell-incorporated collagen gels. *Cell Transplant.* 6, 109–118. doi: 10.1016/s0963-6897(96)00255-2

Okano, T., and Matsuda, T. (1998). Tissue engineered skeletal muscle: preparation of highly dense, highly oriented hybrid muscular tissues. *Cell Transplant.* 7, 71–82. doi: 10.1016/s0963-6897(97)00067-5

Oleaga, C., Bernabini, C., Smith, A. S., Srinivasan, B., Jackson, M., Mclamb, W., et al. (2016). Multi-organ toxicity demonstration in a functional human in vitro system composed of four organs. *Sci. Rep.* 6:20030.

Osaki, T., Sivathanu, V., and Kamm, R. D. (2018a). Crosstalk between developing vasculature and optogenetically engineered skeletal muscle improves muscle contraction and angiogenesis. *Biomaterials* 156, 65–76. doi: 10.1016/j.biomaterials.2017.11.041

Osaki, T., Uzel, S. G. M., and Kamm, R. D. (2018b). Microphysiological 3D model of amyotrophic lateral sclerosis (ALS) from human iPS-derived muscle cells and optogenetic motor neurons. *Sci. Adv.* 4:eaat5847 doi: 10.1126/sciadv.aat5847

Park, K. H., Brotto, L., Lehoang, O., Brotto, M., Ma, J., and Zhao, X. (2012). Ex vivo assessment of contractility, fatigability and alternans in isolated skeletal muscles. *J. Vis. Exp.* 2:e4198.

Pasut, A., Jones, A. E., and Rudnicki, M. A. (2013). Isolation and culture of individual myofibers and their satellite cells from adult skeletal muscle. *J. Vis. Exp.* 3:e50074.

Patani, R., Hollins, A. J., Wishart, T. M., Puddifoot, C. A., Álvarez, S., De Lera, A. R., et al. (2011). Retinoid-independent motor neurogenesis from human embryonic stem cells reveals a medial columnar ground state. *Nat. Commun.* 2:214.

Patkova, J., Andel, M., and Trnka, J. (2014). Palmitate-induced cell death and mitochondrial respiratory dysfunction in myoblasts are not prevented by mitochondria-targeted antioxidants. *Cell Physiol. Biochem.* 33, 1439–1451. doi: 10.1159/000358709

Patterson, M. F., Stephenson, G. M., and Stephenson, D. G. (2006). Denervation produces different single fiber phenotypes in fast- and slow-twitch hindlimb muscles of the rat. *Am. J. Physiol. Cell Physiol.* 291, C518–C528.

Pavesi, A., Adriani, G., Rasponi, M., Zervantonakis, I. K., Fiore, G. B., and Kamm, R. D. (2015). Controlled electromechanical cell stimulation on-a-chip. *Sci. Rep.* 5:11800.

Pegoraro, E., Hoffman, E. P., Piva, L., Gavassini, B. F., Cagnin, S., Ermani, M., et al. (2011). SPP1 genotype is a determinant of disease severity in Duchenne muscular dystrophy. *Neurology* 76, 219–226. doi: 10.1212/wnl.0b013e318207afeb

Perry, L., Flugelman, M. Y., and Levenberg, S. (2017). Elderly patient-derived endothelial cells for vascularization of engineered muscle. *Mol. Ther.* 25, 935–948. doi: 10.1016/j.ymthe.2017.02.011

Petchey, L. K., Risebro, C. A., Vieira, J. M., Roberts, T., Bryson, J. B., Greensmith, L., et al. (2014). Loss of Prox1 in striated muscle causes slow to fast skeletal muscle fiber conversion and dilated cardiomyopathy. *Proc. Natl. Acad. Sci. U.S.A.* 111, 9515–9520. doi: 10.1073/pnas.1406191111

Phua, W. W. T., Wong, M. X. Y., Liao, Z., and Tan, N. S. (2018). An aPPARent functional consequence in skeletal muscle physiology via peroxisome proliferator-activated receptors. *Int. J. Mol. Sci.* 19:1425. doi: 10.3390/ijms19051425

Picard, M., Hepple, R. T., and Burelle, Y. (2012). Mitochondrial functional specialization in glycolytic and oxidative muscle fibers: tailoring the organelle for optimal function. *Am. J. Physiol. Cell Physiol.* 302, C629–C641.

Pieber, K., Herceg, M., Paternostro-Sluga, T., and Schuhfried, O. (2015). Optimizing stimulation parameters in functional electrical stimulation of denervated muscles: a cross-sectional study. *J. Neuroeng. Rehabil.* 12:51.

Potthoff, M. J., Wu, H., Arnold, M. A., Shelton, J. M., Backs, J., Mcanally, J., et al. (2007). Histone deacetylase degradation and MEF2 activation promote the formation of slow-twitch myofibers. *J. Clin. Invest.* 117, 2459–2467. doi: 10.1172/jci31960

Powell, C. A., Smiley, B. L., Mills, J., and Vandenburgh, H. H. (2002). Mechanical stimulation improves tissue-engineered human skeletal muscle. *Am. J. Physiol. Cell Physiol.* 283, C1557–C1565.

Prado, L. G., Makarenko, I., Andresen, C., Kruger, M., Opitz, C. A., and Linke, W. A. (2005). Isoform diversity of giant proteins in relation to passive and active contractile properties of rabbit skeletal muscles. *J. Gen. Physiol.* 126, 461–480. doi: 10.1085/jgp.200509364

Prosser, B. L., Hernandez-Ochoa, E. O., Lovering, R. M., Andronache, Z., Zimmer, D. B., Melzer, W., et al. (2010). S100A1 promotes action potential-initiated calcium release flux and force production in skeletal muscle. *Am. J. Physiol. Cell Physiol.* 299, C891–C902.

Purves-Smith, F. M., Sgarioto, N., and Hepple, R. T. (2014). Fiber typing in aging muscle. *Exerc. Sport Sci. Rev.* 42, 45–52. doi: 10.1249/jes.0000000000000012

Putman, C. T., Sultan, K. R., Wassmer, T., Bamford, J. A., Skorjanc, D., and Pette, D. (2001). Fiber-type transitions and satellite cell activation in low-frequency-stimulated muscles of young and aging rats. *J. Gerontol. A Biol. Sci. Med. Sci.* 56, B510–B519.

Puttonen, K. A., Ruponen, M., Naumenko, N., Hovatta, O. H., Tavi, P., and Koistinaho, J. (2015). Generation of functional neuromuscular junctions from human pluripotent stem cell lines. *Front. Cell Neurosci.* 9:473.

Quarta, M., Brett, J. O., Dimarco, R., De Morree, A., Boutet, S. C., Chacon, R., et al. (2016). An artificial niche preserves the quiescence of muscle stem cells and enhances their therapeutic efficacy. *Nat. Biotechnol.* 34, 752–759. doi: 10.1038/nbt.3576

Quarta, M., Cromie, M., Chacon, R., Blonigan, J., Garcia, V., Akimenko, I., et al. (2017). Bioengineered constructs combined with exercise enhance stem cell-mediated treatment of volumetric muscle loss. *Nat. Commun.* 8:15613.

Quiat, D., Voelker, K. A., Pei, J., Grishin, N. V., Grange, R. W., Bassel-Duby, R., et al. (2011). Concerted regulation of myofiber-specific gene expression and muscle performance by the transcriptional repressor Sox6. *Proc. Natl. Acad. Sci. U.S.A.* 108, 10196–10201. doi: 10.1073/pnas.1107413108

Rangarajan, S., Madden, L., and Bursac, N. (2014). Use of flow, electrical, and mechanical stimulation to promote engineering of striated muscles. *Ann. Biomed. Eng.* 42, 1391–1405. doi: 10.1007/s10439-013-0966-4

Rao, L., Qian, Y., Khodabukus, A., Ribar, T., and Bursac, N. (2018). Engineering human pluripotent stem cells into a functional skeletal muscle tissue. *Nat. Commun.* 9:126.

Rasbach, K. A., Gupta, R. K., Ruas, J. L., Wu, J., Naseri, E., Estall, J. L., et al. (2010). PGC-1alpha regulates a HIF2alpha-dependent switch in skeletal muscle fiber types. *Proc. Natl. Acad. Sci. U.S.A.* 107, 21866–21871. doi: 10.1073/pnas.1016089107

Renzini, A., Benedetti, A., Bouche, M., Silvestroni, L., Adamo, S., and Moresi, V. (2018). Culture conditions influence satellite cell activation and survival of single myofibers. *Eur. J. Transl. Myol.* 28:7567.

Ronaldson-Bouchard, K., Ma, S. P., Yeager, K., Chen, T., Song, L., Sirabella, D., et al. (2018). Advanced maturation of human cardiac tissue grown from pluripotent stem cells. *Nature* 556, 239–243. doi: 10.1038/s41586-018-0016-3

Rosenblatt, J. D., Parry, D. J., and Partridge, T. A. (1996). Phenotype of adult mouse muscle myoblasts reflects their fiber type of origin. *Differentiation* 60, 39–45. doi: 10.1046/j.1432-0436.1996.6010039.x

Rudolf, R., Deschenes, M. R., and Sandri, M. (2016). Neuromuscular junction degeneration in muscle wasting. *Curr. Opin. Clin. Nutr. Metab. Care* 19, 177–181.

Ryall, J. G., Dell'orso, S., Derfoul, A., Juan, A., Zare, H., Feng, X., et al. (2015). The NAD(+)-dependent SIRT1 deacetylase translates a metabolic switch into regulatory epigenetics in skeletal muscle stem cells. *Cell Stem. Cell* 16, 171–183. doi: 10.1016/j.stem.2014.12.004

Sacco, A., Mourkioti, F., Tran, R., Choi, J., Llewellyn, M., Kraft, P., et al. (2010). Short telomeres and stem cell exhaustion model Duchenne muscular dystrophy in mdx/mTR mice. *Cell* 143, 1059–1071. doi: 10.1016/j.cell.2010.11.039

Sakakibara, I., Santolini, M., Ferry, A., Hakim, V., and Maire, P. (2014). Six homeoproteins and a Iinc-RNA at the fast MYH locus lock fast myofiber terminal phenotype. *PLoS Genet.* 10:e1004386. doi: 10.1371/journal.pgen.1004386

Salmons, S., and Sreter, F. A. (1976). Significance of impulse activity in the transformation of skeletal muscle type. *Nature* 263, 30–34. doi: 10.1038/263030a0

Sances, S., Bruijn, L. I., Chandran, S., Eggan, K., Ho, R., Klim, J. R., et al. (2016). Modeling ALS with motor neurons derived from human induced pluripotent stem cells. *Nat. Neurosci.* 19, 542–553.

Sato, M., Ito, A., Kawabe, Y., Nagamori, E., and Kamihira, M. (2011). Enhanced contractile force generation by artificial skeletal muscle tissues using IGF-I gene-engineered myoblast cells. *J. Biosci. Bioeng.* 112, 273–278. doi: 10.1016/j.jbiosc.2011.05.007

Schiaffino, S. (2010). Fibre types in skeletal muscle: a personal account. *Acta. Physiol. (Oxf).* 199, 451–463. doi: 10.1111/j.1748-1716.2010.02130.x

Schiaffino, S., and Reggiani, C. (2011). Fiber types in mammalian skeletal muscles. *Physiol. Rev.* 91, 1447–1531. doi: 10.1152/physrev.00031.2010

Schuh, R. A., Jackson, K. C., Khairallah, R. J., Ward, C. W., and Spangenburg, E. E. (2012). Measuring mitochondrial respiration in intact single muscle fibers. *Am. J. Physiol. Regul. Integr. Comp. Physiol.* 302, R712–R719.

Schuler, M., Ali, F., Chambon, C., Duteil, D., Bornert, J. M., Tardivel, A., et al. (2006). PGC1alpha expression is controlled in skeletal muscles by PPARbeta, whose ablation results in fiber-type switching, obesity, and type 2 diabetes. *Cell Metab.* 4, 407–414. doi: 10.1016/j.cmet.2006.10.003

Schwaller, B., Dick, J., Dhoot, G., Carroll, S., Vrbova, G., Nicotera, P., et al. (1999). Prolonged contraction-relaxation cycle of fast-twitch muscles in parvalbumin knockout mice. *Am. J. Physiol.* 276, C395–C403.

Sellers, J. R. (2004). Fifty years of contractility research post sliding filament hypothesis. *J. Muscle Res. Cell Motil.* 25, 475–482. doi: 10.1007/s10974-004-4239-6

Selvaraj, S., Mondragon-Gonzalez, R., Xu, B., Magli, A., Kim, H., Laine, J., et al. (2019). Screening identifies small molecules that enhance the maturation of human pluripotent stem cell-derived myotubes. *Elife* 8:e147970.

Seto, J. T., Quinlan, K. G., Lek, M., Zheng, X. F., Garton, F., Macarthur, D. G., et al. (2013). ACTN3 genotype influences muscle performance through the regulation of calcineurin signaling. *J. Clin. Invest.* 123, 4255–4263. doi: 10.1172/jci67691

Shansky, J., Del Tatto, M., Chromiak, J., and Vandenburgh, H. (1997). A simplified method for tissue engineering skeletal muscle organoids in vitro. *In Vitro Cell Dev. Biol. Anim.* 33, 659–661. doi: 10.1007/s11626-997-0118-y

Shen, H. W., Jiang, X. L., Gonzalez, F. J., and Yu, A. M. (2011). Humanized transgenic mouse models for drug metabolism and pharmacokinetic research. *Curr. Drug Metab.* 12, 997–1006. doi: 10.2174/138920011798062265

Shoji, E., Sakurai, H., Nishino, T., Nakahata, T., Heike, T., Awaya, T., et al. (2015). Early pathogenesis of Duchenne muscular dystrophy modelled in patient-derived human induced pluripotent stem cells. *Sci. Rep.* 5:12831.

Sicari, B. M., Rubin, J. P., Dearth, C. L., Wolf, M. T., Ambrosio, F., Boninger, M., et al. (2014). An acellular biologic scaffold promotes skeletal muscle formation in mice and humans with volumetric muscle loss. *Sci. Transl. Med.* 6:234ra258.

Sim, W. Y., Park, S. W., Park, S. H., Min, B. H., Park, S. R., and Yang, S. S. (2007). A pneumatic micro cell chip for the differentiation of human mesenchymal stem cells under mechanical stimulation. *Lab. Chip.* 7, 1775–1782. doi: 10.1039/b712361m

Skardal, A., Murphy, S. V., Devarasetty, M., Mead, I., Kang, H. W., Seol, Y. J., et al. (2017). Multi-tissue interactions in an integrated three-tissue organ-on-a-chip platform. *Sci. Rep.* 7:8837.

Sreetama, S. C., Chandra, G., Van Der Meulen, J. H., Ahmad, M. M., Suzuki, P., Bhuvanendran, S., et al. (2018). Membrane stabilization by modified steroid offers a potential therapy for muscular dystrophy due to dysferlin deficit. *Mol. Ther.* 26, 2231–2242. doi: 10.1016/j.ymthe.2018.07.021

Stearns-Reider, K. M., D'amore, A., Beezhold, K., Rothrauff, B., Cavalli, L., Wagner, W. R., et al. (2017). Aging of the skeletal muscle extracellular matrix drives a stem cell fibrogenic conversion. *Aging Cell* 16, 518–528. doi: 10.1111/acel.12578

Stein, C. A. (2016). Eteplirsen approved for duchenne muscular dystrophy: the FDA faces a difficult choice. *Mol. Ther.* 24, 1884–1885. doi: 10.1038/mt.2016.188

Steinbeck, J. A., Jaiswal, M. K., Calder, E. L., Kishinevsky, S., Weishaupt, A., Toyka, K. V., et al. (2016). Functional connectivity under optogenetic control allows modeling of human neuromuscular disease. *Cell Stem. Cell* 18, 134–143. doi: 10.1016/j.stem.2015.10.002

Stienen, G. J., Kiers, J. L., Bottinelli, R., and Reggiani, C. (1996). Myofibrillar ATPase activity in skinned human skeletal muscle fibres: fibre type and temperature dependence. *J. Physiol.* 493(Pt 2), 299–307. doi: 10.1113/jphysiol.1996.sp021384

Strohman, R. C., Bayne, E., Spector, D., Obinata, T., Micou-Eastwood, J., and Maniotis, A. (1990). Myogenesis and histogenesis of skeletal muscle on flexible membranes in vitro. *In Vitro Cell Dev. Biol.* 26, 201–208. doi: 10.1007/bf02624113

Summermatter, S., Thurnheer, R., Santos, G., Mosca, B., Baum, O., Treves, S., et al. (2012). Remodeling of calcium handling in skeletal muscle through PGC-1alpha: impact on force, fatigability, and fiber type. *Am. J. Physiol. Cell Physiol.* 302, C88–C99.

Sun, C., Choi, I. Y., Gonzalez, Y. I. R., Andersen, P., Talbot, C. C. Jr., Iyer, S. R., et al. (2020). Duchenne muscular dystrophy hiPSC-derived myoblast drug screen identifies compounds that ameliorate disease in mdx mice. *JCI Insight* 5:e134287.

Swoap, S. J., Hunter, R. B., Stevenson, E. J., Felton, H. M., Kansagra, N. V., Lang, J. M., et al. (2000). The calcineurin-NFAT pathway and muscle fiber-type gene expression. *Am. J. Physiol. Cell Physiol.* 279, C915–C924.

Takahashi, H., and Okano, T. (2015). Cell sheet-based tissue engineering for organizing anisotropic tissue constructs produced using microfabricated thermoresponsive substrates. *Adv. Healthc. Mater.* 4, 2388–2407. doi: 10.1002/adhm.201500194

Takahashi, H., Shimizu, T., Nakayama, M., Yamato, M., and Okano, T. (2013). The use of anisotropic cell sheets to control orientation during the self-organization of 3D muscle tissue. *Biomaterials* 34, 7372–7380. doi: 10.1016/j.biomaterials.2013.06.033

Takahashi, H., Shimizu, T., and Okano, T. (2018). Engineered human contractile myofiber sheets as a platform for studies of skeletal muscle physiology. *Sci. Rep.* 8:13932.

Terzis, G., Georgiadis, G., Stratakos, G., Vogiatzis, I., Kavouras, S., Manta, P., et al. (2008). Resistance exercise-induced increase in muscle mass correlates with p70S6 kinase phosphorylation in human subjects. *Eur. J. Appl. Physiol.* 102, 145–152. doi: 10.1007/s00421-007-0564-y

Thelen, M. H., Simonides, W. S., and Van Hardeveld, C. (1997). Electrical stimulation of C2C12 myotubes induces contractions and represses thyroid-hormone-dependent transcription of the fast-type sarcoplasmic-reticulum Ca2+-ATPase gene. *Biochem. J.* 321(Pt 3), 845–848. doi: 10.1042/bj3210845

Thorsteinsdottir, S., Deries, M., Cachaco, A. S., and Bajanca, F. (2011). The extracellular matrix dimension of skeletal muscle development. *Dev. Biol.* 354, 191–207. doi: 10.1016/j.ydbio.2011.03.015

Toli, D., Buttigieg, D., Blanchard, S., Lemonnier, T., Lamotte D'incamps, B., Bellouze, S., et al. (2015). Modeling amyotrophic lateral sclerosis in pure human iPSc-derived motor neurons isolated by a novel FACS double selection technique. *Neurobiol. Dis.* 82, 269–280. doi: 10.1016/j.nbd.2015.06.011

Tsika, R. W., Schramm, C., Simmer, G., Fitzsimons, D. P., Moss, R. L., and Ji, J. (2008). Overexpression of TEAD-1 in transgenic mouse striated muscles produces a slower skeletal muscle contractile phenotype. *J. Biol. Chem.* 283, 36154–36167. doi: 10.1074/jbc.m807461200

Tsukamoto, S., Shibasaki, A., Naka, A., Saito, H., and Iida, K. (2018). Lactate Promotes myoblast differentiation and myotube hypertrophy via a pathway involving MyoD in vitro and enhances muscle regeneration in vivo. *Int. J. Mol. Sci.* 19:3649. doi: 10.3390/ijms19113649

Uezumi, A., Nakatani, M., Ikemoto-Uezumi, M., Yamamoto, N., Morita, M., Yamaguchi, A., et al. (2016). Cell-surface protein profiling identifies distinctive markers of progenitor cells in human skeletal muscle. *Stem Cell Rep.* 7, 263–278. doi: 10.1016/j.stemcr.2016.07.004

Urbanchek, M. G., Kung, T. A., Frost, C. M., Martin, D. C., Larkin, L. M., Wollstein, A., et al. (2016). Development of a regenerative peripheral nerve interface for control of a neuroprosthetic limb. *Biomed. Res. Int.* 2016:5726730.

Uzel, S. G., Platt, R. J., Subramanian, V., Pearl, T. M., Rowlands, C. J., Chan, V., et al. (2016). Microfluidic device for the formation of optically excitable, three-dimensional, compartmentalized motor units. *Sci. Adv.* 2:e1501429. doi: 10.1126/sciadv.1501429

Van Putten, M., Putker, K., Overzier, M., Adamzek, W. A., Pasteuning-Vuhman, S., Plomp, J. J., et al. (2019). Natural disease history of the D2-mdx mouse model for Duchenne muscular dystrophy. *FASEB J.* 33, 8110–8124. doi: 10.1096/fj.201802488r

Vandenburgh, H., and Kaufman, S. (1979). In vitro model for stretch-induced hypertrophy of skeletal muscle. *Science* 203, 265–268. doi: 10.1126/science.569901

Vandenburgh, H., Shansky, J., Benesch-Lee, F., Barbata, V., Reid, J., Thorrez, L., et al. (2008). Drug-screening platform based on the contractility of tissue-engineered muscle. *Muscle Nerve* 37, 438–447. doi: 10.1002/mus.20931

Vandenburgh, H. H. (1982). Dynamic mechanical orientation of skeletal myofibers in vitro. *Dev. Biol.* 93, 438–443. doi: 10.1016/0012-1606(82)90131-2

Vandenburgh, H. H. (1988). A computerized mechanical cell stimulator for tissue culture: effects on skeletal muscle organogenesis. *In Vitro Cell Dev. Biol.* 24, 609–619. doi: 10.1007/bf02623597

Vandenburgh, H. H., Hatfaludy, S., Karlisch, P., and Shansky, J. (1989). Skeletal muscle growth is stimulated by intermittent stretch-relaxation in tissue culture. *Am. J. Physiol.* 256, C674–C682.

Vandenburgh, H. H., Hatfaludy, S., Karlisch, P., and Shansky, J. (1991). Mechanically induced alterations in cultured skeletal muscle growth. *J. Biomech.* 24(Suppl. 1), 91–99. doi: 10.1016/0021-9290(91)90380-6

Vandenburgh, H. H., and Karlisch, P. (1989). Longitudinal growth of skeletal myotubes in vitro in a new horizontal mechanical cell stimulator. *In Vitro Cell Dev. Biol.* 25, 607–616. doi: 10.1007/bf02623630

Vandenburgh, H. H., Karlisch, P., and Farr, L. (1988). Maintenance of highly contractile tissue-cultured avian skeletal myotubes in collagen gel. *In Vitro Cell Dev. Biol.* 24, 166–174. doi: 10.1007/bf02623542

Vandenburgh, H. H., and Kaufman, S. (1981). Stretch-induced growth of skeletal myotubes correlates with activation of the sodium pump. *J. Cell Physiol.* 109, 205–214. doi: 10.1002/jcp.1041090203

VanDusen, K. W., Syverud, B. C., Williams, M. L., Lee, J. D., and Larkin, L. M. (2014). Engineered skeletal muscle units for repair of volumetric muscle loss in the tibialis anterior muscle of a rat. *Tissue Eng. Part A* 20, 2920–2930. doi: 10.1089/ten.tea.2014.0060

Verdijk, L. B., Koopman, R., Schaart, G., Meijer, K., Savelberg, H. H., and Van Loon, L. J. (2007). Satellite cell content is specifically reduced in type II skeletal muscle fibers in the elderly. *Am. J. Physiol. Endocrinol. Metab.* 292, E151–E157.

Verdijk, L. B., Snijders, T., Drost, M., Delhaas, T., Kadi, F., and Van Loon, L. J. (2014). Satellite cells in human skeletal muscle; from birth to old age. *Age (Dordr.)* 36, 545–547.

Verma, M., Asakura, Y., Murakonda, B. S. R., Pengo, T., Latroche, C., Chazaud, B., et al. (2018). Muscle satellite cell cross-talk with a vascular niche maintains quiescence via VEGF and notch signaling. *Cell Stem. Cell* 23, e539.

Vernetti, L., Gough, A., Baetz, N., Blutt, S., Broughman, J. R., Brown, J. A., et al. (2017). Functional coupling of human microphysiology systems: intestine liver, kidney proximal tubule, blood-brain barrier and skeletal muscle. *Sci. Rep.* 7:42296.

Vila, O. F., Uzel, S. G. M., Ma, S. P., Williams, D., Pak, J., Kamm, R. D., et al. (2019). Quantification of human neuromuscular function through optogenetics. *Theranostics* 9, 1232–1246. doi: 10.7150/thno.25735

Wang, J., Khodabukus, A., Rao, L., Vandusen, K., Abutaleb, N., and Bursac, N. (2019). Engineered skeletal muscles for disease modeling and drug discovery. *Biomaterials* 221:119416. doi: 10.1016/j.biomaterials.2019.119416

Wang, X., Ono, Y., Tan, S. C., Chai, R. J., Parkin, C., and Ingham, P. W. (2011). Prdm1a and miR-499 act sequentially to restrict Sox6 activity to the fast-twitch muscle lineage in the zebrafish embryo. *Development* 138, 4399–4404. doi: 10.1242/dev.070516

Wang, Y. X., Feige, P., Brun, C. E., Hekmatnejad, B., Dumont, N. A., Renaud, J. M., et al. (2019). EGFR-aurka signaling rescues polarity and regeneration defects in

dystrophin-deficient muscle stem cells by increasing asymmetric divisions. *Cell Stem. Cell* 24:e416.

Wang, Y. X., Zhang, C. L., Yu, R. T., Cho, H. K., Nelson, M. C., Bayuga-Ocampo, C. R., et al. (2004). Regulation of muscle fiber type and running endurance by PPARdelta. *PLoS Biol.* 2:e294. doi: 10.1371/journal.pbio.0020294

Watanabe, N., Komiya, Y., Sato, Y., Watanabe, Y., Suzuki, T., and Arihara, K. (2020). Oleic acid up-regulates myosin heavy chain (MyHC) 1 expression and increases mitochondrial mass and maximum respiration in C2C12 myoblasts. *Biochem. Biophys. Res. Commun.* 525, 406–411. doi: 10.1016/j.bbrc.2020.02.099

Webster, C., Silberstein, L., Hays, A. P., and Blau, H. M. (1988). Fast muscle fibers are preferentially affected in Duchenne muscular dystrophy. *Cell* 52, 503–513. doi: 10.1016/0092-8674(88)90463-1

Wehrle, U., Dusterhoft, S., and Pette, D. (1994). Effects of chronic electrical stimulation on myosin heavy chain expression in satellite cell cultures derived from rat muscles of different fiber-type composition. *Differentiation* 58, 37–46. doi: 10.1046/j.1432-0436.1994.5810037.x

Weinshilboum, R. M., and Wang, L. (2017). Pharmacogenomics: precision medicine and drug response. *Mayo Clin. Proc.* 92, 1711–1722. doi: 10.1016/j.mayocp.2017.09.001

Westerblad, H., and Allen, D. G. (1991). Changes of myoplasmic calcium concentration during fatigue in single mouse muscle fibers. *J. Gen. Physiol.* 98, 615–635. doi: 10.1085/jgp.98.3.615

Westerblad, H., Duty, S., and Allen, D. G. (1993). Intracellular calcium concentration during low-frequency fatigue in isolated single fibers of mouse skeletal muscle. *J. Appl. Physiol. (1985)* 75, 382–388. doi: 10.1152/jappl.1993.75.1.382

Westgaard, R. H., and Lomo, T. (1988). Control of contractile properties within adaptive ranges by patterns of impulse activity in the rat. *J. Neurosci.* 8, 4415–4426. doi: 10.1523/jneurosci.08-12-04415.1988

Williams, M. L., Kostrominova, T. Y., Arruda, E. M., and Larkin, L. M. (2013). Effect of implantation on engineered skeletal muscle constructs. *J. Tissue Eng. Regen. Med.* 7, 434–442. doi: 10.1002/term.537

Windisch, A., Gundersen, K., Szabolcs, M. J., Gruber, H., and Lomo, T. (1998). Fast to slow transformation of denervated and electrically stimulated rat muscle. *J. Physiol.* 510(Pt 2), 623–632. doi: 10.1111/j.1469-7793.1998.623bk.x

Witzemann, V. (2006). Development of the neuromuscular junction. *Cell Tissue Res.* 326, 263–271.

Woodworth-Hobbs, M. E., Perry, B. D., Rahnert, J. A., Hudson, M. B., Zheng, B., and Russ Price, S. (2017). Docosahexaenoic acid counteracts palmitate-induced endoplasmic reticulum stress in C2C12 myotubes: Impact on muscle atrophy. *Physiol. Rep.* 5:e13530.

Wu, H., Naya, F. J., Mckinsey, T. A., Mercer, B., Shelton, J. M., Chin, E. R., et al. (2000). MEF2 responds to multiple calcium-regulated signals in the control of skeletal muscle fiber type. *EMBO J.* 19, 1963–1973. doi: 10.1093/emboj/19.9.1963

Yamaguchi, M., Izumimoto, M., Robson, R. M., and Stromer, M. H. (1985). Fine structure of wide and narrow vertebrate muscle Z-lines. A proposed model and computer simulation of Z-line architecture. *J. Mol. Biol.* 184, 621–643. doi: 10.1016/0022-2836(85)90308-0

Yang, L., Van Der Werf, K. O., Koopman, B. F., Subramaniam, V., Bennink, M. L., Dijkstra, P. J., et al. (2007). Micromechanical bending of single collagen fibrils using atomic force microscopy. *J. Biomed. Mater. Res. A* 82, 160–168. doi: 10.1002/jbm.a.31127

Yang, N., Macarthur, D. G., Gulbin, J. P., Hahn, A. G., Beggs, A. H., Easteal, S., et al. (2003). ACTN3 genotype is associated with human elite athletic performance. *Am. J. Hum. Genet.* 73, 627–631. doi: 10.1086/377590

Young, C. S., Hicks, M. R., Ermolova, N. V., Nakano, H., Jan, M., Younesi, S., et al. (2016). A Single CRISPR-Cas9 deletion strategy that targets the majority of DMD patients restores dystrophin function in hiPSC-derived muscle cells. *Cell Stem. Cell* 18, 533–540. doi: 10.1016/j.stem.2016.01.021

Young, C. S., Mokhonova, E., Quinonez, M., Pyle, A. D., and Spencer, M. J. (2017). Creation of a novel humanized dystrophic mouse model of duchenne muscular dystrophy and application of a CRISPR/Cas9 gene editing therapy. *J. Neuromuscul. Dis.* 4, 139–145. doi: 10.3233/jnd-170218

Yucel, N., Chang, A. C., Day, J. W., Rosenthal, N., and Blau, H. M. (2018). Humanizing the mdx mouse model of DMD: the long and the short of it. *NPJ. Regen. Med.* 3:4.

Yuzefovych, L., Wilson, G., and Rachek, L. (2010). Different effects of oleate vs. palmitate on mitochondrial function, apoptosis, and insulin signaling in L6 skeletal muscle cells: role of oxidative stress. *Am. J. Physiol. Endocrinol. Metab.* 299, E1096–E1105.

Yuzefovych, L. V., Solodushko, V. A., Wilson, G. L., and Rachek, L. I. (2012). Protection from palmitate-induced mitochondrial DNA damage prevents from mitochondrial oxidative stress, mitochondrial dysfunction, apoptosis, and impaired insulin signaling in rat L6 skeletal muscle cells. *Endocrinology* 153, 92–100. doi: 10.1210/en.2011-1442

Zhang, D., Wang, X., Li, Y., Zhao, L., Lu, M., Yao, X., et al. (2014). Thyroid hormone regulates muscle fiber type conversion via miR-133a1. *J. Cell Biol.* 207, 753–766. doi: 10.1083/jcb.201406068

Zhou, J., Parker, D. C., White, J. P., Lim, A., Huffman, K. M., Ho, J. P., et al. (2019). Thyroid hormone status regulates skeletal muscle response to chronic motor nerve stimulation. *Front. Physiol.* 10:1363.

Conflict of Interest: The author declares that the research was conducted in the absence of any commercial or financial relationships that could be construed as a potential conflict of interest.

Advantages of publishing in Frontiers

OPEN ACCESS
Articles are free to read for greatest visibility and readership

FAST PUBLICATION
Around 90 days from submission to decision

HIGH QUALITY PEER-REVIEW
Rigorous, collaborative, and constructive peer-review

TRANSPARENT PEER-REVIEW
Editors and reviewers acknowledged by name on published articles

Frontiers
Avenue du Tribunal-Fédéral 34
1005 Lausanne | Switzerland

Visit us: www.frontiersin.org
Contact us: frontiersin.org/about/contact

REPRODUCIBILITY OF RESEARCH
Support open data and methods to enhance research reproducibility

DIGITAL PUBLISHING
Articles designed for optimal readership across devices

FOLLOW US
@frontiersin

IMPACT METRICS
Advanced article metrics track visibility across digital media

EXTENSIVE PROMOTION
Marketing and promotion of impactful research

LOOP RESEARCH NETWORK
Our network increases your article's readership